WORLD METEOROLOGICAL ORGANIZATION
GLOBAL OZONE RESEARCH AND MONITORING PROJECT—REPORT NO. 25

Scientific Assessment of Ozone Depletion: 1991

NATIONAL AERONAUTICS AND SPACE ADMINISTRATION
NATIONAL OCEANIC AND ATMOSPHERIC ADMINISTRATION
UNITED KINGDOM DEPARTMENT OF THE ENVIRONMENT
UNITED NATIONS ENVIRONMENT PROGRAM
WORLD METEOROLOGICAL ORGANIZATION

World Meteorological Organization
Ozone Secretariat
41 Avenue Giuseppe Motta
P.O. Box 2300
Geneva 20, CH 1211 Switzerland

United Nations Environment Program
United Nations Headquarters
Ozone Secretariat
P.O. Box 30552
Nairobi, Kenya

United Kingdom Department of the Environment
43 Marsham Street
London, SW1P 3PY
United Kingdom

U.S. Department of Commerce
National Oceanic and Atmospheric Administration
14th Street and Constitution Avenue, NW
Hoover Building, Room 5128
Washington, DC 20230
USA

National Aeronautics and Space Administration
Office of Space Science and Applications
Earth Science and Applications Division
Two Independence Square
300 E Street, SW
Washington, DC 20546
USA

WORLD METEOROLOGICAL ORGANIZATION
GLOBAL OZONE RESEARCH AND MONITORING PROJECT—REPORT NO. 25

Scientific Assessment of Ozone Depletion: 1991

NATIONAL AERONAUTICS AND SPACE ADMINISTRATION
NATIONAL OCEANIC AND ATMOSPHERIC ADMINISTRATION
UNITED KINGDOM DEPARTMENT OF THE ENVIRONMENT
UNITED NATIONS ENVIRONMENT PROGRAM
WORLD METEOROLOGICAL ORGANIZATION

LIST OF INTERNATIONAL CONTRIBUTORS AND REVIEWERS

Assessment Co-Chairs

Daniel L. Albritton and Robert T. Watson

Chapter Coordinators

1: Paul Fraser	2: Richard S. Stolarski	3: Lamont R. Poole
4: William H. Brune	5: Ivar S. A. Isaksen	6: Susan Solomon
7: V. Ramaswamy	8: Michael J. Prather	9: Malcolm K. W. Ko
10: Charles H. Jackman		11: Richard L. McKenzie

Assessment Editors

Daniel L. Albritton • Robert T. Watson • Susan Solomon • Robert F. Hampson • Flo Ormond

Authors, Contributors, and Reviewers

Daniel L. Albritton	US	V. Filyushkin	USSR
Fred N. Alyea	US	Vitali Fioletov	USSR
Roger Atkinson	US	Donald A. Fisher	US
John Austin	UK	John E. Frederick	US
T. Berntsen	Norway	Paul J. Fraser	Australia
Lane Bishop	US	A. Fried	US
Don Blake	US	J. A. Fuglestvedt	Norway
M. Blumthaler	Austria	Sophie Godin	France
Rumen D. Bojkov	Switzerland	Keith Grant	US
Guy Brasseur	US	Robert F. Hampson	US
Christoph H. Brühl	Germany	Anne Hansson	Canada
William H. Brune	US	Neil Harris	UK
Bruce Callander	UK	Robert Harriss	US
Jack G. Calvert	US	Robert S. Harwood	UK
Daniel Cariolle	France	William Hill	US
Marie-Lise Chanin	France	Michio Hirota	Japan
William Chu	US	David J. Hofmann	US
Peter Connell	US	Abdel Moneim Ibrahim	Egypt
R. Anthony Cox	UK	Mohammad Ilyas	Malaysia
Paul J. Crutzen	Germany	Ivar Isaksen	Norway
Derek M. Cunnold	US	Charles H. Jackman	US
John DeLuisi	US	Evgeny A. Jadin	USSR
M. Ding	US	Colin Johnson	UK
Anne Douglass	US	Harols S. Johnston	US
Jae A. Edmonds	US	Rod L. Jones	UK
James W. Elkins	US	Igor L. Karol	USSR

Jack Kaye	US
James B. Kerr	Canada
Leon F. Keyser	US
Vyacheslav Khattatov	USSR
Jeffrey Kiehl	US
Volker Kirchhoff	Brazil
Dieter Kley	Germany
Malcolm K. W. Ko	US
Charles E. Kolb	US
Michael J. Kurylo	US
D. Lashof	US
Yuan-Pern Lee	ROC
Jane Leggett	US
Jos. Lelieveld	Germany
Conway B. Leovy	US
M.-T. Leu	US
Pak Sum Low	Kenya
Evgeny Lysenko	USSR
Sasha Madronich	US
Yoshihiro Makide	Japan
Andrew Matthews	New Zealand
M. Patrick McCormick	US
Mack McFarland	US
Richard L. McKenzie	New Zealand
Gèrard Mègie	France
A. J. Miller	US
Mario Molina	US
P. Muthusubramanian	India
Paul Newman	US
Alan O'Neill	UK
Abraham Oort	US
Michael Oppenheimer	US
D. C. Parashar	India
Stuart A. Penkett	UK
M. C. Pitts	US
Lamont R. Poole	US
Michael J. Prather	US
Margarita Prendez	Chile
Ronald G. Prinn	US
John A. Pyle	UK
Lian Xiong Qiu	PRC
V. Ramaswamy	US
Rei A. Rasmussen	US
A. R. Ravishankara	US
Henning Rodhe	Sweden
Jose M. Rodriguez	US
Joan Rosenfield	US
F. Sherwood Rowland	US
Colin E. Roy	Australia
Nelson Antonio Sabogal	Colombia
Eugenio Sanhueza	Venezuela
Toru Sasaki	Japan
H. Scheel	Germany
Mark R. Schoeberl	US
M. D. Schwartzkopf	US
Wolfgang Seiller	Germany
Keith Shine	UK
Howard Sidebottom	Ireland
P. Simmonds	UK
Susan Solomon	US
Johannes Staehelin	Switzerland
K. Stamnes	Germany
Paul Steele	Australia
Richard S. Stolarski	US
Frode Stordal	Norway
Bhoganahalli Subbaraya	India
A. Sutera	Italy
L. W. Thomason	US
Anne Thompson	US
Margaret A. Tolbert	US
O. Brian Toon	US
Adrian F. Tuck	US
Richard Turco	US
Guido Visconti	Italy
Andreas Wahner	Germany
Wei-Chyung Wang	US
David A. Warrilow	UK
Robert T. Watson	US
Debra Weisenstein	US
Ray F. Weiss	US
Tom Wigley	UK
Steve Wofsy	US
Doug R. Worsnop	US
Donald J. Wuebbles	US
Ahmad Zand	Iran
Rudi J. Zander	Belgium
Joseph M. Zawodny	US
Christos Zerefos	Greece
Evgeny A. Zhadin*	USSR
Xiuji Zhou	PRC
Ya-Hui Zhuang	Thailand
Sergei Zvenigorodsky	USSR

*See Jadin

Table of Contents

FOREWORD

The Montreal Protocol on Substances that Deplete the Ozone Layer entered into force on 1 January 1989. Article 6 of the Protocol: Assessment and Review of Control Measures requires that

> "Beginning in 1990, and at least every four years thereafter, the Parties shall assess the control measures provided for in Article 2 on the basis of available scientific, environmental, technical, and economic information. At least one year before each assessment, the Parties shall convene appropriate panels of experts qualified in the fields mentioned and determine the composition and terms of reference of any such panels. Within one year of being convened, the panels will report their conclusions, through the Secretariat, to the Parties."

The second meeting of the Protocol Parties in London, U.K., in June 1990, asked the Secretariat to reconvene, provided for in Article 6, the assessment panels and outlined their terms of reference and timetables for completing assessments of available scientific, environmental, technology and economic information. In particular, the Parties requested that the Scientific assessment panel include an evaluation of the Ozone Depleting Potentials (ODPs) and Global Warming Potentials (GWPs) of substitutes; ODPs of "other halons" that might be produced in significant quantities; the impact on the ozone layer of revised control measures; and the impact on the ozone layer of engine emissions from high-altitude aircraft, rockets and space shuttles. The Parties also requested that the Technology and Economic panels assess the earliest technically feasible dates and the costs for reductions and total phaseout of 1,1,1-trichloroethane (methylchloroform); evaluation of the need for transitional substances in specific applications; quantity of controlled substances needed by developing countries and availability; and comparison of toxicity, flammability, energy efficiency and safety considerations of chemical substitutes and their availability.

At the third meeting of the Protocol Parties in Nairobi, Kenya, in June 1991, the merged Technology and Economic panel was requested to produce a list of full and complete trade names of substances including mixtures by November 1991; to evaluate the implications, possibilities, and difficulties, in particular for developing countries, of an earlier phaseout of controlled substances, for example by 1997; to identify the areas where transitional substances are required to facilitate the earliest possible phaseout of controlled substances and the quantities of transitional substances required; and to identify those transitional substances with the lowest ODPs required for those areas with, if possible, a feasible timetable for their elimination.

The reports of the assessment panels represent the judgement of several hundred experts of appropriate disciplines from developed and developing countries[1]. The reports of each of the three panels incorporated an extensive peer-review process in their original language (English). They will be published and distributed by UNEP in late 1991/early 1992. Copies will be made available to Parties to the Vienna Convention and Montreal Protocol; all other member states of the United Nations; and to interested organizations, institutions, and individuals worldwide.

---

[1] Australia, Austria, Bahamas, Belgium, Benin, Brazil, Canada, Chile, China, Columbia, Czechoslovakia, Denmark, Ecuador, Egypt, France, Germany, Greece, India, Indonesia, Iran, Ireland, Italy, Japan, Jordan, Kenya, Liechtenstein, Malaysia, Mexico, Netherlands, New Zealand, Nigeria, Norway, Papua New Guinea, Saudi Arabia, Singapore, South Africa, South Korea, Sweden, Switzerland, Thailand, Trinidad and Tobago, Tunisia, Uganda, USSR, United Kingdom, United States of America, Venezuela, and Yugoslavia.

The panel reports were chaired as follows:

- The Report of the Ozone Scientific Assessment Panel, chaired by Dr. Robert Watson and Dr. Daniel Albritton (United States of America). One hundred forty-three scientists from 28 countries contributed to the preparation and review of this report (129 scientists from 27 countries prepared the report, and 79 scientists from 25 countries participated in the peer review process).

- The Report of the Environmental Effects Assessment Panel, chaired by Dr. Jan van der Leun (Netherlands) and Dr. Manfred Tevini (Germany). Fifty-eight scientists from 22 countries participated in the preparation and peer review of the report (22 scientists from nine countries prepared the report, and 36 scientists from 18 countries peer reviewed the report).

- The Report of the Technology and Economic Assessment Panel, chaired by Dr. Stephen Andersen (United States of America) and Mr. Steve Lee-Bapty (United Kingdom). Two hundred forty experts from 38 countries prepared the report. Hundreds of expert advisors and peer reviewers from additional countries participated in the peer review process. The Technology and Economic review panel report is a summary of six detailed Technical and Economic Options reports prepared by international subcommittees of sector specific experts. The six technical reports are: (i) Refrigeration, Air Conditioning and Heat Pumps, chaired by Dr. L. Kuijpers (The Netherlands), Dr. H. Haukas (Norway), Mr. P. Vodianitskaia (Brazil) and Mr. J. Kanyua (Kenya); (ii) Rigid and Flexible Foams, chaired by Ms. J. Lupinacci (US) and Mr. P. Vieira (Brazil); (iii) Solvents, Coatings, and Adhesives, chaired by Dr. S. Andersen (US) and Mr. J. Corona (Mexico); (iv) Aerosols, Sterilants and Miscellaneous Uses of CFCs, chaired by Ms. A. Hinwood (Australia) and Mr. J. Pons Pons (Venezuela); (v) Halon Fire Extinguishing Agents, chaired by Mr. G. Taylor (Canada) and Major T. Morehouse (US); and (vi) Economics, chaired by Dr. R. Van Slooten (UK) and Mrs. M. Holmes-Hanek (Bahamas).

EXECUTIVE SUMMARY OF THE SCIENTIFIC ASSESSMENT OF OZONE DEPLETION

RECENT MAJOR SCIENTIFIC FINDINGS

Over the past few years, there have been highly significant advances in the understanding of the impact of human activities on the Earth's stratospheric ozone layer and the influence of changes in chemical composition on the radiative balance of the climate system. Specifically, since the last international scientific review (1989), there have been five major advances:

- **Global Ozone Decreases:** Ground-based and satellite observations continue to show decreases of total column ozone in winter in the Northern Hemisphere. For the first time, there is evidence of significant decreases in *spring and summer* in both the Northern and Southern Hemispheres at middle and high latitudes, as well as in the southern winter. No trends in ozone have been observed in the tropics. These downward trends were larger during the 1980s than in the 1970s. The observed ozone decreases have occurred predominantly in the *lower* stratosphere.

- **Polar Ozone:** Strong Antarctic ozone holes have continued to occur and, in 4 of the past 5 years, have been deep and extensive in area. This contrasts to the situation in the mid-1980s, where the depth and area of the ozone hole exhibited a quasi-biennial modulation. Large increases in surface ultraviolet radiation have been observed in Antarctica during periods of low ozone. While no extensive ozone losses have occurred in the Arctic comparable to those observed in the Antarctic, localized Arctic ozone losses have been observed in winter concurrent with observations of elevated levels of reactive chlorine.

- **Ozone and Industrial Halocarbons:** Recent laboratory research and reinterpretation of field measurements have strengthened the evidence that the Antarctic ozone hole is primarily due to chlorine- and bromine-containing chemicals. In addition, the weight of evidence suggests that the observed middle- and high-latitude ozone losses are largely due to chlorine and bromine. Therefore, as the atmospheric abundances of chlorine and bromine increase in the future, significant additional losses of ozone are expected at middle latitudes and in the Arctic.

- **Ozone and Climate Relations:** For the first time, the observed global lower-stratospheric ozone depletions have been used to calculate the changes in the radiative balance of the atmosphere. The results indicate that, over the last decade, the observed ozone depletions would have tended to cool the lower stratosphere at middle and high latitudes. Temperature data suggest that some cooling indeed has taken place there. The observed lower-stratospheric ozone changes and calculated temperature changes would have caused a decrease in the radiative forcing of the surface-troposphere system in the middle to high latitudes that is larger in magnitude than that predicted for the chlorofluorocarbon (CFC) increases over the last decade. In addition, the ozone depletion may indeed have offset a significant fraction of the radiative forcing due to increases of all greenhouse gases over the past decade.

- **Ozone Depletion Potentials (ODPs) and Global Warming Potentials (GWPs):** A new semi-empirical, observation-based method of calculating ODPs has better quantified the role of polar processes in this index. In addition, the direct GWPs for tropospheric, well-mixed, radiatively-active species have been recalculated. However, because of the incomplete understanding of tropospheric chemical processes, the indirect GWP of methane has not, at present, been quantified reliably. Furthermore, the concept of a GWP may prove inapplicable for the very short-lived, inhomogeneously mixed gases, such as the nitrogen oxides. Hence, many of the indirect GWPs reported in 1990 by the Intergovernmental Panel on Climate Change (IPCC) are likely to be incorrect.

SUPPORTING EVIDENCE AND RELATED ISSUES

Global Ozone

- Independent observations from the ground-based Dobson and M83/M124 instruments and the Total Ozone Mapping Spectrometer (TOMS) satellite instrument all show, for the first time, that there are significant decreases in total-column ozone, after accounting for known natural variability, in winter and now in spring and summer in both the Northern and Southern Hemispheres at middle and high latitudes, but not in the tropics. The following table illustrates some of these points.

Total Ozone Trends (percent per decade with 95 percent confidence limits)

	TOMS: 1979–91			Ground-based: 26°N–64°N	
Season	**45°S**	**Equator**	**45°N**	**1979–1991**	**1970–1991**
Dec–Mar	–5.2 ± 1.5	+0.3 ± 4.5	–5.6 ± 3.5	–4.7 ± 0.9	–2.7 ± 0.7
May–Aug	–6.2 ± 3.0	+0.1 ± 5.2	–2.9 ± 2.1	–3.3 ± 1.2	–1.3 ± 0.4
Sep–Nov	–4.4 ± 3.2	+0.3 ± 5.0	–1.7 ± 1.9	–1.2 ± 1.6	–1.2 ± 0.6

- There is strong *combined* observational evidence from balloonsondes, ground-based Umkehr, and the Stratospheric Aerosol and Gas Experiment (SAGE) satellite instruments that, over the past decade, annual average ozone has decreased in the middle- and high-latitude stratosphere below 25 km (about 10 percent near 20 km).

- Ozone losses in the upper stratosphere have been observed by ground-based Umkehr and SAGE satellite instruments. Changes in the shape of the vertical distribution of ozone near 40 km are qualitatively consistent with theoretical predictions but are smaller in magnitude.

- Measurements indicate that ozone levels in the troposphere up to 10 km above the few existing balloonsonde stations at northern middle latitudes have increased by about 10 percent per decade over the past two decades. However, the data base for ozone trends in the upper troposphere, where it is an effective greenhouse gas, is sparse and inadequate for quantifying its contribution to the global radiative balance. It should be noted that the response of ozone in the upper troposphere is particularly sensitive to oxides of nitrogen injected by aircraft.

- The temperature record indicates that a small cooling (about 0.3°C per decade, globally averaged) has occurred in the lower stratosphere over the last two decades, which is in the sense of that expected from the observed ozone change.

- Increases continue in the atmospheric abundances of source gases that affect ozone and the radiative balance. Although methane has continued to increase in the atmosphere, the rate of increase has slowed, for reasons that are not understood. Methyl bromide is the major contributor to stratospheric bromine (15 parts per trillion by volume or pptv). The sources of methyl bromide are not well characterized; however, significant anthropogenic emissions have been suggested.

- Recent laboratory studies have identified key heterogeneous reactions and have allowed a more quantitative assessment of the role of global stratospheric sulfate aerosols in leading to enhanced abundances of reactive chlorine species.

- Limited observations suggest that the abundance of chlorine monoxide (ClO) in the lower stratosphere at northern middle latitudes is greater than that predicted by models containing only currently known gas phase chemistry, and the observed seasonal and latitudinal dependences are inconsistent with those pre-

dicted. Some new studies that incorporate currently known heterogeneous processes provide an improved simulation for some observed gases, such as ClO and nitric acid.

- Present models containing only gas phase processes cannot simulate the observed seasonal ozone depletions at middle and high latitudes. However, models incorporating currently known heterogeneous processes on sulfate aerosols predict substantially greater ozone depletion (*e.g.*, a factor of 2 to 3 at middle latitudes) from chlorine and bromine compounds compared to models containing only gas phase processes. Indeed, the heterogeneous models simulate most of the observed trend of column ozone in middle latitudes in summer but only about half of that in winter.

- There is not a full accounting of the observed downward trends in global ozone. Plausible mechanisms include (i) local heterogeneous chemistry on stratospheric sulfate aerosols (as evidenced by, for example, elevated levels of ClO and the presence of sulfate aerosols at the altitudes of the observed ozone depletion) and (ii) the transport of both ozone-depleted and chemically perturbed polar air to middle latitudes (as evidenced by high levels of reactive chlorine and low levels of reactive nitrogen, which are characteristic of chemically perturbed polar air). Although other possible mechanisms cannot be ruled out, those involving chlorine and bromine appear to be largely responsible for the ozone loss and are the only ones for which direct evidence exists.

- Since the middle latitude ozone losses are apparently due in large part to chlorine and bromine, greater ozone losses are expected as long as the atmospheric levels of these compounds continue to increase. With the increases in the levels of chlorine and bromine that are estimated for the year 2000, the additional ozone losses during the 1990s are expected to be comparable to those already observed for the 1980s.

- There are numerous ways in which further increases in stratospheric halogen abundances can be reduced. The following table illustrates the effects of reducing the emissions of several types of halocarbons. Four aspects are shown: (i) the change in peak chlorine loading, (ii) the times at which chlorine abundances have decreased back to 2 parts per billion by volume (ppbv) (the abundance in the late 1970s, which is when the Antarctic ozone hole started and when the accelerated trends in total-column ozone losses in the Northern Hemisphere began), (iii) the times at which chlorine abundances have decreased back to 3 ppbv (the abundance in the middle to late 1980s), and (iv) a measure of the cumulative ozone loss for the time period that the chlorine levels are above 3 ppbv. All of the values in the table are relative to the reference scenario (AA).

- Stratospheric bromine is 30 to 120 times more efficient than stratospheric chlorine in destroying ozone on a per atom basis. Therefore, 1 pptv of stratospheric bromine is equivalent to 0.03–0.12 ppbv of stratospheric chlorine.

Scenarios for Reducing Chlorine Emissions

Scenario	Peak Cl (ppbv)	Years at 3 ppbv	Years at 2 ppbv	Integral (Cl>3 ppbv)
AA	**4.1**	**2027**	**2060**	**22.7**
AA3	–0.18	–10 yrs	–7	–7.6
D	–0.03	0	0	–1.3
D3	–0.10	0	0	–2.9
E	0.00	–7	–3	–2.0*
E3	–0.03*	–10	–3	–4.4*
F20	+0.01	0	0	+0.8
F40	+0.02	+1	0	+1.5
G20	+0.01	+5	+2	+4.2
AA3 + D3	–0.21	–11	–7	–10.4

*These values should be reduced by a factor of about 2 to 3 when evaluating ozone loss rather than chlorine loading.

Definitions of scenarios:

AA: Montreal Protocol (10-year lag of 10 percent of CFCs plus CCl_4; no lag for CH_3CCl_3 and halons). HCFC-22 increases at 3 percent per year from 1991 to 2020, ramps to 0 by 2040. No substitution of CFCs with HCFCs.

Nonsubstitution scenarios:

AA3: 3-year acceleration of CFCs and CCl_4 schedules.
D: 3-year acceleration of CH_3CCl_3 schedule.
D3: CH_3CCl_3 on the accelerated CFC phase-out schedule.
E: HCFC-22 ramp to zero between 2000 and 2020.
E3: HCFC-22 on the accelerated CFC phase-out schedule.

Substitution scenarios:

HCFC substitutions: begin in 1995, no growth to 2000, 3 percent per year to 2020, ramp to zero by 2030. HCFC-A has a 2-year lifetime, one chlorine, and an ODP of 0.013; HCFC-B has a 20-year lifetime, one chlorine, and an ODP of 0.13.

F20: 20 percent initial substitution, HCFC-A.
F40: 40 percent initial substitution, HCFC-A.
G20: 20 percent initial substitution, HCFC-B.

Polar Ozone

- The Antarctic ozone hole in 1991 was as deep and as extensive in area as those of 1987, 1989, and 1990. The low value of total-column ozone measured by TOMS in early October in 1991 was 110 Dobson units, which is a decrease of about 60 percent compared to the ozone levels prior to the late 1970s. The previously noted quasi-biennial modulation of the severity of the ozone hole did not occur during the past 3 years. This apparent lack of variability in recent years may imply that halogen chemistry is becoming dominant over dynamically induced fluctuations on Antarctic ozone depletion.

- Recent laboratory studies of heterogeneous processes, reevaluated field measurements, and modeling studies have strengthened the confidence that the cause of the Antarctic ozone hole is primarily chlorine and bromine emissions.

- High concentrations of ClO have been observed in winter in the Arctic stratosphere between 16 and 20 km. These observations have been incorporated into diagnostic models that have calculated localized ozone depletions of about 10 percent at these altitudes over a period of about a month, which are consistent with concurrent ozone measurements.

Ozone-Climate Relations

- The ozone losses observed in the lower stratosphere over the last decade are predicted to have increased the visible and ultraviolet incoming solar radiation reaching the surface-troposphere system and decreased the downward infrared radiation reaching the surface-troposphere system. For models that allow for the temperature of the stratosphere to adjust to the loss of ozone, the net effect is a decrease in radiative forcing. For middle and high latitudes throughout the year, the magnitude of this decrease may be larger than the predicted increases in the radiative forcing due to the increased abundances of CFCs over the last decade. Indeed, this ozone-induced decrease in radiative forcing could be offsetting a significant fraction of the increased forcing attributed to the increases in the abundances of all greenhouse gases over the same period. Changes in the global annual average radiative forcing due to the observed ozone depletion are predicted to be comparable in magnitude, but opposite in sign, to those attributed to the CFCs over the last decade.

- Current tropospheric models exhibit large differences in their predictions of changes in ozone, the hydroxyl radical, and other chemically active gases due to emissions of methane, nonmethane hydrocarbons, carbon monoxide, and nitrogen oxides. This arises from uncertainties in the knowledge of background chemical composition and an inadequate understanding of chemical reactions and dynamical processes. Hence, these deficiencies limit the accuracy of predicted changes in the abundance and distribution of tropospheric ozone, which is a greenhouse gas, and in the lifetimes of a number of other greenhouse gases, including the HCFCs and HFCs, which depend upon the abundance of the hydroxyl radical.

Ozone Depletion and Global Warming Potentials (ODPs and GWPs)

- Steady-state and time-dependent ODPs have been recalculated with improved models that have incorporated more accurate reaction rate coefficients and absorption cross sections and known heterogeneous processes on sulfate aerosols. The numerical values are generally similar to those in previous assessments.

- A new semi-empirical, observation-based method of calculating ODPs has been developed. The resulting values are generally larger (up to a factor of two as compared to some model-based estimates) for species with long stratospheric lifetimes (*e.g.*, HCFC-22 and HCFC-142b) and slightly smaller for species with short stratospheric lifetimes (*e.g.*, carbon tetrachloride and methyl chloroform). Since this approach utilizes more atmospheric observations and fewer model calculations in characterizing polar ozone losses, it is considered to be better than standard model ODPs, at least in the polar regions.

- The direct GWPs (with five different time horizons: 20, 50, 100, 200, and 500 years) for tropospheric, well-mixed, radiatively active species have been recalculated using updated lifetimes for methane, nitrous oxide, and the halocarbons and following the same methodology of IPCC (1990). With the exception of methane, new GWP results indicate only modest changes from the IPCC values, but uncertainties still exist in these calculations due to limitations in knowledge of the carbon cycle.

- Because of incomplete understanding of tropospheric chemical processes, the indirect GWP of methane has not been quantified reliably at the time of this report, although improvements and quantifications of uncertainties in the near future are highly likely. The signs of the net changes in radiative forcing from known indirect effects have been established for some of the trace gases: methane, carbon monoxide, and nonmethane hydrocarbons, which are all positive. The sign of the changes in radiative forcing due to the nitro-

gen oxides cannot currently be established. Furthermore, the basic concept of a GWP may indeed prove to be inapplicable for the very short-lived, inhomogeneously mixed gases, such as the nitrogen oxides and the nonmethane hydrocarbons. Hence, the IPCC (1990) indirect GWPs are not only uncertain, but many are also likely to be incorrect (*e.g.*, for the nitrogen oxides).

Related Issues

- **Ultraviolet Radiation:** Significant increases in ultraviolet radiation have been observed over Antarctica in conjunction with periods of intense ozone depletion. Under clear-sky conditions, these increases are consistent with theoretical predictions. Furthermore, a erythemal radiative amplification factor of 1.25 ± 0.20 has been deduced from simultaneous measurements of column ozone and surface ultraviolet radiation at a clean air site, which is in agreement with a model-calculated value of 1.1. Therefore, for the first time, the response of ground-level ultraviolet radiation to changes in column ozone has been observed and quantified.

- **Supersonic Aircraft:** A previous, independent assessment of the impact of a projected fleet of supersonic aircraft on stratospheric ozone has reported the prediction that the ozone loss increases with the amount of nitrogen oxides emitted. These models used gas phase chemistry and assessed ozone loss for the case of 500 aircraft flying at Mach 2.4 between 17 and 20 km with an annual fuel use of 7×10^{10} kg/yr. The annual average loss of column ozone at middle latitudes in the Northern Hemisphere is predicted to be 2 to 6 percent. For a comparable fleet operated at Mach 3.2 between 21 and 24 km, the comparable column ozone loss is 7 to 12 percent. However, recent evidence has shown that reactions on sulfate aerosols can change the partitioning of nitrogen oxides. Two model studies incorporating this heterogeneous chemistry have recently reexamined the Mach 2.4 case and found substantially less ozone change (–0.5 to +0.5 percent). These implications are being examined as part of a separate assessment.

- **Shuttles and Rockets:** The increase in the abundance of stratospheric chlorine from one projection of U.S. annual launches of nine Space Shuttles and six Titan rockets is calculated to be less than 0.25 percent of the annual stratospheric chlorine source from halocarbons in the present-day atmosphere (with maximum increases of 0.01 ppbv in the middle and upper stratosphere in the northern middle and high latitudes). The TOMS ozone record shows no detectable changes in column ozone immediately following each of several launches of the Space Shuttles.

- **Volcanoes, Ozone Loss, and Climate Perturbations:** Major volcanic eruptions, such as Mt. Pinatubo, substantially increase the stratospheric abundance of sulfate aerosols for a few years. Since laboratory and field data show that heterogeneous processes can lead to increased levels of reactive chlorine in the stratosphere, such injections have the potential to increase ozone losses temporarily. Furthermore, the increased levels of stratospheric sulfate aerosols are predicted to warm the lower stratosphere by about 4°C (which has been observed) and cool the Earth's surface by a much smaller amount.

- **Tropospheric Sulfate Aerosols and Climate:** Fossil fuel emissions over the past century have increased the tropospheric sulfate aerosol concentrations. Their contribution to the direct radiative forcing of the clear-sky Northern Hemisphere is opposite to that due to the greenhouse gases and is estimated to be a substantial fraction of the trace gas forcing.

IMPLICATIONS FOR POLICY FORMULATIONS

The findings and conclusions of the research of the past few years have several major implications as input to policy decisions regarding human-influenced substances that lead to stratospheric ozone depletions and to changes in the radiative forcing of the climate system:

- **Continued Global Ozone Losses:** Even if the control measures of the amended Montreal Protocol (London, 1990) were to be implemented by all nations, the current abundance of stratospheric chlorine (3.3 to 3.5 ppbv) is estimated to increase during the next several years, reaching a peak of about 4.1 ppbv around the turn of the century. With these increases, the additional middle latitude ozone losses during the 1990s are expected to be comparable to those observed during the 1980s, and there is the possibility of incurring widespread losses in the Arctic. *Reducing these expected and possible ozone losses requires further limitations on the emissions of chlorine- and bromine-containing compounds.*

- **Approaches to Lowering Global Risks:** Lowering the peak and hastening the subsequent decline of chlorine and bromine levels can be accomplished in a variety of ways, including an accelerated phase-out of controlled substances and limitations on currently uncontrolled halocarbons. A significant reduction in peak chlorine loading (a few tenths of a ppbv) can be achieved with accelerated phase-out schedules of CFCs, carbon tetrachloride, and methyl chloroform. Even stringent controls on HCFC-22 would not significantly reduce peak chlorine loading (at most 0.03 ppbv, especially when ODP weighted), but do hasten the decline of chlorine. A 3-year acceleration of the phase-out schedule for the halons would reduce peak bromine loading by about 1 pptv. If the anthropogenic sources of methyl bromide are significant and their emissions can be reduced, then each 10 percent reduction in methyl bromide would rapidly result in a decrease in stratospheric bromine of 1.5 pptv, which is equivalent to a reduction in stratospheric chlorine of 0.045 to 0.18 ppbv. *This gain is comparable to that of a 3-year acceleration of the scheduled phase-out of the CFCs.*

- **Elimination of the Antarctic Ozone Hole:** The phase-out schedule of the amended Montreal Protocol, if fully complied by all nations and if there are no continued uses of HCFCs, affords the opportunity to return to stratospheric chlorine abundances of 2 ppbv sometime between the middle and the end of the next century. This is the level at which the Antarctic ozone hole appeared in the late 1970s and hence is about the level that is thought to be necessary (other conditions assumed constant, including bromine loading) to eliminate the ozone hole. *Such levels could never have been reached under the provisions of the original Protocol (Montreal, 1987).*

- **Uncertain Greenhouse Role of CFCs:** The weight of evidence suggests that a large part of the observed lower stratospheric decrease in ozone is the result of CFC emissions. Furthermore, the radiative impact of this ozone decrease may have largely offset the predicted direct radiative perturbations, at middle to high latitudes, due to the CFC increases over the last decade. *Hence, even the sign of the overall radiative effect of CFC increases on the climate system over the last decade is uncertain.*

- **Utility of GWPs:** The direct GWPs are a useful indicator of the relative radiative effects of long-lived, well-mixed, radiatively active trace species. However, GWPs may be inapplicable for comparing the direct radiative effects of a long-lived, well-mixed gas to the indirect effects of a short-lived gas (for example, carbon dioxide to the nitrogen oxides). *For the latter need, the application of new tools, such as three-dimensional, fully coupled chemistry-climate models may be required.*

CHAPTER 1

Source Gases: Concentrations, Emissions, and Trends

Authors:

P. Fraser
S. Penkett
R. Harriss
Y. Makide
E. Sanhueza

Additional Contributors:

F. Alyea
D. Blake
D. Cunnold
J. Elkins
M. Hirota
R. Prinn
R. Rasmussen
S. Rowland
T. Sasaki
H. Scheel
W. Seiler
P. Simmonds
P. Steele
R. Weiss

Chapter 1

Source Gases: Concentrations, Emissions, and Trends

Contents

Contents (Continued))

SCIENTIFIC SUMMARY

The major anthropogenic source gases implicated directly in halogen induced stratospheric ozone loss, *i.e.*, chlorofluorocarbons (CFCs), hydrochlorofluorocarbon-22 (HCFC-22), the halons, methyl chloroform and carbon tetrachloride, continue to grow in concentration in the background troposphere of both hemispheres. Total tropospheric chlorine is increasing by ≈0.1 parts per billion by volume (ppbv) per year. CFCs contribute approximately 75 percent to this increase, methyl chloroform 13 percent, and HCFC-22 ≈5 percent.

The 1989 global mean concentrations and trends of the various source gases that can directly or indirectly influence the global abundance of stratospheric and tropospheric ozone are given in Table 1-1. In general, the data are similar to those reported for 1987 in the previous assessment (WMO, 1990b), but there have also been some important new developments.

CFC-11 and CFC-12 trends have not changed significantly since the last assessment. The global CFC-113 trend in 1989 (≈5–6 parts per trillion by volume (pptv), 9 percent) is higher than observed in 1987 (≈4–5 pptv, 7 percent). Absolute calibration remains uncertain (±10 percent). The global average CCl_4 concentration for 1989 (≈107 pptv) is lower than that reported for 1987 in the last assessment (≈140 pptv), due essentially to a change in calibration based on a comparison of Atmospheric Lifetime Experiment–Global Atmospheric Gases Experiment (ALE–GAGE) data with data collected in several other programs. Absolute calibration remains uncertain (±10 percent).

The CH_3CCl_3 global trend in 1989 from the ALE–GAGE program (5.5 pptv, 3.7 percent) is lower than that reported for 1987 (6.0 pptv, 4.0 percent). Absolute calibration remains uncertain (±10 percent), and the ALE–GAGE calibration could be high by ≈15 percent, inferring a global mean 1989 concentration of 135 pptv rather than 150 pptv based on the current ALE–GAGE calibration scale. The oceans are a significant sink for CH_3CCl_3, implying that computed OH levels are 5–10 percent too high if this sink is ignored. These variations are well within the uncertainty of the rate of methyl chloroform-hydroxyl radical reaction (±40 percent). By analogy, HCFCs and HFCs may also have an oceanic sink although HCFCs and HFCs are more resistant to hydrolysis than CH_3CCl_3. Assuming that the ALE–GAGE calibration and industrial emissions are accurate, then the CH_3CCl_3 trend implies that the CH_3CCl_3 sink and hence global OH levels are increasing by 1.0±0.8 percent per year.

Spectroscopic and gas chromatographic measurements of HCFC-22 both show similar global increases of 6–7 pptv per year. The calibration uncertainty is ±10 percent.

Exponential increases in the bromine containing chemicals Halon-1211 and -1301 have been observed (≈15 percent and ≈20 percent per year respectively), although absolute calibration remains quite uncertain (±15 and ±40 percent respectively). Methyl bromide is the major source of stratospheric bromine. While the possibility of a trend in methyl bromide cannot be assessed due to lack of data, a large anthropogenic methyl bromide source has been previously suggested.

Nitrous oxide continues to increase globally about 0.8 ppbv per year. New global nitrous oxide sources have been proposed (adipic acid production, legume pastures), but the sum of all known sources is not sufficient to balance the calculated atmospheric sink.

The rate of increase of global tropospheric CH_4 continues to decline, with increases of 17–21 ppbv per year observed during 1978–1982 and 12–14 ppbv per year during 1988–1990, or even lower in the Southern Hemisphere. No satisfactory explanation of this phenomenon has been put forward. Ice core studies indicate that CH_4 growth rates have shown significant temporal variability over the past 100 years. The problem of reconciling atmospheric CH_4 observations with estimates of emission sources is severely limited by the lack of

observations in major source regions. There is significant uncertainty in the direct estimates of CH_4 emissions from rice agriculture. Indian studies suggest that the global CH_4 source from rice agriculture may be significantly lower than 100 Tg per year. Recent methane isotopic studies suggest that approximately 20 percent of the total methane source (500 Tg [10^{12} g] per year) is fossil, and 10 percent is from biomass burning. The CH_4 sink due to OH oxidation may be increasing due to increasing levels of OH radical. Global levels of H_2 are increasing (0.5–0.7 percent per year), presumably partly in response to growing CH_4 levels.

Increasing CO concentrations of about 1 ppbv per year appear to be confined to the Northern Hemisphere. In the Southern Hemisphere there have been periods of CO growth (1986–1988) and decline (1983–1985), with no overall change from 1978 to 1990. Some CO sources are known to be increasing (CH_4) and others decreasing (fuel CO emissions from OECD* countries). The CO sink due to OH oxidation may also be increasing due to increasing levels of OH radical.

* Organization for Economic Cooperation and Development (OECD) countries include Australia, Austria, Belgium, Canada, Denmark, Finland, France, Germany, Greece, Iceland, Ireland, Italy, Japan, Luxembourg, Netherlands, New Zealand, Norway, Portugal, Spain, Sweden, Switzerland, Turkey, U.K., U.S., and Yugoslavia (Special Member).

1.1 INTRODUCTION

Source gases are defined as those gases that influence levels of stratospheric ozone (O_3) by transporting species containing halogen, hydrogen, and nitrogen to the stratosphere that are important in O_3 destruction. Examples are the CFCs, methane (CH_4), and nitrous oxide (N_2O). Other source gases that also come under consideration in an atmospheric O_3 context are those that are involved in the O_3 or hydroxyl (OH) radical chemistry of the troposphere. Examples are CH_4, carbon monoxide (CO) and nonmethane hydrocarbons (NMHCs). Most of the source gases, along with carbon dioxide (CO_2) and water vapor (H_2O), are climatically significant and thus affect stratospheric O_3 levels by their influence on stratospheric temperatures. Carbonyl sulphide (COS) could affect stratospheric O_3 through maintenance of the stratospheric sulphate aerosol layer, which may be involved in heterogeneous chlorine-catalyzed O_3 destruction.

This chapter updates the previous reviews of trends and emissions of source gases, either from the context of their influence on atmospheric O_3 (WMO, 1986; 1990a, b) or global climate change (IPCC, 1990). The current (1989) global abundances and concentration trends of the trace gases are given in Table 1-1.

1.2 CFCs AND CARBON TETRACHLORIDE: GLOBAL DISTRIBUTIONS, TRENDS AND CALIBRATION

The CFCs (-11, -12, and -113) and carbon tetrachloride (CCl_4) compose 70 percent of the anthropogenic organochlorine loading of the troposphere (CFC-12, 28 percent; CFC-11, 23 percent; CCl_4, 13 percent; CFC-113, 6 percent). They are inert in the troposphere but photodissociate in the stratosphere and hence are a major source of stratospheric reactive chlorine. The CFCs are used as refrigerants, foam blowing agents and solvents. CCl_4 is used in the production of CFCs.

1.2.1 CFC-11 and CFC-12

There are several long term measurement programs for CFC-12 and CFC-11. National Oceanic and Atmospheric Administration–Climate Monitoring and Diagnostics Laboratory (NOAA–CMDL) have run a global program since 1977 based on weekly flask measurements at Barrow, AL; Niwot Ridge, CO; Mauna Loa, HI; Cape Matatula, Samoa; and the South Pole. The 1989 global mean concentrations for CFC-12 and CFC-11 were 452 and 268 pptv respectively (mean of hemispheric means; Northern Hemisphere: Barrow, Niwot Ridge and Mauna Loa; Southern Hemisphere, Samoa), increasing at 16.9±0.2 and 10.1±0.1 pptv per year, or 3.7 percent and 3.8 percent per year respectively in 1989, based on linear regressions. The data are reported in the original Oregon Graduate Institute for Science and Technology (OGIST) scale and are shown in Figures 1-1 and 1-2 (Thompson *et al.*, 1990). A possible CFC-12 calibration problem has been identified in the NOAA–CMDL data (J. Elkins, NOAA–CMDL, personal communication). A recent reevaluation of the flask data indicates that the long-term, linear, global growth of CFC-12 was 16.1±0.3 pptv per year, based on data from 1977 to 1991. NOAA–CMDL *in situ* measurements (12 per day) of CFC-12 and CFC-11 commenced at Barrow, Mauna Loa, and Samoa (1986) and at the South Pole (1987) (Thompson *et al.*, 1990; Hall *et al.*, 1990); preliminary CFC-12 data have been reported in the recently prepared NOAA–CMDL gravimetric scale. The 1989 global mean CFC-12 concentration was 462 pptv, increasing at about 20 pptv per year, or 4.4 percent per year in 1989. The differences between the global mean derived from flask and *in situ* measurements presumably reflect differences between the OGIST and NOAA–CMDL CFC-12 calibration scales.

In situ measurements (4–12 per day) of CFC-12 and CFC-11 have been made in Ireland, Oregon, Barbados, Samoa, and Tasmania since 1978 as part of the ALE–GAGE program (Cunnold *et al.*, 1986). The 1989 global mean concentrations for CFC-12 and CFC-11 were 453 and 255 pptv respectively (mean of hemispheric means; Northern Hemisphere: Ireland, Barbados; Southern Hemisphere, Tasmania), increasing at 18.2±0.3 and 9.3±0.1 pptv per year, or 4.0 percent and 3.7 percent per year in 1989, based on linear regressions (Cunnold *et al.*, 1986; Prinn *et al.*, 1991b). The data are in the GAGE scale (CFC-11, GAGE scale = OGIST scale x 0.96; CFC-12, GAGE scale = OGIST scale x 0.95) and are also shown in Figures 1-1 and 1-2. The long term stability of the OGIST CFC-11 scale has been possibly but not abso-

Table 1-1 Updated global trends and tropospheric concentrations of source gases for 1989. Adapted from WMO (1990b).

Source gas	Concentration 1989 (pptv)	Increase 1989 pptv/year	Increase 1989 percent/year	Calibration uncertainty
CH_4	1689×10^3	$(12–14) \times 10^3$	0.7–0.8	±1%
H_2	515×10^3	$(2.7–3.7) \times 10^3$	0.5–0.7	?
N_2O	$(307–308) \times 10^3$	$(0.6–0.9) \times 10^3$	0.2–0.3	±1%
CO NH	$(100–150) \times 10^3$	$(0.4–1.2) \times 10^3$	0.3–1.0	±5%
SH	$(50–60) \times 10^3$	0	0	
CO_2	352.2×10^6	1.6×10^6	0.5	<0.1%
C_2H_6 NH			0.6–1.2	
CCl_2F_2	453	16.9–18.2*	3.7–4.0	±2%
CCl_3F	255–268	9.3–10.1	3.7–3.8	±1%
CCl_2FCClF_2	64	5.4–6.2	9.1	±10%
$CClF_2CClF_2$	15–20	≈1	≈6	
CCl_2FCF_3	≈5	≈0.3	≈6	
$CClF_3$	≈5			
CCl_4	107	1.0–1.5	1.2	±10%
CH_3CCl_3	135	4.8–5.1	3.7	±15%
$CHClF_2$	110	5–6	6–7	±10%
CH_3Cl	600			
$CHCl_3$	≈10			
CH_2Cl_2	≈35			
CCl_2CCl_2	≈30			
CH_2ClCH_2Cl	≈35			
$CHClCCl_2$	≈10			
CH_3Br	10–15	?		
CH_2Br_2	2–3			
$CHBr_3$	2–3			
CH_2BrCl	1–2			
$CHBr_2Cl$	1			
$CHBrCl_2$	1			
$C_2H_4Br_2$	1			
C_2H_5Br	2–3			
$CBrClF_2$	1.6–2.5	0.2–0.4	15	±15%
$CBrF_3$	1.8–3.5	0.4–0.7	20	±40%
COS	≈500	?		
Total Cl	3800	110	2.9	
Percent anthropogenic	≈80			
Total Br	40	0.9	2.3	
Percent anthropogenic	≈12 (halons only)			

*Data subject to revision; significantly lower trends may result (see text).

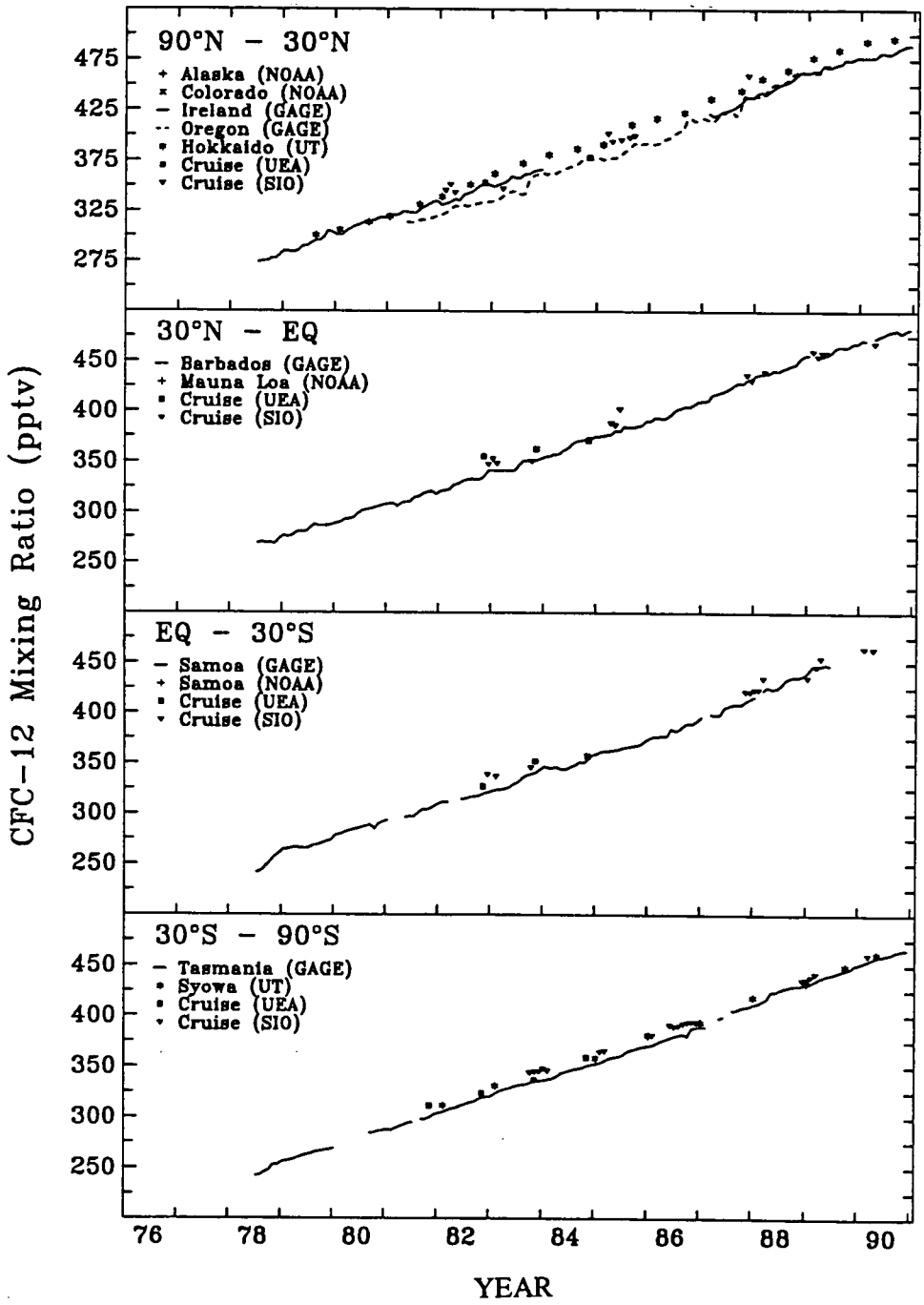

Figure 1-1 CFC-12 observations (pptv) in the four semihemispheres (NOAA: Thompson *et al.*, 1990; GAGE: Cunnold *et al.*, 1986; Prinn *et al.*, 1991b; UT: Makide *et al.*, 1987; Makide 1991). Some of the data are unpublished and are subject to revision. Data should not be used for further analysis without consulting the principal investigators: NOAA, J. Elkins; GAGE, R. Prinn; UT, Y. Makide; UEA, S. Penkett; SIO, R. Weiss.

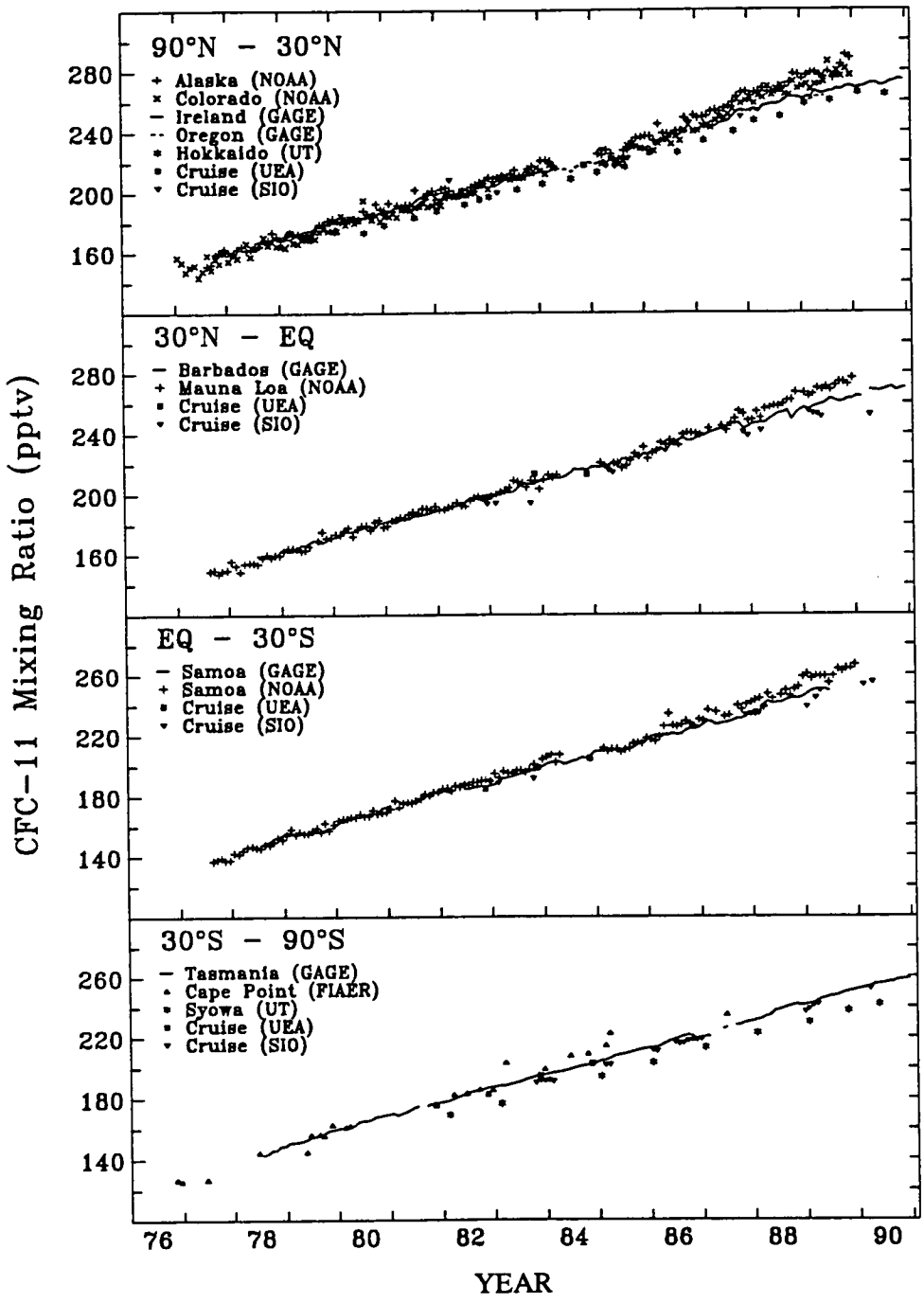

Figure 1-2 CFC-11 observations (pptv) in the four semihemispheres (NOAA: Thompson *et al.*, 1990; GAGE: Cunnold *et al.*, 1986: Prinn *et al.*, 1991b; UT: Makide *et al.*, 1987; Makide 1991) some of the data are unpublished and subject to revision. Data should not be used for further analysis without consulting the principal investigators: NOAA, J. Elkins; GAGE, R. Prinn; UT, Y. Makide; UEA, S. Penkett; SIO, R. Weiss; FIAER, H. Scheel.

lutely demonstrated by extensive, periodic internal comparisons of several original ALE–GAGE calibration gases and by a comparison of measurements made in 1978–1979 in the ALE–GAGE program in Tasmania with modern measurements on air archived from that period. These experiments limit the magnitude of a calibration drift component of the observed trend to about 0.1 percent per year. A possible CFC-12 calibration problem has been identified in the GAGE data, which are currently being reevaluated. Lower trends will probably result (D. Cunnold, GAGE–GIT, personal communication) although the changes are likely to be small.

The global CFC-11 ratio (GAGE (*in situ*) NOAA–CMDL (flask) = 0.95) reflects the difference between the two calibration scales involved (GAGE/OGIST = 0.96), whereas the global CFC-12 ratio (GAGE (*in situ*)/NOAA–CMDL(flask) = 1.00) does not (GAGE/OGIST = 0.95). This requires further investigation. The 1989 mean CFC-12 and CFC-11 concentrations at Tasmania (41°S) were 441 and 247 pptv, which, when compared to the South Pole observations above, suggest that the NOAA–CMDL and GAGE scales agree to within 2 percent (CFC-12) and 1 percent or better (CFC-11).

In situ CFC-11 measurements (24 per day) have been made at Cape Point, South Africa, since 1980 (Scheel *et al.*, 1990; Brunke and Scheel, 1991). The 1989 annual mean CFC-11 concentration at Cape Point (34°S) was 256 pptv, increasing at 9.3±0.1 pptv per year or 3.6 percent per year in 1989 based on a linear regression. The data are reported in the original OGIST scale and are also shown in Figure 1-2. The 1989 mean CFC-11 concentration and trend at Cape Point in the GAGE scale (OGIST x 0.96) are 246 pptv and 9.0 pptv per year respectively, which compare well with the 1989 mean CFC-11 concentration and trend in Tasmania (GAGE program, 41°S), 247 pptv and 9.3±0.1 pptv per year respectively.

Flask measurements of CFC-12 and CFC-11 (1 week every 6 months) have been made on Hokkaido, Japan (40°–45°N), since 1979 (Makide *et al.*, 1987; Makide, 1991) and at Syowa Station, Antarctica (69°S), several times per year since 1982 (Makide 1991). On Hokkaido CFC-11 and CFC-12 increases of 18.6±0.2 and 9.4±0.2 pptv per year respectively have been observed, based on linear regressions. The 1989 mean CFC-12 and CFC-11 concentrations at Hokkaido are 481 and 259 pptv respectively and at Syowa 441 and 235 pptv respectively. The data are reported in independently prepared University of Tokyo (UT) calibration scales and are shown in Figures 1-1 and 1-2. A direct interlaboratory comparison of the GAGE and UT CFC-12 and CFC-11 calibration scales and a comparison of CFC-12 and CFC-11 data collected at Hokkaido (UT), Ireland (GAGE), Syowa (UT), and Tasmania (GAGE) has shown that GAGE data agree to within 2 percent for CFC-12 (GAGE lower) and within 3 percent for CFC-11 (GAGE higher) (Y. Makide and P. Fraser, unpublished data).

Measurements of CFC-12 and CFC-11 have been made in the free troposphere via aircraft over Europe and the North Atlantic Ocean since 1976 (Scheel *et al.*, 1988; Seiler and Scheel, 1991). CFC-12 and CFC-11 increases of 16.3±0.5 and 10.6±0.3 pptv per year have been measured over the period 1976–1987, similar to the trends observed from ground-based observations in the Northern Hemisphere. These aircraft data are based on a commercially available Scott-Marrin standard.

Free tropospheric measurements of CFC-12 and CFC-11 have been made via aircraft over Japan (33°–38°N) since 1978 (Hirota *et al.*, 1988; Hirota and Sasaki, 1991). CFC-12 and CFC-11 increases of 16.2±0.7 and 10.3±0.4 pptv per year have been measured over the period 1978–1990, similar to the trends observed over Europe. These aircraft data are based on a commercially available Seitetsu Kagaku and Nihon Sanso standards, whose absolute concentration is certified to ±5 percent.

A comparison of shipboard measurements of CFC-12 and CFC-11 from 1981 to 1984 on the North and South Atlantic (Penkett, 1991a) to GAGE data from corresponding latitudes shows that the GAGE and Penkett data agree to within 3 percent for CFC-12 (GAGE higher) and to within 1 percent for CFC-11 (GAGE higher). Similarly, a comparison of shipboard measurements of CFC-12 and CFC-11 from 1983 to 1990 on the North and South Atlantic (Weiss, 1991) to GAGE data from corresponding latitudes shows that the GAGE and Weiss data agree to within 2 percent for CFC-12 (GAGE lower) and to within 2 percent for CFC-11 (GAGE higher).

1.2.2 CFC-113

Flask measurements of CFC-113 have been made on Hokkaido, Japan (40°–45°N) since 1980 and at

Syowa Station (69°S) (10 days each winter) since 1987 (Makide *et al.*, 1987; Makide, 1991). On Hokkaido the mean CFC-113 increase over the period 1979–1990 was 5.5±0.2 pptv per year and 7.9±0.3 pptv over the period 1987–1990, based on linear regressions. The data are reported in an independently prepared UT calibration scale and are shown in Figure 1-3.

Real-time measurements (12 per day) of CFC-113 have been made in Ireland, Oregon, Barbados, Samoa, and Tasmania since 1982 as part of the GAGE program (Fraser *et al.*, 1991). The 1989 global mean CFC-113 concentration was 64 pptv (mean of hemispheric means; Northern Hemisphere: Ireland, Barbados; Southern Hemisphere, Tasmania), increasing at 5.8±0.4 pptv per year, or 9.1 percent per year in 1989, based on linear regressions (Fraser *et al.*, 1991). The GAGE CFC-113 data (Figure 1-3) are obtained relative to OGIST calibration gases, but are reported in the GAGE scale, which is based on an interlaboratory comparison to the UT CFC-113 scale (Makide *et al.*, 1987). This comparison showed that the UT/OGIST ratio is 1.4-1.5 (Y. Makide and P. Fraser, unpublished data).

In situ measurements of CFC-113 at Cape Point, South Africa (Brunke and Scheel, 1991) show a lower growth for CFC-113 (2.4±0.2 pptv per year; 7.3 percent per year in 1989). The data are reported in the OGIST scale, so the increase would translate to ≈3.5 pptv per year in the UT scale. Measurements of CFC-113 in the free troposphere over Europe and the North Atlantic during the period 1982–1987 show an increase of 6.6±0.3 pptv per year (Seiler and Scheel, 1991). The data are based on a Scott–Marrin calibration standard, which gives CFC-113 concentrations that are a factor of ≈2 higher than data obtained using OGIST calibration.

NOAA–CMDL have produced a new gravimetric CGC-113 scale, which is about 40 percent higher than the OGIST scale (NOAA–CMDL/OGIST = 1.37) (Thompson *et al.*, 1990) and therefore presumably about 3–5 percent lower than the UT (=GAGE) scale. Measurements of CFC-113 at Cape Grim, Tasmania (41°S), have been compared to CFC-113 measurements on the South Atlantic at similar latitudes and times, which were obtained using an independent calibration scale University of East Anglia (UEA) (Penkett, 1991). The Atlantic data were approximately 10–20 percent lower, which probably reflects the difference in calibration scales (*i.e.*, GAGE/UEA ≈1.1–1.2; thus UEA/OGIST ≈1.2–1.4). It would appear that three independent laboratories (UT, NOAA–CMDL and UEA agree to within ±10 percent on CFC-113 calibration.

1.2.3 CFC-114 and CFC-114a

Rasmussen *et al.*, (1990) has reported growth rates for CFC-114 ($CClF_2CClF_2$) and CFC-114a (CCl_2FCF_3) from the OGIST global flask sampling network from 1979 to 1990 of approximately 6 percent per year. Absolute concentrations were not reported. There have been no new data reported for CFC-115.

1.2.4 Carbon Tetrachloride

In situ CCl_4 measurements have been made at the GAGE stations since 1978 (Simmonds *et al.*, 1988). The data (Figure 1-4) show a global mean 1989 concentration of 134 pptv, based on data from Ireland, Barbados, and Tasmania, and an increase over the entire record of 1.6±0.3 pptv per year, or 1.2 percent per year in 1989.

A similar CCl_4 increase has been observed from *in situ* measurements at Cape Point (1.7±0.1 pptv per year) over the period 1980–1990 (Figure 1-4). This program employs the same calibration scale as the GAGE program. The 1989 mean concentration (128 pptv) at Cape Point (32°S) is very similar to that observed (130 pptv) at Cape Grim, Tasmania (41°S). However *in situ* measurements in 1989 at Samoa (14°S) and the South Pole using the new NOAA–CMDL gravimetric calibration scale gave mean concentrations of 104 and 106 pptv respectively (Thompson *et al.*, 1990; Hall *et al.*, 1990), whereas GAGE measurements at Samoa in 1989 average about 132 pptv, suggesting that concentrations in the NOAA–CMDL scale are ≈20 percent lower than those in the GAGE scale.

Flask measurements of CCl_4 on Hokkaido, (40°–45°N) over the period 1979–1990 show an increase of 1.4±0.2 pptv per year (Makide *et al.*, 1987; Makide, 1991). A direct interlaboratory comparison between GAGE and Makide indicate that the GAGE CCl_4 scale is ≈20 percent higher than Makide (Y. Makide and P. Fraser, unpublished data).

Measurements of CCl_4 in the free troposphere over Europe and the North Atlantic during the period

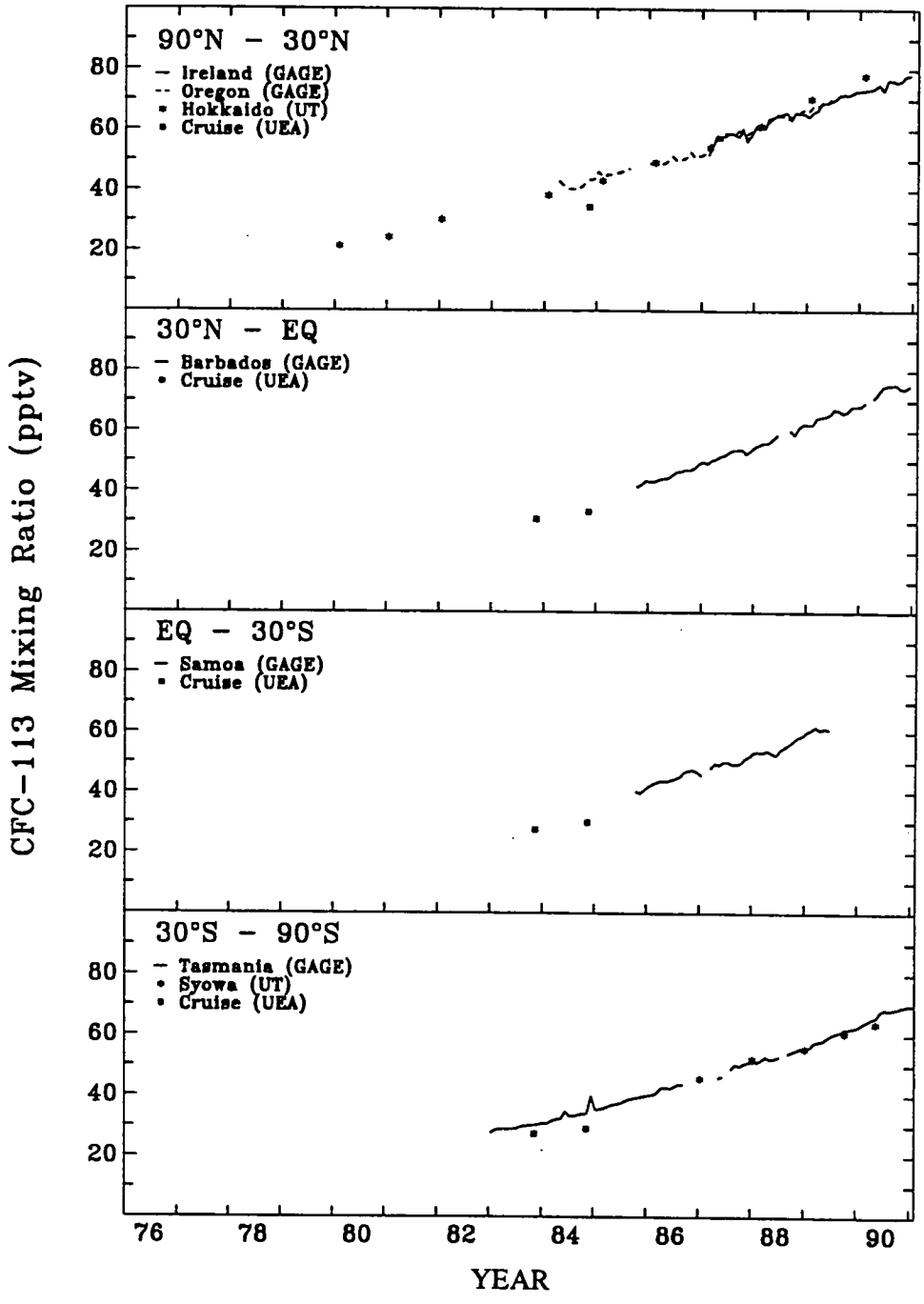

Figure 1-3 CFC-113 observations (pptv) in the four semihemispheres (GAGE: Fraser *et al.*, 1991; Prinn *et al.*, 1991b; UT: Makide, 1991). Some of the data are unpublished and are subject to revision. Data should not be used for further analysis without consulting the principal investigators: GAGE, R. Prinn; UT, Y. Makide; UEA, S. Penkett.

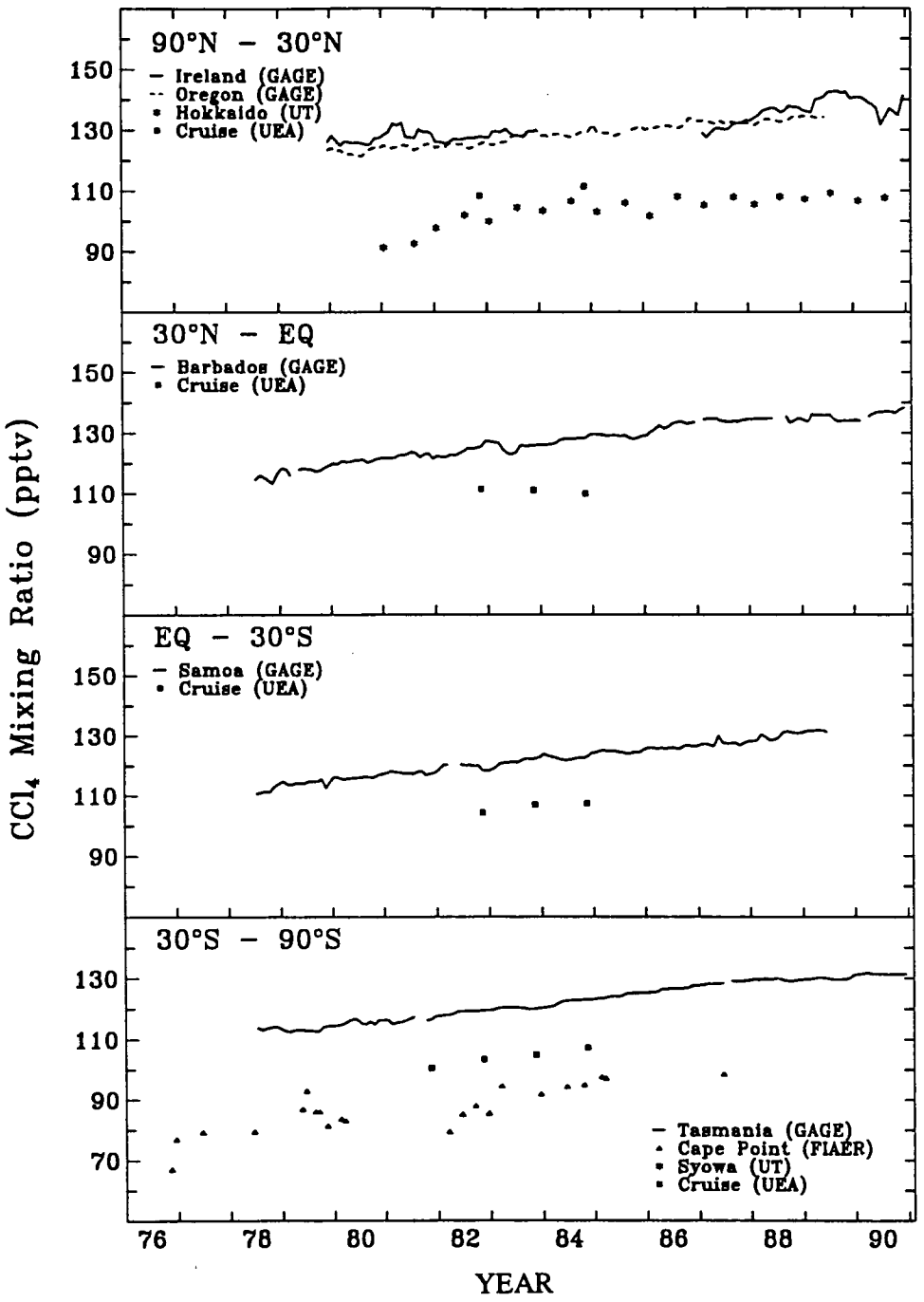

Figure 1-4 Carbon tetrachloride (pptv) in the four semihemispheres. (GAGE: Simmonds *et al.*, 1988; Prinn *et al.*, 1991b; UT: Makide *et al.*, 1987; Makide, 1991; CSIR-FIAER: Scheel *et al.*, 1990). Some of the data are unpublished and are subject to revision. Data should not be used for further analysis withou consulting the principal investigators: GAGE, R. Prinn; UT, Y. Makide; UEA, S. Penkett; FIAER, H. Scheel

1976–1987 show an increase of 2.0±0.3 pptv per year (Seiler and Scheel, 1991). These data are based on a Scott-Marrin calibration standard, which gives CCl_4 concentrations that are a factor of ≈1.15 lower than those based on the GAGE calibration.

Measurements of CCl_4 at Cape Grim (41°S) have been compared to CCl_4 measurements on the South Atlantic at similar latitudes and times, which were obtained using an independent calibration scale (UEA) (Penkett, 1991a). The Atlantic data were approximately 15 percent lower, which probably reflects the difference in calibration scales (*i.e.*, GAGE/UEA ≈1.15). A direct comparison of National Institute of Standards and Technology (NIST) and GAGE CCl_4 standards indicates that the GAGE/NIST ratio is ≈1.35 (Fraser, personal communication, 1991).

It would appear that five independent laboratories (UT, NOAA–CMDL, UEA, Fraunhofer Institute for Atmospheric Environmental Research (FIAER) (Scott-Marrin), and NIST) agree to within ±10 percent on CCl_4 calibration, and are ≈20 percent lower than GAGE.

1.3 METHYL CHLOROFORM AND HCFC-22

Methyl chloroform (CH_3CCl_3) and HCFC-22 ($CHClF_2$) are important trace gases in the global atmosphere. They constitute about 17 percent of the tropospheric anthropogenic organochlorine loading (CH_3CCl_3, 14 percent; $CHClF_2$, 3 percent) and both are partially removed from the atmosphere by reaction with OH. Assuming emissions and absolute abundances of these species are known, they can be used to calculate average tropospheric OH levels (for CH_3CCl_3, see Prinn *et al.*, 1987, 1992). Methyl chloroform is used as an industrial solvent and HCFC-22 is being increasingly used as a substitute for CFCs.

1.3.1 Global distributions and trends

Long-term, high-frequency measurements (4-12 per day) of CH_3CCl_3 have been made in Ireland, Oregon, Barbados, Samoa and Tasmania (Prinn *et al.*, 1987, 1991a) since 1978 as part of the ALE-GAGE program and on Hokkaido twice a year (10 days every 6 months) since 1979 and at Syowa Station in Antarctica (several times per year) (Makide *et al.*, 1987; Makide, 1991). January measurements made in the Pacific North West (PNW) of the United States and at the South Pole since 1975 have been published (Rasmussen and Khalil, 1986; Khalil and Rasmussen, 1990b). Mid-tropospheric CH_3CCl_3 data have been obtained by aircraft air sampling over Europe and the North Atlantic by FIAER since 1978 (Scheel *et al.*, 1988).

The available data are shown in Figure 1-5. Twelve years of ALE–GAGE CH_3CCl_3 data (July 1978 to June 1990) have recently been analyzed (Prinn *et al.*, 1992) showing a global trend of 5.5±0.2 pptv per year or 4.4±0.2 percent per year (mid-1984). The 1989 global mean concentration was 150.0 pptv (based on data from Ireland, Barbados, and Tasmania), and the 1989 increase, based on a linear regression, was 3.7 percent. The free tropospheric data over Europe and the North Atlantic (1978–1987) show a trend of 5.2±0.8 pptv per year or 4.5 percent per year in 1984 (Scheel *et al.*, 1988; Seiler and Scheel, 1991). The Hokkaido data (Makide *et al.*, 1987; Makide, 1991) show an increase of 4 pptv per year over the period 1980–1990 (2.7 percent in 1989) and 5 pptv per year over the period 1987–1990 (3.4 percent in 1989). The concentrations of CH_3CCl_3 observed on Hokkaido are about 15 percent lower than in Ireland or Oregon, although these differences could be due to different calibration scales (see 1.3.2).

The available data on the global distribution and trends of HCFC-22 are limited, reflecting the relative difficulty in making atmospheric HCFC-22 measurements, which can be achieved by spectroscopy (total column) or gas chromatographic techniques involving large volume air samples.

HCFC-22 data have been regularly obtained from the PNW region of the U.S. and from the South Pole (Rasmussen *et al.*, 1980; Khalil and Rasmussen, 1981; Rasmussen and Khalil, 1982, 1983). The PNW data from 1976 to 1981 showed concentrations increasing by about 12±1 percent per year, with an absolute concentration uncertainty of ±10 percent. Combined PNW–South Pole data for 1979–1987 have recently been reported (Khalil and Rasmussen, 1990b), which show a concentration in January 1987 of 105 pptv increasing by 6.4±0.3 pptv per year or 6.1 percent in January 1987. Observations from Cape Grim (1984–1987), show a mean concentration and increase in 1987 of 91 pptv and 6.5±0.3 pptv per year, or 7.1±0.3 percent per year (Fraser *et al.*, 1989). These data are all in the same scale (OGIST)

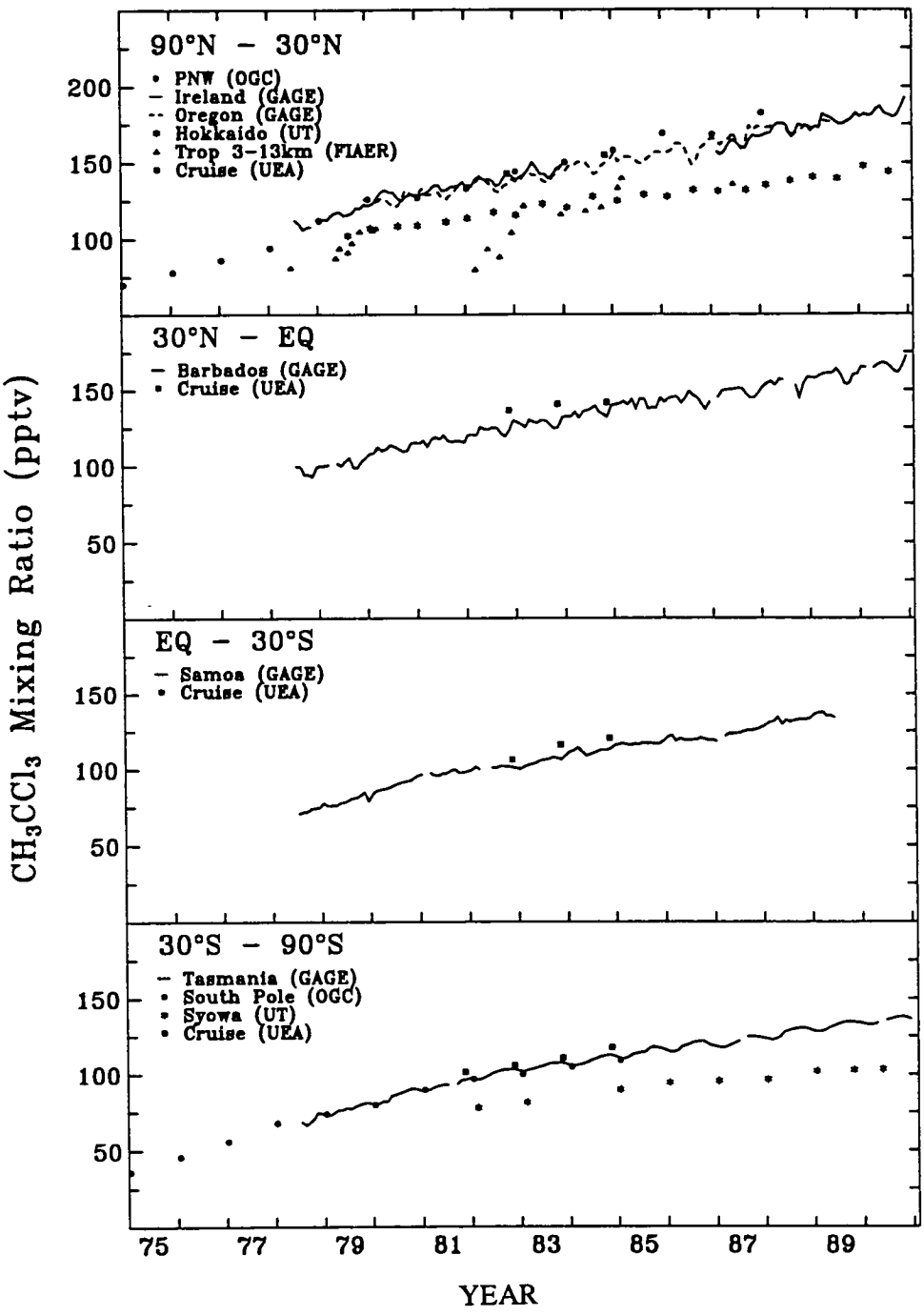

Figure 1-5 Methyl chloroform observations (pptv) in the four semihemispheres (GAGE: Prinn *et al.*, 1991, 1992, UT: Makide *et al.*, 1987 Makide, 1991. FIAER: Scheel *et al.*, 1988; Seiler and Scheel, 1991. OGIST: Rasmussen and Khalil, 1986; Khalil and Rasmussen, 1990b.) Some of the data are unpublished and are subject to revision. Data should not be used for further analysis without consulting the principal investigators: GAGE, R. Prinn; UT, Y. Makide; UEA, S. Penkett; FIAER, H. Scheel.

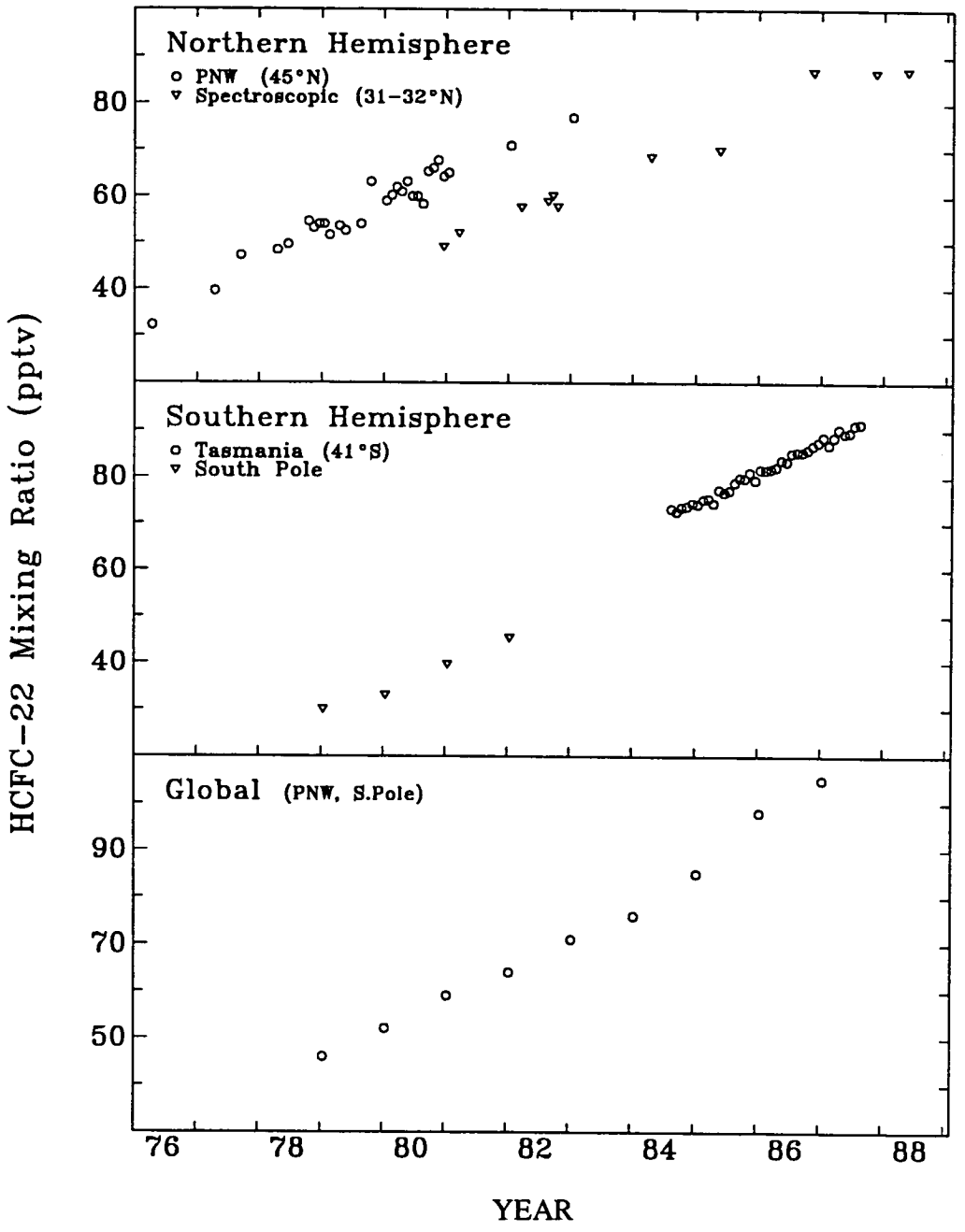

Figure 1-6 Northern Hemispheric, Southern Hemispheric, and global HCFC-22 observations (pptv) (PNW, South Pole: Khalil and Rasmussen, 1981; Rasmussen and Khalil, 1982, 1983; spectroscopic: Rinsland *et al.*, 1989, 1990; Tasmania: Fraser *et al.*, 1989; global: Khalil and Rasmussen, 1990b).

and are shown in Figure 1-6. The OGIST and UEA independent HCFC-calibration 22 scales agree to within 5 percent (Rasmussen *et al.*, 1980).

Solar spectroscopic HCFC-22 measurements from Kitt Peak, AZ (32°N), over the period 1980–1988 show an increase of 7.8±1.0 percent per year, with an absolute error of ±25 percent, arising largely from the uncertainty in the HCFC-22 spectroscopic parameters (Rinsland *et al.*, 1989). These parameters have been refined, and derived concentrations increased by about 30 percent, resulting in reasonable agreement between spectroscopic and gas chromatographic measurements. Additional data from balloon-borne spectrometers and Atmospheric Trace Molecule Spectroscopy Experiment (ATMOS) at 31–32°N (<15km) have been obtained (Rinsland *et al.*, 1990) and the combined data are shown in Figure 1-6. The combined data show a mean concentration in 1989 of 93 pptv and an increase of 5.8±0.4 pptv per year or 6.2 percent per year, based on a linear regression. A trend of ≈10 percent per year has been reported from stratospheric observations for the period 1982–1987 (Fabian *et al.*, 1989).

1.3.2 Methylchloroform Calibration

The absolute calibration of CH_3CCl_3 measurements in the GAGE program is based on the OGIST standard (Khalil and Rasmussen, 1984a). Unfortunately, there have not been any published comparisons of independently derived CH_3CCl_3 standards. A preliminary and as yet unpublished comparison between the GAGE and UT CH_3CCl_3 standards suggests that the latter are lower by ≈25 percent (UT/GAGE = 0.75) (Y. Makide and P. Fraser, unpublished data).

A new gravimetric CH_3CCl_3 standard has been prepared by NOAA–CMDL (Butler *et al.*, 1991). No direct comparisons have been made between this standard and the GAGE standard, but an indirect comparison can be made from observations by both groups in the Southern Hemisphere in early 1990 (Butler *et al.*, 1991; Prinn *et al.*, 1991a). This comparison suggests that the NOAA–CMDL standard is about 10 percent lower than the GAGE standard (NOAA–CMDL/GAGE = 0.9). Shipboard measurements of CH_3CCl_3, based on an independent calibration, have been made on the North and South Atlantic (Penkett, 1991a) between 1981 and 1984. A comparison of ALE–GAGE data at similar latitudes and times indicates that the UEA standard is about 5 percent higher than the GAGE standard (UEA/GAGE = 1.05). Thus, the current range of CH_3CCl_3 measurements based on four independent standards (GAGE, UT, NOAA–CMDL, UEA) would appear to be ±15 percent. The average of the four standards is ≈10 percent lower than GAGE.

The long-term stability of the OGIST CH_3CCl_3 standard has been possibly but not absolutely demonstrated by extensive, periodic internal comparisons of several original ALE–GAGE calibration gases and by a comparison of measurements made in 1978–1979 in the ALE–GAGE program in Tasmania with modern measurements on air archived from that period. These experiments limit the magnitude of a calibration drift component of the observed trend to about 0.2 percent per year, comparable to the uncertainty in the long-term trend due to measurement variability (Prinn *et al.*, 1992).

1.3.3 Methylchloroform Lifetime and the Global OH Abundance

A three-dimensional model has been used to compute tropospheric OH levels from observations of CH_4, CO, O_3, and NO_x (Spivakovsky *et al.*, 1990a) and used to simulate the global distribution of CH_3CCl_3 (Spivakovsky *et al.*, 1990b). The computed OH fields result in a model CH_3CCl_3 lifetime of 5.5 years. The observed CH_3CCl_3 annual cycle south of 25°S is dominated by seasonal changes in OH (CH_3CCl_3 sink), whereas the seasonal variation of CH_3CCl_3 in the tropics and at northern mid–latitudes are dominated by the effects of transport.

The measured ALE–GAGE trends of CH_3CCl_3 have been combined with industrial emission estimates (Midgley, 1989) to deduce a globally averaged CH_3CCl_3 lifetime of 5.7 (+0.7, –0.6) years) and an average tropospheric OH concentration of (8.7±1.0) x 10^5 radicals per cm^3 (Prinn *et al.*, 1992).

Theoretical (Wine and Chameides, 1990) and observational (Butler *et al.*, 1991) studies have suggested that the ocean is a significant sink for CH_3CCl_3. The data of (Butler *et al.* 1991) imply that OH levels computed from CH_3CCl_3 data are 5–10 percent too high if the oceanic sink is ignored. Incorporating an oceanic sink into the GAGE CH_3CCl_3 inversion study results in a lower average OH level of (8.1±0.9) x 10^5 radicals per cm^3 (Prinn *et al.*, 1992).

The ALE–GAGE CH_3CCl_3 trend implies that the globally averaged OH levels have been increasing over the period 1978–1990 by 1.0±0.8 percent per year (Prinn *et al.*, 1992). The deduced positive OH trend is qualitatively consistent with predicted changes in tropical tropospheric OH and O_3 driven by tropical biomass burning (Keller *et al.*, 1991). This possible trend in OH has major implications for other trace gases that are primarily removed by reaction with OH, *e.g.*, CH_4, CO, HCFC-22 and other HCFCs and HFCs.

1.3.4 HCFC-22 lifetime

A three-dimensional model simulation of HCFC-22 estimates the lifetime of HCFC-22 to be 15.5 years (Golombek and Prinn, 1989). With emissions increasing from about 100 million kg per year in 1977 to 220 million kg per year in 1985, good agreement is obtained between observations and model results at Cape Grim in 1984. There is a tendency for the model to overestimate the Cape Grim trend, which is probably due to an overestimation of emissions and/or an underestimation of absolute HCFC-22 concentration.

1.4 OTHER CHLORINATED SPECIES

1.4.1 Methyl Chloride

There have been no data, further to (WMO, 1990a), reported on the global distribution of methyl chloride (CH_3Cl). A global average background concentration of ≈600 pptv is assumed.

1.4.2. Chloroform

Chloroform measurements have been made regularly at Cape Grim as part of the OGIST flask sampling program and as part of the GAGE *in situ* measurement program. The GAGE data have been calibrated with respect to a NIST SRM (Fraser, 1991). The global background concentration in 1989 was ≈10 pptv, based on the previously reported ratio of Northern to Southern Hemispheric measurements (Khalil and Rasmussen, 1983b). Approximately 40 percent of the $CHCl_3$ source required to maintain the observed global concentration (400 million kg per year) is anthropogenic (Khalil and Rasmussen, 1983b). Termite mounds were found to contain elevated levels of $CHCl_3$, which were calculated to emit 100 million kg per year (Khalil *et al.*, 1990).

1.5 HALONS AND OTHER BROMINATED SPECIES

Bromine enters the atmosphere through various processes, both natural and anthropogenic. The bromine source gases that are present in the troposphere are shown in Table 1-1.

The most abundant is methyl bromide (CH_3Br), which has both natural and anthropogenic sources. The main natural sources of CH_3Br are oceanic biological processes (mainly algal), where it is formed with other hydrogen-containing molecules, such as CH_2Br_2, $CHBr_3$, CH_2BrCl, and $CHBrCl_2$. However, measurements of CH_3Br made over the Atlantic Ocean show a marked interhemispheric gradient, with average concentrations of 15 pptv and 10 pptv being recorded in the Northern and Southern Hemispheres respectively (Penkett *et al.*, 1985). This argues for a substantial land-based source, which could well be anthropogenic. The source strength required to produce the observed abundance is 100 million kg per year, whereas the annual anthropogenic production is about 20 million kg (SORG, 1990). There may be other unaccounted sources of anthropogenic CH_3Br.

Observational data records of sufficient frequency and duration to determine possible trends in atmospheric bromine species are rare. The available halon data from the OGIST flask sampling network up to 1986 were recently summarized (WMO, 1990a), which suggested global mean concentrations and rates of increase of 1.7 and 2.0 pptv and 12 and 15 percent per year respectively for $CBrClF_2$ and $CBrF_3$. Thompson *et al.* (1990) have reported NOAA–CMDL shipboard data in 1987 and 1989 of 1.6 and 1.8 pptv, increasing at 8 and 25 percent per year respectively for $CBrClF_2$ and $CBrF_3$.

Rasmussen, *et al.* (1990) has recently revised the global growth rates from the OGIST flask network to be ≈15 and ≈20 percent per year respectively for $CBrClF_2$ and $CBrF_3$, but absolute concentrations were not reported. Based on the 1986 data and the latest growth rates, the concentrations expected in 1989 for $CBrClF_2$ and $CBrF_3$ would be 2.5 and 3.5 pptv respectively. Singh *et al.* (1988) reported tropospheric

concentrations for $CBrClF_2$ and $CBrF_3$ at the mid-latitudes of the Northern Hemisphere in 1987 of 2.0 and 1.3 pptv respectively. The $CBrClF_2$ data compare favorably with the OGIST Northern Hemispheric data (WMO, 1990a), but the $CBrF_3$ data are ≈50 percent lower. These data from three independent laboratories (OGIST, NOAA–CMDL, and Max Planck Institute for Aeronomy, or MPIA) suggest that the uncertainties in calibration of $CBrClF_2$ and $CBrF_3$ are ≈±15 percent and ≈±40 percent respectively.

1.6 CARBONYL SULPHIDE

Chlorine-catalyzed O_3 destruction may be enhanced by heterogeneous processes on the ubiquitous stratospheric aerosol layer (Brasseur *et al.*, 1990). In times of low volcanic activity this stratospheric aerosol layer (sulphate) is maintained by an upward flux of gaseous sulphur precursors, mainly carbonyl sulphide (COS), which are either oxidized or photolyzed in the stratosphere (Crutzen, 1976), while volcanic injections supply sulphur to the stratosphere mainly as sulphur dioxide (SO_2) during individual volcanic eruptions.

COS is the most abundant sulphur gas in the remote atmosphere. Global background concentrations of COS are 510±10 pptv (Khalil and Rasmussen, 1984b). The major sources are the oceans (20–40 percent), via the photooxidation of organic material (Ferek and Andreae, 1984), anthropogenic activities (20 percent), soils (20 percent), biomass burning (10 percent) and the oxidation of carbon disulphide (CS_2) (30 percent), while the major sinks are vegetation (≈80 percent), tropospheric oxidation (≈10 percent) and stratospheric loss (≈10 percent) (Khalil and Rasmussen, 1984b; Servant, 1989). Estimates of the atmospheric lifetime range from 2 to 6 years.

1.7 NITROUS OXIDE

Nitrous oxide is an important component of the background atmosphere, being a climatically significant species and the major source of stratospheric nitrogen oxides, which are significant in regulating stratospheric ozone.

Nitrous oxide is a long-lived atmospheric species, with a lifetime in excess of 150 years (Prinn *et al.*, 1990), whose dominant source is believed to be denitrification in aerobic soils, which has a significant anthropogenic component (deforestation and the use of nitrogenous fertilizers). Biomass burning and fossil fuel combustion are now believed to be only small N_2O sources, although biomass burning may affect subsequent soil N_2O releases (Anderson *et al.*, 1988; Prinn *et al.*, 1990; IPCC, 1990). The oceans are significant sources of N_2O, which vary considerably with location and ocean circulation processes (Butler *et al.*, 1989; IPCC, 1990). The major sinks for N_2O are stratospheric photodissociation and photooxidation.

1.7.1 Atmospheric Distributions and Trends

There are several long-term measurement programs studying N_2O. Shipboard and ground-based measurements have been regularly made by Scripps Institution for Oceanography (SIO) since 1976 (Weiss, 1981; WMO, 1990a). NOAA–CMDL and ALE–GAGE have operated independent five-station networks covering both hemispheres since 1977 and 1978 respectively (Thompson *et al.*, 1990; Prinn *et al.*, 1990). Long-term N_2O measurement programs have been carried out at Cape Point since 1983 (Brunke *et al.*, 1990; Scheel *et al.*, 1990) and in the PNW of the United States and at the South Pole since 1975 (Rasmussen and Khalil, 1986; Khalil and Rasmussen, 1990b). Mid-tropospheric N_2O data have been obtained by aircraft air sampling over Japan (33°–38°N) since 1983 by Meteorological Research Institute (MRI) (Hirota *et al.*, 1988; Hirota and Sasaki, 1991) and over Europe and the North Atlantic by FIAER since 1979 (Scheel *et al.*, 1988).

The available data are shown in Figure 1-7 divided into the four semihemispheres, as well as global data derived by averaging spline fits to the individual CMDL and ALE–GAGE station data sets. From the SIO data (1976–1987) (not shown) a global average concentration and increase (1986) of 304.8 ppbv and 0.61±0.04 ppbv per year or 0.20 percent per year have been deduced (WMO, 1990a). The NOAA–CMDL data (1977–1989) show a global concentration and increase for 1989 of 308.5 ppbv and 0.64±0.06 ppbv per year or 0.21 percent per year (Thompson *et al.*, 1990). The ALE–GAGE data (1978–1989) show a global concentration in 1988 of 307.2 ppbv and an increase (1978–1988) of 0.25–0.31 percent per year (Prinn *et al.*, 1990). The 1989 global mean was 307.0 ppbv (mean of Northern Hemisphere (Ireland, Barbados) and Southern Hemisphere (Tasmania) (Prinn *et al.*, 1991). The Cape Point data (1983–1988) show

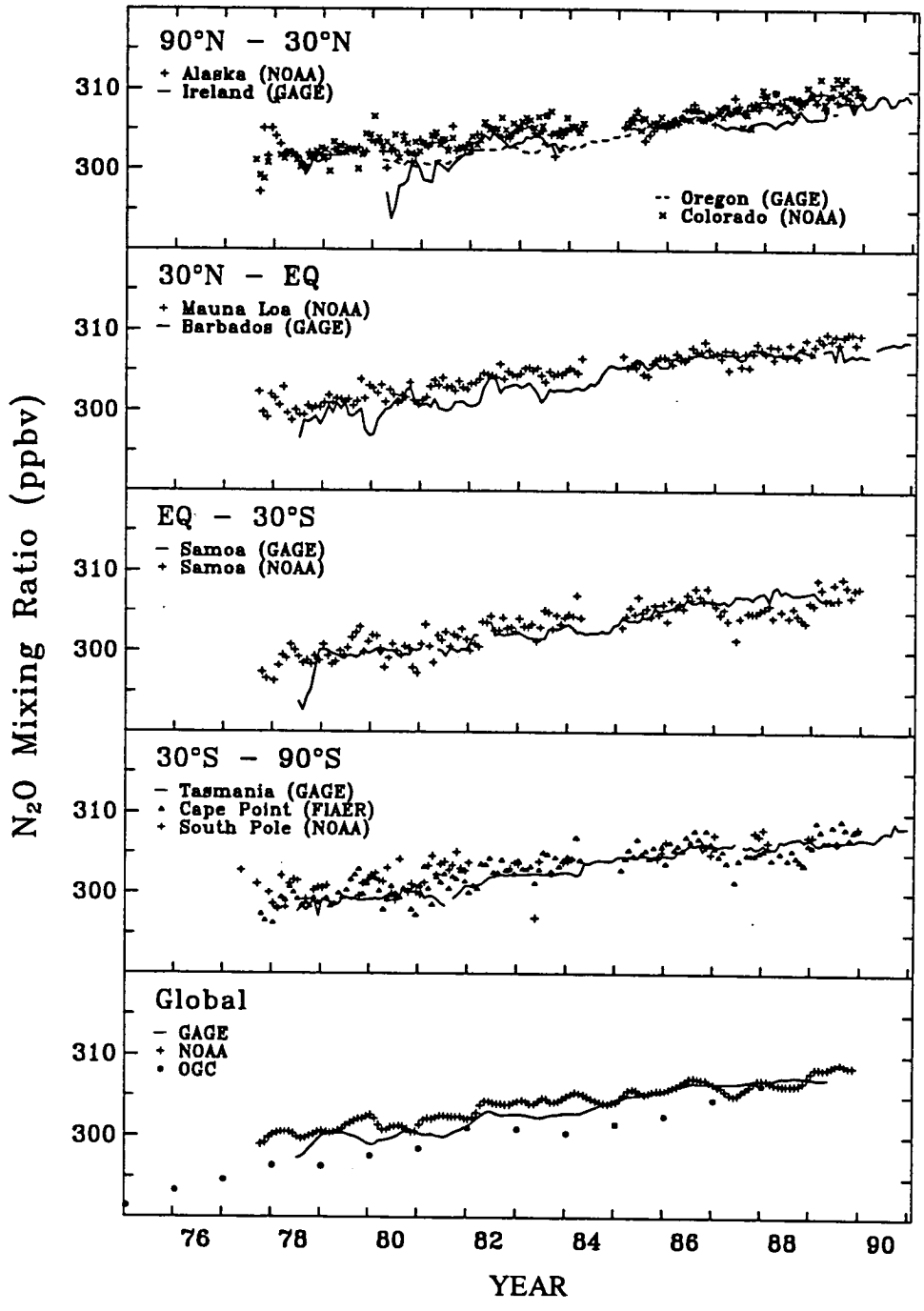

Figure 1-7 Nitrous oxide observations (ppbv) in the four semihemispheres (NOAA: Thompson *et al.*, 1990. OGIST: Khalili and Rasmussen, 1990b) Some of the data are unpublished and are subject to revision. Data should not be used for further analysis without consulting the principal investigators: NOAA, J. Elkins; GAGE, R. Prinn; FIAER, H. Scheel.

an increase of 0.6±0.1 ppbv per year or 0.21 percent per year in 1984 (Brunke *et al.*, 1990; Scheel *et al.*, 1990), while the PNW–South Pole data show an increase of 1.0±0.1 ppbv per year or 0.34 percent per year in January 1985 (Rasmussen and Khalil, 1986). The global data from the OGIST network (1975–1988), (Khalil and Rasmussen, 1990b) show an average increase of 1.0±0.1 ppbv per year or 0.33 percent per year (1988).

The mid-tropospheric N_2O data over Japan show an average increase (1983–1989) of 1.7±0.2 ppbv per year (Hirota and Sasaki, 1991). The free tropospheric data over Europe and the North Atlantic between 1979 and 1987 show an annual average increase of 0.5 ppbv per year or 0.16 percent per year (1987) (Scheel *et al.*, 1988). Spectroscopic observations of N_2O from Kitt Peak between 1979 and 1985 place an upper limit on the growth rate of 0.3 percent per year (Wallace and Livingston, 1990b).

1.7.2. Global Nitrous Oxide Budgets

The ALE–GAGE data have been interpreted (Prinn *et al.*, 1990), using inverse theory and a nine-box model of the global atmosphere, to show that the global distributions and trends are consistent with the hypothesis that stratospheric photodissociation is the major sink for N_2O and that the cause of the N_2O trend appears to be a combination of a growing tropical source (probably tropical land use) and a growing northern mid-latitude source (fertilizer and fossil fuel use). The N_2O budget that best fits the ALE–GAGE observations (not a unique solution) is shown in Table 1-2, together with the budget produced for the IPCC (IPCC, 1990).

The IPCC budget indicates that there are probably unaccounted for or underestimated N_2O sources, while the (Prinn *et al.*) budget is essentially balanced. The difference between the two budgets is largely due to the significant biomass burning-tropical land clearing term in the latter, resulting from large post-burn, postclearing N_2O emissions (Anderson *et al.*, 1988; Luizao *et al.*, 1989; Prinn *et al.*, 1990). The global emissions of N_2O due directly to biomass burning alone have been recently reassessed as less than 2 Tg (N_2O) per year (Cofer *et al.*, 1991) or even less than 1 Tg (N_2O) per year (Crutzen and Andreae, 1990; Hao *et al.*, 1991).

Table 1-2 The global N_2O budget, Tg (10^{12}g) (N_2O) per year (IPCC, 1990; Prinn *et al.*, 1990; Sanhueza, 1991).

	IPCC (1990)	Prinn *et al.* (1990)	Sanhueza (1991)
Sinks			
photodissociation	11–20	13–16	11–20
atmospheric growth	5–7	6–7	5–7
Total	16–27	19–23	16–27
Sources			
oceans	2–4	4	2–4
soils – tropical	4–6	6	4–9
temperate	1–2	1	<1–3
fossil fuel use	<1	2	<1–1
biomass burning	<1	5	<1–2
fertilizer use	<1–4	2	<1–5
adipic acid production	<1		<1–1
Total	7–16	20	8–25

A revised N_2O budget, prepared for IPCC (Sanhueza, 1991) is also given in Table 1-2. The estimates were updated using new information on tropical soil fluxes (Sanhueza *et al.*, 1990; Matson *et al.*, 1990), temperate forest soil fluxes (Bowden *et al.*, 1990), detailed evaluations of cultivated soils (Bouwman, 1990; Eichner, 1990), and new estimates from biomass burning (Lobert *et al.*, 1990; Cofer *et al.*, 1991). Recent results have confirmed that the N_2O emissions from stationary combustion sources are very low (De Soete, 1989; Linak *et al.*, 1990; Sloan and Laird, 1990; Yokoyama *et al.*, 1991).

Other, possibly globally significant, N_2O sources have been identified since the IPCC review and are included in Table 1-3. The worldwide production of nylon could contribute $\leq$ 1 Tg (N_2O) per year (Thiemens and Trogler, 1991), and mobile combustion sources $\approx$0.6 Tg per year (De Soete *et al.*, 1989). The revised N_2O budget still indicates that there are unidentified and/or underestimated N_2O sources.

Some possible candidates are the use of legume pastures as nitrogenous fertilizers, which account for 15 percent of Australian N_2O emissions (Galbally *et al.*, 1992) and the significant, but unidentified, emissions of N_2O (2–3 Tg [N_2O] per year), possibly from stationary sources in Europe (Prather, 1988; Simmonds and Derwent, 1991).

1.8 METHANE

Methane is an important trace gas in the global atmosphere because it absorbs infrared radiation, thus impacting on climate. Methane is involved in tropospheric chemistry via OH and O_3 budgets, and it impacts on stratospheric chemistry as a source of hydrogen (H_2) and H_2O and as a sink for stratospheric chlorine. Methane is produced from a variety of anaerobic processes and is primarily removed by reaction with OH in the troposphere.

1.8.1 Atmospheric Distributions and Trends

There are several long-term CH_4 measurement programs. Ground-based measurements at globally distributed sites have been regularly made by NOAA–CMDL (USA) since 1983 (Steele *et al.*, 1987; Lang *et al.*, 1990a, b), by CSIRO (Australia) since 1978 (Fraser *et al.*, 1986a), by UCI (USA) since 1978 (Blake and Rowland, 1988), and by OGIST (USA) since 1978 (Khalil and Rasmussen, 1983a; 1990a). Long-term CH_4 measurement programs have been carried out at Cape Point, South Africa, since 1983 by CSIR (South Africa)–FIAER (Germany) (Brunke *et al.*, 1990; Scheel *et al.*, 1990), in the PNW and at the South Pole since 1975 (Rasmussen and Khalil, 1986), and at Tsukuba, Japan, since 1985 (Hirota *et al.*, 1989). Mid-tropospheric CH_4 data have been obtained by aircraft air sampling over southeast Australia (Fraser *et al.*, 1984, 1986a) since 1980 and over Europe and the North Atlantic by FIAER since 1979 (FIAER, Scheel *et al.*, 1988).

Selected available CH_4 data are shown in Figure 1-8, divided into the four semi-hemispheres and the published CH_4 trends are summarized in Table 1-3.

The rate of methane increase has slowed during the last decade, as observed at Cape Grim, Tasmania, (1978–1983: >20 ppbv per year; 1983–1990: 12±2 ppbv per year; (Steele *et al.*, 1987; WMO, 1990; Fraser, 1991) and in Antarctica (1983: 13.6 ppbv per year; 1988: 10.4 ppbv per year; (Steele *et al.*, 1989). The global University of California at Irvine (UCI) and Oregon Graduate Center (OGC) data have also shown a decline in CH_4 growth rate, from 19–25 ppbv per year (1981–1983) to 11–20 ppbv per year (1984–1987), with most of the decline in the growth rate occurring in 1983–1984 (Khalil and Rasmussen, 1990a). The observed growth rates as a function of time for the global OGIST and UCI and CSIRO Southern Hemispheric networks are shown in Figure 1-9. The data confirm high growth rates during 1978–1982 (17–21 ppbv per year), which have since declined to 8–13 ppbv per year (1988–1990). Satisfactory explanations for this rapid decline in CH_4 growth rates have yet to emerge.

Prinn *et al.* (1992) have calculated from industry emission estimates and trend observations of CH_3CCl_3 that OH levels in the tropical troposphere are increasing about 1 percent per year. If correct, this has important implications for the CH_4 budget. It suggests that the increasing levels of OH are as important as the approach to equilibrium in determining the slowing down in the CH_4 growth rate. It also allows sources to grow at 1–2 percent per year, rather than the 0–1 percent per year required if OH is constant.

Stevens (1988) has noted that the change in atmospheric CH_4 growth rate was accompanied by changes in its ^{13}C composition. This was true in both the Northern and Southern Hemispheres, where there were

Table 1-3 Global and regional CH_4 trends (ppbv per year, percent per year) from various observational networks.

Network (period)	Region/Location	Increase		Year	Reference
		ppbv per year	percent per year		
Ground–based Measurements					
NOAA–CMDL	Global	12.8	0.8	1984	1–4
(since 1983)	Global	12.9±0.1	0.8	1986	
	South Pole	11.9±0.1	0.7	1988	
CSIRO	Southern	18±2	1.3	1981	3,5,6
(since 1978)	Hemisphere	18±1	1.2	1984	
		11.9±0.2	0.7	1986	
UCI	Global	16±1	1.0	1987	7–9
(since 1978)		12–13	0.7–0.8	1990	
OGIST	Pacific N.W., U.S.	17.5±1.3	1.1	1985	3,10–12
(since 1978)	South Pole				
	Global	13.1±0.1	0.8	1986	
	Global	16.6±0.4	1.0	1988	
1960–1980	Global	13±3	0.8	1979	
FIAER	Cape Point,	10.3±0.3	0.7	1984	13
(since 1983)	South Africa				
MRI	Tsukuba,	9.0	0.5	1987	14
(since 1985)	Japan				
Free Tropospheric Measurements					
CSIRO	S.E. Australia	20±4	1.2	1981	3,5,6
(since 1980)		19±1	1.2	1984	
		12±1	0.8	1986	
FIAER	Europe and	12.7	0.8	1987	15
(since 1987)	North Atlantic				
Total Column Measurements					
1951–1986	Jungfraujoch, Switzerland		0.7		16
1979–1985	Kitt Peak, U.S.		1.1		17
1979–1989			1.0		18

References: 1, Steele *et al.*, 1987; 2, Steele *et al.*, 1989; 3, WMO, 1990a; 4, Novelli *et al.*, 1990; 5, Fraser *et al.*, 1984; 6, Fraser *et al.*, 1986a; 7, Blake and Rowland, 1988; 8, Rowland, 1990; 9, Rowland and Blake, 1991; 10, Rasmussen and Khalil, 1986; 11, Khalil and Rasmussen, 1990a; 12, Khalil *et al.*, 1989; 13, Brunke *et al.*, 1990; 14, Hirota *et al.*, 1989; 15, Scheel *et al.*, 1988; 16, Zander *et al.*, 1989a; 17, Wallace and Livingston, 1990a; 18, Thompson *et al.*, 1990.

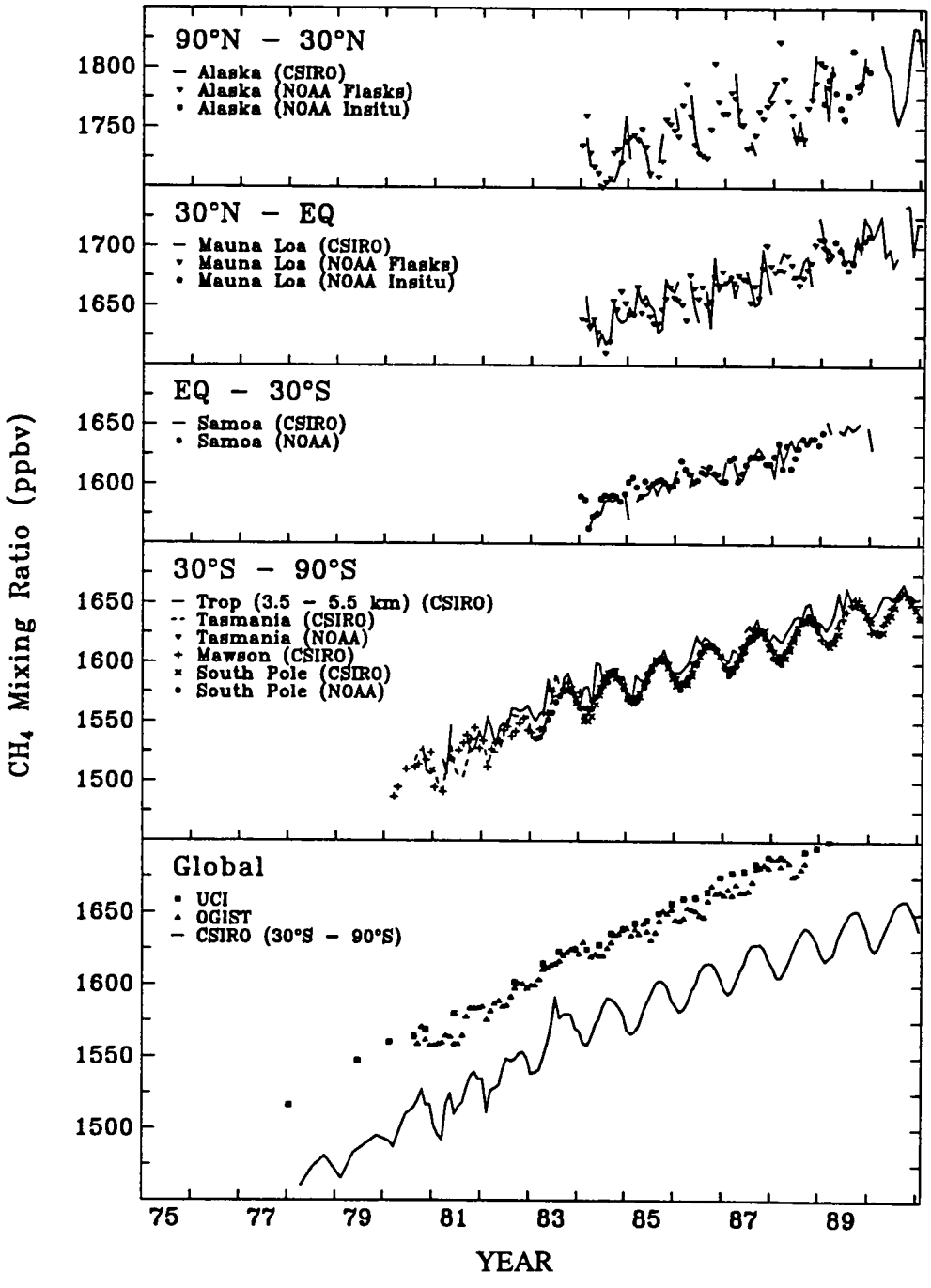

Figure 1-8 Methane observations (ppbv) in the four semihemispheres (NOAA: Steele *et al.*, 1987; Lang *et al.*, 1990a, b. CSIRO: Fraser *et al.*, 1986a, 1990; Fraser, 1991. OGIST: Khalil and Rasmussen, 1990a. UCI: Blake and Rowland, 1988; Rowland, 1990; Blake and Rowland 1991). The CSIRO (30°S–90°S) data are averages of Cape Grim (41°S) and Mawson (67°S) data. Some of the data are unpublished and are subject to revision. Data should not be used for further analysis without consulting the principal investigators: CSIRO, P. Fraser; UCI, D. Blake.

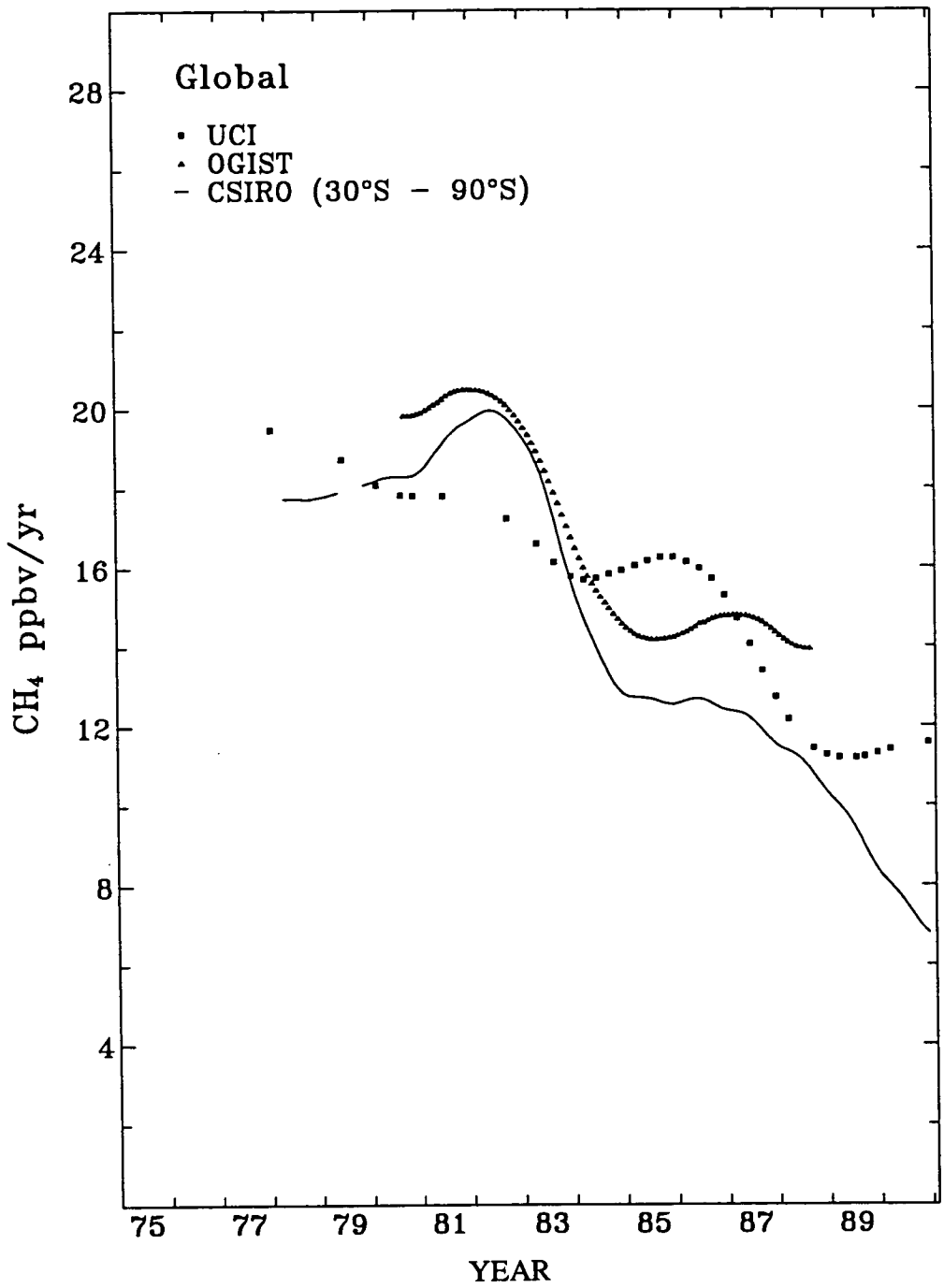

Figure 1-9 The global and Southern Hemispheric CH_4 trends from 1978–1990. The trends are obtained from spline fits to the long–term CH_4 data records (Blake and Rowland, 1988, 1991; Rowland, 1990; Khalil and Rasmussen, 1990a; Fraser *et al.*, 1986a, 1990; Fraser, 1991).

reductions in the ^{13}C depletion. These changes have been tentatively interpreted as indicating that there were changes in the source distribution of CH_4 (probably in the Northern Hemisphere) that were not of anthropogenic origin. It was suggested that there may have been a decrease in the flux of isotopically light (more ^{13}C-depleted) CH_4 of natural origin, such as that from wetlands.

Recent results from a high-accumulation-rate ice core (Etheridge *et al.*, 1992) show that there have been significant variations in the CH_4 growth rate over the period 1840–1980, with accelerating growth from 1890 (≤0.2 percent per year) to 1925 (0.5 percent per year), approximately constant growth from 1925 to 1950 (≈0.5 percent per year), followed by accelerating growth from 1950 (0.5 percent per year) to 1975 (≈1 percent per year). This pattern appears to correlate with the changing production rates of fossil fuels (Keeling, 1973; Marland and Rotty, 1984), perhaps indicating a significant role for this CH_4 source in determining global CH_4 growth rates.

1.8.2 Methane Sinks

The dominant removal process for atmospheric CH_4 is reaction with OH. A new measurement (Vaghjiani and Ravishankara, 1991) of the rate coefficient for the reaction of OH and CH_4 found it to be approximately 25 percent lower than reported previously, implying that the OH-CH_4 sink is approximately 420 Tg per year.

The magnitude of the OH-CH_4 sink is estimated from models whose OH fields are calibrated by the estimated releases and observed trends of methyl chloroform (CH_3CCl_3, see 1.3.3). A further uncertainty in the magnitude of the OH-CH_4 sink has resulted from theoretical (Wine and Chameides, 1990) and observational (Butler *et al.*, 1991) studies suggesting a biological or physical sink for CH_3CCl_3 in oceanic surface waters, which, if confirmed, could further reduce calculated OH levels (and the OH-CH_4 sink) by 10–20 percent.

Modeling studies suggest that OH levels, and hence the relative strength of the CH_4 sink, in preindustrial times were higher than at present. Studies of the ratio of formaldehyde (HCHO), a CH_4 oxidation product, to CH_4 in polar ice cores suggest that OH levels in preindustrial times were 30 percent higher than at present (Staffelbach *et al.*, 1991).

Studies in Arctic, temperate, and tropical environments have firmly established the importance of a global soil sink for atmospheric CH_4 (Steudler *et al.*, 1989; Keller *et al.*, 1990; Mosier *et al.*, 1991; Crill, 1991; Whalen and Reeburgh, 1990). However, there is considerable uncertainty associated with the magnitude of the soil sink for methane (5–60 Tg per year) (Born *et al.*, 1990). The destruction of CH_4 in soils is a biological process that is sensitive to both climatic variations and land use changes. Recent CH_4 soil flux measurements indicate that changes in land use or enhanced nitrogen input to soils by fertilization and/or deposition of atmospheric nitrogen are decreasing the CH_4 uptake by soils (Scharffe *et al.*, 1990; Mosier *et al.*, 1991).

1.8.3 Methane Sources

A recently identified CH_4 source that has not been considered previously is emissions from waste water and animal waste treatment facilities (40–65 Tg per year) (Harriss, 1991). Animal wastes contribute 20–30 Tg per year (Casada and Shafley, 1990). The landfill source may be ameliorated by identified high CH_4 oxidation rates in landfill cover soils (Whalen *et al.*, 1990). The preliminary data on CH_4 emissions from landfills, waste water treatment and animal wastes indicate a total emission of 85±20 Tg per year from anthropogenic waste management systems (Harriss, 1991).

Studies of the ^{14}C and ^{13}C isotopic composition of atmospheric CH_4 have been used to evaluate the contribution to total emissions made by fossil sources. Three independent estimates are (21±3) percent (Whalen *et al.*, 1989), 25 percent (Manning *et al.*, 1990; Lowe *et al.*, 1991) and 16 percent (Quay *et al.*, 1991). The latter value, combined with the reduction in the overall source inferred from the new estimate of the OH-CH_4 sink, would constrain the total fossil source to 90±10 Tg per year. Current estimates of CH_4 emissions from the production and use of oil, natural gas, and coal are compatible with this estimate for the total fossil source. Thus, the contributions of fossil sources such as CH_4 hydrate destabilization and the decomposition of old peat are apparently small.

For ^{13}C, differing amounts of depletion are found for different CH_4 sources. Bacterially produced CH_4, such as that from wetlands, rice paddies, ruminants, and termites, is typically more highly depleted in ^{13}C than is nonbacterial CH_4, such as that produced in biomass burning and in emissions of natural gas. Consideration

of the observed ^{13}C depletion in CH_4 sources together with that of atmospheric CH_4 and the ^{12}C–^{13}C fractionation factor associated with the reaction of CH_4 and OH indicates that bacterial CH_4 makes up some 70 percent of CH_4 sources (Quay *et al.*, 1991).

Methane emission rates from Chinese rice paddies (total emissions: 30 Tg per year, Khalil *et al.*, 1991) were found to be 4–10 times higher than from U.S. and European rice fields. Matthews *et al.* (1991) calculate Chinese and Indian CH_4 emissions from rice production of approximately 20 and 30 Tg per year respectively, assuming a global rice CH_4 source of 100 Tg per year (Fung *et al.*, 1991). By contrast, recent results from the major rice producing areas of India and Japan (Parashar *et al.*, 1991; Mitra, 1991; Yagi and Minami, 1990) indicate emissions that are not significantly different from the U.S. and European data. The Indian data indicate an annual CH_4 flux of only 3–4 Tg per year, an order of magnitude lower than calculated above. Large rice emissions from China and India are consistent with a global rice source of about 100 Tg per year, which is in agreement with constraints imposed by atmospheric observations (Fung *et al.*, 1991, see below). Based on the latest Indian data, Sanhueza (1991) has adopted a lower estimate of CH_4 emissions from rice agriculture (60 Tg per year) for the IPCC review of global CH_4 emissions. R. Cicerone (private communication) estimates that the uncertainty in global emissions from rice is still very large (≈ a factor of seven).

1.8.4 Global Methane Budgets

The NOAA global CH_4 data base have been interpreted with a three-dimensional model incorporating geographic and seasonal emission distributions of the major CH_4 sources and sinks (Fung *et al.*, 1991). Various source and sink scenarios were tested, constrained by the observed geographic and seasonal CH_4 distributions and the observed ^{13}C and ^{14}C composition of atmospheric CH_4. A preferred, but not necessarily unique, budget for CH_4 was derived, which is shown in Table 1-4 along with that derived for IPCC (IPCC, 1990) and also recently by Crutzen (1991), Harriss

Table 1-4 The global CH_4 budget (Tg (CH_4) per year). The numbers in parentheses are the range of uncertainties in sources and sinks. Adapted from: Fung *et al.* (1991); IPCC (1990); Crutzen (1991); Harriss (1991); Sanhueza (1991).

	Fung *et al.* (1991)	IPCC (1990)	Crutzen (1991)	Harriss (1991)	Sanhueza (1991)
Source					
Wetlands	115 (100–200)	115 (100–200)	115 (165–	110 (60–160)	115 (100–200)
Rice	100 (60–170)	110 (25–170)	100 –265)	100 (50–150)	60 (200–100)
Animals	80 (65–100)	80 (65–100)	80 (65–100)	80 (65–95)	80 (65–100)
Fossil fuels	75 (50–95)	80 (45–100)	95 (75–115)	90 (80–100)	95 (80–120)
Biomass burning	55 (50–100)	40 (20–80)	30 (15–45)	30 (15–45)	30 (20–80)
Land fills	40 (30–70)	40 (20–70)	50 (30–70)	85 (65–105)	85 (65–105)
Termites	20 (10–200)	40 (10–100)	20 (10–100)		20 (5–50)
Oceans	10 10 (5–20)	10 (5–20)			10 (5–20)
Others	5 10 (0–120)	5		50 (25–75)	10 (1–30)
Total	500 (380–950)	525 (290–960)	505 (370–720)	545 (360–730)	505 (360–805)
Sink					
Chemical loss	450 (405–495)	500 (400–600)	430 (350–510)	430 (345–515)	430 (350–510)
Soils	10 (5–60)	30 (15–45)	30 (15–45)	30 (15–45)	30 (15–45)
Atmospheric Increase	45 (40–50)	45 (40–50)	45 (40–50)	45 (40–50)	45 (40–48)
Total	505 (450–605)	575 (455–695)	505 (405–605)	505 (400–610)	505 (405–605)

(1991), and Sanhueza (1991). The global CH_4 budget is an underdetermined problem where there are more sources and sinks than there are observations to constrain them. The largest uncertainties in CH_4 emissions are associated with landfills, tropical swamps, rice fields, biomass burning, and termites, due to a lack of direct measurements of fluxes in regions were these sources are concentrated.

In contrast to the IPCC CH_4 budget, there is now fairly good agreement between CH_4 sources and sinks plus atmospheric accumulation. This is due largely to the revised (25 percent lower) atmospheric consumption of CH_4 by OH radicals (Vaghjiani and Ravishankara, 1991). However, there still remains considerable uncertainty associated with the global methane budget. Recent estimates of methane emissions from animal wastes and waste water treatment are included in Table 1-3 only in the Harriss (1991) and Sanhueza (1991) budgets, under landfills. A possibly large methane source from asphalt (Sackett and Barber, 1988), now appears to be less than 1 Tg per year (Tyler *et al.*, 1990).

1.9 HYDROGEN

Oxidation of H_2 in the stratosphere may affect stratospheric O_3 by supplying H_2O vapor to the stratosphere, in addition to that derived from H_2O transported from the troposphere and CH_4 oxidation.

1.9.1 Global Distribution and Trends

Measurement of H_2 in air samples collected in the OGIST global flask sampling program between 1985 and 1989 shows that the concentration of H_2 has increased by 3.2±0.5 ppbv per year (Khalil and Rasmussen, 1990e). The global average concentration in 1989 was ≈515 ppbv, based on the global trend and the 1988 average concentration. The concentration of H_2 in the Southern Hemisphere is about 3 percent higher than in the Northern Hemisphere. The Cape Grim data (1984–1987) from the OGIST network have been reported separately (Fraser *et al.*, 1989).

1.9.2 Sources and Sinks

The global source and sink of H_2 is estimated to be about 90 Tg per year (Khalil and Rasmussen, 1990e), the major sources being CH_4 oxidation (30 percent), oxidation of NMHCs (25 percent), anthropogenic activities (20 percent) and biomass burning (15 percent). The major sinks are removal by soils (85 percent) and oxidation by OH (15 percent). The increasing concentration of H_2 in the atmosphere is probably due to growing sources, for example, the observed CH_4 trend may account for 50 percent of the observed H_2 trend. The higher H_2 concentrations in the Southern Hemisphere compared to the Northern Hemisphere have been interpreted as indicating that the soil sink is the dominant cause of the interhemispheric difference. The observed seasonality in the Southern Hemisphere possibly reflects the local production by CH_4 and NMHC oxidation, while the seasonality in the Northern Hemisphere may reflect the seasonality in the soil sink (Khalil and Rasmussen, 1989).

1.10 CARBON MONOXIDE

Carbon monoxide (CO) is an important trace gas in the troposphere because it plays significant roles in controlling the chemistry of ozone production and hydroxyl radical destruction in the lower atmosphere. It directly affects the oxidizing capacity of the lower atmosphere and can thus influence the concentrations of other important trace gases such as CH_4, CH_3CCl_3, and the HCFCs.

1.10.1 Atmospheric Distributions and Trends

Because of its short residence time (2–3 months), coupled with an inadequate ground-based observational network, the determination of global average concentrations and long-term trends for CO is difficult. Due to larger sources in the Northern Hemisphere, the concentration of CO in the background, marine atmosphere is a factor of about two greater than in the Southern Hemisphere, where the annual average for the background, marine atmosphere is about 50–60 ppbv.

However, over continental sites in both hemispheres, even in clean air, CO concentrations are elevated and highly variable. For example, in the Southern Hemisphere average concentrations of about 100 ppbv over tropical Brazil are typical (Kirchhoff *et al.*, 1989; Kirchhoff and Marinho, 1989).

Remote sensing from space provides a global picture of CO spatial variability (Reichle *et al.*, 1990), indicating large biomass burning sources over South America and tropical Africa, which presumably influence the local production of tropospheric ozone, which is subsequently transported over a significant portion of the Southern Hemisphere (Watson *et al.*, 1990). Long-term CO data are not yet available from space platforms.

There are several long-term CO measurement programs. Ground-based measurements at globally distributed sites have been regularly made by OGIST since 1978 (Khalil and Rasmussen, 1988) and CSIRO since 1980 (Fraser *et al.*, 1986a, b). Long-term CO measurement programs have also been carried out at Cape Point since 1979 (Brunke *et al.*, 1990; Scheel *et al.*, 1990). In the tropics, CO measurements have been made systematically since 1987 in the Brazilian savanna region. Besides a permanent station at Cuiaba (16°S), another station at Natal (6°S) is also maintained for reference (Kirchoff and Rasmussen, 1990).

Mid-tropospheric CO data have been obtained by aircraft air sampling over southeast Australia (Fraser *et al.*, 1986 a, b) since 1980 and over Europe and the North Atlantic by the FIAER since 1979 (Scheel *et al.*, 1988).

Selected available CO data are shown in Figure 1-10, divided into the four semihemispheres. The FIAER–CSIR and CSIRO long-term data in the Southern Hemisphere (Cape Point, 1979–1988; Cape Grim, 1978–1991; middle troposphere, southeastern Australia, 1980–1991; Mawson, 1980–1990) do not show statistically significant trends (Fraser and Coram, 1990; Brunke *et al.*, 1990; Scheel *et al.*, 1990; WMO, 1990b). An earlier report of a significant CO growth at Mawson (1.5±0.6 ppbv per year) (Fraser *et al.*, 1986a) was later proved to be an artifact of the relatively short data record. By contrast, from the OGIST network (Khalil and Rasmussen, 1988, 1990c) a CO trend in the Southern Hemisphere of 0.8±0.4 ppbv per year over the period 1980–1988 has been reported. The Northern Hemispheric data from the OGIST network show a similar positive trend (0.8±0.4 ppbv per year or 0.8–1.4 percent per year) (Khalil and Rasmussen, 1988).

A comparison of spectroscopic data recorded at Jungfraujoch Station, Switzerland, in 1950–1951 with data collected at the same site in 1985–1987 indicates increasing CO levels (0.9±0.2 percent per year, 1950–1987), assuming an exponential growth in CO over this period (Zander *et al.*, 1989b). Spectroscopic data collected at a frequency of about six times per year at Kitt Peak do not show a statistically significant trend for the period 1978–1986 (Wallace and Livingston, 1990b).

It is clear from the long-term ground-based and mid-tropospheric records in the Southern Hemisphere that the rate of CO change exhibits complex interannual variability. Figure 1-11 shows the rate of CO change as a function of time. Between 1978 and 1983, CO concentrations grew about 1 ppbv per year. From 1983 to 1985, CO concentrations declined, on average, 2 ppbv per year; 1986–1988: CO increased by 2 ppbv per year; 1988–1990: CO declined by 3 ppbv per year. Over the period 1978–1990, the overall trend of CO in the mid-to-high latitudes of the Southern Hemisphere is not significantly different from zero.

1.10.2 Carbon Monoxide Calibration

There has been significant progress in the calibration of CO measurements. (Weeks *et al.* 1989) have compared an ambient concentration OGIST calibration gas used in the CSIRO CO program to a dynamically-diluted NIST (formerly NBS) SRM (#2612a, 9.7 ppmv CO in air) and found that ambient levels of CO in the Southern Hemisphere in the NIST scale are ≈30–40 percent higher than those reported in the OGIST scale (≈35–55 ppbv). The CSIRO data reported here (Figure 1-10) are in the NIST scale. Note that there is now good agreement between FIAER and CSIRO measurements at similar latitudes in the Southern Hemisphere. The FIAER CO scale has been found to be within 4 percent of the NIST scale (Brunke *et al.*, 1990). The OGIST scale has recently been revised such that CO concentrations are now reported 20 percent higher than previously (Khalil and Rasmussen, 1990d). A comparison of NIST (U.S.) and National Physical Laboratory (NPL) (U.K.) gravimetric standards indicates agreement to within 0.2 percent at a range of concentrations from 10 ppmv to 8 percent (Hughes *et al.*, 1991).

Novelli *et al.* (1991) at NOAA–CMDL have prepared two series of gravimetric standards of CO in air at 25 to 1,000 ppbv, from pure CO as well as from a NIST SRM at 9.7 ppmv. The two sets of standards

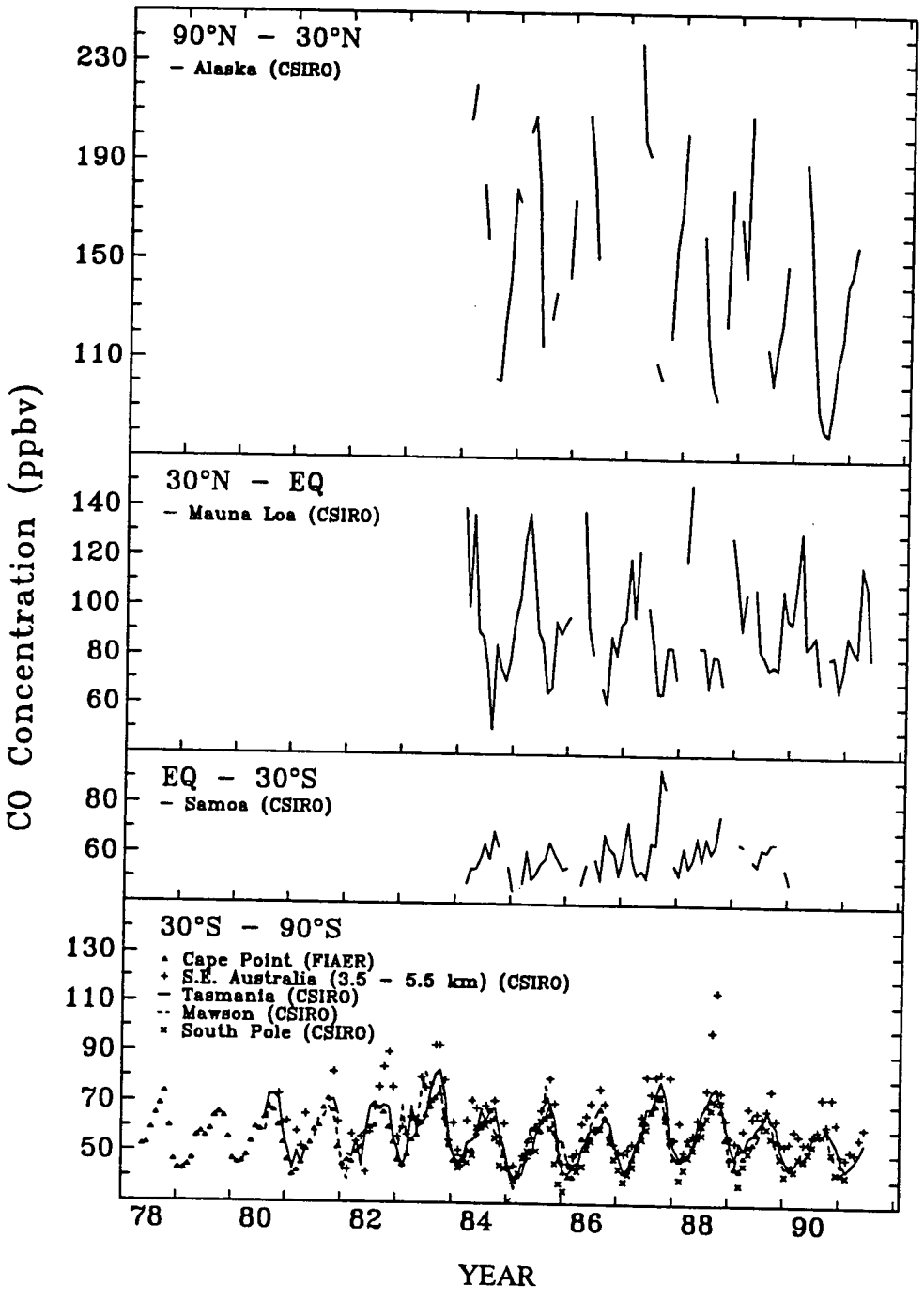

Figure 1-10 Carbon monoxide observations (ppbv) in the four semihemispheres. All data are from the CSIRO global flask network (Fraser *et al.*, 1986a, b; Fraser, 1991), except Cape Point (CSIR-FIAER: Brunke *et al.*, 1990; Scheel *et al.*, 1990). Some of the data are unpublished and are subject to revision. Data should not be used for further analysis without consulting the principal investigators: CSIRO, P. Fraser; FIAER, H. Scheel.

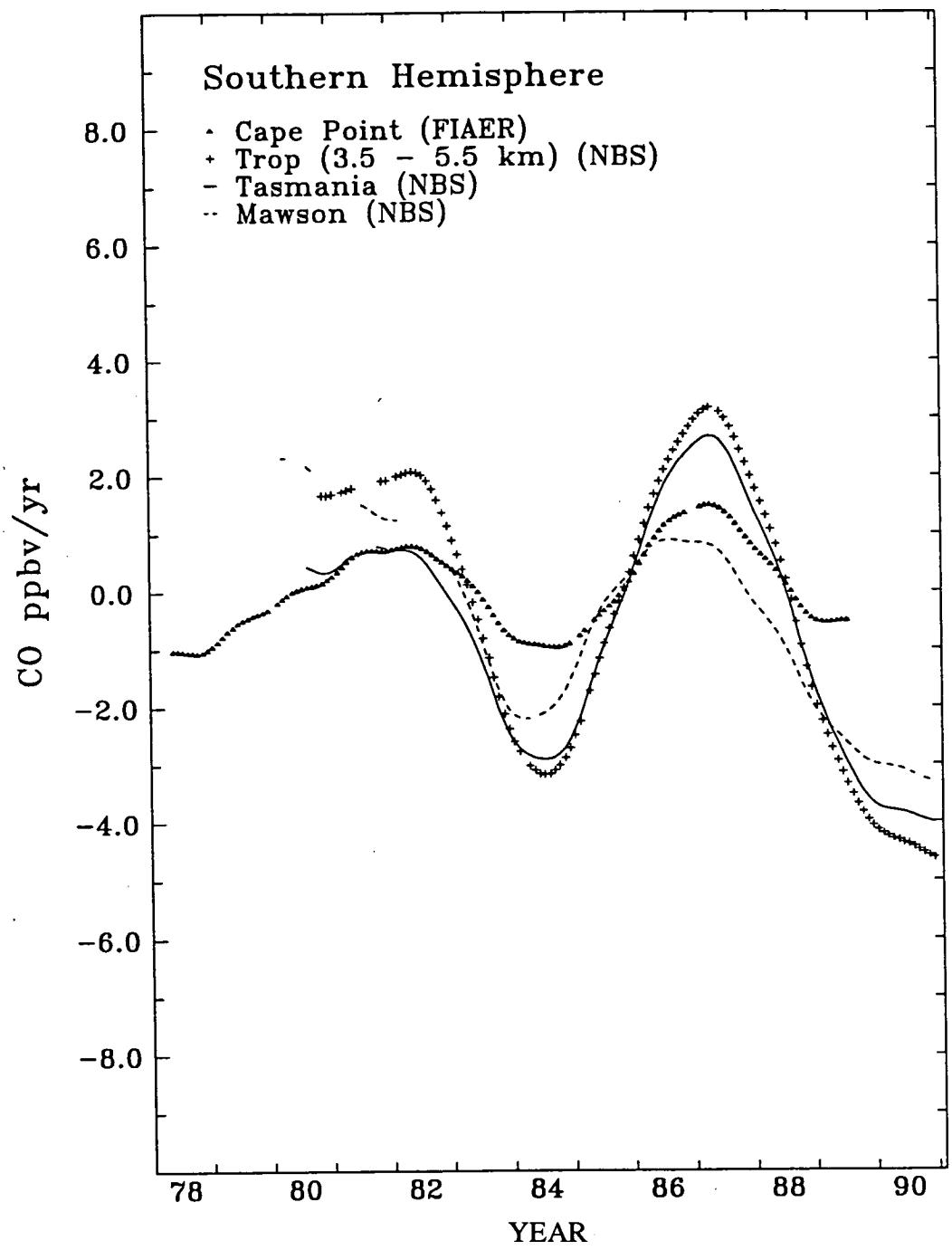

Figure 1-11 The Southern Hemispheric CO trends from 1978–1990. The trends are obtained from spline fits to the long-term CO data records (CSIRO: Fraser *et al.*, 1986a, b; Fraser, 1991. CSIR-FIAER: Brunke *et al.*, 1990; Scheel *et al.*, 1990)

agree to within 1 percent. Comparison of the OGIST and NOAA–CMDL scales at CSIRO showed that CO concentrations determined using the NOAA–CMDL scale are ≈25 percent higher than those obtained in the OGIST scale (before the 20 percent revision).

In summary, the NIST, NPL, and NOAA–CMDL CO standards agree to within 1 percent. The FIAER scale is within 4 percent of NIST, and the revised OGIST scale appears to be within 10–15 percent of the NIST scale.

1.10.3. Global Carbon Monoxide Budgets

At present, there are several uncertainties in evaluating the sources and sinks of atmospheric CO. Carbon monoxide concentrations show a large degree of spatial (Reichle *et al.*, 1990) and temporal (Khalil and Rasmussen, 1988) variability, especially in the Northern Hemisphere over continental regions, which has not yet been adequately described by observational data. This presents serious problems in budget sensitivity studies when trying to match observations and model results (Fraser *et al.*, 1986b). The various CO concentration data sets reported to date in the literature are probably not known to better 10 percent in an absolute sense. According to Lelieveld and Crutzen (1991), the oxidation of formaldehyde (HCHO) in the liquid phase does not produce CO but CO_2 directly. Thus, the fraction of CH_4 and higher NMHCs that produce CO during the oxidation process need to be reevaluated.

Despite these uncertainties in evaluating CO budgets, there have been several attempts to produce global budgets for CO (Table 1-5). The total emissions of CO are probably between 2,000 and 3,000 CO Tg per year, with as much as $^2/_3$ being produced from anthropogenic activities, combustion processes (biomass (30 percent) and fossil fuel (20 percent)) being the dominant sources.

It is interesting to speculate why CO levels are not increasing in the Southern Hemisphere when CO sources are so strongly anthropogenically influenced. However, it is not obvious that all of the anthropogenic CO sources are increasing with time. Data on the temporal change of the magnitude of the biomass

Table 1-5 The global CO budget, Tg per year.

	WMO (1986)	Logan (1990)	Seiler and Conrad (1987)		Khalil and Rasmussen (1990d)		Crutzen and Zimmerman (1991)
Sources							
Primary							
Fossil fuel	440	440	640	(440–840)	500	(400–1000)	500
Biomass burning	700	660	1,000	(400–1600)	680	(340–1400)	600
Vegetation		80	80	(50–100)	100	(50–200)	
Oceans	50	150	100	(10–190)	40	(20–80)	
Secondary							
NMHC oxidn	680	210	900	(400–1300)	690	(300–1400)	600
CH_4 oxidn	610	790	600	(300–900)	600	(400–1000)	630
Total	2480	2,330	3,320	(1,600–4,930)	2,600	(2,000–3,000)	2,330
Sinks							
OH reaction	1,910 (1,200–2,600)	2,020	2,000	(1,400–2,600)	≈2200	2,050	
soils	260	390	390	(150–530)	≈250	280	
stratosphere				110 (80–140)		≈100	
accumulation	20						
Total	2,190 (1,420–2,960)	2,410	2,500	(1,630–3,270)	≈2,550	2,330	

burning source are not readily available and the CO levels in urban areas of the developed countries appear to have declined over the past decade due to cleaner combustion processes (IPCC, 1990). The possibility of increasing levels of OH radical (Prinn *et al.*, 1991a) also complicates the prediction of CO trends.

Crutzen and Zimmerman (1991) have developed a preindustrial CO emission scenario of about 1,000 Tg CO per year, which in a two-dimensional model simulation results in preindustrial CO levels that are 50 percent (Southern Hemisphere) to 60 percent (Northern Hemisphere) of current model levels (2,300 Tg per year CO emissions).

1.11 NON-METHANE HYDROCARBONS (NMHCs)

NMHCs could possibly play a significant role in determining the OH radical concentration in the remote marine boundary layer (Bonsang *et al.*, 1988; Donahue and Prinn, 1990) and act as a significant source of CO. Because of their role in OH chemistry, NMHCs are important in assessing the significance of the OH sink for CH_4, CO, CH_3CCl_3, as well as the HCFCs and HFCs.

The number of NMHCs in the background atmosphere is quite large (in excess of 100), including saturated, unsaturated, and aromatic compounds. The NMHCs can be classified by their atmospheric lifetimes:

- relatively long-lived (lifetimes > week), where the highest concentrations (up to 3 ppbv for ethane (C_2H_6)) are observed in the middle to high northern latitudes;
- more reactive (lifetimes between 12 hours and a week), such as C_2-C_5 alkenes, whose concentrations exhibit significant temporal and latitudinal variability from <0.1 ppbv in remote areas to a few ppbv close to source regions;
- extremely short-lived (lifetimes of hours) such as terpenes or isoprene whose local concentrations only may reach about 10 ppbv close to their sources.

With the exception of C_2H_6, trends in the atmospheric concentrations of NMHCs have not been established. Recently (Ehhalt *et al.*, 1991) have reported a secular trend in the tropospheric concentration of C_2H_6 over the Northern Hemisphere of 0.9±0.3 percent per year, based on spectroscopic observations made at Jungfraujoch in 1951 and from 1984 to 1988, probably due to anthropogenic activities such as the use of fossil fuels and biomass burning.

1.11.1 Sources and Sinks for NMHCs

The oceans are a major source of NMHCs, mainly alkenes. Estimates of the source strength of ethene and propene range from ≈30 to 100 Tg C per year (Penkett, 1982; Bonsang *et al.*, 1988). Emissions of NMHCs from terrestrial vegetation are species dependent, isoprene coming largely from deciduous plants (≈500 Tg C per year) and terpenes from conifers (≈500 Tg C per year) (Rasmussen and Khalil, 1988). These emission estimates are very uncertain. Grasslands emit ≈50 Tg C per year of light alkenes and higher hydrocarbons (Warneck, 1988). Anthropogenic emissions are ≈60 Tg C per year (Warneck, 1988) and biomass burning, 25 Tg C per year (Crutzen and Andreae, 1990). All these emissions have uncertainty factors of 2–3.

It has been generally accepted that the dominant loss mechanism for most NMHCs is reaction with the hydroxyl radical (OH). Other oxidants capable of removing hydrocarbons are ozone (O_3), the nitrate radical (NO_3), and chlorine atoms (Cl). Unsaturated hydrocarbons react rapidly with O_3 and NO_3 such that the atmospheric lifetimes of isoprene for removal by OH, O_3, and NO_3 are 18 hours, 1.2 days, and 20 hours respectively; for a terpene such as α-pinene the lifetimes are respectively 3.4 hours, 4.6 hours, and 2 hours (Corchnoy and Atkinson, 1990). It has also been proposed that chlorine atoms may remove large proportions of some saturated hydrocarbons such as ethane and propane (Singh and Kasting, 1988). This appears to be much less likely now after the findings of low HCl concentration (the source of the Cl atoms over the ocean) (Harris *et al.*, 1991).

To improve our understanding of the role of NMHCs in the tropospheric OH chemistry, a global observational data base of the unsaturated hydrocarbons (up to C_6) at the 1 pptv level is required, both in the atmosphere and surface ocean waters, as well as concurrent O_3, CO, and UV flux observations (Donahue and Prinn, 1990).

1.12 CARBON DIOXIDE

Next to H_2O vapor, CO_2 is the most important greenhouse gas in the atmosphere. Increasing concentrations of CO_2 are predicted to cause a warming of the troposphere and a cooling of the stratosphere, the latter resulting directly in increased levels of stratospheric O_3, or indirectly, through the formation of stratospheric aerosols, reduced levels of stratospheric O_3.

1.12.1 Atmospheric Distributions and Trends

There are several long-term measurement programs for CO_2 in the remote atmosphere. Recent publications from the NOAA–CMDL laboratory describe the results from *in situ* (Mauna Loa, Thoning *et al.*, 1989; Samoa, Waterman *et al.*, 1989) and flask observations (Conway *et al.*, 1988). Data up to 1989 are summarized in Novelli *et al.* (1990).

Concentrations in the Northern Hemisphere are typically 2–3 ppmv higher than in the Southern Hemisphere of CO_2, although the difference between the hemispheres shows substantial interannual variation. The global average CO_2 concentration and increase in 1989, based on the NOAA–CMDL *in situ* data from Barrow, Mauna Loa, Samoa, and the South Pole, was 352.2 ppmv and 1.6 ppmv per year respectively (Novelli *et al.*, 1990). The global average growth rate shows considerable variation from year to year, with values as high as 2.6 ppmv per year (1987–1988) and as low as 0.4 ppmv per year (1981–1982). The long-term growth rate is increasing.

Like CH_4, the observed change in CO_2 amounts has been accompanied by a change in its ^{13}C composition. CO_2 has become more depleted in ^{13}C as isotopically light (more ^{13}C-depleted) CO_2 is added to the lighter pool of atmospheric CO_2 (Kaye *et al.*, 1989).

Variations in atmospheric CO_2 are correlated with El Niño-Southern Oscillation (ENSO) events (Keeling *et al.*, 1989). Some clues to the cause of this correlation may be found in $^{13}C/^{12}C$ ratios of atmospheric CO_2, which allow CO_2 of terrestrial and marine origin to be distinguished. The $^{13}C/^{12}C$ data to date are somewhat contradictory (Keeling *et al.*, 1989; Francey *et al.*, 1990), so that a wide range of CO_2 fluxes associated with ENSO events are possible.

1.12.2 Sources and Sinks of CO_2

The extent to which the terrestrial biota contribute to long-term changes in atmospheric CO_2 has long been a contentious question in carbon cycle studies. Inversion calculations (two-dimensional model), using surface atmospheric CO_2 observations (Enting and Mansbridge, 1989, 1991; Tans *et al.*, 1989), and three-dimensional model studies, supplemented by analysis of surface atmospheric and oceanic partial pressure data (Tans *et al.*, 1990), concluded that there is a large, previously unidentified sink for CO_2 in the Northern Hemisphere, probably biotic uptake. More recently, it has been appreciated that the Tans *et al.* (1990) analysis neglects a natural cycle of CO_2 taken up by the terrestrial biota, transported into the oceans via rivers and then outgased into the atmosphere to close the cycle (Sarmiento and Siegenthaler, 1991). The existence of this cycle represents a correction of perhaps 0.6 Gt to the net ocean uptake calculated by Tans *et al.* (1990). In addition, Enting and Mansbridge (1991) noted that the role of CO in the atmospheric budget implies a correction of about 0.25 Gt to budgets based in interpreting the spatial distribution of CO_2. (The correction needs to be added to southern sinks and subtracted from northern sinks.) The effect of these corrections is to bring the ocean fluxes estimated by Tans *et al.* (1990) into much better agreement with ocean uptake based on global-scale carbon cycle modeling. However, this still implies the need for some biotic uptake of comparable magnitude to the carbon release from deforestation. In particular, estimates of the spatial distribution of CO_2 sources show a tropical source comparable to that expected from ocean outgasing without any additional contribution from tropical deforestation.

REFERENCES

Anderson, I., J. Levine, M. Poth, and P. Riggan, Enhanced biogenic emissions of nitric oxide and nitrous oxide following surface biomass burning, *J. Geophys. Res.*, *93*, 3893–3898, 1988.

Blake, D., and F. Rowland, Continuing worldwide increase in tropospheric methane, 1978–1987, *Science, 239,* 1129–1131, 1988.

Blake D., and F. Rowland, Personal communication, 1991.

Born, M., H. Door, and I. Levin, Methane consumption in aerated soils of the temperate zone, *Tellus, 42B,* 1–8, 1990.

Bonsang, B., M. Kanakidou, G. Lambert, and P. Monfrey, The marine source of C_2–C_6 alphatic hydrocarbons, *J. Atmos. Chem., 6,* 3–20, 1988.

Bouwman, A., Exchange of greenhouse gases between terrestrial ecosystems and the atmosphere, in *Soils and the Greenhouse Effect,* A. Bouwman (ed.), J. Wiley New York, 62–125, 1990.

Bowden, R., P. Steudler, J. Melillo, and J. Durham, Annual nitrous oxide fluxes from temperate forest soils in the northeastern United States, *J. Geophys. Res., 95,* 13997–14005, 1990.

Brasseur, G., C. Granier, and S. Walters, Future changes in stratospheric ozone and the role of heterogeneous chemistry, *Nature, 348,* 626–628, 1990.

Brunke, E., H. Scheel, and W. Seiler, Trends of tropospheric CO, N_2O, and CH_4 as observed at Cape Point, South Africa, *Atmos. Environ., 24A,* 585–595, 1990.

Brunke, E., and H. Scheel, Tropospheric CFC measurements at Cape Point, South Africa, Report prepared for NASA Working Group Meeting on CFC and Halon Concentrations, Trends and Lifetimes, Newport Beach, July, 1991.

Butler, J., J. Elkins, and T. Thompson, Tropospheric and dissolved N_2O of the West Pacific and East Indian Oceans during the El Niño Southern Oscillation event of 1987, *J. Geophys. Res., 94,* 14865–14887, 1989.

Butler, J., J. Elkins, T. Thompson, B. Hall, T. Swanson, and V. Koropalov, Oceanic consumption of CH_3CCl_3: implications for tropospheric OH, *J. Geophys. Res., 96,* 22347-22355, 1991.

Casada, M. and L. Shafley, Global methane emissions from livestock and poultry manure, Report to the Global Change Division, US EPA, Washington, DC, 1990.

Cofer, W., J. Levine, E. Winstead, and B. Stocks, New estimates of nitrous oxide emissions from biomass burning, *Nature, 349,* 689–691, 1991.

Conway, T., P. Tans, L. Waterman, K. Thoning, K. Masarie, and R. Gammon, Atmospheric carbon dioxide measurements in the remote global troposphere, 1981–1984, *Tellus, 40B,* 81–115, 1988.

Corchnoy, S., and R. Atkinson, Kinetics of the gas phase reactions of OH and NO_3 radicals with 2-carine, 1,8-aneole, p-cymene and terpinolene, *Env. Sci. & Tech., 24,* 1497–1502, 1990.

Crill, P., Seasonal patterns of methane uptake and carbon dioxide release from a temperate woodland soil, *EOS Trans., 72,* 80, 1991.

Crutzen, P., The possible importance of COS for the sulfate layer of the stratosphere, *Geophys. Res. Lett., 3,* 73–76, 1976.

Crutzen, P., and M. Andreae, Biomass burning in the tropics: impact on atmospheric chemistry and biogeochemical cycles, *Science, 250,* 1669–1678, 1990.

Crutzen, P., Methane's sinks and sources, *Nature, 350,* 380–381, 1991.

Crutzen, P., and Zimmermann, The changing photochemistry of the troposphere, *Tellus, 43AB,* 136–151, 1991.

Cunnold, D., R. Prinn, R. Rasmussen, P. Simmonds, F. Alyea, C. Cardelino, A. Crawford, P. Fraser, and R. Rosen, Atmospheric lifetime and annual release estimates for CCl_3F and CCl_2F_2 from five years of ALE data, *J. Geophys. Res., 91,* 10797–10817, 1986.

De Soete, G., Updated evaluation of nitrous oxide emissions from industrial fossil fuel combustion. Report to the European Atomic Energy Community, Institut Francais du Petrole, Reference 37–559, 1989.

Donahue, N., and R. Prinn, Nonmethane hydrocarbon chemistry in the remote marine boundary layer, *J. Geophys. Res., 95,* 18387–18411, 1990.

Eichner, M., Nitrous oxide emissions from fertilized soils: summary of available data, *J. Environ. Qual., 19,* 272–280, 1990.

Ehhalt, D., U. Schmidt, R. Zander, P. Demoulin, and C. Rinsland, Seasonal cycle and secular trend of the total and tropospheric column abundance of ethane above the Jungfraujoch, *J. Geophys. Res., 96,* 49875–4994, 1991.

Enting, I., and J. Mansbridge, Seasonal sources and sinks of atmospheric CO_2: Direct inversion of filtered data, *Tellus, 41B,* 111–126, 1989.

Enting, I., and J. Mansbridge, Latitudinal distribution of sources and sinks of CO_2: results of an inversion study, *Tellus, 43B*, 156–170, 1991.

Etheridge, D., G. Pearman, and P. Fraser, Changes in tropospheric methane between 1841 and 1978 from a high accumulation-rate Antarctic ice core, *Tellus*, accepted, 1992.

Fabian, P., R. Borchers, H. Duscha, B. Kruger, S. Lal, and B. Subbaraya, $CHClF_2$ (HCFC-22): distribution, budget and environmental impact, in *Ozone in the Atmosphere*, R. Bojkov and P. Fabian (eds.), 294–297, A. Deepak Publishing, Hampton, Virginia, 1989.

Ferek, R., and M. Andreae, Photochemical production of carbonyl sulphide in marine surface waters, *Nature, 307*, 148–150, 1984.

Francey, R., F. Robbins, C. Allison, and N. Richards, The CSIRO global survey of CO_2 stable isotopes, in Baseline 88, S. Wilson and G. Ayers (eds.), Bureau of Meteorology/CSIRO, 16–27, 1990.

Fraser, P., M. Khalil, R. Rasmussen, and L. Steele, Tropospheric methane in the mid-latitudes of the Southern Hemisphere, *J. Atmos. Chem., 1*, 125–135, 1984.

Fraser, P., P. Hyson, R. Rasmussen, A. Crawford, and M. Khalil, Methane, carbon monoxide and methyl chloroform in the Southern Hemisphere, *J. Atmos. Chem., 4*, 3–42, 1986a.

Fraser, P., P. Hyson, S. Coram, R. Rasmussen, A. Crawford, and M. Khalil, Carbon monoxide in the Southern Hemisphere, Proc. of the Seventh World Clean Air Congress, 2, H. Hartmann (ed.), 341–352, International Union of Air Pollution Preventation Associations/Clean Air Society of Australia and New Zealand, 1986b.

Fraser, P., R. Rasmussen, and M. Khalil, Atmospheric observations of chlorocarbons, nitrous oxide, methane, carbon monoxide and hydrogen from the Oregon Graduate Center flask sampling program, in *Baseline 87*, B. Forgan and G. Ayers (eds.), Bureau of Meteorology/CSIRO, 40–44, 1989.

Fraser, P., and S. Coram, Atmospheric methane, carbon monoxide and carbon dioxide by gas chromatography, 1988, in *Baseline 88*, S. Wilson and G. Ayers (eds.), Bureau of Meteorology/CSIRO, 54–56, 1990.

Fraser, P., P. Steele, R. Francey, and G. Pearman, The CSIRO latitudinal study: methane data from air samples collected at CMDL Baseline Observatories and at Cape Grim, Tasmania, in *Climate Monitoring and Diagnostics Laboratory, No. 18 Summary Report 1989*, W. Komhyr and R. Rosson (eds.), U.S. Department of Commerce, NOAA–ERL, Boulder, Colorado, USA, 97–103, 1990.

Fraser, P., Personal communication, 1991.

Fraser, P., F. Alyea, A. Crawford, D. Cunnold, R. Prinn, R. Rasmussen, R. Rosen, and P. Simmonds, Lifetime and emission estimates of 1,1,2-trichlorotrifluoroethane (CFC-113) from daily global background observations 1982– 1990, to be submitted July 1992.

Fung, I., J. John, J. Lerner, E. Matthews, M. Prather, L. Steele, and P. Fraser, Three-dimensional model synthesis of the global methane cycle, *J. Geophys. Res., 96*, 13033–13065, 1991.

Galbally, I., P. Fraser, C. Meyer, and D. Griffith, Biosphere-atmosphere exchange of trace gases over Australia, Proceedings of the IGBP Workshop No. 14: Utilization of Renewable Biological Resources, October 3–5, 1990, Canberra, Australia, in press, 1992.

Golombek, A., and R. Prinn, Global three-dimensional model calculations of the budgets and present-day atmospheric lifetimes of CCl_2FCClF_2 (CFC-113) and $CHClF_2$ (HCFC-22), *Geophys. Res. Lett., 16*, 1153–1156, 1989.

Hall, B., J. Elkins, J. Butler, T. Thompson, and C. Brunson, Improvements in nitrous oxide and halocarbon measurements at the South Pole, *Ant. J. US., 25*, 252–283, 1990.

Hao, W., D. Scharffe, J. Lobert, and P. Crutzen, Emissions of N_2O from the burning of biomass in an experimental system, *Geophys. Res. Lett., 18*, 999–1002, 1991.

Harris, A.W., D. Klemp, and T. Zenker, An upper limit on the HCl near surface mixing ratio at 28°N 30°W measured using TDLAS., submitted, 1991.

Harriss, R., Personal communication, 1991.

Hirota, M., H. Muramatsu, T. Sasaki, Y. Makino, and M. Asahi, Atmospheric concentrations and distributions of CCl_2F_2, CCl_3F and N_2O over Japan between 1979 and 1986, *J. Meteorol. Soc. Japan, 66*, 703–708, 1988.

Hirota, M., H. Muramatsu, Y. Makino, M. Ikegami and K. Tsutsumi. Gas-chromatographic measurement of atmospheric methane in Japan, *Atmos. Environ, 23*, 1835–1839, 1989.

Hirota, M., and T. Sasaki, Unpublished data presented at the NASA CFC and Halons Trends, Emissions and Lifetimes Meeting, Newport Beach, California, July 1991.

Hughes, E., A. Davenport, P. Woods and W. Zielinski. Intercomparison of a range of primary gas standards of carbon monoxide in nitrogen and carbon dioxide in nitrogen prepared by the National Institute of Standards and Technology and the National Physical Laboratory, *Environ. Sci. Tech.*, *25*, 671–676, 1991.

IPCC, 1990, Watson, R., H. Rodhe, H. Oeschger and U. Siegenthaler. Greenhouse Gases and Aero-sols, Chapter 1, in *Climate Change: the IPCC Scientific Assessment*, WMO–UNEP Intergovernmental Panel on Climate Change, Cambridge University Press, 1–40, 1990.

Kaye, J.A., Stable isotopes as probes of changing atmospheric composition. In *Our Changing Atmosphere* (Proc. 28th International Astrophysical Colloquium, June 26-30, 1989), P. Crutzen, J.-C. Gerard, R. Zander (eds.), pp. 149–161, Universite de Liege, Cointe-Ongree, Belgium, 1989.

Keeling, C., Industrial production of carbon dioxide from fossil fuels and limestone, *Tellus*, *25*, 174–198, 1973.

Keeling, C., R. Bacastow, A. Carter, S. Piper, T. Whorf, M. Heimann, W. Mook, and H. Roeloffzen, A three-dimensional model of atmospheric CO_2 transport based on observed winds: 1. Analysis of observational data, in *Aspects of Climate Variability in the Pacific and in the Western Americas*, D. Peterson (ed.), American Geophysical Union, 165–236, 1989.

Keller, M., M. Mitre, and R. Stallard, Consumption of atmospheric methane in soils of central Panama: effects of agricultural development, *Glob. Biogeochem. Cycl.*, *4*, 21–28, 1990.

Keller, M., D. Jacob, S. Wofsy, and R. Harriss, Effects of tropical deforestation on global and regional atmospheric chemistry, *Climatic Change*, *19*, 139–158, 1991.

Khalil, M., and R. Rasmussen, Increase of $CHClF_2$ in the Earth's atmosphere, *Nature*, *292*, 823–824, 1981.

Khalil, M., and R. Rasmussen, Sources, sinks and seasonal cycles of atmospheric methane, *J. Geophys. Res.*, *88*, 5131–5144, 1983a.

Khalil, M., and R. Rasmussen, Atmospheric chloroform ($CHCl_3$): ocean-air exchange and global mass balance. *Tellus*, *35B*, 266–274, 1983b.

Khalil, M., and R. Rasmussen, Methyl chloroform: global distribution, seasonal cycles and anthropogenic chlorine, *Chemosphere*, *13*, 789–800, 1984a.

Khalil, M., and R. Rasmussen, Global sources, lifetimes and mass balances of carbonyl sulfide (COS) and carbon disulfide (CS_2) in the Earth's atmosphere, *Atmos. Environ.*, *18*, 1805–1813, 1984b.

Khalil, M. and R. Rasmussen, Carbon monoxide in the Earth's atmosphere: indications of a global increase, *Nature*, *332*, 242–245, 1988.

Khalil, M. and R. Rasmussen, Seasonal cycles of hydrogen and carbon monoxide in the polar regions: opposite phase relationships, *Ant. J. US.*, 238–239, 1989.

Khalil, M., R. Rasmussen, and M. Shearer, Trends of atmospheric methane during the 1960s and 1970s, *J. Geophys. Res.*, *94*, 18279–18288, 1989.

Khalil, M., and R. Rasmussen, Atmospheric methane: recent global trends, *Environ. Sci. Technol.*, *24*, 549–553, 1990a.

Khalil, M., and R. Rasmussen, Trace gas data reported in Atmosphere and Climate, Section 24 in: *World Resources 1990–91*, a report by the World Resources Institute, UNEP–UNDP, Oxford University Press, 345–356, 1990b.

Khalil, M., and R. Rasmussen, The global cycle of carbon monoxide: trends and mass balance, *Chemosphere*, *20*, 227–242, 1990c.

Khalil, M., and R. Rasmussen, Atmospheric carbon monoxide: latitudinal distribution of sources, *Geophys. Res. Lett.*, *17*, 1913–1916, 1990d.

Khalil, M. and R. Rasmussen, Global increase of atmospheric molecular hydrogen, *Nature*, *347*, 743–745, 1990e.

Khalil, M., R. Rasmussen, J. French, and J. Holt, The influence of termites on atmospheric trace gases: CH_4, CO_2, $CHCl_3$, N_2O, CO, H_2 and light hydrocarbons, *J. Geophys. Res.*, *95*, 3619–3634, 1990.

Khalil, M., R. Rasmussen, M. Wang, and L. Ren, Methane emissions from rice fields in China, *Environ. Sci. Technol.*, *24*, 979–981, 1991.

Kirchhoff, V., and E. Marinho, A survey of continental concentrations of atmospheric CO in the Southern Hemisphere, *Atmos. Environ.*, *23*, 461–466, 1989.

Kirchhoff, V., A. Setzer, and M. Pereira, Biomass burning in Amazonia: seasonal effects on O_3 and CO, *Geophys. Res. Lett., 16*, 469–472, 1989.

Kirchhoff, V. and R. Rasmussen, Time variations of CO and O_3 concentrations in a region subject to biomass burning, *J. Geophys. Res., 95*, 7521–7532, 1990.

Lang, P., L. Steele, R. Martin, and K. Masarie, Atmospheric methane data for the period 1983–1985 from the NOAA/GMCC global cooperative flask sampling network, NOAA Technical Memorandum ERL CMDL–1, CMDL Boulder, Colorado, 1990a.

Lang, P., L. Steele, and R. Martin, Atmospheric methane data for the period 1986–1988 from the NOAA/CMDL global cooperative flask sampling network, NOAA Technical Memorandum ERL CMDL–2, CMDL, Boulder, Colorado, 1990b.

Lelieveld, J., and P. Crutzen, The role of clouds in tropospheric chemistry, *J. Atmos. Chem., 12*, 229–267, 1991.

Linak, W., J. McSorely, R. Hall, J. Ryan, R. Srivastava, J. Wendt, and J. Mereb, Nitrous oxide emissions from fossil fuel combustion, *J. Geophys. Res., 95*, 7533–7541, 1990.

Lobert, J., D. Scharffe, W. Hao, and P. Crutzen., Importance of biomass burning in the atmospheric budgets of nitrogen-containing gases, *Nature, 346*, 552–556, 1990.

Logan, J., Personal communication, 1990.

Lowe, D., C. Brenninkmeijer, S. Tyler, and E. Dlugokencky, Determination of the isotopic composition of atmospheric methane and its application in the Antarctic, *J. Geophys. Res., 96*, 15435–15467, 1991.

Luizao, F., P. Matson, G. Livingston, R. Luizao, and P. Vitousek, Nitrous oxide flux following tropical land clearing, *Glob. Biogeochem. Cycl. 3*, 281–285, 1989.

Makide, Y., A. Yokohata, Y. Kubo, and T. Tominaga, Atmospheric concentrations of halocarbons in Japan in 1979–1986, *Bull. Chem. Soc. Jpn., 60*, 571–574, 1987.

Makide, Y., Unpublished data presented at the NASA CFC and Halons Trends, Emissions and Lifetimes Meeting, Newport Beach, California, July 1991.

Manning, M., D. Lowe, W. Melhuish, R. Spaarks, G. Wallace, C. Brenninkmeijer, and R. McGill, The use of radiocarbon measurements in atmospheric studies, *Radiocarbon, 32*, 37–58, 1990.

Marland, G., and R. Rotty, Carbon dioxide from fossil fuels: a procedure for estimation and results from 1950–1982, *Tellus, 36B*, 232–261, 1984.

Matson, P., P. Vitousek, G. Livingston, and N. Swanberg, Sources of variation in nitrous oxide flux from Amazonian ecosystems, *J. Geophys. Res., 95*, 16789–16798, 1990.

Matthews, E., I. Fung, and L. Lerner, Methane emission from rice cultivation: geographic and seasonal distribution of cultivated areas and emissions, *Glob. Biogeochem. Cyc., 5*, 3–24, 1991.

Midgley, P., The production and release to the atmosphere of 1,1,1-trichloroethane (methyl chloroform), *Atmos. Environ., 23*, 2663–2665, 1989.

Mitra, A., Overview: Global Change and Indian Experience, in *Impact of Global Climatic Changes on Photosynthesis and Plant Productivity*, Oxford and IBH Publishing Company, 1991.

Mosier, A., D. Schimel, D. Valentine, K. Bronson, and W. Parton, Methane and nitrous oxide fluxes in native, fertilized and cultivated grasslands, *Nature, 350*, 330–332, 1991.

Novelli, P. (ed.), T. Conway, D. Kitzis, P. Lang, R. Martin, K. Masarie, L. Steele, P. Tans, K. Thoning, and L. Waterman, Carbon Cycle Group, Section 4 in *Climate Monitoring and Diagnostics Laboratory, No.18 Summary Report 1989*, W. Komhyr and R. Rosson (eds.), U.S. Department of Commerce, NOAA–ERL, Boulder, Colorado, USA, 31–39, 1990.

Novelli, P., J. Elkins, and P. Steele, The development and evaluation of a gravimetric reference scale for measurements of atmospheric carbon monoxide, *J. Geophys. Res., 96*, 13109–13121, 1991.

Parashar, D., J. Rai, P. Gupta, and N. Singh, Parameters affecting methane emissions from paddy fields, *Ind. J. Radio Space Phys., 20*, 12–17, 1991.

Penkett, S.A., Nonmethane organics in the remote troposphere, in *Atmospheric Chemistry*, E. Goldberg (ed.), 329–355. Dahlem Konferenzen, Berlin, Springer.Verlag, 1982.

Penkett, S., B. Jones, B. Rycroft, and D. Simmons, An interhemispheric comparison of the concentrations of bromine compounds in the atmosphere. *Nature, 318*, 550–553, 1985.

Penkett, S., 1991a, Unpublished data presented at the NASA CFC and Halons Trends, Emissions and

Lifetimes Meeting, Newport Beach, California July 1991.

Prather, M., European sources of halocarbons and nitrous oxide: update 1986, *J. Atmos. Chem.*, *6*, 375–406, 1988.

Prinn, R., D. Cunnold, R. Rasmussen, P. Simmonds, F. Alyea, A. Crawford, P. Fraser, and R. Rosen, Atmospheric trends in methyl chloroform and the global average for the hydroxyl radical, *Science*, *238*, 945–950, 1987.

Prinn, R., D. Cunnold, R. Rasmussen, P. Simmonds, F. Alyea, A. Crawford, P. Fraser, and R. Rosen, Atmospheric emissions and trends of nitrous oxide deduced from 10 years of ALE–GAGE data, *J. Geophys. Res.*, *95*, 18369–18385, 1990.

Prinn, R., F. Alyea, D. Cunnold, P. Fraser, and P. Simmonds, Unpublished, provisional trace gas data from the ALE–GAGE program, 1991b.

Prinn, R., D. Cunnold, P. Simmonds, F. Alyea, R. Boldi, A. Crawford, P. Fraser. D. Gutzler, D. Hartley, R. Rosen, and R. Rasmussen, Global average concentration and trend for hydroxyl radicals deduced from ALE/GAGE trichloro-ethane (methyl chloroform) data for 1978–1990, *J. Geophys. Res,.97*, 2445-2461, 1992.

Quay, P., S. King, J. Stutsman, D. Wilbur, P. Steele, I. Fung, R. Gammon, T. Brown, G. Farwell, P. Grootes, and F. Schmidt, Carbon isotopic composition of atmospheric methane: fossil and biomass burning source strengths, *Glob. Biogeochem. Cyc.*, *5*, 25–47, 1991.

Rasmussen, R., M. Khalil, S. Penkett, and N. Prosser,. $CHClF_2$ (F-22) in the Earth's atmosphere, *Geophys. Res. Letts.*, *7*, 809–812, 1980.

Rasmusssen, R., and M. Khalil, Atmospheric fluorocarbons and methyl chloroform at the South Pole, *Ant. J. US.*, *17*, 203–205, 1982.

Rasmusssen, R, and M. Khalil, Rare trace gases at the South Pole, *Ant. J. US.*, *18*, 250–252, 1983.

Rasmussen, R., and M. Khalil, Atmospheric trace gases: trends and distributions over the last decade, *Science*, *232*, 1623–1624, 1986.

Rasmussen, R., and M. Khalil, Isoprene over the Amazon Basin, *J. Geophys. Res.*, *93*, 1417–1421, 1988.

Rasmussen, R., M. Khalil, R. Gunawordera, L. Dalhige, J. Moher, and K. Walker, Data reported at the Generic Cylinder Workshop, Boulder, Colorado, October 22, 1990.

Reichle, H., V. Connors, J. Holland, R. Sherrill, H. Wallio, J. Casas, E. Condon, B. Gormsen, and W. Seiler, The distribution of middle tropospheric carbon monoxide during early October 1984, *J. Geophys. Res.*, *95*, 9845–9856, 1990.

Rinsland, C., D. Johnson, A. Goldman, and J. Levine, Evidence for a decline in the atmospheric accumulation rate of $CHClF_2$ (HCF-22), *Nature*, *337*, 535–537, 1989.

Rinsland, C., A. Goldman, F. Murcray, R. Blatherwick, J. Kosters, D. Murcray, N. Sze and S. Massie. Long-term trends in the concentrations of SF_6, $CHClF_2$ and COF_2 in the lower stratosphere from analysis of high-resolution infrared solar occultation spectra, *J. Geophys. Res.*, *95*, 16477–16490, 1990.

Rowland, F., Stratospheric ozone depletion by chlorofluorocarbons, *Ambio*, *19*, 281–292, 1990.

Rowland, F., and D. Blake, Changing trends in global methane concentrations, *EOS Trans.*, *72*, 67, 1991.

Sackett, W., and T. Barber, Fossil carbon sources of atmospheric methane, *Nature*, *334*, 201, 1988.

Sanhueza, E., W. Hao, D. Scharffe, L. Donoso, and P. Crutzen, N_2O and NO emissions from soils of the northern part of the Guayana Schield, Venezuela, *J. Geophys. Res.*, *95*, 22481–22488, 1990.

Sanhueza, E., IPCC WG1 Science Update, Section A: CH_4, N_2O, CO and NMHC, in press, 1992.

Sarmiento, J., and U. Siegenthaler, New production and the global carbon cycle, Presented at NATO Advanced Study Institute on Global Carbon Cycle, Il Ciocco, Italy, September, 1991.

Scharffe, D., W. Hao, L. Donoso, P. Crutzen, and E. Sanhueza, Soil fluxes and atmospheric concentration of CO and CH_4 in the northern part of the Guayana Schield, Venezuela, *J. Geophys. Res.*, *95*, 22475–22480, 1990.

Scheel, H., F. Slemr, P. Matuska, J. Werhahn, and W. Seiler, Measurement of the global distribution of tropospheric trace gases and their time dependent variations, Final Report, Fraunhofer Institute for Atmospheric Research, Garmisch– Partenkirchen, Germany, 216pp., 1988.

Scheel, H., E. Brunke, and W. Seiler, Trace gas measurements at the monitoring station Cape Point, South Africa, between 1978 and 1988, *J. Atmos. Chem.*, *11*, 197–210, 1990.

Seiler, W., and R. Conrad, Contribution of tropical ecosystems to the global budget of trace gases,

especially CH_4, H_2, CO and N_2O, in *The Geophysiology of Amazonia*, R. Dickenson (ed.), John Wiley, New York, 133–160, 1987.

Seiler, W., and H. Scheel, Long-term trends and latitudinal distribution of CFCs from aircraft measurements, Report prepared for the NASA Working Group Meeting on CFC and Halon Concentrations, Trends and Lifetimes, Newport Beach, CA, July 1991.

Servant, J., Les sources et les puits d'oxysulfure de carbone (COS) a l'echelle mondiale, *Atmos. Res., b23*, 105–116, 1989.

Simmonds, P., D. Cunnold, F. Alyea, C. Cardelino, A. Crawford, R. Prinn, P. Fraser, R. Rasmussen, and R. Rosen, Carbon tetrachloride lifetimes and emissions determined from daily global measurements during 1978–1985, *J. Atmos. Chem., 7*, 35–58, 1988.

Simmonds, P., and R. Derwent, Measurement of ozone and other radiatively active gases at Mace Head in the Republic of Ireland, *Atmos. Environ., 25A*, 1795–1808, 1991.

Singh, H., and J. Kasting, Chlorine hydrocarbon photochemistry in the marine troposphere and lower stratosphere, *J. Atmos. Chemistry, 7*, 261–285, 1988.

Singh, O., R. Borchers, P. Fabian, S. Lal, and B. Subbaraya, Measurements of atmospheric BrOx radicals in the tropical and mid-latitude atmosphere, *Nature, 334*, 539–542, 1988.

Sloan, S., and C. Laird, Measurements of nitrous oxide emissions from P. F. fired power stations, *Atmos. Environ., 24A*, 1199–1206, 1990.

SORG, 1990, *Stratospheric Ozone 1990*. Report of the UK Stratospheric Ozone Review Group, H. M. Stationery Office, 1990.

Spivakovsky, C., S.Wofsy, and M. Prather, A numerical method for parameterization of atmospheric chemistry: computation of tropospheric OH, *J. Geophys. Res., 95*, 18433–18439, 1990a.

Spivakovsky, C., R. Yevich, J. Logan, S. Wofsy, and M. McElroy, Tropospheric OH in a three-dimensional chemical tracer model: an assessment based on observations of CH_3CCl_3, *J. Geophys. Res., 95*, 18441–18471, 1990b.

Staffelbach, T., A. Neftel, B. Stauffer, and D. Jacob, A record of the atmospheric methane sink from formaldehyde in polar ice cores, *Nature, 349*, 603–605, 1991.

Steele, L., P. Fraser, R. Rasmussen, M. Khalil, T. Conway, A. Crawford, R. Gammon, K. Masarie, and K. Thoning, The global distribution of methane in the troposphere, *J. Atmos. Chem., 5*, 125–171, 1987.

Steele, L., P. Lang, and R. Martin, Atmospheric methane in Antarctica, *Ant. J. U.S., 24*, 239–241, 1989.

Stevens, C., Atmospheric methane, *Chem. Geol., 71*, 11–21, 1988.

Steudler, P., R. Bowden, J. Melillo, and J. Aber, Influence of nitrogen fertilization on methane uptake in temperate forest soils, *Nature, 341*, 314–316, 1989.

Tans, P., T. Conway, and T. Nakazawa, Latitudinal distribution of sources and sinks of atmospheric carbon dioxide derived from surface observations and an atmospheric transport model, *J. Atmos. Chem., 94*, 5151–5172, 1989.

Tans, P., I. Fung, and T. Takahashi Observational constraints on the global atmopspheric CO_2 budget, *Science, 247*, 1431–1438, 1990.

Thiemans, M., and W. Trogler, Nylon production: an unknown source of atmospheric nitrous oxide, *Science, 251*, 932–934, 1991.

Thompson, T. (ed.), J. Elkins, J. Butler, B. Hall, K. Egan, C. Brunson, J. Sczechowski, and T. Swanson, Nitrous Oxide and Halocarbons Group, Section 8, in *Climate Monitoring and Diagnostics Laboratory, No. 18 Summary Report 1989*, W. Komhyr and R. Rosson (eds.), US Department of Commerce, NOAA–ERL, Boulder, Colorado, 64–72, 1990.

Thoning, K., P. Tans, and W. Komhyr, Atmospheric carbon dioxide at Mauna Loa Observatory, 2. Analysis of NOAA GMCC data, 1974–1985, *J. Geophys. Res., 94*, 8549–8565, 1989.

Tyler, S., D. Lowe, E. Diugokeneky, P. Zimmerman, and R. Cicerone, Methane and carbon monoxide emissions from asphalt pavement: measurements and estimates of their importance to global budgets, *J. Geophys. Res., 95*, 14007–14014, 1990.

Vaghjiani, G., and A. Ravishankara, New measurement of the rate coefficient for the reaction of OH with methane, *Nature, 350*, 406–409, 1991.

Wallace, L., and W. Livingston, Spectroscopic observations of atmospheric trace gases over Kitt Peak. 1. Carbon dioxide and methane from 1979 to 1985, *J. Geophys. Res., 95*, 9823–9827, 1990a.

Wallace, L., and W. Livingston, Spectroscopic observations of atmospheric trace gases over Kitt Peak. 2. Nitrous oxide and carbon monoxide from 1979 to 1985, *J. Geophys. Res., 95,* 16383–16390, 1990b.

Warneck, P., In *Chemistry of the Natural Atmosphere,* Academic Press, San Diego, California, 757pp., 1988.

Waterman, L., D. Nelson, W. Komhyr, T. Harris, K. Thoning, and P. Tans, Atmospheric carbon dioxide measurements at Cape Matatula, American Samoa, 1976–1987, *J. Geophys. Res., 94,* 14817–14829, 1989.

Watson, C., J. Fishman, and H. Reichle, The significance of biomass burning as a source of carbon monoxide in the Southern Hemisphere tropics: a satellite analysis, *J. Geophys. Res.,* 95, 16443–16450, 1990.

Weeks, I., I. Galbally, P. Fraser, and G. Matthews,. Comparison of the carbon monoxide standards used at Cape Grim and Aspendale, in *Baseline 87,* B. Forgan and G. Ayers (eds.), Bureau of Meteorology/CSIRO, 21–25, 1989.

Weiss, R., The temporal and spatial distribution of tropospheric nitrous oxide, *J. Geophys. Res.,* 86, 7185–7195, 1981.

Weiss, R., Unpublished data, presented at the NASA CFC and Halons Trends, Emissions and Lifetimes Meetings, Newport Beach, California, USA, July 1991.

Whalen, S., and W. Reeburg, Consumption of atmospheric methane by tundra soils, *Nature, 346,* 160–162, 1990.

Whalen, M., N. Tanaka, R. Henry, B. Deck, J. Zeglen, J. Vogel, J. Southon, A. Shemesh, R. Fairbanks, and W. Broecker, Carbon-14 in methane sources and atmospheric methane: the contribution from fossil carbon, *Science, 245,* 286–290, 1989.

Whalen, S., W. Reeburg, and K. Sandbeck, Rapid methane oxidation in a landfill cover soil, *Appl. Environ. Microbiol., 56,* 3045–3411, 1990.

Wine, P., and W. Chameides, Possible atmospheric lifetimes and chemical reaction mechanisms for selected HCFCs, HFCs, CH_3CCl_3 and their degradation products against dissolution and/or degradation in seawater and cloudwater, in *Scientific Assessment of Stratospheric Ozone: 1989,* WMO Global Ozone Research and Monitoring Project Report Number 20, Volume 2, 269–295, 1990.

WMO, 1986, Gammon, R., S. Wofsy, R. Cicerone, A. Delany, R. Harriss, M. Khalil, J. Logan, P. Midgley, and M. Prather, Tropospheric Trace Gases, Chapter 3, in *Atmospheric Ozone, Assessment of Our Understanding of the Processes Controlling its Present Distribution and Change,* World Meteorological Organization/ Global Ozone Research and Monitoring Project, Report No. 16, Volume 1, 57–116, 1986.

WMO, 1990a, Ehhalt, D., P. Fraser, D. Albritton, R. Cicerone, M. Khalil, Y. Makide, F. Rowland, L. Steele, and R. Zander, Trends in Source Gases, Chapter 8, in *Report of the International Ozone Trends Panel 1988,* World Meteorological Organization/Global Ozone Research and Monitoring Project, Report No. 18, Volume 2, 543–569, 1990.

WMO, 1990b, Chanin, M., D. Ehhalt, P. Fraser, J. Frederick, J. Gille, M. McCormick, G. Megie, and M. Schoeberl, Global Trends, Chapter 2, in *Scientific Assessment of Stratospheric Ozone: 1989,* Volume 1, World Meteorological Organ-ization/Global Ozone Research and Monitoring Project, Report No. 20, 162–281, 1990.

Yagi, K., and K. Minami, Effects of organic matter applications on methane emissions from Japanese paddy fields, in *Soils and the Greenhouse Effect,* A. Bouwman (ed.), 467–473, John Wiley, New York, 1990.

Yokoyama, T., S. Nishinomiya, and H. Matsuda, N_2O emission from fossil fuel fired power plants, *Environ. Sci. Technol., 25,* 347–348, 1991.

Zander, R., P. Demoulin, D. Ehhalt, and U. Schmidt, Secular increase of the vertical column abundance of methane derived from solar spectra recorded at Jungfraujoch Station, *J. Geophys. Res., 94,* 11029–11039, 1989a.

Zander, R., P. Demoulin, D. Ehhalt, U. Schmidt, and C. Rinsland, Secular increase of the total vertical column abundance of carbon monoxide over central Europe since 1950, *J. Geophys. Res., 94,* 11021–11028, 1989b.

CHAPTER 2

Ozone and Temperature Trends

Authors:

R. Stolarski
L. Bishop
R.D. Bojkov
M.-L. Chanin
V. Fioletov
S. Godin
V. Kirchhoff
J. Zawodny
C.S. Zerefos

Additional Contributors:

W. Chu
J. DeLuisi
A. Hansson
J. Kerr
E. Lysenko
M.P. McCormick
P. Newman
M. Prendez
J. Staehelin
B. Subbaraya

Chapter 2

Ozone and Temperature Trends

Contents

SCIENTIFIC SUMMARY

Observational Record: Since the 1989 assessment, the observational record includes an additional 2.5 years of Dobson, Stratospheric Aerosol and Gas Experiment (SAGE) and Total Ozone Mapping Spectrometer (TOMS) data and a complete re-analysis of 29 ground-based M83/M124 stations in the former Soviet Union. This is complemented by a major new advance in the observational record of an internally-calibrated TOMS data set that is now independent of ground-based observations. Trend analyses of SAGE data have been extended to the lower stratosphere and the Umkehr data have been reanalyzed.

Antarctic Ozone: The Antarctic ozone hole in 1991 was as deep and as extensive in area as those of 1987, 1989, and 1990. The low value of total ozone measured in 1991 was 110 Dobson Units, a decrease of 60 percent compared with ozone levels prior to the mid-1970s. The previously noted quasi-biennial modulation of the severity of the ozone hole did not occur during the last 3 years. The area of the ozone hole was similar for these 4 years.

Trends in Total Ozone: Ground-based (Dobson and M83/M124) and satellite (TOMS) observations of total column ozone through March 1991 were analyzed, allowing for the influence of solar cycle and quasi-biennial oscillation (see table). They show that:

- The northern mid-latitude winter and summer decreases during the 1980s were larger than the average trend since 1970 by about 2 percent per decade. A significant longitudinal variance of the trend since 1979 is observed.
- For the first time there are statistically significant decreases in all seasons in both the Northern and Southern Hemispheres at mid- and high-latitudes during the 1980s; the northern mid-latitude long-term trends (1970 to 1991), while smaller, are also statistically significant in all seasons.
- There has been no statistically significant decrease in tropical latitudes from 25°N to 25°S.

Trends in the Vertical Distribution of Ozone: Balloonsonde, ground-based Umkehr, and satellite SAGE observations show that:

- Ozone is decreasing in the lower stratosphere, *i.e.*, below 25 km, at about 10 percent per decade, consistent with the observed decrease in column ozone.
- Changes in the observed vertical distribution of ozone in the upper stratosphere near 40 km are qualitatively consistent with theoretical predictions, but are smaller in magnitude.
- Measurements indicate that ozone levels in the troposphere, over the few existing ozone sounding stations at northern mid-latitudes, have increased about 10 percent per decade over the past two decades.

Trends in Stratospheric Temperature: The temperature record indicates a small cooling (about 0.3°C per decade) of the lower stratosphere in the sense of that expected from the observed change in the stratospheric concentration of ozone.

Total ozone trends in percent per decade with 95 percent confidence limits

	TOMS: 1979–1991			Ground-based: 26°N–64°N	
	45°S	Equator	45°N	1979–1991	1970–1991
Dec–Mar	–5.2 ± 1.5	+0.3 ± 4.5	–5.6 ± 3.5	–4.7 ± 0.9	–2.7 ± 0.7
May–Aug	–6.2 ± 3.0	+0.1 ± 5.2	–2.9 ± 2.1	–3.3 ± 1.2	–1.3 ± 0.4
Sep–Nov	–4.4 ± 3.2	+0.3 ± 5.0	–1.7 ± 1.9	–1.2 ± 1.6	–1.2 ± 0.6

2.1 INTRODUCTION

This chapter is an update of the extensive reviews of the state of knowledge of measured ozone trends published in the Report of the International Ozone Trends Panel: 1988 (WMO, 1990a) and the Scientific Assessment of Stratospheric Ozone: 1989 (WMO, 1990b). The chapter contains a review of progress since these reports, including updating of the ozone records, in most cases through March 1991. Also included are some new, unpublished reanalyses of these records including a complete reevaluation of 29 stations located in the former Soviet Union. The major new advance in knowledge of the measured ozone trend is the existence of independently calibrated satellite data records from the Total Ozone Mapping Spectrometer (TOMS) and Stratospheric Aerosol and Gas Experiment (SAGE) instruments. These confirm many of the findings, originally derived from the Dobson record, concerning northern mid-latitude changes in ozone. We now have results from several instruments, whereas the previously reported changes were dependent on the calibration of a single instrument. This chapter will compare the ozone records from many different instruments to determine whether or not they provide a consistent picture of the ozone change that has occurred in the atmosphere. The chapter also briefly considers the problem of stratospheric temperature change. As in previous reports, this problem received significantly less attention and the report is not nearly as complete. This area needs more attention in the future.

2.2 INSTRUMENTS

2.2.1 Dobson

The Ozone Trends Panel (WMO, 1990a) used data from Dobson stations that had been provisionally revised by R.D. Bojkov using monthly mean corrections (Bojkov *et al.*, 1990).

Since then, a number of the Dobson stations have revised their entire data records making daily corrections based on detailed calibration records. These include Belsk, Hradec Kralove, Ahmedabad, and the four Japanese stations: Sapporo, Tateno, Kagoshima, and Naha. Several other stations have been provisionally revised on a monthly basis by the station. For the rest, this report continues to use Bojkov's provisional revisions. All data have been updated through March 1991.

2.2.2 Filter Ozonometers

The filter ozonometer (M83) was developed in the mid-1950s. In its initial configuration, the instrument had significant systematic errors. In the early 1970s, the instrument was modified and improved light filters were used. Since 1973, this modified instrument has been used in the former Soviet Union portion of ozone monitoring stations. Since 1986, the M83 has been replaced by the M124, which is a modified design but uses the same light filters. The data before 1973 should not be used for the analysis of trends because of large systematic errors. One cause of the instrument problems was the frequent replacement of instruments with new ones about every 2 years. Prior to carrying out the trend analysis reported here, the data from this network were revised by careful checking of calibration records.

2.2.3 TOMS

TOMS was launched on Nimbus-7 in October 1978 and is still working in 1991. The main problem with maintaining a long-term ozone record with TOMS is the degradation of the diffuser plate used to make the solar observation for determination of albedo. Early evaluations of the ozone data from TOMS (Fleig *et al.*, 1986) included a correction for diffuser plate darkening. This correction yielded a TOMS data set that tracked the corresponding Dobson measurements until about 1982 or 1983. After that the TOMS, and the companion solar backscatter ultraviolet spectrometer, began to drift downward with respect to Dobson measurements (WMO, 1990a). A new method has been derived to improve the correction to the diffuser plate (Herman, *et al.*, 1991). The entire data set has been reprocessed (called Version 6) and is estimated to be precise to ± 1.3 percent (2σ) at the end of 1989 relative to the beginning of the record.

2.2.4 Ozonesondes

The previous assessment (WMO, 1990b) analyzed the records from a network of nine ozonesonde stations. This study has not been updated for this

report. The record from Payerne has recently been reanalyzed by Staehelin and Schmid (1991) to correct for changes in the time of day of launch. This reanalyzed record has been used to illustrate some of the features of the observed profile of ozone loss.

2.2.5 Umkehr

The Umkehr technique for measuring the profile of ozone concentration has been in use since its discovery by Götz (1931). In the last assessment report, trends from the records of 10 stations covering the period 1977 to 1987 were analyzed. Mateer and DeLuisi (1991) have devised an improved Umkehr retrieval algorithm. This algorithm is an optimal statistical or maximum likelihood retrieval and uses improved *a priori* profiles and the Paur and Bass (1985) ozone absorption coefficients and their temperature dependence.

2.2.6 SAGE

The SAGE I and SAGE II instruments measure the vertical profile of ozone at sunrise and sunset (McCormick *et al.*, 1989). The SAGE I data set extends over the period from February 1979 through November 1981 and has not been revised since the previous assessment. SAGE II continues to return data since beginning operation in October 1984. The last 6½ years of SAGE II ozone data through mid-1991 are presented here. The SAGE measurement technique is insensitive to drift in instrumental calibration; however, there may be systematic differences between SAGE I and SAGE II. The potential systematic differences are less than 2 percent between 25 and 45 km, increasing to approximately 6 percent at 20 km. The largest change from previous assessments is that the SAGE I and SAGE II ozone profiles below 25 km have now been extensively intercompared with ozonesondes and the trend estimates can be calculated down to 17 km altitude.

2.3 OBSERVED TRENDS

2.3.1 Factors Contributing to Ozone and Temperature Variability

Several natural influences contribute to ozone and temperature variability and must be considered when estimating trends. The following subsections briefly describe those influences thought to be significant.

2.3.1.1 Solar Cycle

The 11-year solar cycle has an influence on stratospheric ozone amounts. Both theoretical calculations and observations (Stolarski *et al.*, 1990) show a 1 to 2 percent peak-to-peak variation in total ozone (WMO, 1990a, Chapter 7). In the upper stratosphere, where theory says most of the variability should occur, the only long-term ozone record is from Umkehr measurements. This record shows a 2 percent peak to peak variation at 40 km rising to 5 percent at 45 km (Reinsel *et al.*, 1989). Details of the analysis of the solar cycle effect have little effect on the deduction of ozone trends from the 35-year Dobson records, but they can be important to deduction of trends from the much shorter 11- to 12-year TOMS and SAGE records. The influence of the 11-year solar cycle effect on temperatures was reviewed by von Cossart and Taubenheim (1987) and Chanin *et al.* (1987). Kokin *et al.* (1990) gave a 3–5 K amplitude in the upper mesosphere and about 1.5 K in the upper stratosphere.

2.3.1.2 Energetic Particles

Another phenomenon related to the solar cycle that has produced observed effects on atmospheric ozone concerns high-energy protons (Zerefos and Crutzen, 1975; Heath *et al.*, 1977; Solomon and Crutzen, 1981; McPeters and Jackman, 1985). These solar proton events (SPEs) are sporadic, and events with a large impact on ozone are rare. Particularly large events were those of August 1972. It has been suggested that the late 1989 events were partially responsible for the low total ozone seen in the north polar region in the spring of 1990 (Reid *et al.*, 1991), and enhancements of NO_2 and decreases in ozone were observed by SAGE during this period (Zawodny and McCormick, personal communication).

2.3.1.3 Quasi-Biennial Oscillation

There is a clear quasi-biennial oscillation (QBO) signal in total ozone data at the equator, with magni-

tude of about 4 to 5 percent peak to peak (Bojkov, 1987; WMO, 1990a; Hilsenrath and Schlesinger, 1981). As a function of altitude, the ozone profile changes due to the QBO are much larger (Bojkov, 1987; Zawodny and McCormick, 1991). Two separate equatorial peak QBO amplitudes are found at 24 km (20 percent peak to peak) and 34 km (15 percent peak to peak). Although these variations are large, they largely cancel out in the total ozone column.

2.3.1.4 El Niño–Southern Oscillation

A relationship of total ozone to El Niño–Southern Oscillation (ENSO) has also been suggested. The tropical Dobson data show 3 to 4 percent variations which correlate with the Southern Oscillation Index (SOI) (Zerefos *et al.*, 1991a,b). The SOI shows a major ENSO event in 1982–1983 that has been suggested to be partly responsible for the negative ozone deviations at high latitudes in the Northern Hemisphere (Bojkov, 1987a).

2.3.1.5 Atmospheric Nuclear Tests

Chemical models predict that the atmospheric nuclear test series of the late 1950s and early 1960s may have had an observable effect on the baseline amount of ozone measured by the Dobson instruments during the 1960s.

2.3.1.6 Volcanic Eruptions

Finally, explosive volcanic eruptions are a sporadic and unpredictable potential perturbation of ozone or cause interference with ozone measurements. There have been several major eruptions and a number of minor eruptions during the period of the ozone data record. The eruption of Gunung Agung in 1963 is near the beginning of most of the ground-based ozone records. The only major eruption during the period of most of the ozone data records was El Chichón in Mexico in 1982. El Chichón has had at most a 2 percent effect on measured total ozone (Chandra and Stolarski, 1991). Indications from recent measurements of the volcanic eruptions of Mt. Pinatubo are that it may have injected two to three times more material than El Chichón. The current analysis does not include any ozone measurements during or after the June 1991 eruption of Mt. Pinatubo. The aerosol increase in the lower stratosphere from large volcanic eruptions has also produced a large (4K) temperature rise (Labitzke *et al.*, 1983; Michelangeli *et al.*, 1989).

2.3.2 Antarctic Trends

The springtime Antarctic ozone hole has been observed since the late 1970s (Farman, *et al.*, 1985; Chubachi, 1985). Measurements by ground-based instruments, balloonsondes, and satellites have shown that the depletion occurs mainly during September with the ozone concentration in the lower stratosphere between about 14 and 22 km declining to nearly zero concentrations by early October.

The Antarctic ozone holes of 1989 and 1990 were both characterized by low total ozone values over much of the south polar region (Stolarski, *et al.*, 1990; Newman *et al.*, 1991). The depth and extent of the hole in each of these years were comparable to the large 1987 ozone hole discussed in WMO (1990b). In 1990, the hole lasted a particularly long time, through December (Newman *et al.*, 1991). The vortex appeared to have been weakened by wave events in August, but it persisted because very little wave activity was propagated upward from the troposphere. Figure 2-1 shows the TOMS daily minimum total ozone (for a 2° latitude by 5° longitude bin) measured in the south polar region from August through November (updated from Newman *et al.*, 1991, by Schoeberl, personal communication). The shaded area in Figure 2-1 indicates the range of minimum values for all years from 1979 through 1990. Also indicated are the minima for 1979, 1987, 1988, 1989, and 1990. The 1991 data, shown as dots, show a decline through early October that is similar to the previous deep ozone hole years 1987, 1989, and 1990. A minimum value of 110 Dobson units (DU), slightly lower than in previous years, was reached in early October 1991. This was the preliminary number available in October from real time processing. The final number from the regular processing system was 108 DU (Krueger, personal communication). The recovery through the middle of November 1991 has closely followed that of 1989. The quasi-biennial modulation of the depth of the ozone hole that has been previously noted (Garcia and Solomon, 1987; Lait *et al.*, 1987) is not evident in the data for the last 3 years.

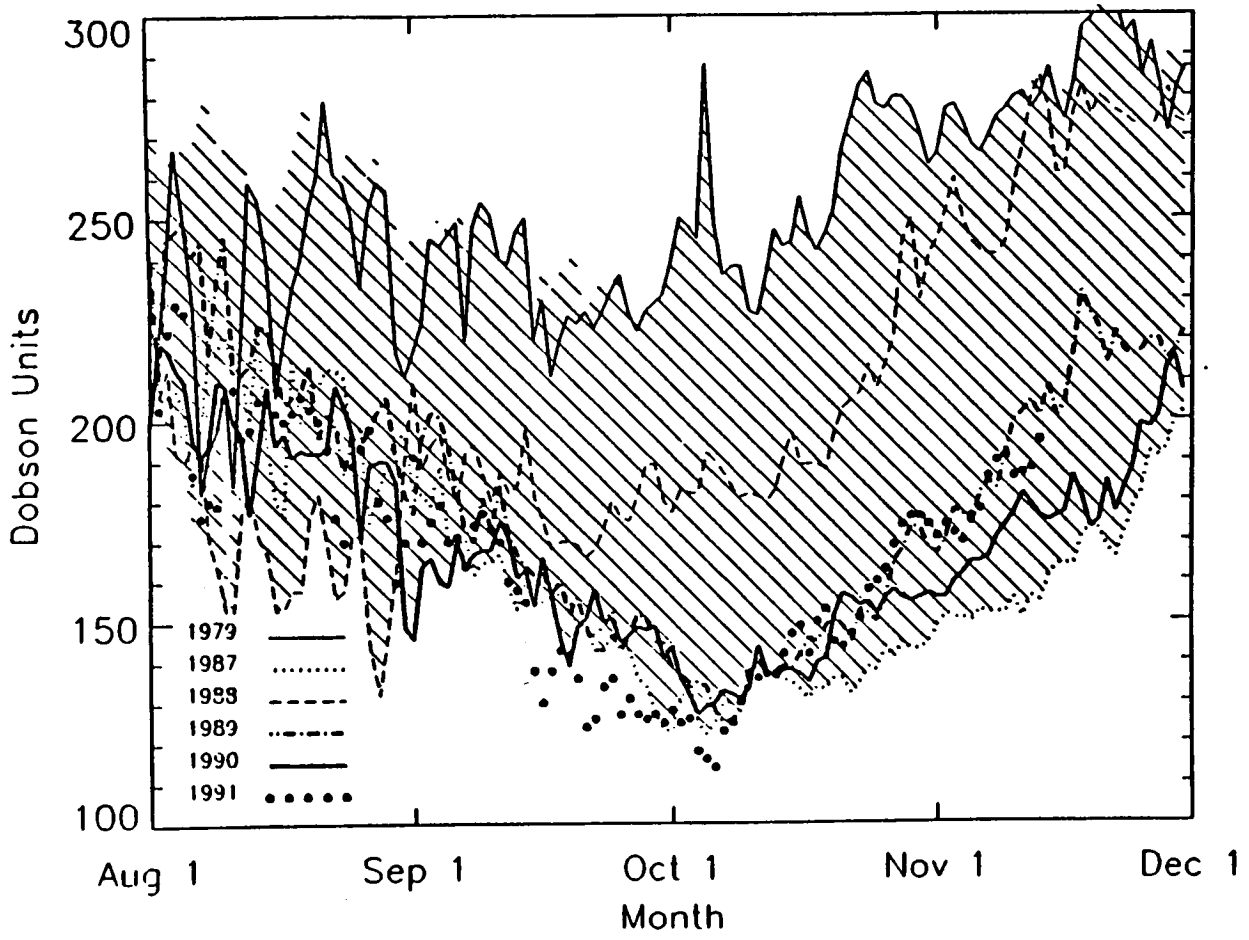

Figure 2-1 TOMS daily minimum total ozone measured south of 30°S from August through November. The individual years 1979, 1987, 1988, 1989, 1990, and 1991 are shown. The shaded area indicates the range of daily minima for all years from 1979 through 1990 (Schoeberl, personal communication, 1991).

The September decrease in Antarctic ozone has been clearly shown to be a lower stratospheric phenomenon (mainly between 14 and 22 km altitude) with nearly all of the ozone being removed in cold years with deep ozone holes (Hofmann *et al.*, 1987; Gardiner, 1988; Komhyr *et al.*, 1988). This was again the case in 1989 and 1990 (Deshler *et al.*, 1990; Deshler and Hofmann, 1991). The lower stratospheric ozone decrease detected by balloon ozonesondes has been confirmed by measurements from SAGE (McCormick and Larsen, 1986, 1988), from lidar (Browell *et al.*, 1988), and from *in situ* measurements on aircraft (Proffitt *et al.*, 1989).

The Antarctic ozone hole is occurring during the spring when sunlight reaches the vortex while it is still intact. There is a strong correlation of low total ozone amounts with low temperatures in the lower stratosphere. An example is shown in Figure 2-2 for the data over the Japanese station Syowa. The cold years are dynamically less active with a more stable vortex, which results in a stronger and more persistent ozone depletion. During the period when the vortex is warming (September through December), there appears to be a significant negative temperature trend if only the cold years are considered. The warmer years are dynamically active, with consequent variability that overwhelms any possible trend (Newman *et al.*, 1990; Randel, 1988).

For the recent 4 years with deep ozone holes (1987, 1989–1991), the area covered by the ozone

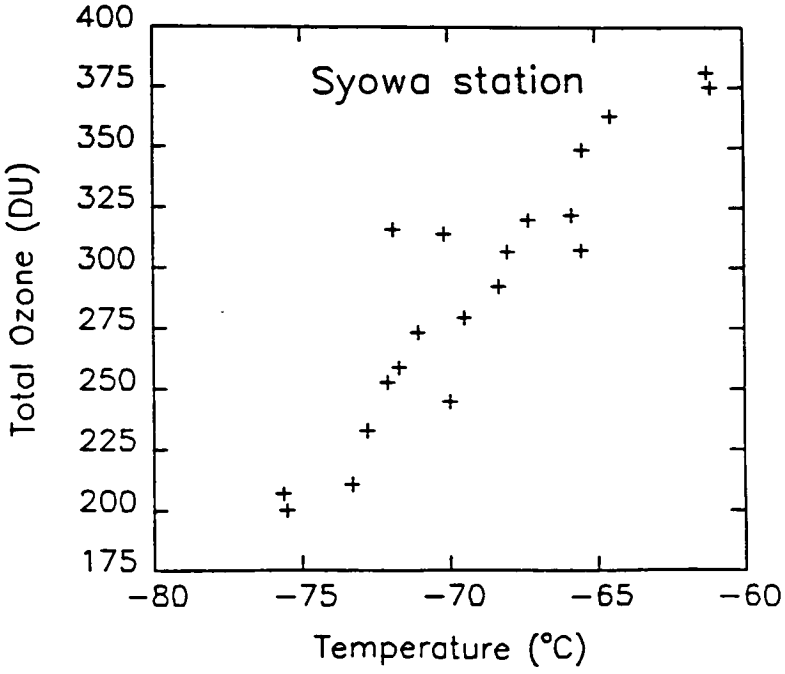

Figure 2-2 Correlation of October monthly mean 100-hPa temperatures and total ozone amounts measured above Syowa, Antarctica.

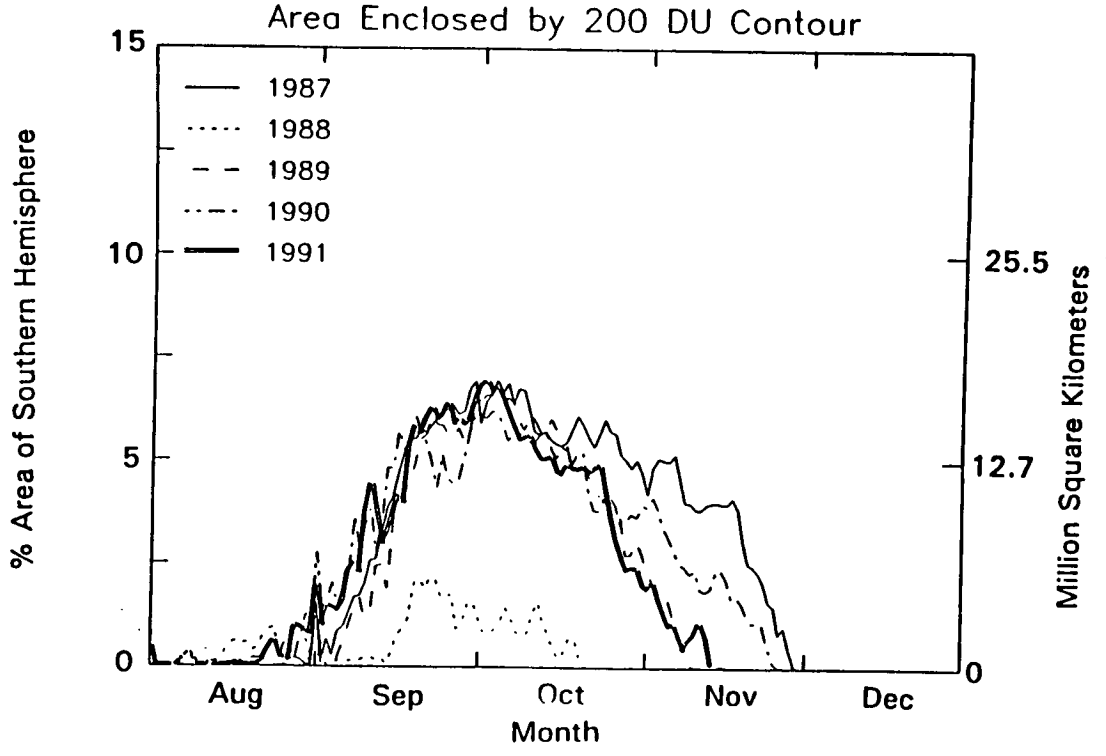

Figure 2-3 The area of the south polar region with total ozone amount less than 200 DU as measured by TOMS on a daily basis for each of the last 5 years.

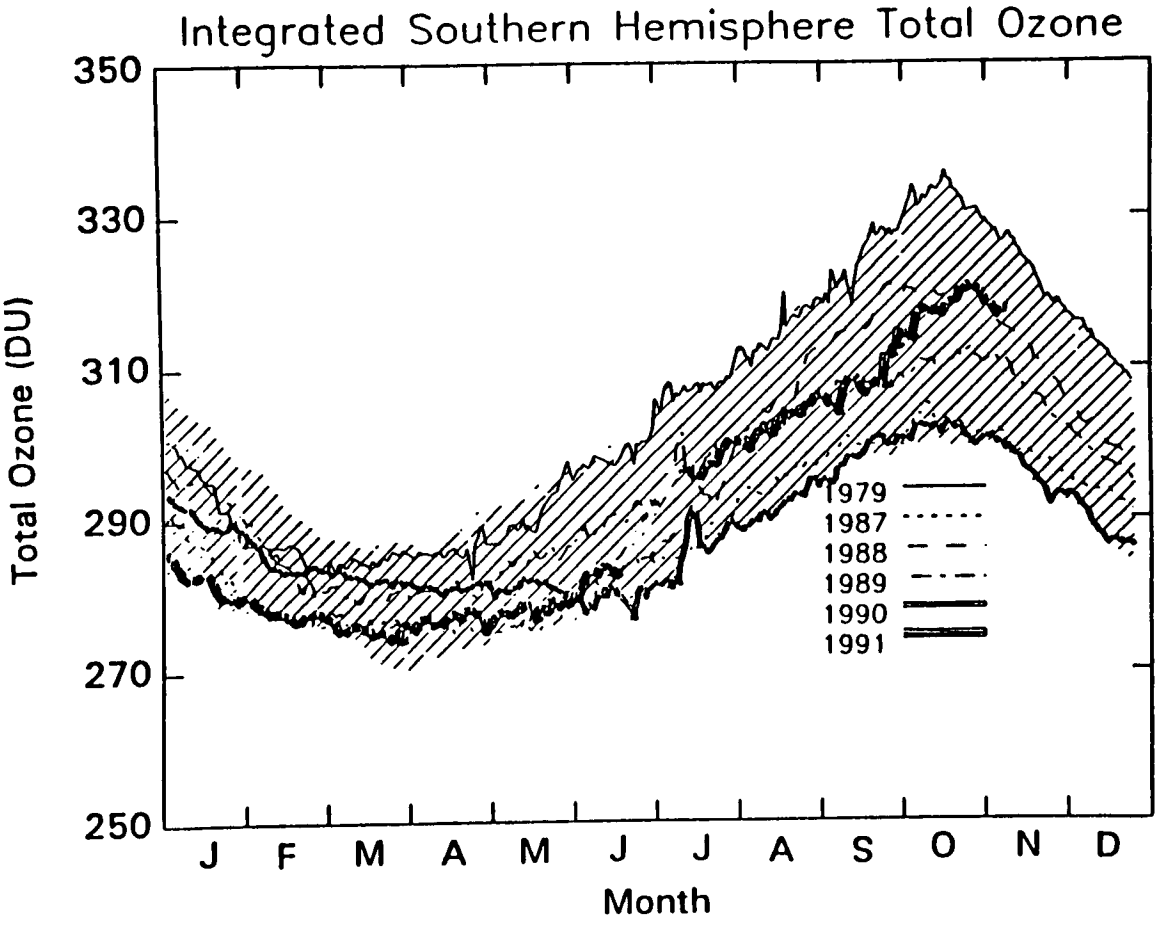

Figure 2-4 Daily average Southern Hemisphere total ozone as measured by TOMS for the years 1979, 1987, 1988, 1989, 1990, and 1991. The shaded area indicates the range for all years from 1979 through 1990.

hole is more or less constant. As a measure of the size of the ozone hole, Figure 2-3 shows the area for which the TOMS total ozone measurements are less than 200 DU. The area for 1988, the shallow ozone hole year, is very small. For the other 4 years, the rise in the area of less than 200 DU occurs during the first half of September. The area reaches a maximum of about 14 million square kilometers, or approximately the size of the Antarctic continent. The variations in the rate of decline from late October through November indicate differences in the vortex weakening and breakup. The recovery in 1991 closely follows that of 1989.

The area-weighted average of Southern Hemisphere total ozone measured by TOMS is shown in Figure 2-4. From January through May of 1991, the Southern Hemisphere average ozone was near the minimum observed for the last 12 years. In early June, the average ozone began to recover towards more normal values. Data from TOMS were not available for the end of June and beginning of July. By mid-July, the average total ozone was in the middle of the range observed for the last 12 years. This results from a strong mid-latitude maximum of total ozone related to planetary wave activity.

Figure 2-5 shows a comparison of the October monthly mean TOMS Southern Hemisphere maps for the last 5 years. The 1991 map shows a deep minimum with lowest value of just over 150 DU. The contours are offset from the pole and a strong maximum of >450 DU is observed. The pattern is very similar to that of 1989. In contrast, 1987 and 1990 showed a much more symmetric pattern about the south pole. Averaged over the month of October, the 1987 ozone hole had the lowest measured ozone amounts with a region around the pole of <150 DU.

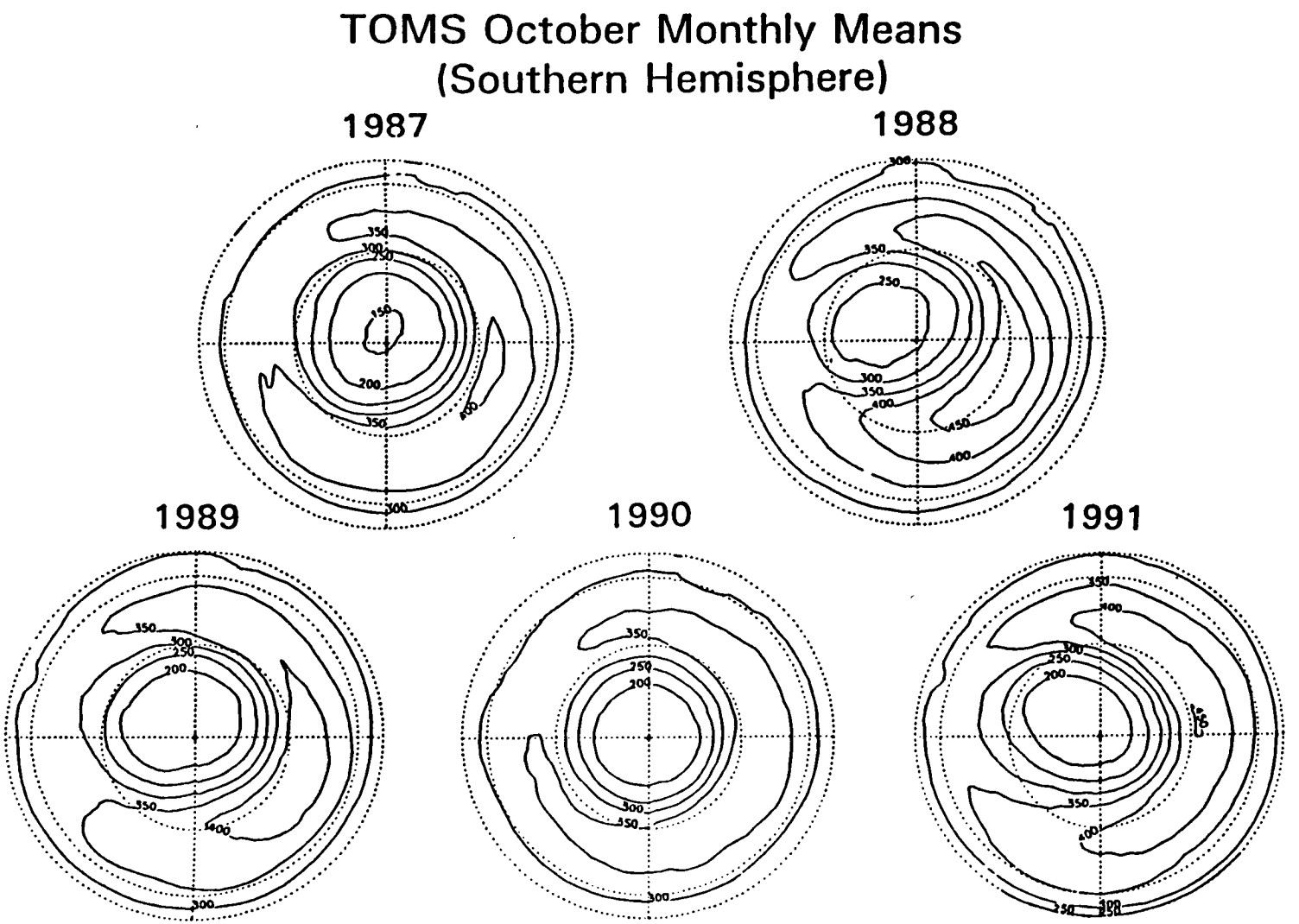

Figure 2-5 Polar orthographic projections of TOMS Southern Hemisphere maps of October mean total ozone for each of the last 5 years. The south pole is at the center; the equator, 30° S, and 60° S latitude circles are shown; and Greenwich is to the top. The contours are in Dobson units.

2.3.3 Global Trends in Total Ozone

2.3.3.1 Ground Station Trends

As in the previous reports (WMO 1986; WMO, 1990a,b), the trend analysis of ozone series uses a statistical model that fits terms for seasonal variation in mean ozone, seasonal variation in ozone trends, and the effects of the QBO, solar cycles, atmospheric nuclear tests (where appropriate), and autocorrelated noise (see, *e.g.*, Reinsel *et al.*, 1987; Bojkov *et al.*, 1990). In some cases, simplified versions of the full model were fit. For the longer Dobson series, the trend fitted for each month was a "hockey stick," with a level baseline prior to December 1969 and a linear trend after 1970. For series that began after 1970, the trend is a simple linear monthly trend.

The Ozone Trends Panel Report (WMO, 1990a) analyzed the available Dobson data through the end of 1986. An update through October of 1988 was given in the 1989 WMO–UNEP assessment report (WMO, 1990b). Dobson data are now available through March of 1991. The earlier reports used published data, some of which had been "provisionally revised" by R.D. Bojkov in an attempt to remove the effect of some obvious changes due to calibrations. Since that time a number of stations have reevaluated their data and calibrations and have issued what could be called "officially reevaluated" data sets. The last column and footnotes in Table 2-1 indicate the data source used for each station. Also available now are reevaluated data from 29 stations using the M83/M124 filter instruments in the former Soviet Union (Bojkov and Fioletov, 1991). During the second half of the 1980s, Brewer spectrophotometers replaced Dobson instruments at some stations with long ozone records (Canada); continuity of ozone records at these stations used in the present assessment was achieved by reporting simulated Dobson data to the World Ozone Data Center based on a 3-year overlap study of the instruments.

Two different forms of analysis have been performed on the ground-based data. The standard analysis performs a trend analysis as described previously at each ground-based station. The results of these analyses are reported as Table 2-1, which gives trend results for the seasons December–March (Northern Hemisphere winter), May–August (Northern Hemisphere summer), September–November (Northern Hemisphere fall), and a year-round trend that is the average trend over all months of the year. As a continuation of this form of analysis, individual station trends can be appropriately averaged over regions to yield regional trends as reported in Table 2-2 for North America, Europe, and the Far East.

A second form of analysis forms a composite ozone series for a region, or a latitude belt, by a combination of the individual ozone series at the stations within that region or latitude belt. The primary advantage of this approach is the ability to include data from stations with records too short to analyze with the normal trend analysis, or which stopped taking data before the beginning of the trend period, in order to stabilize the regional or belt average. In the case of the filter (M83/M124) data, the ozone records are so variable that regional averages supply considerable stabilization. The method of producing these series was to average the deseasonalized series together, and then to add back in an average seasonal component in order to calculate percentage trends. A problem with this construction is that series with data starting after the beginning of the trend period (usually taken to be 1970) are adjusted to have monthly means of zero, and this has the effect of muting any negative trend in the composite series when a late starting series is averaged in with the rest. Other methods of seasonal adjustment have been investigated, but no completely satisfactory technique has been found. Trends from the zonal series appear to be sensitive to the method of composition of the aggregate series, and these will be used for illustration and sensitivity studies only. However, trends obtained from the composite filter series are not very sensitive to the method of construction, since the individual series have a common time span.

Table 2-1 shows the results of the individual station analysis, and the trends for the mid-latitude northen stations are plotted versus latitude in Figure 2-6. The trends are negative in all seasons, and year-round, at nearly all stations. There is also a clear gradient with latitude for the bulk of the stations, with more northerly stations exhibiting the largest negative trends. The two most northerly stations, Reykjavik and Lerwick, break the pattern, with positive trends in the winter, and positive or nearly zero trends in the summer. This may reflect difficulty in very low sun measurements or be an indication of longitudinal

Table 2-1 Long-term trends derived from ground-based total ozone data for individual stations. These estimates were derived from the Allied statistical model using data from January 1958 through March 1991 where possible, with a linear trend fit to the period 1970–1991.

		Year Round		Dec–Mar		May–Aug		Sep–Nov		
	Lat	Trend	SE	Trend	SE	Trend	SE	Trend	SE	Code*
North America:										
Churchill	59 N	–3.4	.5	–4.3	.8	–3.2	.6	–2.4	.8	2
Edmonton	54 N	–1.4	.4	–2.6	.8	–0.7	.6	–0.4	.7	2
Goose Bay	53 N	–1.3	.4	–1.4	.8	–1.5	.5	0.1	.6	2
Caribou	47 N	–2.2	.4	–3.7	.8	–1.2	.4	–1.1	.6	2
Bismarck	47 N	–2.4	.4	–3.5	.7	–2.0	.5	–1.0	.6	2
Toronto	44 N	–1.5	.4	–3.1	.8	–1.3	.4	0.1	.7	2
Boulder	40 N	–2.7	.4	–3.1	.8	–2.6	.4	–1.8	.6	2
Wallops Is.	38 N	–1.5	.6	–2.9	1.2	–0.8	.7	–1.3	.8	2
Nashville	36 N	–2.1	.4	–3.3	.8	–2.0	.4	–1.6	.6	2
Tallahasse	30 N	–2.0	.5	–3.5	.9	–1.5	.5	–1.7	.6	3
Europe:										
Reykjavik	64 N	–0.3	.7	.2	1.4	–0.7	.6	–0.2	1.1	3
Lerwick	60 N	–0.1	.7	.9	1.5	–1.0	.6	.7	1.1	1,2
St. Petersburg	60 N	–3.1	.5	–4.5	1.1	–1.8	.6	–2.5	.8	2
Belsk	52 N	–2.2	.5	–3.8	1.0	–1.0	.6	–1.6	.8	1
Bracknell	51 N	–3.4	.5	–4.3	1.0	–3.1	.6	–2.3	.9	1,2
Hradec Kralove	50 N	–1.8	.5	–4.0	.9	–0.3	.5	–0.7	.7	1
Uccle	51 N	–2.9	.6	–2.5	1.3	–2.7	.7	–3.4	1.1	3
Hohenpeissenberg	48 N	–2.3	.5	–3.1	1.0	–1.7	.5	–1.2	.8	1,2
Arosa	47 N	–2.4	.4	–3.4	.8	–1.8	.4	–1.8	.6	2
Vigna di Valle	42 N	–0.8	.4	–2.3	.9	.4	.5	–0.2	.5	2
Cagliari/Elmas	39 N	–0.4	.5	–1.8	1.0	.7	.6	–0.1	.8	2
Far East:										
Nagaevo**	60 N	–3.4	1.0	–2.5	1.9	–4.6	1.2	–0.8	2.0	1,2
Petropavlosk**	53 N	–2.4	.8	–2.0	1.4	–1.8	1.6	–3.0	1.1	1,2
Sahalin**	47 N	–2.0	.8	–2.7	1.4	–0.9	1.2	–2.4	1.1	1,2
Sapporo	43 N	–1.3	.5	–2.4	.8	–1.1	.6	–0.2	.6	1
Tateno	36 N	–0.9	.4	–2.1	.8	–0.6	.4	0.3	.5	1
Kagoshima	32 N	.4	.5	–0.4	.8	.7	.5	1.0	.6	1
Naha	26 N	–0.3	.7	–0.8	1.2	–0.1	.8	–0.3	.9	1
Low Latitude:										
Quetta	30 N	–0.2	.6	–0.1	.9	.2	.6	–0.4	.7	2
Cairo	30 N	–0.0	.8	–0.5	1.7	–0.4	.9	1.0	.8	2
Ahmedabad	23 N	.4	.5	–0.7	.8	1.0	.7	1.3	.6	1
Mauna Loa	20 N	–0.2	.5	–0.8	.8	.3	.5	–0.4	.5	2
Mexico City	19 N	1.6	1.3	1.7	2.3	0.7	1.7	2.1	.8	3
Huancayo	12 S	–0.5	.2	–0.7	.3	–0.6	.3	–0.2	.3	2
Samoa	14 S	–1.2	1.0	–1.8	.9	1.8	1.5	.4	1.4	2
Southern Hemisphere:										
Aspendale	38 S	–2.6	.4	–3.1	.4	–2.5	.6	–2.3	.6	1,2
Hobart	43 S	–2.2	.4	–1.6	.6	–3.4	.6	–1.2	.7	2
Invercargill	46 S	–3.5	.5	–3.8	.7	–3.8	.8	–2.7	.9	1
MacQuarie Is.	54 S	–0.1	.8	1.0	1.0	–1.2	1.1	.1	1.3	3

*Codes: 1 = Reevaluated by the operating agency, 2 = Provisionally reevaluated (R. Bojkov)
3 = Needs further reevaluation

** M-83 Station

Table 2-2 Regional and zonal long-term ozone trends trends derived from ground-based total ozone data. These estimates were derived from the Allied statistical model using data from January 1958 through March 1991 where possible (January 1973–March 1991 for the filter series), with a linear trend fit over the period 1970–1991.

	Year Round		Dec–Mar		May–Aug		Sep–Nov	
	Trend	SE	Trend	SE	Trend	SE	Trend	SE
Dobson Regional Trends[1]:								
North America	–2.1	.3	–3.2	.4	–1.7	.4	–1.1	.3
Europe	–1.8	.3	–2.9	.4	–1.2	.3	–1.2	.3
Far East*	–1.2	.4	–1.8	.5	–0.9	.5	–0.4	.4
26°–64° N combined	–1.8	.2	–2.7	.3	–1.3	.2	–1.0	.2
Filter (M-83/124) Regional Trends[2]:								
Central Asia	–1.4	.6	–2.1	1.1	–0.7	.8	–1.8	.7
Eastern Siberia	–2.1	.6	–2.2	1.2	–1.0	.7	–2.2	.6
European Region	–3.2	.6	–4.1	1.2	–2.5	.7	–2.1	.5
Western Siberia	–1.6	.6	–1.9	1.3	–1.0	.6	–1.6	.7
Average filter	–2.1	.3*	–2.6	.6*	–1.3	.4**	–1.9	.3*
Combined Regional[3]:	–1.8	.3	–2.7	.4	–1.3	.2	–1.2	.3
Zonal Bands[4]:								
53°–64° N	–1.6	.4	–2.1	.7	–1.2	.4	–0.9	.3
40°–52° N	–1.6	.3	–2.8	.7	–1.0	.3	–0.7	.3
30°–39° N	–0.7	.4	–1.3	.6	–0.4	.4	–0.2	.3

Notes:

1. The Dobson regional trends, and the corresponding 26°–64° N average, are obtained as weighted averages of the trends at each station from Table 2-1. The weights and standard errors take into account the different series lengths and precision at each station.
2. The U.S.S.R. regional trends and the zonal band trends are calculated by applying the standard trend analysis model to average total ozone series for each region or zone, computed from the individual ozone deviations from monthly means at each station.
3. The combined regional trends include the former Soviet Union (average filter) as a fourth region to be combined with the Dobson regional trends.
4. The zonal band series include the former U.S.S.R. stations, and also a number of Dobson stations additional to those in Table 2-1, whose records are too short to be of use in direct trend analyses. The zonal band results are included here for completeness, but the trend values are sensitive to the exact method of construction of the series (see text).

*Includes 3 Dobson stations

**Estimated standard error, not calculated

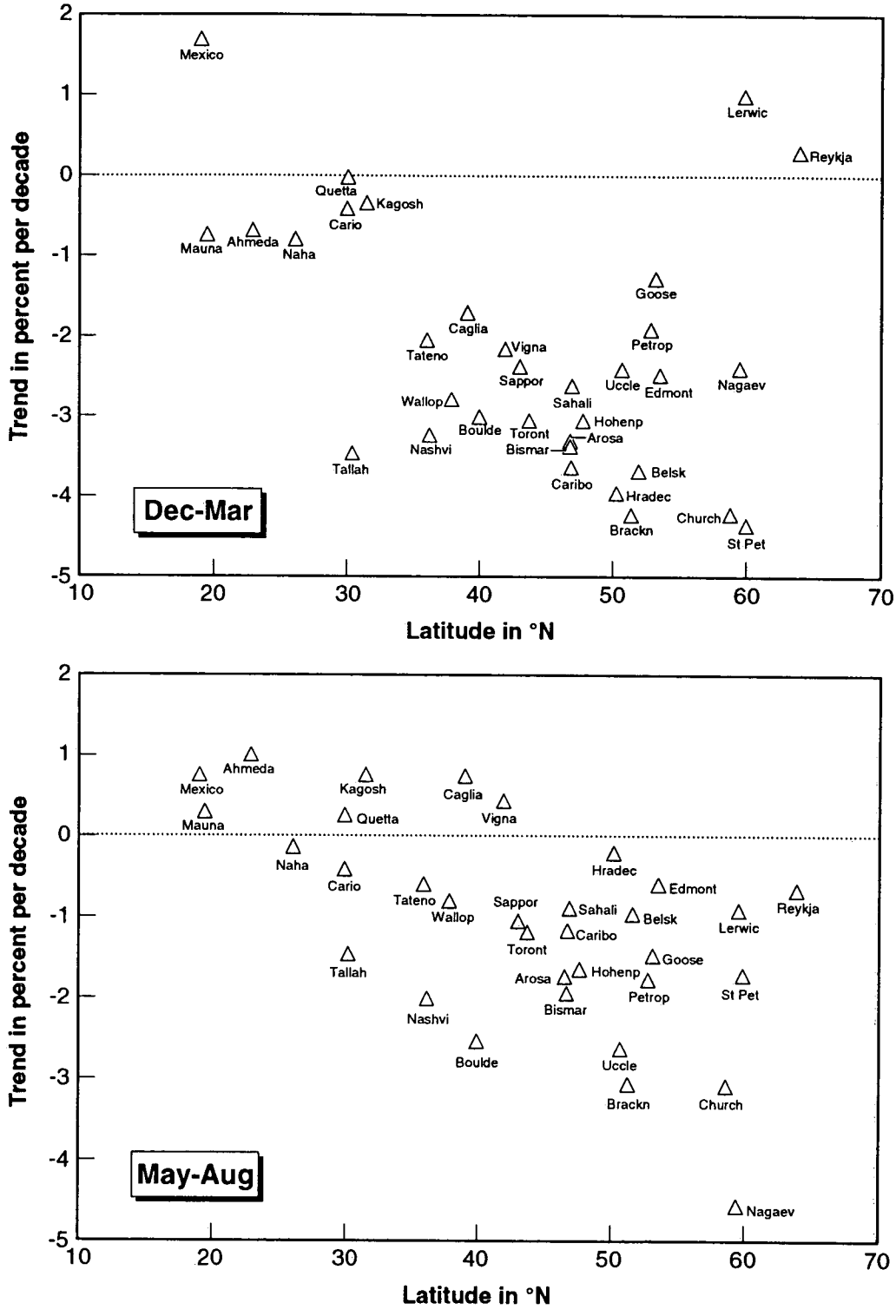

Figure 2-6a Individual station long-term trends, by season, for 39 Northern Hemisphere stations, versus station latitude. The estimates were derived from the standard seasonal model using data from 1958 through 1969 as a baseline, and monthly linear trends over the period 1970 through March 1991.

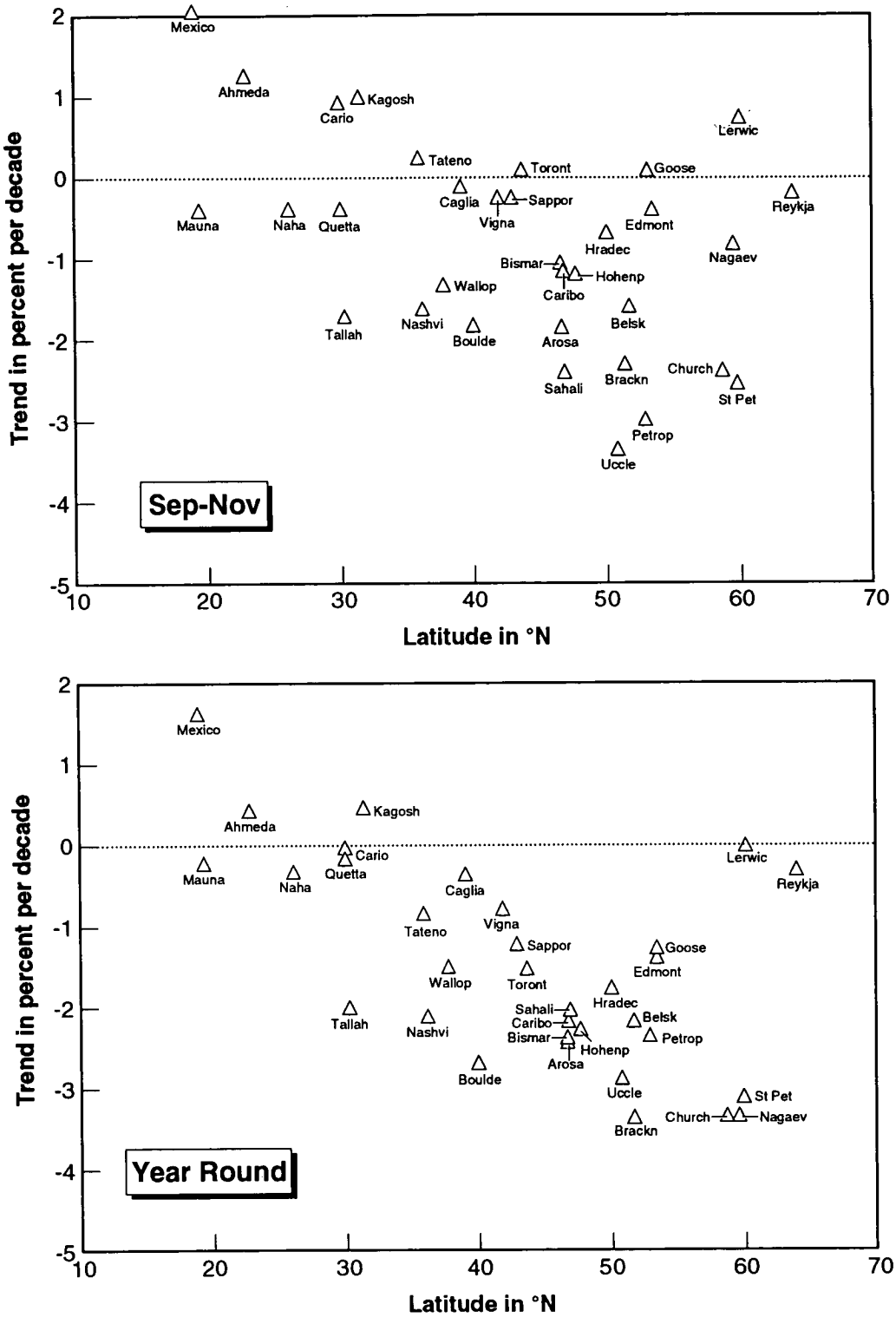

Figure 2-6b Individual station long-term trends, by season, for 39 Northern Hemisphere stations, versus station latitude. The estimates were derived from the standard seasonal model using data from 1958 through 1969 as a baseline, and monthly linear trends over the period 1970 through March 1991.

variation in trends, which is discussed below in conjunction with the TOMS data analysis.

Average trends in North America, Europe, and the Far East have been calculated using a variance components model described in Reinsel *et al.* (1981), which takes into account the precision of the trend estimate at each station (primarily length of record and natural variability) and variablility of the station trends inside a region. These average trends are presented in Table 2-2 as the 26°–64°N combined Dobson trend. This average trend is –2.7 percent per decade in the winter, –1.3 percent per decade in the summer, and –1.0 percent per decade in the fall. All three of these results are statistically significant.

This represents a significant new finding versus the last assessment (WMO, 1990b) and the results of Bojkov *et al.* (1990). Significant winter trends were also found in those studies (as well as in the Ozone Trends Panel report, WMO, 1990a), and the current winter trends are slightly more negative than found then. The summer trends found in the last assessment were much smaller and not statistically significant (fall trends were not given). Bojkov *et al.* (1990) found a (barely) significant summer trend, but the fall trend was nearly zero. The current trends are much larger and statistically significant in all three seasons.

For visualizing the results for these three regions, Figure 2-7 shows composite series for North America, Europe, and the Far East with a strong statistical smoother drawn through the data. (These composite series were constructed slightly differently from those described above—they have solar, QBO, and nuclear testing effects subtracted as well as the seasonal effect, before averaging the series.) The trends are evident in all three regions, and an apparent increase in slope after 1980 is quite noticeable in North America and Europe. This increase in the trend in the 1980s is discussed again later when the TOMS data are considered.

Composite series (the second method described previously) were constructed for the filter (M83/M124) data for four major regions of the former Soviet Union where the characteristics of the ozone regime have shown some distinguishable differences (Bojkov and Fioletov, 1991). The results of fitting trends to these regional series are also given in Table 2-2. The results are very similar to the Dobson regional results, with significant negative trends in every season.

Given the close match of the Dobson and filter results, it makes sense to combine these estimates, although they derive from different types of analyses. If we consider the former Soviet Union as a fourth region, we can compute an omnibus mid-latitude Northern Hemisphere trend, which is given in Table 2-2 as "Combined Regional Trends." The trend estimates from this combination are –2.7 percent per decade in the winter, –1.3 percent per decade in the summer, and –1.2 percent per decade in the fall. All of these are statistically very significant. These combined regional results probably represent the best estimates of the overall mid-latitude Northern Hemisphere seasonal trends.

The latitude belt composite series were analysed with the full standard statistical model, and the trend results are reported in Table 2-2. The trend results are similar to, but slightly less negative than, the average of trends calculated at individual stations from the Dobson network. Figure 2-8 shows the 40°–52° N zonal trends by month, calculated from a simpler statistical model and with a slightly different construction, both with and without the M83/M124 filter data, by month of the year. The results are seen to be essentially identical regardless of whether or not the filter data are included. The belt trends are reported here primarily for comparison with previous assessments (WMO, 1990a,b).

2.3.3.2 Comparison of Ground Station and Satellite Data

While the trends reported above are based on a 33-year record from 1958 to 1991, the satellite record is only a little over 12 years in length. This raises the question of interpreting the 12-year trends in the context of the longer Dobson record. Fioletov (1989, updated 1991) has examined this question by utilizing the zonal series (40°–52°N and 53°–64°N) described above and calculated a sliding 11-year trend starting with the first 11 years of the data set, *i.e.*, from 1958 through 1968. The results are shown on Figure 2-9 for the annual average, winter, and summer trends at 40°–52° and 53°–64°N. The most recent 11-year trends are more negative than in the past, although substantial negative winter trends occurred in the 11-year periods ending in the range 1975–1980.

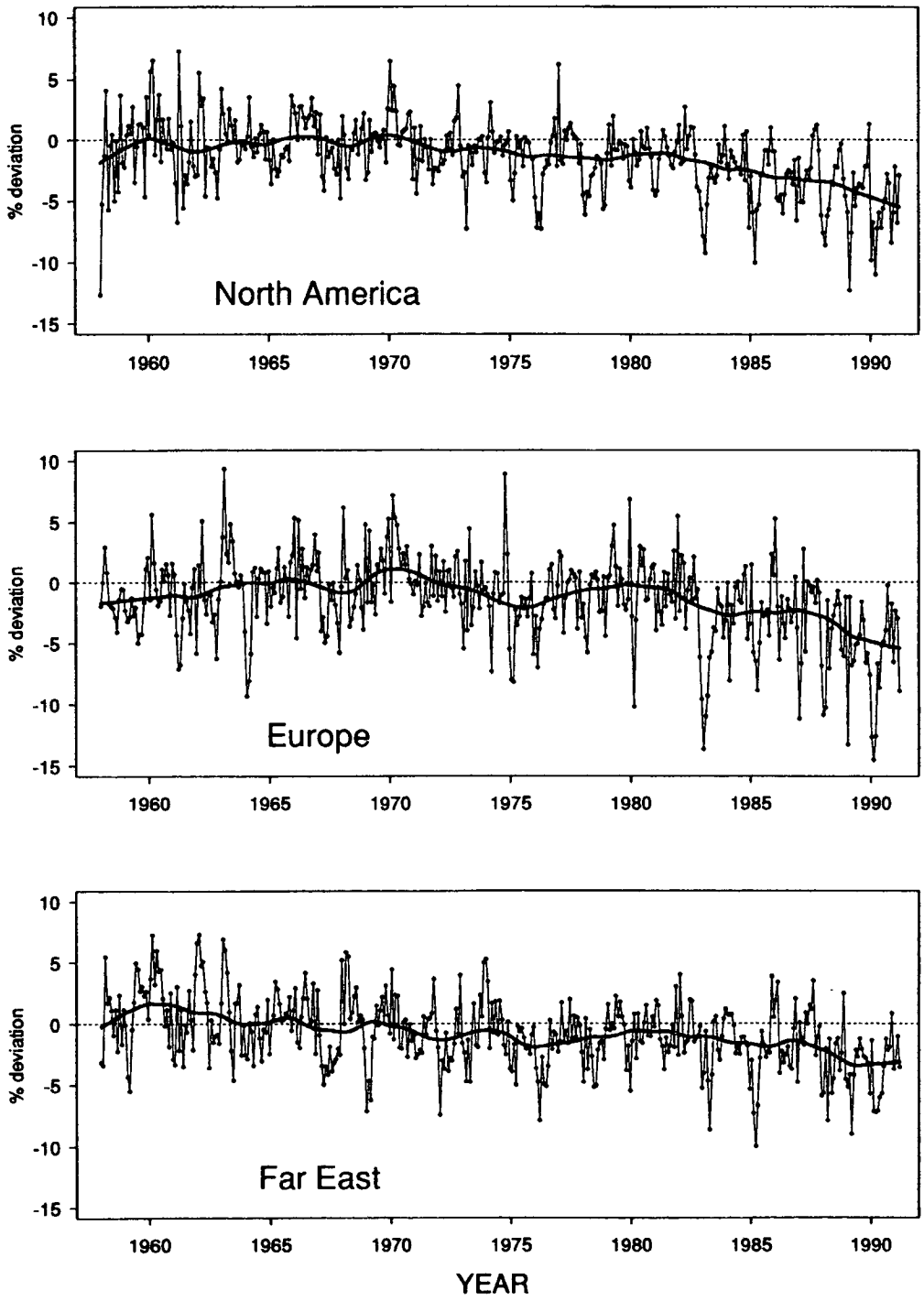

Figure 2-7 Regional average ozone series versus time. The series were calculated by taking seasonal, solar, QBO, and nuclear components at each station as determined from the full standard model (including trends) and subtracting these components (but not the trend component) from the ozone series at each station. The resulting series with seasonal, solar, etc., components removed, were averaged over all stations in the respective regions. The thick line is a strong statistical smoother (a 4-year moving robust regression) intended to bring out the slowly changing features in the data.

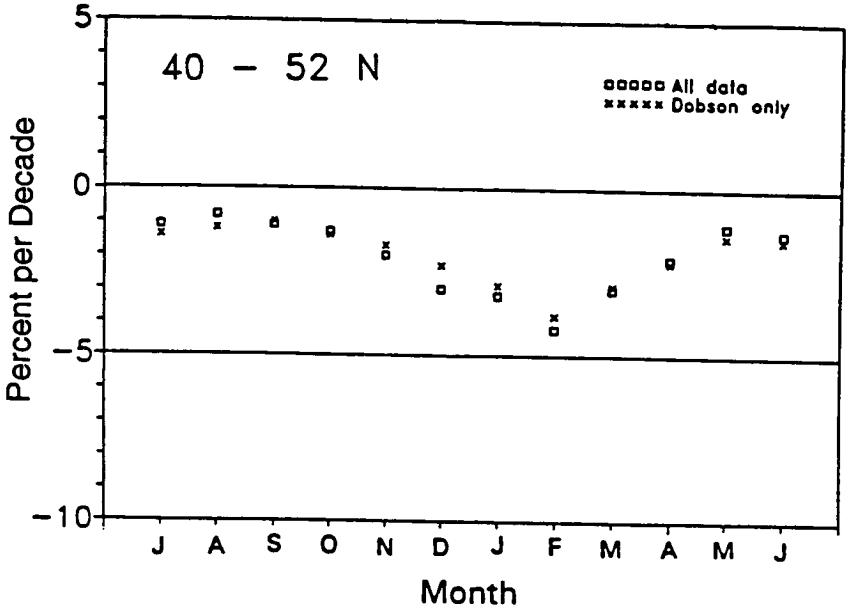

Figure 2-8 Ozone trends versus month obtained using the full statistical model on the 40°–52° N latitude band series with and without the inclusion of the filter ozonometer data (Fioletov, personal communication, 1991).

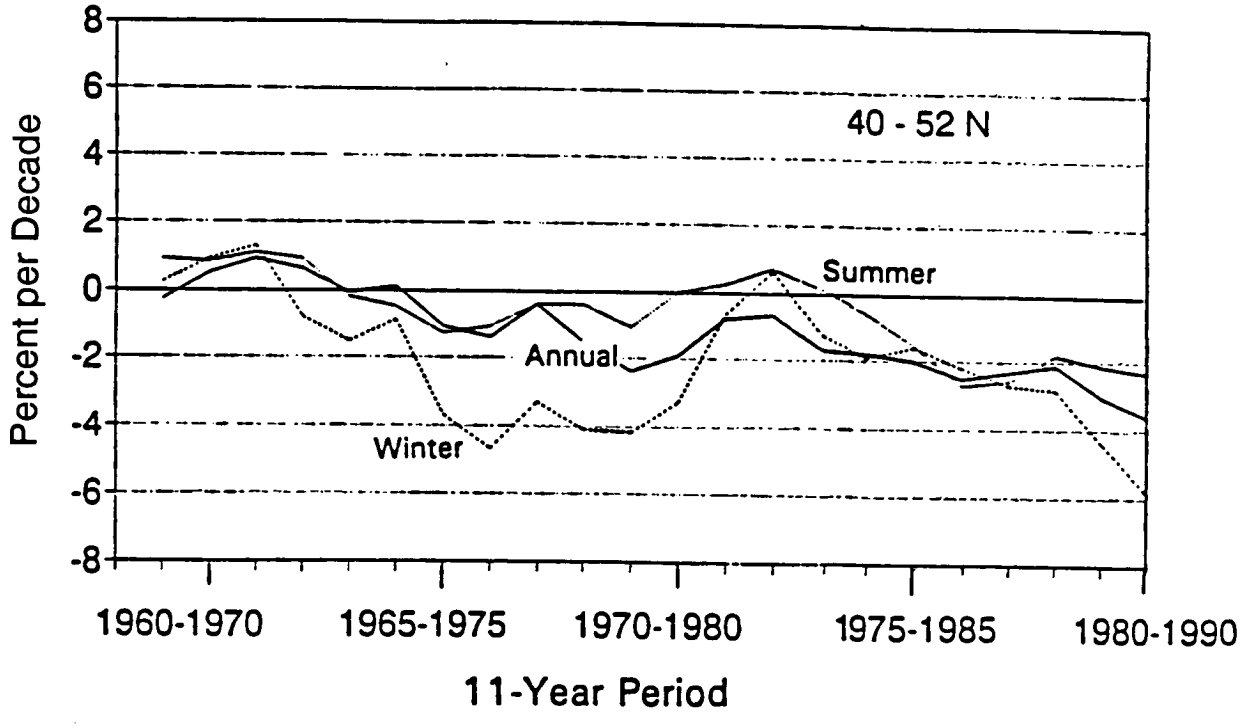

Figure 2-9 Sliding 11-year trend determined from Dobson series for the latitude band 40°–52° N. The series was deseasonalized and had the 11-year solar cycle removed before fitting of the trends. Each point on the graph was obtained by fitting a linear 11-year trend through the given time period, *i.e.*, 1960 through 1970 or 1980 through 1990 (Fioletov, personal communication, 1991).

A significant new data set is the internally recalibrated TOMS global total ozone, called Version 6. The previous TOMS data set, Version 5, also was internally calibrated, but the method broke down with increasing length of the data record, and TOMS was found to drift significantly with respect to the ground-based Dobson network. The drift was as much as 5 percent by 1987, leading to use of TOMS data in the Ozone Trends Panel Report in only "normalized to Dobson" mode. The TOMS Version 6 data have been compared to the World Primary Standard Dobson Instrument (#83) when TOMS passes over that instrument during its calibration each summer at Mauna Loa (McPeters and Komhyr, 1991). These comparisons show agreement over the time period 1979 to 1990 to within the stated error bars. Comparison of TOMS with an aggregate of stations is reported later in this chapter, indicating that TOMS has drifted downward relative to those stations by 0.5 to 1 percent per decade, which is within the quoted error bar.

Table 2-3 shows a comparison of the trend derived from TOMS over a number of Dobson stations along with the trend from the Dobson data for the same time period (November 1978 to March 1991). The Dobson trends over this time period show more variability, as would be expected, and average less in magnitude than the TOMS trends over the same stations; –3.5 versus –4.6 percent per decade in December–March, and –3.0 versus –3.5 percent per decade in May–August. Comparison of the Dobson trends over the TOMS time period with the Dobson trends in Table 2-1 from 1970 through 1991, shows the recent short-term trends to be consistently more negative for the nonequatorial stations (poleward of 25° north or south): 30 out of 34 stations are more negative in both seasons.

Figure 2-10 compares the time series of deviations from the seasonal average for TOMS with that for the Dobson instruments averaged over the latitude band, 40°–52°N. An important point to note is the shortness of the TOMS record compared with the Dobson; therefore, firm conclusions regarding total ozone trends rely on both records. The TOMS record provides global coverage while the Dobson provides a long record and frequent calibration checks. The two series exhibit almost identical features over their common timespan. The trends are nearly the same, as seen in Table 2-3, and the maxima and minima are highly correlated. In most cases, the TOMS record has somewhat less pronounced maxima and minima. This is particularly evident in the winter of 1982–1983.

2.3.3.3 Trends from Satellite Data

The TOMS data were analyzed by Stolarski *et al.* (1991) for trends over the period November 1978 to May 1990. They found no ozone trend near the equator, and an increasing trend towards high latitudes in both hemispheres. The Northern Hemisphere midlatitude trend is the most important new result from this study. An update of those results through March of 1991 is shown in Figure 2-11. Trends have been shown only to within about 10° of the terminator because of possible high solar zenith angle problems with TOMS (see *e.g.*, Pommereau *et al.*, 1989; Lefèvre and Cariolle, 1991a,b). The figure shows the trend as a function of latitude and season obtained from a statistical model including a fit to the 11-year solar cycle, the quasi-biennial oscillation, and a linear trend. The results are similar to those obtained by Stolarski *et al.* (1991) showing a winter to early spring maximum in the trend at northern mid-latitudes, although the trend through March of 1991 is smaller than that through May of 1990. The wintertime peak rate of ozone decrease near 40°N is slightly greater than 6 percent per decade in Figure 2-11 as compared to a value of greater than 8 percent per decade in Stolarski *et al.* (1991).

Because of the global coverage of the TOMS data, it can also be used to map the latitudinal and longitudinal structure of the ozone change. Figure 2-12 shows a global map of the average trend, obtained from the TOMS data through March of 1991, for the season comprising the months from December through March (Northern Hemisphere winter and Southern Hemisphere summer). Superimposed are the trend results obtained from the Dobson stations listed in Table 2-1 analyzed over the same time period as TOMS. The TOMS results show strong longitudinal variations at high northern latitudes, which are also seen in the ground-based data. The longitudinal variations at 60°N are marginally statistically significant, but there is no obvious way to determine whether or not they indicate a longitudinal variation in the cause of the trend.

Figure 2-13 shows the equivalent global map of the TOMS trends with superimposed Dobson trends

Table 2-3 A comparison of TOMS ozone trends with short-term trends (over the same data period, November 1978–March 1991) derived from ground-based total ozone data for individual stations. The TOMS trends given in the table are calculated for the 5° latitude by 10° longitude block containing the station.

		December–March				May–August			
		Ground		TOMS		Ground		TOMS	
	Lat	Trend	SE	Trend	SE	Trend	SE	Trend	SE
North America									
Churchill	58 N	–5.4	2.3	–2.3	2.1	–6.7	1.5	–6.4	1.5
Edmonton	53 N	–5.5	2.1	–5.5	2.2	–7.5	1.0	–5.2	1.2
Goose Bay	53 N	2.1	2.6	–1.1	2.4	–5.1	1.4	–4.3	1.3
Caribou	47 N	–4.7	2.4	–3.5	2.6	–3.4	1.1	–4.3	1.2
Bismarck	46 N	–4.4	1.9	–4.6	1.8	–5.1	1.4	–5.2	1.3
Toronto	43 N	–4.3	2.0	–6.6	2.4	–2.8	1.1	–3.1	0.9
Boulder	40 N	–2.4	2.0	–4.4	1.9	–2.5	1.2	–3.6	1.2
Wallops Island	38 N	–6.8	1.8	–7.4	2.1	–1.9	1.6	–2.6	1.0
Nashville	36 N	–7.3	1.9	–6.8	2.1	–2.0	1.2	–1.8	0.9
Tallahassee	30 N	–5.8	2.8	–6.3	1.9	–2.8	2.0	–1.7	0.9
Average:		–4.5		–4.8		–4.0		–3.8	
Europe									
Reykjavik	64 N	–0.0	5.6	–0.8	4.1	–4.8	1.3	–4.5	1.4
Lerwick	60 N	1.3	14	–2.9	3.6	–5.6	1.9	–5.7	1.5
St. Petersburg	60 N	–4.6	2.7	–5.8	2.6	–4.0	1.6	–4.7	1.4
Belsk	52 N	–5.4	2.8	–5.9	2.9	–5.3	1.3	–4.1	1.6
Bracknell	51 N	–3.8	2.5	–4.4	2.7	–5.9	1.3	–5.0	1.4
Uccle	50 N	–4.4	2.7	–6.3	2.6	–4.3	1.3	–4.7	1.3
Hradec Kralove	50 N	–5.0	2.6	–6.6	2.6	–3.5	1.1	–4.4	1.4
Hohenpeissenberg	47 N	–3.8	2.9	–6.9	2.7	–2.4	1.1	–3.7	1.2
Arosa	46 N	–5.9	2.5	–6.1	2.7	–2.8	1.3	–4.4	1.4
Vigna di Valle	42 N	–6.0	2.8	–6.3	2.5	–4.4	1.3	–3.4	1.1
Cagliari/Elmas	39 N	–3.8	3.4	–4.4	2.5	–0.8	2.3	–2.7	1.2
Average		–3.8		–5.1		–4.0		–4.3	
Far East									
Nagaevo	60 N	–4.3	2.5	–4.4	2.1	–3.0	2.0	–3.9	1.5
Petropavlovsk	53 N	–5.2	2.1	–6.8	1.7	–1.8	2.7	–3.8	1.5
Sahalin	47 N	–4.2	1.5	–7.6	1.5	–1.1	1.7	–4.3	1.5
Sapporo	43 N	–3.7	2.1	–6.8	2.1	–4.0	1.6	–3.9	1.7
Tateno	36 N	–3.3	2.3	–6.2	2.2	–2.2	1.2	–3.3	1.2
Kagoshima	31 N	–2.9	1.9	–5.0	2.0	–1.5	1.1	–2.6	1.1
Naha	26 N	–3.2	1.8	–3.5	1.6	–1.3	1.1	–2.2	1.0
Average		–3.8		–5.8		–2.1		–3.4	
Low Latitudes									
Quetta	30 N	–3.0	2.6	–4.8	2.4	–0.9	1.5	–2.6	1.3
Cairo	30 N	–1.6	2.5	–3.2	2.2	–1.2	1.2	–3.0	1.0
Ahmedabad	23 N	–0.3	2.4	–2.3	1.6	–2.3	1.5	–0.9	1.0
Mauna Loa	19 N	1.0	2.3	–1.8	2.1	2.0	1.4	0.3	1.0
Mexico City	19 N	3.8	4.8	–1.8	1.8	3.7	4.0	0.1	1.1
Huancayo	12 S	1.2	0.6	0.1	0.6	–0.5	0.8	–0.3	0.9
Samoa	14 S	–0.4	1.1	–1.1	1.1	0.5	2.0	–1.1	1.5
Average		+0.1		–2.1		+0.2		–1.1	
Southern Hemisphere									
Aspendale	38 S	–4.6	1.0	–3.2	0.9	–2.9	1.4	–3.0	1.7
Hobart	42 S	–5.5	1.3	–3.7	1.0	–5.5	1.6	–4.8	1.7
Invercargill	46 S	–7.1	1.4	–5.0	1.0	–6.1	1.7	–6.6	1.9
MacQuarie Island	54 S	–6.1	2.1	–5.9	1.1	–4.5	2.8	–5.8	2.1
Average		–5.8		–4.5		–4.8		–5.0	
Average all stations		–3.5		–4.6		–3.0		–3.5	

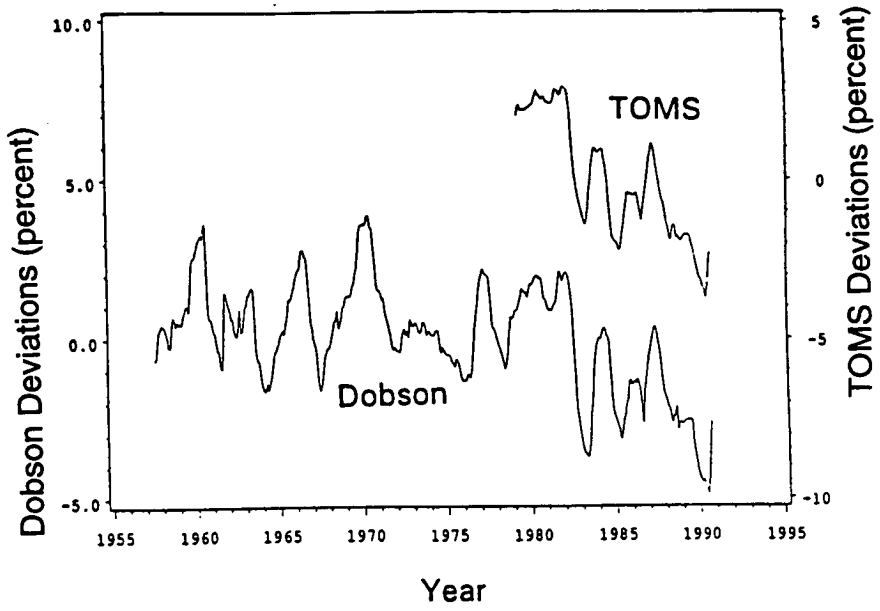

Figure 2-10 A comparison of TOMS and Dobson data for northern middle latitudes. The TOMS series is deseasonalized mean ozone over 40°–52° N. The Dobson series is the composite series constructed from deseasonalized ozone for stations in the latitude range 40°–52° N. The data plotted are a 1-year moving mean, which smooths high-frequency variations, but broadens and decreases the amplitude of large excursions such as that of the winter of 1982–1983.

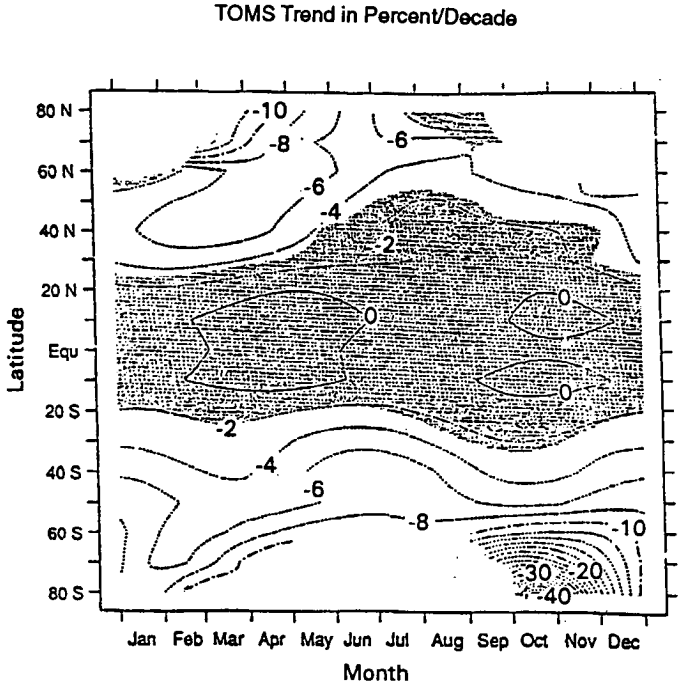

Figure 2-11 Trend obtained from TOMS total ozone data as a function of latitude and season. Data included extends from November 1978 through March 1991. Unshaded area indicates where trends are statistically significant at the 2σ level (Bloomfield, personal communication, 1991).

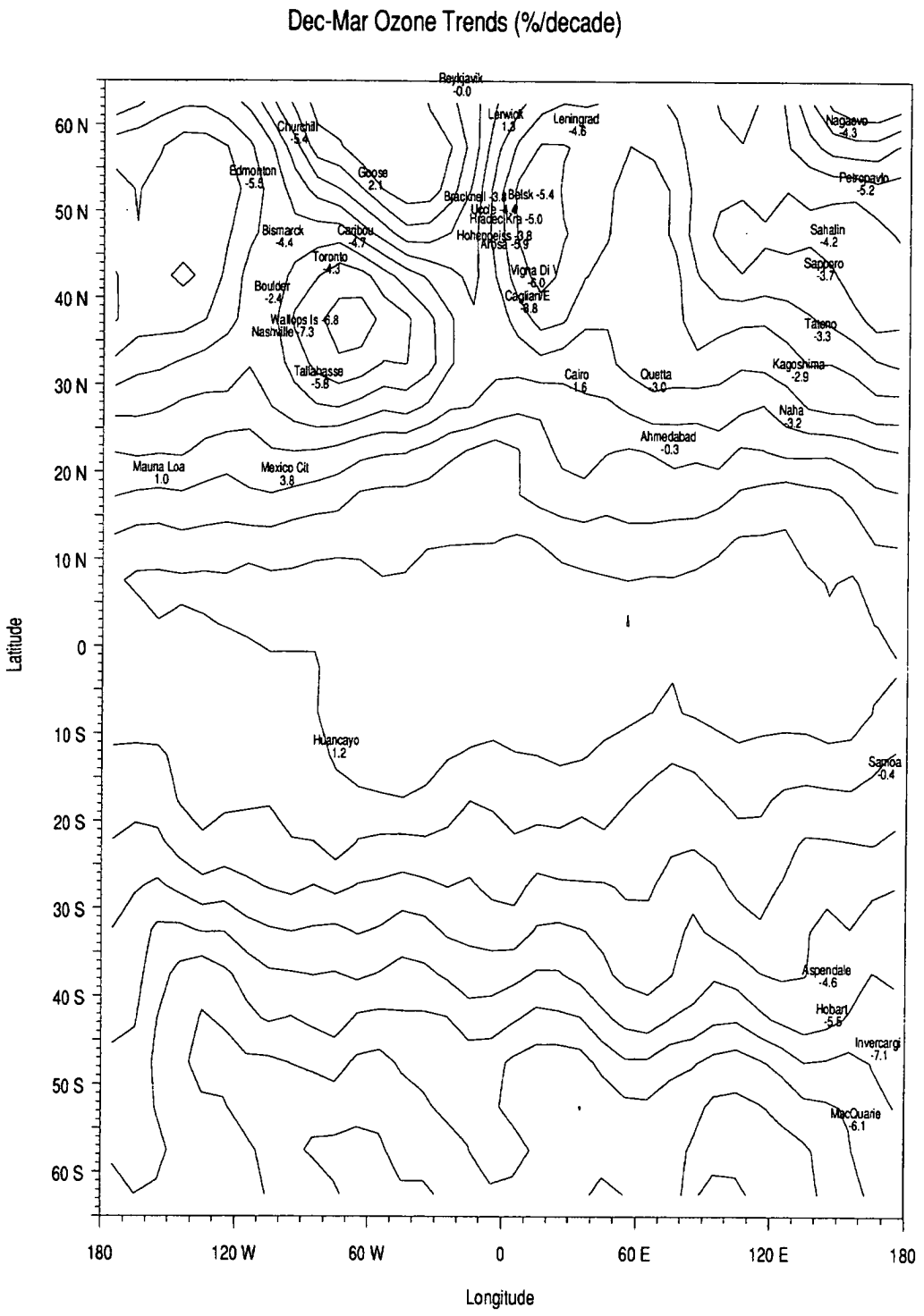

Figure 2-12 Contours of constant TOMS average trend for December through March over the period November 1978—March 1991, versus latitude and longitude. Superimposed are the corresponding short-term (also November 1978—March 1991) ground-based trends. The numerical value of the ground-based trend is centered as nearly as possible over the station's location. All trends in percent per decade.

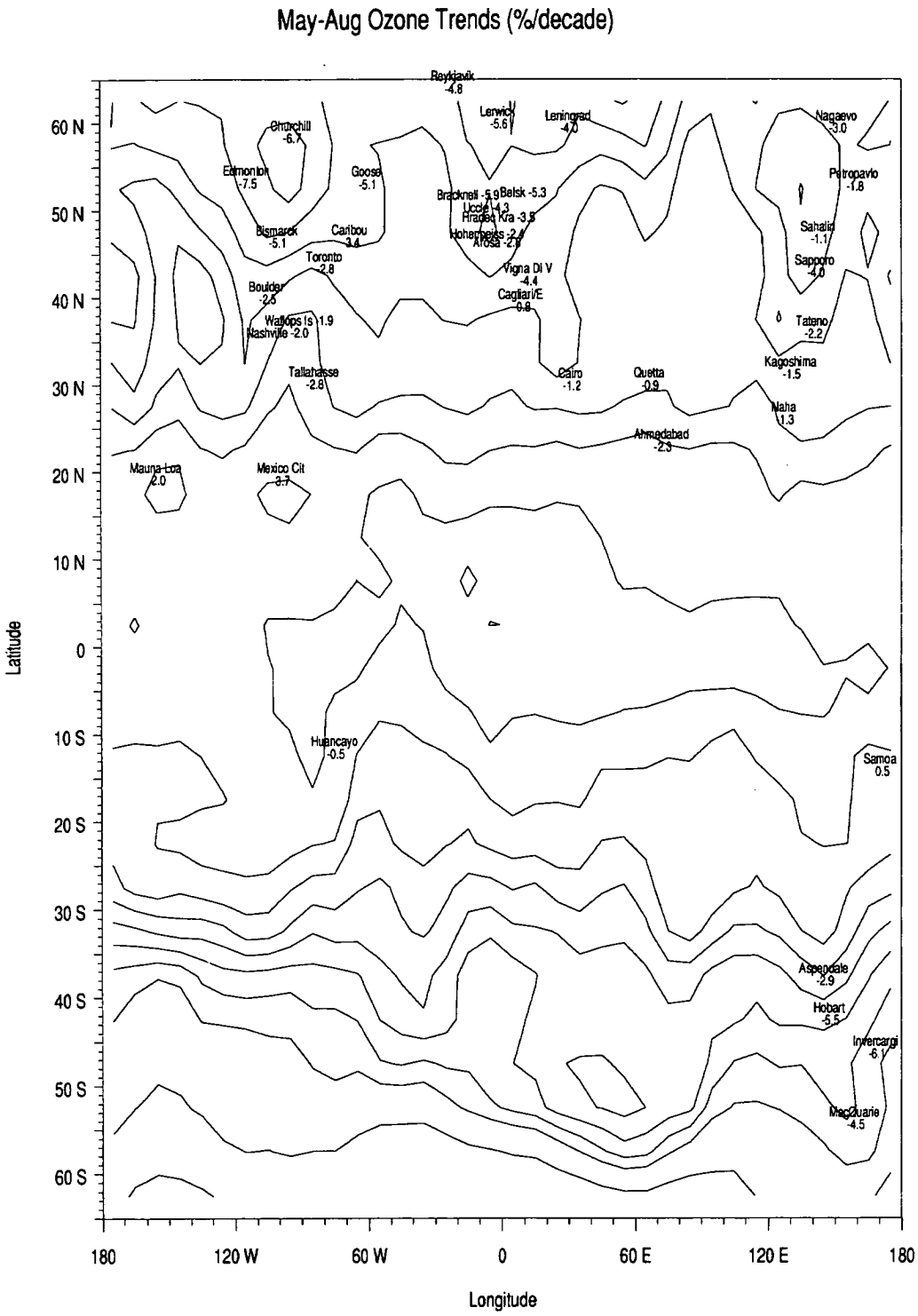

Figure 2-13 Contours of constant TOMS average trend for May through August over the period November 1978–March 1991, versus latitude and longitude. Superimposed are the corresponding short-term (also November 1978–March 1991) ground-based trends. The numerical value of the ground-based trend is centered as nearly as possible over the station's location. All trends in percent per decade.

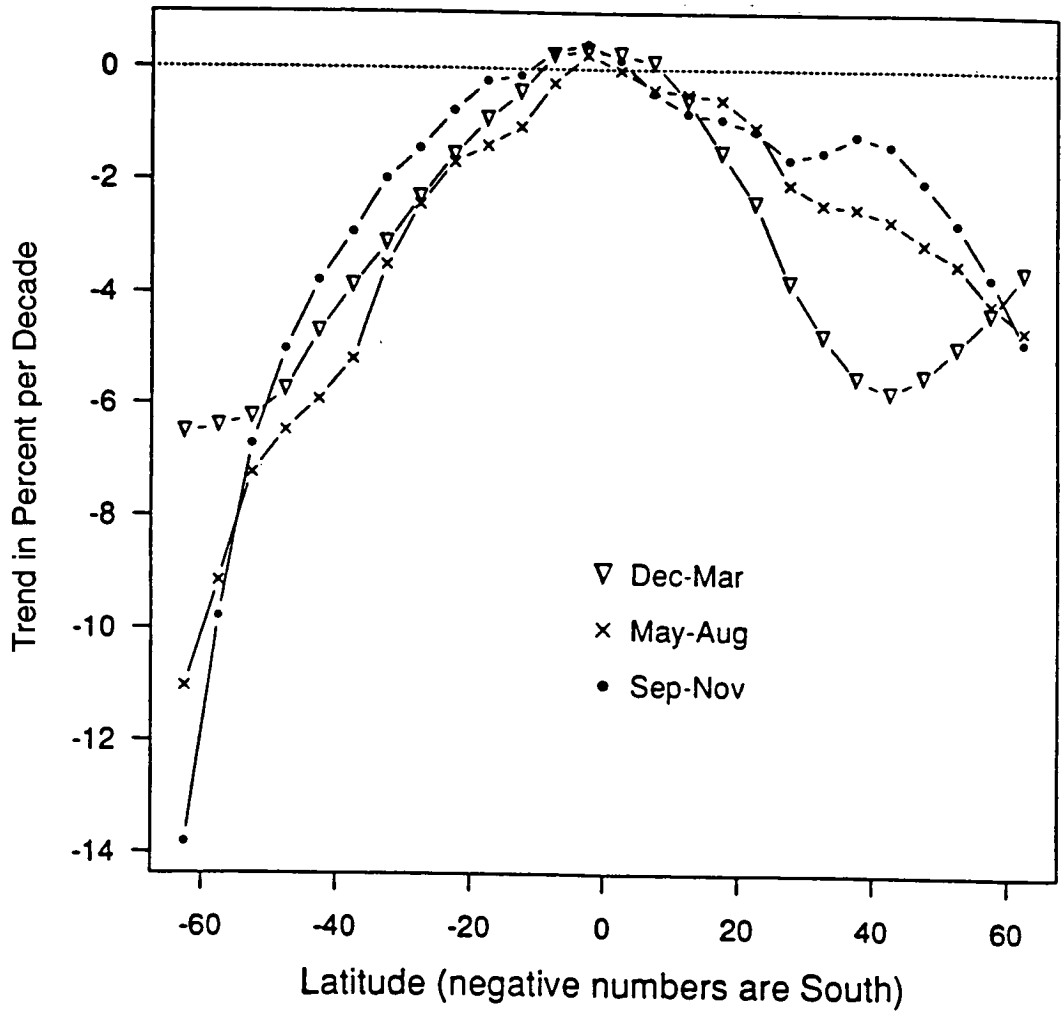

Figure 2-14 TOMS trends in zonal mean ozone versus latitude, by season. The data period is November 1978 through March 1991.

at each station for the season May–August (Southern Hemisphere winter and Northern Hemisphere summer). Longitudinal variations are seen in both hemispheres, but are not as pronounced as those in the December–March northern high latitudes.

The zonal mean seasonal trends obtained from TOMS are shown in Figure 2-14 as a function of latitude. The three seasons shown all have near-zero trends around the equator. The December–March trend reaches just about –6 percent per decade at high southern latitudes (summer) and nearly –6 percent per decade at northern middle latitudes (winter). The northern winter negative trend maximizes at about 40°N and then decreases poleward as the longitudinal variations increase. The May–August (summer) trend in the Northern Hemisphere increases steadily as latitude increases until it is actually larger than the winter trend at 60°N. This steady increase with latitude is consistent with the summer trend found for the Dobson stations over the longer time period 1970–1991, as shown in Figure 2-6. The September–November (fall) trend is smaller in the Northern Hemisphere than the summer or winter trends except near 60°N. In the Southern Hemisphere, the September–November trend is for spring and the large trends (–14 percent per decade) are indicative of the region near the Antarctic ozone hole.

2.3.4 Trends in the Ozone Profile

2.3.4.1 Ozonesondes

In the 1989 assessment report (WMO, 1990b), analyses of nine ozonesonde stations were presented for data through the end of 1986. These were an update of previous work with data through 1982 (Tiao *et al.*, 1986). The results showed a statistically significant negative trend between about 17 and 24 km, but extreme caution was urged in drawing conclusions on a global scale, because there were considerable differences in trend profiles from station to station.

The ozonesonde time series from Payerne, Switzerland has recently been analyzed by Dütsch *et al.* (1991) and by Staehelin and Schmid (1991) using data through 1988. They found statistically significant positive trends in the troposphere and statistically significant negative trends in the lower stratosphere. Figure 2-15 (Staehelin, personal communication, 1991) shows the trends obtained from 1967 through 1990 as a function of altitude for three seasons, winter (December to March), summer (May to September) and fall (October to November). A large positive trend (statistically significant) was obtained for all seasons in the troposphere. The trend in tropospheric ozone seen in Figure 2-15 is consistent with that found at other stations when regional variations in air pollution are considered. The data were reviewed in the 1989 WMO–UNEP Assessment Report (WMO, 1990b) and previously by Logan (1985), Bojkov (1987b), and Penkett (1988). Although a trend in tropospheric ozone is not unexpected, the evidence for a global scale increase is still not conclusive. A crossover to a negative trend was found for all seasons with the crossover occurring at the lowest altitude in winter (~200 mbar) and the highest altitude in fall (~100 mbar). The trend in all three seasons goes to near zero between about 10 and

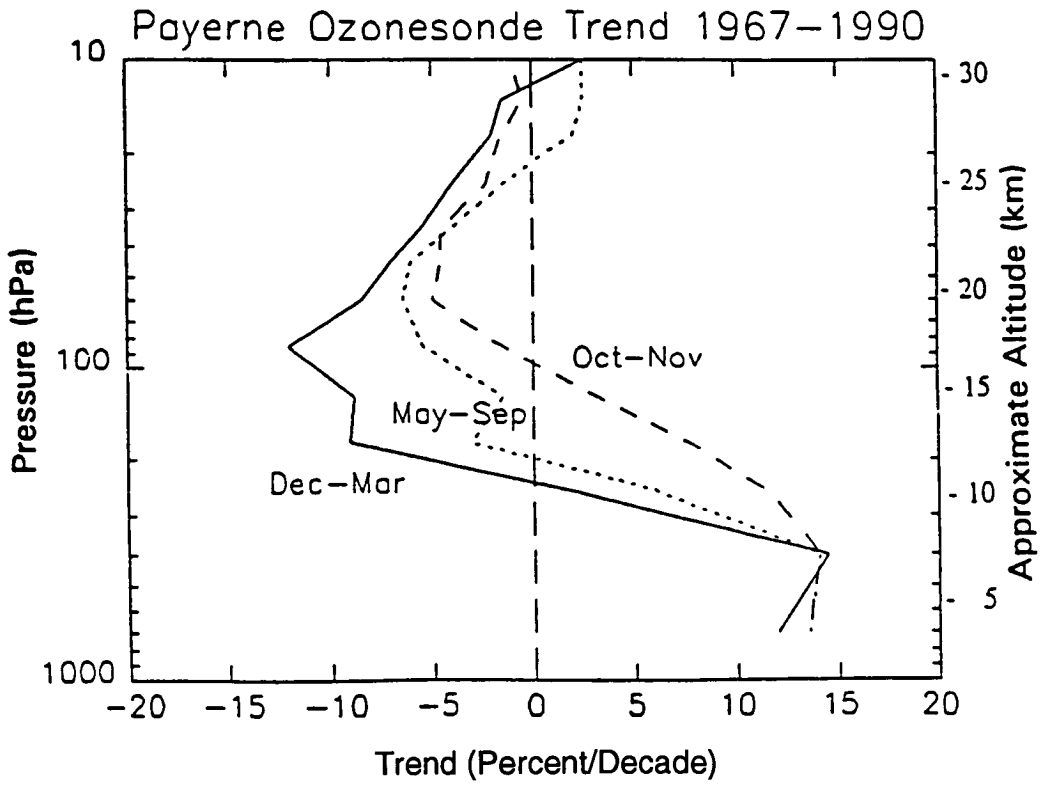

Figure 2-15 Trend versus altitude derived from Payerne ozonesonde record. Shown are linear trends for the period 1967 through 1990 for three seasons, winter (December through March), summer (May through September), and fall (October through November) (Staehelin, personal communication, 1991).

20 mbar. Since the total ozone column from each ozonesonde profile is normalized to Dobson column measurements, the integrated effect of the sonde trend profile is necessarily quantitatively consistent with the Dobson trends.

The change in the altitude profile of ozone is graphically illustrated in Figure 2-16 (Staehelin, personal communication, 1991), which shows the profile obtained from the Payerne ozonesondes averaged over three different 2-year time periods. The time periods, 1969–70, 1979–80, and 1989–90 were chosen to be near the maxima of three consecutive solar cycles. Two-year time periods were chosen to remove seasonal variations and to approximately remove the effects of the quasi-biennial oscillation. The profiles in Figure 2-16 clearly show that lower ozone concentrations are measured throughout the ozone peak region in the lower stratosphere during 1989–90.

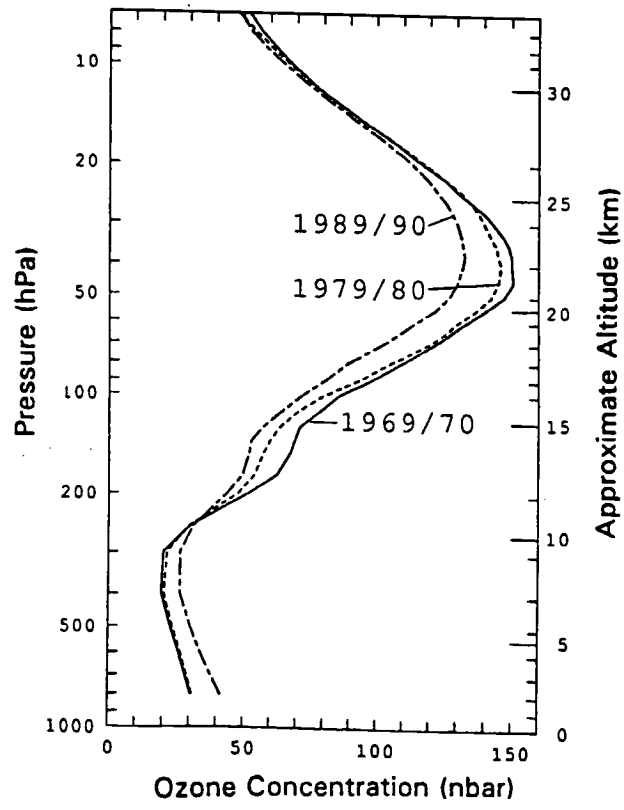

Figure 2–16 Average ozone concentration versus altitude measured over Payerne for three 2-year periods, 1969–1970, 1979–1980, and 1989–1990. Periods were chosen to be approximately during solar maximum and 2 years was used to remove most of any QBO effect (Staehelin, personal communication, 1991).

2.3.4.2 SAGE

The Ozone Trends Panel Report showed ozone changes as a function of altitude above 25 km obtained by differencing 3 years of SAGE II data from the more than 2 years of SAGE I data. Since that report, the SAGE I and SAGE II ozone profiles below 25 km have been validated (Veiga and Chu, 1991) and trends down to 17 km altitude can be evaluated. Additionally, there are now more than 6 years of SAGE II data which, when combined with SAGE I data, can be used to give an independent determination of the altitude profile of ozone change.

Figure 2-17 is a latitude-altitude plot of the annual average trends deduced from the combined SAGE I/SAGE II data set (McCormick *et al.*, 1992). Ozone trends deduced from SAGE in the middle stratosphere (25–35 km) are small and not significantly different from zero. Above 35 km, the trends are generally negative. The maximum decrease is found near 42 km at 20°S latitude and changes in the Southern Hemisphere are larger than those in the Northern Hemisphere. The latitudinal dependence and magnitude of the upper stratospheric trends is at variance with model predictions (see Figure 2-18). In the lower stratosphere, strong negative trends are seen with a weak latitude dependence. The strongest lower stratospheric trends appear near about 25° in each hemisphere.

2.3.4.3 Umkehr

The Umkehr record was analyzed in the Ozone Trends Panel Report and in the 1989 WMO–UNEP assessment. Data from 10 stations were evaluated for the time period 1977–1987 using two different assumptions concerning data immediately after El Chichón. One assumption was to delete the data for 2 years after the eruption and the other was to include a statistical term in the analysis with the shape of the lidar optical thickness. These procedures led to similar results: a decrease in Levels 7 and 8 (~35–45 km), which is statistically significant, or nearly so, at the two σ level. The Umkehr records have now been updated through 1990 and analyzed by DeLuisi (personal communication).

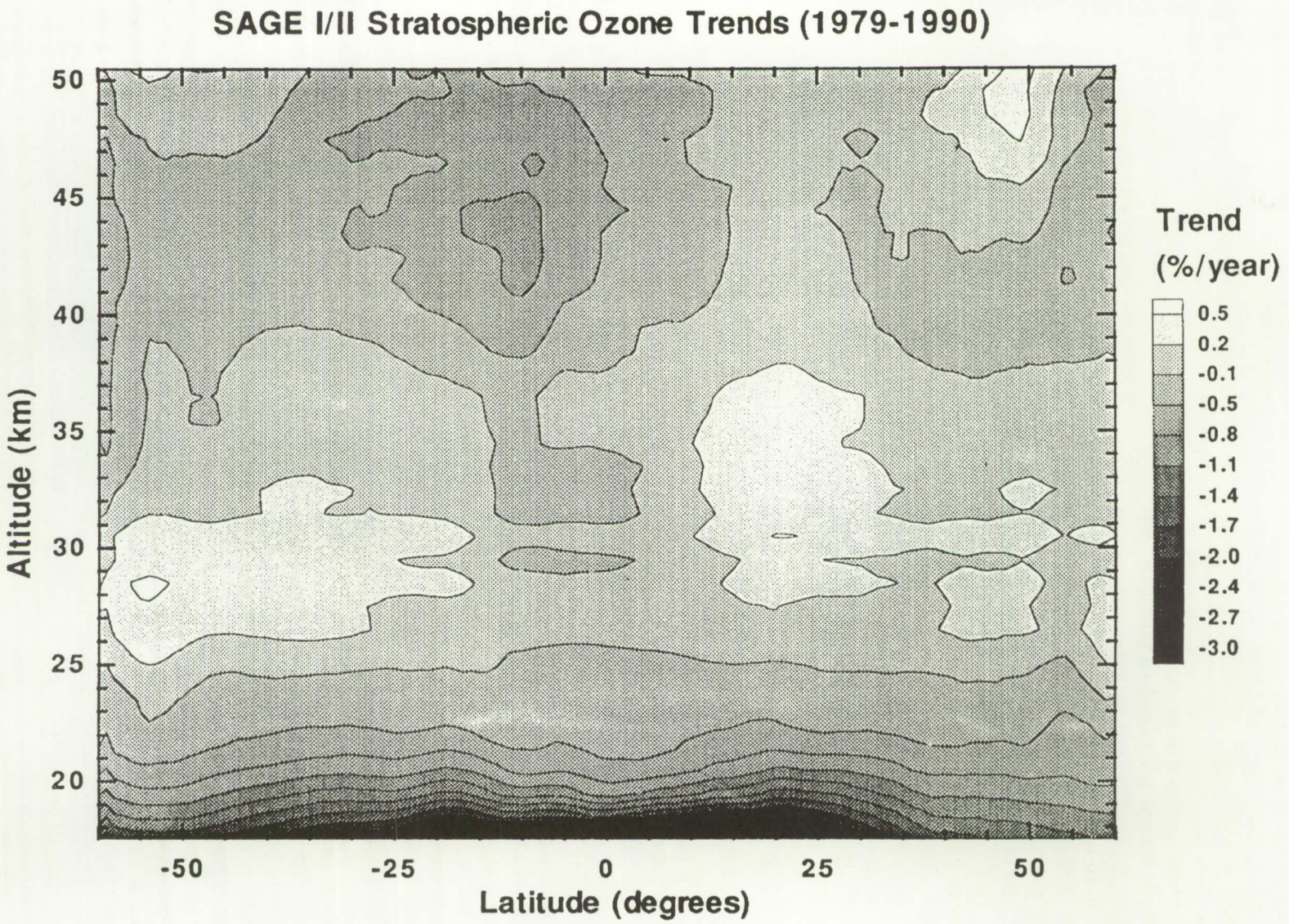

Figure 2-17 Trends derived from the SAGE I and SAGE II measurements of the ozone profile in percent per decade as a function of latitude and altitude (McCormick *et al.*, 1992).

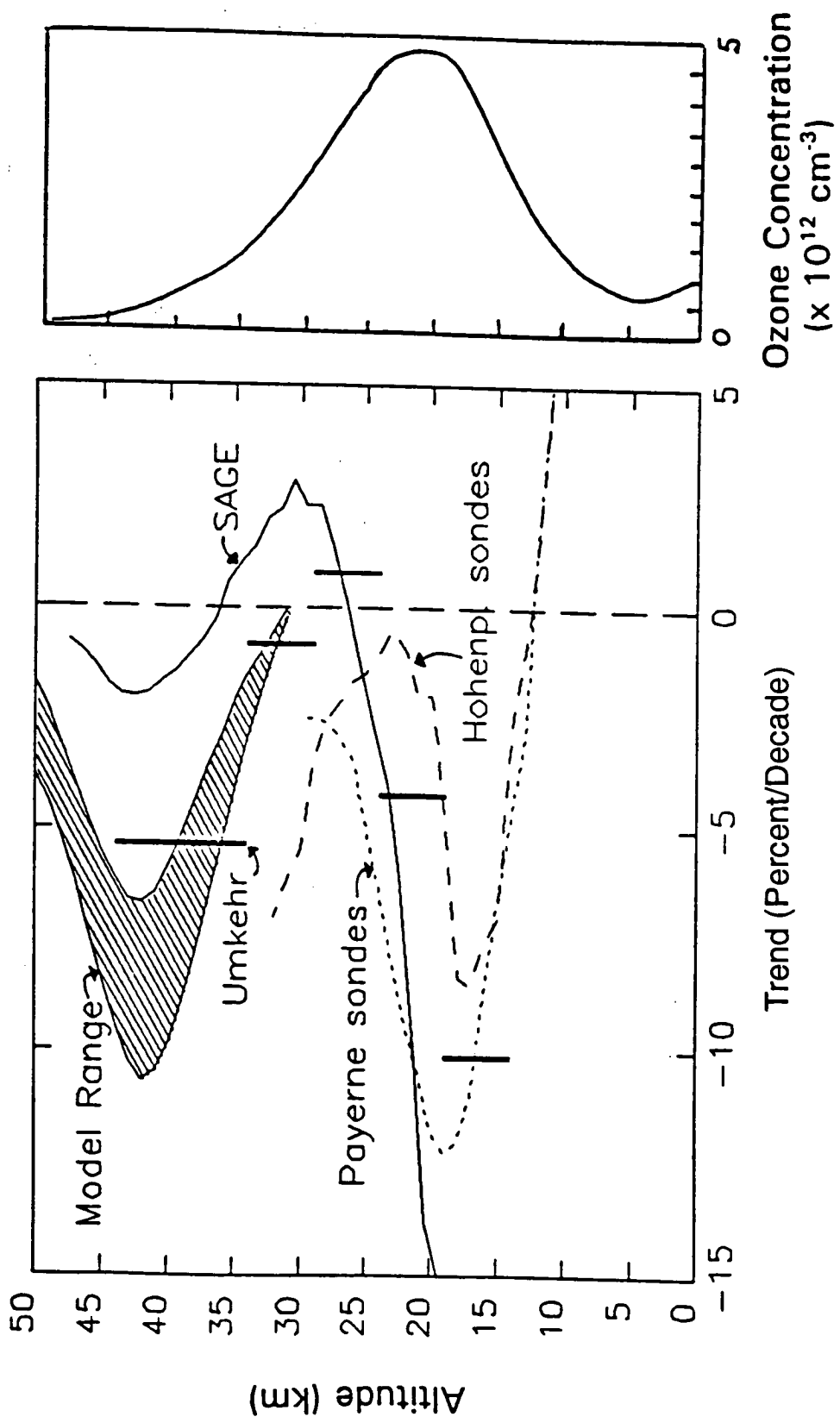

Figure 2-18 Comparison of ozone profile trend estimates from several measurement systems, SAGE, Umkehr, and two ozonesonde stations. SAGE data is an average over the latitude ranges 20°–50° N and 20°–50° S. The Umkehr is the average over five northern mid-latitude stations. Shaded area shows the range of two model calculations at 50° N and 50° S. The panel on the right shows a typical ozone concentration versus altitude.

2.3.4.4 Comparison of Profile Trends

To facilitate a direct comparison with SAGE, the Umkehr record has been analyzed from 1979 through 1990. The resulting trend and error bars are shown in Figure 2-18 along with the SAGE trends. Following WMO (1990a,b), only the Umkehr results in Layers 4 through 8 are shown. The trend profiles from Umkehr and SAGE agree to within their uncertainties and show a maximum decrease of $-1/2$ percent per year in Layers 7 and 8 (35–45 km), which is approximately half of the change predicted by models. No significant trend is observed in the 25–30-km region. SAGE and Umkehr independently confirm the large negative trends in the lower stratosphere (below 25 km) seen in the ozonesonde data.

2.3.5 Temperature

Ozone and temperature generally correlate positively in the lower stratosphere and negatively in the upper stratosphere, but the respective responses to various forcings may complicate this relationship. Temperature is subject to frequent fluctuations whether of external (solar, volcanic) or internal origin (planetary and gravity waves, QBO, etc.). This temperature variability may result in fluctuations in either total ozone or in ozone concentration. Conversely ozone changes, such as those reported in this chapter, will affect the absorption rate of ultraviolet and infrared radiation and can lead to temperature changes in response. It is important to compare trends in the temperature with those observed in ozone concentration.

Even though the number of measurements is very large, the search for temperature trends has received far less attention. The previous assessment report (WMO, 1990b) concluded that there was some evidence of a generally negative trend in the lower stratosphere, with large spatial variability. The upper-limit zonal-average trend was given as –0.6 to –0.8 K per decade between the 100 and 10 hPa levels, respectively. Recently, Labitzke and van Loon (1991), who had earlier indicated a cooling of 0.4 K per decade at 20 and 24 km in October–November between 20° and 50°N, have cast some doubts about their results from radiosondes due to the high variability observed, mostly in winter.

Two studies of trends deduced from radiosondes have been performed since the last assessment

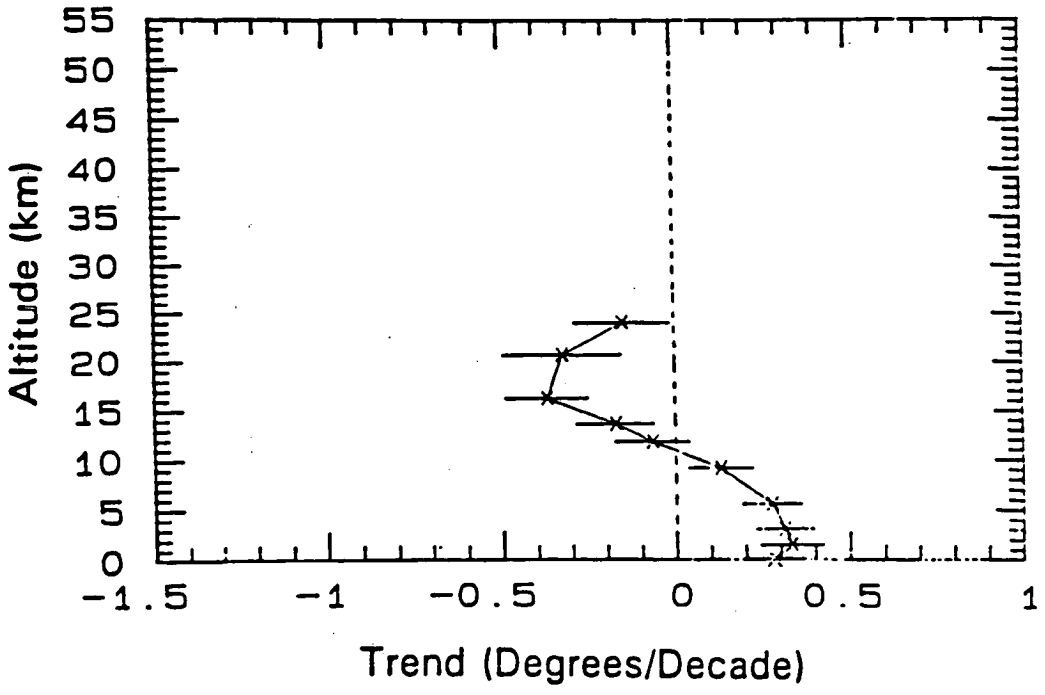

Figure 2-19 Rawinsonde temperature trend estimates in °C per decade as a function of altitude. Horizontal bars represent 95 percent confidence limits of estimated trends (Miller *et al.*, 1991).

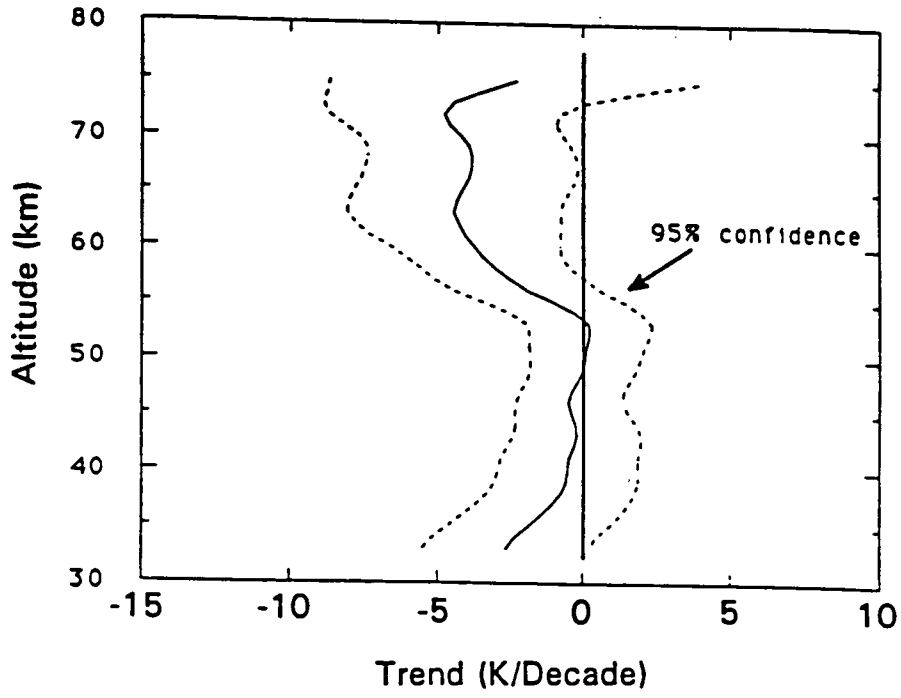

Figure 2-20 Temperature trend versus altitude for 6-month summer season from April through September obtained by lidar measurements above Observatoire de Haute Provence in southern France. Data period was from 1979 through 1990 (Hauchecorne *et al.*, 1991).

(Miller *et al.*, 1991; and Oort and Liu, 1991). Both use the data set already used by Angell (1988); *i.e.*, 62 stations extending from 80°N to 80°S. Miller *et al.* (1991) deduced a warming of the order of 0.3° per decade between the surface and 5 km (500 mb) and a maximum cooling of 0.4° per decade between 16 km (100 mb) and 20 km (50 mb) as shown in Figure 2-19. Oort and Liu (1991) treated the two hemispheres and deduced a trend of –0.38° per decade in the Northern Hemisphere compared to –0.43° per decade in the Southern Hemisphere.

These recent analyses support a global cooling of the lower stratosphere of between 0.3 K and 0.5 K per decade. Significantly more work needs to be done on temperature trends but it appears that a relatively conservative conclusion can be reached that there has been a global mean cooling of the lower stratosphere of about 0.3 K per decade over the last 2 to 3 decades.

Other recent results concerning the upper stratosphere and mesosphere (Kokin *et al.*, 1990; Aikin *et al.*, 1991; Hauchecorne *et al.*, 1991) have been obtained. Figure 2-20, from Hauchecorne *et al.* (1991), illustrates the results obtained in summer by lidar at 44°N, 61°E. Whereas a clear cooling of 4 K per decade associated with CO_2 increase is observed in the mesosphere, the ~1 K per decade seen between 35 and 50 km is below the significance level. The same type of result is observed from four rocket sites by Kokin *et al.* (1991). In those two cases the quite significant response to the 11-year solar forcing has been taken into account and extracted independently. Aikin *et al.* (1991) examined satellite data using the synthesized Stratospheric Sounding Unit (SSU) channel 47x centered near 0.5 hPa or 55 km and they confirmed that the mesospheric cooling of Figure 2–20 was global scale. The comparison with models at 40 km, which indicates between 1 and 2 K per decade, due half to the O_3 depletion and half to the CO_2 increase, is within the error bars of the observations, but the cooling observed above 50 km is much larger than expected from models.

2.4 SUMMARY

The Antarctic ozone hole of 1989 was deep and long-lasting, demonstrating that 1987 was not unique. The 1990 ozone hole was also quite deep, similar to

both 1987 and 1989. It lasted through December, the latest disappearance yet of the springtime ozone hole. The 1991 ozone hole was again deep and long-lasting, very similar to 1989. Thus, four of the last five years have had deep long-lasting ozone holes. The previously noted quasi-biennial modulation of the severity of the ozone hole did not occur during the last 3 years. The area of the ozone hole has remained constant for the years 1987, 1989, 1990, and 1991.

For the first time statistically significant decreases in total ozone are being observed in all seasons in both the Northern and Southern Hemispheres at middle and high latitudes. Southern mid-latitude total ozone trends from the TOMS data are statistically significant in all seasons south of about 25°S. This is consistent with the analyses from the few existing Dobson stations with long records. The northern mid-latitude winter decrease found by the Ozone Trends Panel has continued and is now somewhat larger than previously reported, extending into the spring and summer. The majority of Dobson stations now show a statistically significant summer trend since 1970. The Dobson measurements have now been confirmed by independent measurement systems, *i.e.*, TOMS and SAGE. The TOMS negative trends are about 1 percent more negative than those from the Dobson instruments at the same latitude. There is longitudinal structure to the trends derived from TOMS for northern mid-latitudes. The longitudinal structure in the Dobson data is less clear, but reasonably consistent with that from TOMS. No statistically significant decreases are seen in tropical latitudes, from 25° S to 25° N.

SAGE and ozonesonde measurements have demonstrated that the northern middle latitude trends are occurring in the lower stratosphere. The negative trend in the lower stratosphere, below 25 km, is about 10 percent per decade, consistent with the observed decrease in column ozone. The measured upper stratospheric trend from both SAGE and Umkehr have a shape with altitude that is similar to model predictions, but the magnitude is somewhat smaller than that of the models. Tropospheric ozone increases of 10 percent per decade over the last 2 decades are seen over the few existing ozone sounding stations at northern middle latitudes.

The temperature record and understanding of changes in temperature are not in nearly as good shape as the ozone record. The existing record indicates a small cooling (about 0.3 K per decade) of the lower stratosphere in the sense of that expected from the observed change in the stratospheric concentration of ozone.

REFERENCES:

Aikin, A.C., M.L. Chanin, J. Nash, and D.J. Kendig, Temperature trends in the lower mesosphere, *Geophys. Res. Lett., 18*, 416–419, 1991.

Angell, J.K. Variations in trends in tropospheric and stratospheric global temperatures, 1958-87, *J. Climate, 12*, 1296-1313, 1988.

Bojkov, R.D., The 1983 and 1985 anomalies in ozone distribution in perspective, *Mon. Wea. Rev., 115*, 2187–2201, 1987a.

Bojkov, R.D., Ozone changes at the surface and in the free troposphere, in Tropospheric Ozone: Proceedings of the NATO Workshop, ed. by I.S.A. Isaksen, pp. 83–96, D. Reidel, Boston, 1987b.

Bojkov, R.D., L. Bishop, W.J. Hill, G.C. Reinsel, and G.C. Tiao, A statistical trend analysis of revised Dobson total ozone data over the Northern Hemisphere, *J. Geophys. Res., 95*, 9785–9807, 1990.

Bojkov, R.D., and V.E. Fioletov, The ozone changes over mid-latitude Eurasia based on re-evaluated filter ozonometer data, *J. Geophys. Res.*, submitted, 1991.

Browell, E.V., L.R. Poole, M.P. McCormick, S. Ismail, C.F. Butler, S.A. Kooi, M.M. Szedlmayer, R.L. Jones, A. Krueger, and A.F. Tuck, Large-scale variations in ozone and polar stratospheric clouds measured with airborne lidar during formation of the 1987 ozone hole over Antarctica, Polar Ozone Workshop, NASA Ref. Publ. 10014, 61–64, 1988.

Chandra, S., and R.S. Stolarski, Recent trends in stratospheric total ozone: implications of dynamical and El Chichón perturbations, *Geophys. Res. Lett., 18*, 2277–2280, 1991.

Chanin, M.L., N. Smires, and A. Hauchecorne, Long-term variation of the temperature of the middle atmosphere at mid-latitude: dynamical and radiative causes, *J. Geophys. Res., 92*, 10933–10941, 1987.

Chubachi, S., A special ozone observation at Syowa Station, Antarctica from February 1982 to

January 1983, in Atmospheric Ozone, Ed. by C. S. Zerefos and A.M. Ghazi, Reidel, Dordrecht, 285–289, 1985.

Deshler, T., and D.J. Hofmann, Ozone profiles at McMurdo Station, Antarctica, the Austral spring of 1990, *Geophys. Res. Lett., 18*, 657–660, 1991.

Deshler, T., D.J. Hofmann, J.V. Hereford, and C. B. Sutter, Ozone and temperature profiles over McMurdo Station, Antarctica, in the spring of 1989, *Geophys. Res. Lett., 17*, 151–154, 1990.

Dütsch, H.U., J. Bader, and J. Staehelin, Separation of solar effects on ozone from anthropogenically produced trends, *J. Geomagnetism and Geoelectricity*, in press, 1991.

Farman, J.C., B.G. Gardiner, and J.D. Shanklin, Large losses of total ozone in Antarctica reveal seasonal ClO_x/NO_x interaction, *Nature, 315*, 207–210, 1985.

Fioletov, V.E., Total ozone content variations on various temporal scales, Proceedings of the 28th Liege International Astrophysical Colloquium, Liege, Belgium, 1989 (updated 1991).

Fleig, A.J., P.K. Bhartia, C.G. Wellemeyer, and D.S. Silberstein, Seven years of total ozone from the TOMS instrument—a report on data quality, *Geophys. Res. Lett., 13*, 1355–1358, 1986.

Garcia, R.R., and S. Solomon, A possible relationship between interannual variability in Antarctic ozone and the quasi-biennial oscillation, *Geophys. Res. Lett., 14*, 848–851, 1987.

Gardiner, B.G., Comparative morphology of the vertical ozone profile in the Antarctic spring, *Geophys. Res. Lett., 15*, 901–904, 1988.

Götz, F.W.P., Zum Strahlungsklima des Spitzbergen Sommers, *Gerlands Beitrage zur Geophys., 31*, 119–154, 1931.

Hauchecorne, A., M.L. Chanin, and P. Keckhut, Climatology and trends of the middle atmospheric temperature (33–87 km) as seen by Rayleigh lidar over the south of France, *J. Geophys. Res., 96*, 15297–15309, 1991.

Heath, D.F., A.J. Krueger, and P.J. Crutzen, Solar proton event: influence on stratospheric ozone, *Science, 197*, 886–888, 1977.

Herman, J.R., R. Hudson, R. McPeters, R. Stolarski, Z. Ahmad, X.-Y. Gu, S. Taylor, and C. Wellemeyer, A new self-calibration method applied to TOMS/SBUV backscattered ultraviolet data to determine long-term global ozone change, *J. Geophys. Res., 96*, 7531–7545, 1991.

Hilsenrath, E., and B.M. Schlesinger, Total ozone seasonal and interannual variations derived from the 7-year Nimbus-4 BUV data set, *J. Geophys. Res., 86*, 12087–12096, 1981.

Hofmann, D.J., J.W. Harder, J.M. Rosen, J.V. Hereford, and J.R. Carpenter, Ozone profile measurements at McMurdo Station, Antarctica during the spring of 1987, *J. Geophys. Res., 94*, 16527–16536, 1989.

Jäger, H., and K. Wege, Stratospheric ozone depletion at northern midlatitudes after major volcanic eruptions, *J. Atmos. Chem., 10*, 273–20, 1990.

Kokin, G.A., Ye. V. Lysenko, and S.Kh. Rozenfeld, Temperature changes in the stratosphere and mesosphere in 1964–1988 based on rocket sounding data, *Izvestiya, Atmospheric and Oceanic Physics, 26*, 518, 1990.

Komhyr, W.D., R.D. Grass, and R.K. Leonard, Total ozone, ozone vertical distribution, and stratospheric temperatures at South Pole, Antarctica, in 1986 and 1987, *J. Geophys. Res., 94*, 11429–11436, 1988.

Labitzke, K., B. Naujokat, and M.P. McCormick, Temperature effects on the stratosphere of the April 4, 1982, eruption of El Chichón, Mexico, *Geophys. Res. Lett., 10*, 24–26, 1983.

Labitzke, K., and H. van Loon, Some complications in determining trends in the stratosphere, *Adv. Space Res., 11*, (3)21–(3)30, 1991.

Lait, L.R., M.R. Schoeberl, and P.A. Newman, Quasi-biennial modulation of Antarctic ozone, *J. Geophys. Res.*, 94, 11559–11571, 1989.

Lapworth, A., Report of a re-evaluation of total ozone data from the UK Dobson network for the last decade, UK Meteorological Office Manuscript, 1991.

Lefèvre, F,. and D. Cariolle, Total ozone measurements and stratospheric cloud detection during the AASE and the TECHNOPS Arctic balloon campaign, *Geophys. Res. Lett., 18*, 33–36, 1991a.

Lefèvre, F., D. Cariolle, S. Muller, and F. Karcher, Total ozone from TOVS/HIRS2 infrared radiances during the formation of the 1987 "ozone hole", *J. Geophys. Res., 96*, 12893–12911, 1991b.

Logan, J.A., Tropospheric ozone: seasonal behavior, trends, and anthropogenic influence, *J. Geophys. Res., 90*, 10463–10482, 1985.

Mateer, C.L., and J.J. DeLuisi, A new Umkehr inversion algorithm, Manuscript, 1991.

McCormick, M.P., and J.C. Larsen, Antarctic springtime measurements of ozone, nitrogen dioxide, and aerosol extinction by SAM II, SAGE, and SAGE II, *Geophys. Res. Lett., 13*, 1280–1283, 1986.

McCormick, M.P., and J.C. Larsen, Antarctic measurements of ozone by SAGE II in the spring of 1985, 1986, and 1987, *Geophys. Res. Lett., 15*, 907–910, 1988.

McCormick, M.P., J.M. Zawodny, R.E. Veiga, J.C. Larsen, and P. H. Wang, An overview of SAGE I and II ozone measurements, *Planet. Space Sci., 37*, 1567–1586, 1989.

McCormick, M.P., R.E. Veiga, and W.P. Chu, Stratospheric ozone profile and total ozone trends derived from the SAGE I and SAGE II data, *Geophys. Res. Lett., 19*, 269–272, 1992.

McPeters, R.D., and C.H. Jackman, The response of ozone to solar proton events during solar cycle 21: the observations, *J. Geophys. Res., 90*, 7945–7954, 1985.

McPeters, R.D., and W.D. Komhyr, Long-term changes in TOMS relative to World Primary Standard Dobson Spectrometer 83, *J. Geophys. Res. 96*, 2987-2993, 1991.

Michelangeli, D.V., M. Allen, and Y.L. Yung, El Chichón volcanic aerosols: impact of radiative, thermal, and chemical perturbations, *J. Geophys. Res., 94*, 18429–18444, 1989.

Miller, A.J., R.M. Nagatani, G.C. Tiao, X.F. Niu, G.C. Reinsel, D. Wuebbles, and K. Grant, Comparisons of observed ozone and temperature trends, submitted to *Geophys. Res. Lett.*, 1991.

Newman, P.A., M.R. Schoeberl, and L.R. Lait, Comparison of the Southern Hemisphere springs of 1988 and 1987, Proceedings of the NATO Advanced Research Workshop on Dynamics, Transport and Photochemistry in the Middle Atmosphere of the Southern Hemisphere, San Francisco, CA, USA, April 15–17, 1989, Kluwer Academic Publishers, Dordrecht, The Netherlands, 1990.

Newman, P., R. Stolarski, M. Schoeberl, R. McPeters, and A. Krueger, The 1990 Antarctic ozone hole as observed by TOMS, *Geophys. Res. Lett., 18*, 661–664, 1991.

Oort, A.H., and H. Liu, Upper air temperature trends over the globe, 1958–1989, *J. Climate*, submitted, 1991.

Paur, R.J., and A.M. Bass, The ultraviolet cross-sections of ozone: II. Results and temperature dependence, in Atmospheric Ozone, Ed. by C.S. Zerefos and A.M. Ghazi, Reidel, Dordrecht, 611–616, 1985.

Penkett, S.A., Indications and causes of ozone increases in the troposphere, in The Changing Atmosphere, edited by F.S. Rowland and I.S.A. Isaksen pp. 91–103, Wiley-Interscience, New York, 1988.

Pommereau, J.P., F. Goutail, H. LeTexier, and T.S. Jorgensen, Stratospheric ozone and nitrogen dioxide monitoring at southern and northern polar latitudes, Proc. of the 28th International Astrophysical Colloquium, Liege, Belgium, 1989.

Proffitt, M.H., M.J. Steinkamp, J.A. Powell, R.J. McLaughlin, O.A. Mills, A.L. Schmeltekopf, T L. Thompson, A.F. Tuck, T. Tyler, R.H. Winkler, and K.R. Chan, In-situ ozone measurements within the 1987 Antarctic ozone hole from a high altitude ER-2 aircraft, *J. Geophys. Res., 94*, 16547–16556, 1989.

Randel, W.J., The anomalous circulation in the Southern Hemisphere stratosphere during spring 1987, *Geophys. Res. Lett., 15*, 911–914, 1988.

Reid, G.C., S. Solomon, and R.R. Garcia, Response of the middle atmosphere to the solar proton events of August–December, 1989, *Geophys. Res. Lett., 18*, 1019–1022, 1991.

Reinsel, G.C., G.C. Tiao, A.J. Miller, D.J. Wuebbles, P.S. Connell, C.L. Mateer, and J.J. DeLuisi, Statistical analysis of total ozone and stratospheric Umkehr data for trends and solar cycle relationship, *J. Geophys. Res., 92*, 2201–2209, 1987.

Reinsel, G., G.C. Tiao, M.N. Wang, R. Lewis, and D. Nychka, Statistical analysis of stratospheric ozone for the detections of trends, *Atmos. Envir., 15*, 1569–1577, 1981.

Reinsel, G.C., G.C. Tiao, J.J. DeLuisi, S. Basu, and K. Carreise, trend analysis of aerosol-corrected Umkehr ozone profile data through 1987, *J. Geophys. Res., 94*, 16373–16386, 1989.

Solomon, S., and P.J. Crutzen, Analysis of the August 1972 solar proton event including chlorine chemistry, *J. Geophys. Res., 86*, 1140–1146, 1981.

Staehelin, J., and W. Schmid, Trend analysis of tropospheric ozone concentrations utilizing the 20-year data set of ozone balloon soundings over Payerne (Switzerland), *Atmos. Envir., 25a*, 1739–1749, 1991.

Stolarski, R.S., M.R. Schoeberl, P.A. Newman, R.D. McPeters, and A.J. Krueger, The 1989 Antarctic ozone hole as observed by TOMS, *Geophys. Res. Lett., 17*, 1267–1270, 1990.

Stolarski, R.S., P. Bloomfield, R.D. McPeters, and J. R. Herman, Total ozone trends deduced from Nimbus-7 TOMS data, *Geophys. Res. Lett., 18*, 1015–1018, 1991.

Tiao, G.C., G.C. Reinsel, J.H. Frederick, G.M. Allenby, C.L. Mateer, A.J. Miller, and J.J. DeLuisi, A statistical trend analysis of ozonesonde data, *J. Geophys. Res., 91*, 13121–13136, 1986.

Veiga, R.E., and W.P. Chu, Validation of SAGE I and SAGE II ozone in the lower stratosphere, EOS Trans. of the AGU, 72, 68, 1991.

von Cossart, G., and J. Taubenheim, Solar cycle and long-period variations of mesospheric temperatures, *J. Atmos. Terr. Phys., 49*, 303–307, 1987.

WMO, Report of the International Ozone Trends Panel: 1988, World Meteorological Organization Global Ozone and Monitoring Network Report #18, WMO, Washington, DC, 1990a.

WMO, International Ozone Assessment: 1989, World Meterological Organization Global Ozone and Monitoring Network Report #20, WMO, Washington, DC, 1990b.

Zawodny, J.M., and M.P. McCormick, Stratospheric aerosol and gas experiment II measurements of the quasi-biennial oscillations in ozone and nitrogen dioxide, *J. Geophys. Res., 96*, 9371–9378, 1991.

Zerefos, C.S., and P.J. Crutzen, Stratospheric thickness variations over the Northern Hemisphere and their possible relation to solar activity, *J. Geophys. Res., 80*, 5041–5043, 1975.

Zerefos, C.S., A.F. Bais, L.C. Ziomas, and R.D. Bojkov, On the relative importance of QBO and ENSO in the revised Dobson total ozone records, *J. Geophys. Res.*, submitted, 1991a.

Zerefos, C.S., A.F. Bais, K. Ziomas, and R.D. Bojkov, Total ozone forcing from El Niño events, Paper presented at the XV IUGG General Assembly, Vienna, Austria., 1991b.

CHAPTER 3

Heterogeneous Processes: Laboratory, Field, and Modeling Studies

Authors:

L.R. Poole
R.L. Jones
M.J. Kurylo
A. Wahner

Additional Contributors:

J.G. Calvert
A. Fried
R.F. Hampson
D.J. Hofmann
L.F. Keyser
C.E. Kolb
M.-T. Leu
M.J. Molina
M.C. Pitts
A.R. Ravishankara
L.W. Thomason
M.A. Tolbert
D.R. Worsnop

Chapter 3

Heterogeneous Processes: Laboratory, Field, and Modeling Studies

Contents

SCIENTIFIC SUMMARY

Since the previous assessment, there have been major advances in understanding the role of heterogeneous reactions on Polar Stratrospheric Clouds (PSCs) and stratospheric sulfate (H_2SO_4/H_2O) aerosols in increasing the abundance of active chlorine compounds in the lower stratosphere.

Reaction Efficiencies: Direct chlorine activation, *e.g.*, via $ClONO_2(g) + HCl(s) \rightarrow Cl_2(g) + HNO_3(s)$ is very efficient on surfaces which mimic PSCs. Denoxification, *e.g.*, $N_2O_5(g) + H_2O(s) \rightarrow 2\ HNO_3(s)$, is very efficient on H_2SO_4/H_2O surfaces typical of mid-latitude stratospheric aerosols and indirectly enhances active chlorine by inhibiting formation of the reservoir $ClONO_2$. Direct chlorine activation on sulfate aerosols may also occur under volcanic conditions or at very cold temperatures, the latter becoming more important with expected future increases in stratospheric H_2O vapor. Furthermore, there may be other important heterogeneous processes that have not yet been identified.

PSC Physical Characteristics: Additional laboratory studies have confirmed that HNO_3/H_2O clouds can form above the frost point. Significant HNO_3 supersaturation may be required for Type 1 PSC formation, implying that heterogeneous processing by sulfate aerosols may be more important at lower temperatures than previously thought. Type 1 PSCs may exist in two subclasses, which, in turn, may have different surface area characteristics and different heterogeneous processing efficiencies. HNO_3 has been shown to stick readily on pure ice and retard its sublimation, supporting the idea that falling ice crystals are responsible for stratospheric denitrification.

SAM II PSC Climatology:
Antarctic: Average PSC sighting frequency peaks at about 60 percent near 18 km in August. Sighting frequency remains at 10 to 20 percent at lower altitudes—under dehydrated and denitrified conditions—well past the spring equinox. Individually or collectively, the high PSC frequency and persistence of the clouds into sunlit conditions provide firm evidence of a direct link between heterogeneous chlorine activation and South Polar ozone losses.

Arctic: Appreciable PSC sightings occur only from December through February, and the peak average sighting frequency is only about 10 percent. However, the limited spatial coverage of Stratospheric Aerosol Measurements (SAM) II likely yields an underestimate of cloud frequency in the polar region as a whole. More robust PSC statistics will be required before the relationship between lower stratospheric ozone losses in the Northern Hemisphere and heterogeneous chlorine activation on Arctic PSCs can be quantified.

Stratospheric Sulfate Aerosols: Long-term observational records all show a 40 to 50 percent increase in loading over the decade from 1979 to 1989. The effective aerosol surface area available for heterogeneous chemical processing most likely increased by a comparable amount on a global scale during the same period. Additional loading from the June 1991 Mt. Pinatubo eruption will most likely be the greatest of the century to date (exceeding that of El Chichón) and is expected to persist for several years.

Heterogeneous processes must be included in stratospheric chemistry models. Measurements of ClO and HNO_3 are better explained by model calculations that include heterogeneous processing on PSCs and sulfate aerosols. Since there have been more extensive measurements of chemical changes in the polar regions, the picture of heterogeneous processing on PSCs is clearer. Direct heterogeneous chlorine activation in these clouds appears to be rapid and may not be dependent on detailed particle characteristics. Experimental opportunities provided by the Mt. Pinatubo injection should yield the data required to examine this issue more fully with regard to sulfate aerosols.

3.1 INTRODUCTION

The efficiencies of chemical families such as ClO_x and NO_x for altering the total abundance and distribution of stratospheric ozone are controlled by a partitioning between reactive (active) and nonreactive (reservoir) compounds within each family. Gas phase thermodynamics, photochemistry, and kinetics would dictate, for example, that only about 1 percent of the chlorine resident in the lower stratosphere would be in the form of active Cl or ClO, the remainder existing in the reservoir compounds HCl and $ClONO_2$. The consistency of this picture has recently been challenged by the recognition that important chemical transformations take place on polar stratospheric cloud (PSC) particles in both polar regions (The Airborne Antarctic Ozone Experiment (AAOE), Parts 1 and 2, 1989; The Airborne Arctic Stratospheric Expedition (AASE), 1990). Following the discovery of the Antarctic ozone hole, Solomon *et al.* (1986) suggested that the heterogeneous chemical reaction:

$$ClONO_2(g) + HCl(s) \rightarrow Cl_2(g) + HNO_3(s) \qquad (3\text{-}1)$$

could play a key role in converting chlorine from inactive forms into a species (Cl_2) that would rapidly dissociate in sunlight to liberate atomic chlorine and initiate ozone depletion. The symbols (s) and (g) denote solid phase, or adsorbed onto a solid surface, and gas phase, respectively, and represent the approach by which such a reaction is modeled rather than the microscopic details of the reaction. Reaction (3-1) was expected to be most important at altitudes where PSCs were most prevalent (10 to 25 km), thereby extending the altitude range over which chlorine compounds can efficiently destroy ozone from the 35 to 45 km region (where concentrations of active chlorine are usually highest) to lower altitudes where the ozone concentration is at its peak.

Direct measurements of ozone depletion and enhancements of ClO have strongly supported the Solomon *et al.* (1986) hypothesis and have prompted laboratory studies of Reaction (3-1), and several others on surfaces that mimic the suspected composition of the two main types of PSCs (nitric acid trihydrate, or NAT, Type 1; and water ice, Type 2):

$$ClONO_2(g) + H_2O(s) \rightarrow HOCl(g) + HNO_3(s) \qquad (3\text{–}2)$$
$$N_2O_5(g) + HCl(s) \rightarrow ClNO_2(g) + HNO_3(s) \qquad (3\text{–}3)$$
$$N_2O_5(g) + H_2O(s) \rightarrow 2\,HNO_3(s) \qquad (3\text{–}4)$$

Since both PSC types are likely to be doped with HCl in the stratosphere, studies have also examined the direct role of HCl on the surface reactions. In addition to the effect that Reactions (3-1) to (3-3) have on chlorine partitioning, all four reactions play an equally important role in sequestering odd nitrogen species as HNO_3, a process that has been popularly termed "denoxification." Although the condensed HNO_3 may be released as vapor if the PSCs evaporate, HNO_3 vapor is quite inert photochemically in the winter polar stratosphere. The sequestration of odd nitrogen helps to maintain high levels of active chlorine by retarding the reformation of the reservoir $ClONO_2$ via the gas phase reaction between ClO and NO_2. Furthermore, if the PSC particles involved grow large enough to undergo appreciable sedimentation, the odd nitrogen is irreversibly transferred (denitrification) from a higher altitude region to a lower one (Hübler *et al.*, 1990).

The efficiencies of such heterogeneous reactions on PSCs coupled with observations of significant ozone loss and ClO enhancement outside of the polar regions have prompted speculation about the role of the H_2SO_4/H_2O (sulfate) stratospheric aerosol layer in promoting similar chemical repartitioning. Studies have focused on Reactions (3-1) to (3-4) occurring on H_2SO_4/H_2O surfaces as well as the physical uptake of HCl and HNO_3 (where 1 = liquid):

$$HCl(g) + H_2SO_4/H_2O(l,s) \rightarrow HCl(l,s) + H_2SO_4/H_2O(l,s) \qquad (3\text{-}5)$$
$$HNO_3(g) + H_2SO_4/H_2O(l,s) \rightarrow HNO_3(l,s) + H_2SO_4/H_2O(l,s) \qquad (3\text{-}6)$$

This chapter will briefly review the current state of knowledge of heterogeneous processes in the stratosphere, emphasizing those results obtained since WMO (1990). Sections are included on laboratory investigations of heterogeneous reactions, the characteristics and climatology of PSCs, stratospheric sulfate aerosols, and evidence of heterogeneous chemical processing.

3.2 LABORATORY MEASUREMENTS

Laboratory studies of heterogeneous reactions generally result in a determination of the mass accommodation coefficient (α), or the fractional loss of a species from the gas phase upon collision with a surface. If such surface contact results in an irreversible transformation of the species, then the mass accommodation coefficient can be equated to a reac-

tion probability (γ). While the interpretation of the results from these studies can be quite complex, the field has matured rapidly since the initial reports by Molina *et al.* (1987) and Tolbert *et al.* (1987). Based on some of the most recent measurements, a reasonable consensus of reaction probabilities on PSC-like surfaces for Reactions (3-1) to (3-4) can be presented (Table 3–1). As will be pointed out, inconsistencies among some previous results can possibly be attributed to concentration effects whereby either the nature of the surface is altered or the experimental conditions are not completely representative of the stratosphere. This underscores the importance of determining reactant loss rates and the effects of the incorporation of HCl and HNO_3 into the solid surface at stratospheric concentration levels. Nevertheless, it should be emphasized that no measurements of reaction probabilities have yet been made on realistic PSC particles. Hence, there may be subtle differences in γ values among various laboratory studies and between laboratory results and the real atmosphere that can be attributed to actual surface characteristics. The reader should note that a far more extensive review and evaluation of laboratory data for heterogeneous processes is being conducted by the NASA Panel for Data Evaluation as part of its assessment of kinetic and photochemical data for use in stratospheric modeling. This review will be published as a 1992 Jet Propulsion Laboratory report and should be consulted by those seeking more detailed information, including estimates of uncertainties.

An explanation for the wide range of γ values for Reaction (3–2) on water ice and NAT surfaces that have appeared in the literature has been proposed by Hanson and Ravishankara (1991a), who suggest that passivation of the water-ice surface by the product HNO_3 at high reactant concentrations would account for the earlier low values of γ (Leu, 1988a; Molina *et al.*, 1987; Tolbert *et al.*, 1987). Similar saturation effects have been noted by M. A. Tolbert (private communication, 1991). While this issue can be fully reconciled only by further study, the plausibility of this explanation provides the basis for the recommended values of γ given here.

Hanson and Ravishankara (1991a) observed no measurable difference in γ for Reactions (3–1) and (3–2) on water ice and interpreted the HCl enhancement of previous studies (Leu, 1988a; Molina *et al.*, 1987) to be associated with a passivated HNO_3/H_2O surface rather than one of pure ice. Hanson and Ravishankara (1991b) and Abbatt *et al.* (1992) report that HOCl produced in Reaction (3–2) rapidly reacts with HCl on ice to yield $Cl_2(g)$ and $H_2O(s)$. Thus, the mechanism for Reaction (3–1) on ice probably involves two steps (*i.e.*, the formation of HOCl, followed by its immediate heterogeneous conversion into Cl_2), and the differentiation between reactions (3–1) and (3–2) is perhaps moot. However, the HOCl + HCl heterogeneous reaction itself provides a mechanism for the conversion of HCl into active chlorine under low NO_x conditions when $ClONO_2$ is suppressed (Prather, 1992). Such a mechanism has not been quantitatively investigated in atmospheric models to date with respect to polar ozone depletion.

Table 3–1: Reaction Probabilities (γ) on PSC-like Surfaces

Reaction	γ_{ice}	γ_{NAT}
(3–1) $ClONO_2 + HCl$	0.3	0.3
(3–2) $ClONO_2 + H_2O$	0.3	0.006
(3–3) $N_2O_5 + HCl$	see text	0.003
(3–4) $N_2O_5 + H_2O$	0.03	0.0006

The γ for Reaction (3–2) was determined to be significantly lower on NAT surfaces than on water ice (Hanson and Ravishankara, 1991a; Moore *et al.*, 1990; Leu *et al.*, 1991). These groups also report a subsequent enhancement of γ with HCl present on the NAT surface (Reaction 3–1), approaching that obtained on pure water ice. Thus, unlike the case for the reaction $ClONO_2 + H_2O$, the direct heterogeneous reaction between $ClONO_2$ and HCl does apparently occur on Type1 PSCs.

On water ice, values for γ recently measured for Reaction (3–4) are in good agreement (Hanson and Ravishankara, 1991a; Leu, 1988b; and Quinlan *et al.*, 1990). Because of the lower reaction probability, saturation effects are less pronounced than in the case of Reaction (3–2). However, there is some evidence that Reaction (3–4) may be somewhat faster in a liquid water droplet than on water ice (Van Doren *et al.*, 1990). Hanson and Ravishankara (1991a) observed no enhancement of γ when HCl was present in the ice (Reaction 3–3) at concentrations representative of the stratosphere and suggested that the enhancements observed by Leu (1988b) might be attributable to the very high concentrations of HCl used. Thus, there is no unequivocal evidence for chlorine activation via

Reaction (3–3) on water ice surfaces under stratospheric conditions. On NAT surfaces, Hanson and Ravishankara (1991a) obtained a value of γ for Reaction (3–4) a factor of 50 lower than that on water ice. The much larger value determined by Quinlan *et al.* (1990) at higher reactant concentrations may be associated with formation of a condensed phase of supercooled HNO_3 liquid on which the reaction probability may be much greater than on NAT. Finally, Hanson and Ravishankara (1991a) observed a factor of 5 increase in γ for the reaction of N_2O_5 on NAT when HCl is present (Reaction 3–3), suggesting that N_2O_5 preferentially reacts with HCl rather than with H_2O on Type 1 PSCs.

Reactions (3–1), (3–2), and (3–4) have also been studied extensively on H_2SO_4/H_2O surfaces, as has the physical uptake of HCl and HNO_3 (Reactions 3–5 and 3–6). (See Tables 3–2 and 3–3). For Reaction (3–2), the measurements by Reihs *et al.* (1991) and by Hanson and Ravishankara (1991c) as a function of H_2SO_4 weight percentage (W) yield values for γ that are in excellent agreement and imply that this reaction is an unlikely source of perturbed stratospheric chemistry on a global scale. Relative to Reaction (3–2), a 10-fold reduction in γ was observed by Hanson and Ravishankara (1991c) and Tolbert *et al.* (1988) for the reaction with HCl to produce chlorine (Reaction 3–1). Since these measurements were made for surface compositions typical of mid-latitude stratospheric aerosols (~60 to 75 percent H_2SO_4 by weight), the results are not necessarily valid for surfaces rarer in H_2SO_4. With regard to this point, Hanson and Ravishankara (1991c) and M.-T. Leu, S.B. Moore, and L.F. Keyser (private communication, 1991) confirm the observations of Watson *et al.* (1990) that the uptake of HCl on sulfuric acid aerosols (Reaction 3–5) is strongly dependent on the H_2SO_4 fraction and that there is a rapid equilibration with gas phase HCl in the stratosphere (see Table 3–3). Thus, $ClONO_2$ is more likely to react with H_2O in a H_2SO_4/H_2O particle than with the dissolved HCl. While these combined observations suggest that Reaction (3–1) on stratospheric aerosols will not be a significant source of active chlorine, Hofmann and Solomon (1989) point out that large increases in aerosol surface area following volcanic eruptions could lead to important enhancements in the production of HOCl via Reaction (3–2). In the polar regions, direct chlorine activation on H_2SO_4/H_2O aerosols can possibly take on added significance. For example, Wolff and Mulvaney (1991) have suggested that water-rich aerosols (<60 percent H_2SO_4 by weight), which can absorb significant levels of HCl, may be present under polar stratospheric conditions. Should stratospheric H_2O vapor content increase with time, such as from the oxidation of CH_4, aerosols in these cold regions would become even more water rich (Steele and Hamill, 1981), which could lead to enhanced direct chlorine activation.

Table 3–2: Reaction Probabilities (γ) on Sulfuric Acid/Water Surfaces

Reaction	Probability
(3–1) $ClONO_2 + HCl + H_2SO_4/H_2O$	0.1 x γ for Reaction (3–2)
(3–2) $ClONO_2 + H_2SO_4/H_2O$	$\log_{10}(\gamma) = 1.87 - 0.074W$*
(3–4) $N_2O_5 + H_2SO_4/H_2O$	0.1

* W = wt. % H_2SO_4

Unlike Reactions (3–1) and (3–2), Reaction (3–4) appears to occur quite rapidly on sulfuric acid/water surfaces with a γ that is relatively independent of temperature and of H_2SO_4 fraction (Hanson and Ravishankara, 1991b; Mozurkewich and Calvert, 1988; Reihs *et al.*, 1991; Van Doren *et al.*, 1991; and A. Fried, M. Mozurkewich, B. Henry, and J.G. Calvert, private communication, 1991). Thus, this reaction represents an important loss process for NO_x and a source of HNO_3 the condensed phase concentration of which is limited by its solubility (Van Doren *et al.*, 1991; Reihs *et al.*, 1990). Such NO_y repartitioning affects stratospheric ozone through both the NO_x and ClO_x cycles (reducing the efficiency of the former and increasing that of the latter).

With respect to data on mass accommodation coefficients alone (see Table 3–3), values of α for HCl (Hanson and Ravishankara, 1991a; Leu, 1988a) and HNO_3 (Leu, 1988a) on pure ice are large, as is that for HNO_3 on concentrated sulfuric acid surfaces (Van Doren *et al.*, 1991). Direct uptake of HNO_3 on H_2SO_4/H_2O is, however, subject to the same solubility limitations as the HNO_3 produced in Reaction (3–4) (Van Doren *et al.*, 1991; Reihs *et al.*, 1990). It is also of note that direct HNO_3 uptake on water ice leads to NAT formation, which reduces further HNO_3 uptake. Such direct uptake may be important in denitrification of the stratosphere (Wofsy *et al.*, 1990) and in contrails of high-speed civil transports (HSCTs).

The uptake of HCl on NAT surfaces is unresolved at present, with reported α values ranging from ≥ 0.3 (Hanson and Ravishankara, 1991b) to between 8×10^{-3} and 9×10^{-7} (Leu *et al.*, 1991). While the latter measurements may have been subject to solubility limitations, further work is required to reconcile this issue.

The role of these heterogeneous reactions has greatly revised current thinking about stratospheric chemistry and continues to be investigated through direct laboratory studies and intensive atmospheric measurement campaigns. The latter are aimed at assessing the cause(s) of enhanced ozone loss in the Northern Hemisphere, the potential for ozone changes associated with CFC substitute usage or commercial HSCTs, and the role that severe polar ozone loss plays in altering total ozone at neighboring mid-latitudes.

Table 3–3: Mass Accommodation Coefficients (α) on Ice and Sulfuric Acid/Water Surfaces

	Reaction	On Ice	On 60–75 wt. % H_2SO_4
(3–5)	$HCl + H_2SO_4/H_2O$	> 0.2	$4x10^{-4*}$–10^{-5*}
(3–6)	$HNO_3 + H_2SO_4/H_2O$	> 0.2	> 0.1

*Effective uptake coefficient; mass accommodation coefficient has not been measured at low HCl solubilities; for Reaction (3–5), increases by 10^2–10^3 below 50 percent H_2SO_4.

3.3 POLAR STRATOSPHERIC CLOUD CHARACTERISTICS AND CLIMATOLOGY

Data collected during recent Arctic field campaigns have provided additional insight into PSC formation mechanisms and physical characteristics. Particle measurements during AASE (Dye *et al.*, 1991) showed some Type 1 PSC particles formed at temperatures around 195 K, or near HNO_3 saturation with respect to NAT, the suspected composition of Type 1 particles. However, extensive cloud particle formation was not observed until saturation ratios were near 10, a finding supported by balloon-borne observations of Schlager *et al.* (1990) and Hofmann *et al.* (1990). These results suggest that relatively few H_2SO_4/H_2O aerosols are frozen at HNO_3 saturation and that further cooling (to about 192 K) is required for the remainder to freeze and serve as PSC nuclei. It should be noted that there is no direct observational evidence to date of frozen H_2SO_4/H_2O particles in the stratosphere. Analyses of AASE lidar data (Browell *et al.*, 1990; Toon *et al.*, 1990a) revealed two subclasses of Type 1 PSCs, both appearing at temperatures at or below the equilibrium threshold for NAT. Type 1a PSCs are composed of nonspherical particles having a volume equivalent radius ≥ 1.0 µm, while Type1b clouds have spherical or nearly spherical particles with typical radii near 0.5 µm. Toon *et al.* (1990a) suggested that air parcel cooling rate and the extent to which parcels cool below the initial condensation point were important factors in determining particle characteristics. Other lidar data (McCormick *et al.*, 1990; Poole *et al.*, 1990) showed broad spatial coverage of Type 1b PSCs and systematic evolution of cloud optical properties with decreasing temperature.

A great deal has been learned (and many questions have been raised) about PSC physical chemistry from recent laboratory studies. New vapor pressure measurements (D. R. Worsnop, private communication, 1991) have confirmed that NAT forms at temperatures some 4 to 6 K above the ice point, in support of a previous finding of Hanson and Mauersberger (1988). The new measurements have also observed saturation ratios up to 10 for HNO_3 vapor over ice surfaces, suggestive of the ratio required for Type 1 PSC nucleation on H_2SO_4/H_2O aerosols as discussed above. Ritzhaupt and Devlin (1991), Tolbert and Middlebrook (1990), and Smith *et al.* (1991) have measured the infrared spectra of thin films of condensed H_2O/HNO_3 mixtures. Each group has reported a set of three similar spectra, although with different chemical assignments. Ritzhaupt and Devlin (1991) and Tolbert and Middlebrook (1990) identified nitric acid monohydrate, trihydrate, and dihydrate spectra, while Smith *et al.* (1991) ascribed the same spectra to monohydrate, trihydrate, and mixed ice/trihydrate phases. In addition, Koehler *et al.* (1991) suggest that two forms of NAT are possible: an α-NAT formed at colder temperatures, and a β-NAT formed at warmer temperatures and higher H_2O vapor pressures or, alternatively, by heating α-NAT. There are no direct atmospheric observations of these forms, nor is there laboratory evidence to suggest that they would exhibit differences in heterogeneous reactivity. Tolbert and

Middlebrook (1990) and Worsnop have also observed solid-diffusion-limited evaporation of water through thin (0.02–μm) films of NAT over ice, a finding that supports the notion of Wofsy *et al.* (1990) that falling ice crystals are responsible for denitrification of the winter polar stratosphere (as discussed in Section 3.5.3).

An updated yearly average PSC climatology has recently been derived (Pitts *et al.*, 1991) using 1–μm aerosol extinction data for 1979–1989 from the SAM II sensor aboard Nimbus 7. The Nimbus 7 orbit has degraded to a point such that no SAM II measurements have been possible during Arctic winter since early 1990. Thus, data beyond 1989 were excluded from the analysis, as were some data from 1982 to 83 which were masked by El Chichón volcanic aerosols. The latitude of SAM II measurements varies slowly from about 64° at the winter solstices to about 80° at the spring equinoxes. Hence, early to midwinter observations are typical of conditions near the edge of the polar vortex and likely yield an underestimate of PSC frequencies in the polar regions as a whole. Observations in late winter are more representative of the vortex interior. In light of this systematic variation, it is impractical to use SAM II data to derive seasonal statistics on the fraction of PSCs that form outside the polar vortices.

The results (Figure 3–1) show hemispheric differences in PSC sighting frequency that are consistent with seasonal temperature patterns as well as with the behavior reported in WMO (1990). Antarctic sightings normally begin in May, and average sighting frequency generally increases at all altitudes as winter progresses, reaching a seasonal peak of about 60 percent near 18 km in August. The frequency falls sharply at higher altitudes (as local temperatures rise) after August, but continues at the 10 to 20 percent level well into October at the lower altitudes. Thus, it is clear that Antarctic PSCs continue to form even under dehydrated and denitrified conditions and, on average, persist well past the spring equinox. Individually or collectively, the high PSC frequency and the persistence of the clouds into sunlit conditions provide firm evidence of a direct link between heterogeneous chlorine activation and South Polar ozone losses.

The season for appreciable Arctic PSC sightings extends only from December through February, and the peak average sighting frequency is only about 10 percent. The sighting frequency for Arctic PSCs in March is well below 1 percent on average and exceeded 1 percent in only 2 of the 10 years of measurements analyzed. There have been no Arctic PSC sightings by SAM I during the month of April. While these lower frequencies are consistent with warmer average temperatures (relative to the Antarctic), absolute values are more uncertain due to possible systematic underestimation caused by the limited spatial coverage of SAM II. More robust PSC statistics will be required before the relationship between lower stratospheric ozone losses in the Northern Hemisphere and heterogeneous chlorine activation on Arctic PSCs can be quantified.

3.4 STRATOSPHERIC SULFATE AEROSOLS

Routine balloon-borne and lidar measurements of H_2SO_4/H_2O (sulfate) stratospheric aerosols have been conducted at several Northern Hemisphere sites since the early 1970s. These have been supplemented in a more global sense since the late 1970s with spaceborne observations by the SAM II (1978 to present), SAGE I (1979 to 1981), and SAGE II (1984 to present) sensors. Long-term trends in sulfate aerosols will be examined and discussed in this section, along with perturbations induced by major volcanic eruptions (including the June 1991 eruption of Mt. Pinatubo). There will also be a brief discussion of the use of multi-wavelength SAGE II aerosol extinction data to estimate total aerosol surface area, a critical parameter in model calculations of the efficiency of aerosols for catalyzing heterogeneous chemical reactions.

3.4.1 Long-Term Trends and Volcanic Perturbations

The record of integrated aerosol column from 15 to 20 km at Laramie, Wyoming (41° N), is shown in Figure 3–2 for particles with radii (r) ≥ 0.15 μm and ≥ 0.25 μm respectively (D.J. Hofmann, private communication, 1991). The figure also includes integrated backscatter (from the tropopause + 2 km to ≈ 30 km) obtained by the NASA Langley Research Center 48-inch ruby (λ = 0.6943 μm) lidar system (at 37°N) and is annotated to mark the occurrence of volcanic eruptions during the past two decades. The 1978 to 1979 period is commonly referred to as the "quies-

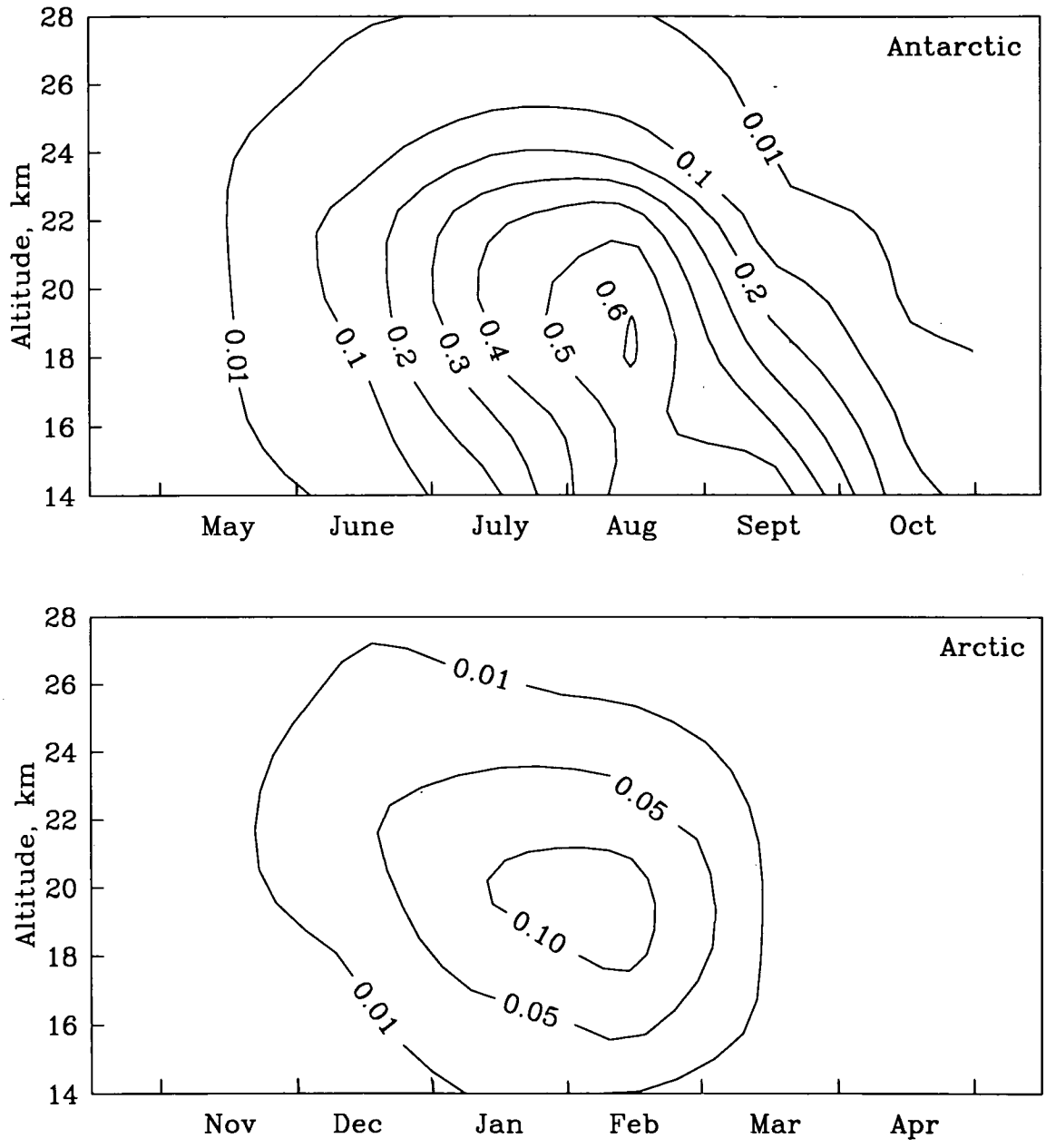

Figure 3–1 Yearly average polar stratospheric cloud sighting frequency by SAM II for the period 1979 to 1989. Sighting frequency is defined, at a particular altitude and time, as the number of observations classified as PSCs divided by the total number of observations.

cent" or "background" aerosol state since it followed by some 5 years the 1974 eruption of Fuego and preceded the series of eruptions in the early 1980s. Hofmann (1990) suggested that such a background state had again been reached by 1989 and calculated that non-volcanic aerosol mass at the stratospheric maximum had increased by 5 ± 2 percent per year over the previous decade, ostensibly due to an increase solely in the number of larger particles. The aerosol columns shown here support this earlier finding in that only the larger particles have increased (by some 40 to 50 percent) over the decade. The Langley backscatter record shows a similar decadal increase, thus demonstrating consistency between the different aerosol monitoring techniques at separate sites.

Figure 3–3 shows 1–μm optical depth (aerosol extinction integrated upward from the tropopause + 2 km) records from SAM II and SAGE I and SAGE II. The SAM II data are weekly Antarctic and Arctic (from ≈ 64° to 80°) averages, while the SAGE data are monthly Northern and Southern Hemisphere averages. The SAM II record shows distinct extrema that are not representative of subpolar sulfate aerosols and do not appear in the SAGE records. The maxima seen during winter in both hemispheres reflect PSC activity, and the sharp minima appearing during Antarctic spring signify downward transport of aerosols (likely a combination of subsidence and sedimentation) inside the Antarctic polar vortex. Away from these extrema, there has been a 40 to 50 percent increase in average optical depth in the polar regions over the decade. This is virtually matched on a global scale by the difference in the average optical depth between SAGE II in 1989 to 1990 and SAGE I in 1979.

The cause of such a consistent increase among the various data records is open to question. Hofmann (1991) suggested that the aerosol mass increase was too large to be caused by increased OCS transport from the troposphere and speculated that the remainder might be due to increases in sulfur emissions from commercial aircraft flying in the upper troposphere and lower stratosphere. Hofmann (personal communication, 1991) found that there had been no appreciable increase over the decade in the 20 to 25 km aerosol column for particles with $r \geq 0.15$ μm or $r \geq 0.25$ μm, suggesting that a lower stratospheric source may indeed be responsible for the observed mass increase. However, since the impact of major volcanic eruptions (*e.g.*, El Chichón) is very large initially and persists for several years, it is not certain that the stratosphere had totally recovered by 1989 from the combined effects of volcanoes El Chichón and Ruiz.

The stratospheric aerosol loading from the eruptions of Mt. Pinatubo will most likely be the greatest of the century to date, well in excess of that induced by the El Chichón eruption (McCormick and Veiga, 1992). Figure 3–4 shows the zonal mean (from 60°S to 60°N) 1–μm stratospheric aerosol extinction coefficient measured by SAGE II from mid-September to mid-October in 1990 (part a) and 1991 (part b). The 1991 values in the tropics and mid-latitudes are generally 1 to 2 orders of magnitude larger than corresponding 1990 values, with the increases attributable solely to the Mt. Pinatubo eruption. Since this perturbation is expected to last for several years, it is unlikely that the causes of the apparent long-term trend in aerosol loading will be clarified for some years to come.

It is reasonable to estimate that the effective aerosol surface area available for heterogeneous chemical processing likely increased globally during the 1980s by an amount comparable to the increase observed in aerosol column and optical depth. By the same token, a relatively short-term increase in total sulfate surface area of a factor of 10 to 100 can be expected from the Mt. Pinatubo eruption. One might also expect, purely from cloud microphysical principles, that such increases in sulfate aerosols would lead to similar secular increases in total PSC surface area, since the aerosols serve as PSC nuclei. This notion has not been examined (and is likely unresolvable) using current PSC observational data.

3.4.2 Estimation of Surface Area

In addition to the basic 1–μm channel, near-global aerosol extinction measurements are made by SAGE II at wavelengths of 0.385, 0.453, and 0.525 μm. These data can be coupled with Mie scattering theory to estimate total (geometric) aerosol surface area if a form for the underlying particle size distribution is assumed. Since the SAGE II measurements are not very sensitive to particles with $r < 0.1$ μm, the choice of aerosol models is somewhat arbitrary. The lognormal distribution has been more or less the standard model for past analyses of SAGE observations

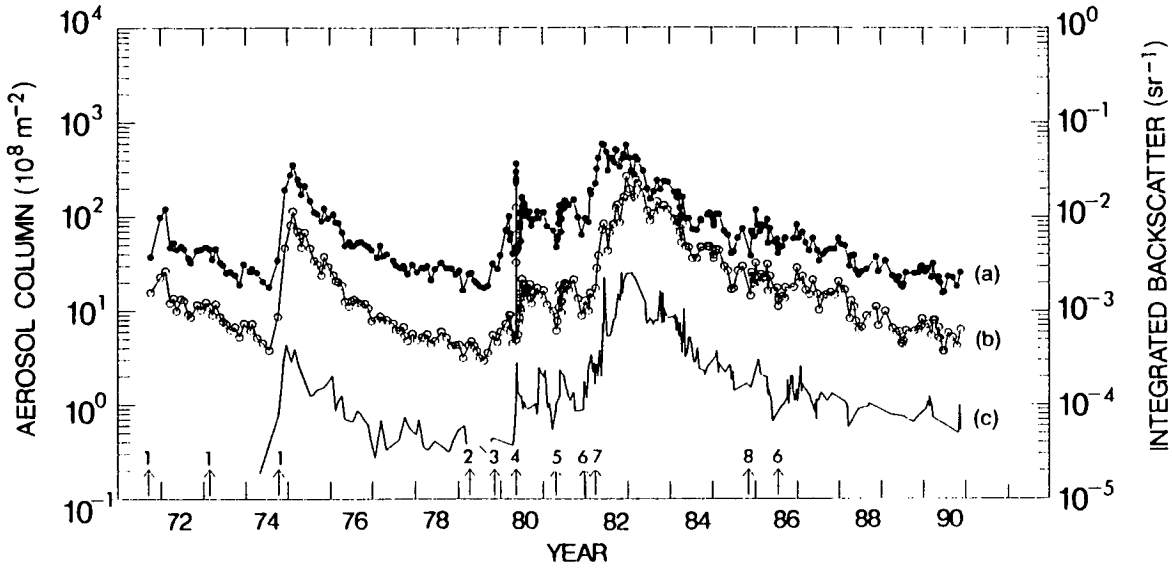

Figure 3–2 Long-term records of: (a) the aerosol column from 15 to 20 km at Laramie, Wyoming, for particles with $r \geq 0.15$ μm; (b) as in (a), but for particles with $r \geq 0.25$ μm; (c) integrated backscatter ($\lambda = 0.6943$μm) measured at NASA Langley Research Center. Volcano key: 1–Fuego, 2–La Soufriere, 3–Sierra Negra, 4–Mt. St. Helens, 5–Alaid, 6–Nyamuragira, 7–El Chichón, 8–Ruiz.

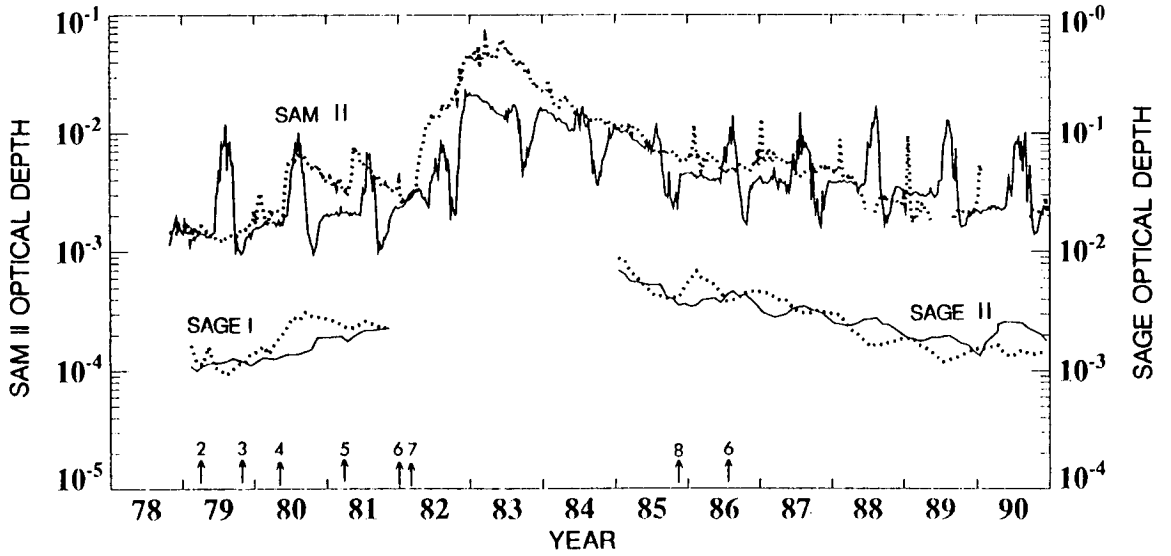

Figure 3–3 Records of 1.0–μm optical depth measured by SAM II in the Antarctic (solid curve) and Arctic (dotted curve) and by SAGE I and SAGE II in the Southern (solid curves) and Northern (dotted curves) Hemispheres. Arrows along x-axis denote volcanic eruptions, key as in Figure 3–2.

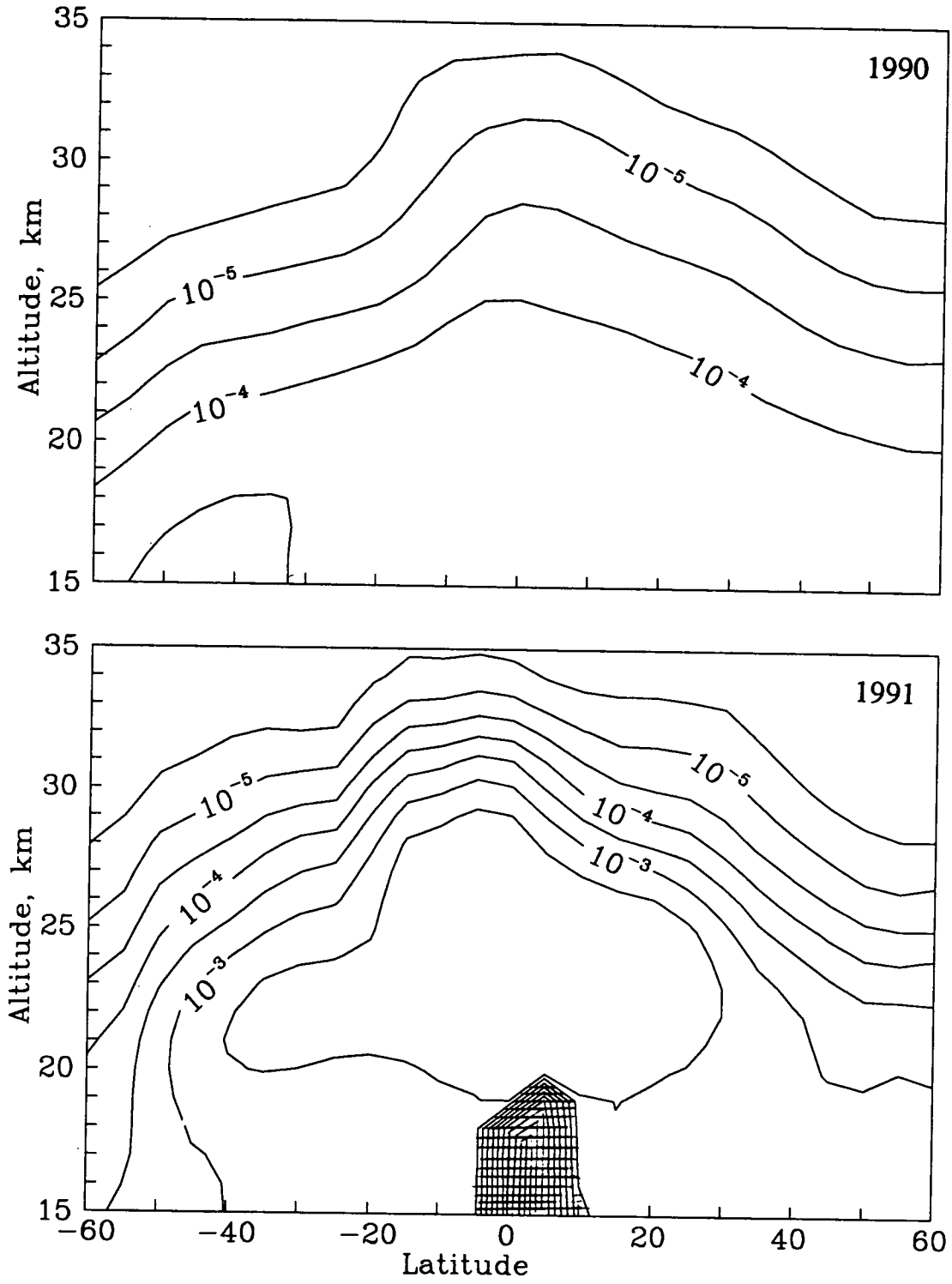

Figure 3–4 Zonal mean (60°S to 60°N) stratospheric aerosol extinction coefficient (km^{-1}) at 1 μm measured by SAGE II from mid-September to mid-October in 1990 and 1991. Values in cross-hatched region exceed the sensitivity of the instrument.

(*e.g.*, Yue and Deepak, 1983) and of *in situ* measurements as well. However, a recent study (Thomason, 1991) showed that a segmented power law model more accurately reproduces the spectral variation in SAGE II data. Total surface areas estimated using the two models exhibit similar spatial and seasonal features, and agree quantitatively to within the uncertainty of the extinction measurements. Figure 3–5 shows sample areas derived by applying the segmented power law to SAGE II data from January to March 1989. Similar estimates (smoothed for simplicity) are used in theoretical calculations described in Chapter 8 to study the efficiency of sulfate aerosols in catalyzing heterogeneous chemical reactions and, hence, in promoting ozone loss. A note of caution is in order, namely that there is no assurance that the surface area available for heterogeneous reactions on aerosols (or PSCs, for that matter) equals the geometric surface area. Discrepancies here would greatly impact the accuracy of calculated heterogeneous reaction rates.

3.5 EVIDENCE FOR HETEROGENEOUS PROCESSES IN THE STRATOSPHERE

The extensive measurements of chemical changes obtained in the polar regions during recent years have firmly established a link between heterogeneous processing by PSCs and ozone loss, especially in the Antarctic. The picture is not clear with regard to the relationship between heterogeneous processing by sulfate aerosols and observed global ozone decreases (as discussed more thoroughly in Chapter 4). Experimental opportunities provided by the Mt. Pinatubo eruption should yield a wealth of data on this issue over the next few years. In either case, many details of (and relationships between) individual mechanisms are not clear at this time. For example, the observation of elevated ClO concentrations provides in itself neither direct evidence nor quantitative information on the efficiency of individual reactions. A complete assessment of a given reaction would require that rates of change in both reactant and product concentrations be measured simultaneously. Since this has not been possible in the lower stratosphere to date, those quantitative tests that have been performed have been necessarily incomplete and indirect. The extent of such indirect tests of heterogeneous processes is described in this section.

3.5.1 Heterogeneous Reactions on PSCs

An increase in ClO concentration observed in Type 1 PSCs during the AASE ER–2 flight of January 24, 1989, was interpreted by Jones *et al.* (1990a) as *in situ* heterogeneous chlorine activation, principally via Reaction (3–1). The rate of ClO increase was quantitatively consistent with the probability for that reaction given in Table 3–1, implying a time constant for release of reactive chlorine of several hours. This verification is indirect as any concurrent decay in HCl or $ClONO_2$, or increase in Cl_2 and HNO_3, could not be monitored. No comparable test has been performed for Type 2 PSCs. The rapid rate of release compared with the time constant for reactive chlorine to return to more benign forms (days to weeks) implies that uncertainties in the precise rates of individual heterogeneous reactions may not be the major source of uncertainty in calculating ClO concentrations. Recent model calculations (*e.g.* Drdla *et al.*, 1991) generally confirm this view, indicating that heterogeneous release of reactive chlorine on PSCs is both rapid and not critically dependent on detailed particle characteristics. This may not be the case, however, if the PSCs are very sporadic or very limited in spatial extent. Finally, observations inside both the Antarctic and Arctic polar vortices of anomalously low ratios of the HCl column content to that of HF have been interpreted as a clear signature of heterogeneous removal of gaseous HCl (Coffey *et al.*, 1989; Toon *et al.*, 1989; Mankin *et al.*, 1990).

3.5.2 Heterogeneous Reactions on Sulfate Aerosols

Since stratospheric sulfate aerosols are ubiquitous rather than episodic in nature (except for periods immediately following major volcanic eruptions), direct estimation of reaction rates on these particles in the lower stratosphere is normally impossible. Although several comparisons between observed and modeled chlorine and odd nitrogen species have been performed recently, it must be noted that these represent a test of both the perturbing (heterogeneous) reactions and the coupled gas phase reactions (primarily the release of NO_2 from HNO_3). Considering chlorine partitioning first, Mather and Brune (1990) analyzed observations of ClO outside the northern polar vortex and deduced that direct heterogeneous

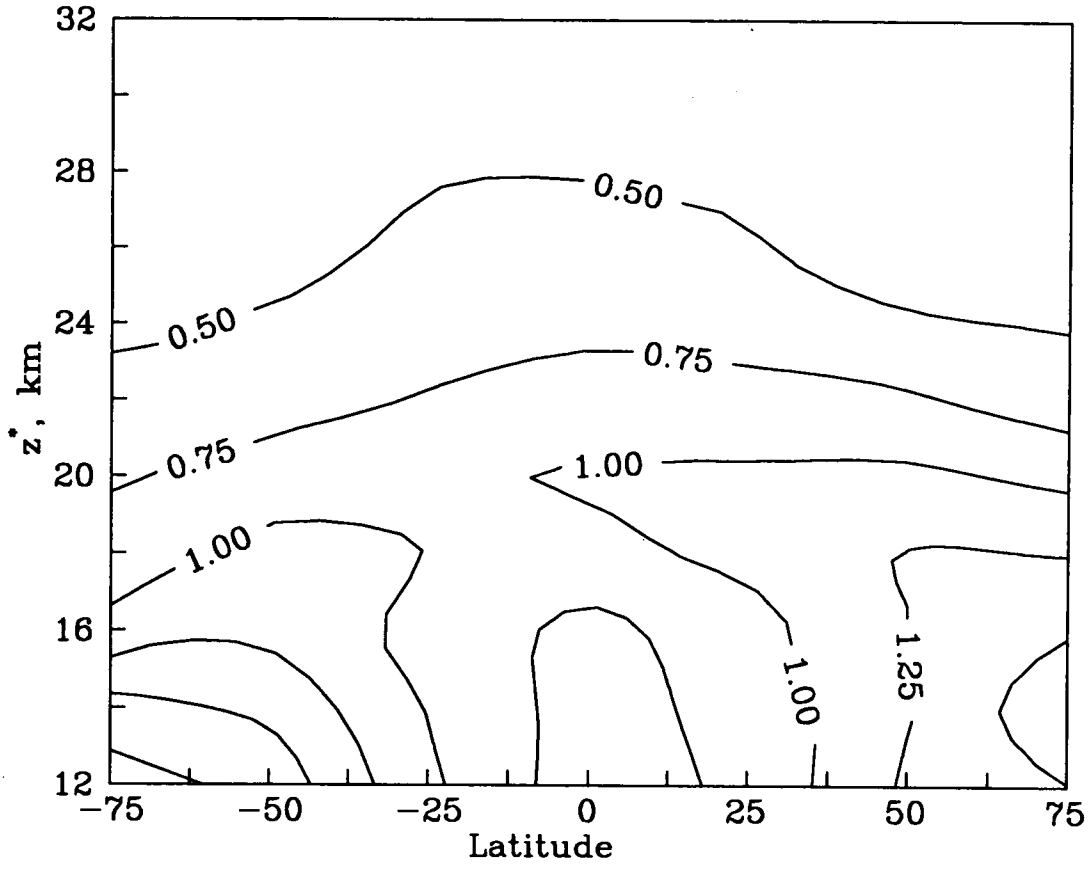

Figure 3–5 Sulfate aerosol surface area ($\mu m^2 cm^{-3}$) derived from SAGE II data for January to March 1989 using segmented power law size distribution model. $z^* = 16 \log_{10}(1000/\text{pressure [mbar]})$.

activation of chlorine is inefficient on background aerosols. This is consistent with the low measured reaction probabilities for direct release of reactive chlorine via Reactions (3–1) and (3–2) of Table 3–2. Chlorine partitioning can also be perturbed (ClO concentrations elevated) indirectly by the heterogeneous conversion of N_2O_5 to HNO_3 (Reaction 3–4, Table 3–2). The study by Rodriguez *et al.* (1991) showed that ClO mixing ratios of up to 150 ppbv that had been observed at 57°N could be reproduced solely via this path using a γ of ≈0.1, consistent with the recommended value in Table 3–2.

In terms of odd nitrogen species, model calculations assuming only gas phase chemistry have for some time been unable to simulate the HNO_3 distribution in the stratosphere, particularly the appearance of higher mid-latitude abundances in the winter hemisphere than in the summer hemisphere (Austin *et al.*, 1986; Jackman *et al.*, 1987). More recently, similar three-dimensional simulations have been unable to reproduce the spatial and temporal variability of HNO_3 in northern mid-latitudes, and comparison with LIMS data shows that HNO_3 does not behave as a tracer in the lower stratosphere as would be expected on the basis of gas phase chemistry (Rood *et al.*, 1990). Measurements of the NO_2 column at high latitudes (66°S, 78°S) under non-PSC conditions (Pommereau and Goutail, 1988; Solomon and Keys, 1991) strongly suggest that N_2O_5 is converted heterogeneously on background aerosols to a longer-lived reservoir, probably HNO_3 (as by Reaction (3–4), Table 3–2). A preliminary assessment of *in situ* NO measurements at mid-latitudes in the Northern Hemisphere (Kawa *et al.*, 1991) also suggests that some heterogenous conversion of N_2O_5 is required. A further complication has been introduced by recent measurements of the temperature dependence of the HNO_3 photolysis cross section (Rattigan *et al.*, 1991),

which suggest that HNO_3 is photolyzed some 2 to 3 times slower in the lower stratosphere than previously thought. As this process is the dominant loss mechanism for HNO_3 in the lower stratosphere, a change in photolysis rate will influence significantly the odd nitrogen partitioning and, hence, the level of consistency between observations and model results discussed above.

3.5.3 Denitrification Mechanisms

Several viable mechanisms have now been suggested for denitrification and dehydration of the lower stratosphere. Wofsy *et al.* (1990) suggest that denitrification is initiated by sedimentation of ice particles formed at higher altitudes, a notion supported by recent laboratory results (Section 3.2) that show that HNO_3 vapor readily sticks to ice surfaces, forming a layer of NAT, which retards sublimation of the underlying ice. Calculations by Toon *et al.* (1990b) do not assume scavenging of vapor by falling particles, yet suggest that HNO_3 and H_2O vapor removal can occur either separately or simultaneously, depending on the period and extent of cooling. Neither mechanism has been tested comprehensively using analyzed wind and temperature fields and observed H_2O and NO_y measurements, and features have been observed that, at first sight, may not be consistent with either approach. For example, the appearance everywhere of dehydration in denitrified air masses over the Antarctic during AAOE might not be expected if the processes were coupled in a manner as suggested by Wofsy *et al.* (1990b). It must be noted, however, that the earliest AAOE observations were made in mid-August of 1987, or several months after the observed denitrification and dehydration features likely began to evolve. On the other hand, the sudden appearance of denitrification in the Northern Hemisphere during AASE well after Type 1 PSCs were first observed might argue against the Toon *et al.* (1990b) approach. In this case, it must be noted that ER–2 measurements during the early phase of AASE were generally at latitudes south of the region in which denitrification may have occurred via Type 1 PSC formation alone.

A reliable prediction of the spatial extent of denitrification may not be as critical in explaining Antarctic ozone losses to zeroth order as it is in understanding the interannual variation in the severity of these losses or in assessing the potential for ozone depletion in the Northern Hemisphere. This raises the important question of whether denitrification is essential for significant Northern Hemisphere ozone losses. It is now recognized that synoptically- and orographically-forced PSCs can process quite large volumes of lower stratospheric air (Cariolle *et al.*, 1989; McKenna *et al.*, 1989; Jones *et al.*, 1990b; Lefèvre *et al.*, 1991). In the Arctic, an air parcel typically executes a circuit of the periphery of the vortex in about 5 days, a time scale that is likely much shorter than that required to return reactive chlorine to more benign forms, particularly in light of the newly measured reduced photolysis rates of HNO_3. Thus, if PSCs are present at high northern latitudes, the periodic exposure of parcels to the clouds is likely to affect chlorine partitioning over large volumes of the lower stratosphere. Even in the absence of denitrification, such processing could maintain a highly perturbed, high-ClO_x state, leading to ozone destruction. It may be expected that in such a case, denitrification would lead to only minor increases in ClO_x and ozone loss.

REFERENCES

Abbatt, J., K. Beyer, A. Fucaloro, J. McMahon, L. Molina, P. Wooldridge, R. Zhang, and M. Molina, Interactions of HCl vapor with water ice: Stratospheric implications, *J. Geophys. Res.*, in press, 1992.

The Airborne Antarctic Ozone Experiment (AAOE), Part 1, *J. Geophys. Res., 94, D9,* August 30, 1989.

The Airborne Antarctic Ozone Experiment (AAOE), Part 2, *J. Geophys. Res., 94, D14,* November 30, 1989.

The Airborne Arctic Stratospheric Expedition (AASE), *Geophys. Res. Lett., 17,* 4, March Supplement, 1990.

Austin, J., R.R. Garcia, J.M. Russell III, S. Solomon, and A.F. Tuck, On the atmospheric photochemistry of nitric acid, *J. Geophys. Res., 91,* 5477-5485, 1986.

Browell, E.V., C.F. Butler, S. Ismail, P.A. Robinette, A.F. Carter, N.S. Higdon, O.B. Toon, M.R. Schoeberl, and A.F. Tuck, Airborne lidar observations in the wintertime Arctic stratosphere:

polar stratospheric clouds, *Geophys. Res. Lett., 17*, 385-388, 1990.

Cariolle, D., S. Muller, F. Cayla, and M.P. McCormick, Mountain waves, polar stratospheric clouds, and the ozone depletion over Antarctica, *J. Geophys. Res., 94*, 11233-11240, 1989.

Coffey, M.T., W.G. Mankin, and A. Goldman, Airborne measurements of stratospheric constituents over Antarctica in the austral spring, 1987, 2. Halogen and nitrogen trace gases, *J. Geophys. Res., 94*, 16597-16613, 1989.

Drdla, K., R.P. Turco, and S. Elliot, Heterogeneous chemistry on Antarctic PSCs: A microphysical estimate of the extent of chemical processing, submitted for publication to *J.Atmos. Sci.*, 1991.

Dye, J.E., D. Baumgardner, B.W. Gandrud, S.R. Kawa, K.K. Kelly, M. Loewenstein, G.V. Ferry, K.R. Chan, and B.L. Gary, Particle size distributions in Arctic polar stratospheric clouds, growth and nucleation of sulfuric acid droplets and implications for cloud formation, to appear in *J. Geophys. Res.*, 1991.

Hanson, D.R., and K. Mauersberger, Laboratory studies of the nitric acid trihydrate: Implications for the South polar stratosphere, *Geophys. Res. Lett., 15*, 855-858, 1988.

Hanson, D.R., and A.R. Ravishankara, The reaction probabilities of $ClONO_2$ and N_2O_5 on polar stratospheric cloud materials, *J. Geophys. Res., 96*, 5081-5090, 1991a.

Hanson, D.R., and A.R. Ravishankara, Investigation of the reactive and nonreactive processes involving $ClONO_2$ and HCl on water and nitric acid doped ice, submitted for publication to *J. Phys. Chem.*, 1991b.

Hanson, D.R. and A.R. Ravishankara, The reaction probabilities of $ClONO_2$ and N_2O_5 on 40 to 75 percent sulfuric acid solutions, *J. Geophys. Res., 96*, 17307-17314, 1991c.

Hofmann, D.J., Increase in the stratospheric background sulfuric acid aerosol mass in the past 10 years, *Science, 248*, 996-1000, 1990.

Hofmann, D.J., Aircraft sulphur emissions, *Nature, 349*, 659, 1991.

Hofmann, D.J. and S. Solomon, Ozone destruction through heterogeneous chemistry following the eruption of El Chichón, *J. Geophys. Res., 94*, 5029-5041, 1989.

Hofmann, D.J., T. Deshler, F. Arnold, and H. Schlager, Balloon observations of nitric acid aerosol formation in the Arctic stratosphere: II. Aerosol, *Geophys. Res. Lett., 17*, 1279-1282, 1990.

Hübler, G., D.W. Fahey, K.K. Kelly, D.D. Montzka, M.A. Carroll, A.F. Tuck, L.E. Heidt, W.H. Pollock, G.L. Gregory, and J.F. Vedder, Redistribution of reactive odd nitrogen in the lower Arctic stratosphere, *Geophys. Res. Lett., 17*, 453-456, 1990.

Jackman, C.H., P.D. Guthrie, and J.A. Kaye, An intercomparison of nitrogen-containing species in Nimbus 7 LIMS and SAMS data, *J. Geophys. Res., 92*, 995-1008, 1987.

Jones, R.L., S. Solomon, D.S. McKenna, L.R. Poole, W.H. Brune, D.W. Toohey, J.G. Anderson, and D.W. Fahey, The polar stratospheric cloud event of January 24, 1989, part 2, photochemistry, *Geophys. Res. Lett., 17*, 541-544, 1990a.

Jones, R.L., D.S. McKenna, L.R. Poole, and S. Solomon, On the influence of polar stratospheric cloud formation on chemical composition during the 1988/89 Arctic winter, *Geophys. Res. Lett., 17*, 545-548, 1990b.

Kawa, S.R., D.W. Fahey, L.E. Heidt, W.H. Pollock, S. Solomon, D.E. Anderson, M. Loewenstein, M.H. Proffitt, J.J. Margitan, and K.R. Chan, Photochemical partitioning of the reactive nitrogen and chlorine reservoirs in the high latitude stratosphere, *J. Geophys. Res*, in press, 1991.

Koehler, B.G., A.M. Middlebrook, and M.A. Tolbert, Characterization of model polar stratospheric cloud films using Fourier transform infrared spectroscopy and temperature programmed desorption, *J. Geophys. Res.*, in press, 1991.

Lefèvre, F., L.P. Riishojgaard, D. Cariolle, and P. Simon, Modelling the February 1990 polar stratospheric cloud event and its potential impact on the northern hemisphere ozone content, *J. Geophys. Res., 96*, 22509-22534, 1991.

Leu, M.-T., Laboratory studies of sticking coefficients and heterogeneous reactions important in the Antarctic stratosphere, *Geophys. Res. Lett., 15*, 17-20, 1988a.

Leu, M.-T., Heterogeneous reactions of N_2O_5 with H_2O and HCl on ice surfaces: Implications for Antarctic ozone depletion, *Geophys. Res. Lett., 15*, 851-854, 1988b.

Leu, M.-T., S.B. Moore, and L.F. Keyser, Heterogeneous reactions of chlorine nitrate and hydrogen chloride on Type 1 polar stratospheric clouds, *J. Phys. Chem., 95,* 7763-7771, 1991.

Mankin, W.G., M.T. Coffey, A. Goldman, M.R. Schoeberl, L.R. Lait, and P.A. Newman, Airborne measurements of stratospheric constituents over the Arctic in the winter of 1989, *Geophys. Res. Lett., 17,* 473-476, 1990.

Mather, J.H., and W.H. Brune, Heterogeneous chemistry on liquid sulfate aerosols: A comparison of *in situ* measurements with zero-dimensional model calculations, *Geophys. Res. Lett., 17,* 1283-1286, 1990.

McCormick, M.P., and R.E. Veiga, SAGE II measurements of early Pinatubo aerosols, *Geophys. Res. Lett., 19,* 155-158, 1992.

McCormick, M.P., G.S. Kent, W.H. Hunt, M.T. Osborn, L.R. Poole, and M.C. Pitts, Arctic polar stratospheric cloud observations by airborne lidar, *Geophys. Res. Lett., 17,* 381-383, 1990.

McKenna, D.S., R.L. Jones, J. Austin, E.V. Browell, M.P. McCormick, A.J. Krueger, and A.F. Tuck, Diagnostic studies of the Antarctic vortex during the 1987 Airborne Antarctic Ozone Experiment: Ozone miniholes, *J. Geophys. Res., 94,* 11641-11668, 1989.

Molina, M.J., T.-L. Tso, L.T. Molina, and F.C.-Y. Yang, Antarctic stratospheric chemistry of chlorine nitrate, hydrogen chloride, and ice: Release of active chlorine, *Science, 238,* 1253-1257, 1987.

Moore, S.B., L.F. Keyser, M.-T. Leu, R.P. Turco, and R.H. Smith, Heterogeneous reactions on nitric acid trihydrate, *Nature, 345,* 333-335, 1990.

Mozurkewich, M., and J.G. Calvert, Reaction probability of N_2O_5 on aqueous aerosols, *J. Geophys. Res., 93,* 15889-15896, 1988.

Pitts, M.C., L.R. Poole, and M.P. McCormick, Polar stratospheric cloud sightings by SAM II, 1979-89: Contrasts between the Antarctic and Arctic, Paper presented at the American Geophysical Union Spring Meeting, Baltimore, MD, 1991.

Pommereau, J.P., and F. Goutail, Stratospheric O_3 and NO_2 observations at the southern polar circle in summer and fall 1988, *Geophys. Res. Lett., 15,* 895-897, 1988.

Poole, L.R., G.S. Kent, M.P. McCormick, W.H. Hunt, M.T. Osborn, S. Schaffner, and M.C. Pitts, Dual-polarization airborne lidar observations of polar stratospheric cloud evolution, *Geophys. Res. Lett., 17,* 389-392, 1990.

Prather, M.J., More rapid polar ozone depletion through the reaction of HOCl with HCl on polar stratospheric clouds, *Nature, 355,* 534-537, 1992.

Quinlan, M.A., C.M. Reihs, D.M. Golden, and M.A. Tolbert, Heterogeneous reactions on model polar stratospheric cloud surfaces: Reaction of N_2O_5 on ice and nitric acid trihydrate, *J. Phys. Chem., 94,* 3255-3260, 1990.

Rattigan, O., E. Lutmann, R.L. Jones, R.A. Cox, C. Clemitshaw, and J. Williams, Temperature-dependent absorption cross sections of gaseous nitric acid and methyl nitrate, submitted for publication to *J. Photochem. Photobiol.*, 1991.

Reihs, C.M., D.M. Golden, and M.A. Tolbert, Nitric acid uptake by sulfuric acid solutions under stratospheric conditions: Determination of Henry's law of solubility, *J. Geophys. Res., 95,* 16545-16550, 1990.

Reihs, C.M., J.A. Manion, D.M. Golden, and M.A. Tolbert, Heterogeneous reaction of N_2O_5 and $ClONO_2$ on sulfuric acid surfaces representative of global stratospheric particulate, to be submitted to *J. Geophys. Res.*, 1991.

Ritzhaupt, G., and J.P. Devlin, Infrared spectra of nitric and hydrochloric acid-hydrate thin films, *J. Chem. Phys., 90,* 90-95, 1991.

Rodriguez, J.M., M.K. Ko, and N.D. Sze, Role of heterogeneous conversion of N_2O_5 on sulfate aerosols in global ozone losses, *Nature, 352,* 134-137, 1991.

Rood, R.B., J.A. Kaye, A.R. Douglass, D.J. Allen, S. Steenrod, and E.M. Larson, Wintertime nitric acid chemistry: Implications from 3-dimensional model calculations, *J. Atmos. Sci., 47,* 2696-2709, 1990.

Schlager, H., F. Arnold, D. Hofmann, and T. Deshler, Balloon observations of nitric acid aerosol formation in the Arctic stratosphere: I. Gaseous nitric acid, *Geophys. Res. Lett., 17,* 1275-1278, 1990.

Smith, R.H., M.-T. Leu, and L.F. Keyser, Infrared spectra of solid films formed from vapors containing water and nitric acid, *J. Phys. Chem., 95,* 5924-5930, 1991.

Solomon, S., and J.G. Keys, Seasonal variations in Antarctic NO_x chemistry, *J. Geophys. Res.*, in press, 1991.

Solomon, S., R.R. Garcia, F.S. Rowland, and D.J. Wuebbles, On the depletion of Antarctic ozone, *Nature, 321*, 755-758, 1986.

Steele, H.M., and P. Hamill, Effects of temperature and humidity on the growth and optical properties of sulphuric acid-water droplets in the stratosphere, *J. Aerosol Sci., 12*, 517-528, 1981.

Thomason, L.W., A diagnostic stratospheric aerosol size distribution inferred from SAGE II measurements, *J. Geophys. Res., 96*, 22501-22508, 1991.

Tolbert, M.A., and A.M. Middlebrook, Fourier transform infrared studies of model polar stratospheric cloud surfaces: Growth and evaporation of ice and nitric acid/ice, *J. Geophys. Res., 95*, 22423-22431, 1990.

Tolbert, M.A., M.J. Rossi, R. Malhotra, and D.M. Golden, Reaction of chlorine nitrate with hydrogen chloride and water at Antarctic stratospheric temperatures, *Science, 238*, 1258-1260, 1987.

Tolbert, M.A., M.J. Rossi, and D.M. Golden, Heterogeneous interactions of chlorine nitrate, hydrogen chloride, and nitric acid with sulfuric acid surfaces at stratospheric temperatures, *Geophys. Res. Lett., 15*, 847-850, 1988.

Toon, G.C., C.B. Farmer, L.L. Lowes, P.W. Schaper, J.-F. Blavier, and R.H. Norton, Infrared aircraft measurements of stratospheric composition over Antarctica during September 1987, *J. Geophys. Res., 94*, 16571-16596, 1989.

Toon, O.B., E.V. Browell, S. Kinne, and J. Jordan, An analysis of lidar observations of polar stratospheric clouds, *Geophys. Res. Lett., 17*, 393-396, 1990a.

Toon, O.B., R.P. Turco, and P. Hamill, Denitrification mechanisms in the polar stratospheres, *Geophys. Res. Lett., 17*, 445-448, 1990b.

Van Doren, J.M., L.R. Watson, P. Davidovits, D.R. Worsnop, M.S. Zahniser, and C.E. Kolb, Temperature dependence of the uptake coefficients of HNO_3, HCl, and N_2O_5 by water droplets, *J. Phys. Chem., 94*, 3265-3269, 1990.

Van Doren, J.M., L.R. Watson, P. Davidovits, D.R. Worsnop, M.S. Zahniser, and C.E. Kolb, Uptake of N_2O_5 and HNO_3 by aqueous sulfuric acid droplets, *J. Phys. Chem., 95*, 1684-1689, 1991.

Watson, L.R., J.M. Van Doren, P. Davidovits, D.R. Worsnop, M.S. Zahniser, and C.E. Kolb, Uptake of HCl molecules by aqueous sulfuric acid droplets as a function of acid concentration, *J. Geophys. Res., 95*, 5631-5638, 1990.

Wofsy, S.C., R.J. Salawitch, J.H. Yatteau, M.B. McElroy, B.W. Gandrud, J.E. Dye, and D. Baumgardner, Condensation of HNO_3 on falling ice particles: Mechanism for denitrification of the polar stratosphere, *Geophys. Res. Lett., 17*, 449-452, 1990.

Wolff, E.W., and R. Mulvaney, Reactions on sulfuric acid aerosol and on polar stratospheric clouds in the Antarctic stratosphere, *Geophys. Res. Lett., 18*, 1007-1010, 1991.

WMO, Scientific Assessment of Stratospheric Ozone: 1989, Global Ozone Research and Monitoring Project, Report No. 20, 1990.

Yue, G.K., and A. Deepak, Retrievals of stratospheric aerosol size distribution from atmospheric extinction of solar radiation at two wavelengths, *Appl. Opt., 22*, 1639-1645, 1983.

CHAPTER 4

Stratospheric Processes: Observations and Interpretation

Authors:

W.H. Brune
R. Turco
W.A. Matthews
A. Douglass
M. Prendez
B.H. Subbaraya
R.A. Cox
G. Brasseur
X. Zhou
R.J. Zander
J.M. Rodriguez
A. O'Neill

Additional Contributors:

S. Solomon
A.F. Tuck
A.R. Ravishankara
M.K.W. Ko
M.J. Prather
J. Austin
M.R. Schoeberl

Chapter 4

Stratospheric Processes: Observations and Interpretation

Contents

SCIENTIFIC SUMMARY

The primary cause of the Antarctic ozone hole is firmly established to be halogen chemistry. Increased confidence in this mechanism results from analyses using reevaluated field measurements, new laboratory data, and modeling studies.

The year-to-year fluctuation in the area and depth of the ozone hole over the last decade, which has been attributed to dynamical effects, is not fully explained. The apparent lack of variability in recent years—extensive ozone holes have been observed in four of the last five years—may imply that halogen chemistry is becoming dominant over dynamically-induced fluctuations in Antarctic ozone depletion.

High concentrations of ClO between 16 and 20 km have been observed in wintertime in the Arctic lower stratosphere. These observations have been incorporated into diagnostic models that have calculated localized ozone depletions of about 10 percent at these altitudes over a period of about 1 month, which are consistent with concurrent ozone measurements.

Should an unusually cold and long winter occur in the Arctic polar vortex, the appearance of clearly detectable ozone depletions there will be more likely.

Limited observations suggest that the abundance of ClO in the lower stratosphere at mid-latitudes is greater than that predicted by current models containing only gas phase chemistry, and the observed seasonal and latitudinal dependences are opposite to those predicted. Some new studies that incorporate currently known heterogeneous processes provide an improved simulation for some observed gases, such as ClO and nitric acid.

There is not a full accounting of the observed downward trend in global ozone. Plausible mechanisms include heterogeneous chemistry on sulfate aerosols and the transport of chemically perturbed polar air to middle latitudes. Although other mechanisms cannot be ruled out, those involving catalytic destruction of ozone by chlorine and bromine appear to be largely responsible for the ozone loss and are the only ones for which direct evidence exists.

The potential importance of ozone loss in the lower stratosphere due to bromine, through bromine-chlorine interaction, is significantly increased by the widespread enhanced ClO abundances.

Because heterogeneous processes are important and the levels of chlorine in the stratosphere are increasing, volcanic injections into the stratosphere could have a substantial effect on global ozone.

Increasing levels of atmospheric chlorine and bromine are expected to lead to significantly more ozone depletion.

4.1 INTRODUCTION

Explaining the observed ozone trends discussed in Chapter 2 and predicting future trends requires an understanding of the stratospheric processes that affect ozone. Stratospheric processes occur on both large and small spatial scales and over both long and short periods of time. Because these diverse processes interact with each other, only in rare cases can individual processes be studied by direct observation. Generally the cause and effect relationships for ozone changes have been established by comparisons between observations and model simulations. Increasingly, these comparisons rely on the developing, observed relationships among trace gases and dynamical quantities to initialize and constrain the simulations.

The goal of this chapter on stratospheric processes is to describe the causes for the observed ozone trends as they are currently understood. At present, we understand with considerable confidence the stratospheric processes responsible for the Antarctic ozone hole but are only beginning to understand the causes of the ozone trends at middle latitudes. Even though the causes of the ozone trends at middle latitudes have not been clearly determined, it is likely that they, just as those over Antarctica, involve chlorine and bromine chemistry that has been enhanced by heterogeneous processes.

This chapter generally presents only an update of the discussions and observations that have occurred for stratospheric processes since the last assessment (WMO, 1990), and is not a complete review of all the new information about stratospheric processes. It begins with an update of the previous assessment of polar stratospheres (WMO, 1990), followed by a discussion on the possible causes for the ozone trends at middle latitudes and on the effects of bromine and of volcanoes.

4.2 ANTARCTIC OZONE DEPLETION

Significant advances in our understanding of the processes of the lower stratosphere have come from our attempts to understand the Antarctic ozone hole. We know that the ozone loss each spring over Antarctica is in large part caused by chlorine and bromine catalysis, that the enhanced chlorine catalysis results from the alteration of the chemical environment near and inside the Antarctic polar vortex by heterogeneous processes, and that these processes occur in the meteorological conditions of the wintertime stratosphere at high latitudes (Solomon *et al.*, 1986; McElroy *et al.*, 1986a; Toon *et al.*, 1986; WMO, 1990).

The basic catalytic cycles responsible for most of the observed ozone loss are (Molina and Molina, 1987):

$$ClO + ClO + M^* \rightarrow Cl_2O_2 + M$$
$$Cl_2O_2 + \text{sunlight} \rightarrow Cl + ClOO$$
$$ClOO + M \rightarrow Cl + O_2 + M$$
$$Cl + O_3 \rightarrow ClO + O_2$$

and (McElroy *et al.*, 1986b):

$$ClO + BrO \rightarrow Br + Cl + O_2$$
$$Cl + O_3 \rightarrow ClO + O_2$$
$$Br + O_3 \rightarrow BrO + O_2$$

*M represents N_2 and O_2

Other catalytic cycles, one containing the reaction $ClO + HO_2 \rightarrow HOCl + O_2$ (Solomon *et al.*, 1986) and another containing $ClO + O \rightarrow Cl + O_2$, make smaller contributions.

Our confidence in the validity of these processes, which were postulated with little initial support from laboratory and field measurements, has continually increased as laboratory and field studies have been completed. At the time of the last assessment (WMO, 1990), most of the reaction rate constants and the reaction products were known for the catalytic cycles. The products of the photolysis of ClOOCl, previously unknown, have now been identified as Cl and ClOO (Molina *et al.*, 1990). Although, in 1989, heterogeneous reactions affecting chlorine and nitrogen were known to be fast, computer models using these data were hard pressed to simulate features of the ozone hole (Rodriguez *et al.*, 1989; Prather, 1991). Laboratory data taken since 1989 indicate that chlorine nitrate reactivity with H_2O is slow on nitric acid trihydrate, that the reaction between HOCl and HCl is fast on ice surfaces, and that chlorine and nitrogen chemistry occurs on cold liquid sulfate aerosols that exist in the polar regions prior to the onset of polar stratospheric clouds (PSCs) (see Chapter 3 for details and references). These heterogeneous reactions lead to more mechanisms for converting chlorine from reservoir to reactive forms than were previously known.

4.2.1 Quantitative Estimates of Ozone Loss

The observed increase in the reactive ClO and the concurrent decrease in ozone as measured from outside to inside of the chemically perturbed region over Antarctica (Figure 4-1) gave a strong indication that the proposed chlorine chemistry was involved in the ozone loss (Anderson *et al.*, 1989a). However, at the time of the 1989 assessment (WMO, 1990), the ozone loss calculated using the observed abundances of ClO and BrO and measured reaction rate constants produced expected ozone losses that were somewhat less than the ozone losses that were concurrently observed. (Anderson *et al.*, 1989b; deZafra *et al.*, 1989; Sander *et al.*, 1989). These calculations all assumed that abundances of ClO and BrO were zonally symmetric, and that the vortex edge restricted the flow of polar air to middle latitudes, thus forming a "containment vessel." Other model calculations that did not depend upon the observed ClO abundances and simple assumptions about halogen radical distributions were capable of reproducing the observed ozone destruction because they calculated ClO abundances that were larger than those observed (Jones *et al.*, 1989; Austin *et al.*, 1989; Ko *et al.*, 1989). These models, however, were not definitive because of the uncertainties in the spatial and temporal distributions of PSCs and heterogeneous chemistry. As a result, a number of other catalytic ozone loss mechanisms involving chlorine were proposed.

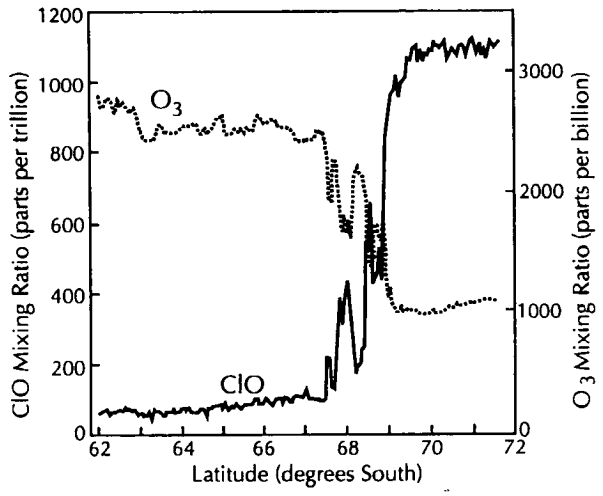

Figure 4-1 The observed variation of ClO and O_3 across the edge of the Antarctic ozone hole on Sept. 16, 1987 (Anderson *et al.*, 1990a). The edge of the chemically perturbed region is at 68°S. The ClO abundance inside the chemically perturbed region exceeds 1,000 pptv, which is sufficient to rapidly destroy ozone. This observation is one of a series that illustrates the development of the anticorrelation between ClO and O_3 in August and September 1987.

Recent calculations of ozone loss (Anderson *et al.*, 1991) using reevaluated *in situ* ClO and BrO measurements show that the observed ozone loss can be described completely by chlorine and bromine catalysis, to within experimental errors, for a zonally symmetric air flow within a containment vessel (Figure 4-2). This reevaluation resulted from additional, careful laboratory calibrations of the pressure and temperature dependences of the instrument used to measure ClO and BrO from the National Aeronautics and Space Administration (NASA) ER-2 aircraft during the Airborne Antarctic Ozone Experiment (AAOE) campaign (Anderson *et al.*, 1991). As a result, the measured *in situ* values of ClO and BrO are larger than was earlier reported, and the calculated rate of ozone destruction is increased, particularly for potential temperatures below 400 K (Murphy, 1991).

Agreement between observed and calculated ozone loss is also obtained from other data. An analysis of OClO column abundances and diurnal variations from McMurdo, Antarctica, during September 1987 shows that the observed ozone loss can be accounted for by the catalytic mechanisms involving Cl_2O_2 and ClO + BrO (Solomon *et al.*, 1990). In another study, model calculations using ground-based and *in situ* ClO measurements and aircraft HCl and $ClONO_2$ column measurements were used to synthesize the expected ClO abundances well inside the Antarctic vortex (Rodriguez *et al.*, 1990). Visual agreement was obtained between the observed and the calculated ozone decline.

Verification, with even less uncertainty, of the processes that cause the Antarctic ozone hole will require additional information (Solomon, 1990). The temporal and spatial distribution of ClO and BrO should be mapped globally. The amount of air that flows through the vortex in winter—whether the vortex is a flowing processor (Tuck, 1989; Proffitt, 1989) or a containment vessel (Hartmann *et al.*, 1989; Schoeberl and Hartmann, 1991)—needs to be definitively settled. The mixing of air parcels must be better understood. The characteristics of the large PSCs,

composed mainly of water ice, and the amount of cloudiness in the troposphere over Antarctica need to be quantified, so that the radiative effects of PSCs, which may be small on average, can be better understood (WMO, 1990; Rosenfield, 1991).

Nonetheless, since the first observations of the ozone hole, we have been able to state to within the uncertainties of the laboratory and field measurements and the models that the ozone hole is caused largely by halogen chemistry. The difference between this assessment and the previous one (WMO, 1990) is that the uncertainties in our knowledge of stratospheric processes have been reduced by the reevaluated field measurements, new laboratory data, and modeling studies. We now have greater confidence that the ozone hole is caused by halogen chemistry.

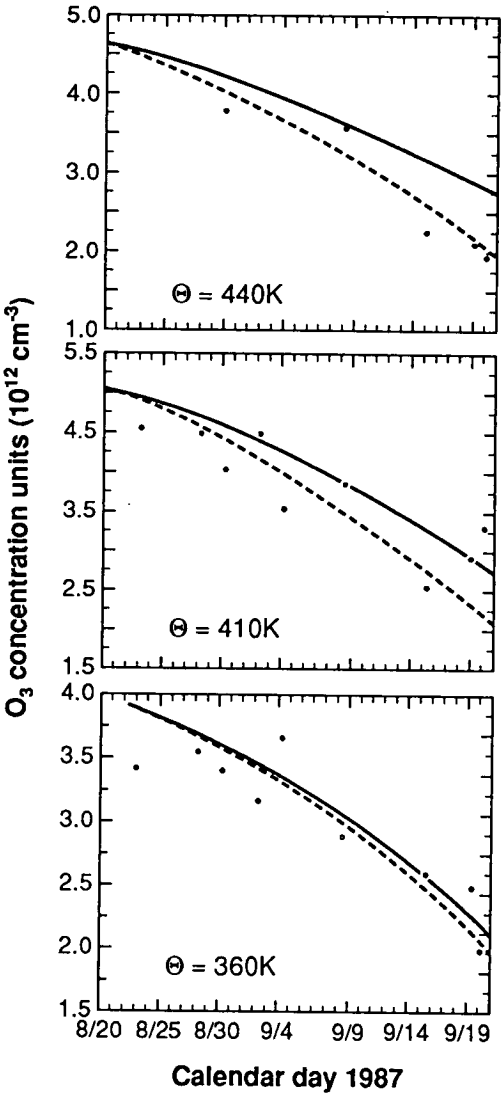

Figure 4-2 Comparison between the observed disappearance of O_3 over the 4-week period of the AAOE mission and the calculated amount of ozone removed, based on simultaneous observed concentrations of ClO and BrO for two catalytic cycles (Anderson *et al.*, 1991). The catalytic cycle involving Cl_2O_2 (solid line) and the sum of catalytic cycles involving the Cl_2O_2 and ClO + BrO mechanisms (dotted line) match the observed O_3 decline (dots).

4.2.2 Year-to-Year Variability in the Severity of the Ozone Hole

The fundamental mechanisms that determine the interannual variability of the severity of the Antarctic ozone hole have so far not been identified. Evidence has been presented for a correlation between one dynamical effect, the tropical quasi-biennial oscillation (QBO), and total ozone amounts in the extratropics, although the relationship is not well understood (Garcia and Solomon, 1987; WMO, 1990; Gray and Ruth, 1991; Lait *et al.*, 1989; Angell, 1990). The QBO may modulate the transport of inorganic chlorine and reactive nitrogen or may modulate the propagation of planetary waves, thus affecting the temperatures and winds associated with the polar vortex. The modulation of the observed total ozone loss may be related to others factors as well. These dynamical couplings are complex, and attempts to establish connections on the basis of simple correlations have not been successful (Dunkerton and Baldwin, 1991; Angell, 1990).

In three of the last four years, the ozone hole has been as extensive and as intense as the ozone hole in 1987. The correlation of the easterly phase of the QBO and a less intense ozone hole was observed in 1988 but has not been observed in 1991 (Figure 4-3). This diminished effect of the QBO on ozone loss may result from the shift in the phase of the QBO cycle (a period of 22 to 34 months) relative to the austral winter over the course of several years (Gray and Ruth, 1991). On the other hand, this recent series of deep ozone holes may be an early indication that the fluctuating dynamical effects on the stability, temperatures,

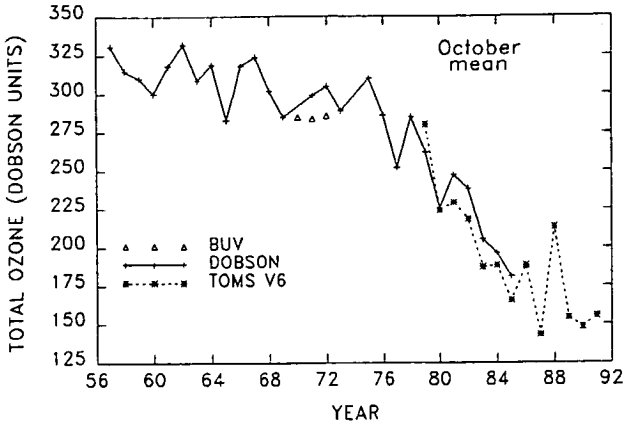

Figure 4-3 Year-to-year variations of the mean ozone observed in the southern polar region for October (R.S. Stolarski, private communication). Satellite and ground-based measurements of the October mean total ozone show the development of the Antarctic ozone hole. The measurements are by the Dobson Instrument at Halley Bay (plusses); the Nimbus 7 TOMS satellite instrument, processed as Version 6 on a 2° latitude by 5° longitude grid (asterisks with a dashed line); and the Nimbus 4 Backscatter Ultraviolet instrument for the first 3 years (triangles).

and thus annual ozone loss of the Antarctic polar vortex may not moderate ozone loss in the future.

As the chlorine loading of the stratosphere increases in the future, the amount of time required for significant ozone depletion by these chemical mechanisms will decrease. Under these circumstances, significant ozone depletion would eventually occur even for a warmer, shorter-lived vortex that might be expected in the easterly phase of the QBO. Although it is plausible that this chemical control has already begun, such speculation must be quantified and verified by continued observations of yearly, intense ozone holes.

4.3 THE PERTURBED CHEMISTRY AND OZONE LOSS IN THE ARCTIC

4.3.1 Observations of the Arctic Polar Vortex

No ozone decline similar to the Antarctic ozone hole has yet been observed in the Arctic. Yet the observations of the Arctic polar vortex in January and February 1989 indicate that the Arctic polar vortex was almost as chemically perturbed as the Antarctic polar vortex (Figure 4-4) (see *Geophys. Res. Lett., 17,* No. 4, 1990, special issue on the Airborne Arctic Stratospheric Experiment (AASE); *Geophys. Res. Lett., 18,* No. 4, 1991, Chemistry of Ozone in the Polar Stratosphere, special section on CHEOPS–III). First of all, enhanced abundances of ClO were observed near and inside the Arctic polar vortex (Brune *et al.*, 1988, 1990) with values inside the vortex at altitudes of 16 to 20 km as large as those observed over Antarctica. Estimates of the amount of available chlorine indicate that inside the Arctic polar vortex, the amount of chlorine in the forms of ClO or Cl_2O_2 was at least 85 percent of the total amount of available chlorine (Figure 4-5) (Kawa *et al.*,

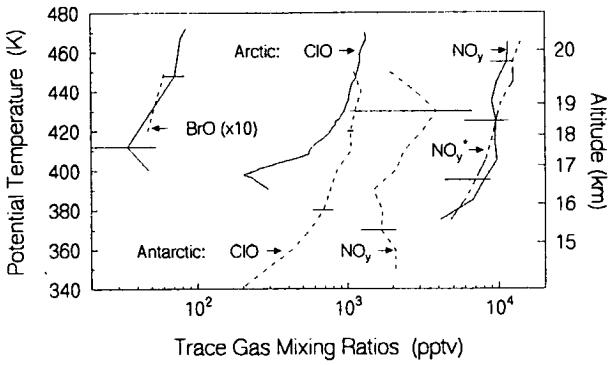

Figure 4-4 Comparison of Antarctic and Arctic in situ data taken during the AAOE in 1987 and the AASE in 1989 (Brune *et al.*, 1991). Arctic data are represented by solid lines; Antarctic data by dashed lines. The dot-dash line represents the NO_y abundances predicted by the measurement of N_2O and the empirical relationship between N_2O and NO_y, called NO_y^* (Fahey *et al.*, 1990c). The Arctic abundances shown are about 1,000 pptv larger than the Antarctic abundances. All data have been averaged over the flights except for ClO over the Arctic, which are only from one flight on Feb. 10, 1989. In relation to the spring equinox for the respective hemispheres, the Arctic mission (Jan. 3–Feb. 10) ended before the Antarctic mission (Aug. 17–Sept. 23) started. Error bars are the variability ($+1\sigma$) of the results for all flights. The ClO abundances observed in the Antarctic vary little from flight to flight and were similar to the abundances observed in the Arctic. The Antarctic abundances of NO_y had large variability, as shown by the error bars at 430 K and 370 K.

1991; Brune *et al.*, 1990, 1991; Salawitch *et al.*, 1990; McKenna *et al.*, 1990). Measurements of the depleted HCl reservoir (Mankin *et al.*, 1990; Adrian *et al.*, 1991) and the increased column abundances of $ClONO_2$ near the edge of the vortex and decreases inside (Mankin *et al.*, 1990) are consistent with widespread conversion of chlorine to reactive forms. The abundances of BrO were also found to be similar to those observed over Antarctica (Toohey *et al.*, 1990; Wahner *et al.*, 1990a).

At altitudes between 16 and 20 km inside the Arctic polar vortex, these observed, enhanced abundances of reactive chlorine and bromine in the presence of sunlight dictate the instantaneous rate of ozone loss. The integrated amount of ozone loss by

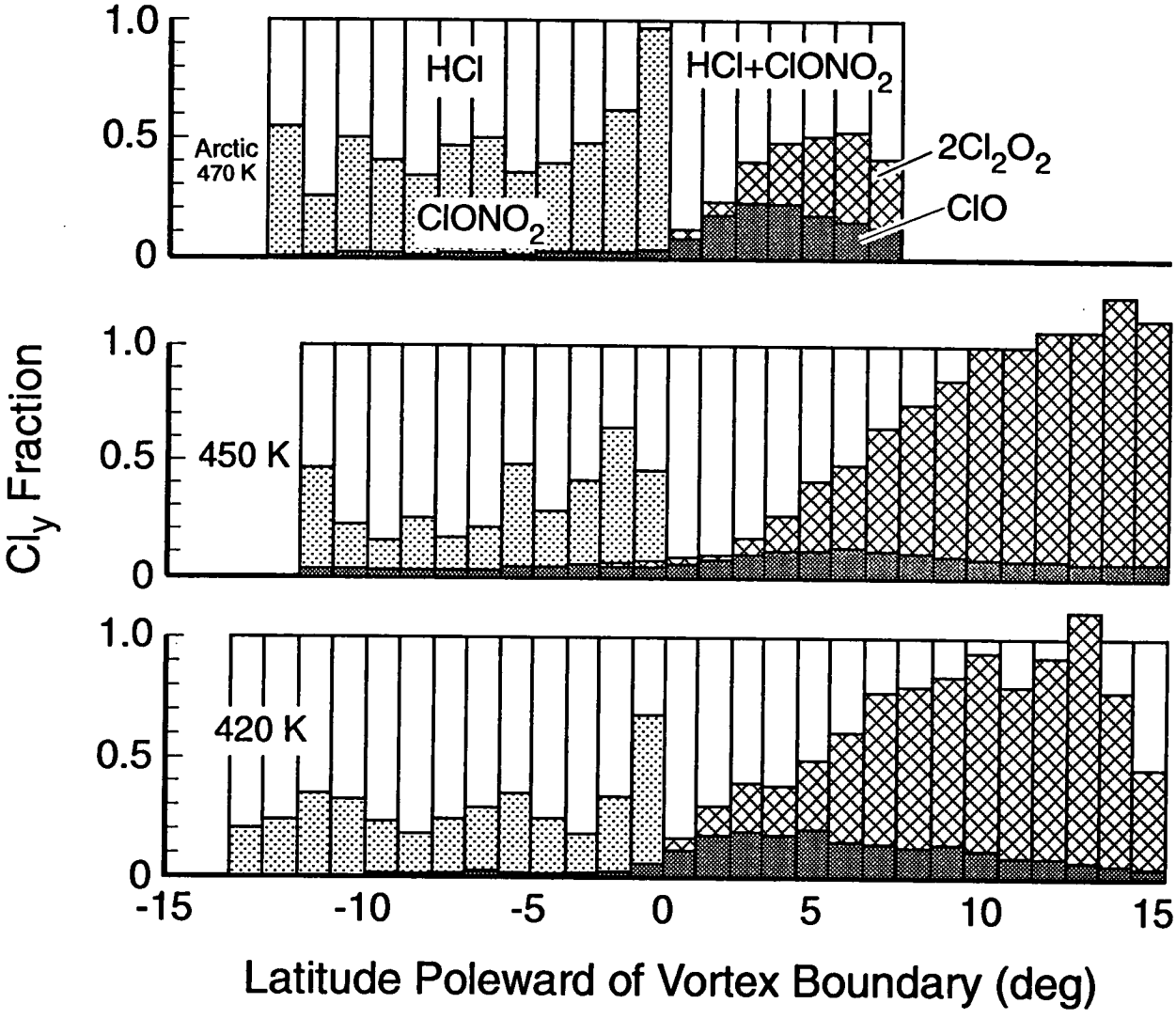

Figure 4-5 Fractional partitioning that is derived for reactive chlorine in the Arctic during AASE at three potential temperatures (Kawa *et al.*, 1991). Photochemical stationary steady state is assumed to determine $ClONO_2$ and Cl_2O_2 abundances from observations of ClO and NO. Data are averaged for several flights, for which the maximum wind has been used to define the vortex edge at 0° latitude. Positive values of the latitude are inside the vortex. The values of ClO are low because the illumination of the vortex was weak during much of this mission. Note that ClO and Cl_2O_2 make up essentially all of the total available chlorine for potential temperatures below 470 K at 5° to 10° latitude inside the vortex.

chlorine and bromine catalysis, however, is also dictated by the abundances of NO_x, which control ClO and BrO through the formation of $ClONO_2$ and $BrONO_2$. Inside the Arctic polar vortex, the amounts of the reactive nitrogen species NO_2 (Mount *et al.*, 1988; Pommereau and Goutail, 1988; Mankin *et al.*, 1990; and Wahner *et al.*, 1990b) were very low, and the amount of NO was unmeasurable (<10 pptv) by *in situ* techniques (Fahey *et al.*, 1990a). The Arctic polar vortex was only occasionally observed to be denitrified, and then, usually only partially so (Arnold and Knop, 1989; Kawa *et al.*, 1990; Fahey *et al.*, 1990b; Schlager and Arnold, 1990; Mankin *et al.*, 1990; Kondo *et al.*, 1990). This amount of denitrification is significantly different from the almost complete denitrification observed over Antarctica. This difference in denitrification means that more HNO_3 was available to be photolyzed into NO_2 in the Arctic, thus speeding the chemical conversion of ClO into $ClONO_2$, and slowing the halogen catalytic destruction of ozone.

4.3.2 Estimates and Observations of Ozone Loss in the Arctic Polar Vortex

Diagnostic models based on the observations of ClO, BrO, and NO_y suggest that losses of ozone at altitudes between 16 and 20 km inside the Arctic polar vortex in 1989 were about 10 percent for the 35 days between January 6 and February 10 (McKenna *et al.*, 1990; Salawitch *et al.*, 1990). These local losses are consistent with the analyses of the ozone losses deduced from the ozone observations made concurrently (Proffitt *et al.*, 1990; Browell *et al.*, 1990; Schoeberl *et al.*, 1990; Hofmann *et al.*, 1989). Additional local losses that might have occurred in mid-February were estimated to be about 2 percent per day (McKenna *et al.*, 1990; Murphy, 1991; Brune *et al.*, 1991).

Total ozone loss can be estimated from calculated and measured local ozone loss rates by integrating through the region affected by polar stratospheric clouds. The effects of PSCs on reactive chlorine and reactive nitrogen were observed for altitudes below 20 km and must be estimated for higher altitudes where no measurements of reactive chlorine and bromine exist. However, losses in the total ozone for 60°N to 70°N in 1989 have been calculated to be 5 percent to 8 percent by two-dimensional models (Isaksen *et al.*, 1990; Chipperfield and Pyle, 1990; Pitari and Visconti, 1991). These losses of total ozone are roughly consistent with the observations and calculations of the local ozone losses discussed above, although these calculations are sensitive to the characteristics and chemistry of PSCs. Ozone changes of this magnitude can be determined when data are averaged over large spatial and temporal scales but are difficult to separate from the natural, seasonal ozone fluctuations when the ozone changes are observed for only one to two months.

A difference between the Arctic polar vortex and the Antarctic chemically perturbed region is that the Arctic vortex does not get as cold and thus is not as denitrified. Further, the Arctic vortex often breaks up a month before the spring equinox, whereas the Antarctic polar vortex breaks up 1 or 2 months or after the spring equinox. However, the observations show that even the rather limited number of PSCs of the Arctic polar vortex is sufficient to activate the reactive chlorine. In 1989, the vortex was as cold as had been observed in January in 30 years of records, but rapidly warmed in mid-February (Nagatani *et al.*, 1990). The breakup of the vortex in early March restricted the amount of ozone loss. However, the Arctic polar vortex was more stable and colder in the winters of 1966–1967 and 1975–1976 (Nagatani *et al.*, 1990. If the conditions of these years were repeated, with the increased amount of stratospheric chlorine that exists today (Zander *et al.*, 1987; Wallace and Livingston, 1991), then an Arctic ozone hole, probably smaller and less intense than an Antarctic ozone hole, would most likely occur. This probability will increase as the amount of stratospheric chlorine increases from 3.5 to 4.1 parts per billion by volume (ppbv) in the near future.

4.3.3 Dynamics of the Arctic Polar Vortex

The issue of the amount of air that is exchanged between the polar vortex and middle latitudes, previously examined for the Antarctic, has now been examined for the Arctic (Proffitt *et al.*, 1990; Tuck *et al.*, 1991; Schoeberl *et al.*, 1991). The amount of air transported between the polar vortex and middle latitudes affects not only the actual ozone loss within the vortex, but also that in middle latitudes. The effects on ozone in middle latitudes will be examined in the next section.

The polar vortex could be viewed as a flowing processor of air. The diabatic cooling that produces transport from the vortex exterior to the interior has been used to explain the observed distributions of N_2O from the AASE mission (Proffitt *et al.*, 1990). In addition, high-resolution analyses of potential vorticity from the European Center for Medium-Range Weather Forecasts (ECMWF), in combination with trajectory calculations, have been used to support the notion that air may be chemically processed within the Arctic polar vortex and then transported to the middle latitudes (Tuck *et al.*, 1991) (Figure 4-6). Measurements of water vapor near the Antarctic and Arctic polar vortices may also indicate a substantial flow of air through the polar vortices (Kelly *et al.*, 1990).

However, the polar vortex may also be viewed as a leaky containment vessel. Plumb (1990) contends that the large meridional flow proposed by Proffitt *et al.* (1990) is probably inconsistent with the angular momentum budget. Schoeberl *et al.* (1991) have combined data analyses, trajectory calculations, and radiative transfer computations to diagnose the residual polar circulation. They conclude that the polar vortex is essentially isolated from the middle latitudes. Their model of the vortex has rather rapid mixing outside the vortex, weak mixing across the vortex boundary, and modest mixing inside the vortex (Figure 4-7). However, rapid radiative cooling due to large PSCs, even if it occurs infrequently, may affect these conclusions. In support of the concept of weak mixing from inside to outside the vortex, three-dimensional model calculations using assimilated data fields (Rood *et al.*, 1991) indicate that only a small amount of the chemically perturbed polar air passes from inside the vortex to the middle latitudes. This model has only modest spatial resolution, however, and so may not quantitatively represent the transport of the observed small-scale polar air parcels to the middle latitudes.

4.4 OZONE DEPLETION AT MIDDLE LATITUDES

The ozone loss at the middle latitudes has well-defined characteristics that must be explained by any proposed stratospheric processes (see Chapter 2 for details). The decadal trend is greatest at high latitudes and in winter and spring, although significant trends occur as far south as 30°N and in summer. Further, the observed ozone decreases predominantly occur in the lower stratosphere below 25 km. Computer models containing only the currently understood gas phase chemistry cannot reproduce these characteristics of the observed ozone trends (see Chapter 8). As a result, some other chemistry or dynamics that are not properly represented in these models must be involved.

Isolating the causes of this decadal change in ozone at middle latitudes is considerably more difficult than establishing the link between stratospheric chlorine and the Antarctic ozone hole. While the ozone decreases in the Antarctic ozone hole are measured in percent per day, the ozone decreases at middle latitudes are measured in percent per decade. Subtle changes in either the dynamics or chemistry could possibly cause such ozone changes.

At present, the only proposed cause of the downward trends in total ozone at middle latitudes that can satisfy most current observations involves enhanced chlorine and bromine catalysis that is initiated by heterogeneous chemistry. These processes based on halogen photochemistry are appealing as the cause for a couple of reasons. First, they occur in the lower stratosphere where both PSCs and stratospheric aerosols are concentrated, precisely at the altitudes where the observed ozone trend is occurring. Second, the observed increases in stratospheric chlorine and bromine that have occurred over the last few decades could, by these processes, result in the observed ozone trend.

4.4.1 Transport of Polar Air to the Middle Latitudes

One reasonable postulate for the total ozone decrease at middle latitudes is that the chemically perturbed polar air is being transported to middle latitudes in the lower stratosphere. In the Southern Hemisphere, the mixing of the polar air, depleted of ozone, with the middle latitude air (the dilution effect) (Chipperfield and Pyle, 1988; Sze *et al.*, 1989; Prather *et al.*, 1990; Cariolle *et al.*, 1990) would cause ozone loss at the middle latitudes at the breakup of the vortex in November or December. A second effect, which can occur in both hemispheres, is the transport to middle latitudes of air that has enhanced levels of reactive chlorine and deplet-

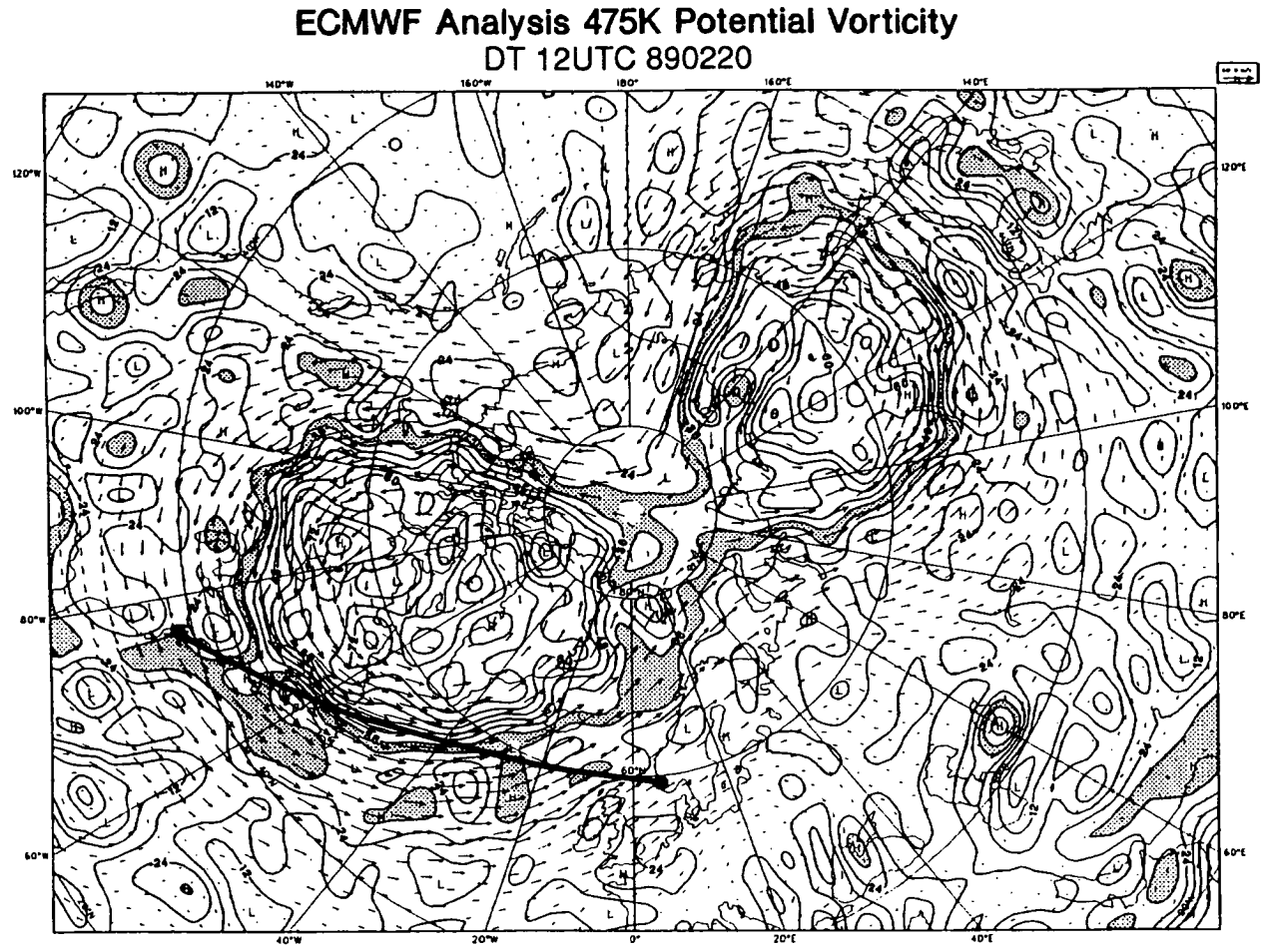

Figure 4-6 The potential vorticity (PV) map at the 475 K potential temperature surface for Feb. 20, 1989, from the European Center for Medium-Range Weather Forecasts (ECMWF) analysis model run at the T63 resolution (horizontal resolution of 210 km) (Tuck *et al.*, 1991). PV contours are marked every 6 x 10^{-6} K kg^{-1} m^2 s^{-1}, and the area between the PV contours of 30 x 10^{-6} and 36 x 10^{-6} K kg^{-1} m^2 s^{-1} has been shaded. This band corresponds to a conservative view of the Arctic polar vortex edge. Arrows mark the direction and relative speed of the horizontal wind. The butterfly shape of the polar vortex is evident, and small features of high PV are scattered over the map. The heavy line indicates the flight track of the NASA ER–2 aircraft from Stavanger, Norway, to Wallops Island, VA.

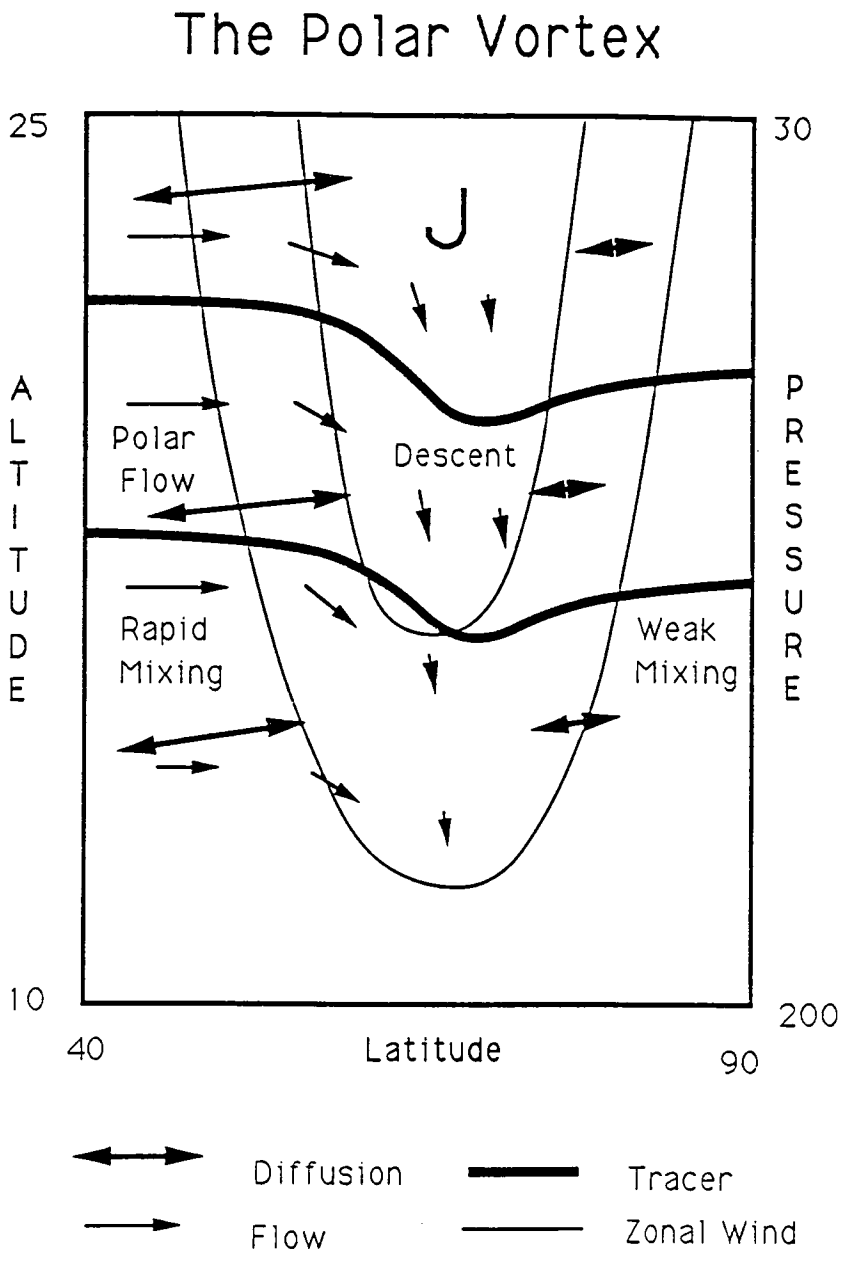

Figure 4-7 A schematic diagram of the circulation and mixing associated with the generic polar vortex, based on mixing rate estimates and radiative transfer computations (Schoeberl *et al.*, 1991). Thin lines show the zonal contours; J indicates the jet core. Double arrows indicate mixing, with the longer arrows representing larger mixing rates. Mixing rates vary from 10^4 m^2 sec^{-1} or less inside the vortex to greater than 10^5 m^2 sec^{-1} outside. Single arrows indicate flow directions, with the lengths approximately indicating magnitude. Maximum poleward flow (on the order of 0.1 m sec^{-1}) occurs equatorward of the wind jet. The largest descent zone (with vertical velocities of about 0.05 cm sec^{-1}) is roughly coincident with the jet core. Long-lived tracer isopleths are shown by thick lines. This picture of the polar vortex is relevant to the Arctic midwinter period or the Antarctic early spring. Approximate altitudes and pressures (in mb) are given along the ordinate.

ed levels of reactive nitrogen (called chemical propagation) (Prather and Jaffe, 1990). In these air parcels, the reactive chlorine would be constantly depleting ozone at an accelerated pace until the ClO is converted to $ClONO_2$ and HCl by gas phase chemistry. This conversion occurs over a period of weeks either by photolysis of any nitric acid remaining in the air parcel or by mixing of the polar air with middle latitude air.

The mixing of the polar air with the middle latitude air at the breakup of the vortices in the late winter and early spring can explain some of the ozone loss at the middle latitudes for these times. However, significant flow of air through the vortex, as proposed by Tuck *et al.* (1991) and Proffit *et al.* (1990), is required if the ozone losses during the winter are to be explained mainly by this mechanism. Tuck *et al.* (1991) estimate that 5 percent to 25 percent of the area north of 30°N consists of air that has come from the vortex. Conflicting results are reported from a three-dimensional model study capable of reproducing the observed ClO abundances at modest resolution (Douglass *et al.*, 1991; Kaye *et al.*, 1991). This study indicates that the transport of polar air masses contributes little to the ozone change at middle latitudes. In addition to any ozone loss that may be caused by transport of polar air, some ozone loss occurs in air parcels that come from the middle latitudes and pass through cold regions, in which PSCs form, that are outside the Arctic polar vortex (Jones *et al.*, 1990; Lefèvre *et al.*, 1991). The amount of ozone that is being removed by all these processes at middle latitudes during winter and after the vortex breakup, perhaps even into summer, needs to be quantified.

The chemical signatures of air parcels from the vortices are enhanced levels of reactive chlorine, low levels of NO_x, and possibly NO_y, low levels of long-lived tracers such as N_2O, and high values of the dynamical tracer, potential vorticity. In the Southern Hemisphere after mid-September, these air parcels would also exhibit low levels of ozone. Such air masses, with spatial extents of 10 to 100 km, have been observed outside of both polar vortices (Tuck *et al.*, 1991, and references therein; Atkinson *et al.*, 1989), as is shown for outside the Arctic polar vortex in 1989 (Figure 4-8). The observations of spikes of chemically perturbed air imply that some ozone is being lost at middle latitudes by the transport of polar air.

4.4.2 Photochemistry of the Sulfate Aerosol Layer

A newly proposed mechanism for explaining at least part of the observed ozone trends at middle latitudes involves heterogeneous reactions occurring on the global sulfate aerosols, as discussed in Chapter 3. In the current theory, the rapid reaction,

$$N_2O_5(g) + H_2O(\text{aerosol}) \rightarrow 2 \times HNO_3(g)$$

happens on the sulfate aerosol, and its reaction efficiency, $\gamma = \sim 0.1$, is independent of temperature. The direct conversion of the reservoir chlorine species on sulfate aerosols by the reactions, $ClONO_2 + H_2O \rightarrow HOCl + HNO_3$ and $ClONO_2 + HCl \rightarrow Cl_2 + HNO_3$, is thought to be unimportant for most of the stratosphere (Watson *et al.*, 1990; Mather and Brune, 1990; Rodriguez *et al.*, 1991), except perhaps near the polar vortices where the temperatures are lower than 205 K (Wolff and Mulvaney, 1991; Drdla *et al.*, 1991), or after large volcanic eruptions (Hofmann and Solomon, 1989; Brasseur *et al.*, 1990; Pitari *et al.*, 1991).

For a typical sulfate aerosol surface area of 0.5 $\mu m^2\ cm^{-3}$, the time constant for the conversion of N_2O_5 to nitric acid is ~5 days. The immediate result is that NO_x is diminished, particularly at the high latitudes in seasons when the sunlight is too weak to photolyze the nitric acid significantly. Due to the coupling among the chlorine, nitrogen, and hydrogen families, concentrations of reactive chlorine and HO_x increase. As a result, the negative ozone trends calculated by models that include the heterogeneous conversion of N_2O_5 on sulfate aerosols increase by almost a factor of two, not only for high latitudes in winter, but also at middle latitudes in summer (Rodriguez *et al.*, 1991; see also Chapter 8). These models simulate the observed ozone trends substantially better than models with only gas phase chemistry (see the discussion in Chapter 8).

Preliminary evidence exists for the conversion of N_2O_5 to nitric acid on the global sulfate aerosols and the subsequent enhancement of ClO. First of all, from a limited set of measurements (King *et al.*, 1991; Toohey *et al.*, 1991), the observed abundances and latitudinal gradient of ClO are better simulated by models containing heterogeneous chemistry on sulfate aerosols than by models with only gas phase

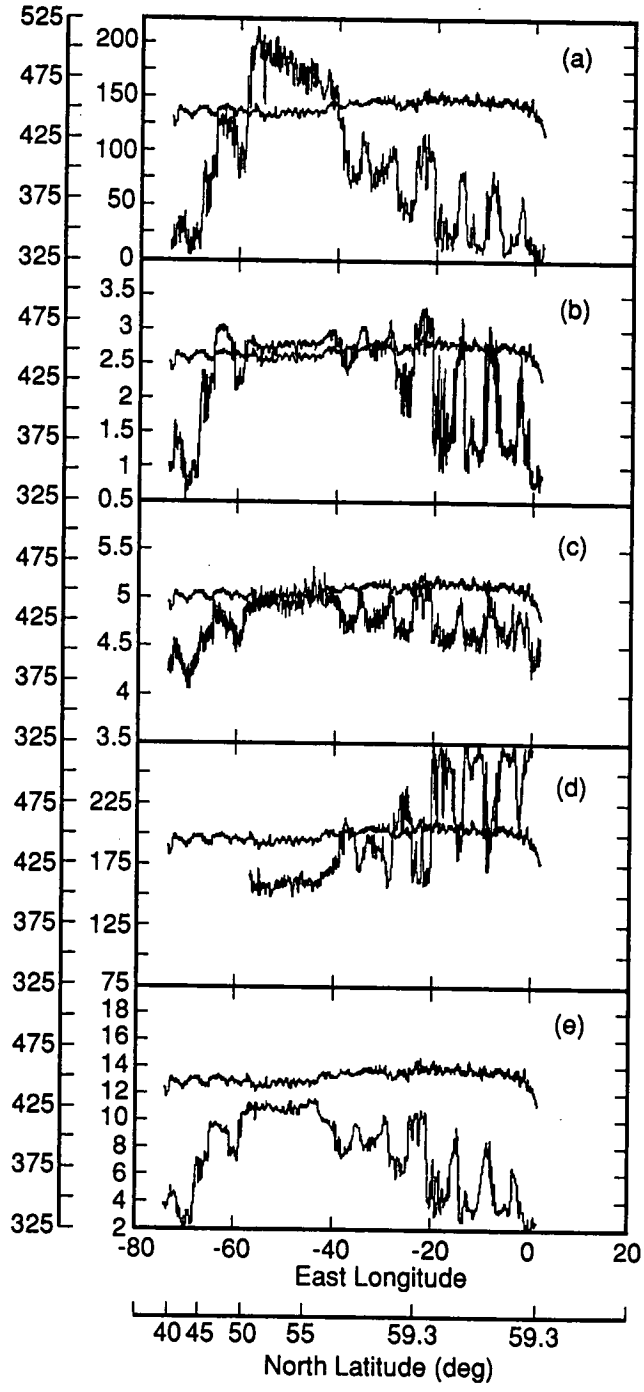

Figure 4-8 Measurements of trace gases from the NASA ER–2 aircraft versus longitude, taken on Feb. 20, 1989, along the flight track shown as a heavy line in Figure 4-6 (Tuck *et al.*, 1991). Measurements are: (a) ClO (pptv); (b) O_3 (ppmv); H_2O (ppmv); (d) N_2O (ppbv); and (e) NO_y (ppbv). Superimposed on each plot is the potential temperature along the flight track. Note that sharp increases in ClO, O_3, NO_y, and H_2O occur simultaneously with sharp decreases in N_2O in the spikes. These chemical signatures indicate that the air in the spikes has been altered by heterogeneous chemistry and comes from the polar vortex.

chemistry (Figure 4-9) (King *et al.*, 1991; Toohey *et al.*, 1991). This conclusion appears to be robust despite the inability of the models to simulate the downwelling of the stratosphere (Heidt *et al.*, 1989; Loewenstein *et al.*, 1990; Schmidt *et al.*, 1991). Some observations of reactive nitrogen gases, when compared with model results, also indicate that these heterogeneous processes on sulfate aerosols are occurring. These observations include nitric acid measurements from the Limb Infrared Monitor of the Stratosphere (LIMS) (Austin *et al.*, 1986; Jackman *et al.*, 1987; Rood *et al.*, 1990) and Atmospheric Trace Molecule Spectroscopy Experiment (ATMOS) (Natarajan and Callis, 1991), N_2O_5 measurements (Natarjan and Callis, 1991; Evans *et al.*, 1985), and the high-latitude column measurements of NO_2 (Pommereau and Goutail, 1988; Solomon and Keys, 1991).

On the other hand, some discrepancies between model results and observations suggest that more work is required to understand all the processes that affect the abundances of reactive chlorine and nitrogen in the lower stratosphere. First, the observed abundances of ClO at low latitudes (<30°N) are better represented by the model with only gas phase chemistry (Figure 4-9). Second, the abundances of ClO obtained in summertime during only a few observations at 40°N latitude are smaller than predicted by models with heterogeneous chemistry on sulfate aerosols. Also, studies of *in situ* NO measurements (Considine *et al.*, 1991; Kawa *et al.*, 1991) indicate that the observed NO levels may be higher than predicted by models containing the $N_2O_5 + H_2O$ reaction but are smaller than predicted by models containing gas phase chemistry only.

4.4.3 Halogen Photochemistry as a Cause of the Observed Ozone Decline

Comparisons between observations and model results will become more definitive in establishing the role of heterogeneous chemistry on sulfate aerosols when more measurements are made and the models are improved. In addition, the impact of new laboratory data, such as the measurements of smaller, temperature-dependent absorption cross sections for HNO_3 (Rattigan *et al.*, 1991), must be carefully assessed. Nevertheless, the characteristics of the ozone trends and of the ClO and HNO_3 abundances place tight constraints on any proposed mechanism. Thus, although proposed dynamical mechanisms might explain the observed ozone changes in the lower stratosphere, they would also have to simultaneously explain the observed abundances of ClO, NO_x, and HNO_3. The assertion that dynamics alone is probably not responsible for the observed ozone trend is supported by an analysis of total ozone in the Southern Hemisphere for July–September from 1963 to the present (Lehmann *et al.*, 1991). In this study, the changes in the tropopause height and the transient eddy heat flux, used to represent dynamical influences, explain the interannual variability, but not the

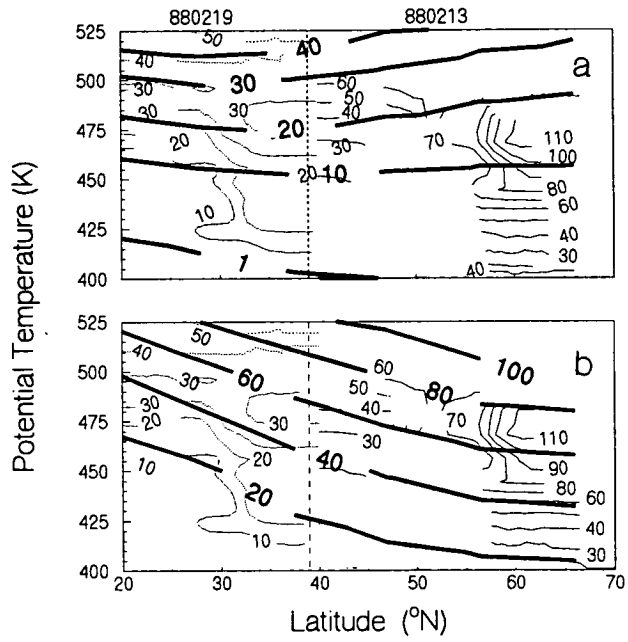

Figure 4-9 Comparisons between the observed ClO mixing ratios (pptv) in February 1988 with the results of model calculations (heavy lines) that contain gas phase chemistry only (a) and those that contain currently-known heterogeneous chemistry ($N_2O_5 + H_2O$) on sulfate aerosols (b) (King *et al.*, 1991). ClO data from Feb. 19 (21°N to 38°N) and Feb. 13 (39°N to 61°N) were separately converted to contours and then plotted together, separated by a vertical dotted line. These few ClO observations are better simulated at latitudes >30°N by the model with heterogeneous chemistry on sulfate aerosols and at latitudes <30°N by the model with only gas phase chemistry.

observed negative trend in total ozone over the last decade.

The proposed enhanced halogen catalysis that is initiated by heterogeneous chemistry currently appears to be the most likely cause of the declining ozone trend at middle latitudes. The summer trends and about one-half of the winter trends in ozone are simulated by models with heterogeneous chemistry on sulfate aerosols; the other half of the winter trend may result from transport of chemically-processed polar air to middle latitudes (see Chapter 8). If halogen chemistry is the cause, then as the atmospheric abundances of chlorine and bromine increase in the future, significant additional losses of ozone are expected not only in the Arctic, but also at middle latitudes.

4.5 BROMINE PHOTOCHEMISTRY

This current assessment (in Chapter 6), as well as the last assessment (WMO, 1990), has pointed to the greater potential of bromine than chlorine per molecule to destroy stratospheric ozone. This greater ozone depletion potential for the lower stratosphere happens because ~50 percent of the available bromine is in the reactive forms (Br and BrO), compared with chlorine, which has only a few percent in the reactive ClO form. Moreover, BrO primarily reacts synergistically with ClO in the fast catalytic cycle already shown to destroy ozone, even in the absence of oxygen atoms. Finally, bromine catalysis is most efficient in the lower stratosphere where the ozone concentration is largest. Thus, as the abundances of chlorine increase throughout the stratosphere, ozone destruction by bromine catalysis will increase proportionally to the increases in the abundances of both stratospheric chlorine and bromine.

Reactive bromine has been detected directly in the stratosphere, particularly inside the Antarctic chemically perturbed region and the Arctic polar vortex (Toohey *et al.*, 1990; Wahner *et al.*, 1990a; Carroll *et al.*, 1989). Direct measurements of the reaction of BrO with ClO in these polar regions come from the ground- and aircraft-based measurements of OClO (Solomon *et al.*, 1988; Wahner *et al.*, 1989; Perner *et al.*, 1991), for which the only known source is the reaction between BrO and ClO. Analyses of these measurements indicate that the BrO + ClO catalytic cycle is responsible for roughly 25 percent of the observed total ozone loss in the Antarctic ozone hole, with the Cl_2O_2 mechanism responsible for roughly 70 percent. Outside the polar vortices, or when the ClO abundances are only a few hundred pptv, the BrO + ClO catalytic cycle is more important, relative to the Cl_2O_2 cycle, than when ClO abundances exceed 1,000 pptv.

4.6 EFFECTS OF VOLCANIC ERUPTIONS ON OZONE

A large increase in the aerosol surface area caused by the injection of gas and debris from El Chichón in 1982, and the subsequent heterogeneous reactions may have lead to a decrease in the total ozone in the years that followed (Hofmann and Solomon, 1989; Brasseur *et al.*, 1990). The ozone depletion resulted from chlorine catalysis that followed heterogeneous reactions on sulfate aerosols in the El Chichón cloud (see Chapter 3). Direct evidence for heterogeneous conversions—the shifts in the trace gas concentrations in the El Chichón cloud—has been collected (Arnold *et al.*, 1991). Such eruptions could have a large impact in the future as the chlorine and bromine content of the stratosphere continue to increase.

Mt. Pinatubo in the Philippines erupted violently in June 1991, injecting a cloud of sulfur into the stratosphere. Analysis of early satellite observations suggest that Mt. Pinatubo injected two to three times as much sulfur into the stratosphere as El Chichón (Bluthetal, 1992). In the following few months, the aerosols from the eruption were observed as far north as Wyoming (Deshler *et al.*, 1992, Sheridan *et al.*, 1992), and a thick cloud encircled the Earth equatorward of 30° latitude (McCormick and Veiga, 1992).

The potential impact of the Mt. Pinatubo eruption on total ozone has been modeled. The calculated decline in total ozone is predicted to be in the range of 3 to 12 percent in the northern middle latitudes between 30°N and 60°N, depending on which model was used (J.M. Rodriguez, private communication; G.P. Brasseur, private communication). At high latitudes (>70°N) in February, these models predict maximum ozone losses in the range of 8 to 24 percent. Ozone reductions of 2 percent or less result from chlorine chemistry that is initiated by the reaction of $N_2O_5 + H_2O$ on the sulfate aerosols. The largest impact appears to result from chlorine chemistry that

is initiated by the reactions of $ClONO_2 + H_2O$ on the volcanic sulfate aerosols. The rates of these latter processes depend heavily on the temperature and the water vapor mixing ratio and are thus somewhat uncertain. However, the assessment models do indicate that volcanic injections into the stratosphere could have a substantial effect on global ozone, at least for one or two years.

A positive aspect of the volcanic injection into the stratosphere is that it presents an opportunity to study these processes on sulfate aerosols. Sharp gradients in aerosol abundances that are present in the early stages of the spread of the volcanic plume are excellent for testing theories about chemical processes that occur on time scales of less than a few weeks. They also present an excellent opportunity to test theories about the motion and mixing of air parcels in the lower stratosphere. These studies will help shape our understanding of the heterogeneous processes that are occurring on sulfate aerosols and will give us greater predictive capability of the future trends of total ozone.

REFERENCES

Adrian, G.P., T. Blumenstock, H. Fischer, L. Gerhardt, T. Gulde, H. Oelhaf, P. Thomas, and O. Trieschmann, Column amounts of trace gases derived from ground-based measurements with MIPAS during CHEOPS III, *Geophys. Res. Lett., 18,* 783, 1991.

Anderson, J.G., W.H. Brune, and M.H. Proffitt, Ozone destruction by chlorine radicals within the Antarctic vortex: The spatial and temporal evolution of ClO–O_3 anticorrelation based on *in situ* ER–2 data, *J. Geophys. Res., 94,* 11465, 1989a.

Anderson, J.G., W.H. Brune, S.A. Lloyd, D.W. Toohey, S.P. Sander, W.L. Starr, M. Loewenstein, and J.R. Podolske, Kinetics of O_3 destruction by ClO and BrO within the Antarctic vortex: An analysis based on *in situ* ER–2 data, *J. Geophys. Res., 94,* 11480, 1989b.

Anderson, J.G., D.W. Toohey, and W.H. Brune, Free radicals within the Antarctic vortex: The role of CFCs in Antarctic ozone loss, *Science, 251,* 39, 1991.

Angell, J.K., Influence of equatorial QBO and SST on total polar ozone, and the 1990 Antarctic Ozone Hole, *Geophys. Res. Lett., 17,* 1569, 1990.

Arnold, F., and G. Knop, Stratospheric nitric acid vapor measurements in the cold arctic vortex—implications for nitric acid condensation, *Nature, 338,* 746, 1989.

Arnold, F., T. Buhrke, and S. Qiu, Trace gas measurements in the stratospheric eruption cloud of volcano El Chichón using a balloon-borne mass spectrometer: Evidence for heterogeneous chemistry? submitted to *Nature,* 1991.

Atkinson, R.J., W.A. Matthews, P.A. Newman, and R.A. Plumb, Evidence of the middle latitude impact of Antarctic ozone depletion, *Nature, 340,* 290, 1989.

Austin, J., R.R. Garcia, J.M. Russell, S. Solomon, and A.F. Tuck, On the atmospheric photochemistry of nitric acid, *J. Geophys. Res., 91,* 5477, 1986.

Austin, J., R.L. Jones, D.S. McKenna, A.T. Buckland, J.G. Anderson, D.W. Fahey, C.B. Farmer, L.E. Heidt, M.H. Proffitt, A.F. Tuck, and J.F. Vedder, Lagrangian photochemical modeling studies of the 1987 Antarctic spring vortex, 2, Seasonal trends in ozone, *J. Geophys. Res., 94,* 16717, 1989.

Brasseur, G.P., C. Granier, and S. Walters, Future changes in stratospheric ozone and the role of heterogeneous chemistry, *Nature, 348,* 626, 1990.

Browell, E.V., C.F. Butler, S. Ismail, M.A. Fenn, S.A. Kooi, A.F. Carter, A.F. Tuck, O.B. Toon, M.H. Proffitt, M. Loewenstein, M.R. Schoeberl, I. Isaksen, and G. Braathen, Airborne lidar observations in the wintertime Arctic stratosphere: Ozone, *Geophys. Res. Lett. 17,* 325, 1990.

Brune, W.H., D.W. Toohey, J.G. Anderson, W.L. Starr, J.F. Vedder, and E.F. Danielsen, *In situ* northern middle latitude observations of ClO, O_3, and BrO in the wintertime lower stratosphere, *Science, 242,* 558, 1988.

Brune, W.H., D.W. Toohey, J.G. Anderson, and K.R. Chan, *In situ* observations of ClO in the Arctic stratosphere: ER–2 aircraft results from 59°N to 80°N latitude, *Geophys. Res. Lett., 17,* 505, 1990.

Brune, W.H., J.G. Anderson, D.W. Toohey, D.W. Fahey, S.R. Kawa, R.L. Jones, D.S. McKenna, and L.R. Poole, The potential for ozone depletion in the Arctic polar stratosphere, *Science, 252,* 1260, 1991.

Cariolle, D., A. Lasserre-Bigorry, and J.F. Royer, A general circulation model simulation of the springtime Antarctic ozone decrease and its impact on middle latitudes, *J. Geophys. Res., 95,* 1883, 1990.

Carroll, M.A., S. Solomon, R.W. Sanders, and A.L. Schmeltekopf, Visible and near-ultraviolet spectroscopy at McMurdo Station, Antarctica, 6, Observations of BrO, *J. Geophys. Res., 94,* 16633, 1989.

Chipperfield, M.P., and J.A. Pyle, Two-dimensional modeling of the Antarctic lower stratosphere, *Geophys. Res. Lett., 15,* 875, 1988.

Chipperfield, M.P., and J.A. Pyle, Two-dimensional modeling of the Northern Hemisphere high latitude lower stratosphere, *J. Geophys. Res., 95,* 11865, 1990.

Considine, D.B., A.R. Douglass, and R.S. Stolarski, Heterogeneous conversion of N_2O_5 to HNO_3 on background sulfate aerosols, submitted to *Geophys. Res. Lett.*, 1991.

de Zafra, R.L., M. Jaramillo, J. Barrett, L.K. Emmons, P.M. Solomon, and A. Parrish, New observations of a large concentration of ClO in the springtime lower stratosphere over Antarctica and its implications for ozone-depleting chemistry, *J. Geophys. Res., 94,* 11423, 1989.

Douglass, A.R., R.B. Rood, J.A. Kaye, R.S. Stolarski, D.J. Allen, and E.M. Larson, The influence of polar heterogeneous processes on reactive chlorine at middle latitudes: Three-dimensional model implications, *Geophys. Res. Lett., 18,* 25, 1991.

Drdla, K., R.P. Turco, and S. Elliott, Heterogeneous chemistry on Antarctic PSCs: A microphysical estimate of the extent of chemical processing, submitted to *J. Geophys. Res.,* 1991.

Dunkerton, T.J., and M.P. Baldwin, Quasi-biennial modulation of planetary-wave fluxes in the Northern Hemisphere winter, *J. Atmos. Sci., 48,* 1043, 1991.

Evans, W.F.J., C.T. McElroy, and I.E. Galbally, The conversion of N_2O_5 to HNO_3 at high latitudes in winter, *Geophys. Res. Lett.,12,* 825–828, 1985.

Fahey, D.W., S.R. Kawa, and K.R. Chan, Nitric oxide measurements in the Arctic winter stratosphere, *Geophys. Res. Lett.,17,* 489, 1990a.

Fahey, D.W., K.K. Kelly, S.R. Kawa, A.F. Tuck, M. Loewenstein, K.R. Chan, and L.E. Heidt, Observations of denitrification and dehydration in the winter polar stratospheres, *Nature, 344,* 321, 1990b.

Fahey, D.W., S. Solomon, S.R. Kawa, M. Loewenstein, J.R. Podolske, S.E. Strahan, and K.R. Chan, A diagnostic for denitrification in the winter polar stratosphere, *Nature, 345,* 698, 1990c.

Garcia, R.R., and S. Solomon, A possible relationship between the interannual variability in Antartic ozone and the quasi-biennial oscillation, *Geophys. Res. Lett., l4,* 848, 1987.

Gray, L.J., and S. Ruth, The two-dimensional modeling of the high latitude ozone QBO, *J. Atmos. Sci.*, in press, 1991.

Hartmann, D.L., L.E. Heidt, M. Loewenstein, J.R. Podolske, J. Vedder, W.L. Starr, and S.E. Strahan, Transport into the south polar vortex in early spring, *J. Geophys. Res., 94,* 16779, 1989.

Heidt, L.E., J.F. Vedder, W.H. Pollock, R.A. Lueb, and B.E. Henry, Trace gases in the Antarctic atmosphere, *J. Geophys. Res., 94,* 11599, 1989.

Hofmann, D.J., T.L. Deshler, P. Aimedieu, W.A. Matthews, P.V. Johnston, Y. Kondo, W.R. Sheldon, G.J. Byrne, and J.R. Benbrook, Stratospheric clouds and ozone depletion in the Arctic during January, 1989, *Nature, 340,* 117, 1989.

Hofmann, D.J., and S. Solomon, Ozone destruction through heterogeneous chemistry following the eruption of El Chichón, *J. Geophys. Res., 94,* 5029, 1989.

Isaksen, I.S.A., B. Rognerud, F. Stordal, M.T. Coffey, and W.G Mankin, Studies of Arctic stratospheric ozone in a two-dimensional model including some effects of zonal asymmetries, *Geophys. Res. Lett., 17,* 557, 1990.

Jackman, C.H., P.D. Guthrie, and J.A. Kaye, An intercomparison of nitrogen-containing species in Nimbus-7 LIMS and SAMS data, *J. Geophys. Res., 92,* 995, 1987.

Jones, R.L., J. Austin, D.S. McKenna, J.G. Anderson, D.W. Fahey, C.B. Farmer, L.E. Heidt, K.K. Kelly, D.M. Murphy, M.H. Proffitt, A.F. Tuck, and J.F. Vedder, Lagrangian photochemical modeling studies of the 1987 Antarctic spring vortex, 1, Comparison with AAOE observations, *J. Geophys. Res., 94,* 11529, 1989.

Jones, R.L., D.S. McKenna, L.R. Poole, and S. Solomon, Simulating the evolution of the chemical composition of the 1988/89 winter vortex, *J. Geophys. Res. Lett., 17,* 549, 1990.

Kawa, S.R., D.W. Fahey, L.C. Anderson, M. Loewenstein, and K.R. Chan, Measurements of total reactive nitrogen during the Airborne Arctic

Stratospheric Expedition, *Geophys. Res. Lett., 17,* 485, 1990.

Kawa, S.R., D.W. Fahey, L.E. Heidt, S. Solomon, D.E. Anderson, M. Loewenstein, M.H. Proffitt, J.J. Margitan, and K.R. Chan, Photochemical partitioning of the reactive nitrogen and chlorine reservoirs in the high latitude stratosphere, *J. Geophys. Res.,* in press, 1991.

Kaye, J.A., A.R. Douglass, R.B. Rood, R.S. Stolarski, P.A. Newman, D.J. Allen and E.M. Larson, Spatial and temporal variability of the extent of chemically processed stratospheric air, *Geophys. Res. Lett., 18,* 29–32, 1991.

Kelly, K.K., A.F. Tuck, L.E. Heidt, M. Loewenstein, J.R. Podolske, S.E. Strahan, and J.F. Vedder, A comparison of ER–2 measurements of stratospheric water vapor between the 1987 Antarctic and 1989 Arctic airborne missions, *Geophys. Res. Lett., 17,* 465, 1990.

King, J.C., W.H. Brune, D.W. Toohey, J.M. Rodriguez, W.L. Starr, and J.F. Vedder, Measurements of ClO and O_3 from 21°N to 61°N in the lower stratosphere during February 1988: Implications for heterogeneous chemistry, *Geophys. Res. Lett.,* in press, 1991.

Ko, M.K.W., J.M. Rodriguez, N.D. Sze, M.H. Proffitt, W.L. Starr, A. Krueger, E.V. Browell, and M.P. McCormick, Implications of the AAOE observations for proposed chemical explanations of the seasonal and interannual behavior of Antarctic ozone, *J. Geophys. Res., 94,* 16705, 1989.

Kondo, Y., P. Aimedieu, W.A. Matthews, D.W. Fahey, D.G. Murcray, D.J. Hofmann, P.V. Johnston, Y. Iwasaka, A. Iwata, and W.R. Sheldon, Balloon-borne measurements of total reactive nitrogen, nitric acid, and aerosol in the cold Arctic stratosphere, *Geophys. Res. Lett., 17,* 437, 1990.

Lait, L.R., M.R. Schoeberl, and P.A. Newman, Quasi-biennial modulation of Antarctic ozone depletion, *J. Geophys. Res., 94,* 11559, 1989.

Lefèvre, F., and D. Cariolle, Total ozone measurements and stratospheric cloud detection during the AASE and the TECHNOPS arctic balloon campaign, *Geophys. Res. Lett., 18,* 33–36, 1991.

Lefèvre, F., L.P. Riishojgaard, D. Cariolle, and P. Simon, Modeling the February 1990 type II event and its potential impact on the northern hemisphere ozone content, to be published in *J. Geophys. Res.,* 1991.

Lehmann, P., D.J. Koroly, P.A. Newman, T.S. Clarkson, and W.A. Matthews, An investigation into the reduction of stratospheric ozone in the Southern Australasian region, submitted to *Nature,* 1991.

Loewenstein, M., J.R. Podolske, K.R. Chan, and S.E. Strahan, N_2O as a dynamical tracer in the Arctic vortex, *Geophys. Res. Lett., 17,* 477, 1990.

Mankin, W.G., M.T. Coffey, A. Goldman, M.R. Schoeberl, L.R. Lait, and P.A. Newman, Airborne measurements of stratospheric constituents over the Arctic in the winter of 1989, *Geophys. Res. Lett., 17,* 473, 1990.

Mather, J.H., and W.H. Brune, Heterogeneous chemistry on liquid sulfate aerosols: A comparison of in-situ measurements with zero-dimensional model calculations, *Geophys. Res. Lett., 17,* 1283, 1990.

McElroy, M.B., R.J. Salawitch, and S.C. Wofsy, Antarctic O_3: Chemical mechanisms for the spring decrease, *Geophys. Res. Lett., 13,* 1296, 1986a.

McElroy, M.B., R.J. Salawitch, S.C. Wofsy, and J.A. Logan, Antarctic ozone: reductions due to synergistic interactions of chlorine and bromine, *Nature, 321,* 759, 1986b.

McKenna, D.S., R.L. Jones, L.R. Poole, S. Solomon, D.W. Fahey, K.K. Kelly, M.H. Proffitt, W.H. Brune, M. Loewenstein, and K.R. Chan, Calculations of ozone destruction during the 1988/89 Arctic winter, *Geophys. Res. Lett., 17,* 553, 1990.

Molina, L.T., and M.J. Molina, Production of Cl_2O_2 from the self-reaction of the ClO radical, *J. Phys. Chem., 91,* 433, 1987.

Molina, M.J., A.J. Colussi, L.T. Molina, R.N. Schindler, and T.-L. Tso, Quantum yield of chlorine-atom formation in the photodissociation of chlorine peroxide (ClOOCl) at 308 nm, *Chem. Phys. Lett., 173,* 310, 1990.

Mount, G.H., S. Solomon, R.W. Sanders, R.O. Jakoubek, and A.L. Schmeltekopf, Observations of stratospheric NO_2 and O_3 at Thule, Greenland, *Science, 242,* 555, 1988.

Murphy, D.M., Ozone loss rates calculated along ER–2 flight tracks, *J. Geophys. Res., 96,* 5045, 1991.

Nagatani, R.M., A.J. Miller, M.E. Gelman, and P.A. Newman, A comparison of Arctic lower stratospheric winter temperatures for 1988–89 with temperatures since 1964, *Geophys. Res. Lett., 17,* 333, 1990.

Natarajan, M., and L.B. Callis, Stratospheric photochemical studies with Atmospheric Trace Molecule Spectroscopy (ATMOS) measurements, *J. Geophys. Res., 96*, 9361–9370, 1991.

Perner, D., T. Klupfel, U. Parchatka, A. Roth, and T. Jorgensen, Ground-based UV-VIS spectrometry: Diurnal OClO profiles during January 1990 above Sondre Stromfjord, Greenland, *Geophys. Res. Lett., 18*, 787–790, 1991.

Pitari, G., and G. Visconti, Ozone trend in Northern Hemisphere: A numerical study, *J. Geophys. Res, 96*, 10931–10940, 1991.

Pitari, G., G. Visconti and V. Rizi, Sensitivity of stratospheric ozone to heterogeneous conversion of N_2O_5 on sulphate aerosols, *Geophys. Res. Lett., 18*, 833–836, 1991.

Plumb, A., Ozone depletion in the Arctic, *Nature, 347*, 20, 1990.

Pommereau, J.P., and F. Goutail, O_3 and NO_2 ground-based measurements by visible spectroscopy during Arctic winter and spring, 1988, *Geophys. Res. Lett., 15*, 891, 1988.

Prather, M.J., Polar stratospheric chemistry: HOCl reaction with HCl on clouds, submitted to *Nature*, 1991.

Prather, M.J., and A.H. Jaffe, Global impact of the Antarctic ozone hole: Chemical propagation, *J. Geophys. Res., 95*, 3473, 1990.

Prather, M., M.M. Garcia, R. Suozzo, and D. Rind, Global impact of the Antarctic ozone hole: dynamical dilution with a three-dimensional chemical transport model, *J. Geophys. Res., 95*, 3449, 1990.

Proffitt, M.H., K.K. Kelly, J.A. Powell, B.L. Gary, M. Loewenstein, J.R. Podolske, S.E. Strahan, and K.R. Chan, Evidence for diabatic cooling and poleward transport within and around the 1987 Antarctic ozone hole, *J. Geophys. Res., 94*, 16797, 1989.

Proffitt, M.H., J.J. Margitan, K.K. Kelly, M. Loewenstein, J.R. Podolske, and K.R. Chan, Ozone loss in the Arctic polar vortex inferred from high-altitude aircraft measurements, *Nature, 347*, 31, 1990.

Rattigan, O., E. Lutmann, R.L. Jones, R.A. Cox, C. Clemitshaw, and J. Williams, Temperature dependent absorption cross-sections of gaseous nitric acid and methyl nitrate, submitted to *J. Phys. Chem.*, 1991.

Rodriguez, J.M., M.K.W. Ko, N.D. Sze, S.D. Pierce, J.G. Anderson, D.W. Fahey, K.K. Kelly, C.B. Farmer, G.C. Toon, M.T. Coffey, L.E. Heidt, W.G. Mankin, K.R. Chan, W.L. Starr, J.F. Vedder, and M.P. McCormick, Nitrogen and chlorine species in the spring Antarctic stratosphere: Comparisons of models with Airborne Antarctic Ozone Experiment observations, *J. Geophys. Res., 94*, 16683, 1989.

Rodriguez, J.M., M.K. W. Ko, and D.D. Sze, The role of chlorine chemistry in the Antarctic ozone loss: Implications of new kinetic data, *Geophys. Res. Lett., 17*, 255, 1990.

Rodriguez, J.M., M.K. W. Ko, and N.D. Sze, Role of heterogeneous conversion of N_2O_5 on sulphate aerosols in global ozone losses, *Nature, 352*, 134-137, 1991.

Rood, R.B., J.A. Kaye, A.R. Douglass, D.J. Allen, S. Steenrod, and E.M. Larson, Wintertime nitric acid chemistry: Implications from three-dimensional model calculations, *J. Atmos. Sci., 47*, 2696, 1990.

Rood, R.B., J. Eric Nielsen, R.S. Stolarski, A.R. Douglass, J.A. Kaye, and D.J. Allen, Episodic total ozone minima and associated effect on heterogeneous chemistry and lower stratospheric transport, to be published in *J. Geophys. Res.*, 1991.

Rosenfield, J.E., Radiative effects of polar stratospheric clouds during AAOE and AASE, submitted to *J. Geophys. Res.*, 1991.

Salawitch, R.J., M.B. McElroy, J.H. Yatteau, S.C. Wofsy, M.R. Schoeberl, L.R. Lait, P.A. Newman, K.R. Chan, M. Loewenstein, J.R. Podolske, S.E. Strahan, and M.H. Proffitt, Loss of ozone in the Arctic vortex for the winter of 1989, *Geophys. Res. Lett., 17*, 561, 1990.

Sander, S.P., R.R. Friedl, and Y.L. Yung, Rate of formation of the ClO dimer in the polar stratosphere: Implications for ozone loss, *Science, 245*, 1095, 1989.

Schlager, H., and F. Arnold, Measurements of stratospheric gaseous nitric acid in the winter arctic vortex using a novel rocket-borne mass spectrometic method, *Geophys. Res. Lett., 17*, 433, 1990.

Schmidt, U., R. Bauer, A. Khedim, E. Klein, G. Kulessa and C. Shiller, Profile observations of long-lived trace gases in the arctic vortex, *Geophys. Res. Lett., 18*, 767–770, 1991.

Schoeberl, M.R., and D.L. Hartmann, The dynamics of the stratospheric polar vortex and its relation to springtime ozone depletion, *Science, 251,* 46, 1991.

Schoeberl, M.R., M.H. Proffitt, K.K. Kelly, L.R. Lait, P.A. Newman, J.E. Rosenfield, M. Loewenstein, J.R. Podolske, S.E. Strahan, and K.R. Chan, Stratospheric constituent trends from ER–2 profile data, *Geophys. Res. Lett., 17,* 469, 1990.

Schoeberl M.R., L.R. Lait, P.A. Newman, and J.E. Rosenfield, The structure of the polar vortex, *J. Geophys. Res.,* in press, 1991.

Solomon, S., Antarctic ozone: Progress toward a quantitative understanding, *Nature, 347,* 347, 1990.

Solomon, S., and J.G. Keys, Seasonal variations in Antarctic NO_x chemistry, *J. Geophys. Res.,* in press, 1991.

Solomon, S., R.R. Garcia, F.S. Rowland, and D.J. Wuebbles, On the depletion of Antarctic ozone, *Nature, 321,* 755, 1986.

Solomon, S., G.H. Mount, R.W. Sanders, R.O. Jakoubek, and A.L. Schmeltekopf, Observations of the nighttime abundance of OClO in the winter stratosphere above Thule, Greenland, *Science, 242,* 550, 1988.

Solomon, S., R.W. Sanders, and H.L. Miller, Jr., Visible and near-ultraviolet spectroscopy at McMurdo Station, Antarctica, 7, OClO diurnal photochemistry and implications for ozone destruction, *J. Geophys. Res., 95,* 13807, 1990.

Sze, N.D., M.K. W. Ko, D.K. Weisenstein, J.M. Rodriguez, R.S. Stolarski, and M.R. Schoeberl, Antarctic ozone hole: Possible implications for ozone trends in the Southern Hemisphere, *J. Geophys. Res., 94,* 11521, 1989.

Toohey, D.W., J.G. Anderson, W.H. Brune, and K.R. Chan, *In situ* measurements of BrO in the Arctic stratosphere, *Geophys. Res. Lett., 17,* 513, 1990.

Toohey, D.W., W.H. Brune, K.R. Chan, and J.G. Anderson, *In situ* measurements of midlatitude ClO in winter, *Geophys. Res. Lett., 18,* 21–24, 1991.

Toon, O.B., P. Hamill, R.P. Turco, and J. Pinto, Condensation of HNO_3 and HCl in the winter polar stratosphere, *Geophys. Res. Lett., 13,* 1284, 1986.

Tuck, A.F., Synoptic and chemical evolution of the Antarctic vortex in late winter and early spring, 1987, *J. Geophys. Res., 94,* 11687, 1989.

Tuck, A.F., T. Davies, S.J. Hovde, M. Noguer-Alba, D.W. Fahey, S.R. Kawa, K.K. Kelly, D. M. Murphy, M.H. Proffitt, J.J. Margitan, M. Loewenstein, J.R. Podolske, S.E. Strahan, and K.R. Chan, PSC-processed air and potential vorticity in the Northern Hemisphere lower stratosphere at middle latitudes during winter, *J. Geophys. Res.,* in press, 1991.

Wahner, A., R.O. Jakoubek, G.H. Mount, A.R. Ravishankara, and A.L. Schmeltekopf, Remote sensing observations of nighttime OClO column during the Airborne Antarctic Ozone Experiment, *J. Geophys. Res., 94,* 11405, 1989.

Wahner, A., J. Callies, H.-P. Dorn, U. Platt, and C. Schiller, Near UV atmospheric absorption measurements of column abundances during Airborne Arctic Stratospheric Expedition, January–February 1989: 3. BrO observations, *Geophys. Res. Lett., 17,* 517, 1990a.

Wahner, A., J. Callies, H.-P. Dorn, U. Platt, and C. Schiller, Near UV atmospheric absorption measurements of column abundances during Airborne Arctic Stratospheric Expedition, January–February 1989: 1. Technique and NO_2 observations, *Geophys. Res. Lett., 17,* 497, 1990b.

Wallace, L., and W. Livingston, Spectroscopic observations of atmospheric trace gases over Kitt Peak, 3, Long-term trends of hydrogen chloride and hydrogen fluoride from 1978 to 1990, *J. Geophys. Res., 96,* 15513, 1991.

Watson, L.R., J.M. Van Doren, P. Davidovits, D.R. Worsnop, M.S. Zahniser, and C.E. Kolb, Uptake of HCl molecules by aqueous sulfuric acid droplets as a function of acid concentration, *J. Geophys. Res., 95,* 5631, 1990.

Wolff, E.W., and R. Mulvaney, Reactions on sulphuric acid aerosol and on polar stratospheric clouds in the Antarctic stratosphere, *Geophys. Res. Lett., 18,* 1007–1010, 1991.

WMO, *Scientific Assessment of Stratospheric Ozone: 1989, Vol. I,* Global Ozone Research and Monitoring Project, Report No. 20, World Meteorological Organization, Washington, 1990.

Zander, R., G. Roland, L. Delbouille, A. Sauval, C.B. Farmer, and R.H. Norton, Column abundance and the long-term trend of hydrogen chloride (HCl) above the Jungfraujoch Station, *J. Atmos. Chem., 5,* 395, 1987.

CHAPTER 5

Tropospheric Processes: Observations and Interpretation

Authors:

I.S.A. Isaksen
Y.-P. Lee
R. Atkinson
H. Sidebottom
J.A. Fuglestvedt
C. Johnson
J. Lelieveld
A. Thompson

Additional Contributors:

W. Brune
J. Kaye
M. Oppenheimer
T. Berntsen

Chapter 5

Tropospheric Processes: Observations and Interpretation

Contents

SCIENTIFIC SUMMARY

- **Calculated O_3 changes:** Models predict increasing tropospheric ozone in the Northern Hemisphere in response to increasing emissions of NO_x, CO, CH_4, and NMHC that vary markedly with latitude, altitude, and season. These variations have to be taken into account if indirect climate effects are to be estimated.

  Model differences in the calculated ozone increase from NO_x emissions are large (~factor of 3). In addition the spatial and temporal variations are particularly large, and the model results are highly sensitive to the adopted background concentrations. All this precludes a quantitative assessment at the present time. NO_x emitted from aircrafts produces ozone much more efficiently than ground-based emission (by > a factor 10).

  Model differences and spatial variations in the O_3 increase in response to CH_4 emissions are moderate (both within 50 percent). The sensitivity to background assumptions is also moderate. Calculations of ozone changes can be done with reasonable accuracy.

- **Calculated OH changes:** Increases in CH_4, CO and HC emissions lead to reduced OH values, while increased NO_x emissions lead to enhanced OH levels. As a result of these opposing effects the sign of future OH changes cannot be predicted. The indirect effect of CH_4 emission on the CH_4 distribution, through its effect on OH, is estimated to be ~35 percent.

- **Indirect effects on global warming potential (GWP):** The indirect effects from CH_4 emissions on O_3 and CH_4 concentrations can be estimated with moderate accuracy. At present no estimates can be made of the indirect effects of NO_x surface emissions, as uncertainties in the calculations are too large. Furthermore, the impact on O_3 and CH_4 from NO_x emissions is in opposing directions.

- **Tropospheric chemistry of hydrochlorofluorocarbons (HCFCs) and hydrofluorocarbons (HFCs):** Experimental studies show that the breakdown of the HCFCs and HFCs is generally as expected from analogy with the C_1 haloalkanes, and alkanes. However, several of the intermediate oxidation products (COFCl, COF_2, CF_3COF, CCl_3COF, and the halogenated peroxyacyl nitrates) may have long lifetimes in the upper troposphere, and transport to the stratosphere could occur. This could influence the stratospheric ozone chemistry and radiation. Although future changes in OH, which cannot yet be estimated, will affect the breakdown of HCFCs and HFCs, these compounds will not have an effect on OH and the tropospheric O_3 chemistry.

Impact of increased emission on climate gases (+ gives increases in global averages, – gives decreases):

Incr. emission	OH	O_3	τ (CH_4, HCFC, HCF)
CH_4	–	+	+
NO_x	+	+	–
CO	–	+	+
HC	–	+	+

5.1 INTRODUCTION

In the present chapter three aspects of tropospheric chemical processes imposed by man-made emission of source gases will be discussed. First, we will look at the implications for the OH distribution and thereby for the lifetime of source gases which are controlled by reactions with OH in the troposphere (*e.g.*, CH_4 and HCFC). This is of importance for stratospheric ozone and for climate. Second, we will study the impact of source gas emission on tropospheric ozone and discuss the possibility to estimate indirect climate effects from the changes in ozone and other climate gases. Finally, the degradation of HFC and HCFCs is discussed.

Recent observations of ozone indicate substantial increases in the free tropospheric distribution over the last 1 to 2 decades (see Chapter 2 on measured trends in Ozone and Temperature). Ozone sonde observations over central Europe show that the increase occurs at least up to heights of approximately 10 km. Unfortunately, free tropospheric ozone changes are less well documented over other areas. Nevertheless, the observed ozone increases point to a fundamental change in the oxidation processes in the troposphere as ozone is a key player in tropospheric chemical processes.

Changes in the OH distribution in the troposphere could be of particular importance as OH provides the main sink for a large number of gases. It controls the distribution of CO and CH_4 (Weinstock, 1969) which are significant for tropospheric chemistry and also for gases affecting stratospheric ozone like HCFCs and HFCs (see the discussion later in this chapter and WMO, 1990). Changes in OH may also have a significant impact on climate change through the same loss reactions (IPCC, 1990). For instance, reduced OH enhances CH_4 concentrations and those of other radiatively active gases which are controlled by OH.

This chapter will be an update and extension of previous reviews of the tropospheric O_3 and OH chemistry (WMO, 1989; WMO, 1990). Recent studies have highlighted the importance of tropospheric chemical changes (*e.g.*, changes in O_3 and OH) for the stratospheric ozone and climate issues. We are particularly interested in assessing our capability to predict changes in O_3 and OH resulting from changed emission of source gases (CH_4 and other hydrocarbons, CO and NO_x), in order to predict their contribution to climate and stratospheric chemical changes. The emphasis will be on model estimates of such changes.

5.2 PROCESSES CONTROLLING TROPOSPHERIC O_3 AND OH

The chemistry of the troposphere is primarily driven by ultraviolet (UV) radiation with wavelengths shorter than about 320 nm. The OH radicals are formed by photodissociation of O_3 in the presence of water vapor:

$$O_3 + h\nu\ (\lambda \lesssim 320\ nm) \rightarrow O(^1D) + O_2 \qquad R1$$

$$O(^1D) + H_2O \rightarrow 2OH \qquad R2$$

Tropospheric ozone may be produced by *in situ* chemistry (Crutzen, 1973; Chameides and Walker, 1973; Fishman and Crutzen, 1978) or by transfer from the stratosphere, where O_3 is generated by the photodissociation of molecular oxygen at altitudes above 25 km, followed by combination of the ground state oxygen atoms with O_2:

$$O_2 + h\nu\ (\lambda < 242\ nm) \rightarrow 2O(^3P) \qquad R3$$

$$O(^3P) + O_2 + M \rightarrow O_3 + M \qquad R4$$

The *in situ* source of tropospheric ozone is the reaction of HO_2 with NO followed by the photodissociation of the nitrogen dioxide produced and the $O(^3P) + O_2$ reaction (R4).

$$HO_2 + NO \rightarrow NO_2 + OH \qquad R5$$

$$NO_2 + h\nu\ (\lambda < 400\ nm) \rightarrow O(^3P) + NO \qquad R6$$

Although NO and NO_2 concentrations are very low throughout most of the troposphere, the effect of this reaction sequence can provide a significant O_3 source. Ozone may also be produced by reaction sequences where organic peroxy radicals are involved instead of HO_2.

Reaction R1 followed by reaction R2 is of significance for the ozone distribution in the troposphere, as it provides a major sink for ozone.

There is also an *in situ* loss of ozone through reaction with NO_2 (to give NO_3), HO_2, and unsaturated hydrocarbons. The most important of these reactions is the one with HO_2

$$HO_2 + O_3 \rightarrow OH + 2O_2 \qquad (R7)$$

Although tropospheric O_3 only makes up about 10 percent of all ozone in the atmosphere, its amount is clearly central to the problem of the oxidizing efficiency of the troposphere, since O_3 photolysis is the primary source of OH radicals as well as being an oxidizing species itself. Through the formation of OH it determines the cleansing efficiency of the troposphere. Therefore, ozone ultimately maintains the chemical composition of the troposphere. Because of the central role of OH, the chemistry of many species, notably of CO, CH_4 and NO_x is strongly intertwined. In the background troposphere, remote from most of the direct effects of human activities, probably as much as 70 percent of the OH radicals react with CO, and a substantial part of the rest with CH_4. It follows that the future trends of oxidizing capacity will be tied to the future tropospheric burdens of CO, CH_4, nonmethane hydrocarbons, and other organics, as well as nitrogen oxides.

An understanding of tropospheric chemistry and estimating of the impacts of human activities require detailed knowledge of the photochemical reactions affecting CH_4, CO and O_3. Catalytic reactions with nitrogen oxides strongly affect photochemical processes. NO_x has natural and strong anthropogenic sources, most importantly the combustion of fossil fuels. Atmospheric environments are called NO_x-rich when NO volume-mixing ratios exceed those of O_3 by much more than the ratio of the rate coefficients between the ozone destruction reaction R7 and the ozone production reaction R5.

This ratio of k_{R7}/k_{R5} is about 2.5×10^{-4}. Since the O_3 mixing ratio near the earth's surface in the background atmosphere is roughly 20 ppbv, O_3 can be produced at NO mixing ratios exceeding $\approx$ 5 pptv, approximately equivalent to 15 to 20 pptv NO_x. Because of ozone loss by reactions R1 and R2, however, net ozone production takes place at larger NO_x volume-mixing ratios, depending on latitude and season. Especially in warm humid air, reaction R2 becomes so important that net production of O_3 requires quantities of NO_x that are several times larger. Over large parts of the Northern Hemisphere, where NO_x emissions are considerably enhanced by anthropogenic activities, net photochemical O_3 production is commonplace. In more pristine oceanic environments, in much of the Southern Hemisphere, where observations show low NO_x values (Ehhalt *et al.*, 1991; WMO, 1990), and in the middle troposphere, ozone destruction becomes more important.

Although OH radicals react with CH_4 and CO, these reactions do not always lead to a net loss of OH. They are merely the starting points for various, often lengthy reaction chains, which may partly compensate or even overcompensate, the initial removal of OH. For instance, in the presence of a sufficiently large amount of NO_x, the oxidation of CH_4 initiates reactions that lead to the formation of ozone without net loss of OH and NO_x. In NO_x-rich environments the dominant pathway to the first stable oxidation product, formaldehyde (CH_2O) yields NO_2 and HO_2. The hydroperoxyl radical (HO_2) reacts with NO, forms NO_2 and regenerates OH (reaction R5). UV radiation photodissociates the NO_2 molecules and produces O_3 (reaction R4). Further breakdown of CH_2O (which has a lifetime of less than a day) yields more HO_2 radicals, which, through the catalytic action of NO_x, also generate O_3 and OH. In the presence of sufficient NO_x, oxidation of one molecule of CH_4 yields more than one molecule of O_3, whereas further conversion of CO into CO_2 leads to additional O_3 production (Crutzen, 1988).

In NO_x-poor environments, on the other hand, alternative oxidation pathways to CH_2O become important, proceeding over the intermediate CH_3O_2H; no ozone is formed. Further breakdown of CH_2O again yields HO_2 radicals. In the absence of NO to react with, these radicals destroy O_3 (reaction R7). The net effect of the entire reaction sequence is loss of both O_3 and OH. Since anthropogenic emissions from the industrialized continents constitute the dominant source of NO_x, and because NO_x has a lifetime in the atmosphere of only a few days (during which it can travel at most a few thousand kilometers), we believe that a large part of the troposphere is in a NO_x-poor state. This is supported by NO_x measurements over the Pacific Ocean (McFarland *et al.*, 1979; Ridley *et al.*, 1987). Note, however, that in the upper troposphere

downward transport of NO_x derived from N_2O oxidation in the stratosphere and production from lightning can become important. Nevertheless, a substantial fraction of the background troposphere contains so little NO_x that there is little or no ozone produced. Under these circumstances we may also expect that OH radicals are lost by the oxidation of CO and CH_4. An increase in CH_4 and CO emissions can thus, via reduction of OH, amplify the growth of these species, an important positive feedback. It is therefore clear that understanding the distribution of NO_x in the troposphere is crucial for our ability to predict chemical changes in the troposphere.

5.3 COMPLEXITIES IN O_3 AND OH PREDICTIONS

The large variations in regional NO_x distributions have important implications for our understanding of the location of NO_x sources relative to their importance in ozone production. First of all, because water occupies such a large fraction of the earth's surface, more than 90 percent of the volume of the troposphere is contained in the region that we classify as the remote free troposphere. Second, because of the nonlinearity in the ozone production, a NO_x molecule in the remote free troposphere is much more effective in producing ozone than if such a molecule is introduced in more industrialized regions (Liu *et al.*, 1987). This nonlinearity is illustrated in Figure 5-1. Here, the ozone production efficiency, which is defined as the amount of ozone produced for the amount of NO_x released, is plotted as a function of the NO_x mixing ratio. Values in this figure were calculated for summer conditions at 40°N. However, the values are not expected to be significantly different at other latitudes. It should be noted that, depending on the assumption made concerning heterogeneous and nighttime chemistry of NO_x, these values are rather uncertain and may depend on meteorology and season. Nevertheless, from the figure, one can see that a molecule of NO_x released in areas with 10 pptv of NO_x mixing ratio (*e.g.* remote oceanic areas) will produce about 10 times as much ozone as an NO_x molecule released in areas with more than 10 ppbv of NO_x (*e.g.*, an urban center). In other words, for a constant NO_x source strength, NO_x entering or being transported to the remote atmosphere is more efficient in producing ozone than if it were introduced into the atmosphere in an industrialized region and oxidized there.

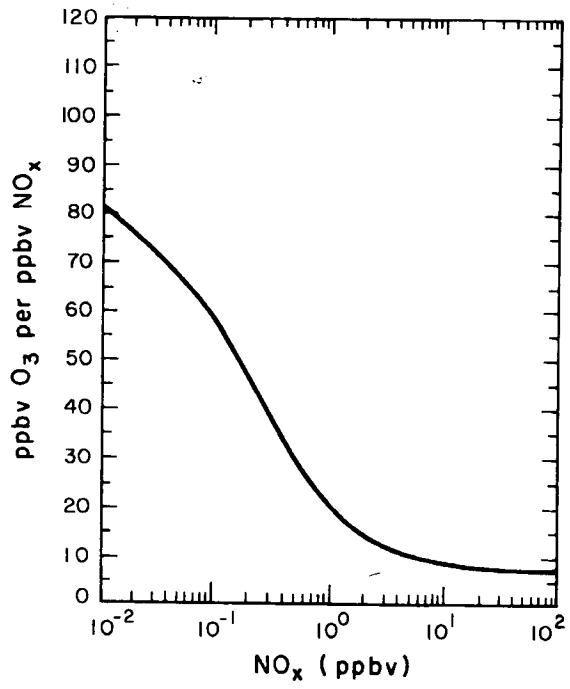

Figure 5-1 Ozone increases per NO_x molecule as a function of NO_x levels.

5.4 RECENT DEVELOPMENTS IN PROCESSES AFFECTING O_3 AND OH

5.4.1 CH_4 and CH_3CCl_3 Chemistry: Implications for OH

Chemical destruction of CH_4 in the atmosphere is about 97 percent accounted for by reaction with OH radicals, of which 90 percent occurs in the troposphere. An additional small, but still significant biological CH_4 sink is microbial oxidation in soil surface layers. Various compilations of methane sources and sinks have been developed; a frequently quoted study is that by Cicerone and Oremland (1988), in which a global CH_4 sink by OH of 400 to 600 Tg yr^{-1} is presented. However, recently, the rate coefficient of the reaction between CH_4 and OH has been revised, reducing it by about 20 percent (Vaghjiani and Ravishankara, 1991). This implies that

the CH_4 sink through OH is most likely in the lower part of the above range.

The accuracy of the CH_4 lifetime is largely determined by our ability to reproduce realistic OH distributions with global-scale chemistry-transport models, which in turn are tested against measurements of methylchloroform (CH_3CCl_3). This compound is emitted in relatively well known quantities (± 20 percent) by the chemical industry. Until now, it has been generally assumed that CH_3CCl_3 is destroyed only by reactions with OH radicals, so that agreement between measured and modeled CH_3CCl_3 concentrations has been interpreted as validation of the model predicted OH distributions. However, Wine and Chameides (1990) have suggested that the oceans constitute an additional sink of CH_3CCl_3, so that global average OH abundances may have been overestimated by up to several tens of percent. Also, for the reaction rate coefficient for CH_3CCl_3 + OH, only a few measurements are available, so that it cannot be ruled out that this reaction will be revised in the future (see also the discussion in Chapter 1).

5.4.2 Changes in Global OH

The importance of knowing OH distributions accurately is underscored by considering that hydrogen containing halocarbon (HCFC, HFC) concentrations in the atmosphere are determined by OH abundances. HCFCs and HFCs are the likely replacements of the long-lived CFCs that will be phased out by the turn of the century, because of the ability of CFCs to reach the stratosphere, where they contribute to ozone depletion. In fact, one compound, F-21, is already in widespread use and its concentration is measured to be approximately 100 pptv (1987) and increasing rapidly (WMO, 1990). Since the hydrogen atom in HCFCs and HFCs can be abstracted by OH, the chemical lifetimes of some of these compounds are short enough to prevent large amounts from being transported into the stratosphere. However, several of these compounds have still large enough lifetimes to be of importance for the chlorine loading of the stratosphere.

Significant changes in the global distribution of OH may have occurred over the last two centuries as the composition of the troposphere is documented to have evolved dramatically. Current changes in key compounds like CH_4 and CO which are observed to increase (see Chapter 1) and NO_x are expected to affect the OH abundances. Future change in global OH abundance would critically affect predictions of future trends in CH_4, CH_3CCl_3 and the HCFCs (Chapter 8).

Direct measurements of OH in the troposphere giving global distribution is difficult due to short lifetime (< 1 s) and low concentrations. One method of deriving an average global distribution is to use a tropospheric photochemical model for an appropriate range of global conditions (*e.g.*, Logan *et al.*, 1981; Isaksen and Hov, 1987; Thompson *et al.*, 1989). Such calculations require observations or calculations of sunlight as well as a large number of key species involved in the tropospheric OH chemistry (O_3, NO_x, H_2O, CO, CH_4, ...). The OH global fields thus derived have considerable uncertainties (Prather and Spivakovsky, 1990; Spivakovsky *et al.*, 1990a, 1990b), probably of the order of 30 percent to 50 percent (see discussion in WMO, 1990).

A second approach is to adopt a set of calculated OH distributions and to recalibrate or scale them with global tracer model experiments using species with known sources and with chemical losses proportional to OH. This approach has been applied successfully to ^{14}CO and ^{12}CO in a global two-dimensional tracer model (Volz *et al.*, 1981; Derwent and Volz-Thomas, 1990). This work has been followed up by a three-dimensional chemical tracer model study using the global distribution of CH_3CCl_3 to recalibrate the OH fields. Any such recalibration of the OH fields is highly sensitive to the underlying model: errors in the formulation, numerics, circulation, or spatial averaging of the model are usually unspecified or unknown, and they are difficult to propagate to the derived OH fields.

The Atmospheric Lifetime Experiment/Global Atmospheric Gases Experiment (ALE/GAGE) analysis of CH_3CCl_3 (Prinn *et al.*, 1987, 1992) presents a derivation of the overall atmospheric lifetime for CH_3CCl_3. By assuming that the loss is due solely to tropospheric OH (with a small, 10 percent correction for stratospheric losses), they infer a global mean OH concentration. Due to the coarse spatial resolution used in this study, the concept of a global mean value is not very meaningful nor well defined without specifying the spatial dependence of the rate coefficient and the tracer distribution. Nevertheless, the globally averaged loss of CH_3CCl_3

attributed to reaction with OH can be scaled to other reactions such as CH_4 and the HCFCs with similar distributions and rate coefficients to a high degree of accuracy. Therefore, the derivation of a CH_3CCl_3 atmospheric residence time from the ALE/GAGE analysis places a strong single constraint on the integrated tropospheric OH distribution. Unfortunately, stratospheric losses and other sinks such as oceanic uptake (Wine and Chameides, 1990) complicate the interpretation of the ALE/GAGE results. Prinn *et al.* (1992) deduce a trend in global OH from the ALE/GAGE CH_3CCl_3 record of + 1.0 percent ± 1.2 percent per year over the past decade. Their result may depend on the choice of a simple tropospheric box model. For example the shift in CH_3CCl_3 use over the past decade from the United States to Japan and the Far East is predicted (using a three-dimensional chemical transport model, Prather, 1991) to have caused a geographical redistribution of the CH_3CCl_3 which reduce the inferred global burden, and thereby leading to an assumed increase in the tropospheric loss comparable to that derived.

Given the complexities in determining a global OH concentration today and difficulties in interpreting the past record of trace gas change empirically-derived values for OH will be model dependent and have large uncertainties connected to errors in kinetics, trace gas concentrations, etc.

5.4.3 Other Processes Affecting Tropospheric Ozone

A. Heterogeneous chemistry

As discussed above, the possibility exists that global chemistry-transport models validated indirectly through CH_3CCl_3 analysis overpredict OH concentrations. The same might be true for model-derived OH distribution where only gas phase chemistry is considered. For example, it has been shown by Lelieveld and Crutzen (1990) that chemical reactions in clouds reduce photochemical production of O_3, due to separation of the insoluble NO from the soluble HO_2 between gas and aqueous phase, thus hampering reaction R5. Further, aqueous phase destruction of O_3 is significant, via

$$O_3(aq) + O_2^- \xrightarrow{H_2O} OH + 2O_2 + OH^- \qquad (R8)$$

Another important reaction in the aqueous phase is that between dissolved, hydrolyzed formaldehyde and OH. This reaction yields HO_2 that, after dissociation to O_2^-, contributes to O_3 destruction via reaction R8. Thus, a catalytic cycle is set up, in which O_3 and CH_2O are destroyed through aqueous phase OH and O_2^- regeneration. As a consequence of this cloud-induced O_3 reduction and that of CH_2O (being a source of HO_2) the oxidizing capacity of the troposphere is decreased. Furthermore, during the night N_2O_5 is formed via the reactions

$$NO_2 + O_3 \rightarrow NO_3 + O_2 \qquad (R9)$$

$$NO_3 + NO_2 \xrightarrow{M} N_2O_5 \qquad (R10)$$

(during daytime NO_3 is rapidly photolyzed). If the N_2O_5 comes into a cloud, HNO_3 is formed almost instantaneously. HNO_3 has a long chemical lifetime and, due to its high solubility, is efficiently removed by deposition processes, so that HNO_3 formation is a sink for NO_x. Reduction of NO_x through N_2O_5 scavenging in clouds additionally decreases O_3 production via reactions R5 and R6, whereas OH regeneration by reaction R5 is decreased.

B. Hydrocarbons and PAN

Another aspect that has received increased attention recently, is the role of higher hydrocarbons in global scale tropospheric chemistry (*e.g.*, Kanakidou *et al.*, 1991). It has long been recognized that these compounds are precursors of peroxyacetyl-nitrate (PAN), which can act as a globally important reservoir species of NO_x (Crutzen, 1979). PAN is thermally instable, and rapidly broken up at high temperatures. But after upward transport to higher, colder air layers its lifetime can increase up to several months, during which long-range transport can take place. Recent measurements show that the PAN levels can exceed NO_x by a factor of 2 to 6 in the free troposphere, with typical values of 100 to 200 pptv, and could thus contribute significantly to the redistribution of active nitrogen compounds in the free troposphere.

Very reactive natural hydrocarbons, such as isoprene and terpenes, which are emitted in large quantities by terrestrial ecosystems, can also contribute significantly to the formation of ozone and

PAN (Liu *et al.*, 1987; Chameides *et al.*, 1988). Blake *et al.* (1991) measured enhanced ozone levels (>90 ppbv) in the planetary boundary layer over the Eastern United States extending into the free troposphere, during a period with high isoprene levels. Isoprene was found to dominate the OH and ozone chemistry in the area. A main question to be answered is to what extent such natural production of hydrocarbons contributes significantly to free tropospheric ozone formation.

C. Radiative effects on ozone

Recent developments with respect to the influence of sulfate particles on climate change processes have indicated that, by enhancing backscattering of solar shortwave radiation, anthropogenic sulfur emissions may have counteracted climate warming by the increased emissions of greenhouse gases (Wigley, 1991). Since about 90 percent of the anthropogenic sulfur releases to the atmosphere occur in the Northern Hemisphere, and because SO_2 and sulfate have lifetimes of less than a week, the process is limited to the Northern Hemisphere. Charlson *et al.* (1991) have shown that anthropogenic sulfate enhances the hemispherically reflected solar radiation to such an extent, that the current warming by growth of CO_2 may be strongly reduced on a hemispheric scale. Although this estimate is still uncertain, based on incomplete scientific understanding, it seems possible that the decreased shortwave radiative flux in the Northern Hemisphere also reduces OH formation, and thus affects the oxidizing capacity of the troposphere.

The large reductions in lower stratospheric ozone observed over the last decade, could, according to the observations by Schnell *et al.* (1991) be significant for tropospheric O_3 and OH formation. Shortwave UV radiation could be strongly enhanced and increase OH production (R1) with varying effect on O_3 formation (Liu and Trainer, 1988).

In regions already high in NO_x, hydrocarbons and O_3, higher levels of UV imply higher rates of O_3 formation, assuming no other radiative changes are occurring. This is because photodissociation leading to OH and HO_2 increases the processes R5 and R6, leading to O_3 formation. In hydrocarbon and NO_x-poor environments the additional UV implies net O_3 loss through the reactions R1, R2, and R7. Indeed, tropospheric O_3 loss caused by perturbed UV during recent years of Antarctic ozone hole may have been observed at the South Pole, a NO_x-poor environment (Schnell *et al.*, 1991; Thompson, 1991). In either case; the effect on tropospheric OH resulting from stratospheric ozone depletion is to give higher levels through reactions R1 and R2.

A further consideration to be taken into account when future O_3 and OH levels are to be estimated is the possible effect of a global warming. This could affect moisture levels, cloud amount and distribution, precipitation, and dynamics on different scales. It is difficult to predict the consequences for O_3 and OH formation as a number of processes are likely to be affected, some leading to increases in O_3 or OH and some leading to decreases (Thompson *et al.*, 1989).

5.5 MODELING TROPOSPHERIC OZONE CHANGES

Ozone sonde measurements reported in chapter 10 of this assessment indicate that ozone has increased by 1 to 1.5 percent per year in the free troposphere over Europe during the last 20 to 25 years. This is likely an increase due to increased emissions of the ozone precursors NO_x, CO, CH_4, and other hydrocarbons during this time period.

In order to quantify the potential for tropospheric ozone formation by these gases, several model studies have been performed in which the emissions of the source gases were changed one by one. The impact on the tropospheric OH distribution, and thereby on methane, as a major greenhouse gas, has also been studied.

The following perturbation calculations have been carried out by several model groups:

- Doubled NO_x surface emission.
- Doubled CH_4 surface mixing ratio or surface fluxes.
- Increase of 0.5 Tg N/yr NO_x emission from airplanes.
- Doubled CO surface emission.
- Doubled NMHC surface emission.

5.5.1 Source Gases

The calculated changes in tropospheric ozone and in OH will be determined by the changes in

source strength and distribution of the source gases. A thorough discussion of methane, the nonmethane hydrocarbons, and carbon monoxide is given in Chapter 1, and these species will be mentioned only briefly in this Chapter.

• **Methane**: The long chemical lifetime of methane makes it a well mixed gas in the troposphere, with hemispheric differences less than 10 percent. Its impact on the ozone chemistry is therefore not very sensitive to the source distribution, but rather to the total methane emission, which is best determined indirectly by the global methane distribution (mean global concentration is at present 1.72 ppmv in the troposphere) and the loss through the OH reaction. The limiting factor is the accuracy with which we can estimate the tropospheric OH distribution (see the discussion above). Changes in methane emission are therefore expected to have a global effect on the ozone chemistry. Observed methane increase has been 0.7 to 0.8 percent per year during the last years (Table 1-1 in Chapter 1).

• **Nonmethane hydrocarbons:** These source gases are, first of all, expected to affect the ozone and OH chemistry in polluted regions where the anthropogenic emission is large. Due to the wide range of reactivity of NMHC their impact on the chemistry outside polluted regions depends strongly on the partitioning between the individual hydrocarbons. Such considerations are taken into account in model calculations of the impact of these sources on tropospheric chemistry. All the anthropogenically released NMHC have lifetimes short enough to show strong latitudinal and seasonal variations in concentrations, in most cases reflecting enhanced Northern Hemispheric mid-latitude emissions.

Outside the more polluted regional areas natural biogenic sources like isoprene could be the dominant ozone precursors as demonstrated by Blake *et al.* (1991). Although these compounds are very reactive and therefore predominantly are oxidized in the atmospheric boundary layer, they could contribute to free tropospheric ozone formation through ozone transport. However, estimates of their contribution to the free tropospheric ozone formation and OH changes are to be made, and require realistic descriptions of the transport of gases between the boundary layer and the free troposphere.

Anthropogenic emissions of NMHC are estimated to be 100 to 120 Tg/yr. Natural emissions are highly uncertain, but probably substantially larger than the anthropogenic emissions.

• **CO:** This is a major compound in tropospheric ozone chemistry, providing the main loss reaction for OH as well as enhancing the ozone formation by reaction R7 through the regeneration of HO_2:

$$OH + CO \rightarrow H + CO_2 \qquad (R11)$$

$$H + O_2 + M \rightarrow HO_2 + M \qquad (R12)$$

Observations of CO (see, Cicerone, 1988) show that Northern Hemispheric CO distribution is strongly influenced by large anthropogenic emissions (see Table 1-4 in Chapter 1), while Southern Hemispheric distribution is dominated by the production from methane oxidation, with additional production at low latitudes from natural sources (oxidation of natural hydrocarbons) as well as anthropogenic biomass burning which are not well quantified. Since the lifetime of CO is only a few months, large latitudinal variations in concentrations are found, reflecting the variation in the source distribution. Typical mixing ratios of 150 to 200 ppbv are observed in the Northern Hemisphere. In the Southern Hemisphere its mixing ratios are in the range 50 to 70 ppbv.

• **NO_x compounds.** The tropospheric lifetime of NO_x is very short (days or less) compared to the other gases we have discussed. The concentrations therefore vary strongly in space and in time, depending on the strengths and distribution of the sources. It is thus not very meaningful to define an average global or hemispheric distribution. From a modeling point of view it is important to have a good representation of the source distribution as ozone and OH distributions depend critically on the NO_x levels.

Several sources contribute to the formation of tropospheric NO_x as shown below.

The emission estimates of the natural sources (biogenic emission from soils, lightning) are connected with large uncertainties. Emission from soil has large temporal and spatial variations (Sanhueza *et al.*, 1990). This source may grow due to increased use of N-fertilizers. Production from lightning (and from airplanes) is of particular

importance as the NO_x is emitted directly into the free troposphere.

Table 5-1 Estimated emission of NO_x (Tg N/yr) (Sanhueza, 1991).

A. Natural	
—Soils	10–20
—Lightning	2–8
—Transport from stratosphere	1
B. Anthropogenic	
—Fossil fuel combustion	21
—Biomass burning	2.5–8.5
—Tropospheric aircraft	0.6
	37.1–59.1

The following source strengths are used in the reference calculations:

Fossil fuel combustion	21	Tg N/yr
Biomass burning/Soils	16	"
Lightning	6	"
Trsp. from stratosphere	0.6	"
Airplanes	0.7	"

Figure 5-2 shows a comparison between a measured NO profile at northern mid-latitudes (Ehhalt *et al.*, 1991) and calculated height distribution at the same latitudes. Although we should expect large variations in NO, making it difficult to compare model results with observations, some common features emerge. NO has a minimum in the middle troposphere (4 to 8 km) where mixing ratios are sufficiently low to expect *in situ* ozone loss. There is a marked increase above these heights which is assumed to be a result of NO_x production from lightning, airplanes and from transport from the stratosphere.

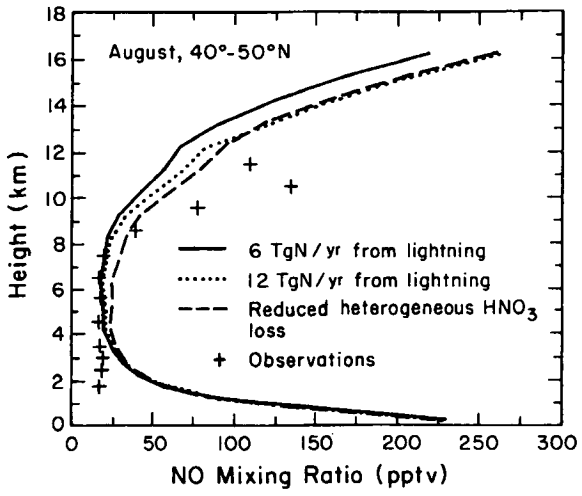

Figure 5-2 Height profile for the NO distribution at 40-50°N, with observed NO profiles from the same latitudes.

The results are seen to be sensitive to the strength of the lightning source and the the removal efficiency of HNO_3 in the middle and upper troposphere. The results indicate that calculations underestimate NO_x levels at these heights. Drummond *et al.* (1988) and Ehhalt *et al.* (1991) suggest that fast convective transport from the surface could contribute significantly to NO_x at these heights. It should be mentioned that transport by convective processes could be an effective pump of NO_x, CO, and other insoluble gases from the boundary layer to the upper troposphere (Dickerson *et al.*, 1987; Pickering *et al.*, 1991). These types of processes are not included in the calculations, and the given profile could therefore represent an underestimate of NO_x.

5.5.2 Calculated Ozone Perturbations

Figure 5-3 gives the global and yearly average height profiles of ozone changes due to increased emissions of NO_x from surface sources, increased emission of CH_4, and increased NO_x emission from aircraft. With the exception of airplane emission all model perturbations give smallest increases in the upper troposphere. Ozone changes show the fastest drop with height in the case of increased surface NO_x emissions.

There are substantial differences in the calculated ozone production from the different models. The "multiregion one-dimensional model" (National Aeronautics and Space Administration/Goddard Space Flight Center) seems to give somewhat larger ozone increases than the two-dimensional models (Harwell, Oslo), but there are also pronounced differences between the two-dimensional models in the cases of increased NO_x emissions, particularly in the upper troposphere. Calculated ozone changes due to increased CH_4 show more consistency between the models.

Ozone changes will, since it has a relatively short lifetime, depend on the distribution of the precursor

gas emissions. Anthropogenic influences are strongest in the Northern Hemisphere, hence ozone changes are most pronounced in this hemisphere. Figure 5-4 shows height profiles for ozone changes at 40°N latitude and 40°S latitude for NO_x increases and CH_4 increases. The hemispheric, seasonal and height differences in ozone increases are particularly strong in the case of increased NO_x emissions. Any impact on climate from tropospheric ozone changes will therefore be highly variable.

In these perturbation studies the source strength of the different gases emitted is highly different. In order to make comparisons of the efficiencies in producing ozone, all increases are given relative to emission of one mass unit and normalized to the

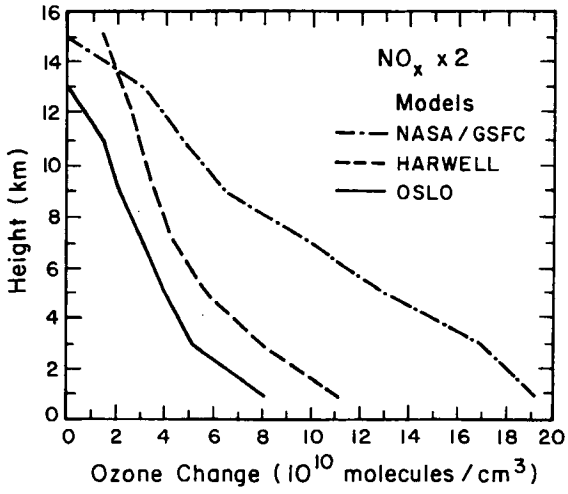

Figure 5-3a Global average height profiles of O_3 increases for doubled NO_x surface emission.

Table 5-2 Calculated average global changes in tropospheric ozone (percent) due to the increased emission of ozone precursors given in Table 5-1.

Model	NASA/GSFC	HARWELL	OSLO
2 x NO_x	13.8	6.6	3.7*(5.0)
2 x CH_4	15.2	11.3**	10.4**
2 x AIRPL.		3.4	0.8*
2 x CO			8.9*
2 x NMHC			6.8*

*Refers to calculations where surface fluxes of methane are kept constant.

**Refers to doubling in surface fluxes. All other calculations have a fixed methane mixing ratio at the lower boundary. (In the case of doubled CH_4, surface methane concentrations are twice the current values).

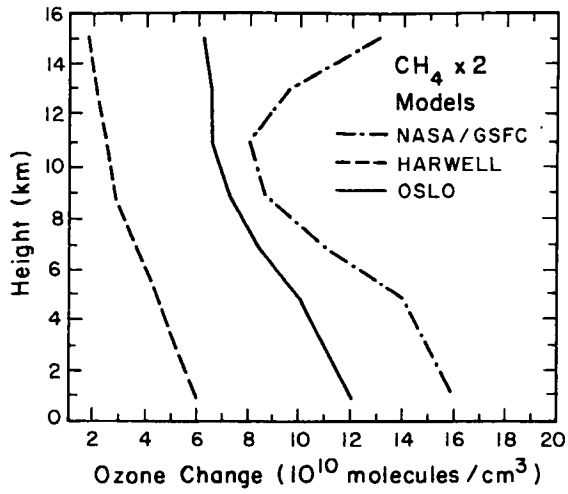

Figure 5-3b Global average height profiles of O_3 increases for doubled CH_4 emission.

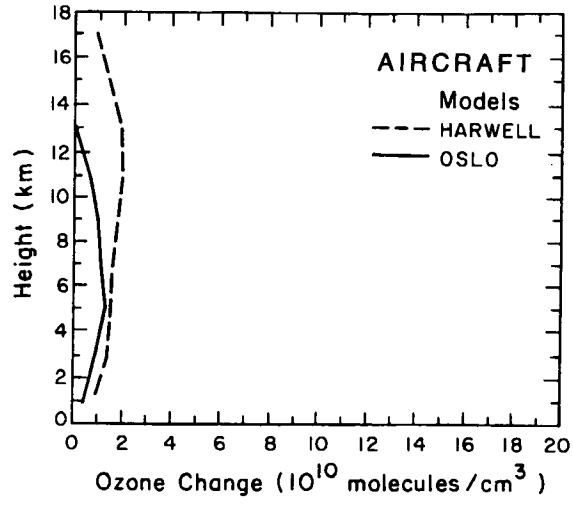

Figure 5-3c Global average height profiles of O_3 increases for increased emission from airplanes.

impact from methane. The results are given in Table 5-3.

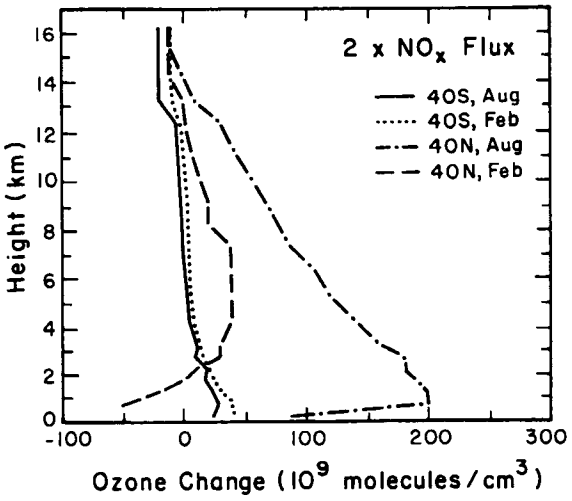

Figure 5-4a Height profiles for ozone increases at 40°N latitude and 40°S latitude for February and August for doubled NO_x surface emission.

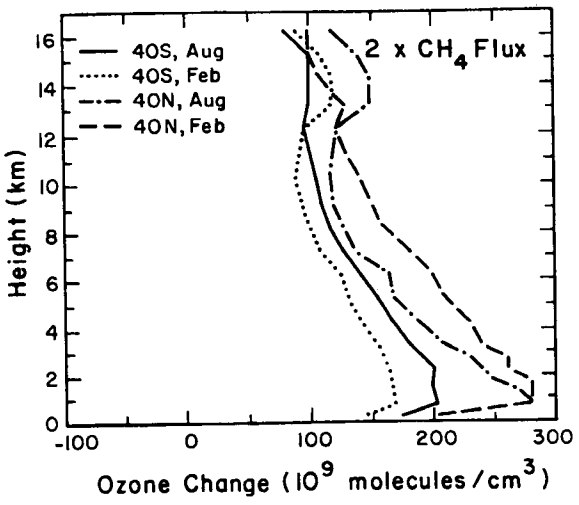

Figure 5-4b. Height profiles for ozone increases at 40°N latitude and 40°S latitude for February and August for doubled CH_4 emission.

Table 5-3 Efficiencies of the source gas emissions in producing tropospheric ozone. The numbers are given relative to the efficiency of methane emission. (Calculated with the Oslo model.)

	2 x NO_x	2x AIRPL	2 x CH_4	2 x CO	2 x NMHC
Rel.eff	3.0	50	1	0.2	0.5

It is clear that NO_x emitted from airplanes in the upper troposphere is much more efficient in enhancing ozone than ground based emissions of NO_x (a factor of 17 in these calculations). We should notice that we are here looking at the tropospheric average production. In the context of climate impact, upper tropospheric O_3 changes are more important than changes in the lower troposphere (Wang *et al.*, 1980; Lacis *et al.*, 1990). NO_x emissions from airplanes are therefore even more important than ground based releases as changes occur predominantly in the upper troposphere (see Figure 5-3). Both CO and NMHC are less efficient ozone producers than methane.

5.5.3 Changes in OH and in the Oxidation Potential of the Troposphere

Changes in the ozone distribution are accompanied by changes in OH and in source gases that are controlled by OH. From a climate point of view we are especially interested in the impact of OH changes on methane, we therefore concentrate our discussion on the interaction of chemical changes with methane through the reaction:

$$OH + CH_4 \rightarrow CH_3 + H_2O \qquad (R13)$$

This reaction is of importance because it provides the dominating loss mechanism for methane in the atmosphere as well as being an important loss reaction for OH.

We should remember that changes in OH also have impact on the abundances of other greenhouse gases like the HCFCs and the HFCs.

Table 5-4 gives calculated changes in the globally averaged OH concentrations in the model cases studied.

Table 5-4 OH changes (percent)

	NASA/GSFC	HARWELL	OSLO
2 x NO_x	17.4	15.2	15.4*(14.3)
2 x CH_4	-17.7	-10.2	-16.9*(-10.8)
2 x AIRPL		2.6	2.0*
2 x CO			-21.3*
2 x NMHC			-5.5*

*Refers to fluxes as lower-boundary values, otherwise the lower-boundary concentrations are fixed.

There is a consistent picture emerging from the calculations showing that increased NO_x emissions lead to enhanced OH and thereby increased oxidation in the troposphere, while increases in the emissions of the other source gases lead to reduced OH values.

A substantial part of the increase in methane concentrations could result from the positive feedback imposed by increasing methane on OH through reaction R13 (Chameides *et al.*, 1977; Sze, 1977; Isaksen, 1988). The magnitude of this feedback depends on how important reaction R13 is for the OH loss. The effect of the feedback increases with increasing methane levels as methane becomes more important for the OH loss at higher methane values. This is illustrated in Figure 5-5 where the relation between increased fluxes and increased mixing ratios of CH_4 in the atmosphere is given. The feedback is given by the expression

$$f = [(c-c1)/c1]/[(F-F1)/F1] - 1 \qquad \text{(R14)}$$

where c1 and F1 are present day concentrations and fluxes respectively, and c and F are perturbed levels.

At present day methane levels the feedback amounts to about 35 percent. This feedback accounts for an indirect effect that adds to the GWP of methane. In a similar way the feedback will affect the concentrations when emissions are reduced, but it will become less significant at lower concentrations.

5.5.4 Sensitivity Tests

As previously pointed out, there might be large nonlinear effects connected to formation of ozone in the atmosphere (see Figure 5-1) due to the large spatial and temporal variations of NO_x and the interaction with methane. Two sets of sensitivity tests have been performed. Calculations of the efficiency of ozone formation for: a) 10 percent increases in NO_x and CH_4 emissions instead of a doubling, and b) double NO_x and CH_4 emissions with a background production of 12 Tg N/yr from lightning (instead of 6 Tg N/yr). The results of these comparisons are shown in Table 5-5.

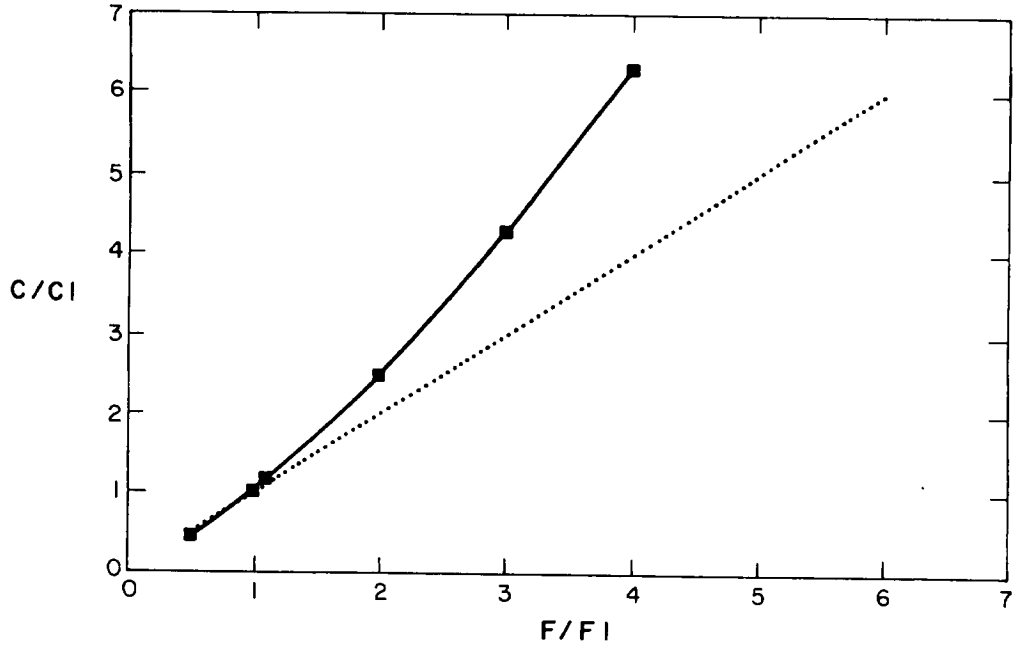

Figure 5-5 Calculated changes in average global mean concentration of CH_4 as a function of changes in fluxes. The straight line represents no feedback between OH and CH_4.

Table 5-5 Calculation of the efficiency of ozone formation from increased emissions of NO_x and CH_4. All numbers in (a) and (b) are compared to the efficiency of doubling CH_4 fluxes with a lightning production of 6 Tg N/yr. The numbers should therefore be compared with the numbers given in Table 5-3.

(a)	10 percent NO_x incr.	4.1
	10 percent CH_4 incr.	1.2
(b)	2 x NO_x	1.6
	2 x CH_4	1.07
	2 x AIRPL	24.8

When NO_x emissions from lightning are increased from 6 to 12 Tg N/yr in the model calculations and the CH_4 surface mixing rations are kept at fixed levels, the CH_4 emissions increase by 11 percent showing that the OH concentrations have increased.

Table 5-5 shows that tropospheric ozone production from NO_x increases is sensitive to the levels of NO_x in the atmosphere as well as the increase in the emissions. Small increases in emissions lead, as we could expect, to more efficient ozone production. When NO_x fluxes are increased by 10 percent, ozone production increases by approximately 40 percent, compared to the production when NO_x fluxes are doubled. Higher background levels of NO_x reduce the efficiency of ozone production from increased NO_x fluxes markedly. The sensitivity of methane induced ozone production to the adapted background levels of NO_x and to changes in fluxes is moderate. It is seen that CH_4 produces ozone slightly more efficiently at higher NO_x background levels, and the efficiency varies little with changes in the surface fluxes.

Tests of the response of ozone changes to changes in emissions of pollutants reveal that efficiencies are sensitive to the region where emission takes place (*e.g.*, NO_x emitted in polluted regions, gives different ozone production efficiency than NO_x emitted in less polluted regions).

5.5.5 Recent Changes in Tropospheric O_3 and OH

It has been pointed out that tropospheric OH could have decreased substantially over the past several decades due to suppression by increasing CH_4 and CO (Levine *et al.*, 1985; Thompson and Cicerone, 1986). On the other hand, increasing O_3 and NO_x since pre-industrial times may have caused OH to increase in certain parts of the troposphere (Isaksen and Hov, 1987; Crutzen and Zimmermann, 1991), making predictions of present trends difficult to make. Simulations of eight scenarios with varying rates of

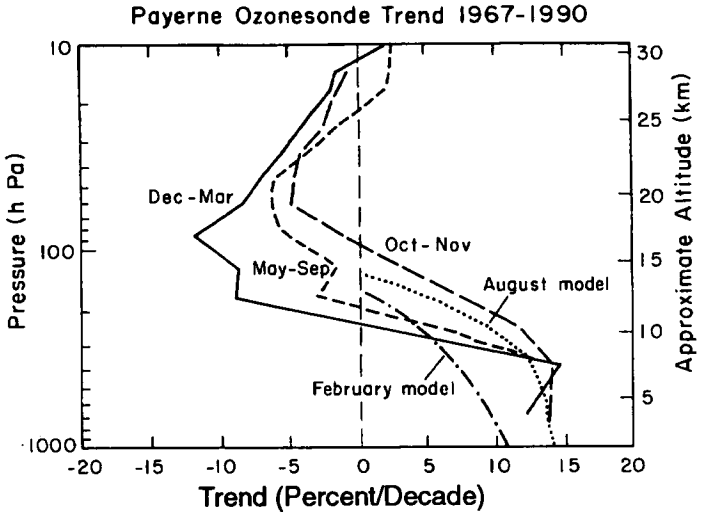

Figure 5-6 Height profile for the calculated and observed decadel ozone increases over the last 20 years at northern mid-latitudes (40–50°). Observations are from Payerne, Switzerland.

CH_4, CO, and NO emissions performed for a 1990 U.S. Assessment (USEPA, 1990) showed a small increase in global OH over the next 50 years (Isaksen *et al.*, 1989) whereas two other models (Prather, 1989; Thompson *et al.*, 1990) projected moderate losses over that period.

Ozone is probably increasing due to enhanced emissions of hydrocarbons, CO, and NO.

A model simulation of the chemical development of the troposphere over the last 20 years, assuming a doubling of anthropogenic emission of NO_x in this period, whereas emissions of CO and CH_4 have been increased by 0.8 and 1.0 percent per year respectively, and similar increases in anthropogenic NMHC, give global average ozone increases of 9.4 percent and a negligible change in OH (~1 percent). The mid-latitudinal height profile of the O_3 increase is shown in Figure 5-6, and is compared with Payerne, Switzerland, ozone sonde observations. The strong decadel ozone increase observed in the free troposphere up to approximately 10 km is also reflected in the model calculations.

Table 5-6 shows globally-averaged long-term future O_3 growth rates from several recent model studies that assume roughly current CH_4 and CO growth levels. Tropospheric O_3 increases are predicted to continue in the 0.2–1.5 percent/year range. Rates are different depending on how the models treat regional inhomogenities.

Table 5-6 Model ozone predictions with "business-as-usual" increases in CH_4, CO, and NO, 1985–2040.

Model	%Annual Increase, Global Mean
2D-Hough & Derwent (1990	0.2–0.4
2D-Law & Pyle (1991)	1–1.5
2D-Valentin (1990)	>0.2
USEPA (1990): 2D-Isaksen	0.1
USEPA (1990): M-1D-Thompson	0.3
USEPA (1990): OD-Prather AMAC	0.3

5.6 TROPOSPHERIC DEGRADATIONS OF HFCs AND HCFCs

The dominant loss process for the HFCs and HCFCs in the atmosphere is through reaction with the OH radical in the troposphere. Photolysis and reaction with the $O(^1D)$ atom in the stratosphere will also contribute a minor additional loss process. The rate constants for the OH radical reactions with the HFCs and HCFCs are now reasonably well known (DeMore *et al.*, 1990; IUPAC, 1991). The calculated tropospheric lifetimes are inversely proportional to the OH radical reaction rate constants at ~270 K, and are tabulated elsewhere in this report. Since these lifetimes are predominantly determined by the tropospheric OH radical concentration, any change in tropospheric OH will directly impact the fraction transported into the stratosphere (see discussion above for future tropospheric OH trends).

These OH radical reactions proceed by H-atom abstraction to form a haloalkyl radical (taking the compound CX_3CHYZ as an example, where X, Y and Z are H, Cl, Br and/or F)

$$OH + CX_3CHYZ \rightarrow H_2O + CX_3CYZ \qquad (R15)$$

The reactions subsequent to this initial H-atom abstraction have not been completely elucidated to date, and our present knowledge of the tropospheric degradations of the HFCs and HCFCs is in part based on analogy with the reasonably well understood reactions of the alkanes and the C_1 haloalkanes (WMO, 1990). A generalized reaction scheme is shown in Figure 5-7, leading to the first-generation products. If the carbonyl $CX_3C(O)Y$ is an aldehyde (Y = H), then a further reaction sequence can occur, as shown in Figure 5-8, and the CX_3 radical produced in these reactions then undergoes an analogous series of reactions as outlined for the CX_3CYZ radical in Figure 5-7.

Recent available experimental data obtained for the C_1 and C_2 HFCs and HCFCs are consistent with this general degradation scheme. The various steps in this degradation scheme are discussed briefly below, with an emphasis on the potential for transport of chlorine- and bromine-containing intermediate product species into the stratosphere.

- **Reaction of the Haloalkyl Radical, CX_3CYZ:** The sole reaction under tropospheric conditions is with O_2 to form the peroxy radical, CX_3CYZOO (WMO, 1990).

- **Reactions of the Peroxy Radical, CX_3CYZOO:** The peroxy radicals may react with NO, NO_2, and HO_2 radicals under tropospheric conditions. Given

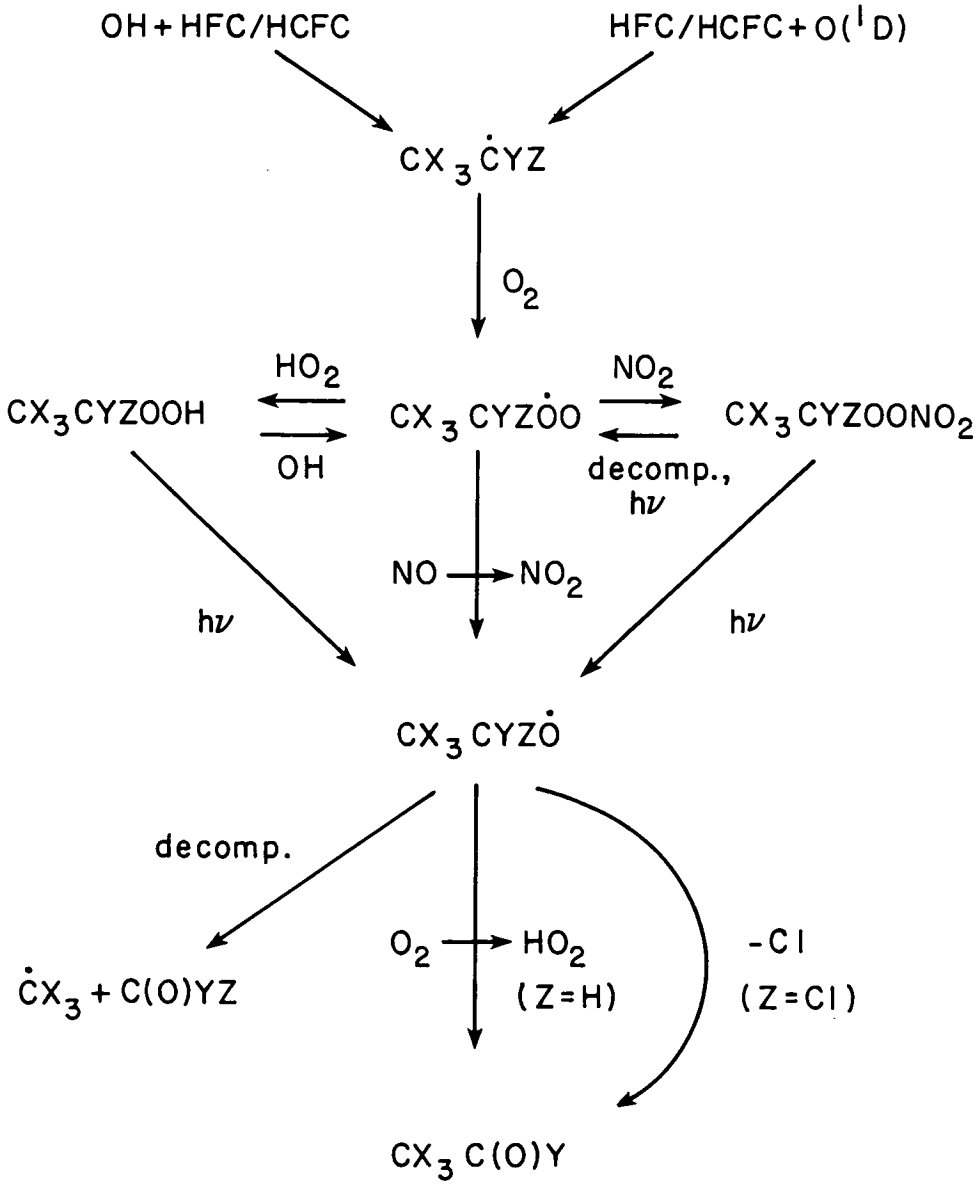

Figure 5-7 Degradation scheme for HFC/HCFC initiated by the reactions with OH and O(1D).

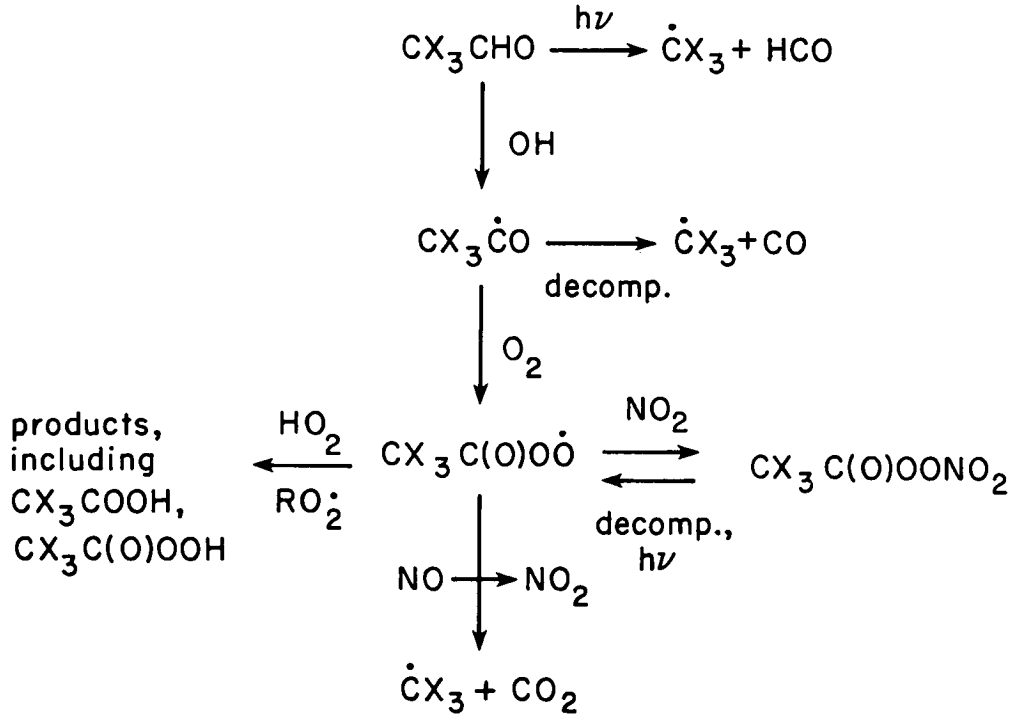

Figure 5-8 Example of oxidation scheme for HFC/HCFC oxidation products (aldehydes).

the relative magnitudes of the rate constants for reactions of peroxy radicals with these species and their atmospheric concentrations, the major loss process for CX_3CYZOO radicals in the atmosphere will be with NO (WMO, 1990; Hayman *et al.*, 1991). While the reaction with NO is expected to form mainly the alkoxy radical, CX_3CYZO, formation of the organic nitrate, $CX_3CYZONO_2$, from the pathway

$$CX_3CYZOO + NO \xrightarrow{M} CX_3CYZONO_2 \qquad (R16)$$

may also occur to a minor extent. Formation of ethyl nitrate from the reaction of NO with the ethyl peroxy radical accounts for approximately 1percent of the overall reaction at 298°K and atmospheric pressure (Atkinson *et al.*, 1982). The products and quantum yields of photolysis of alkyl nitrates have not been extensively studied, although the lack of structure in the absorption spectra of these compounds suggests that the quantum yield for decomposition is close to unity. The available evidence indicates that the major reaction channel involves breaking of the $O\text{-}NO_2$ bond generating the alkoxy radical (Roberts, 1990). Thus, it is unlikely that halogenated nitrates will have significant atmospheric lifetimes but will photolyze to give the corresponding alkoxy radical.

The reactions of the peroxy radical with HO_2 and NO_2 lead to the formation of hydroperoxides and peroxynitrates, respectively (Figure 5-7).

• **Hydroperoxides:** The hydroperoxides are expected to undergo photolysis and reaction with the OH radical.

$$CX_3CYZOOH + h\nu \rightarrow CX_3CYZO + OH \qquad (R17)$$

$$OH + CX_3CYZOOH \rightarrow H_2O + CX_3CYZOO \qquad (R18)$$

$$OH + CX_3CYZOOH \rightarrow H_2O + CX_3CYOOH \ (Z = H) \qquad (R19)$$

$$CX_3CYOOH \rightarrow CX_3C(O)Y + OH \qquad (R20)$$

To date, kinetic and photolysis data are available only for CH_3OOH and these data indicate lifetimes of ~5 days for each of these processes, with an overall lifetime due to photolysis and OH radical reaction of ~2 to 3 days. In addition, wet deposition of the hydroperoxides is expected to be efficient, and dry deposition may also be rapid (*WMO*, 1990). The tropospheric residence times of the halogenated hydroperoxides are then expected to be short, of the order of a few days or less, and the potential for transport of chlorine into the stratosphere through the intermediacy of the hydroperoxides is very low.

• **Haloalkyl Peroxynitrates:** The haloalkyl peroxynitrates, $ROONO_2$, thermally decompose back to the peroxy radical and NO_2

$$CX_3CYZOONO_2 \rightleftarrows CX_3CYZOO + NO_2 \qquad (R21)$$

The lifetimes of methyl and ethyl peroxynitrate due to this thermal decomposition range from ~1 sec at the earth's surface (288 K) to ~10^6 sec (10 days) in the upper troposphere (Zabel *et al.*, 1989; IUPAC, 1989, 1991; WMO, 1990). For the haloalkyl peroxynitrates $ROONO_2$, where R = CF_2Cl, $CFCl_2$, and CCl_3, the thermal decomposition rates are slower, and the lifetimes due to thermal decomposition range from 5-20 sec at 298 K to 0.1 to 1 year in the upper troposphere (Köppenkastrop and Zabel, 1991). The thermal decomposition rates for $CF_2ClCH_2OONO_2$ and $CFCl_2CH_2OONO_2$ have been measured (Kirchner *et al.*, 1991) and the data indicate a lifetime due to thermal decomposition of ~2 days in the upper troposphere (*i.e.*, less than those of $CF_2ClOONO_2$, $CFCl_2OONO_2$, and CCl_3OONO_2). This limited set of thermal decomposition data show that the haloalkyl peroxynitrates of structure $ROONO_2$, where R = CF_2Cl, $CFCl_2$ and CCl_3, are thermally stable over a time period of months to a few years in the upper troposphere, especially at high NO_2/NO concentration ratios, and suggest that this may also be the case for compounds of the structure RCX_2OONO_2, where X = Cl and/or F.

In addition to thermal decomposition, the peroxynitrates are expected to undergo photolysis, based on the limited data of Cox and Tyndall (1979), Morel *et al.* (1980) and Sander and Watson (1980) for CH_3OONO_2, $CFCl_2OONO_2$, and CCl_3OONO_2, with calculated lifetimes of ~5 days in the lower troposphere. These data indicate that the lifetimes of the peroxynitrates will be sufficiently short that significant transport to the stratosphere will not occur, except possibly at high latitudes during wintertime nighttime conditions for $CF_2ClOONO_2$, $CFCl_2OONO_2$, and CCl_3OONO_2 (and possibly other, as yet not studied, peroxynitrates).

• **Acyl Peroxynitrates:** For the halogen-containing acyl peroxynitrates, $RC(O)OONO_2$, the thermal decomposition lifetimes are expected, by analogy with those for peroxyacetyl and peroxypropionyl nitrates (PAN and PPN, respectively), to be much longer than those for the peroxynitrates $ROONO_2$. Rate data for the thermal decomposition of $CF_2ClC(O)O_2NO_2$ reported by Kirchner *et al.* (1991) support this conclusion. The results show that the thermal lifetime is extremely long, varying from ~3 hour at 298 K to ~5000 year in the upper troposphere (220 K) and its total lifetime in the upper troposphere will be limited by its photolysis rate. Thus, as for the alkyl peroxynitrates, halogenation appears to increase the thermal stability of acyl peroxynitrates. Since photolysis is also likely to be slow (by analogy with peroxyacetyl nitrate) (IUPAC, 1989, 1991), the lifetimes of the haloperoxyacyl nitrates due to chemical processes are likely to be long in the upper troposphere, and the potential for transport of chlorine to the stratosphere exists. This is possible for the peroxyacyl nitrates which may be formed in the tropospheric degradation reactions of HCFC-141b and 142b.

• **Acids and Acyl Hydroperoxides**: By analogy with the reactions of the $CH_3C(O)OO$ radical, haloacyl peroxy radicals, $CX_3C(O)OO$, may react with HO_2 and also with CH_3O_2 in the lower troposphere (WMO, 1990). The products of these reactions are expected to be acids, $CX_3C(O)OOH$. Reaction with the OH radical is likely to be slow, and the most probable fate of these species is via wet deposition and rain out.

• **Reactions of Haloalkoxy Radicals**: There are a number of potential reaction pathways for the atmospheric degradation of haloalkoxy radicals.

C-Cl or C-Br bond cleavage: (i)

$$CX_3CYClO \rightarrow CX_3C(O)Y + Cl$$
$$CX_3CYBrO \rightarrow CX_3C(O)Y + Br$$

C-C bond cleavage:

$$CX_3CYZO \rightarrow CX_3 + C(O)YZ \quad \text{(ii)}$$

Hydrogen abstraction:

$$CX_3CHYO+O_2 \rightarrow CX_3C(O)Y + HO_2 \quad \text{(iii)}$$

For example, for the $CF_2ClCHClO$ radical formed from HCFC-132b

$$CF_2ClCHClO \rightarrow CF_2ClCHO + Cl \quad \text{(R22)}$$

$$CF_2ClCHClO \rightarrow CF_2Cl + HC(O)Cl \quad \text{(R23)}$$

$$CF_2ClCHClO + O_2 \rightarrow CF_2ClC(O)Cl + HO_2 \quad \text{(R24)}$$

The majority of the experimental data concerning the reactions of haloalkoxy radicals has come from chlorine atom-initiated oxidation of halogenated alkanes and alkenes. Most of this work has been carried out at 298 K and atmospheric pressure in air. It is assumed that the removal processes for these radicals determined in chlorine-rich systems are applicable to atmospheric conditions. A number of general conclusions concerning the relative importance of the available reaction pathways may be drawn from the available experimental data (Bertrand *et al.*, 1971; Sanhueza *et al.*, 1976; Carr *et al.*, 1986; Lesclaux *et al.*, 1987; WMO, 1990; Nelson *et al.*, 1990; Edney *et al.*, 1991; Hayman *et al.*, 1991; Jemi-Alade *et al.*, 1991; Libuda *et al.*, 1991; Meller *et al.*, 1991; Scollard *et al.*, 1991; Tuazon and Atkinson, 1991; Zellner *et al.*, 1991).

(i) CX_2ClO radicals (X = H, Cl or F) eliminate a Cl atom, except for CH_2ClO where reaction with O_2 is the dominant reaction. The reactions for the CH_2BrO and $CHBr_2O$ radicals are totally analogous to those for the corresponding chlorine-containing radicals.

(ii) CF_3O radicals are believed to be the product of the reaction of CF_3O_2 with NO under atmospheric conditions. However, the mechanism for oxidation of the CF_3O radical is uncertain. Fluorine atom loss and reaction with O_2 are improbable since both reactions are appreciably endothermic. It is generally assumed that the final product of the tropospheric degradation of CF_3O radicals will be $C(O)F_2$, although the formation of other products cannot be discounted.

(iii) CX_3CH_2O radicals (X = H, Cl or F) react either with O_2 to form the aldehyde and an HO_2 radical, or undergo C-C bond cleavage.

(iv) CX_3CCl_2O and CX_3CFClO radicals decompose by Cl atom elimination rather than by C-C bond fission. From the available data this type of reaction occurs whatever the substituent X.

(v) CX_3CF_2O radicals underdo C-C bond cleavage.

(vi) CX_3CHYO radicals (Y = Cl or F) have two important reaction channels. The relative importance of the C-C bond breaking process and reaction with O_2 appears to be a function of both the nature of X and Y and is expected to be temperature dependent. Recent results for the CF_3CHFO radical show that at 298 K and one atmosphere of air C-C bond fission is the dominant reaction channel (~75 percent) (Meller *et al.*, 1991; Tuazon and Atkinson, 1991; Zellner *et al.*, 1991). For atmospheric modeling purposes both the effect of O_2 pressure and temperature on the relative importance of the two pathways is required.

- **Carbonyl Compounds:**

Aldehydes. The absorption spectra of HC(O)Cl and HC(O)Br extend beyond 290 nm (Libuda *et al.*, 1990, 1991) and lead to calculated photolysis lifetimes in the troposphere of 50 days and ~4 days, respectively, assuming unit photodissociation quantum yields. HC(O)F will not photolyze in the troposphere (Libuda *et al.*, 1991). Only for HC(O)Cl has the OH radical reaction been studied (Libuda *et al.*, 1990), with an upper limit to the rate constant of $<3.2 \times 10^{-13}$cm^{3}molecule^{-1}s^{-1} at 298°K being reported. These OH radical and absorption cross-section data indicate that HC(O)Cl and HC(O)Br will have short lifetimes in the troposphere. HC(O)F is, however, expected to have a much longer lifetime with respect to OH radical reaction and photolysis.

The tropospheric lifetimes of the halogenated acetaldehydes due to reaction with OH radicals are calculated to range from about four days for CH_2ClCHO to around 20 days for CF_3CHO (Dóbé *et al.*, 1989; Nelson *et al.*, 1990; Starcke *et al.*, 1990; Balestra-Garcia *et al.*, 1991; Scollard *et al.*, 1991). The absorption cross sections have been measured for several Cl and Br-containing acetaldehydes (Starcke *et al.*, 1990; Libuda *et al.*, 1991; Rattigan *et al.*, 1991). Photolysis lifetimes in the troposphere are about 1 to 7 hours, based on unit photodissociation quantum yields. Assuming the halogenated acetaldehydes have similar quantum yields to acetaldehyde, their photolysis lifetimes may be several days. These available OH rate constant and photolysis data for halogenated acetaldehydes indicate that they will rapidly degrade in the troposphere, and not be important reservoirs for halogen atoms.

Carbonyl halides. Reaction of the OH radical with $C(O)Cl_2$ has been shown to be slow, with an upper limit to the rate constant of $<1 \times 10^{-15}$ cm^3 molecule^{-1} s^{-1} having been determined at 298 K (Nelson *et al.*, 1990), and the analogous reactions with C(O)FCl and $C(O)F_2$ are expected to be similarly slow. The absorption cross sections of the carbonyl halides have been measured (CODATA, 1982; Libuda *et al.*, 1991; Meller *et al.*, 1991). The absorption spectrum of $C(O)Br_2$ extends beyond 290 nm, and leads to a calculated photolysis lifetimes in the troposphere of less than one week (Libuda *et al.* 1991). The absorption spectrum of $C(O)Cl_2$ extends to 290 nm (Meller *et al.*, 1991), with the longwavelength limits of C(O)FCl and $C(O)F_2$ being 250 nm and 230 nm, respectively (Meller *et al.*, 1991). The calculated lower tropospheric lifetime of $C(O)Cl_2$ due to photolysis is approximately 50 days, assuming a unit quantum yield. For C(O)FCl and $C(O)F_2$, photolysis will not occur in the troposphere. Thus these carbonyl halides are expected to have long tropospheric lifetimes due to chemical loss processes. Uptake into water droplets and oceans with subsequent hydrolysis could be a possible removal process in competition with transport to the stratosphere. It has generally been assumed that removal in cloudwater and the oceans is relatively efficient, leading to a low flux of these species into the stratosphere (WMO, 1990). However, Worsnop *et al.* (1991) have only been able to obtain upper limits for the uptake coefficients for $C(O)F_2$ and $C(O)Cl_2$ into aqueous droplets of less than 10^{-3}. Furthermore, the calculated washout ratio W of W = 4.1 for $C(O)Cl_2$ at 278 K reported by Dana *et al.* (1985) is consistent with only slow or very slow rain-out of $C(O)Cl_2$ (compare with W = 5–6 for CH_3CCl_3 at 298 K and with washout ratios of 10^4 to 10^6 for very efficiently rained-out chemicals (Dana *et al.*, 1985)). These results indicate that if indeed wet deposition is important, removal into the oceans may dominate over cloudwater uptake. Further studies of the uptake of these compounds to water droplets is urgently needed.

Acetyl halides. As for the carbonyl halides, the fully halogenated acetyl halides, $CX_3C(O)Y$, are not expected to react with the OH radical at significant rates. Moreover, those acetyl halides containing H atoms, such as $CH_3C(O)Cl$, are expected to react only slowly with the OH radical, as observed for $CH_3C(O)Cl$ (Nelson *et al.*, 1990). Hence the major

tropospheric loss processes for the acetyl halides will be photolysis and/or wet deposition. Absorption cross sections have been measured for several acetyl halides ($CF_3C(O)Cl$, $CF_3C(O)F$, $CH_3C(O)F$, $CH_3C(O)Cl$, $CH_2ClC(O)Cl$, $CHCl_2C(O)Cl$ and $CCl_3C(O)Cl$) (Libuda *et al.*, 1991; Meller *et al.*, 1991; Rattigan *et al.*, 1991). Assuming unit quantum yields for photodissociation, the calculated tropospheric lifetimes are approximately: $CF_3C(O)Cl$, 85 days (Rattigan *et al.*, 1991); $CF_3C(O)F$, 1700 years (Rattigan *et al.*, 1991); $CH_3C(O)F$, 24 years (Rattigan *et al.*, 1991); $CH_3C(O)Cl$, 75 days (Libuda *et al.*, 1991); $CH_2ClC(O)Cl$, 30 days (Libuda *et al.*, 1991); $CHCl_2C(O)Cl$, 9 days (Libuda *et al.*, 1991); and $CCl_3C(O)Cl$, 6 days (Libuda *et al.*, 1991).

These data indicate that photolysis of the acetyl chlorides, $CX_3C(O)Cl$, will be important in the troposphere, whereas the removal of the acetyl fluorides via photolysis is likely to be negligible. There is no evidence at the present time to indicate that photolysis of the acetyl halides leads to the formation of chlorofluorocarbons, as for example (Meller *et al.*, 1991):

$$CF_3C(O)Cl + h\nu \rightarrow CF_3Cl + CO \qquad (R25)$$

As for $C(O)Cl_2$ and $C(O)F_2$, (Worsnop *et al.*, 1991) have found no evidence for uptake of CF_3 $C(O)Cl$ and $CCl_3C(O)Cl$ into water droplets, leading to uptake coefficients of less than 10^{-3}. Direct measurements of wet deposition rates are of vital importance in order to assess the possibility of transport of these species to the stratosphere.

5.7 CONCLUSIONS

Increases in emissions of pollutants like NO_x, CH_4, NMHC and CO can all lead to increases in tropospheric ozone, and could explain the observed ozone increases registered over northern hemispheric latitudes. The efficiencies of these source-gases vary markedly, depending on where the emissions take place, particularly for NO_x emissions. Furthermore, estimates of ozone production resulting from NO_x emission seem to be model-dependent, setting limitations on the use of such calculations. Calculations of ozone changes from methane increases are more uniform, and thus easier to perform.

Taking into account the strong variability of tropospheric NO_x, the limited sets of NO_x observations that are available, and the key role NO_x plays in tropospheric ozone chemistry, high priority should be given to observations of NO_x compounds.

Only limited observations of free tropospheric ozone increases exist. A better coverage of free tropospheric ozone variations and trends is essential in order to understand and predict ozone changes resulting from changes in source gas emissions.

It seems to be difficult to predict how tropospheric OH is going to change with the present accuracy of our models. While increased emission of CH_4, NMHC and CO tend to suppress tropospheric OH, increased emission of NO_x has the opposite effect. Predictions of how future combined changes in emissions may affect OH are therefore difficult to make.

On the other hand, increased emissions of CH_4 are likely to have a marked positive feedback effect on its concentrations through the reaction with OH, leading to an enhanced climate effect.

The impact (+ gives increases in global averages, – gives decreases) of anthropogenic emissions on OH, O_3 and the lifetime τ of climate gases which are controlled by OH in the troposphere are summarized in the table below.

Incr. emission	OH	O_3	τ (CH_4, HCFC, HCF)
CH_4	–	+	+
NO_x	+	+	–
CO	–	+	+
HC	–	+	+

REFERENCES

Atkinson, R., S.M. Aschmann, W.P.L. Carter, A.M. Winer, and J.N. Pitts, Alkyl nitrate formation from the NO_x-air photooxidations of C_2-C_8 n-alkanes, *J. Phys. Chem.*, *86*, 4563–4569, 1982.

Balestra-Garcia, C., G. Poulet, G. Le Bras, and H. Mac Leod, Kinetic study of the reaction OH + CH_3CFCl_2(HCFC-141b) and OH + CH_3CCl_3, STEP-HALOCSIDE/AFEAS Workshop, Dublin, May 14-16, 1991.

Bertrand, L., L. Exsteen-Meyers, J.A. Franklin, G. Huybrechts, and J. Olbregts, Chlorine-photosensitized oxidations of chloromethanes and chloromethylenes in the gas phase, *Int. J. Chem. Kinet.*, *3*, 89–96, 1971.

Blake, N.J., D.R. Blake, D.F. Hurst, T.W. Smith Jr., W.J. Whipple, T.Y. Chen, I.S.A. Isaksen, and F.S. Rowland, Summertime measurements of selected nonmethane hydrocarbons in the arctic and subarctic during the 1988 Arctic Boundary Layer Experiment (ABLE-3A), AGU Fall Meeting, 1991.

Carr, R.W. Jr., D.G. Peterson, and F.K. Smith, Flash photolysis of 1.3-dichlorotetrafluoroacetone in the presence of oxygen kinetics and mechanism of the oxidation of the chlorodifluoromethyl radicals, *J. Phys. Chem., 90*, 607–614, 1986.

Chameides, W.L., and J.C.G. Walker, A photochemical theory of tropospheric ozone, *J. Geophys. Res., 78*, 8751–8760, 1973.

Chameides, W.L., S.C. Liu, and R.J. Cicerone, Possible variations in atmospheric methane, *J. Geophys. Res., 82*, 1795–1798, 1977.

Chameides, W.L., R.W. Lindsay, J. Richardson, and C.S. Kiang, The role of biogenic hydrocarbons in urban photochemical smog: Atlanta as a case study, *Science, 241*, 1473–1475, 1988.

Charlson, R.L., J. Langner, H. Rodhe, C.B. Leovy, and S.G. Warren, Perturbation of the Northern Hemisphere radiative balance by backscattering from anthropogenic sulfate aerosols, *Tellus, 43AB, No. 4*, 152–163, Aug./Sep. 1991.

Cicerone, R.J., and R.S. Oremland, Biogeochemical aspects of atmospheric methane, *Global Biogeochemical Cycles, Vol. 2, No. 4*, 299–327, Dec. 1988.

Cicerone, R.J., How has the atmospheric concentrations of CO changed?, The Changing Atmosphere, F. S. Rowland and I.S.A. Isaksen (Eds.) Wiley-Interscience, 49–61, 1988.

CODATA, Evaluated Kinetic and Photochemical Data for Atmospheric Chemistry: Supplement I, *J. Phys. Chem. Ref. Data, 11*, 327–496, 1982.

Cox, R.A., and G.S. Tyndall, Rate constants for reactions of CH_3O_2 in the gas phase, *Chem. Phys. Lett., 65*, 357–360, 1979.

Crutzen, P.J., A discussion of the chemistry of some minor constituents in the stratosphere and troposphere, *Pure App. Geophys., 106–108*, 1385–1399, 1973.

Crutzen, P.J., The role of NO and NO_2 in the chemistry of the troposphere and stratosphere, *Ann. Rev. Earth Planet. Sci., 7*, 443, 1979.

Crutzen, P.J., Tropospheric ozone: An overview, NATO ASI Series, (Ed. I. S. A. Isaksen), Series C, Vol. 227, 3–32, D. Reidel Publ. Company, Dordrecht, Holland, 1988.

Crutzen, P.J., and P.H. Zimmermann, The changing photochemistry of the troposphere, *Tellus, 43A-B*, 136–151, 1991.

Dana, M.T., R.N. Lee, and J.M. Hales, Hazardous Air Pollutants: Wet removal rates and mechanisms, U. S. Environmental Protection Agency Report EPA–600/3–84–113, Research Triangle Park, NC, 1985.

DeMore, W.B., S.P. Sander, D.M. Golden, M.J. Molina, R.F. Hampson, M.J. Kurylo, C.J. Howard, and A.R. Ravishankara, Chemical kinetics and photochemical data for use in stratospheric modeling, NASA Evaluation No. 9, Jet Propulsion Laboratory Publication 90–1, Pasadena, CA, January 1, 1990.

Derwent, R.G., and A. Volz-Thomas, The tropospheric lifetimes of halocarbons and their reactions with OH radicals: an assessment based on the concentration of ^{14}CO, in Alternative Fluorocarbon Environmental Acceptability Study, Scientific Assessment of Stratospheric Ozone: 1989, Vol. II, Appendix, Global Ozone Research and Monitoring Project, Report 20, 125–146, World Meteorological Organization, 1990.

Dickerson, R R., G.J. Huffman, W.T. Luke, L.J. Nunnermacker, K.E. Pickering, A.C.D. Leslie, C.G. Lindsey, W.G.N. Slinn, T.J. Kelly, P.H. Daum, A.C. Delany, J.P. Greenberg, P.R. Zimmermann, J.F. Boatman, J.D. Ray, and D.H. Stedman, Thunderstorms: an important mechanism in the transport of air pollutants, *Science, 235*, 460–465, 1987.

Dóbé, S., L. Khachatryan, and T. Berces, Kinetics of reactions of hydroxyl radicals with a series of aliphatic aldehydes, *Ber. Bunsenges. Phys. Chem., 93*, 847–848, 1989.

Drummond, J.W., D.H. Ehhalt, and A. Volz, Measurements of nitric oxide between 0 to 12 km altitude and 67°N to 60°S latitude obtained during STRATOZ-III, *J. Geophys. Res., 93*, 15831–15849, 1988.

Edney, E.O., B.W. Gay Jr., and D.J. Driscoll, Chlorine initiated oxidation studies of hydrochlorofluorocarbons: Results for

HCFC–123 (CF_3CHCl_2) and HCFC-141b ($CFCl_2CH_3$), *J. Atmos. Chem.*, *12*, 105–120, 1991.

Ehhalt, D.H., F. Rohrer, and A. Wahner, Sources and distribution of NO_x in the upper troposphere at northern mid-latitudes. Submitted to *J. Geophys. Res.*, June 1991.

Fishman, J. and P.J. Crutzen, The origin of ozone in the troposphere, *Nature*, *274*, 855, 1978.

Hayman, G.D., M.E. Jenkin, T.P. Murrells, and S.J. Shalliker, Kinetic and mechanistic studies associated with the atmospheric degradation of HCFC–123, STEP-HALOCSIDE/AFEAS Workshop, Dublin, May 14–16 , 1991.

Hough, A.M., and R.G. Derwent, Changes in the global concentration of tropospheric ozone due to human activities, *Nature*, *344*, 645–648, 1990.

IPCC, Climate Change, The IPCC Scientific Assessment, World Meteorological Organization United Nations Environment Programme, 1990.

Isaksen, I.S.A., and Q. Hov, Calculation of trends in the tropospheric concentration of O_3, OH, CO, CH_4, and NO_x, *Tellus, Ser. B.*, *39*, 271–285, 1987.

Isaksen, I.S.A., Is the oxidizing capacity of the atmosphere changing?, The Changing Atmosphere, F. S. Rowland and I. S. A. Isaksen (Eds.) Wiley-Interscience, 141–157, 1988.

Isaksen, I.S.A, T. Berntsen, and S. Solberg, Estimates of past and future tropospheric ozone changes from changes in human released source gases, in ozone in the atmosphere, ed. by R. Bojkov and P. Fabian, pp. 576–579, A. Deepak, Hampton, Va, 1989.

IUPAC, Evaluated Kinetic and Photochemical Data for Atmospheric Chemistry: Supplement III (1989), *J. Phys. Chem. Ref. Data*, *18*, 881–1097.

IUPAC, Evaluated Kinetic and Photochemical Data for Atmospheric Chemistry: Supplement IV (1991), *J. Phys. Chem. Ref. Data*, submitted for publication.

Jemi-Alade, A.A., P.D. Lightfoot, and R. Lesclaux, UV absorption spectra of the peroxy radical derivatives of hydrohalocarbons, STEP-HALOCSIDE/AFEAS Workshop, Dublin, May 14–16, 1991.

Kanakidou, M., H.B. Singh, K.M. Valentin, and P.J. Crutzen, A two-dimensional study of ethane and propane oxidation in the troposphere, *J. Geophys. Res.*, *96*, No. D8, 15395–15413, August 20, 1991.

Kirchner, F., F. Zabel, and K.H. Becker, Thermal stability of $CClF_2CH_2O_2NO_2$, $CCl_2FCH_2O_2NO_2$ and $CClF_2C(O)O_2NO_2$, STEP-HALOCSIDE /AFEAS Workshop, Dublin, May 14–16 , 1991.

Köppenkastrop, D., and F. Zabel, Thermal decomposition of chlorofluoromethyl peroxynitrates, *Int. J. Chem. Kinet.*, *23*, 1–15, 1991.

Lacis, A.A., D.J. Wuebbles, and J.A. Logan, Radiative forcing of climate by changes in the vertical distribution of ozone, *J. Geophys. Res.*, *95*, D7, 9971–9981, 1990.

Law, K.S., and J.A. Pyle, Modelling the response of tropospheric trace species to changing source gas concentrations, *Atmos. Environ.*, *25A*, 1863–1871, 1991.

Lelieveld, J., and P.J. Crutzen, Influences of cloud photochemical processes on tropospheric ozone, *Nature*, *343*, 227–233, January 18, 1990.

Lesclaux, R., A. M. Dognon, and F. Caralp, Photooxidation of halomethanes at low temperature: The decomposition rate of CCl_3O and $CFCl_2O$ radicals, *J. Photochem. Photobiol., A: Chemistry*, *41*, 1–11, 1987.

Levine, J.S., C.P. Rinsland, and G.M. Tennillé, The photochemistry of methane and carbon monoxide in the troposphere in 1950 and 1985, *Nature*, *318*, 254–27, 1985.

Libuda, H.G., K.H. Becker, E.H. Fink, and F. Zabel, Formyl chloride: UV absorption cross sections at rate constants for the reactions with Cl and OH, *J. Phys. Chem.*, *94*, 5860, 1990.

Libuda, H.G., F. Zabel, and K.H. Becker, UV spectra of some organic chlorine and bromine compounds of atmospheric interest, STEP-HALOCSIDE/AFEAS Workshop, Dublin, May 14–16, 1991.

Liu, S.C., M. Trainer, F.C. Fehsenfeld, D.D. Parrish, E.J. Williams, D.W. Fahey, G. Hubler, and P.C. Murphy, Ozone production in the rural troposphere and the implications for regional and global ozone distributions, *J. Geophys. Res.*, *92*, 4, 191–4, 207, 1987.

Liu, S.C., and M. Trainer, Responses of the tropospheric ozone and odd hydrogen radicals to column ozone change, *J. Atmos. Chem.*, *6*, 221–234, 1988.

Logan, J.A., M.J. Prather, S.C. Wolfsy, and M.B. McElroy, Tropospheric chemistry: A global perspective, *J. Geophys. Res.*, *86*, 7210–7254, 1981.

McFarland, M., D. Kley, J.M. Drummond, A.L. Schmeltekopf, and R.H. Winkler, Nitric oxide measurements in the equatorial Pacific, *Geophys. Res. Let.*, *6*, 605–608, 1979.

Meller, R., D. Boglu, and G.K. Moortgat, UV spectra of several halogenated carbonyl compounds and FTIR studies on the degradation of CF_3COCl, HCFC–123, and HFC-134a, STEP-HALOCSIDE/ AFEAS Workshop, Dublin, May 14–16, 1991.

Morel, O., R. Simonaitis, and J. Heicklen, Ultraviolet absorption spectra of HO_2NO_2, $CCl_3O_2NO_2$, $CCl_2FO_2NO_2$, and $CH_3O_2NO_2$, *Chem. Phys. Lett.*, *73*, 38–42, 1980.

Nelson, L., I. Shanahan, H. Sidebottom, J. Treacy, and O. J. Nielsen, Kinetics and mechanism for the oxidation of 1,1,1-trichloroethane, *Int. J. Chem. Kinet.*, *22*, 577–590, 1990.

Pickering, K.E., A. Thompson, J.R. Scala, W.-K. Tao, J. Simpson, and M. Garstang, Photochemical ozone production in tropical squall line convection during NASA Global Tropospheric Experiment/Amazon Boundary Layer Experiment 2A, *J. Geophys. Res.*, *96*, D2, 3099–3114, 1991.

Prather, M.J., ed., An assessment model for atmospheric composition, NASA Conf. Pub., 3023, 1989.

Prather, M.J., Personal communication, 1991.

Prather, M., and C.M. Spivakovsky, Tropospheric OH and the lifetimes of hydrochlorofluorocarbons, *J. Geophys. Res.*, *95*, No. D11, 18723–18729, Oct. 20, 1990.

Prinn, R., D. Cunnold, R. Rasmussen, P. Simmonds, F. Alyea, A. Crawford, P. Fraser, and R. Rosen, Atmospheric trends in methylchloroform and the global average for the hydroxyl radical, *Science*, *238*, 945–950, 1987.

Prinn, R., D. Cunnold, R. Rasmussen, P. Simmonds, F. Alyea, A. Crawford, P. Fraser, and R. Rosen, Global average concentration and trend for hydroxyl radicals deduced from ALE/GAGE trichloroethane (methyl chloroform) data: 1978–1990, *J. Geophys. Res.*, *97*, 2445–2461, 1992.

Rattigan, O., R.A. Cox, and R.L. Jones, The UV absorption cross-sections of CF_3COCl, CF_3COF, CH_3COF, and CCl_3CHO, STEP-HALOCSIDE/ AFEAS Workshop, Dublin, May 14–16, 1991.

Ridley, B.A., M.A. Carroll, and G.L. Gregory, Measurements of nitric oxide in the boundary layer and free troposphere over the Pacific ocean, *J. Geophys. Res.*, *92*, 2025–2047, 1987.

Roberts, J.M., The atmospheric chemistry of organic nitrates, *Atmos. Environ.*, *24A*, 243–287, 1990.

Sander, S.P., and R.T. Watson, Kinetics Studies of Reactions of CH_3O_2 with NO, NO_2, and CH_3O_2 at 298 K, *J. Phys. Chem.*, *84*, 1664–1674, 1980.

Sanhueza, E., I.C. Histatsune, and J. Heicklen, Oxidation of haloethylenes, *Chem. Rev.*, *76*, 801–826, 1976.

Sanhueza, E., W.M. Hao, D. Scharffe, L. Donoso, and P.J. Crutzen, N_2O and NO emissions from soils of the Northern part of the Guayana Shield, Venezuela, *J. Geophys. Res.*, *95*, 22481–22488, 1990.

Sanhueza, E., Prepared for the 1991 IPCC report, Personal communication, 1991.

Schnell, R. C., S. C. Liu, S. J. Oltmans, R. S. Stone, D. J. Hofmann, E. G. Dutton, T. Deshler, W.T. Sturges, J. W. Harder, S. D. Sewell, M. Trainer, and J. M. Harris, Decrease of summer tropospheric ozone concentrations in Antarctica, *Nature*, *35*, 726–729, 1991.

Scollard, D., M. Corrigan, H. Sidebottom, and J. Treacy, Kinetics and mechanisms for the oxidation of halogenated aldehydes, STEP-HALOCSIDE/AFEAS Workshop, Dublin, May 14–16, 1991.

Spivakovsky, C.M., S.C. Wolfsy, and M.J. Prather, A numerical method for parameterization of atmospheric chemistry: Computation of tropospheric OH, *J. Geophys. Res.*, *95*, No. D11, 18433–18439, Oct. 20, 1990a.

Spivakovsky, C. M., R. Yevich, J. A. Logan, S. C. Wolfsy, M. B. McElroy, and M. J. Prather, Tropospheric OH in a three-dimensional chemical tracer model: An assessment based on observations of CH_3CCl_3, *J. Geophys. Res.*, *95*, No. D11, 18441–18471, Oct. 20, 1990b.

Starcke, J., F. Zabel, L. Elsen, W. Nelson, I. Barnes, and K.H. Becker, Proc. European Symposium on the physio-chemical behaviour of atmospheric pollutants, G. Restelli and G. Angeletti, eds.,

Kluwer Academic Publishers, Dordrech, Boston, London, 172–176, 1990.

Sze, N.D., Anthropogenic CO emissions: Implications for the atmospheric CO-OH-CH_4 cycle, *Science, 195*, 673–675, 1977.

Thompson, A.M., and R J. Cicerone, Possible perturbations to atmospheric CO, CH_4, and OH. *J. Geophys. Res., 91*, 10853–10864, 1986.

Thompson, A.M., M.A. Owens, R.W. Stewart, and J.A. Herwehe, Sensitivity of tropospheric oxidants to global chemical and climate change, *Atmos. Environ., 23*, 516–532, 1989.

Thompson, A.M., M.A. Huntley, and R.W. Stewart, Perturbations to tropospheric oxidants, 1985-2035: 1. Calculations of ozone and OH in chemically coherent regions, *J. Geophys. Res., 95*, 9829–9844, 1990.

Thompson, A.M., New ozone hole phenomenon, *Nature, 352*, 282–283, 1991.

Tuazon, E.C., and R. Atkinson, Investigation of tropospheric degradation of alternative fluorocarbons, STEP-HALOCSIDE/AFEAS Workshop, Dublin, May 14–16, 1991.

U.S. Environmental Protection Agency (USEPA), Policy options for stabilizing global climate, Technical Appendices, D. Tirpak and D. Lashof, eds., Report to Congress, Washington DC, 1990.

Vaghjiani, G.L., and A.R. Ravishankara, New measurements of the rate coefficient for the reaction of OH with methane, *Nature, 350*, 406–409, 1991.

Valentin, K.M., Numerical modeling of the climatological and anthropogenic influences on the chemical composition of the troposphere since the last glacial maximum, Ph. D. Thesis, Johannes-Gutenburg-Univ. Mainz, FRG, 1990.

Volz, A., D.H. Ehhalt, and R.G. Derwent, Seasonal and latitudinal variation of ^{14}CO and the tropospheric concentration of OH-radicals, *J. Geophys. Res., 86*, 5163–5171, 1981.

Wang, W.-C., and N.D. Sze, Coupled effects of atmospheric N_2O and O_3 on earth's climate, *Nature, 286*, 589–590, 1980.

Weinstock, B., Carbon monoxide: residence time in the atmosphere, *Science, 166*, 224–225, 1969.

Wigley, T.M.L., Could reducing fossil-fuel emissions cause global warming?, *Nature, 349*, 503–506, 1991.

Wine, P.H., and W.L. Chameides, Possible atmospheric lifetimes and chemical reaction mechanisms for selected HFFCs, HFCs, CH_3CCl_3, and their degradation products against dissolution and/or degradation in seawater and cloudwater, in Alternative Fluorocarbon Environmental Acceptability Study, Scientific Assessment of Stratospheric Ozone: 1989, Vol. II, Appendix, WMO Global Ozone Research and Monitoring Project, Report 20, 271–295, World Meteorological Organization, 1990, AFEAS, 1990.

WMO, Report of the international ozone trends panel 1988, Global ozone research and monitoring project, World Meteorological Organization, Report No. 18, Vol. I and II, 1989.

WMO, Scientific assessment of stratospheric ozone: 1989, Global Ozone Research and Monitoring Proj., World Meteorological Organization, Report 20, Vol. I and II (Appendix: AFEAS Report), 1990.

Worsnop, D.R., G.N. Robinson, M.S. Zahniser, C.E. Kolb, S.X. Duan, W. DeBruyn, X. Shi, and P. Davidovits, Heterogeneous chemistry of alternative CFC oxidation intermediates, STEP-HALOCSIDE/AFEAS Workshop, Dublin, May 14–16, 1991.

Zabel, F., A. Reimer, K. H. Becker, and E. H. Fink, Thermal decomposition of alkyl peroxynitrates, *J. Phys. Chem., 93*, 5500–5507, 1989.

Zellner, R., A. Hoffman, D. Bingemann, V. Mors, and J. P. Kohlmann, Time-resolved studies in the oxidation of HCFC-22 and HFC–134a under simulated tropospheric conditions, STEP-HALOCSIDE/AFEAS Workshop, Dublin, 14–16 May, 1991.

CHAPTER 6

Ozone Depletion and Chlorine Loading Potentials

Authors:

J.A. Pyle
D. Wuebbles
S. Solomon
S. Zvenigorodsky

Additional Contributors:

P. Connell
M.K.W. Ko
D. Fisher
F. Stordal
D. Weisenstein

Chapter 6

Ozone Depletion and Chlorine Loading Potentials

Contents

SCIENTIFIC SUMMARY

The recognition of the roles of chlorine and bromine compounds in ozone depletion has led to the regulation of their source gases. Some source gases are expected to be more damaging to the ozone layer than others, so that scientific guidance regarding their relative impacts is needed for regulatory purposes. Parameters used for this purpose include the steady-state and time-dependent chlorine loading potential (CLP) and the ozone depletion potential (ODP). Chlorine loading potentials depend upon the estimated value and accuracy of atmospheric lifetimes and are subject to significant (~20–50 percent) uncertainties for many gases. Ozone depletion potentials depend on the same factors, as well as the evaluation of the release of reactive chlorine and bromine from each source gas and corresponding ozone destruction within the stratosphere.

ODPs have generally been calculated with two-dimensional numerical models, which have limitations in the treatments of atmospheric transport and chemistry required for evaluation of ozone losses. In particular, such models do not fully represent the transport processes of the lower stratosphere (so that the calculated release of reactive chlorine from the source gases there is subject to uncertainties) nor do they reproduce in detail the large observed ozone losses in the lower stratosphere, especially in polar regions. The sensitivity of modeled ODPs to these problems is reduced by virtue of the fact that the ODP is a relative parameter, but is not completely eliminated, so that the more conservative assessment parameter represented by the CLP has also been considered. In this assessment, ODPs are estimated both from models and with a new semi-empirical approach that uses measurements and/or deduced correlations between source gases (to evaluate reactive chlorine release) together with observations of ozone losses. A critical assumption in the semi-empirical approach is that observed lower stratospheric ozone losses are due to halogen chemistry. This assumption is well justified in polar regions and likely to be largely true at mid-latitudes. Therefore, the semi-empirical ODPs are expected to be more realistic than those derived from current models, at least in polar regions.

Modeled steady-state ODPs and CLPs have been evaluated using improved kinetic schemes. Further, some preliminary model results include a treatment of known heterogeneous chemistry on mid-latitude sulfate aerosols. The numerical values of these modeled ODPs are close to those of previous assessments.

Semi-empirical steady-state ODPs are given for the polar lower stratosphere and, in a few cases, for the global average. The semi-empirical ODPs are generally larger than the modeled values for chlorocarbons whose stratospheric loss rates are slower than that of CFC-11 and smaller for those whose loss rates are faster than that of CFC-11. For example, the semi-empirical ODP for HCFC-22 is between about 20 and 80 percent greater than the range of the model values. For some halons (brominated halocarbons), the semi-empirical ODPs for polar regions exceed some model estimates by as much as a factor of two. For all of the HCFCs considered here, the inferred ODP values are well below the CLPs and show that the upper limit to ozone loss represented by the CLP is not realized in the stratosphere for these species. This narrows significantly the uncertainties in the ODPs for HCFCs.

During the next decade, stratospheric chlorine abundances are expected to rise substantially. This increase in chlorine will likely lead to further global ozone loss including larger reductions in the Arctic and perhaps in northern mid-latitudes. In this near-term period, the HCFCs and many halons will have an impact that is considerably larger than their steady-state ODPs, in some cases and over some time horizons by as much as a factor of two to five.

6.1 INTRODUCTION

Understanding of the depletion of stratospheric ozone by anthropogenic halocarbons has led to the need for simple measures for comparing the impact of one halocarbon source gas against others as a scientific guide to public policy. The simplest of these is the chlorine loading potential, or CLP. This index represents the amount of total chlorine delivered from the troposphere to the stratosphere due to emission of a given halocarbon, relative to that from a reference molecule, generally CFC-11 (see, e.g., Prather and Watson, 1990). CLPs can be considered upper limits to the steady-state relative effect on ozone depletion for most gases, and are defined by:

$$\mathrm{CLP} = \frac{\mathrm{Cl\ (trop)\ for\ compound\ x}}{\mathrm{Cl\ (trop)\ for\ CFC\text{-}11}} = \frac{\tau_x}{\tau_{\mathrm{CFC\text{-}11}}} \frac{M_{\mathrm{CFC\text{-}11}}}{M_x} \frac{n_x}{3} \qquad (6\text{-}1)$$

where Cl (trop) is the chlorine transported across the tropopause to the stratosphere per unit mass of halocarbon emitted; τ_x, $\tau_{\mathrm{CFC\text{-}11}}$, $M_{\mathrm{CFC\text{-}11}}$ and M_x denote the lifetime and molecular weights of CFC-11 and the compound in question, respectively; and n_x is the number of chlorine atoms per molecule of compound x. Similarly, the steady-state bromine loading potential (BLP) represents the total bromine delivered to the stratosphere relative to the chlorine due to CFC-11, and can be defined as:

$$\mathrm{BLP} = \frac{\mathrm{Br\ (trop)\ for\ compound\ x}}{\mathrm{Cl\ (trop)\ for\ CFC\text{-}11}} = \frac{\tau_x}{\tau_{\mathrm{CFC\text{-}11}}} \frac{M_{\mathrm{CFC\text{-}11}}}{M_x} \frac{k_x}{3} \qquad (6\text{-}2)$$

where k_x is the number of bromine atoms per molecule of compound x. The chlorine loading for many HCFCs is determined largely by their decomposition within the troposphere through reaction with the reactive OH radical. Effective tropospheric OH concentrations can be estimated from observations of the trend in methyl chloroform together with information on its releases (e.g., Prinn *et al.*, 1991). The lifetimes of other species similarly destroyed by reaction with tropospheric OH can then be inferred using laboratory measurements of their respective rate coefficients (e.g., Prather and Spivakovky, 1990). Estimates of the uncertainties in lifetimes and hence in CLPs will be discussed in Section 6.2.2.

Ozone depletion due to halocarbons depends not only upon the amount of chlorine or bromine delivered to the stratosphere from the troposphere (the CLP), but also on the following stratospheric processes: (i) the breakdown of the halocarbon within the stratosphere, which is responsible for liberating reactive halogen gases and (ii) the subsequent chemistry of the reactive halogens that controls the magnitude of the ozone depletion. Source gases with long stratospheric lifetimes will break down to release their chlorine or bromine less effectively than CFC-11, making their net impact on ozone smaller than their CLPs. It is important to distinguish between the tropospheric and stratospheric lifetimes, particularly for the HCFCs, which have relatively short tropospheric lifetimes but long stratospheric lifetimes (see Table 6-2). The need to consider stratospheric ozone loss processes in the assessment of relative impacts of halocarbons on the ozone layer has led to the use of numerical models for evaluation of the ozone depletion potential as first suggested by Wuebbles (1983). The ODP represents the amount of ozone destroyed by emission of a gas over its entire atmospheric lifetime (i.e., at steady state) relative to that due to emission of the same mass of CFC-11, and is defined in modeling calculations as follows:

$$\mathrm{ODP} = \frac{\mathrm{Global}\ \Delta\ O_3\ \mathrm{due\ to\ x}}{\mathrm{Global}\ \Delta\ O_3\ \mathrm{due\ to\ CFC\text{-}11}} \qquad (6\text{-}3)$$

Because the ODP is a relative measure, it is likely that it can be calculated by present stratospheric models with greater reliability than the absolute ozone depletion, but it is important to quantify that reliability. The accuracy and reliability of ODP estimates will be addressed in this chapter by considering both statistical ranges of likely uncertainties and by examining observations.

The ODP/CLP ratio represents the efficiency of particular compounds for ozone destruction once in the stratosphere and allows for separation of the effects of stratospheric processes on the ozone depletion potential from those related to tropospheric removal and uncertainties in lifetimes. This will be discussed in more detail in Sections 6.2 and 6.3.

Two-dimensional models have become one of the principal tools for assessing the impact of anthropogenic emissions on the ozone layer. Such models generally include rather detailed representations of

gas-phase photochemical processes and parameterized descriptions of stratospheric transport. These models have achieved significant successes in representing the chemical composition of the stratosphere, particularly at mid-latitudes above perhaps 25 km. However, recent research has demonstrated that current ozone depletion takes place largely below 25 km and is not well simulated by gas phase models (WMO, 1990; and Chapters 2 and 8 of this report). This occurs in part because current models do not contain satisfactory descriptions of the complicated microphysical processes governing the development of polar stratospheric clouds, the heterogenous reactions that occur on them, and the important processes of dehydration and denitrification, nor do they simulate in detail the transport processes that link polar and mid-latitude regions.

The breakdown of halocarbons within the stratosphere depends heavily upon both the modeled atmospheric transport and chemistry. It has been shown (e.g., Podolske *et al.*, 1989) that current models fail to predict the very low concentrations of source gases and the correspondingly high concentrations of inorganic chlorine observed in the polar lower stratosphere in late winter. Without a realistic representation of the distributions of source gases and thus their chlorine (or bromine) release, the ODP cannot be calculated reliably even if the heterogeneous chemical processes leading to ozone depletion are considered in complete detail. The fact that the ODP is a relative measure alleviates, but does not eliminate, the role of shortcomings in model transport and ozone loss processes for modeling studies of ODPs, suggesting the need to examine observations to better constrain ODP estimates.

ODPs from gas phase model calculations were presented in WMO (1990) and by Fisher *et al.* (1990). Calculations by a variety of modeling groups were included. The general behavior, e.g., significantly higher ODPs for CFCs compared with HCFCs, was reproduced by all the models. However, there were also systematic differences between the models. For example, the Atmospheric and Environmental Research, Inc. (AER) two-dimensional model calculated somewhat smaller ODPs for the CFCs than the Oslo two-dimensional model, presumably a reflection of differences in stratospheric processes, whereas, for the HCFCs, the AER model calculated higher ODPs than the Oslo model, presumably a reflection of differences in tropospheric processes in the two models. These differences suggest that, for any particular model, the relative variation among ODPs of similar compounds (e.g., HCFCs) may be more accurately calculated than that for different types of compounds (e.g., a CFC versus an HCFC). Section 6.2 describes new calculations of ODPs and CLPs including some from models that consider heterogenous chemistry.

An alternative new approach to modeling studies of ODPs is to use observations of source gases to evaluate the chlorine or bromine release; such information coupled with observations of ozone loss can be used to deduce semi-empirical ODPs as described in Section 6.3. While subject to important uncertainties and assumptions, this semi-empirical method avoids the demanding requirements of accurate numerical simulation of source gas distributions and ozone destruction, and is therefore expected to be more realistic than present models, at least in the polar lower stratosphere where a significant fraction of contemporary ozone loss is found.

The time scale for the atmosphere to attain steady state with respect to injections of halocarbons ranges from a few years to many centuries, depending upon the lifetime of the species in question. Steady-state ODPs represent the best current understanding of the long-term impacts of such releases, but they do not describe short-term (decades or less) responses (WMO, 1990; SORG, 1990). When specific short-term time horizons are considered, time-dependent ODPs provide a more appropriate measure of impacts. Section 6.4 presents estimates of time-dependent ODPs for several halocarbons of interest over a range of time horizons.

6.2 MODEL CALCULATIONS OF CLPs AND ODPs

6.2.1 Compounds and Chemistry Considered

The list of compounds considered in this assessment (Table 6-1) is similar to that in WMO (1990), comprising most of the chlorofluorocarbons (CFCs) and other chlorinated halocarbons of interest, including several already being used or considered as replacements for CFCs, such as HCFC-22, HCFC-225ca, and HCFC-225cb. The list of halons considered here is much more extensive than the previous report, reflecting the increased interest in the environ-

Table 6-1 Spectroscopic and chemical rate data used in the ODP calculations at Lawrence Livermore National Laboratory (LLNL).

Species	Chemical Formula	UV Absorption Cross-section Reference	OH Reaction Rate Constant A (cm^3 $molecules^{-1}s^{-1}$)	E/R (K)	Reference
CFCs					
CFC-11	$CFCl_3$	a			
CFC-12	CF_2Cl_2	a			
CFC-113	$CFCl_2CF_2Cl$	b			
CFC-114	CF_2ClCF_2Cl	b			
CFC-115	CF_2ClCF_3	b			
HCFCs, etc.					
HCFC-22	CF_2HCl	b	1.2 (–12)	1.65 (3)	a
HCFC-123	CF_3CHCl_2	m	6.4 (–13)	8.50 (2)	a
HCFC-124	CF_3CHFCl	d	6.6 (–13)	1.25 (3)	a
HCFC-141b	CH_3CFCl_2	m	9.4 (–13)	1.50 (3)	h
HCFC-142b	CH_3CF_2Cl	m	1.4 (–12)	1.80 (3)	i
HCFC-225ca	$CF_3CF_2CHCl_2$	n	2.0 (–12)	1.30 (3)	j
HCFC-225cb	CF_2ClCF_2CHFCl	n	6.7 (–13)	1.30 (3)	j
Carbon Tetrachloride	CCl_4	a			
Methyl Chloroform	CH_3CCl_3	b,c	5.0 (–12)	1.80 (3)	a
Brominated Compounds					
H-1301	CF_3Br	b			
H-1211	CF_2ClBr	e			
H-1202	CF_2Br_2	e			
H-2402	CF_2BrCF_2Br	e			
H-1201	CF_2HBr	f	7.4 (–13)	1.30 (3)	f
H-2401	CF_3CHFBr	g	7.4 (–13)	1.08 (3)	k
H-2311	$CF_3CHClBr$	b	7.0 (–13)	7.30 (2)	l
Methyl bromide	CH_3Br	b	6.8 (–13)	8.50 (2)	a

[a] JPL 90-1
[b] Gillotay and Simon (1990)
[c] Vanlaethem-Meuree et al. (1979)
[d] Orlando et al. (1991) as quoted in Gillotay and Simon (1990); see also Gierczak et al. (1991)
[e] Burkholder et al. (1991)
[f] Talukdar et al. (1991a)
[g] Brown et al. (1989)
[h] Recommended for this report (See Chapter 8); ~30 percent smaller than WMO (1990) value @ 277K
[i] Recommended for this report (See Chapter 8); ~15 percent smaller than WMO (1990) value @ 277K
[j] Recommended for this report (See Chapter 8)
[k] Orkin et al. (1990)
[l] Based on value at 300K in Brown et al. (1989)
[m] Gillotay and Simon (1991)
[n] Braun et al. (1991)

mental effects of these compounds. Since WMO (1990), the uncertainties in photolysis cross sections and reaction rate constants for many compounds have been narrowed considerably by improved laboratory studies. Table 6-1 shows the adopted kinetic parameters for the compounds evaluated in the Lawrence Livermore National Laboratory (LLNL) atmospheric models. It was not possible to ensure that all models presented here used the same kinetic parameters, but most of these differences are expected to be minor.

Detailed information is now available regarding the full temperature dependence of the ultraviolet (UV) and visible cross sections for many of the compounds examined, whereas models used in the WMO (1990) assessment were restricted to a single set of temperature-independent absorption coefficients for nearly all compounds. Inclusion of the temperature dependence can affect the altitude of Cl and Br release in the stratosphere. The temperature dependence of the absorption cross sections also affects the atmospheric lifetimes for several species, including H-1202, H-1211, and H-2402. Many of the bromoalkanes exhibit smooth continuum UV absorption cross sections in the region of 280–400 nm (near ultraviolet and visible). As pointed out by Burkholder *et al.* (1991), this region contributes significantly to atmospheric photoprocesses (because of the greatly increased transmitted flux there relative to shorter wavelengths) but the absolute absorption coefficients there are often small and difficult to measure. As an example, lifetimes ranging from 10 to greater than 50 years were calculated for H-1211 with the LLNL one-dimensional model, depending on the inclusion or exclusion of the temperature dependence of the cross sections and the extension of the long-wavelength tail, emphasizing the need for accurate measurements in this region.

Improved laboratory studies have changed the understanding of reaction rates with OH and hence the lifetimes and CLPs for several of the HCFCs. For example, reaction rates of OH with HCFC-141b (Talukdar *et al.*, 1991b) and HCFC-142b (Gierczak *et al.*, 1991) are about 30 percent and 15 percent smaller, respectively, than in the previous assessment.

All of the past calculations of ODPs were based on models including only gas phase chemistry and did not consider heterogeneous chemistry on sulfate aerosols or polar stratospheric cloud particles. In order to provide a historical perspective and because of limited time for preparing this report, most of the model results presented here are still based on gas phase chemistry. Some preliminary calculations are presented that attempt to consider heterogeneous processes (see Chapter 8).

Two-dimensional model calculations of atmospheric lifetimes, chlorine loading potentials, and ozone depletion potentials are included from five modeling groups: LLNL, AER, University of Oslo/Norsk Institute for Luftforskning, Norway (Oslo/NILU), and E.I. Du Pont de Nemours and Company (Du Pont). Most of the compounds have been evaluated with both the LLNL and AER models; the other groups evaluated a limited number of compounds.

6.2.2 Atmospheric Lifetimes and Chlorine Loading Potentials

Calculated lifetimes are shown in Table 6-2. The estimated lifetimes of the HCFCs are generally shorter than in the previous assessment, largely as a result of increases in calculated tropospheric hydroxyl concentrations due to new, more accurate measurements of the rate of the reaction of OH with CH_4 (Vaghjiani and Ravishankara, 1991). Differences of 20–30 percent are obtained for the calculated lifetimes for the HCFCs between the models used, reflecting the extreme difficulty and uncertainty associated with evaluation of tropospheric OH chemistry (see Chapter 5). Due to these problems, the lifetimes of compounds that react predominantly with OH are generally constrained by scaling to an assumed CH_3CCl_3 lifetime deduced from observations. In this chapter, lifetimes for all species in each model will be scaled to match the best estimates given in Chapter 8 and shown in Table 6-2. While such scaling imposes uniform CLPs, it fails to standardize other processes important to determining ODP values. For example, if different models calculate different tropospheric OH densities, then they are also likely to exhibit different stratospheric OH abundances. Stratospheric OH distributions have a minor impact on the lifetimes of the HCFCs, but control their stratospheric breakdown, subsequent chlorine release, and hence the ODP/CLP ratio. Similarly, many of the differences in calculated lifetimes for species destroyed by stratospheric photolysis (e.g., CFC-113) likely reflect differences in model transport and/or radiative transfer

Table 6-2 Lifetimes and Chlorine Loading Potentials. The range of atmospheric lifetimes calculated in the two-dimensional models used for the ODP analyses are shown, along with the corresponding standardized lifetimes and stratospheric lifetimes used in this report (see Chapter 8), and the CLPs derived with the standardized lifetimes.

Species	Model Total Lifetimes (yrs)	Best Estimate Total Lifetimes (yrs)	Approximate Stratospheric Lifetime (yrs)	Adopted CLPs
CFCs				
CFC-11	48.6–66	55	55	1.0
CFC-12	104–113	116	116	1.597
CFC-113	85–109	110	110	1.466
CFC-114	182–200	220	220	2.143
CFC-115	414–522	550	550	2.964
HCFCs, etc.				
HCFC-22	13.5–17.7	15.8	240	0.152
HCFC-123	1.3–1.6	1.7	47	0.0185
HCFC-124	5.7–7.1	6.9	129	0.0421
HCFC-141b	9.0–10.9	10.8	76	0.154
HCFC-142b	19.3–23.4	22.4	215	0.185
HCFC-225ca	2.2–2.7	2.8	60	0.0230
HCFC-225cb	6.7–8.1	8.0	120	0.0656
CCl_4	40–58	47	47	1.018
CH_3CCl_3	5.0–6.0	6.1	47	0.114
Brominated Compounds				
H-1301	65.5–68.6		67	
H-1211	18.5–20.1		40	
H-1202	3.9 (1 model)		33	
H-2402	22.1–30.4		38	
H-1201	5.6 (1 model)		58	
H-2401	2.0 (1 model)		46	
H-2311	0.8 (1 model)		29	
CH_3Br	1.2–1.8		35	

treatments that influence stratospheric chlorine release and ODP/CLP ratios, at least to some degree. These important model differences are not improved by standardizing the model lifetimes. In the following, ODP/CLP ratios will be taken directly from the individual model results, but the CLPs used to calculate ODPs will be based upon the standardized lifetimes.

A recent study using observations of CH_3CCl_3 together with estimates of its emissions suggests that the lifetime of CH_3CCl_3 may be shorter than previously thought due to changes in measurement calibrations (Prinn *et al.*, 1992), while others have noted the possible importance of oceanic hydrolysis as a sink for this compound (Wine and Chameides, 1990; Butler *et al.*, 1991). In contrast, many of the HCFCs are expected to undergo less oceanic hydrolysis, so that the fraction of their total lifetime attributable to loss with OH may differ from that of methyl chloroform. These considerations imply that the use of methyl chloroform to deduce an effective average tropospheric OH concentration is less certain than previously thought, with attendant uncertainties for estimates of CLPs and ODPs for compounds destroyed by reaction with OH. The lifetimes of compounds destroyed by stratospheric photolysis (including the

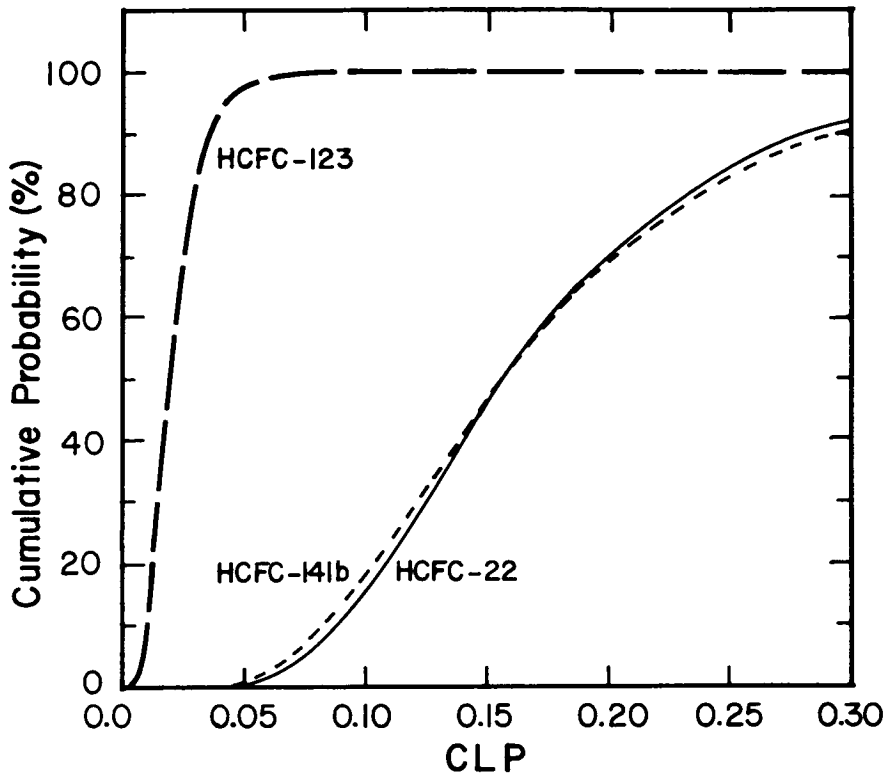

Figure 6-1 Cumulative probability distribution functions estimated for the CLPs of HCFCs 22, 123, and 141b. Uncertainties considered were as follows: The CH_3CCl_3 oceanic hydrolysis time scale was assumed to be 72 years, with an uncertainty of ±50 percent. The rates of reaction of HCFCs 22, 123, and 141b with tropospheric OH were assumed to be uncertain by ±44 percent, ±50 percent, and ±51 percent, respectively (includes an estimated ±13 percent uncertainty in the tropospheric OH deduced from CH_3CCl_3 measurements). The stratospheric lifetimes of CH_3CCl_3, HCFC-22, HCFC-124, and HCFC-141b were assumed to be uncertain by about ±30 percent.

reference molecule for ODP calculations, CFC-11) also have significant uncertainties. These are due in part to uncertainties in the dynamical processes responsible for transporting these compounds to the altitudes where their chemical destruction is rapid. The range of model values shown in Table 6-2 is likely to be representative of these uncertainties.

The range of total uncertainty in chlorine loading potentials for some species is illustrated explicitly in Figure 6-1, wherein estimated accuracies were used to deduce cumulative probability distribution functions (e.g., Lindgren, 1968). The uncertainties considered are indicated on the figure. This approach assumes that these errors are randomly distributed and is intended only to illustrate the current best estimate of the range of statistically probable error. The figure illustrates the fact that uncertainties in steady-state CLPs can be large for some compounds, and that the CLPs for HCFC-123, HCFC-22, and HCFC-141b are likely (>90 percent probability) to lie below 0.035, 0.26, and 0.29, respectively.

Additional uncertainties exist, but most of these are related to fundamental understanding rather than numerical accuracy and are not included in Figure 6-1. In deriving the CLPs shown in Figure 6-1 and Table 6-2, it has been assumed that the products of all

decomposition reactions in the troposphere are too short-lived to reach the stratosphere. However, some HCFCs (e.g., HCFC-141b and 142b) likely produce halogen-containing acyl peroxynitrates as products of their oxidation with tropospheric OH (see Chapter 5). If these peroxynitrates are sufficiently long-lived to be transported to the stratosphere to some degree, then an effective increase in CLPs will result. Further, it is possible that OH and/or HO_2 radicals may be removed on aerosol surfaces in the troposphere and/or stratosphere, affecting the lifetimes of compounds removed by tropospheric OH and perhaps their stratospheric chlorine release. Although observations of CH_3CCl_3 place some constraints on the magnitude of tropospheric OH in an averaged sense and thus upon such reactions, they cannot be ruled out. Further, CLPs represent best estimates for the contemporary atmosphere but neglect possible changes that may occur over the lifetimes of the compounds in question. For example, future changes in tropospheric water vapor and hence OH concentrations (due, for example, to atmospheric climatic change) would affect the CLPs of many compounds but are not considered here.

6.2.3 Calculated ODPs

Table 6-3 presents ODPs for CFCs, HCFCs, halons and other halocarbons calculated with the two-dimensional models considered. The model-calculated ODPs for CH_3CCl_3 and the HCFCs are generally less than 0.15, while those for the CFCs and halons are much larger. Chlorinated compounds with stratospheric lifetimes comparable to or shorter than that of CFC-11 display ODP/CLP ratios close to 1, reflecting the fact that they release their chlorine in a manner similar to the reference gas and hence have similar impacts on ozone once in the stratosphere. As mentioned in Section 6.1, chlorinated compounds with stratospheric lifetimes longer than that of CFC-11 release their chlorine more slowly and display ODP/CLP ratios that are less than 1. Many of the HCFCs have relatively small ODP/CLP values due to their slow stratospheric breakdown by reaction with OH (see Table 6-2). Clearly, the least damaging chlorinated substances are those that are destroyed rapidly within the troposphere (thus limiting their CLPs) but slowly in the stratosphere (reducing the ODP/CLP ratio).

For the halons, the ODP/BLP ratios depend on the efficiency of bromine as compared to chlorine in destroying ozone as well as on the stratospheric lifetime (hence the bromine release). The efficiency of bromine relative to chlorine in depleting ozone is hereafter referred to as α, and is expected to be close to the ODP/BLP ratio for all of the halons considered here. It is important to note that α is dependent on the absolute amount of reactive chlorine, due to chemical coupling between chlorine and bromine that controls the impact of bromine on ozone. The α values given here pertain to conditions of total reactive chlorine loading close to contemporary levels. The scenarios presented in Chapter 8 suggest that the future chlorine loading is likely to change by less than 20 percent for at least the next several decades. The calculated globally-averaged α values suggested by the ODP/BLP ratios in Table 6-3 range from about 10 to 80. These illustrate the extreme effectiveness of bromine in catalyzing ozone destruction (first noted by Yung *et al.*, 1980). The model-calculated α values for the halons depend critically on the portion of bromine species found in the active form (BrO), which in turn depends on the formation and removal rates of the reservoir species, HBr and $BrONO_2$. Some measurements of HBr appear difficult to reconcile with present theory (Park *et al.*, 1989). However, measurements of BrO by Brune *et al.* (1988) are in general agreement with model predictions, lending some support to the calculated α values and current photochemical schemes for bromine. The precise values of α for mid-latitudes also depend on calculated concentrations of atomic oxygen, OH, and HO_2 in the lower stratosphere, which are subject to considerable uncertainties. The values reported in the table should therefore be considered as preliminary. Note, however, that the value of α in the polar lower stratosphere is much better understood as discussed later (see Section 6.3).

Most of the calculations include gas phase chemistry only, but some calculations have also been carried out with the AER, LLNL, and Du Pont models, including a parameterization of known heterogeneous chemistry on sulfate aerosols, and with a treatment of PSC chemistry for the Oslo model (see Chapter 8). The ODP/CLP and ODP/BLP ratios calculated with heterogeneous chemistry in Table 6-3 are very similar

Table 6-3 Derived ODPs scaled to UNEP-standardized lifetimes and the model-derived ODP/CLP ratio from the two-dimensional models for each of the compounds examined. Results were based on gas phase chemistry- only results unless indicated otherwise. Brackets indicate derived values with heterogeneous chemistry in the model. For all halons, model-derived ODPs are presented without reference to the standardized lifetime.

Species	LLNL		AER		Oslo		Du Pont	
	ODP	ODP/CLP or BODP/BLP	ODP	ODP/CLP or BODP/BLP	ODP	ODP/CLP	ODP	ODP/CLP
CFCs								
CFC-11	1.0	1.0	1.0	1.0	1.0	1.0	1.0	1.0
CFC-12	0.88	0.551	0.93	0.586	0.95 (0.93)	0.595 (0.582)	1.06 (1.01)	0.665 (0.635)
CFC-113	0.92	0.631	1.01	0.690	0.99 (0.98)	0.675 (0.668)		
CFC-114	0.57	0.266	0.82	0.382				
CFC-115	0.29	0.099	0.48	0.161				
HCFCs, etc.								
HCFC-22	0.034	0.221 (0.231)	0.045 (0.039)	0.276 (0.255)	0.032 (0.082)	0.221	0.048 (0.043)	0.314 (0.286)
HCFC-123	0.019 (0.016)	0.944 (0.878)	0.020	1.05			(0.013)	(0.709)
HCFC-124	0.016	0.358	0.020	0.449			(0.034)	(0.793)
HCFC-141b	0.12 (0.11)	0.720 (0.731)	0.12	0.767			(0.105)	(0.650)
HCFC-142b	0.035 (0.037)	0.186 (0.200)	0.057	0.305			(0.054)	(0.289)
HCFC-225ca	0.020	0.856	0.021	0.920			(0.016)	(0.714)
HCFC-225cb	0.023	0.348	0.031	0.474			(0.024)	(0.370)
CCl_4	1.03	1.014	1.15 (1.13)	1.13 (1.11)				
CH_3CCl_3	0.11 (0.13)	0.968 (1.12)	0.13	1.13			0.12 (0.12)	1.032 (1.08)
Halons, etc.								
H-1301	12.7	32.2	10.03	23.9				
H-1211	5.0	49.6	1.8	16.3				
H-1202	1.7	52.9						
H-2402	6.4	42.1	10.2	47.8				
H-1201	1.4	35.1						
H-2401	0.44	66.4						
H-2311	0.28	79.9						
CH_3Br	0.74	67.7	0.62 (0.53)	35.8(30.6)				

to those from the gas phase models presented here for nearly all species. However, as discussed in more detail below and in Chapter 8, the models including heterogeneous chemistry still do not fully describe the chlorine release nor the ozone loss observed in the lower stratosphere at mid and high latitudes, so that their calculated ODPs remain subject to uncertainties.

6.3 COMPARISON OF MODELED ODPs AND INFERENCES FROM OBSERVATIONS

In this section, semi-empirical information useful for estimating the ratio between ODP and CLP will be briefly described, the results presented, and compared to the models used here. Briefly, the approach used (Solomon *et al.*, 1992) consists of using direct measurements of halocarbons to evaluate chlorine release and hence local ODP/CLP ratios, particularly in the polar lower stratosphere. When direct measurements are limited, correlations are used to infer abundances for some halocarbons from those of other tracers and hence their ODP/CLP ratios. Globally-averaged ODP/CLP ratios are estimated for some compounds using local ODP/CLP values together with an observationally-derived ozone loss distribution assuming that the ozone loss is due only to halogen chemistry.

The fraction of halocarbon dissociated within the stratosphere (F) can be defined as:

$$F = \frac{\mu_{entry} - \mu_{\theta,z}}{\mu_{entry}} \qquad (6\text{-}4)$$

where μ_{entry} denotes the mixing ratio of halocarbon entering the stratosphere and $\mu\vartheta,z$ indicates the mixing ratio at any latitude and altitude. Measurements of the distributions of halocarbons within the stratosphere can be used to define $\mu\vartheta,z$. Since the tropical troposphere is rather well-mixed for species with lifetimes longer than a few months, μ_{entry} is likely to be nearly equal to the surface mixing ratio. Time lags for transport between the troposphere and stratosphere influence the value of μ_{entry} for any molecule whose abundance is changing with time (e.g., HCFC-22, CFC-11). Such lags are believed to be short (2 years or less) over much of the atmosphere, but measurements of CO_2 suggest time lags of about 3-5 years in the polar lower stratosphere (Heidt *et al.*, 1991; Schmidt and Khedim, 1991).

As noted in WMO (1990), the local ozone depletion in regions of rapid chlorine-catalyzed destruction of ozone is proportional to the relative stratospheric chlorine release (Cl_{rel}) per unit of surface emission of substance, which can be defined as the ratio of fractional dissociation of a particular molecule to that of CFC-11, multiplied by the chlorine loading potential. This implies that the local ozone depletion potential [$ODP(\vartheta,z)$] at any point can be defined as follows (see Solomon *et al.*, 1992):

$$ODP(\vartheta,z) \approx Cl_{rel} = \frac{\{(\mu_{entry} - \mu_{\vartheta,z}) / \mu_{entry\ for\ X}\}}{\{(\mu_{entry} - \mu_{\vartheta,z}) / \mu_{entry\ for\ CFC\text{-}11}\}} \cdot CLP \qquad (6\text{-}5)$$

Equation (6-5) allows estimation of the local ODP/CLP ratio from available measurements of CFC-11 together with other halocarbons. This approach has been taken for a number of halocarbons of interest, particularly HCFC-22, CCl_4, CFC-113, and CH_3CCl_3 in polar regions (Solomon *et al.*, 1992). Simultaneous airborne measurements of these species together with CFC-11 were obtained by Heidt and coworkers (see, Heidt *et al.*, 1989) during the Airborne Arctic Stratospheric Expedition (AASE) in January–February 1989. The polar measurements of CH_4, N_2O, and CFC-11 used here have been stringently intercompared with other calibration standards and are believed to be accurate to within a few percent. Because of the large ozone losses in the Arctic and Antarctic as described in Chapter 2, the local ozone depletion potentials of the polar lower stratospheres are of considerable importance in determining the globally-averaged ODP as well as in understanding requirements for reducing or eliminating ozone losses such as the Antarctic ozone hole. Table 6-4 presents Arctic lower stratospheric local ozone depletion potentials from these direct measurements, averaged over the region from 15-21 km; similar numbers have been obtained from Antarctic lower stratospheric measurements obtained in September 1987. Growth rates for these source gases have been taken from WMO (1990) and results are shown for several cases assuming no time lag between the troposphere and stratosphere and assuming a 3-year lag as discussed earlier.

Table 6-4 Semi-empirical ODPs for Chlorine Compounds (adapted from Solomon *et al.*, 1992).

Polar Lower Stratosphere

Molecule	Input data	Test Case	ODP/CLP	ODP
HCFC-22	HCFC-22, CFC-11	Arctic (Jan) 15–21 km, no lag	0.55	0.084
	Direct obs 15-21 km	Arctic (Jan) 15–21 km, 3-yr lag	0.38	0.058
CH_3CCl_3	CH_3CCl_3, CFC-11	Arctic (Jan) 15–21 km, no lag	1.07	0.122
	Direct obs 15-21 km	Arctic (Jan) 15–21 km, 3-yr lag	1.09	0.124
CCl_4	CCl_4, CFC-11	Arctic (Jan) 15–21 km, 3-yr lag	1.05	1.069
	Direct obs 15-21 km			
CFC-113	CFC-113, CFC-11	Arctic (Jan) 15–21 km, 3-yr lag	0.75	1.100
	Direct obs 15-21 km			
HCFC-22	CH_4, CFC-11	Arctic (Jan) 15–21 km, no lag	0.34	0.052
	model correlation to CH_4	Arctic (Jan) 15–21 km, 3-yr lag	0.34	0.052
HCFC-142b	CH_4, CFC-11	Arctic (Jan) 15–21 km, 3-yr lag	0.36	0.067
	model correlation to CH_4			
CH_3Cl	CH_4, CFC-11	Arctic (Jan) 15–21 km, no lag	0.86	0.022
	model correlation to CH_4	Arctic (Jan) 15–21 km, 3-yr lag	0.89	0.023
HCFC-141b	N_2O, CFC-11	Arctic (Jan) 15–21 km, no lag	0.70	0.108
	model correlation to N_2O	Arctic (Jan) 15–21 km, 3-yr lag	0.72	0.111

Global

Molecule	Input data	Test Case	ODP/CLP	ODP
HCFC-22	Global CFC-11, CH_4 data	Global with polar loss, processor	0.372–0.389	0.056–0.059†
	observed Δozone	Global with polar loss, no processor	0.333–0.344	0.051–0.052†
	model correlation w/CH_4			
	3-year lag in vortex			
HCFC-142b	Global CFC-11, CH_4 data	Global with polar loss, processor	0.377–0.394	0.070–0.073†
	observed Δozone	Global with polar loss, no processor	0.336–0.345	0.062–0.064†
	model correlation w/CH_4			
	3-year lag in vortex			
CCl_4	Global CFC-11 data	Global with polar loss, processor	1.03–1.05	1.049–1.069†
	observed Δozone	Global with polar loss, no processor	1.05–1.09	1.069–1.110†
	model correlation w/CFC-11			
	3-year lag in vortex			

†Range shows the effect of different assumptions regarding the magnitude of upper stratospheric ozone losses (see Solomon *et al.*, 1992).

Direct observations of HCFCs and halons are, however, extremely limited for many species. In the absence of direct information, correlations among long-lived tracers provide a useful means to infer the distribution of one compound from observations of another, thus extending the possible range in space and in compounds evaluated (see Fahey *et al.*, 1990; Solomon *et al.*, 1992; Plumb and Ko, 1991). Plumb and Ko (1991) have shown that the correlations between long-lived tracers are likely to be robust parameters that depend largely on the ratio of stratospheric loss rates and not upon the details of transport processes. The correlations between species can therefore be calculated in models with far greater confidence than the absolute tracer abundances or ODPs. In the following, abundances of several HCFCs and their corresponding local ODPs are inferred from observations of CH_4 or N_2O using cor-

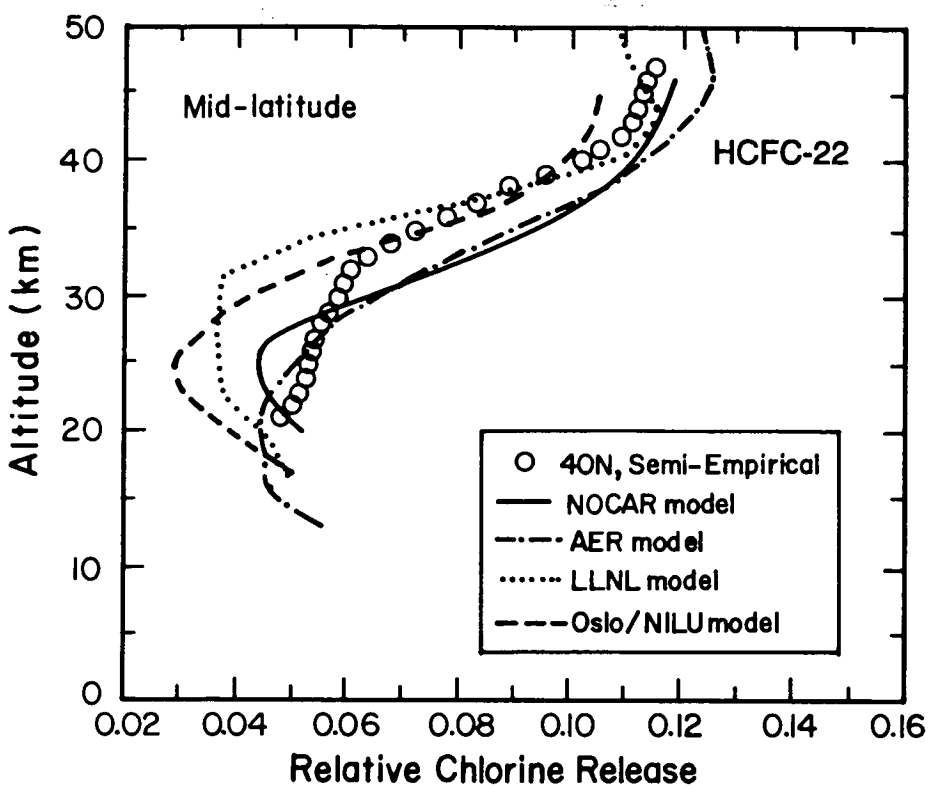

Figure 6-2 Model calculations of the local chlorine release in mid-latitudes for HCFC-22 in winter along with those inferred from an analysis of measured CFC-11 and CH_4 distributions and the correlation between CH_4 and HCFC-22 (Solomon *et al.*, 1992).

relations from model calculations (see Solomon *et al.*, 1992 for details). Table 6-4 shows that the polar ODP inferred for HCFC-22 using an assumed correlation with CH_4 gave results close to that obtained with direct measurements of HCFC-22 when a 3-year lag time was assumed. The calibration standard used here for HCFC-22 has not yet been intercompared in detail with others. This comparison nonetheless strengthens confidence in the correlation approach. Further, it is important to note that the semi-empirical ODP deduced from direct measurements of HCFC-22 is sensitive to the assumed age of the air due to the rapid (order 7–10 percent per year) rate of increase of this compound in the contemporary atmosphere, while the values derived from CH_4 display little dependence on the assumed age since the CH_4 growth rate is only about 0.7 percent per year.

Figure 6-2 presents the local chlorine release profile inferred for mid-latitude winter for HCFC-22 (based upon measurements of CFC-11 and CH_4 together with an adopted correlation between CH_4 and HCFC-22 that is in good agreement with available direct measurements as described in Solomon *et al.*, 1992). Values taken from several models used in this assessment are shown for comparison. Because of the possibility of sharp latitude gradients, detailed comparisons between models and measurements should be carried out as a function of latitude as well as altitude, so that Figure 6-2 provides only general guides to the comparisons between models, and between models and quantities inferred from measurements. Figure 6-2 reveals overall consistency between the shapes of the vertical profiles of the modeled and inferred relative chlorine release but many differences in detail. The discrepancies in the lower stratosphere where much of present-day ozone loss occurs (see Chapter 2) are of the greatest importance to estimates of ODPs.

Comparison of Tables 6-3 and 6-4 shows that the observationally-based polar lower stratospheric ODP/CLP ratios are generally *larger* than the globally-averaged values obtained in gas phase models for chlorocarbons whose stratospheric lifetimes are longer than that of CFC-11 (e.g., HCFC-22 and HCFC-142b), while the observationally-based values tend to be slightly *smaller* than the model calculations for chlorocarbons that exhibit stratospheric loss time scales that are shorter than that of CFC-11 (e.g., CCl_4). This primarily reflects differences in the time-dependent breakup of these molecules within the stratosphere relative to CFC-11, coupled with the fact that the air within the polar lower stratosphere is likely to be relatively 'old' compared to other regions where much of the modeled ozone depletion takes place.

The extrapolation of the local approach to the global scale requires empirically-based specifications of the global distributions of both long-lived tracers and ozone loss. A global semi-empirical ozone depletion potential may be defined (Solomon *et al.*, 1992) as:

$$ODP = \frac{\sum_z \sum_\theta \sum_t \Delta O_{3(z,\theta,t)} \cdot \cos\theta \cdot Cl_{rel}(z,\theta,t)}{\{\sum_z \sum_\theta \sum_t \Delta O_{3(z,\theta,t)} \cdot \cos\theta\}} \quad (6\text{-}6)$$

where $\Delta O_3(z,\vartheta,t)$ is the estimated decrease in ozone concentration observed in today's atmosphere at each altitude, latitude, and time of year (see Solomon *et al.*, 1992 for details of the ozone loss distribution imposed). This equation involves the important assumptions that all of the observed ozone depletion in the contemporary atmosphere is due to halogen chemistry and that the depletion is proportional to the local relative chlorine and/or bromine release (see also, Solomon *et al.*, 1992). These assumptions are well justified in polar regions and likely at mid-latitudes.

Table 6-4 presents semi-empirical global ODPs for the following compounds: HCFC-22, HCFC-142b, and CCl_4. A range of values is presented, showing the effects obtained if it is assumed (as extreme cases) that the polar vortex acts as a processor (i.e., assuming that mid-latitude lower stratospheric ozone losses have their origin entirely in the polar region) and assuming that the polar vortex is completely isolated (see the discussion in Chapter 4 of this assessment). The global ODP/CLP ratios inferred are dominated by ozone losses in the lower stratosphere and are similar to those obtained from the direct Arctic measurements. Thus the polar ODPs are likely to be close approximations to the global values.

Observations can also be used to place constraints on local ozone depletion potentials for halons in the polar regions. The lifetimes of most halons are rather short within the stratosphere due to rapid photolysis (see Table 6-2), and grab-sampling measurements of, for example, Halon-1211 during AASE suggest that it is nearly completely dissociated in the Arctic over the height range from about 15 to 21 km (W. Pollock and L. Heidt, personal communication, 1991). Assuming that the halons will be dissociated by at least as large a fraction compared to their input values to the stratosphere as CFC-11 in the polar lower stratosphere, the ozone depletion potentials for halons (or BODP) in the contemporary stratosphere can be defined as:

$$BODP \approx BLP \cdot \alpha \quad (6\text{-}7)$$

Direct measurements of BrO, ClO, and OClO in the polar stratosphere confirm the role of bromine in polar ozone loss and constrain the value of α there considerably better than the global estimates from models discussed earlier. These show that it is at least 40 in this region (see Chapter 8 and references in Solomon *et al.*, 1992). A value of 40 is thus adopted here.

Table 6-5 presents the semi-empirical ODPs inferred from equation 6-7 for the halons, compares the semi-empirical and modeled ODPs for all compounds, and presents the recommended ODPs for this assessment, based mainly on the semi-empirical approach with guidance from the models. Semi-empirical ODPs for HCFC-123, HCFC-124, HCFC-225ca, and HCFC-225cb were obtained using the correlation between these molecules and CH_4 from the LLNL model, using the approach of Solomon *et al.* (1992). The ODPs for the halons derived both semi-empirically and from some models shown in Table 6-3 are considerably larger than the estimates of the previous assessment. The semi-empirical ODP/CLP values for HCFC-22 are larger than the range of the models shown here by about 20 to 80 percent, while for HCFC-142b, the inferred values are as much as a

Table 6-5 Range of modeled and semi-empirical steady-state ODPs and recommended best estimates.

Species	Model Range		Semi-empirical Range		Best Estimate ODP
	ODP	ODP/CLP or ODP/BLP	ODP	ODP/CLP or ODP/BLP	
CFCs					
CFC-11	1.0	1.0	1.0	1.0	1.0
CFC-12	0.88–1.06	0.551–0.665			≈1.0
CFC-113	0.92–1.01	0.631–0.690	1.07	0.75	1.07
CFC-114	0.57–0.82	0.266–0.382			≈0.8
CFC-115	0.29–0.48	0.099–0.161			≈0.5
HCFCs, etc					
HCFC-22	0.032–0.048	0.221–0.314	0.05–0.08	0.33–0.55	0.055
HCFC-123	0.013–0.020	0.709–1.050	0.02	1.112	0.02
HCFC-124	0.016–0.034	0.358–0.793	0.022	0.523	0.022
HCFC-141b	0.10–0.12	0.650–0.767	0.11	0.70–0.72	0.11
HCFC-142b	0.035–0.057	0.186–0.305	0.06–0.07	0.33–0.39	0.065
HCFC-225ca	0.016–0.020	0.714–0.920	0.025	1.093	0.025
HCFC-225cb	0.023–0.031	0.348–0.474	0.033	0.50	0.033
CCl_4	1.03–1.15	1.014–1.130	1.05–1.11	1.03–1.09	1.08
CH_3CCl_3	0.11–0.13	0.968–1.130	0.122–0.124	1.07–1.09	0.12
Brominated Compounds					
H-1301	10.0–12.7	23.9–32.2	15.2–17.2	40	≈16
H-1211	1.8–5.0	16.3–49.6	3.9–4.4	40	≈4
H-1202	1.7	52.9	1.25	40	≈1.25
H-2402	6.4–10.2	42.1–47.8	5.9–8.5	40	≈7
H-1201	1.4	35.1	1.4	40	≈1.4
H-2401	0.4	66.4	0.25	40	≈0.25
H-2311	0.3	79.9	0.14	40	≈0.14
CH_3Br	0.5–0.7	30.6–67.7	0.44–0.69	40	≈0.6

factor of two greater than some model values. For all of the HCFCs considered here, the inferred ODP/CLP values are, however, far below one, showing that the upper limit represented by the CLPs is not realized.

The uncertainty in the semi-empirical polar ODP/CLP ratios for most species considered is mainly dependent on the relative calibration of the tracer measurements and is estimated to be on the order of ±10 percent for compounds inferred from CH_4 measurements. Combining this uncertainty with that of the CLPs discussed earlier allows estimation of the statistically probable error range for ODP values. Figure 6-3 presents the cumulative probability distribution functions for the ODPs of several molecules of interest based upon the known uncertainties considered. The figure shows that current uncertainties suggest that the ODP is highly likely (>90 percent) to lie below 0.04 for HCFC-123, below 0.11 for HCFC-22, and below 0.23 for HCFC-141b. However, it should be emphasized that these ranges are likely to be underestimates since they are based purely on statistical errors in present understanding and do not include chemical and physical processes whose influences could be large but cannot currently be quantified (see Section 6.2.2).

6.4 TIME DEPENDENT EFFECTS

The ODP of compound x, defined in Section 6.1, refers to conditions when the two compounds, x and CFC-11, have reached their steady-state concentrations. Consider the example of compound x, an

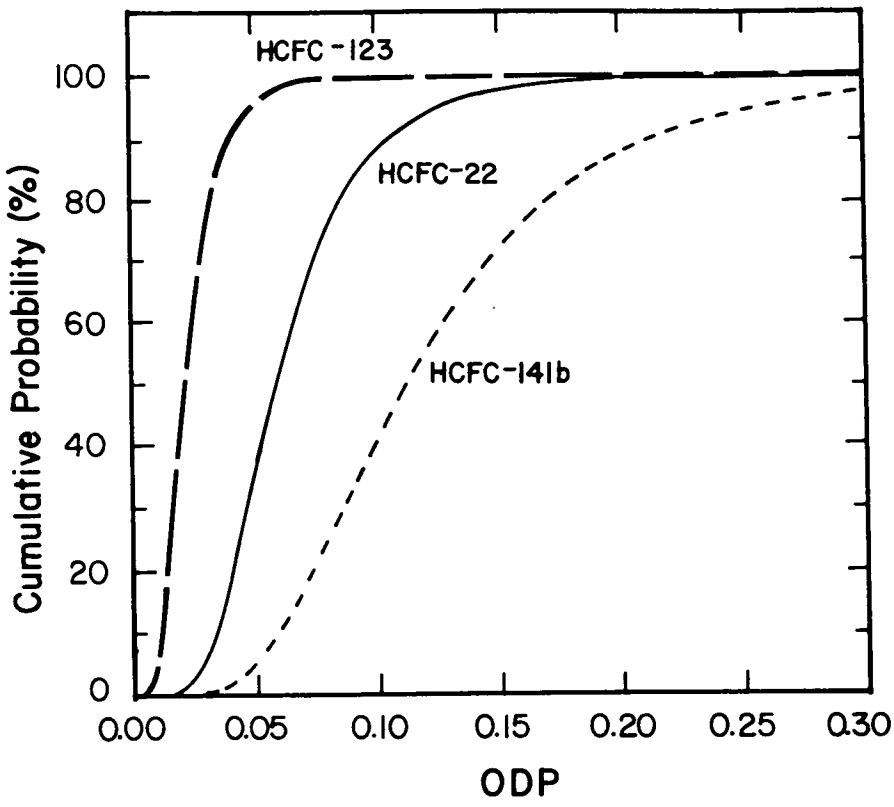

Figure 6-3 Cumulative probability distribution functions estimated for the ODPs of HCFCs-22, 123, and 141b, based on adopted accuracies in CLPs from Figure 6-1 and an estimated ±10 percent accuracy for the ODP/CLP ratios of these species.

HCFC with a relatively short tropospheric lifetime. The steady-state ODP compares the calculated steady-state ozone loss due to x, which will be realized within perhaps a decade or so, with the ozone loss due to CFC-11, realized on the time scale of centuries. On the other hand, the ratio of the ozone loss due to compound x compared to that from CFC-11, if calculated after about a decade, will be much larger than the steady-state ODP of compound x. All of x's ozone depletion has already occurred while the CFC-11 depletion is still increasing. Thus, while the ODPs for some short-lived compounds, including the HCFCs, may suggest only a modest impact on the chronic response by ozone, the acute response over the next several years will be more substantial.

As in estimations of greenhouse warming potentials (see Chapter 7), relative impacts can be assessed not just for steady state, but also for specific time horizons. The time-dependent, semi-empirical ODP can be defined as follows (see Solomon and Albritton, 1992):

$$\mathrm{ODP}(t) = \frac{\{(\mu_{\mathrm{entry}} - \mu_{0,z})/\mu_{\mathrm{entry\ for\ x}}\}}{\{(\mu_{\mathrm{entry}} - \mu_{0,z})/\mu_{\mathrm{entry\ for\ CFC\text{-}11}}\}} \cdot \frac{M_{\mathrm{CFC\text{-}11}}}{M_x} \cdot \frac{n_x}{3} \cdot \frac{\int_0^t e^{-t/\tau_x}\,dt}{\int_0^t e^{-t/\tau_{\mathrm{CFC\text{-}11}}}\,dt} \qquad (6\text{-}8)$$

where t is the time horizon and the other symbols have all been defined previously. The terms in brackets represent the fractional dissociation of x and CFC-11, respectively (equation 6-4) in the region considered. As in the previous section, these will be evaluated below using polar semi-empirical estimates based on observations. In principle, time lags for

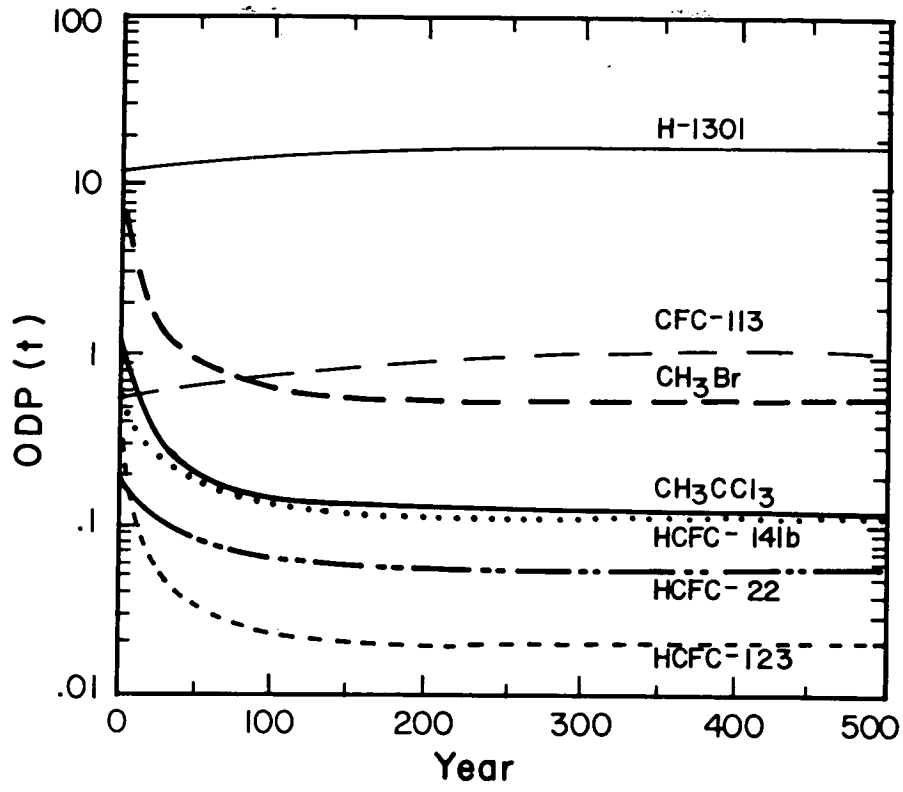

Figure 6-4 ODPs for several representative compounds as a function of time horizon based upon best estimate CLPs of this assessment and the semi-empirical ODP/CLPs.

transport to the stratosphere could be considered in evaluating ODPs over specific time horizons but these are not expected to change the results greatly and were neglected for simplicity in the calculations presented here.

Figure 6-4 shows polar lower stratospheric ODPs for several HCFCs and halons as a function of time horizon using the CLPs of Table 6-2. The large ODPs for bromine-containing compounds reflect the large value of α. Compounds with relatively short lifetimes display reduced impacts over long time scales but large ODPs over short time horizons. Note that although CH_3Br displays a relatively small ODP over long time horizons, it has a very large ODP for short time scales by virtue of its short lifetime and the large value of α. The large ODPs for CH_3CCl_3 obtained over short time horizons reflect the very short lifetimes of this gas, allowing for large and rapid impacts on ozone. The HCFCs have relatively short lifetimes, and generally display small ODPs over long time horizons, but exhibit ODPs over short time scales that can be as much as 3 to 10 times greater than their steady-state ODPs. The opposite is true for compounds with lifetimes comparable to or longer than that of CFC-11 (e.g., CFC-113), which display smaller ODPs over short time horizons than they do over time scales of centuries.

The calculations presented here illustrate the roles of various compounds in depleting ozone both over the long and short term. Likely future changes in atmospheric chlorine and bromine are described in Chapter 8, where various emission scenarios are considered. Current restrictions on emissions of halocarbons suggest that the chlorine content of the stratosphere will continue to increase for at least the next decade, implying that further ozone reductions are likely in the near future. During this period, ODPs for the specific time horizon in question are expected to

best represent the anticipated relative ozone response to releases of various compounds.

REFERENCES

Braun, W., A. Fahr, R. Klein, M.J. Kurylo, and R.E. Huie, UV gas and liquid phase absorption cross section measurements of hydrochlorofluorocarbons HCFC-225ca and HCFC-225cb, *J. Geophys. Res., 96*, 13009-13015, 1991.

Brown, A.C., C.E. Canosa-Mas, A.D. Parr, J.M.T. Pierce, and R.P. Wayne, Tropospheric lifetimes of halogenated anaesthetics, *Nature, 341*, 635–637, 1989.

Brune, W.H., D.W. Toohey, J.G. Anderson, W.L. Starr, J.F. Vedder, and E.F. Danielson, *in situ* northern mid-latitude observations of ClO, O_3, and BrO in the wintertime lower stratosphere, *Science, 242*, 558-562, 1988.

Burkholder, J.B., R.R. Wilson, T. Gierczak, R. Talukdar, S.A. McKeen, J.J. Orlando, G.L. Vaghjiani, and A.R. Ravishankara, Atmospheric fate of CF_3Br, CF_2Br_2, CF_2ClBr, and CF_2BrCF_2Br, *J. Geophys. Res., 96*, 5025–5043, 1991.

Butler, J.H., J.W. Elkins, T.M. Thompson, B.D. Hall, T.H. Swanson, and V. Koropalov, Oceanic consumption of CH_3CCl_3: Implications for tropospheric OH, *J. Geophys. Res., 96*, 22347–22355, 1991.

Fahey, D.W., S. Solomon, S.R. Kawa, M. Loewenstein, J.R. Podolske, S.E. Strahan, and K.R. Chan, Reactive nitrogen and nitrous oxide in the lower polar stratosphere: a case study in the coupling of photochemistry and dynamics, *Nature, 345*, 698, 1990.

Fisher, D.A., C.H. Hales, D.L. Filkin, M.K. W. Ko, N.D. Sze, P.S. Connell, D.J. Wuebbles, I.S.A. Isaksen, and F. Stordal, Model calculations of the relative effects of CFCs and their replacements on stratospheric ozone, *Nature, 344*, 508, 1990.

Gierczak, T.,R. Talukdar, G.L. Vaghjiani, E.R. Lovejoy and A.R. Ravishankara, Atmospheric chemistry of hydrofluoroethanes and hydrochlorofluoroethanes: 1. Rate coefficients for reactions with OH, *J. Geophys. Res., 96*, 5001, 1991.

Gillotay, D. and P.C. Simon, Ultraviolet absorption cross sections of photoactive species of stratospheric interest, Part 1: The Halocarbons, *Aeronomica Acta A, No. 356*, Institut D'Aeronomic Spatiale De Belgique, 173, 1990.

Gillotay, D. and P.C. Simon, Temperature-dependence of ultraviolet absorption cross sections of alternative chlorofluoroethanes, *J. Atm. Chem., 12*, 269–285, 1991.

Heidt, L.E., J.F. Vedder, W.H. Pollock, R.A. Lueb, and B.E. Henry, Trace gases in the Antarctic atmosphere, *J. Geophys. Res., 94*, 11599, 1989.

Heidt, L.E., S.J. Hovde, A.F. Tuck, J. Vedder, and R. Weiss, The age of the air in the Arctic lower stratospheric vortex during late winter 1988/9, in preparation for submission to *J. Geophys. Res.*, 1991.

JPL 90-1, Chemical kinetics and photochemical data for use in stratospheric modeling, NASA Panel for Data Evaluation, evaluation number 9, JPL Publ. 90-1, 1990.

Lindgren, B.W., *Statistical theory*, McMillan Press, New York, 1968.

Orkin, V.L., V.G. Khamaganov, and E.E. Kasimobskaya, Investigation of elementary processes which determine the Ozone Depletion Potential of some halogenated hydrocarbons, 11th International Symposium on Gas Kinetics, Assissi, Italy, 1990.

Orlando, J.J., J.B. Burkholder, S.A. McKeen, and A.R. Ravishankara, Atmospheric fate of several hydrofluoroethanes and hydrochloroethanes: 2. UV absorption cross sections and atmospheric lifetimes, *J. Geophys. Res., 96*, 5013–5023, 1991.

Park, J.H., B. Carli, and A. Barbis, Stratospheric HBr mixing ratio obtained from far infrared emission spectra, *Geophys. Res. Let., 16*, 787-790, 1989.

Plumb, R.A., and M.K. W. Ko, Interrelationships between mixing ratios of long-lived stratospheric constituents, submitted to *J. Geophys. Res.*, 1991.

Podolske, J.R., M. Loewenstein, S.E. Strahan, and K.R. Chan, Stratospheric nitrous oxide distribution in the Southern Hemisphere, *J. Geophys. Res., 94*, 16767, 1989.

Prather, M.J., and C.M. Spivakovsky, Tropospheric OH and the lifetimes of hydrochlorofluorocar-

bons (HCFCs), *J. Geophys. Res.*, *95*, 18723-18729, 1990.

Prather, M.J., and R.T. Watson, Stratospheric ozone depletion and future levels of atmospheric chlorine and bromine, *Nature*, *344*, 729–734, 1990.

Prinn, R., D. Cunnold, P. Simmonds, F. Alyea, R. Boldi, A. Crawford, P. Fraser, D. Gutzler, D. Hartley, R. Rosen, and R. Rasmussen, Global average concentration and trend for hydroxyl radicals deduced from ALE/GAGE trichloroethane (methyl chloroform) data for 1978-1990, *J. Geophys. Res.*, *97*, 2445–2462, 1992.

Schmidt, U., and A. Khedim, In-situ measurements of carbon dioxide in the winter arctic vortex and at mid-latitudes: an indicator of the 'age' of stratospheric air, *Geophys. Res. Lett.*, *18*, 763-766, 1991.

Solomon, S., M. Mills, L.E. Heidt, W.H. Pollock, and A.F. Tuck, On the evaluation of ozone depletion potentials, *J. Geophys. Res.*, *97*, 825-842, 1992.

Solomon, S., and D.L. Albritton, A new analysis of time-dependent ozone depletion potentials, submitted to *Nature*, 1992.

SORG (U. K. Stratospheric Ozone Review Group), Stratospheric Ozone 1990, Crown Copyright, 1990.

Talukdar, R., A. Mellouki, T. Gierczak, J.B. Burkholder, S.A. McKeen, and A.R. Ravishankara, Atmospheric lifetime of CHF_2Br, a proposed substitute for halons, *Science*, *252*, 693–695, 1991a.

Talukdar, R., A. Mellouki, T. Gierczak, J.B. Burkholder, S.A. McKeen, and A.R. Ravishankara, Atmospheric fate of CF_2H_2, CH_2CF_3, CHF_2CF_3, and CH_3CFCl_2: Rate coefficients for reactions with OH and UV absorption cross sections of CH_3CFCl_2, *J. Phys. Chem.*, *95*, 5815–5821, 1991b.

Vaghjiani, G.L., and A.R. Ravishankara, New measurement of the rate coefficient for the reaction of OH with methane, *Nature*, *350*, 406-409, 1991.

Vanlaethem-Meuree, N., J. Wisemberg, and P.C. Simon, Ultraviolet absorption spectrum of methylchloroform in the vapor phase, *Geophys. Res. Lett.*, *6*, 451–454, 1979.

Wine, P.H., and W.L. Chameides, Possible atmospheric lifetimes and chemical reaction mechanisms for selected HCFCs, HFCs, CH_3CCl_3 and their degradation products against dissolution and/or degradation in seawater and cloudwater, in *Scientific assessment of stratospheric ozone: 1989*, World Meteorological Organization, report number 20, volume 2, p. 269, 1990.

WMO, *Scientific assessment of stratospheric ozone: 1989*, World Meteorological Organization, report number 20, vols. 1 and 2, 1990.

Wuebbles, D.J., Chlorocarbon emission scenarios: potential impact on stratospheric ozone, *J. Geophys. Res.*, *88*, 1433, 1983.

Yung, Y.L., J.P. Pinto, R.T. Watson, and S.P. Sander, Atmospheric bromine and ozone perturbations in the lower stratosphere, *J. Atmos. Sci.*, *37*, 339, 1980.

CHAPTER 7

Radiative Forcing of Climate

Authors:

V. Ramaswamy
C. Leovy
H. Rodhe
K. Shine
W.-C. Wang
D. Wuebbles

Additional Contributors:

M. Ding
J.A. Edmonds
P. Fraser
K. Grant
C. Johnson
D. Lashof
J. Leggett
J. Lelieveld
M.P. McCormick
A. Oort
M.D. Schwarzkopf
A. Sutera
D.A. Warrilow
T. Wigley

Chapter 7

Radiative Forcing of Climate

Contents

SCIENTIFIC SUMMARY

Global Warming Potentials

Direct Effect. Direct global warming potentials (GWP) have been recalculated for tropospheric, well-mixed, radiatively active species (CH_4, N_2O and the halocarbons). We use updated lifetimes of these species and follow the same methodology as in the Intergovernmental Panel on Climate Change report (IPCC, 1990), for time horizons corresponding to 20, 50, 100, 200, and 500 years. The new GWP results include a correction in the values for methane arising due to a typographical error in the IPCC (1990) report, as well as changes in values for other species that are a manifestation of the updated lifetimes. However, there still exist uncertainties in these calculations due to uncertainties in the carbon cycle.

Indirect Effect. While chemical reactions involving the radiatively active atmospheric species can contribute to the GWPs, our ability to estimate them is restricted at present owing to complexities in the chemical processes and uncertainties in the temporal and spatial variations of various species. While the sign of the radiative forcing due to some of the indirect effects can be evaluated with a fair measure of confidence (Chapter 5), the quantitative aspects of the indirect effects are more difficult to ascertain than was anticipated earlier in IPCC (1990) and we do not recommend the use of those values.

Radiative forcing due to trace gases, including ozone (1979–1990)

Stratospheric Ozone. The observed global ozone losses in the lower stratosphere cause a significant forcing of the climate system. The physical effects due to this loss consist of an increase in the solar and a decrease in the longwave forcing of the surface-troposphere system, together with a tendency to cool the lower stratosphere. The latter effect amplifies the longwave influences and can thereby give rise to a significant net negative radiative forcing of the surface-troposphere system, but the magnitude of the induced forcing is very sensitive to the change in the lower stratospheric temperatures. This tendency is opposite to the direct positive (greenhouse) forcing exerted by the well-mixed gases and is pronounced in the mid-to-high latitudes of both hemispheres, and during all seasons. In fact, if the tendency to cool the lower stratosphere is fully realized as equilibrium temperature change, the magnitude of the negative ozone radiative forcing in the mid-to-high latitudes can be larger than the decadal greenhouse forcing due to the CFCs over this period, and could also be a significant fraction of the total decadal greenhouse forcing due to the non-ozone gases.

Tropospheric Ozone. Ozone in the troposphere, although present in smaller amounts than that in the stratosphere, has a significant opacity and exerts a greenhouse effect (positive forcing), with the sensitivity being greatest for ozone changes in the upper troposphere. However, the databases for tropospheric ozone trends are sparse and therefore inadequate for quantifying the global radiative influences due to changes in tropospheric ozone.

Radiative forcing due to sulfate aerosols

Tropospheric Aerosols. Fossil fuel emissions over the past century have increased significantly the tropospheric sulfate aerosol concentrations. The contribution of this species to the direct clear-sky radiative forcing of the Northern Hemisphere is opposite to that due to the greenhouse gases and is estimated to be a significant fraction of the trace gas forcing. Although we are confident of the sign of the forcing, uncertainties exist owing to the spatial inhomogeneity of the aerosol distributions and a lack of understanding of the aerosol effects in cloudy regions.

Stratospheric Aerosols. With the eruption of Mt. Pinatubo in mid-1991, there is again a radiative forcing of the climate system due to increases in the concentrations of the stratospheric sulfate aerosols. These aerosols produce a net negative radiative forcing of the climate system which is comparable to the positive ones due to the greenhouse gases, but this forcing is short-lived. The presence of the aerosols in the stratosphere also contributes to a warming tendency in the lower stratosphere. Preliminary observations indicate about a 4 K warming of the tropical lower stratosphere two months following the Mt. Pinatubo eruption.

7.1 INTRODUCTION

This chapter is an update of the scientific discussions presented in Chapter 2 of the Intergovernmental Panel on Climate Change report (IPCC,1990; hereafter referred to as IPCC) concerning the atmospheric radiative and chemical species of significance for climate change. There are two major objectives of the present update. The first is an extension of the discussion on the Global Warming Potentials (GWPs), including a reevaluation in view of the updates in the lifetimes of the radiatively active species. The second important objective is to underscore major developments in the radiative forcing of climate due to the observed stratospheric ozone losses occurring between 1979 and 1990. The contents of this chapter are in the following sections:

7.2 Definitions of radiative forcing,
7.3 GWPs of the well-mixed trace gases using new lifetimes; also included is the sensitivity of the radiative forcing to the absolute concentrations of greenhouse gases, and the radiative forcing due to increase of water vapor in the stratosphere resulting from the oxidation of methane,
7.4 Radiative forcing due to the increases in non-ozone trace gases (1979–1990),
7.5 Characterization of the radiative forcing due to changes in atmospheric ozone that have occurred over the past decade (1979–1990),
7.6 Radiative forcing induced by increases in tropospheric sulfate aerosol concentrations, and
7.7 Stratospheric aerosol effects following the eruption of the Mt. Pinatubo volcano.

Several radiative transfer models have been employed to obtain the results described here. Those that performed calculations exclusively for this study are listed in Table 7-1.

Table 7-1 Radiative transfer models employed in this study. Models I and III have a spectral resolution of 10 cm^{-1}. Model V includes a one-dimensional chemistry model as well.

Model	Institution	References
I	Geophysical Fluid Dynamics Laboratory	Fels *et al.* (1980); Mahlman and Umscheid (1984); Ramaswamy *et al.* (1990)
II	Geophysical Fluid Dynamics Laboratory	Ramaswamy and Ramanathan (1989)
III	University of Reading	Shine (1991)
IV	State University of New York at Albany	Wang and Molnar (1985); Fisher *et al.* (1990)
V	Lawrence Livermore National Laboratory	Miller *et al.* (1991)

7.2 RADIATIVE FORCING

The radiative forcing due to a perturbation in the concentration of a gas is defined by the net radiative flux change induced at the tropopause. The forcing is usually interpreted as a gain (positive) or a loss (negative) for the surface-troposphere system as a whole. The rationale for this concept arises from exercises with one-dimensional radiative-convective models where the change in the surface temperature can be related simply to the net radiative flux change at the tropopause (WMO, 1986). This has led to the adoption of the surface-troposphere system as a convenient means to obtain a perspective of the trace gas radiative effects. The instantaneous radiative forcing is given by the change obtained keeping all parameters (including temperature and water vapor) fixed in both the troposphere and the stratosphere, with the meteorological conditions conforming to an assumed atmospheric state.

A second definition of radiative forcing, emerging from the discussions in WMO (1986) and IPCC relates to the case when the stratospheric temperatures are allowed to relax to a new equilibrium under the assumption of a constant dynamical heating—the so-called Fixed Dynamical Heating (FDH) concept (Fels and Kaplan, 1975; Ramanathan and Dickinson, 1979, Fels *et al.*, 1980). This also constitutes a generalization of the global mean concept of relaxing the stratosphere back to a radiative equilibrium (Hansen *et al.*, 1981), with the proviso that the tropospheric temperatures as well as the water vapor everywhere remain unchanged, being the same as in the unperturbed state. This definition makes use of the fact that the model stratosphere adjusts or comes to equilibrium more rapidly (usually within 60 to 90 days) to the perturbation induced by a change in a specific trace

gas concentration than do the troposphere and the surface (several years to possibly several decades).

For the purposes of this assessment, we will term the *instantaneous* forcing resulting from the first definition as *Mode A*, and that from the second definition involving the *stratospheric temperature adjustment* as *Mode B*. It is the Mode B result that describes more appropriately the long-term (seasonal and longer time scales) forcing of the surface-troposphere system (WMO, 1986; IPCC, 1990). Further, Mode A can be interpreted as the case without temperature feedback in the stratosphere while, in Mode B, there is a temperature feedback in the stratosphere. In both modes, tropospheric feedback mechanisms are excluded.

7.3 GLOBAL WARMING POTENTIAL

7.3.1 Definition

As a relative measure of the possible warming effect of the surface and the troposphere arising due to the emissions of each greenhouse gas, IPCC presented the concept of the Global Warming Potential. The GWP of a greenhouse gas takes into account the radiative forcing due to a single pulsed emission of that gas, as well as its lifetime within the atmosphere. It is thus related to the emissions of greenhouse gases and their lifetimes. Since IPCC discusses the GWP concept in considerable detail, only the salient features of the GWP are emphasized here.

The GWP of a well-mixed gas is defined (IPCC, page 58) formally as the time-integrated commitment to radiative forcing from the instantaneous release of 1 kg of a trace gas expressed relative to that from the release of 1 kg of CO_2. This definition requires a consideration of the following factors:

- choice of a reference molecule and its lifetime, as well as the lifetimes of other gases,
- the radiative forcing due to a change in the concentration of a gas,
- the time horizon over which the radiative forcings have to be integrated,
- the background concentrations of various species, and the atmospheric temperature and moisture profiles, and
- the indirect effects due to chemical reactions that are accompanied by changes in the concentrations of the radiatively active species.

The GWP concept is derived from the globally- and annually-averaged net radiative flux change at the tropopause. Accordingly, the surface-troposphere radiative forcing employed in GWP determinations is obtained from a radiative transfer model for global mean atmospheric conditions. The principal significance of the GWP concept lies in the fact that it offers a simple yet reasonable characterization of the relative global mean radiative effects due to changes in the concentrations of the well-mixed species. This renders it particularly useful in the context of policy-making decisions concerning the emissions of the well-mixed greenhouse gases. However, as noted subsequently (section 7.3.8), this concept does have serious limitations.

7.3.2 Reference Molecule and its Lifetime

Given the conceptual framework of the GWP and its implications for policy-making, the choice of a reference molecule is dictated by the need for simplicity and the need to evaluate the results in terms of the dominant contributor in the greenhouse gas problem. IPCC chose CO_2 as the reference molecule for the GWP determinations. Although another gas or surrogate would have a simpler atmospheric decay rate compared to CO_2 (*e.g.*, CFCs; see Fisher *et al.*, 1990) and can equally well be chosen as the reference, the evaluation of GWPs presented here continues to use CO_2 as the reference gas. The chief reason for this is the importance of CO_2 as the gas of primary concern to future climate change. Further, again following IPCC and notwithstanding the uncertainties in the carbon cycle, the results from the Siegenthaler (1983) model are employed to estimate the lifetimes of CO_2.

7.3.3 Time Horizons for GWPs

Since greenhouse gases differ in their relative reactivity and their sink mechanisms, they remain in the atmosphere for different time periods, *i.e.*, they have different lifetimes. The calculation of GWPs, thus, depends on the time-period of integration chosen for the analysis. There is, however, no given value of integration time for determining GWPs that is ideal over the range of uses of this concept.

The choice of a time-scale for integration of the GWP calculation, however, need not be totally arbi-

trary. The risks of climate change are associated with different kinds of undesirable changes. For example, rapid climate changes over successive decades may have adverse impacts to biological systems as climate zones shift more quickly than natural systems can migrate. Likewise, a several degree increase in surface temperature over the next century or two, a somewhat longer time horizon, could have adverse effects on both human communities and natural ecosystems. Each type of system has its own characteristic thresholds of sensitivity to different types of damage. The choice of the yardstick for measuring the risks of climate change depends on the type of undesirable changes that are of greatest interest to the analyst or policymaker.

Although most of the public attention to the climate problem has been concentrated on one indicator of risk (*i.e.*, the global average surface temperature change), several other indicators of unwanted change, too, could have important climate change ramifications. Also, they could be of importance from the policymaker's perspective. The choice of which indicator to use (and which time horizon to employ) for the GWP analyses is determined by the type of undesirable change that is under consideration.

The effect of the surface inertia of the climate system associated with the world's oceans influences the time-scales associated with a given climatic response and the resulting impacts. Within the climate system, the exchange of energy between the oceans and the atmosphere results in a lag in the temperature response to a given forcing. The lag in the climate response is estimated to be between 10 and 100 years (IPCC).

Several possible indicators of change (and the associated time horizons for analyses of GWPs) are shown below. The column on the right illustrates the characteristic integration periods that would be appropriate to capture the important aspects of these different indicators:

Climate Change Indicator	Integration Time Period
Maximum change in temperature	~100 years
Rate of change in temperature	~ 20–50 years
Maximum change in sea level	> 100 years
Rate of change in sea level	> 50 years

GWPs in this report are calculated over time horizons of 20, 50, 100, 200, and 500 years (as compared to 20, 100, and 500 years only in IPCC). These five different time horizons ought to provide a useful set of reference values for policy decisions. As suggested above, the GWPs estimated for long time periods provide a measure of the cumulative chronic effects on climate. Integrations to extremely long times (*i.e.*, 500 years) are subject to significant uncertainties in the decay rate of atmospheric CO_2. On the other hand, the 20 and 50-year integrations are representative of the time scales for the maximum rate of response of temperature.

The GWPs evaluated over the 100-year period appear generally to provide a balanced representation of the various time horizons for climate response. This is a time scale that includes due consideration of the ocean thermal inertia and its impacts on the global mean surface temperature. In addition, carbon cycle models also indicate that this time period broadly represents the time scale over which a significant fraction of CO_2 is removed from the atmosphere. However, policy analyses emphasizing the rate of temperature change or the rate of sea level rise may find the 50-year integration period to provide a better representation of the climate responses. Considerations of the shortest time scale (*i.e.*, 20 years) suggest one way to reduce the rate of increase of the radiative forcing, particularly for short-lived species.

7.3.4 Direct GWPs of Well-Mixed Trace Gases

Based on the above considerations, and employing the updated lifetimes of the various species (Chapter 8), and the radiative forcings given in Table 2-3 of IPCC, new direct (*i.e.*, in the absence of atmospheric chemistry considerations) GWPs of several well-mixed species are determined. These are listed in Table 7-2 for the five time horizons and may be compared with Table 2-8 in IPCC. The forcings employed here conform to the Mode B definition discussed in Section 7-2, thus implicitly allowing for the temperature feedback in the stratosphere due to the particular greenhouse gas. Changes in the lifetime and variations of radiative forcing with changes in the background concentrations of species are neglected.

The direct GWPs for methane in Table 7-2 are substantially higher than those inferred from IPCC owing to a typographical error in that report. The

Table 7-2 Direct global warming potentials of several well-mixed trace gases relative to CO_2. The GWPs of the various non-CO_2 species are calculated for each of five time horizons (20, 50, 100, 200 and 500 years) using, as in IPCC, the carbon cycle model of Siegenthaler (1983). (Note that IPCC contained a typographical error which led to incorrect values for the direct GWP of methane.)

Gas	Lifetime (years)	Time Horizons				
		20 years	50 years	100 years	200 years	500 years
CO_2	#	1	1	1	1	1
CH_4	10.5	35	19	11	7	4
N_2O	132	260	270	270	240	170
CFC-11	55	4500	4100	3400	2400	1400
CFC-12	116	7100	7400	7100	6200	4100
HCFC-22	15.8	4200	2600	1600	970	540
CFC-113	110	4600	4700	4500	3900	2500
CFC-114	220	6100	6700	7000	7000	5800
CFC-115	550	5500	6200	7000	7800	8500
HCFC-123	1.71	330	150	90	55	30
HCFC-124	6.9	1500	760	440	270	150
HFC-125	40.5	5200	4500	3400	2200	1200
HFC-134a	15.6	3100	1900	1200	730	400
HCFC-141b	10.8	1800	980	580	350	200
HCFC-142b	22.4	4000	2800	1800	1100	620
HFC-143a	64.2	4700	4500	3800	2800	1600
HFC-152a	1.8	530	250	150	89	49
CCl_4	47	1800	1600	1300	860	480
CH_3CCl_3	6.1	360	170	100	62	34
CF_3Br	77	5600	5500	4900	3800	2300

#(see Table 2.8, IPCC, 1990)

other differences between Table 7-2 and Table 2-8 of IPCC are a manifestation of the changes in the lifetimes. Species whose lifetimes have changed substantially include F-125 (45 percent higher) and F-141b (35 percent higher), F-143a (57 percent higher) and CF_3Br (30 percent less). The new direct GWPs in Table 7-2 are generally within 20 percent of the IPCC values. The exceptions are the above-mentioned species viz., F-125, F-141b and F-143a, all of which have an increase in GWP exceeding 20 percent for the 100- and the 500-year time horizons, while CF_3Br has a decrease of more than 20 percent for the 500-year horizon.

7.3.5 Sensitivity of Radiative Forcing to Background Trace Gas Concentrations

One important parameter determining the radiative forcing due to changes in the concentrations of trace gases is the background concentrations of the trace species themselves. The effect of this parameter is investigated here using one-dimensional radiative-convective models. Specifically, the perturbation in the radiative fluxes is examined for two different background concentrations, one corresponding to present (1990) atmosphere and the other to a postulated 2020 atmospheric profile (Chapter 8). Each atmosphere is brought to a model-determined radiative-convective equilibrium. To each of these atmospheres in equilibrium, an identical perturbation is applied corresponding to an increase in the concentration of a particular trace gas, keeping the concentrations of the other species fixed. The perturbations are evaluated for the Mode A condition, *i.e.*, without the stratospheric temperature feedback.

Models I, II, and IV performed computations for specified perturbations (see Table 7-3) in the concentrations of CO_2, CH_4, N_2O, F-11 and F-12. The results,

listed in Table 7-3, are quoted as the ratio by which the radiative forcing in 2020 changes with respect to that in 1990. The perturbations applied are arbitrary and correspond to changes in the concentrations of each trace gas occurring between 1980 and 1990 (Chapter 8).

The results from the various models agree well with each other and are completely understandable in terms of the nonlinearities in the radiative properties of the individual species (IPCC). The decrease in the forcing due to CH_4 and N_2O is less than that for CO_2, so that the GWPs of CH_4 and N_2O would be greater in 2020 than in 1990. The changes for F-11 and F-12 are negligible. These examples confirm the dependence of the GWPs on the assumed background atmospheric concentrations of the trace species.

Table 7-3 Ratio of the Mode A radiative forcings due to an increase in the concentration of a trace gas, as computed for the atmospheric profiles in the years 2020 and 1990. The atmospheres correspond to those obtained from a one-dimentional radiative-convective model, with the background concentrations of the trace gases in 1990 and 2020 following Chapter 8. The perturbation applied to the 1990 and 2020 atmospheres in radiative-convective equilibrium are listed below. The ratios are derived from Models I, II and IV, respectively.

Gas	Perturbation applied	Model I	Model II	Model IV
CO_2	17 ppmv	0.85	0.86	0.87
CH_4	15 ppmv	0.89	0.87	0.95
N_2O	8 ppbv	0.95	0.92	0.94
CFC-11	111 pptv	1.0	1.0	1.0
CFC-12	170 pptv	1.0	1.0	1.0

7.3.6 Indirect GWP Effects

While a sizable body of knowledge is available to indicate the sign of the indirect effects as induced by chemical processes, the magnitudes of these effects are still not easily quantified without considerable uncertainties. Chapter 5 presents estimates of the changes in species concentrations induced by chemical interactions. Some of these could contribute to the GWP of certain species listed in Table 7-2. We recognize that these indirect effects are more difficult to estimate than the direct effects owing to the complexity of the chemical reactions and the temporal and spatial dependence of the involved species' concentrations. While the sign of the indirect effects can be estimated with a fair degree of confidence (Chapter 5), the quantitative aspects merit further detailed investigations. In fact, the values for the indirect effects in IPCC could be very uncertain and their use is not recommended. It is now known that the value for NO_x, in particular, may have been overestimated substantially in the IPCC report (Johnson *et al.*, 1992). It is possible that, for methane, some progress in quantifying the uncertainties in the indirect effects may be possible in the near future. As an example, the indirect enhancement in the methane radiative forcing due to a specific chemical transformation is discussed in the next section.

7.3.7 Indirect GWP of Methane Due to Oxidation to Water Vapor

As noted in IPCC, the oxidation of methane in the stratosphere results in an increase in the water vapor content at those altitudes, which, in turn, contributes to the greenhouse effect. In this study, a one-dimensional chemistry algorithm (Model V) was used to compute the increase in the stratospheric water vapor content resulting from the oxidation of methane. The change in the vertical profile of water vapor, corresponding to increases in methane of 30 and 100 percent, respectively, is shown in Figure 7-1. These changes contribute to the indirect GWP effects of methane (IPCC). The change in the surface-troposphere radiative flux (Mode A; W/m^2) due to the direct effect of methane, and that due to the considered indirect effect, as obtained by Model V, is shown below. The accompanying changes in stratospheric column ozone (ΔO_3) are also shown.

	Direct	Indirect	ΔO_3
+30 % increase	0.18	0.04	0.7%
+100 % increase	0.52	0.12	2.1%

Indirect effects were also reported in IPCC and have also been calculated in a recent study by Lelieveld and Crutzen (1992). The amplification in the methane radiative forcing due to this indirect effect from the various calculations is summarized below. Models IV and V employ the same perturbation but differ in the radiation schemes employed:

$$RF(H_2O \text{ from } CH_4) = X \bullet RF(CH_4\text{-direct}),$$

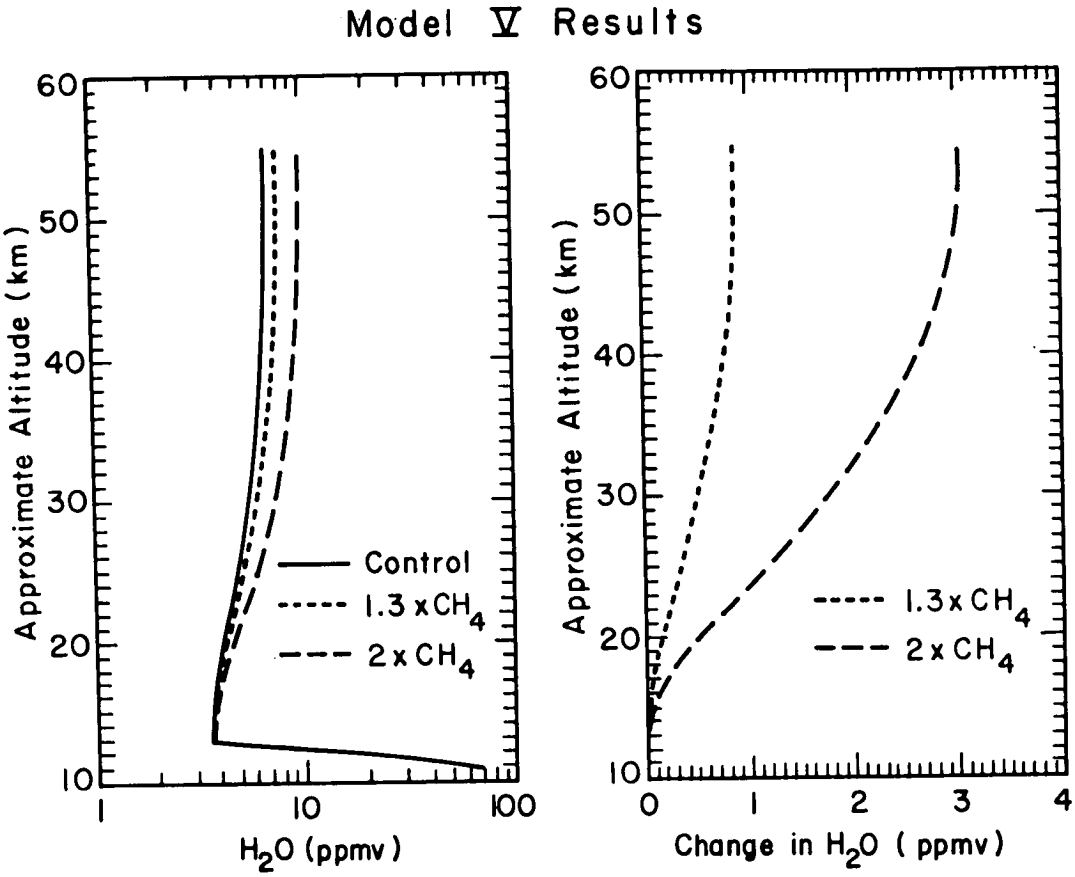

Figure 7-1 Changes in the vertical profile of water vapor due to 30 and 100 percent increase, respectively, in methane, as obtained by Model V.

where "X" reflects the enhancement in the GWP of methane and "RF" refers to radiative forcing;

X = 0.3 (IPCC)
= 0.22 (Model V-this report)
= 0.31–0.38 (Model IV)
= 0.05 (Lelieveld and Crutzen, 1992)

There are considerable differences between the results. While the first three results are approximately similar, the differences between the fourth result and the others have not been satisfactorily resolved as yet. The differences may partly reflect the different types of numerical experiments performed to calculate the effect. The difference between Model V and IV, which employed identical perturbations, are likely due to differences in the radiative transfer schemes. Further analyses are required to resolve all these differences. It is noted that the actual effect involving the oxidation of methane to water vapor will depend not only on photochemical factors but also on the transport processes, and could have a latitudinal dependence.

7.3.8 Limitations and Uses of GWPs

While the GWP, as defined in IPCC, is a convenient yet reasonable practical index for ranking the relative and aggregated greenhouse gas emission impacts, it has the following limitations, some of which are very serious:

A) The radiative forcing employed in the determination of the GWP does not purport to characterize the latitudinal and seasonal dependence of the change in the surface-troposphere radiative fluxes. Nor does the GWP describe explicitly the partitioning of the surface-troposphere flux changes into that at the surface and that within the troposphere.

B) The GWP definition considers only the surface-troposphere radiative forcing rather than a particular response (*e.g.*, surface temperature) of the climate sys-

C-3

tem. While the surface-troposphere radiative flux perturbations can be related to temperature changes at the surface in the context of the one-dimensional radiative-convective models (WMO, 1986), such a general interpretation for the temperature response in the three-dimensional general circulation models or in the actual surface-atmosphere system must be approached with caution. Further, although the GWP of a well-mixed gas can be regarded as a first-order indicator of the potential global mean temperature change due to that gas, it is inappropriate for predicting or interpreting the regional climate responses.

C) Different well-mixed gases can yield characteristically different spatial patterns of radiative forcings and climate responses (Wang *et al.*, 1991). Since the GWP is a measure of the global effect of a given greenhouse gas emission, it is most appropriate for well-mixed gases in the troposphere (*e.g.*, CO_2, CH_4, N_2O and halocarbons). The global perspective of the concept raises doubts about its applicability to species that have pronounced spatial and temporal variations such as sulfate aerosols.

D) The accounting of the indirect effects (*e.g.*, due to changes in water vapor and ozone) is more problematic than the direct effects. At present, there exist uncertainties in the details of the chemical processes as well as in the spatial and temporal variations of species involved in such transformations. Further, while the GWP concept thus far has been applied to gases with perturbations only in the longwave spectra, it may not adequately account for the radiative effects due to inhomogeneously-distributed species with significant interactions in both the solar and the longwave spectra (*e.g.*, ozone).

E) GWP values are sensitive to significant uncertainties regarding atmospheric residence times and indirect effects. Thus, revisions to the GWP values should be expected as scientific understanding improves. In particular, the sinks for anthropogenic CO_2 emissions are poorly understood and cannot be characterized by a single exponential decay term. Because CO_2 is used as the reference gas, any revision to the calculation of its integrated radiative forcing over time will change all GWP values.

F) GWP values will change as the composition of the trace species in the atmosphere changes with time. Hence, GWP indices evaluated with respect to, say 2020, may differ significantly from those for 1990. One way of getting around this is to calculate GWP values on the basis of an emission scenario. However, such scenarios are also subject to uncertainties so that GWP revisions due to changes in atmospheric composition cannot be avoided.

Given the above limitations, care must be exercised in applying GWPs in the policy arena. Some possible applications are identified below.

- Technology Assessment: Alternative technologies may each emit a number of greenhouse gases in different quantities. GWPs are useful in evaluating the overall greenhouse impact of these technologies. This assessment should consider the total emissions (rather than the annual emissions) affected by the technology choice.
- Emission Inventories: GWPs can be used to sum emissions of different gases to develop estimates of overall greenhouse gas emissions in "CO_2 equivalents." The different character of emissions from different sources and the different levels of uncertainty associated with the emission estimates should be considered in conducting such an analysis.
- Limitation Policies: Policies to limit greenhouse gases could be formulated in terms of the GWP of some set of gases rather than individual gases. Uncertainties in both the GWPs and the baseline emission estimates must be carefully considered in developing this approach.

GWPs should be used with caution and with other viable approaches in evaluating policy options. In particular, the use of GWPs should not substitute for scenario analyses to evaluate the implications of different emission paths over time. It is also recognized that alternative formulations of GWPs (*e.g.*, use of continuous rather than pulsed emissions) are possible and that there is necessarily no unique definition of GWPs which can satisfy all policy needs simultaneously.

7.4 RADIATIVE FORCINGS DUE TO NON-OZONE TRACE GASES (1979–1990)

Standard atmospheric profiles, including temperature and moisture (McClatchey *et al.*, 1972), are used to determine the clear-sky radiative forcing due to the increases in the non-ozone gases (CO_2, CH_4,

N_2O and CFCs) occurring between ~1979 and 1990 (Chapter 8). The CFCs considered here include CFC-11, CFC-12, CFC-113, CFC-115, and HCFC-22. All these gases primarily interact with the terrestrial infrared (longwave) radiation. The increases in the surface-troposphere forcing (Mode A) are listed in Table 7-4.

First, it is noted that the 10 cm^{-1} spectral resolution results from Model I have been compared with the 'benchmark' line-by-line results (Ellingson *et al.*, 1991) and found to be in excellent agreement (Ramaswamy *et al.*, 1990). Also, results from Models I and IV agree quite well with each other. The results in Table 7-4 emphasize that the trace gas radiative forcing depends on latitude and season, as was pointed out for CO_2 in WMO (1986). This occurs because of the dependence of the longwave radiative transfer on the molecular absorption and emission processes, and on the Planck function, both of which, in turn, depend on the atmospheric profiles (WMO, 1986). Since no feedbacks are considered, the contrasts in the forcings should not be associated with temperature responses actually occurring at the various latitudes and during the different seasons.

Table 7-4 Clear-sky Mode A radiative forcing (W/m^2) due to the increase in the non-ozone trace gases between 1979 and 1990. Both Models employ the Roberts *et al.* (1976) continuum while Model IV in addition considers the Clough *et al.* (1989) continuum (values within parenthesis). The atmospheric profiles follow McClatchey *et al.* (1972).

Case	Model I	Model IV
Tropics	0.71	0.64 (0.68)
Mid-latitude summer	0.66	0.61 (0.65)
Mid-latitude winter	0.50	0.51 (0.52)
Subarctic summer	0.60	0.57 (0.60)
Subarctic winter	0.39	0.41 (0.41)

An important aspect of the trace gas forcings is the vertical partitioning between the surface and the troposphere. It is known, for example that while, for CO_2, most of the effect in the surface-troposphere system is felt within the troposphere, the CFCs exert their major effect at the surface (WMO, 1986). Table 7-5 demonstrates that, in the tropics, the troposphere rather than the surface "feels" most of the instantaneous radiative forcing (Mode A) due to the trace gas increases. This is primarily because of the large water vapor amount present in the tropical troposphere which tends to have a high optical opacity (Ramanathan *et al.*, 1979). At higher latitudes, the lesser moisture amounts serve to decrease the trapping of the flux in the troposphere and instead focus the forcing mainly at the surface. Thus, the latitudinal and seasonal dependence of the radiative forcing, and its partitioning between the surface and the troposphere, are significant aspects of the global radiative perturbations. They deserve adequate attention in the analyses of global mean quantities (*e.g.*, GWPs).

The trace gas forcings also depend on the assumptions made about the water vapor continuum absorption in the 8 to 12 micron region of the infrared spectrum. This is an important component of the longwave radiative transfer that is still not completely understood (Ellingson *et al.*, 1991). While the above discussions were with respect to one assumption (Roberts *et al.*, 1976), the forcing and the partitioning using another assumption (Clough *et al.*, 1989) can be different (Tables 7-4 and 7-5). This emphasizes the need for further investigations regarding the water vapor continuum. It is also pertinent to point out that there are other spectroscopic issues that have not been adequately resolved as yet which, too, can have a non-negligible bearing on the radiative forcing computations, such as assumptions about line shape and line mixing, temperature dependence of the halocarbon absorption, etc. (see Ellingson *et al.*, 1991 for a state-of-the-art assessment of longwave radiative transfer algorithms, and IPCC, 1990).

Table 7-5 Partitioning of the Mode A radiative forcing (W/m^2) between surface and troposphere, as obtained by Model IV, using the Roberts *et al.* (1976) and the Clough *et al.* (1989) continuum (in parenthesis).

Case	Troposphere	Surface
Tropics	0.50 (0.48)	0.14 (0.20)
Mid-latitude summer	0.41 (0.37)	0.20 (0.27)
Mid-latitude winter	0.16 (0.09)	0.35 (0.43)
Subarctic summer	0.32 (0.27)	0.25 (0.33)
Subarctic winter	0.04 (–0.02)	0.37 (0.43)

7.5 RADIATIVE FORCING DUE TO OZONE (1979–1990)

7.5.1 Lower Stratosphere Ozone Losses (Clear Skies)

The recent Total Ozone Mapping Spectrometer (TOMS) and Stratospheric Aerosol and Gas Experiment (SAGE) results show a significant global depletion of ozone between 1979 and 1990 (Chapter 2). While the TOMS trends analysis (Stolarski *et al.*, 1991) shows a decrease in the column ozone over the middle and high latitudes of both hemispheres, ozonesonde, Umkehr and SAGE satellite analysis (McCormick *et al.*, 1992) indicate that most of this loss occurs in the lower stratosphere (Chapter 2).

In this section, the results from the trends analyses are employed to perform a series of clear-sky sensitivity studies and determine the radiative impact of the ozone decreases. These are compared with the non-ozone gas increases described in section 7-4. The study was performed for seven cases involving different geographical locations, time of the year, and atmospheric profiles (McClatchey *et al.*, 1972), as listed in Table 7-6. The conditions chosen include low and high ozone depletion cases. Two of the models listed in Table 7-1 (I and IV) performed the calculations. In both models, the ozone loss amount is confined to a layer between tropopause and 7 km above it. This is approximately consistent with the observed vertical profile of the ozone loss in the lower stratosphere.

The results under Mode A and Mode B conditions are tabulated in Table 7-7. This table lists the forcings for three different changes: CO_2+CH_4+N_2O, CFCs only and O_3 only. A histogram plot of the forcings, as obtained by Model I, appears in Figure 7-2. Results from the two models listed are in fair agreement and yield similar conclusions for Mode A. Mode B results were unavailable from Model IV.

The effects due to the non-ozone species (CO_2, CH_4, N_2O, and CFC) are solely due to their absorption bands in the infrared, with solar absorption being small and arising due to CO_2 alone. As in Table 7-4, the latitudinal dependence for the non-ozone gases is evident again. In comparing Mode B with Mode A results, an important distinction occurs for the CFCs and the other non-ozone species. Since the CFCs tend to warm the region near the tropopause (Dickinson *et*

Table 7-6 Cases selected for analyzing the radiative forcing arising due to ozone depletion in clear skies, based on the TOMS data (Stolarski *et al.*, 1991). The ozone change during the decade at the particular latitude and time, and the atmospheric profile used in the computations are listed.

Case	Latitude	Time of year	Profile*	ΔO_3 (%)
1	0°N	July 1	T	–0.5%
2	45°N	July 1	MLS	–2.0%
3	45°N	Feb. 1	MLW	–8.0%
4	45°S	Jan. 1	MLS	–6.0%
5	45°S	Aug.1	MLW	–5.0%
6	70°N	Mar.1	SAW	–17.0%
7	75°S	Oct. 1	SAW	–32.0%

*T–Tropical, MLS–Mid-latitude Summer, MLW–Mid-latitude Winter, SAW-Subarctic Winter; see McClatchey et al., (1972).

Table 7-7 Radiative forcings (W/m^2) due to the non-ozone trace gas increases, CFC only increases, and that due to ozone decreases for each of the cases cited in Table 7-6. The ozone loss is assumed to occur in a layer between the tropopause and extending upward to 7 km above it. The results listed are obtained by Models I and IV (within parentheses).

Case	CO_2+ CH_4+N_2O		CFCs only		O_3 only	
	A	B	A	B	A	B
1	0.54 (0.54)	0.49	0.16 (0.14)	0.17	0.01 (0.02)	–0.01
2	0.51 (0.51)	0.47	0.13 (0.12)	0.15	0.08 (0.12)	–0.11
3	0.41 (0.44)	0.38	0.08 (0.09)	0.10	0.03 (0.07)	–0.42
4	0.51 (0.53)	0.47	0.13 (0.12)	0.15	0.27 (0.32)	–0.30
5	0.41 (0.44)	0.37	0.08 (0.09)	0.10	0.05 (0.07)	–0.22
6	0.34 (0.36)	0.30	0.05 (0.05)	0.06	–0.17 (–0.22)	–0.90
7	0.34 (0.36)	0.31	0.05 (0.05)	0.06	–0.41 (–0.39)	–2.38

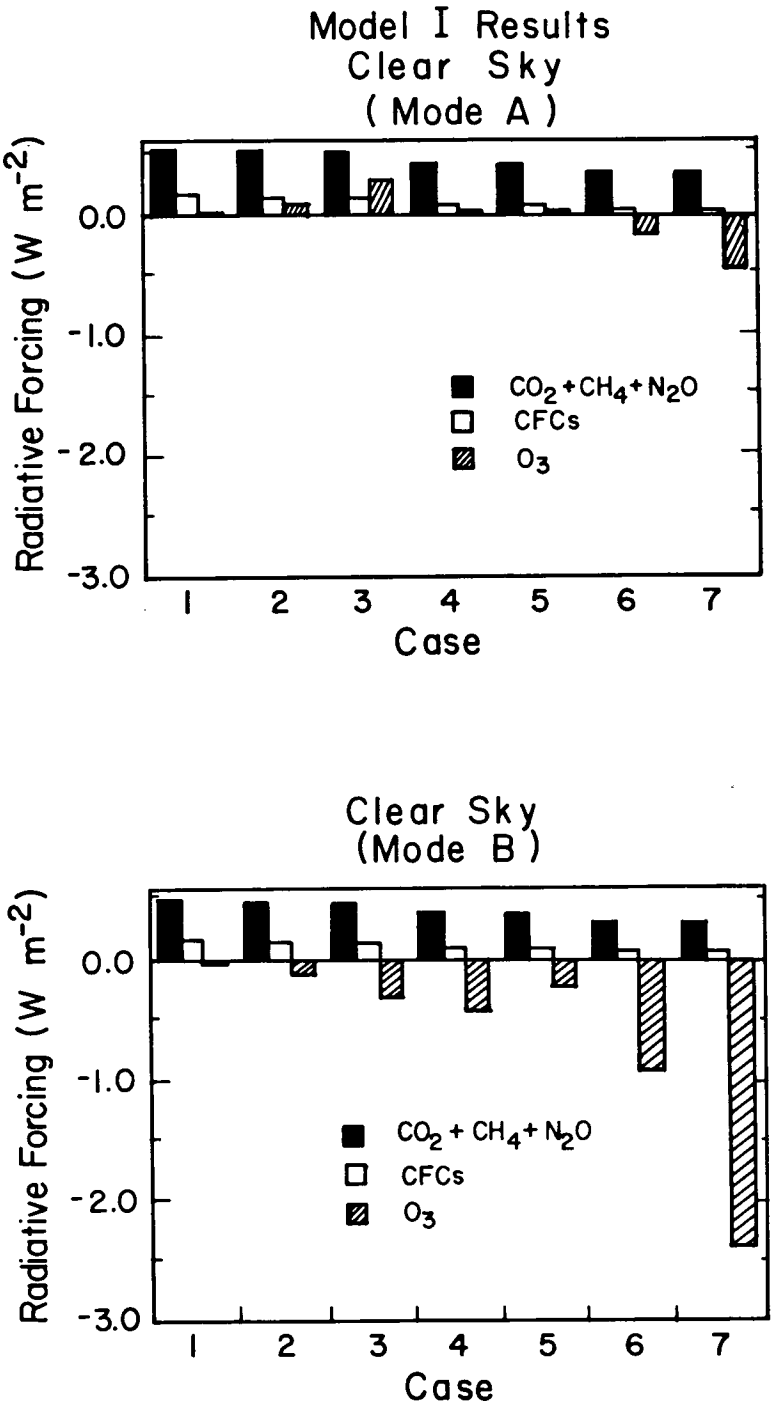

Figure 7-2 Radiative forcing due to CO_2+CH_4+N_2O, CFCs only, and that due to lower stratospheric ozone losses (see 7.5.1) at various locations and times of the year listed in Table 7-6. The seven cases employ clear-sky atmospheric profiles (McClatchey *et al.*, 1972). Upper panel shows Mode A results and the lower panel Mode B results (Model I computations). Numerical values are tabulated in Table 7-7.

al., 1978; Ramanathan *et al.*, 1985), the forcing in Mode B is associated with a warming of those altitude regimes. This leads to increased longwave emission by the lower stratosphere into the surface-troposphere system which yields a greater forcing than in Mode A. In contrast, for CO_2+CH_4+N_2O, the overall effect in the stratosphere is dominated by the cooling due to CO_2 (WMO, 1986) which consequently yields a lesser forcing in Mode B than in Mode A.

Unlike the other trace gases, changes in ozone perturb both solar and longwave radiation substantially (WMO, 1986). The effect in the solar spectrum is one of a decrease in the stratospheric absorption, resulting in more radiation becoming available for absorption in the surface-troposphere system; this constitutes a positive forcing on the system. While the solar effects due to ozone losses are determined solely by the total column ozone amounts, the longwave effects are determined both by the amount and its vertical location (Ramanathan and Dickinson, 1979; WMO, 1986; Wang *et al.*, 1980; Lacis *et al.*, 1990). In Mode A, the decrease of ozone in the lower stratosphere leads directly to a decreased emission into the surface-troposphere system which offsets, to some extent, the increase in the solar absorption there.

The reduction in the solar absorption and the change in the longwave convergence within the lower stratosphere would yield a radiatively-induced cooling tendency. This tendency due to ozone losses is similar to that due to the increases in the non-ozone gases. If this is not compensated in some manner, such as by dynamical changes, the ozone losses would lead to a cooling of the lower stratosphere (Ramanathan and Dickinson, 1979; Fels *et al.*, 1980; Lacis *et al.*, 1990). This process acts to further reduce the longwave emission into the surface-troposphere system (Ramanathan *et al.*, 1985). The solar effect is practically independent of temperature so that it is identical in both the Mode A and B determinations. However, the solar effect does affect the magnitude of the temperature change in the lower stratosphere. Thus, as far as the surface-troposphere system is concerned, both the effect of reduction in absorber amount and the reduction in temperature lead to a change in the longwave radiative transfer that competes with the solar effect. The net radiative forcing in Mode B becomes negative, being opposite in sign to the effects due to the non-ozone gases. This effect is more marked at the higher latitudes where the ozone losses are larger. The resulting forcing at the higher latitudes acquires a substantially large negative value relative to the non-ozone forcing there. Because the forcings depend on the solar insolation, the results in both Mode A and B depend on the time of year and the geographical region.

7.5.2 Sensitivity of the Radiative Forcing to Ozone Amount and Tropospheric Cloudiness

This section highlights briefly two factors that govern the ozone radiative forcing. For this purpose, Model II was employed to analyze the quantitative influences due to the amount of ozone loss and the amount of cloudiness in the troposphere. The summary of the tests is listed in Table 7-8. The tests assume the clear-sky, mid-latitude summer (MLS) atmospheric profile (McClatchey *et al.*, 1972) and a 10 percent ozone loss as the nominal case. Solar insolation corresponds to annually-averaged conditions at the mid-latitudes. The vertical profile of the loss is as in section 7.5.1. The low, middle and high cloud amounts, their heights and properties for the 'partly cloudy' case in Table 7-8 follow the prescription in Ramaswamy and Ramanathan (1989), except that all

Table 7-8 Summary of the sensitivity tests performed using Model II to explore the dependence of the ozone-induced forcing (W/m²). The nominal case is the clear-sky mid-latitude summer profile (McClatchey *et al.*, 1972) with a surface temperature of 294 K.

Comment	O_3 forcing	
	Mode A	Mode B
Dependence on O_3 amount lost		
–2%	.06	–.02
–10%	.30	–.21
–20%	.61	–.48
Dependence on Clouds (10% loss)		
Clear	.30	–.21
Partly cloudy	.24	–.18
Overcast	.23	–.03

clouds are assumed to be 'black' in the longwave. For the 'overcast case,' the high cloud amount is unity and its top is placed at the tropopause, thus yielding a condition which is the opposite extreme of a clear sky in the following sense—the upwelling longwave tropospheric flux in the lower stratosphere is the least; *i.e.*, the troposphere is optically opaque in the longwave as far as the lower stratosphere is concerned.

The results in Table 7-8 show that the net radiative forcing due to the lower stratospheric ozone losses increases markedly with the amount of ozone loss in Mode A due to the solar effect, as pointed out above. In Mode B, the temperature decreases are enhanced with increases in the ozone loss, thus yielding increasingly negative ozone forcings. The experiments with clouds indicate that Mode B results are sensitive to cloud properties. This is due to the upwelling flux from the troposphere playing an important role in the changes in the longwave flux convergence within the lower stratosphere. This, in turn, determines the magnitude of the temperature reduction there, with a concomitant effect upon the changes in the stratospheric longwave emission into the troposphere. The larger the upwelling flux from the troposphere, the larger are the resultant effects. Thus, for the extreme overcast case, there results the least forcing, and the difference from the clear-sky results is quite pronounced. Although the studies here are by no means exhaustive, they indicate that the Mode B results, owing to their dependence on the lower stratospheric temperatures, are sensitive to tropospheric radiative influences. In contrast, since Mode A does not depend on the temperature feedbacks in the stratosphere, it is not influenced by the tropospheric longwave processes.

7.5.3 Lower Stratospheric Ozone Losses (General Atmospheric Conditions)

As the third part of the stratospheric ozone loss study, the sensitivity examination was extended to study the zonal impacts due to the decadal ozone decreases for general atmospheric conditions. Also considered again for comparisons are the forcings due to greenhouse gases other than ozone. Cloud amounts in the troposphere for Models I and III follow London (1957) while the Stowe *et al.* (1989) climatology is adopted in Model IV. All the models employed in the calculations of this section have different initial climatologies of ozone and water vapor. The altitude range of ozone loss employed at each latitude for the model simulations are again similar to those employed in section 7.5.1. The latitudinal dependence of the column ozone loss amounts follow the TOMS percentage trends at each latitude. The vertical distribution of the loss applied differs among the models. Models III and IV applied equal ozone loss amounts in each layer within the altitude of depletion while Model I applies an equal percentage loss in the concerned layers. Also, Model I employs an ozone climatology that, when combined with the TOMS percentage trends, may be overestimating the column loss amount at latitudes poleward of 70 degrees. Most of the results in this section pertain to January and July conditions. However, Models I and IV have simulated the perturbations corresponding to all four seasons and these are considered below in some of the discussions. (Note: A slightly different sensitivity experiment, which leads to the same implications as discussed below, is reported in Ramaswamy *et al.*, 1992).

The Mode A results, as obtained by Models I and IV, are shown, respectively, in Figures 7-3 and 7-4. Note that Figure 7-3 illustrates the non-ozone and ozone forcings separately while Figure 7-4 illustrates the non-ozone and the non-ozone + ozone forcings. The characteristics of Mode A, as in section 7.5.1, can be summarized as follows: there is an increase of solar radiation into the surface-troposphere system, and there is a decrease of the longwave emission, with the net effect dependent on the latitude. The impacts on the surface-troposphere forcing are greater for latitudes having larger ozone losses.

The Mode B results have been obtained by Models I and III (latter only for Northern Hemisphere) and the results appear in Figures 7-5 and 7-6, respectively. Note that Mode B results were unavailable from Model IV while Mode A results from Model II are not plotted. The forcings are shown for the non-ozone gases taken together, and for the ozone losses. Model III yields somewhat more negative ozone forcings than does Model I poleward of 30° in the Northern Hemisphere. Both models indicate a heightened sensitivity with latitude. The most important reason for this feature is the increasing ozone loss at the higher latitudes. The differences between Models I and IV in Mode A and between Models I and III in Mode B are attributable in general to a

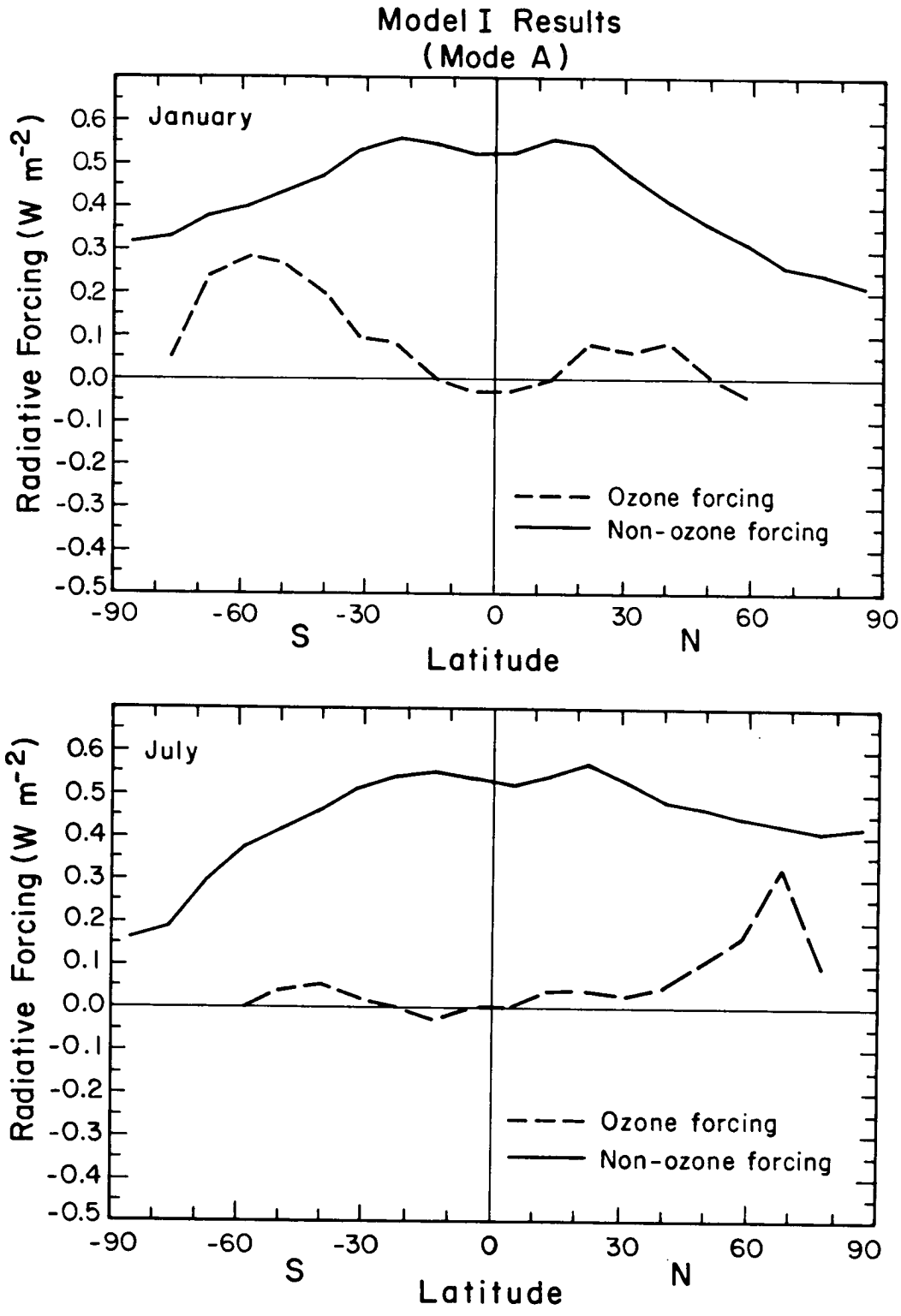

Figure 7-3 Mode A January and July radiative forcing as obtained by Model I for the 1979 to 1990 increases in all the non-ozone gases (Chapter 8) and that due to the lower stratospheric ozone losses (Stolarski *et al.*, 1991; McCormick *et al.*, 1992).

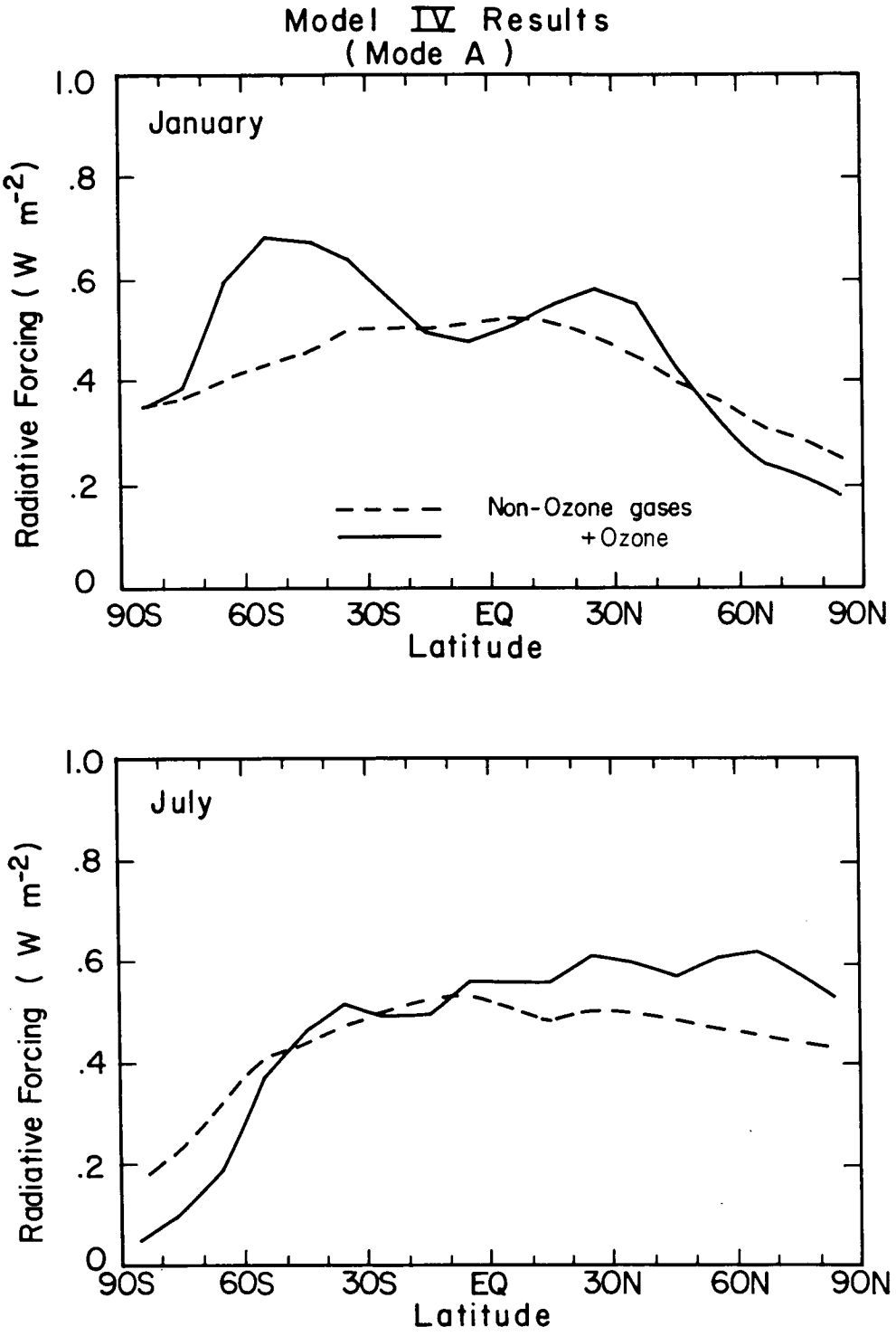

Figure 7-4 Same as Figure 7-3, except as obtained by Model IV. Note that the results are plotted for non-ozone gas increases only, and for non-ozone + ozone changes.

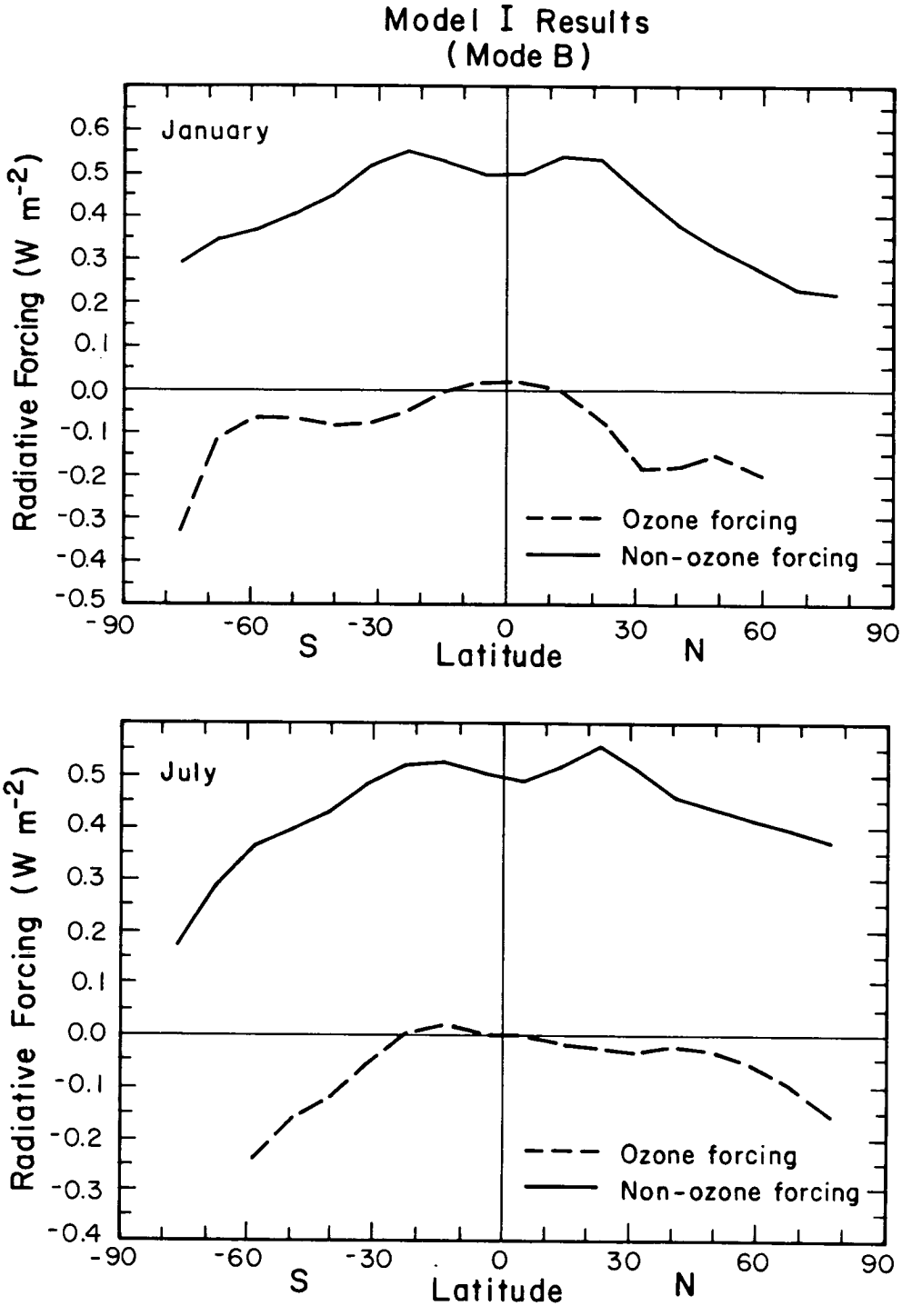

Figure 7-5 Mode B January and July radiative forcings due to non-ozone gas increases and ozone losses as obtained by Model I. Compare with the corresponding Mode A results in Figure 7-3.

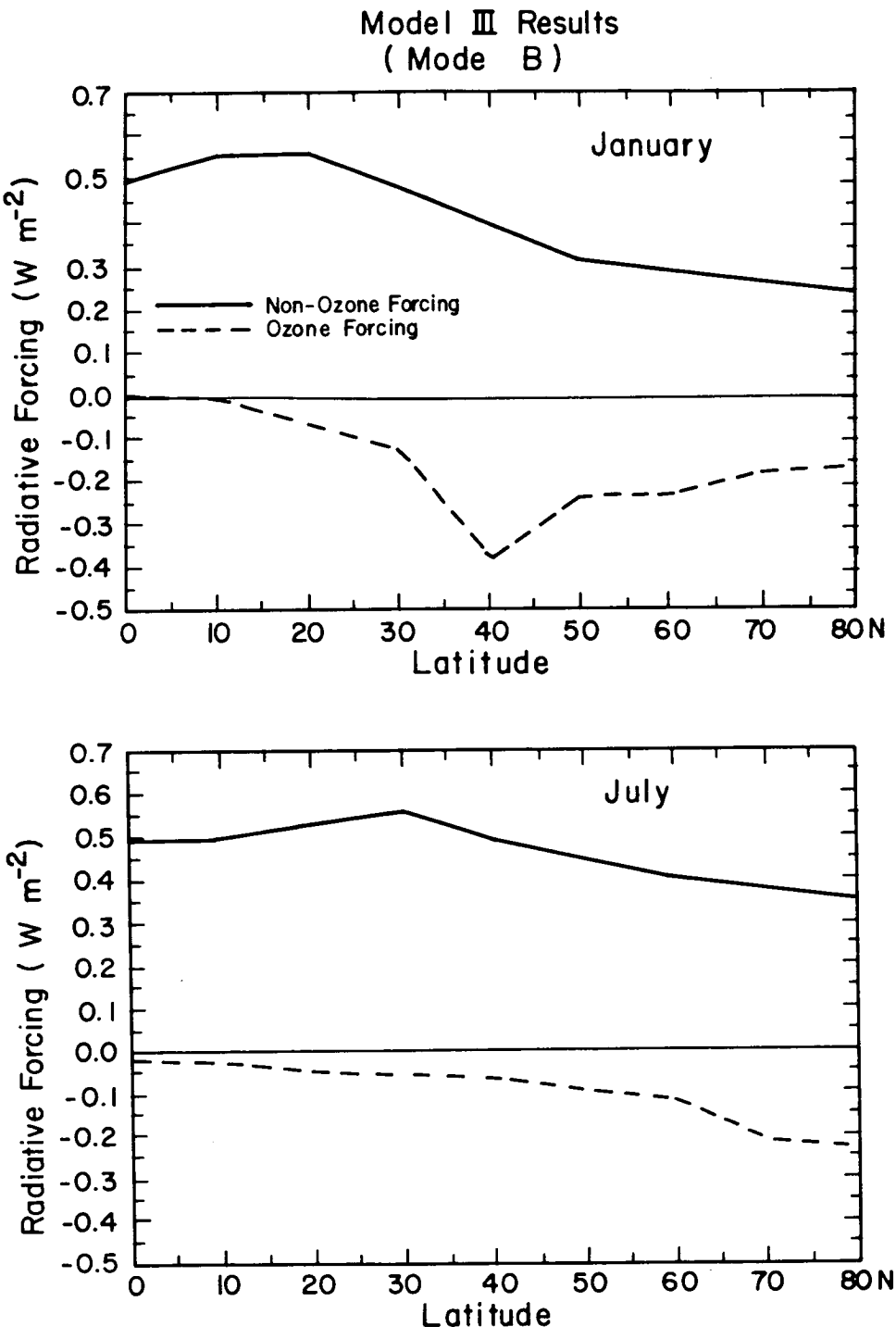

Figure 7-6 Mode B January and July radiative forcings due to non-ozone gas increases and ozone losses as obtained by Model III.

number of factors, *e.g.*, different initial climatologies including tropospheric conditions, vertical resolution, tropopause location, vertical distribution of the ozone loss, radiative transfer algorithms, etc.

The temperature change in the lower stratosphere at ~40°N (January), obtained in Mode B after stratospheric equilibrium in the presence of a fixed dynamical heating, is shown in Figure 7-7. The temperature decrease due to the ozone losses in the lower stratosphere exceeds substantially that due to the non-ozone gas increases. Comparing Models I and III, the temperature decrease in the latter is shifted more to the lower altitudes in the stratosphere because of the manner of the vertical distribution of the loss, as mentioned above. Specifically, Model III has a greater amount of loss in the lower portion of the stratosphere than does Model I. It is this ozone-induced temperature decrease that is responsible for the enhancement in the decrease of the stratospheric longwave emission to the troposphere in Mode B, thus resulting in a net negative surface-troposphere radiative forcing at this latitude.

To emphasize the relative importance of the 1979 to 1990 Mode B ozone radiative forcings, the ratio of the ozone to all the non-ozone forcing and that of ozone to CFC only forcing, as obtained by Model I, is shown in Figure 7-8. Poleward of 30 degrees, the magnitude of the (negative) ozone forcing become increasingly comparable to and can even exceed the (positive) CFC forcing. At these latitudes, the ozone forcings can also be a significant fraction of the (positive) non-ozone forcing during all seasons and in both hemispheres.

The globally averaged forcings due to changes in the radiatively active gaseous species between 1979 and 1990 are listed in Table 7-9. They suggest that the instantaneous ozone forcing, without any stratospheric temperature feedback (Mode A), enhances the direct CFC radiative forcing by more than 40 percent. However, considering the stratosphere to be in equilibrium, which is more appropriate to derive the climatically significant surface-troposphere forcing (WMO, 1986; IPCC), and assuming that there is no change in the dynamical heating of the stratosphere (Mode B), the ozone forcing is comparable but opposite in magnitude to the CFC forcing, besides being about 20 percent of the entire 1979 to 1990 trace gas forcing.

7.5.4 Characteristic Features of the Ozone Forcing

The forcing due to ozone is unique in two respects when compared to the forcings by the other gases (section 7.4). First, although there is a global mean offset of the CFC direct forcing by the ozone losses for the 1979 to 1990 period (Table 7-9, Mode B results), it is evident from Figures 7-5, 7-6 and 7-8 that this arises because of a significant negative forcing by ozone occurring in the higher latitudes only. In particular, the radiative forcing due to CFCs + ozone changes, as inferred from Figure 7-8, ranges from a net positive one at the low latitudes to a net negative one at the higher latitudes for the period considered. Further, the ozone losses suggest that the latitudinal dependence of the forcing due to changes in all trace gases between 1979 and 1990 could have had a meridional gradient quite different from that expected for the non-ozone species only.

Table 7-9 Globally and annually averaged radiative forcing (W/m^2) of the surface-troposphere system due to changes in the concentrations of the trace gases between 1979 and 1990: a) increases in CFCs only, b) combined effects of increases in CO_2, CH_4, N_2O and CFCs and c) decreases in ozone. Results obtained from both Mode A and B are listed. Model I averages employ each of the four midseason months in both hemispheres. Model III results are only for January and July perturbations in the Northern Hemisphere. Model IV results are available only for Mode A averaged over the four seasons.

Mode A			
Model	CFCs	All non-ozone gases	Ozone
I	0.09	0.49	0.06
III	0.10	0.51	0
IV	0.07	0.51	0.03

Mode B			
Model	CFCs	All non-ozone gases	Ozone
I	0.10	0.46	–0.08
III	0.11	0.47	–0.11

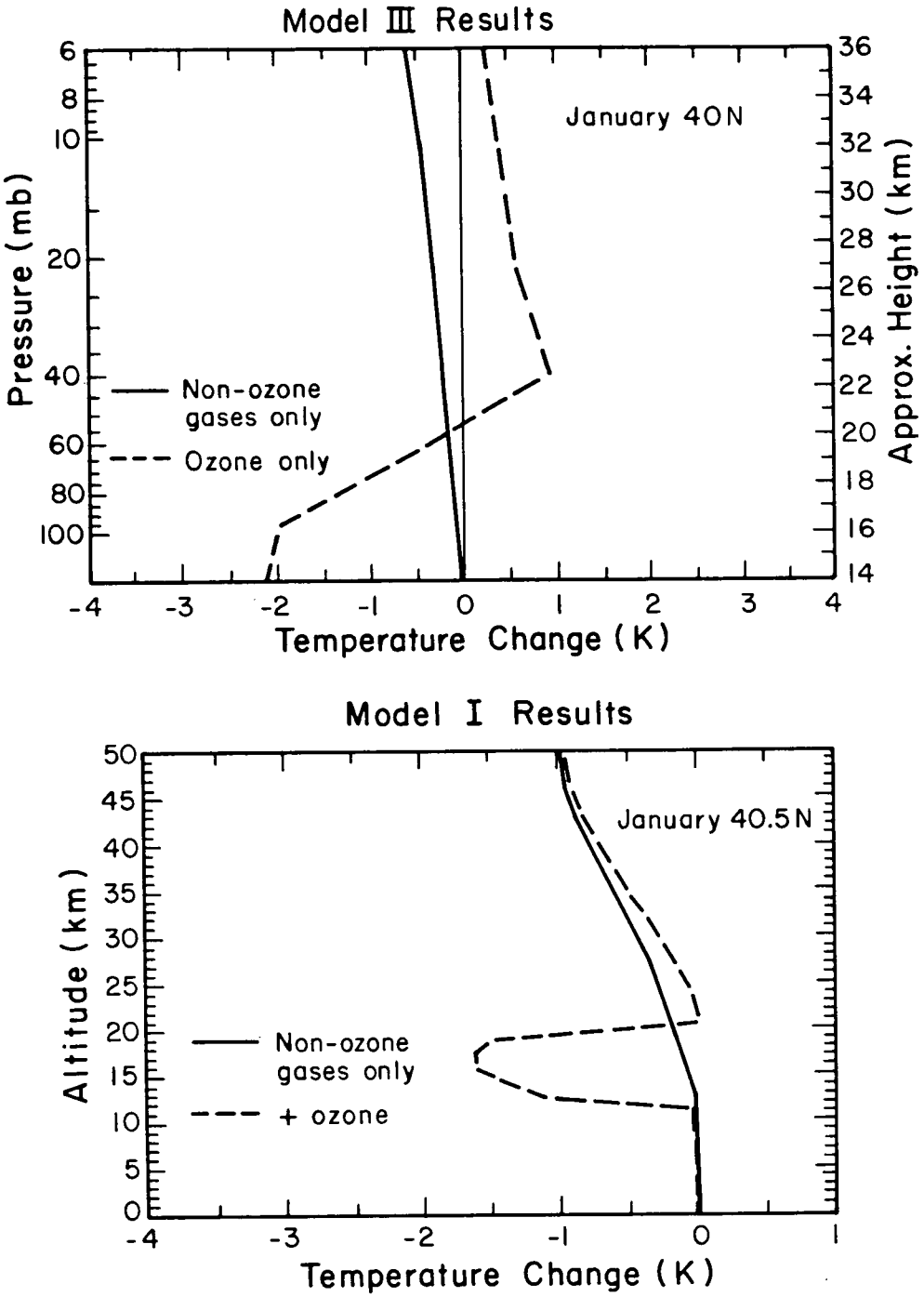

Figure 7-7 Temperature change at ~40°N for January conditions as obtained by Model III and Model I due to increases in the non-ozone gases (Chapter 8) and due to the lower stratospheric ozone losses occurring between 1979 and 1990 (Stolarski *et al.*, 1991; McCormick *et al.*, 1992). Note that, for Model III, the results are plotted for the two components separately while, for Model I, the results are plotted for non-ozone gases only, and for ozone + non-ozone gases.

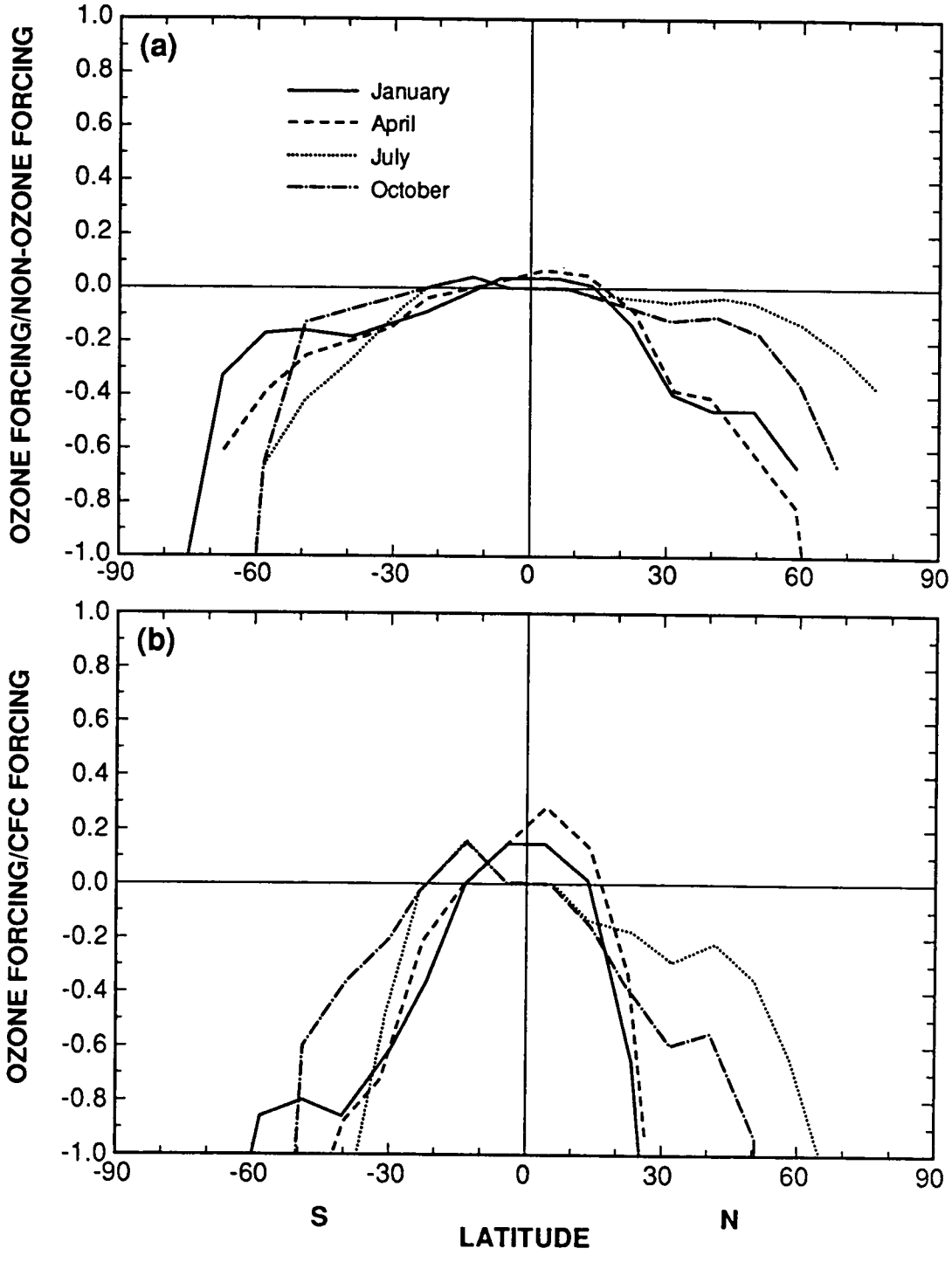

Figure 7-8 Ratio of the Mode B ozone forcing to that due to a) the non-ozone gas increases and b) CFCs alone for all seasons, as obtained by Model I.

There is yet another unique aspect concerning the ozone forcing which concerns the partitioning of the effect between the surface and the troposphere. For ozone, unlike the other radiatively active species, both solar and the longwave interactions are significant. As shown by Ramanathanan and Dickinson, (1979), most of the solar forcing is "felt" at the surface, while the longwave forcing is "felt" primarily within the upper troposphere. While that study considered a different ozone loss profile, yet the same features are seen even for the present lower stratospheric losses. Table 7-10 indicates this to be true in both Mode A and Mode B. The negative Mode B surface-troposphere forcing at the mid-to-high latitudes thus consists of a dipole-like feature, with a solar-induced warming at the surface, combined with a longwave-induced cooling tendency of the troposphere. There is a greater decrease for the troposphere in Mode B than in Mode A due to the temperature decreases in the lower stratosphere. Comparing with the effects for the non-ozone gases (Table 7-5), ozone stands out not only in terms of being able to cause a negative radiative forcing (Lacis *et al.*, 1990), but also in imparting a distinctively different vertical partitioning of this forcing.

Table 7-10 Mode A and Mode B surface and troposphere ozone forcing (W/m^2) in different latitude belts, as obtained by Model I.

Latitude	Mode A Surface	Troposphere
90–60°S	0.31	–0.13
60–30°S	0.16	–0.05
30–10°S	0.006	0.
10S–10°N	–0.02	0.
10–30°N	0.04	0.
30–60°N	0.15	–0.06
60–90°N	0.25	–0.10
Latitude	**Mode B Surface**	**Troposphere**
90–60°S	0.27	–0.76
60–30°S	0.15	–0.24
30–10°S	0.005	–0.01
10S–10°N	–0.02	–0.03
10–30°N	0.04	–0.07
30–60°N	0.14	–0.26
60–90° N	0.22	–0.49

The negative surface-troposphere Mode B forcing due to ozone can be interpreted as a cooling of the surface only if the convective coupling between the surface and the troposphere is strong, as is assumed in one-dimensional radiative-convective models. In the polar regions and for the upper troposphere, this need not be true (Dickinson *et al.*, 1978; Ramanathan and Dickinson, 1979; WMO, 1986). Three-dimensional General Circulation Model (GCM) studies are required to comprehensively determine the effect of this coupling on the response of the climate system to the ozone forcing.

7.5.5 Greenhouse Implications of the 1979 to 1990 Observed Ozone Losses

Since the ozone losses are suspected to be due to heterogeneous chemical reactions involving chlorine- and bromine-containing chemicals, the Mode B results here suggest that the ozone-depleting substances, which include the anthropogenic emissions of CFCs, have substantially reduced the radiative contributions of the CFCs to the greenhouse forcing over the past decade. Thus, the overall greenhouse effect attributed to the CFCs taken together must recognize this potential indirect contribution due to the chemically induced destruction of ozone.

The Mode B results here for ozone are in the same sense as those estimated by Lacis *et al.*(1990) for mid-latitudes during the decade of the 1970s. They are, however, different from those obtained using one-dimensional gas-phase only photochemistry models that predicted losses of ozone primarily in the middle and upper stratosphere (Ramanathan *et al.*, 1985) and led to a positive forcing. Since the observed ozone losses over the 1979 to 1990 period are indicating losses in a different region of the stratosphere than predicted earlier, this leads to a substantially different ozone radiative impact, and a different implication about the overall effect of the CFCs taken together in the global greenhouse forcing. The differences are entirely due to the differences in the assumed vertical profile of the ozone loss.

It is emphasized that the ozone forcing are extremely sensitive to the altitude of the losses (Ramanathan *et al.*, 1985; Lacis *et al.*, 1990). In the

computations here, it has been assumed that all the losses occur in the lower stratosphere. Detailed analyses from SAGE (McCormick *et al.*, 1992) and ozonesondes (Chapter 2) reveal that there are additional losses occurring in the middle stratosphere (~40 km) together with a small increase at ~30 km. There still is some uncertainty regarding the exact profile and the magnitude of the loss in the immediate vicinity of the tropopause. The SAGE profiles are available only from ~17 km and above globally, and indicate an increasing percentage of loss with decreasing altitude in the lower stratosphere. While the assumptions in the model sensitivity calculations of this section serve to infer the general implications of the radiative forcing due to lower stratospheric ozone losses, more precise estimates of the climate forcing need to consider carefully the details of the vertical loss profile. As an example of this sensitivity, if the hypothetical assumption were made that the TOMS observed losses are uniformly distributed in the entire stratospheric column (as in WMO, 1986), then the longwave effects become considerably less than the one obtained in the Mode B calculations here, leading to a small global ozone forcing (–0.01 W/m² from Model I and –0.04 W/m² from Model III; compare with Table 7-9). Thus, inferences about ozone forcings depend crucially on both the total column change as well as the change in the vertical profile and both these entities need to be monitored very carefully.

7.5.6 Effect of Dynamics on Stratospheric Temperature Changes

The indirect effect of CFCs on the climate system due to depletion of ozone in the lower stratosphere is critically sensitive to the actual temperature change and its distribution in the lower stratosphere. While Mode B generally provides more realistic assessments of forcing than Mode A, it too, may be unrealistic if the predicted stratospheric temperature change is not realized. Because atmospheric circulation can change in response to radiative perturbations, the dynamical contribution to the heating could also change, thereby contributing to the actual temperature change (Dickinson, 1974). This dynamical contribution is most likely to be significant when the forcing has strong spatial gradients, as does the observed ozone depletion.

A better estimate of temperature change may be obtained from three-dimensional general circulation models combined with careful diagnostic studies of the behavior of the real atmosphere. The observed global ozone depletion has not yet been simulated in a GCM, but simulations for the following scenarios of ozone changes have been performed: a) a uniform decrease of O_3 throughout the stratospheric column (Fels *et al.*, 1980; Kiehl and Boville, 1988), b) a homogeneous gas phase chemical model prediction of ozone depletion (Kiehl and Boville, 1988), which is different from the observed losses, and c) observed springtime depletion in the Antarctic region (Kiehl *et al.*, 1988). The resulting stratospheric temperature changes in these studies indicate that, unless the column depletions are large (>50 percent), the fixed dynamical heating (FDH) temperature response (*i.e.*, Mode B) closely resembles the GCM response, but there are some latitude-dependent departures. The GCM studies of Rind *et al.* (1990, 1991) show that dynamically forced temperature changes can result from subtle interactions between changes in the atmospheric structure, upper tropospheric latent heat release, and the forcing and transmission of planetary waves and gravity waves.

Lacking appropriate GCM simulations corresponding to the observed ozone loss, we turn to the observed temperature trend for an assessment of the stratospheric temperature changes due to the observed ozone depletion. Unfortunately, this trend is ambiguous because of the large natural variability in the lower stratospheric temperatures. Two different analyses suggest that there has been a cooling of the global lower stratosphere (50–100 mb layer) over the past two decades, which is more significant in the southern polar regions and less so for the Northern Hemisphere mid-latitudes. For the 1973–1987 period, Angell (1988) obtains a global mean trend of -0.62 ± 0.48 K/decade while, for the 1964–1988 period, Oort and Liu (1992) obtain a global mean trend of -0.40 ± 0.12 K/decade. The global mean of the decadal temperature change, averaged over the 50–100 mb layer, as obtained in the Mode B results of section 7.5.3, is –0.46 K from Model I and –0.63 K from Model III. Although the model results appear to be within the uncertainty limits present in the global mean trends, it must be recognized that there are other physical factors (*e.g.*, changes in tropospheric state, aerosols, etc.), not accounted for here, which could also be

contributing to the trends. Thus, the question of the horizontal and vertical distribution, and the magnitude of the stratospheric temperature change at each latitude produced by the observed ozone depletion remains open and requires further investigations, including GCM simulations.

7.5.7 Sensitivity to Increases in Tropospheric Ozone

Thus far, only the stratospheric decrease in O_3 has been considered. However, there is some evidence from ground-based stations of increases in tropospheric ozone during the past decade (Chapter 2). The greenhouse effect of tropospheric ozone has been anticipated and investigated in earlier reports (WMO, 1986). Even though tropospheric ozone amounts are less than the stratospheric ones, the effective longwave optical depths are greater in the troposphere (Ramanathan and Dickinson, 1979).

In order to investigate the forcing upon the surface-troposphere system due to increases in tropospheric ozone, Model I performed a sensitivity study which employs the stratospheric loss at 40°N as a base. Tropospheric ozone is then increased at this latitude from 0 to 17 percent, the latter being the reported decadal increase by the Hohenpeissenberg station. The vertical profile of the tropospheric ozone change follows the Hohenpeissenberg trends. Figure 7-9 illustrates the reduction of the stratospheric impacts due to increases in tropospheric ozone. There is almost a linear increase of the greenhouse effect with a percentage increase in the tropospheric ozone concentration. Although the greenhouse effect of increases in tropospheric ozone can be significant, there is at present insufficient evidence that such changes are taking place globally, especially in the radiatively important upper tropospheric regions (Lacis, *et al.*, 1990). In the absence of statistically significant global trends, it is not possible at this stage to quantify the global greenhouse effect due to tropospheric ozone.

7.6 RADIATIVE FORCING DUE TO TROPOSPHERIC SULFATE AEROSOLS

Sulfur-containing gases emitted into the atmosphere through natural and anthropogenic processes do not contribute significantly to the greenhouse effect. However, a large fraction of these gases are transformed into sulfate aerosol particles in the atmosphere. These aerosol particles may affect climate in several ways, the most important being:

- scattering of sunlight back to space in clear skies, thereby reducing the amount reaching the surface,
- increasing the number of cloud condensation nuclei (CCN), thereby potentially altering the physical characteristics of clouds (*e.g.*, albedo, precipitation), and
- altering the chemical balance (*e.g.*, ozone concentrations) by providing surfaces for chemical transformations. This could be particularly important in the lower stratosphere.

The most important new information that has become available since IPCC refers to the first of the above three mechanisms. Based on simulations of the global distribution of sulfate aerosols, Charlson *et al.* (1990, 1991) used previously acquired information on backscattering coefficients per unit mass of sulfate to estimate the impact on the shortwave radiation balance of anthropogenic sulfur emissions. They concluded that the clear-sky effect alone, averaged over the Northern Hemisphere, corresponds to a negative forcing at the Earth's surface of approximately 1 W/m^2. This is comparable to and of the opposite sign to the forcing due to the buildup of CO_2 in the atmosphere. Even though this estimate needs to be refined through further calculations and measurements, it is based on relatively few basic assumptions and is probably not uncertain by more than a factor of 2.

A very important implication of this finding is that the effective anthropogenic climate forcing in the Northern Hemisphere during the past century is likely to have been smaller than previously believed. A meaningful quantitative comparison between the positive forcing of the well-mixed greenhouse gases and the negative forcing due to sulfate aerosols is complicated by the nonuniform spatial distribution of the latter, in contrast to the uniform geographical distribution of the well-mixed gases.

Anthropogenic sulfur emissions in the Southern Hemisphere are much smaller and the resulting concentrations correspondingly lower so that no compensating cooling tendency is likely to have taken place there. The expected hemispheric difference in forcing is qualitatively consistent with an observed small difference in temperature trends between the hemi-

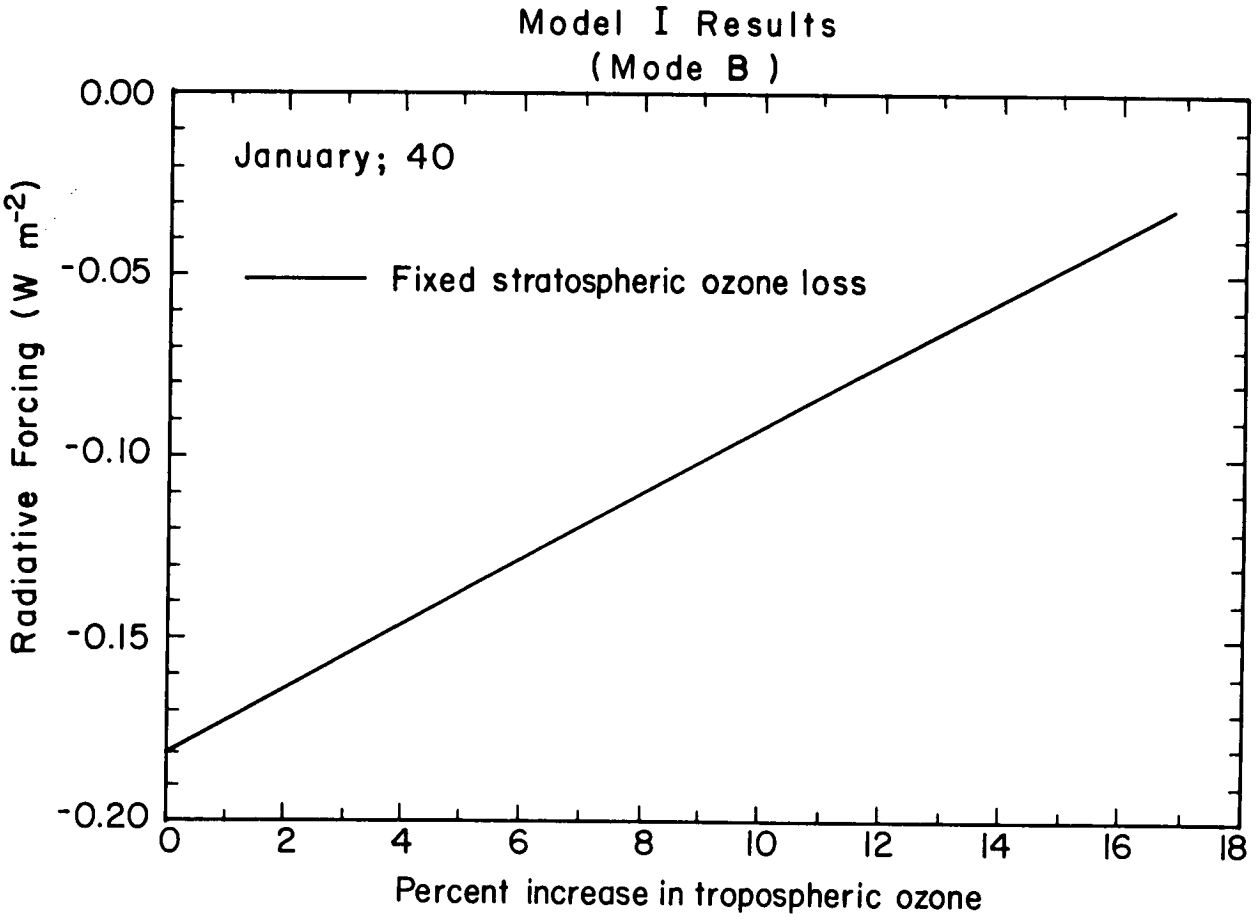

Figure 7-9 Radiative forcing due to increases in tropospheric ozone as obtained from Model I. The vertical profile of tropospheric ozone changes conforms to the Hohenpeissenberg observations. The base state (*i.e.*, the forcing for a 0 percent increase) corresponds to the stratospheric losses at 40°N for January conditions (see section 7.5.7).

spheres over the past century (Wigley, 1989). A more detailed analysis will also have to take into account the potential effect of aerosol particles from biomass burning in both hemispheres (Crutzen and Andrae, 1990).

Further changes in the forcing due to sulfate aerosols and greenhouse gases will depend on the variations in their respective emission sources. Because of the short atmospheric residence times of sulfates and their precursors, the atmospheric concentrations will adjust within weeks to changes in emissions. This is different from the case for the greenhouse gases which have effective lifetimes ranging from decades up to centuries. For example, the concentration of CO_2 will continue to rise for more than a century even if emissions are kept constant at today's level. This difference has been examined by Wigley (1989) and Charlson *et al.* (1991), who show how the climate forcings due to CO_2 and sulfate aerosol would change if the global fossil fuel consumption leveled off and was eventually reduced. Because of the rapid growth in emissions during the past decades, both the greenhouse forcing due to CO_2 and the opposite forcing due to aerosols have grown accordingly. During a leveling off phase, the greenhouse forcing will continue to grow whereas the aerosol forcing will remain constant. During a decay phase, the greenhouse forcing will start to level off and the aerosol forcing will decline. This simple example demonstrates that the relative importance of these two major anthropogenic forcing agents in the future will depend critically on changes in the use of fossil fuel (large-scale desulfurization measures would, of course, also have to be considered).

Because of the very different character of the forcing due to aerosols as compared to that of the well-mixed greenhouse gases, no attempt is made to define a GWP for anthropogenic sulfur emissions. It is also considered that there is no meaningful use of a GWP value for sulfur; trade-offs between reduction in greenhouse gases and increases in sulfur emissions do not seem reasonable.

7.7 RADIATIVE FORCING DUE TO STRATOSPHERIC AEROSOLS

Observations of the past decade (lidar, satellite, balloon, sunphotometer) indicate that the stratospheric aerosol concentration remained higher than that measured in 1979 (a relatively quiescent period) throughout most of the 1980s. This was probably in part attributable to the major El Chichón volcanic eruption in 1982 plus few other minor ones (McCormick and Trepte, 1987). An additional contribution could also have been due to anthropogenic means (Hofmann, 1990). With the recent major eruption of the Mt. Pinatubo volcano, there is now a fresh accumulation of particulates in the stratosphere that can be expected to yield a radiative forcing (WMO, 1990). The radiative effects may be already manifest in the tropical lower stratosphere where there has been a temperature increase of 3–4 K (McCormick, M. P., private communication) in the 2 months following the eruption. These aerosols can also be expected to exert a radiative forcing on the surface-troposphere system. It has been suggested that global coolings have occurred following major eruptions in the past but are of the order of a few tenths of a Kelvin or less (Mass and Portman, 1989). In the case of the aerosols from the Mt. Pinatubo eruption, the magnitude of the surface cooling, if any, has yet to be confirmed.

REFERENCES

Angell, J.K., Variations and trends in tropospheric and stratospheric global temperatures, 1958–1987, *J. Clim, 1*, 1296–1313, 1988.

Charlson, R.J., J. Langner, and H. Rodhe, Sulfate aerosol and climate, *Nature, 348*, 22, 1990.

Charlson, R.J., J. Langner, H. Rodhe, C.B. Leovy, and S.G. Warren, Perturbation of the Northern Hemisphere radiative balance by backscattering from anthropogenic sulfate aerosols, *Tellus, 43B*, 152–163, 1991.

Clough, S.A., F.X. Kneizys, and R.W. Davies, Line shape and the water vapor continuum, *IRS '88: Current problems in Atmospheric Radiation*, eds. J. Lenoble and J.-F. Geleyn, pp 355–359, A. Deepak Publishing, Hampton, VA, 1989.

Crutzen, P.J., and M.O. Andrae, Biomass burning in the tropics: Impact on atmospheric chemistry and biogeochemical cycles, *Science, 250*, 1669–1678, 1990.

Dickinson, R.E., Climate effects of stratospheric chemistry, *Can. J. Chem., 52*, 1616–1624, 1974.

Dickinson, R.E., S.C. Liu, and T.M. Donahue, Effects of chlorofloromethane infrared radiation on zonal atmospheric temperature, *J. Atmos. Sci., 35*, 2142–2152, 1978.

Ellingson, R., J. Ellis, and S.B. Fels, The intercomparison of radiation codes used in climate models: Longwave results, *J. Geophys. Res., 96*, 8929-8953, 1991.

Fels, S.B., and L.D. Kaplan, A test of the role of longwave radiative transfer in a general circulation model , *J. Atmos. Sci., 33*, 779-789, 1975.

Fels, S.B., J.D. Mahlman, M.D. Schwarzkopf, and R.W. Sinclair, Stratospheric sensitivity to perturbations in ozone and carbon dioxide: Radiative and dynamical response, *J. Atmos. Sci., 37*, 2266–2297, 1980.

Fisher, D.A., C.H. Hales, W-C. Wang, M.K.W. Ko, and N.D. Sze, Model calculations of the relative effects of CFCs and their replacements on global warming, *Nature, 344*, 513–516, 1990.

Hansen, J., D. Johnson, A. Lacis, S. Lebedeff, P. Lee, D. Rind, and G. Russell, Climatic impact of increasing atmospheric carbon dioxide, *Science, 213*, 957–966, 1981.

Hofmann, D.J., Increase in the stratospheric background sulfuric acid aerosol mass in the past 10 years, *Science, 248*, 996–1000, 1990.

Intergovernmental Panel on Climate Change, *Climate Change: The IPCC Scientific Assessment* (eds. Houghton, J.T., G.J. Jenkins, and J.J. Ephraums), 41-68, Cambridge University Press, 1990.

Johnson, C., J. Henshaw, and G. McInnes, The impact of aircraft NO_x emissions on tropospheric ozone and global warming, *Nature, 355*, 69–71, 1992.

Kiehl, J.T., and B.A. Boville, The radiative-dynamical response of a stratospheric-tropospheric general circulation model to changes in ozone, *J. Atmos. Sci., 45*, 1798–1817, 1988.

Kiehl, J.T., and S. Solomon, On the radiative balance of the stratosphere, *J. Atmos. Sci., 43*, 1525–1534, 1986.

Kiehl, J.T., B.A. Boville, and B.P. Briegleb, Response of a general circulation model to a prescribed Antarctic ozone hole, *Nature, 332*, 501–504, 1988.

Lacis, A.A., D.J. Wuebbles, and J.A. Logan, Radiative forcing by changes in the vertical distribution of ozone, *J. Geophys. Res., 95*, 9971–9981, 1990.

Lelieveld, J., and P.J. Crutzen, Indirect chemical effects of methane on climate warming, *Nature, 355*, 339-342, 1992.

London, J., A study of the atmospheric heat balance. Final report, Contract AF19 (122–165), New York University, 99 pp., 1957.

Mahlman, J.D., and L.J. Umscheid, Dynamics of the middle atmosphere: Successes and problems of the GFDL "SKYHI" general circulation model, in *Dynamics of the Middle Atmosphere*, eds. J. R. Holton and T. Matsuno, pp. 501–525, Terra Sci. Publ. Co., Japan, 1984.

Mass, C., and D. Portman, The effect of major volcanic eruptions of the last century on surface temperature, pressure, and precipitation, *J. Clim., 2*, 566–593, 1989.

McClatchey, R.A., R.W. Fenn, J.E.A. Selby, F.E. Volz, and J. S. Garing, *Optical properties of the atmosphere*, Rep. AFCRL–72–0497, 85 pp., Air Force Cambridge Research Lab., Bedford, Mass., 1972.

McCormick, M.P., and C.R. Trepte, Polar stratospheric optical depth observed between 1978 and 1985, *J. Geophys. Res., 92*, 4297–4307, 1987.

McCormick, M.P., R.E. Veiga, and W.P. Chu, Stratospheric ozone profile and total ozone trends derived from the SAGE I and SAGE II data, *Geophys. Res. Lett. 19*, 269-272, 1992.

Miller, A.J., R.M. Nagatani, G.C. Tiao, X.F. Niu, G. C. Reinsel, D. Wuebbles, and K. Grant, Comparisons of observed ozone and temperature trends in the lower stratosphere, submitted to *Geophys. Res. Lett.*, 1991.

Oort, A.H., and H. Liu, Upper air temperature trends over the globe, 1958–1989, in press *J. Clim*, 1992.

Ramanathan, V., and R.E. Dickinson, The role of stratospheric ozone in the zonal and seasonal radiative energy balance of the earth-troposphere system, *J. Atmos. Sci., 36*, 1084–1104, 1979.

Ramanathan, V., M.S. Lian and R.D. Cess, Increased atmospheric CO_2: Zonal and seasonal estimates of the effect on the radiation energy balance and surface temperature, *J. Geophys. Res., 84*, 4949–4958, 1979.

Ramanathan, V., R.J. Cicerone, H.B. Singh and J.T. Kiehl, Trace gas trends and their potential role in climate change, *J. Geophys. Res., 90*, 5547–5566, 1985.

Ramaswamy, V., and V. Ramanathan, Solar absorption by cirrus clouds and the maintenance of the tropical upper troposphere thermal structure, *J. Atmos. Sci., 46*, 2293-2310, 1989.

Ramaswamy, V., M.D. Schwarzkopf, and K.P. Shine, Radiative forcing from global stratospheric ozone loss, *Nature, 355*, 810-812, 1992.

Ramaswamy, V., M.D. Schwarzkopf and D.L. Trueman, Line-by-line characterization of the radiative effects and the greenhouse warming potential due to various halogenated compounds, *Preprints, American Meteorological Society Seventh Conference on Atmospheric Radiation*, San Francisco, 438–441, 1990.

Rind, D., N.K. Balachandran, and R. Suozzo, Climate change and the middle atmosphere. Part II: The impact of volcanic aerosols, *J. Clim.*, in press, 1991.

Rind, D., R. Suozzo, N.K. Balachandran, and M.J. Prather, Climate change and the middle atmosphere. Part I: The doubled CO_2 climate, *J. Atmos. Sci., 47*, 475–494, 1990.

Roberts, R.E., L.M. Bieberman, and J.E. A. Selby, Infrared continuum absorption by atmospheric water vapor in the 8 to 10 μm window, *Appl. Opt., 15*, 2085–2090, 1976.

Shine, K.P., On the cause of the relative greenhouse strength of gases such as the halocarbons, *J. Atmos. Sci., 48*, 1513–1518, 1991.

Siegenthaler, U., Uptake of excess CO_2 by an outcrop-diffusion model of the ocean, *J. Geophys. Res., 88*, 3599–3608, 1983.

Stolarski R.S., P. Bloomfield, R.D. McPeters, and J.R. Herman, Total ozone trends deduced from Nimbus-7 TOMS data, *Geophys. Res. Lett., 18*, 1015–1018, 1991.

Stowe, L.L., H. Yeh, T.F. Eck, C.G. Wellemeyer, and H.L. Kyle, NIMBUS-7 global cloud climatology. Part II: First year results, *J. Clim., 2*, 671-709, 1989.

Wang, W-C., and G. Molnar, A model study of the greenhouse effects due to increasing atmospheric CH_4, N_2O, CF_2Cl_2, and $CFCl_3$, *J. Geophys. Res., 90*, 12971-12980, 1985.

Wang, W-C., J.P. Pinto and Y.L. Yung, Climatic effects due to halogenated compounds in the earth's atmosphere, *J. Atmos. Sci., 37*, 333–338, 1980.

Wang, W-C., M.P. Dudek, X.Z. Liang, and J.T. Kiehl, Inadequacy of effective CO_2 as a proxy in simulating the greenhouse effect of other radiatively active gases, *Nature, 350*, 573–577, 1991.

Wigley, T.M.L., Possible climate change due to SO_2-derived cloud condensation nuclei, *Nature, 339*, 365–367, 1989.

World Meteorological Organization (WMO), *Atmospheric Ozone 1985*, Chapter 15, Global ozone research and monitoring project, Rep. 16, Geneva, 1986.

World Meteorological Organization (WMO), Report of the *International Ozone Trends Panel 1988*, Chapter 6, Global ozone research and monitoring project, Rep. 18, Geneva, 1990.

CHAPTER 8

Future Chlorine-Bromine Loading and Ozone Depletion

Authors:

M.J. Prather
T. Sasaki
A.M. Ibrahim
F. Stordal
G. Visconti

Model Contributors:

G.P. Brasseur
C.H. Bruehl
D.A. Fisher
I.S.A. Isaksen
C.H. Jackman
M.K.W. Ko
T. Sasaki
S. Solomon
G. Visconti
D.J. Wuebbles
E. Zhadin
S. Zvenigorodsky

Chapter 8

Future Chlorine-Bromine Loading and Ozone Depletion

Contents

SCIENTIFIC SUMMARY

The atmospheric loading of chlorine and bromine compounds and corresponding predictions of current and future ozone changes are examined using global two-dimensional models of stratospheric chemistry and transport. There has been a major advance in the two-dimensional assessment models used here: most models now include currently-known heterogeneous chemical reactions on the stratospheric sulfate layer. Further, three models also incorporate a parametric formulation of the chemistry involving polar stratospheric clouds (PSCs), but PSC simulations remain incomplete. Results are shown from these three types of models, denoted GAS (gas phase chemistry only), HET (includes reactions of N_2O_5 and $ClONO_2$ on sulfate-layer aerosols), and PSC (includes parameterization of PSC-chemistry). The HET models predict a substantially different balance among the chlorine, bromine, odd-hydrogen, and odd-nitrogen cycles for ozone destruction in the lower, mid-latitude stratosphere than do the GAS models, with important implications for the ozone response to a variety of perturbations in trace gases (*e.g.*, chlorofluorocarbons (CFCs), halons, methane, nitrous oxide, and nitric oxides from aircraft). The only forcing considered in the model scenarios is the evolving atmospheric composition, which over the past decade has been dominated by the increase in halocarbon chlorine loading from 2.5 to 3.6 ppbv.

GAS models predict integrated column depletions and vertical profiles of ozone loss from 1980 to 1990 that are much less than those observed at middle latitudes over all seasons in both hemispheres.

HET models simulate most of the observed column ozone loss from 1980 to 1990 for the northern middle latitudes in summer, but only about half of that in winter (see Table 8-A below). Unlike previous assessments, the predicted vertical profile of ozone loss from 1980 to 1990 has the same structure as observed, including substantial losses in the lower middle latitude stratosphere. Largest relative ozone losses at 45°N from 1980 to 1990 are predicted to range from 7 percent to 16 percent near 44-km altitude, and, compared with observations, are similar in shape (loss versus altitude) but greater in magnitude. The sensitivity of these results to substantial (factor of 4) changes in the sulfate layer area is small (about 1/2 percent change in column ozone over the past decade). Similar results hold for the Southern Hemisphere, except near 60°S in winter–spring, where observed losses greatly exceed those predicted.

PSC models are still under development; current versions predict greater ozone loss at northern middle latitudes in winter.

Table 8-A Approximate Ranges of Column Ozone Losses (percent) for 1980–1990

	TOMS*		GAS		HET		PSC	
lat./months	JFM	JAS	JFM	JAS	JFM	JAS	JFM	JAS
60°N	6–8	3–4	1–2	1	3–4	3	5–7	3–4
30°N	4–5	1–2	1	< 1	2–3	1–2	2	1–2

*TOMS (Total Ozone Mapping Spectrometer) from Figure 2-11.

We expect that atmospheric loading of chlorine and bromine will peak in the late 1990s at levels of about 4.1 ppbv and 25 pptv, respectively. The HET models predict the maximum ozone loss circa 2000, with the additional losses for the period 1990–2000, will be equal to or slightly less than those for 1980–1990. Predictions for the year 2050 depend on many competing changes in Cl_y, Br_y, NO_y (through nitrous oxide), CH_4, and stratospheric temperatures (through CO_2 and O_3 changes), and thus the model predictions show large differences.

FUTURE Cl-Br LOADING AND OZONE DEPLETION

The peak chlorine loading in the late 1990s may vary over a range of 0.2 ppbv in response to a wide variety of options for halocarbon phaseouts and hydrochlorofluorocarbon (HCFC) substitution. A significant reduction in peak chlorine loading can be achieved with accelerated phase-out schedules of CFCs, carbon tetrachloride, and methyl chloroform. The times at which chlorine loading falls below 3 and 2 ppbv can be shifted by at most 10 years with such an acceleration of the phaseout. The integral of high chlorine levels (*i.e.*, cumulative exposure to ozone loss and, hence, ultraviolet (UV) increases) is more sensitive to the differences between certain policy options: heavy substitution with HCFCs can increase this number by at most 20 percent, whereas accelerated phaseouts can reduce it by as much as 50 percent. Acceleration of the halon phaseout by 3 years would reduce peak bromine loading by 1 pptv (about 4 percent). Stringent controls on current use of HCFC-22, or on substitution with alternative HCFCs, would not significantly reduce peak chlorine, but would accelerate the decay in chlorine loading in the decades following the peak. Scenarios in Table 8-B show the sensitivity of tropospheric chlorine loading to a range of halocarbon phase-out schedules.

To represent the differences in effectiveness of halocarbons in destroying ozone, we define a new quantity: the stratospheric free halogen content (FH in ppbv), the weighted sum of the free chlorine (FC in ppbv), and free bromine (FB) in the stratosphere, which are measures of the Cl_y and Br_y, respectively, available in the stratosphere to contribute to ozone depletion (*e.g.*, particularly in the lower, high-latitude stratosphere). The FC is calculated from the chlorine loading by weighting individual chlorocarbons by a factor proportional to their relative ozone depletion potentials (ODPs). All of the bromine in the halons and methyl bromide is assumed to be available in the stratosphere as Br_y, which is 30 to 120 times more effective per atom than Cl_y in catalyzing ozone loss (*i.e.*, the scale factor to convert FB into the same units as FC and FH, effective ppbv of Cl_y). These preliminary calculations of FH demonstrate that a large proportion (0.8 to 2.8 ppbv) is due to bromine, predominantly methyl bromide. But, the Br_y/Cl_y scale factor is highly uncertain due to large uncertainties in the bromine chemistry and to differences in the model calculations of Br_y-catalyzed ozone destruction.

Table 8-B Scenarios for Reducing Chlorine and Bromine Emissions

Case	Peak (ppbv Cl_y)			Year when		Integral > 1985 Value (ppbv–year)		
	CL	FC	FH	CL<3	CL<2	CL	FC	FH
AA	**4.11**	**3.24**	**4.17**	**2027**	**2061**	**22.8**	**12.6**	**16.8**
AA/X	–0.18	–0.12	–0.14	–10	–7	–33%	–28%	–24%
D	–0.03	–0.04	–0.04	0	0	–6%	–9%	–7%
D/X	–0.10	–0.07	–0.09	0	0	–13%	–21%	–16%
E	0.00	0.00	0.00	–7	–3	–8%	–1%	–1%
E/X	–0.03	–0.01	–0.01	–10	–3	–18%	–6%	–5%
AA+D/X	–0.21	–0.13	–0.16	–11	–7	–45%	–46%	–39%
AA+D+E/X	–0.21	–0.13	–0.16	–18	–13	–53%	–48%	–41%
AA+HH/X	–0.18	–0.12	–0.17	–10	–7	–33%	–28%	–29%
XX	–0.21	–0.13	–0.18	–22	–19	–64%	–59%	–59%
F20	+0.01	0.00	0.00	+1	0	+3%	+3%	+3%
F40	+0.02	0.00	0.00	+1	0	+6%	+6%	+5%
G20	+0.01	0.00	0.00	+5	+2	+18%	+15%	+14%

CL = Chlorine loading (in ppbv) is the sum of the mean tropospheric mixing ratio of chlorine in the form of chlorocarbons. The 1985 value for CL is 3.00 ppbv.

FC = Free chlorine in the lower stratosphere is the weighted sum of the chlorocarbons (CFC-11 x 2.70, CFC-12 x 1.08, CFC-113 x 1.8, CFC-114 x 1.16, CFC-115 x 0.12, CCl_4 x 3.80, CH_3CCl_3 x 2.94, CH_3Cl x 0.99, HCFC-22 x 0.32, HCFC-A/B x 0.99). The 1985 value for FC is 2.45 ppbv.

FH = Free halogen in the lower stratosphere is equal to FC plus 40 times the bromocarbon concentrations (halons 1211 and 1301, CH_3Br). The 1985 value for FH is 3.18 ppbv.

Scenario AA: Protocol (10-year lag of 10 percent of CFCs and CCl_4, no lag for CH_3CCl_3 and halons. HCFC-22 (+3 percent/year 1991 → 2020, ramps to 0 by 2040), *No* other HCFCs.

Other Scenarios (all relative to AA):

AA/X: CFC and CCl_4 schedules accelerated 3 years, (1994+ → 1991+)

HH/X: Halon schedule accelerated 3 years (1994+ → 1991+)

D: CH_3CCl_3 schedule accelerated 3 years

D/X: CH_3CCl_3 phaseout on accelerated CFC schedule (1993+ only)

E: HCFC-22 ramp to 0 from 2000 to 2020

E/X: HCFC-22 phaseout on accelerated CFC schedule (1993+ only)

XX: CUT ALL halocarbon emissions in 1993.

Substitution with HCFCs begin in 1995 (percent of 1985 CFC prod.), +3 percent/year to 2020, ramp to 0 by 2030:

F20: 20 percent substitution with HCFC-A (molecular weight 135, 1 Cl, 2-year lifetime)

F40: 40 percent substitution with HCFC-A

G20: 20 percent substitution with HCFC-B (molecular weight 135, 1 Cl, 20-year lifetime)

8.1 INTRODUCTION

The prediction of future ozone requires three elements: (1) a scenario for the net emissions of chemically and radiatively active trace gases from the land and oceans; (2) a global atmospheric model that projects the accumulation of these gases; and (3) a chemical transport model that describes the distribution of ozone for a prescribed atmospheric composition and climate. This chapter, of necessity, presents models for all three elements and focuses on the: (1) atmospheric abundance of chlorine and bromine in the form of halocarbons; and (2) the associated perturbations to stratospheric ozone.

Primary emissions of the trace gases are the cornerstone of any model of atmospheric composition. We are concerned only with those gases that are transported readily into the stratosphere and that play important roles in the chemical or dynamical processes there. This chapter deals primarily with chlorine and bromine whose atmospheric abundances are dominated by known industrial sources. Scenarios for the future emissions of currently used halocarbons ($CFCl_3$, CF_2Cl_2, $CF_2ClCFCl_2$, CF_2ClCF_2Cl, CF_3CF_2Cl, CCl_4, CH_3CCl_3, CHF_2Cl, CF_2ClBr, CF_3Br) and possible chlorine-containing substitutes (CF_3CHCl_2, CF_3CHFCl, CH_3CFCl_2, CH_3CF_2Cl) are based on the current Montreal Protocol (1987, revised 1990, London) and on simple assumptions about future regulations and market growth. Other halocarbons (CH_3Cl, CH_3Br) are held fixed. No attempt is made to derive emissions scenarios for the other important trace gases (CO_2, N_2O, CH_4) for which concentrations are extrapolated into the next century using current trends.

The atmospheric concentrations of trace gases may be predicted from the net emissions using an atmospheric model describing both transport and the chemical-physical losses. The scientific community has developed two- and three-dimensional chemical transport models for the purposes of interpreting observations or defining sources and sinks of all the major trace gases. Here we must simplify our treatment of atmospheric composition by compressing the detailed, multidimensional chemical losses into a single, bulk atmospheric lifetime (e-folding time). For species that are not predominantly of industrial origin, we adopt an even simpler approach of specifying future abundances based on current trends. For the past two decades, we can define the bulk tropospheric (average) composition from observations.

Stratospheric ozone is the focus of this assessment, and this chapter reports predictions of ozone changes using the best global two-dimensional models of stratospheric chemistry and transport currently in use within the international scientific community. These models are not three-dimensional and thus cannot include the full range of dynamical coupling, *e.g.*, between the large Antarctic ozone losses and the circulation itself. Results presented here are, however, a significant step beyond those reported in previous United Nations Environment Program-World Meteorological Organization (UNEP-WMO) assessments (WMO, 1990a; 1990b). The models now incorporate heterogeneous chemical reactions expected to occur on the ubiquitous stratospheric sulfate layer, and some models have included a parametric formulation of the chemistry involving PSCs. Calculations are shown for the past decade and into the next century. We examine not only perturbations to column ozone (and hence solar ultraviolet at the ground), but also changes in local ozone concentrations and in key species that drive stratospheric chemistry.

8.2 ATMOSPHERIC COMPOSITION AND CHEMISTRY

In this assessment, the stratospheric ozone models are forced by specifying the composition of the bulk troposphere from 1970 through 2050. Observations are used for the period 1970–1990. After 1990, we adopt a single projection for those species unaffected by the Montreal Protocol and its revisions, but examine a range of options for those halocarbons likely to fall under regulation.

The lower troposphere in these scenarios is treated as a single, well-mixed box (of uniform composition) that acts as a lower boundary condition for the chemical transport models. This assumption is reasonable for the time scales considered here, but ignores the well-defined latitudinal gradients and other spatial variations in trace gas concentrations throughout the lower atmosphere. The troposphere mixes vertically and within hemispheres on time scales of a few months (*e.g.*, Mahlman *et al.*, 1980); interhemispheric transport is slower, taking about a

year (*e.g.*, Cunnold *et al.*, 1986). The observed and expected interhemispheric gradients in the important trace gases are small (less than 10 percent with the exception of CH_3Br, see Chapter 1) and are not expected to induce significant hemispheric asymmetries in the stratosphere.

Transport of trace gases from the troposphere to the stratosphere is predicted to take as long as 5 years depending upon where in the stratosphere and which model (see Jackman *et al.*, 1989a). This time lag in stratospheric response to tropospheric forcing is simulated automatically by the stratospheric models used here when the calculations are performed in a time-dependent manner (*i.e.*, the lower boundary conditions are reset annually according to the scenario). In this case, the model simulation must continuously calculate every year in the scenario, from the initialization (1970) to the final year (2050). (Results from the different models for the initial year, 1970, are not easily compared because they depend so much on the individual initializations of each model, rather than on the universally adopted boundary conditions from the scenario.) When models are used to study a specific year, the calculation is often done as a steady-state atmosphere (*i.e.*, periodically repeating annual cycle with the same fixed boundary conditions). For these stratosphere models, we have chosen steady-state boundary conditions corresponding to the time-dependent scenario of 2.5 years previous in order to approximate the time lag in stratospheric transport (Holton, 1990). The true delay will be shorter than 2 years in the lower stratosphere, and may be longer at high altitudes and within the wintertime polar vortex (Schmidt and Khedim, 1991).

This section summarizes the scenario model for trace gas composition (all mixing ratios are vol/vol), including the lifetimes of the halocarbons, the historical record, the options for control of future halocarbon abundances, and the assumed stratospheric chemical model.

8.2.1 Lifetimes of the Halocarbons

The lifetimes of those gases with only stratospheric destruction (*i.e.*, the chlorofluorocarbons, carbon tetrachloride, Halon-1301, and nitrous oxide) should, in principle, be calculated directly from the global stratospheric chemical transport models. The model-derived lifetimes for these gases are in basic agreement, but no better than ±20 percent. The range of calculated lifetimes for the principal halocarbons are presented in Table 8-1. The empirically derived lifetimes from a budget analysis of the Atmospheric Lifetime Experiment-Global Atmospheric Gases Experiment (ALE-GAGE) observations (Cunnold *et al.*, 1986) provides no further constraint.

For this assessment, we have had to agree on a single set of lifetimes for the halocarbons. A midrange value of 55 years was selected for $CFCl_3$. The other stratospheric lifetimes (with the exception of Halon-1211) were scaled to the 55-year lifetime for $CFCl_3$ by noting that for most models the ratios of lifetimes for the CFCs were in better agreement than their absolute values. The relative lifetimes for different CFCs within a model are believed to be mainly independent of the specific circulation. The circulation patterns vary substantially from model to model (see Jackman *et al.*, 1989a) and are believed to be the cause of the large range in CFC lifetimes reported in Table 8-1. Nevertheless, this assumption is too simple. For example, the $CFCl_3$ lifetime is sensitive to transport below 25 km whereas the CF_2Cl_2 lifetime is determined by the transport to altitudes above 25 km, and transport in these different regimes does not scale similarly in all models.

Several currently important halocarbons (CH_3CCl_3, CHF_2Cl) and all proposed substitutes (the HCFCs) are destroyed in the troposphere by reaction with OH. Losses in the lower atmosphere dominate; stratospheric destruction is minor, see Table 8-2. Tropospheric chemistry models for the global distribution of OH have significant uncertainties, about ±30 percent (see AFEAS, 1990; WMO, 1990). These chemistry models can be based on the observed climatologies of important species such as O_3, NO + NO_2, H_2O, CO, and sunlight (Spivakovsky *et al.*, 1990) or they can be calibrated against other trace species that react primarily with OH such as ^{14}CO (Derwent and Volz-Thomas, 1990) or CH_3CCl_3 (Prinn *et al.*, 1987). Considering the estimates of tropospheric OH from a combination of such models, we have arbitrarily chosen a tropospheric OH distribution that corresponds to a CH_3CCl_3 lifetime of exactly 7 years with respect to reaction with OH in the troposphere. (A unique mean OH concentration cannot be derived from this assumption.) Based on

Table 8-1 Stratospheric Lifetimes and Halocarbons Scenarios

Species	Abbreviation	Lifetime (yr)	Lifetime (range)	Emissions (kt/year)	Factor (kt/pptv)
$CFCl_3$	F11	55	(42–66) (57–105)$^{A/G}$	360	23.2
CF_2Cl_2	F12	116	(95–130) (67–333)$^{A/G}$	450	20.4
$CF_2ClCFCl_2$	F113	110	(75–144)	165	31.6
CF_2ClCF_2Cl	F114	220	(197–264)	15	28.9
CF_3CF_2Cl	F115	550	(400–800)	10	26.1
CCl_4	CTC	47	(30–58)	80	25.9
CF_2ClBr	1211	11	(10–20)	10	27.9
CF_3Br	1301	77	(69–88)	9	25.1
CF_2BrCF_2Br	2402	20*	(22–30)		
N_2O		132*	(110–168)		
CH_3CCl_3	MCF	6.1	(5.1–6.4)$^{A/G}$	600	22.4
CHF_2Cl	H22	15.8		140	14.6
$C_xH_yF_xCl$	HX	20		(tbd)	22.
$C_xH_yF_xCl_2$	HY	2		(tbd)	22.

Note: A/G = ALE/GAGE. The quoted range in lifetimes refers to calculations by the participating models, including those used in Chapter 6; lifetimes derived empirically from a budget analysis of the ALE/GAGE data (Cunnold *et al.*, 1986; Prinn *et al.*, 1992) are noted. The short lifetime for Halon 1211 is due to photolysis in the upper tropical troposphere. The quoted lifetimes(*) for Halon 2402 and N_2O are not used in these scenarios but are needed for ODP and GWP calculations. For the lifetimes of CH_3CCl_3 and CHF_2Cl, see Table 8-2 Lifetimes for Tropospheric Loss. The base level of emissions assumed for 1985 are given. Factor is the global budget relationship of species mass (kilotons) per tropospheric average mixing ratio (pptv). The properties of the two surrogate substitutes, HX and HY, are also given. Here and throughout this document, the notation for mixing ratio (pptv = 10^{-12}, ppbv = 10^{-9}, ppmv = 10^{-6}) refer to number density (vol/vol). Emissions refer to the 1985 baseline levels.

the analysis of Prather and Spivakovsky (1990), the tropospheric lifetimes of other trace gases that react with OH can be accurately calculated by scaling the ratio of their respective rate coefficients evaluated at a temperature of 277 K. The contribution of stratospheric losses are added on (inverse sum), and the net atmospheric lifetimes are given in Table 8-2. The resulting lifetime for CH_3CCl_3 is in excellent agreement with the most recent ALE/GAGE analysis (Prinn *et al.*, 1992). If recalibration of the CH_3CCl_3 data from ALE/GAGE reduces concentrations by 10 percent (see Chapter 1), then it is likely that analyses (currently underway) may recommend a shorter lifetime and hence greater tropospheric OH levels.

It must be recognized that the mean atmospheric residence time describing the decay rate of a specific halocarbon, denoted here simply as the lifetime, is inherently a variable quantity. Stratospheric losses may change in a future atmosphere with a different circulation and ozone columns. Similarly, we may expect that the lifetimes of the HCFCs would change as tropospheric OH responds to the overall global changes in composition and climate.

An international scientific working group is currently reexamining the CFC and HCFC atmospheric lifetimes, focusing on both *ab initio* model calculations and empirical analyses of global budgets. Results from this study will be available in early 1992 and may lead to a revision in the lifetimes adopted here.

8.2.2 Historical Record and Projections

The important non-halocarbon species for stratospheric modeling are N_2O, CH_4 and CO_2. Nitrous oxide is the primary stratospheric source of

Table 8-2 Lifetimes for Tropospheric Loss

Species	Abbreviation	k (OH + Species) A	B	Lifetimes (year) τ trop	τ strat	τ Net*
CH_3CCl_3	MCF	5.0E-12	1800	7.00	47	6.1
CHF_2Cl	H22	1.2E-12	1650	17.0	240	15.8
CH_2F_2	H32	2.8E-12	1650	7.3	infinite	7.3
CF_3CHCl_2	H123	6.4E-13	850	1.77	47	1.71
CF_3CHFCl	H124	6.6E-13	1250	7.28	129	6.9
CHF_2CF_3	H125	6.0E-13	1700	40.7	infinite	40.7
CF_3CH_2F	H134a	1.3E-12	1650	15.7	infinite	15.7
CH_3CFCl_2	H141b	9.4E-13	1500	12.6	76	10.8
CH_3CF_2Cl	H142b	1.4E-12	1800	25.0	215	22.4
CH_3CF_3	H143a	1.6E-12	2100	64.6	infinite	64.6
CH_3CHF_2	H152a	1.3E-12	1050	1.80	infinite	1.80
$CF_3CF_2CHCl_2$	H225ca	2.0E-12	1300	2.88	120*	2.81
CF_2ClCF_2CHClF	H225cb	6.7E-13	1300	8.59	120*	8.0
CH_4	methane	3.9E-12	1885	12.2	147	11.3
C_2H_6	ethane	1.1E-11	1100	0.25	50	0.25
C_3H_8	propane	1.4E-11	750	0.06	50	0.06
CH_3Cl	methyl chloride	2.1E-12	1150	1.59	50	1.54
CH_3Br	methyl bromide	6.8E-13	850	1.67	50	1.62
CH_2Cl_2	methylene chloride	5.8E-12	1100	0.48		0.48
C_2Cl_4	perchlor-ethylene	9.4E-12	1200	0.43		0.43
C_2HCl_3	trichlor-ethylene	4.9E-13	–450	0.021		0.021

Note: The notation H is an abbreviation for hydrochlorofluorocarbon (HCFC). The rate coefficients for reaction with OH, k = A exp(–B/T(K) cm^3s^{-1}, are taken from the most recent reviews (JPL-90, IUPAC-91, see Chapter 3). We assume a global tropospheric OH corresponding to a CH_3CCl_3 tropospheric lifetime equal to 7 years; the tropospheric lifetimes for other species are scaled by the ratio of the rate coefficients at 277 K (Prather and Spivakovsky, 1990). Stratospheric lifetimes are based on direct or scaled model calculations, except for infinite (assumed no stratospheric loss) and for H225c isomers (120* is an estimate). The Net lifetime is the inverse average of the tropospheric and stratospheric lifetimes. The Net lifetime for CH_3CCl_3 is in agreement with the most recent ALE-GAGE empirical value of 5.1 to 6.4 year, (Prinn *et al.*, 1991). If there were an additional loss process for CH_3CCl_3 such as oceanic hydrolysis, the Net derived lifetime for CH_3CCl_3 alone would be reduced, but still fall within the empirically derived range.

Using current estimates for emissions of CH_2Cl_2 (500 kt/year), C_2Cl_4 (500 kt/year), and C_2HCl_3 (300 kt/year), these gases would contribute 0.035, 0.032, and 0.001 ppbv, respectively, to the tropospheric chlorine loading.

*$1/\tau_{Net} = 1/\tau_{Trop} + 1/\tau_{Strat}$

odd-nitrogen compounds (NO_y = NO + NO_2 + NO_3 + $2xN_2O_5$ + HNO_3 + HO_2NO_2 + HONO + $ClONO_2$ + $BrONO_2$). NO_y-related chemistry is responsible for a large fraction of stratospheric O_3 loss, controls partitioning in the Cl_y family (Cl_y = HCl + ClO + $2xCl_2O_2$ + Cl + $2xCl_2$ + OClO + HOCl + $ClONO_2$ + BrCl), and suppresses the odd-hydrogen abundance (HO_x = OH + HO_2 + $2xH_2O_2$). Methane plays a direct role in the HO_x chemistry and couples with Cl_y chemistry through the formation of HCl, as well as adding to stratospheric H_2O when oxidized. Carbon dioxide does not participate directly in stratospheric chemistry, but does affect the radiative balance of both stratosphere and troposphere. Some of the participating stratospheric models include the enhanced cooling and reduced stratospheric temperatures associated with increasing concentrations of CO_2 (and global tropospheric warming).

Observations of N_2O, CH_4 and CO_2 over the past 2 decades reasonably define their global tropospheric abundances (see Chapter 1). Table 8-3 gives the bulk tropospheric concentrations at 5-year intervals from 1970 through 1990; a linear interpolation is assumed for intermediate years. The currently-observed trends

in N_2O (+0.25 percent/year) and CH_4 (+13 ppbv/year) are continued at the same rate until 2050. Predicting future CH_4 growth is a guessing game, but there seems to be an overall trend to lower growth rates. There is strong evidence that human activities are responsible for these increases, but a satisfactory reconciliation of the sources for these gases is not yet possible. The CO_2 increases (+0.6 percent/year) are based on a fit to the Intergovernmental Panel on Climate Change (IPCC) (1990) business-as-usual (BaU) scenario.

We have assumed that the only natural source of stratospheric chlorine, methyl chloride, remains constant throughout these scenarios at 600 pptv. Nevertheless, we have only limited observational evidence that CH_3Cl has remained constant over the past two decades. Similarly, the abundance of CH_3Br is assumed to remain constant at 15 pptv. Methyl bromide, however, presents a particular problem: it is used as a grain fumigant with potentially large emissions; the large north–south gradient and high variability in northern mid-latitudes (Penkett *et al.*, 1985) also point to an industrial source; and it is the predominant source of stratospheric bromine in these calculations. Thus, the lack of a good historical record for CH_3Br, or of an understanding of the industrial emissions, introduces significant uncertainty into the bromine-loading scenarios used here.

The adopted abundances of the industrial halocarbons for the period 1970–1990 are given in Table 8-3. Data are not adequate to define tropospheric abundances in the early 1970s, and we have extrapolated backward smoothly, based in some cases on estimates of emissions. The projected concentrations of these halocarbons are calculated from several emission scenarios discussed in the following section, using the lifetimes described above.

Table 8-3 Historical Record (1970–1990) and Projections

Year	CO_2 (ppmv)	N_2O (ppbv)	CH_4 (ppbv)	CH_3Cl (pptv)	CH_3Br (pptv)
1970	325	295	1420	600	15
1975	331	298	1495	600	15
1980	337	302	1570	600	15
1985	345	306	1650	600	15
1990	354	310	1715	600	15
1991+	x1.006	x1.0025	+13	fixed	fixed

Year	F11	F12	F113	F114	F115	1211	1301	H22	CTC	MCF
1970	60	120	2	1	0	0.1	0.1	10	85	40
1975	115	205	6	2	1	0.2	0.2	27	90	70
1980	173	295	15	4	2	0.5	0.6	54	95	100
1985	222	382	30	5	4	1.5	1.7	80	100	130
1990	284	485	57	8	6	2.5	3.5	104	106	159
(1990 obs)	263	470	71	20				115	107	155
1991+	Use Scenarios A, B, or C below with data from Table 8-1									

Note: All halocarbons are in pptv.

These scenarios were based on previous assessments (WMO, 1990b; IPCC, 1990) and defined prior to the work in Chapter 1; they have minor differences for the 1990 observed atmosphere shown here as (1990 obs). See Chapter 1 for references. The large difference in CFC-113 is due to a change in the calibration scale of GAGE measurements. The total tropospheric chlorine loading in the year 1990 from this scenario (3.62 ppbv) and observations (3.56 ppbv) are almost equal since the observations also include some minor halocarbons not part of the scenario.

These scenarios do not include any other year-to-year variability that is known to affect ozone (*e.g.*, solar cycle, quasi-biennial oscillation, or volcanoes). For a more detailed analysis of the period 1955–1985, see Chapter 7 of Report of the International Ozone Trends Panel (WMO, 1990a).

8.2.3 Montreal Protocol: Halocarbon Scenarios

The model for future concentrations of the industrially-produced halocarbons is based on three options for future growth and regulation: the baseline reference case (M) attempts to approximate the current Montreal Protocol (1987, revised 1990, London), as summarized in Table 8-4, are implemented globally with no exception; that CHF_2Cl (HCFC-22) is phased out similarly to CH_3CCl_3 (see Table 8-4); and that no additional chlorine-containing halocarbons are produced. This baseline results in a complete phaseout of all halocarbon production by the year 2005. Note that the phaseout of CFCs is expected to begin substantially before the year 2000, and thus peak chlorine loading is almost 1 ppbv below previous expectations (*e.g.*, Figure 4 of Prather and Watson, 1990).

Three variations of this minimum, baseline scenario are chosen for the stratospheric model calculations. They are summarized in Table 8-5. Scenario A assumes near-global compliance with the Protocol but allows for 10 percent of the CFC market to continue without growth until a complete phaseout in the year 2010. Scenario B is similar to A except that the 10 percent of the CFC market grows at a rate of 5 percent/year until the year 2020 (reaching 430 kton/year). Scenario C examines one possibility when the world market replaces CFC use with alternative HCFCs in addition to conservation, not-in-kind use, and HFCs (hydrofluorocarbons). Scenario C follows Scenario A, except that one long-lived HCFC alternative, H_x with a lifetime of 20 years, is assumed to replace about 30 percent of the CFC plus HCFC-22 market beginning in the year 2000 with 360 kton/year. H_x production is assumed to grow at 3 percent/year until the year 2020, whereupon it is replaced with a short-lived HCFC alternative, H_y, with lifetime of 2 years, and allowed to continue growth at 3 percent/year to the year 2050 (1578 kton/year). Scenario C is an attempt to simulate chlorine loadings that might result from global compliance to a CFC phaseout and market-based projections of HCFC uses.

The calculation of halocarbon concentrations follows the simple box-model integration of Prather and Watson (1990) using lifetimes given in Table 8-1 and emission rates equal to the production as defined in Scenarios A, B, and C above. The assumption that emission equals production can introduce a phase error in the scenarios because some halocarbons are used in products that do not rapidly release the gas to the atmosphere (*e.g.*, hermetic refrigeration, closed-cell foams). This effect needs to be examined with a more complete model of halocarbon use, but should not induce substantial error in the modeling and comparison of scenarios studied here.

The tropospheric trace gas concentrations for Scenarios A, B, and C are given in Tables 8-6a and 8-6b for the time-dependent and steady-state calculations. The chlorine loading (*i.e.*, total tropospheric chlorine mixing ratio in the form of halocarbons) and bromine loading (similarly defined) are shown in Table 8-7.

8.2.4 Gas Phase and Heterogeneous Stratospheric Chemistry

One key to understanding the chemical processes responsible for the Antarctic ozone hole was the recognition that reactions on the surfaces of stratospheric particles (*i.e.*, heterogeneous chemistry) could activate chlorine-catalyzed ozone loss (see Chapters 3 and 4). It has also been noted recently that reactions on the ubiquitous stratospheric sulfate layer may compete with gas phase photochemistry in the lower stratosphere (see discussion in Chapter 3; Hofmann and Solomon, 1989; Rodriguez *et al.*, 1991; Pitari *et al.*, 1991). Unfortunately, such heterogeneous processes, particularly PSCs, are especially difficult to incorporate (in a generally agreed upon manner) into the global stratosphere models used in these assessments. An attempt was made to formulate a simplified, uniform PSC chemistry for the two-dimensional models, but instead some of the models incorporated polar chemistry in their own way (see model references). The basically non-zonal nature of both PSCs and the circulation of the vortex make the incorporation of polar stratospheric chemistry in a two-dimensional formalism an extremely difficult, possibly intractable, problem (see later discussion and Chapter 4).

Heterogeneous chemistry on the sulfate layer, however, can be defined in a straightforward manner as a homogeneous process, and most of the participating modelers agreed to adopt a standard form. The sulfate-layer chemistry is described in

Table 8-4 Production Factors for Baseline to Approximate the Montreal Protocol

Year	CFCs	CCl_4	Halons	CH_3CCl_3	CHF_2Cl*
1985*	1.00	1.00	1.00	1.00	1.00
1986*	1.05	1.05	1.05	1.05	1.05
1987*	1.10	1.10	1.10	1.10	1.10
1988*	1.15	1.15	1.15	1.15	1.15
1989*	1.20	1.20	1.20	1.20	1.20
1990*	1.25	1.25	1.25	1.25	1.25
1991	1.00	1.00	1.00	1.30	1.00
1992	1.00	1.00	1.00	1.35	1.00
1993	0.80	1.00	1.00	1.00	1.00
1994	0.80	1.00	1.00	1.00	1.00
1995	0.50	0.15	0.50	0.70	1.00
1996	0.50	0.15	0.50	0.70	1.00
1997	0.15	0.15	0.50	0.70	1.00
1998	0.15	0.15	0.50	0.70	1.00
1999	0.15	0.15	0.50	0.70	1.00
2000	0	0	0	0.30	1.00
2001				0.30	1.00
2002				0.30	1.00
2003				0.30	1.00
2004				0.30	1.00
2005				0	0

*Denotes years or species not explicitly part of the current protocol. The Montreal Protocol invokes 1.00 as the upper limit in midyear of 1990. These factors represent upper limits of production by the participating parties; some countries have already reduced production and may phase out some halocarbons earlier than this schedule.

Table 8-5 Basic Halocarbon Scenarios

M =Baseline scenario assumes emissions equal production as defined in Tables 8-1 and 8-4. Assumes global compliance with the Montreal Protocol plus additional phaseout of all other industrial halocarbons. All halocarbon emissions cease in 2005.

Peak CL = 4.08 ppbv $\int$ CL (above 3 ppbv) = 17.9 ppbv-year

A = Baseline scenario, but part of CFC-only market (about 10 percent of 1985 CFC production with the same mix of CFCs) is allowed a 20-year delay in compliance. This CFC production of 100 kton/year continues from 1991 to 2010 with no growth. No HCFC substitutes.

Peak CL = 4.13 ppbv $\int$ CL (above 3 ppbv) = 20.8 ppbv-year

B = Baseline scenario, but the CFC noncompliance (as in A, 100 kton/year in 1990) grows at 5 percent/year, reaching 430 kton/year in 2020. Phaseout of all CFCs in 2020. No HCFC substitutes.

Peak CL = 4.14 ppbv $\int$ CL (above 3 ppbv) = 22.4 ppbv-year

C = Baseline scenario, including limited non-compliance (as in A), but with an aggressive substitution policy including HCFCs. Begin in 2000 with 360 kton/year (about 30 percent of CFC+HCFC-22 market) of the alternate halocarbon H_x (20-year lifetime), allow growth at 3 percent/year, replace in 2020 with short-lived alternate H_y (2-year lifetime), and continue growth at 3 percent/year (1578 kton/year of H_y in 2050).

Peak CL = 4.13 ppbv $\int$ CL (above 3 ppbv) = 22.6 ppbv-year

Table 8-6a Trace Gas Scenarios: Time-Dependent

A (without H_x and H_y) and C (including H_x and H_y)

Year	F11	F12	F113	F114	F115	1211	1301	H22	CCl_4	MCF	H_x*	H_y*
1985	222	382	30	5	4	1.5	1.7	80	100	130	0	0
1990	284	485	57	8	6	2.5	3.5	104	106	159	0	0
1995	337	577	81	10	8	3.2	5.2	119	111	176	0	0
2000	337	595	87	11	9	2.9	6.0	127	102	141	0	0
2005	315	581	86	11	9	2.0	5.8	134	91	90	77	0
2010	295	567	85	11	9	1.4	5.6	98	82	40	149	0
2015	271	545	81	11	9	0.9	5.3	71	74	17	220	0
2020	247	522	78	11	9	0.6	4.9	52	66	8	291	0
2025	226	500	74	10	9	0.4	4.6	38	60	3	227	59
2030	206	479	71	10	9	0.2	4.3	28	54	1	177	73
2035	188	459	68	10	9	0.1	4.0	20	48	1	138	86
2040	172	439	65	10	8	0.1	3.8	15	43	0	107	99
2045	157	421	62	9	8	0.1	3.6	11	39	0	83	115
2050	143	403	59	9	8	0.0	3.3	8	35	0	65	133

B

Year	F11	F12	F113	F114	F115	1211	1301	H22	CCl_4	MCF
1985	222	382	30	5	4	Same as in A and C				
1990	284	485	57	8	6					
1995	338	578	81	10	8					
2000	340	600	88	11	9					
2005	323	593	89	11	9					
2010	311	592	91	12	9					
2015	305	597	94	12	10					
2020	305	610	99	13	10					
2025	284	593	96	13	10					
2030	260	568	92	12	10					
2035	237	544	88	12	10					
2040	216	521	84	12	10					
2045	198	499	80	12	10					
2050	180	478	77	11	10					

*In the stratospheric models, H_x is treated as one-half molecule of CF_2Cl_2; H_y as one molecule of CF_2Cl_2.

Table 8-6b Trace Gas Scenarios: Steady State

Year	F11	F12	F113	F114	F115	1211	1301	H22	CCl_4	MCF	CO_2	N_2O	CH_4
A Steady State													
'80SS	149	250	11	3	2	0.4	0.4	41	93	85	334	300	1538
'90SS	253	434	44	7	5	2.0	2.6	92	103	145	350	308	1685
'00SS	337	586	84	11	9	3.0	5.6	123	106	158	372	316	1815
'20SS	259	533	79	11	9	0.7	5.1	62	70	12	419	332	2075
'50SS	150	412	60	9	8	0.0	3.4	9	37	0	501	358	2465
B Steady State													
'80SS	149	250	11	3	2	0.4	0.4	41	93	85	334	300	1538
'90SS	253	434	44	7	5	2.0	2.6	92	103	145	350	308	1685
'00SS	339	589	85	11	9	3.0	5.6	123	106	158	372	316	1815
'20SS	305	604	97	13	10	0.7	5.1	62	70	12	419	332	2075
'50SS	189	489	78	11	10	0.1	3.4	9	37	0	501	358	2465

C Steady State

	Same as A except												
							H_X*	H_Y*					
'80SS							0	0					
'90SS							0	0					
'00SS							0	0					
'20SS							256	0					
'50SS							74	124					

*In the stratospheric models, H_X is treated as one-half molecule of CF_2Cl_2; H_Y as one molecule of CF_2Cl_2.

Table 8-7 Tropospheric Chlorine and Bromine Loading

Year	Chlorine (ppbv) A	B	C	Bromine (pptv) A–B–C
1985	3.00	3.00	3.00	18.2
1990	3.62	3.62	3.62	21.0
1995	4.13	4.13	4.13	23.4
2000	4.05	4.07	4.05	23.9
2005	3.76	3.82	3.84	22.8
2010	3.45	3.57	3.60	22.0
2015	3.20	3.44	3.42	21.2
2020	2.99	3.41	3.28	20.5
2025	2.82	3.25	3.16	20.0
2030	2.67	3.07	2.99	19.5
2035	2.53	2.91	2.84	19.1
2040	2.41	2.76	2.71	18.9
2045	2.29	2.63	2.61	18.7
2050	2.19	2.51	2.52	18.3

Table 8-8. One key uncertainty in the formulation is the surface area of sulfate aerosols (see Chapter 3). We gave upper and lower limits for the surface area: the lower limit corresponds to baseline, clean conditions (*i.e.*, several years after any significant volcanic injection of sulfur), and the upper limit, a factor of four greater, is approximately the median value over the past two decades (*i.e.*, about half of the time the surface area exceeded the upper limit). For example, the sulfate layer's optical depth (closely related to surface area) has increased by factors of 20 or more during the past decade following the eruption of El Chichón, (see Figure 3-2). The stratospheric model calculations of the trace gas scenarios included both a gas phase only chemistry using JPL–90

Table 8-8 Heterogeneous Chemistry on the Sulfate Layer

Aerosol Surface Area (10^{-8} cm^2cm^{-3})

z*	Jan-Feb-Mar-Apr-May-Jun					Jul-Aug-Sep-Oct-Nov-Dec				
km	60–90N	30–60N	30N–30S	30–60S	60–90S	60–90N	30–60N	30N–30S	30–60S	60–90S
					Enhanced (Median)					
32	0.1	0.1	0.4	0.2	0.1	0.1	0.1	0.4	0.3	0.1
30	0.2	0.3	0.7	0.4	0.2	0.2	0.3	0.7	0.6	0.2
28	0.5	0.7	1.3	0.8	0.5	0.5	0.7	1.3	1.0	0.5
26	1.0	1.0	1.7	1.2	1.0	1.0	1.0	1.7	1.5	1.0
24	1.4	1.5	2.0	1.7	1.4	1.4	1.5	2.0	2.0	1.4
22	1.8	2.0	2.5	2.5	2.0	1.8	2.0	2.5	2.5	2.0
20	2.5	2.5	3.0	3.2	3.0	2.5	2.5	3.0	3.0	2.5
18	3.0	3.0	3.0	4.0	4.0	3.0	3.0	3.0	4.0	4.0
16	3.5	3.5	2.0	4.0	4.5	3.0	3.0	2.0	4.0	5.0
14	4.5	4.5	2.0	4.0	5.0	3.5	3.5	2.0	5.0	6.0
12	5.0	5.0	2.0	4.0	5.0	4.0	4.0	2.0	5.0	7.0
					Baseline (Lower Limit)					
32										
...					...Divide All Numbers by Four ...					
12										

Note: Surface areas based on analysis of SAGE II data by Poole, Thomason, and Yue, see Chapter 3.

Reactions:

(1) N_2O_5 (+ H_2O in aerosol) → $2xHNO_3$

(2) $ClONO_2$ (+ H_2O in aerosol) → HNO_3 + HOCl

Probabilities:

$G_1 = 0.1$

$G_2 = 0.006 \exp[-0.15 \times (T - 200)]$

where G is the probability of reaction per collision. G_2 depends on the water content of the sulfuric acid. This formula has been fitted to the laboratory data of Tolbert *et al.* (1988) under stratospheric conditions.

Rates:

k = 5200 cm/s x G x Surface-Area (/cm)

where 5200 cm/s is an effective collision velocity.

kinetics (DeMore *et al.*, 1990) with updates noted in Table 8-2 (denoted GAS), and a sulfate chemistry using the same gas phase kinetics plus the specifications in Table 8-8 (denoted HET for the lower limit of sulfate aerosol areas and HET-E for the enhanced levels of sulfate aerosols).

8.3 THE CURRENTLY OBSERVED ATMOSPHERE: 1980–1990

This section examines the model simulations of stratospheric ozone concentrations for the current epoch. We focus on the period 1980–1990 for which we have the most extensive global observations of ozone from satellites (see Chapter 2). The change in ozone over the past decade is predicted by the participating two-dimensional stratospheric models using different chemical formulations. The models and their chemistries are summarized in Tables 8-9a and b.

Ozone loss prior to 1980 is not discussed here; the choice of 1970 as the initial atmosphere precluded such comparisons. A best estimate of the predicted perturbations prior to 1980 would be that they are comparable to those reported here for the period 1980 to 1990 (*i.e.*, the predicted ozone loss from 1960 to 1990 would be larger, possibly twice as large as that shown here for 1980–1990, but would require additional studies to quantify). There is evidence from the long-term record at Dobson sites (see Chapter 2) that ozone depletion in the 1980s was significantly greater than that in the 1970s. The existence of a high threshold for chlorine levels, above 15 ppbv at which there would be rapidly nonlinear ozone loss (Prather *et al.*, 1984), may need to be reexamined in light of the impact of heterogeneous chemistry on the coupling of the NO_y and Cl_y families in the lower stratosphere.

These scenarios do not include any year-to-year variability that is known to affect ozone (*e.g.*, solar cycle, quasi-biennial oscillation, and volcanoes). For a more detailed analysis of the period 1955–1985, see Chapter 7 of *Report of the International Ozone Trends Panel* (WMO, 1990a). Comparison of these model calculations (which do not include a solar cycle) with observations for the decade 1980–1990 is appropriate because it began and ended near the maximum of the solar cycle.

8.3.1 Chlorine and Bromine Loading

The atmospheric composition has evolved steadily since 1980 (see Chapter 1). As summarized in Table 8-3, CO_2 has increased by about 5 percent, N_2O by 2.5 percent, and CH_4 by about 9 percent. These relative changes are dwarfed by the large increases in halocarbons, leading to a growth in the atmospheric chlorine loading from 1.5 ppbv in 1970 to 2.5 ppbv in 1980 to 3.6 ppbv today. Bromine loading before the year 1980 would have been dominated by natural sources and industrial CH_3Br; but by 1990 the halons contribute about 40 percent to stratospheric bromine.

In the models, ozone perturbations over this period are due, first, to chlorine nearly doubling and, second, to CH_4 and bromine increases. The observed trend over this period cannot be used to calibrate the chlorine-induced ozone depletion calculated by the models without a more exhaustive search to rule out other causes not included in these calculations. For example, we do not include directly any observed temperature trends or climatic "red noise" over this period that might induce changes in stratospheric circulation (see Chapter 2). Likewise, we have neglected other changing influences due to human activity (*e.g.*, aircraft exhaust, combustion by-products, hydrocarbons). The systematic decrease in stratospheric temperatures over these 20 years (–2 K near the stratopause, much less in the lower stratosphere except near the Antarctic ozone hole) is predicted to be primarily a product of O_3 depletion rather than CO_2 cooling and is included in some of the models.

8.3.2 Observed and Calculated Ozone: 1980 Baseline

The column abundance of ozone (1 Dobson Unit = 2.687×10^{16} ozone molecules cm^{-2}) is often displayed as a traditional Dobson map showing contours of zonally-averaged column O_3 as a function of latitude and month. The ozone columns calculated by the participating models for the year 1980 are shown in Figure 8-1. Also in Figure 8-1 we present the observations from the Total Ozone Mapping Spectrometer (TOMS) averaged over the years 1979 and 1980. Most models show the same basic pattern as the observed column ozone. The Northern

Table 8-9a Participating Two-Dimensional Stratospheric Chemistry Models

Group	Investigators/References	Location /References
AER	Malcolm Ko Debra Weisenstein Jose Rodriguez Nien Dak Sze	Atmospheric and Environmental Research, U.S. Ko *et al.* (1984, 1985, 1989)
DuPont	Don Fisher	DuPont, USA
GSFC	Charles Jackman Anne Douglass	NASA Goddard Space Flight Center, U.S. Douglass *et al.* (1989), Jackman *et al.* (1989b, 1990)
ITALY	Guido Visconti Giovanni Pitari Eva Mancini	University of Aquila, Italy Pitari and Visconti (1985, 1991), Pitari *et al.* (1991)
JMRI	Toru Sasaki	Meteorological Research Institute, Japan
LLNL	Don Wuebbles Peter Connell Doug Kinnison	Lawrence Livermore National Laboratory, U.S.
MPI	Christoph Bruehl Paul Crutzen	Max Planck Institute for Chemistry, Germany Bruehl and Crutzen (1988)
NCAR	Guy Brasseur Claire Granier	National Center for Atmospheric Research, U.S.
NOCAR	Susan Solomon Rolando Garcia	NOAA Aeronomy Lab, U.S. NCAR, U.S.
Oslo	Ivar Isaksen Björg Rognerud Frode Stordal	University of Oslo, Norway Stordal *et al.* (1985), Isaksen *et al.* (1990) NILU, Norway
SPB	Sergey Zvenigorodsky Sergey Smyshlayev	Environ. Branch, St. Petersburg, Russia Krecov and Zvenigorodsky (1990)

Table 8-9b Chemical Model Calculations

Group	Chemical Models
AER	GAS TD, GAS SS, HET/E SS
GSFC	GAS TD, HET TD, HET/E TD
ITALY	GAS SS, HET SS, HET/E+PSC SS
JMRI	GAS SS
LLNL	GAS SS, HET SS, HET/E SS
MPI	GAS TD
NCAR	GAS SS, HET SS, HET/E SS, HET/E+PSC SS
NOCAR	GAS SS, HET SS
Oslo	GAS TD, HET/E+PSC TD
SPB	GAS TD, GAS SS

Note: The GAS and HET chemical formulations are described in section 8.2.4. Some models simulate enhanced polar ozone loss through PSC-type processing (+PSC). The HET chemistry includes both lower limits (baseline) and higher levels (enhanced or /E) of sulfate surface area, see Table 8-8. The term SS refers to steady state (*i.e.*, single-year run); TD, to time-dependent (*i.e.*, full 70-year) scenario. The NOCAR model (lower boundary at 100 mbar) does not calculate O_3 columns.

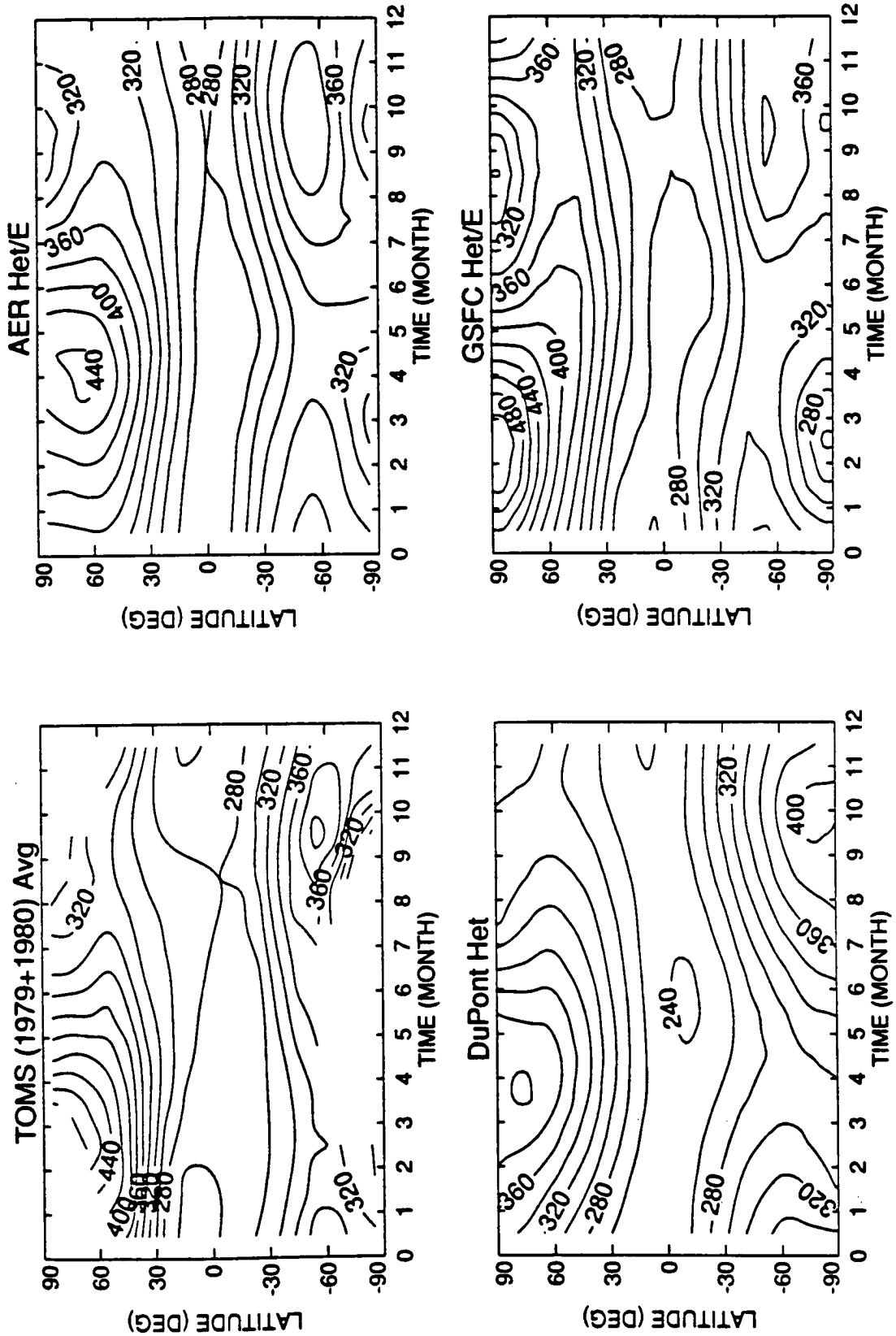

Figure 8-1a Column ozone abundances (Dobson Units) circa 1980 from observations (TOMS) and models.

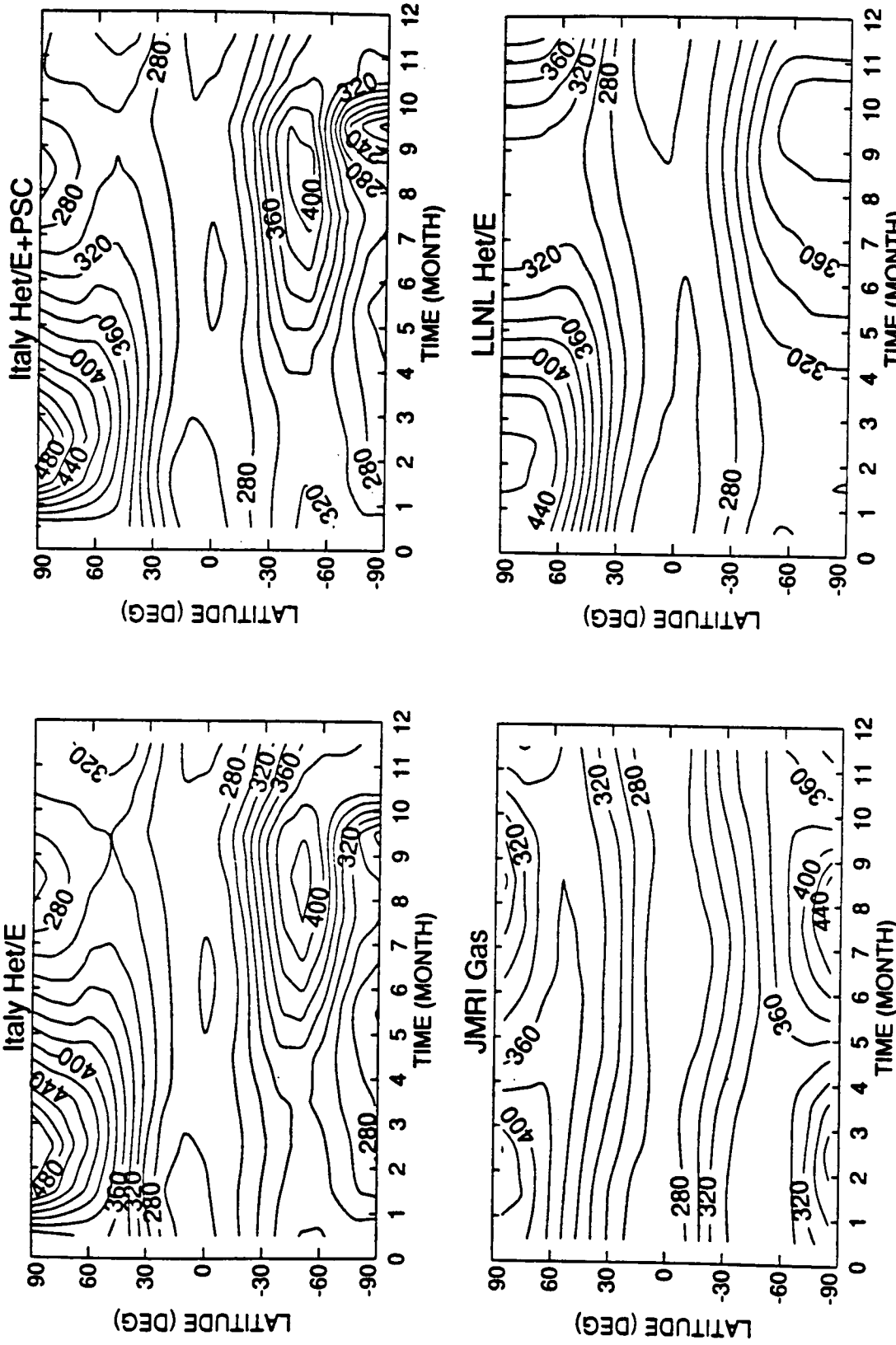

Figure 8-1b Column ozone abundances (Dobson Units) circa 1980 from observations (TOMS) and models.

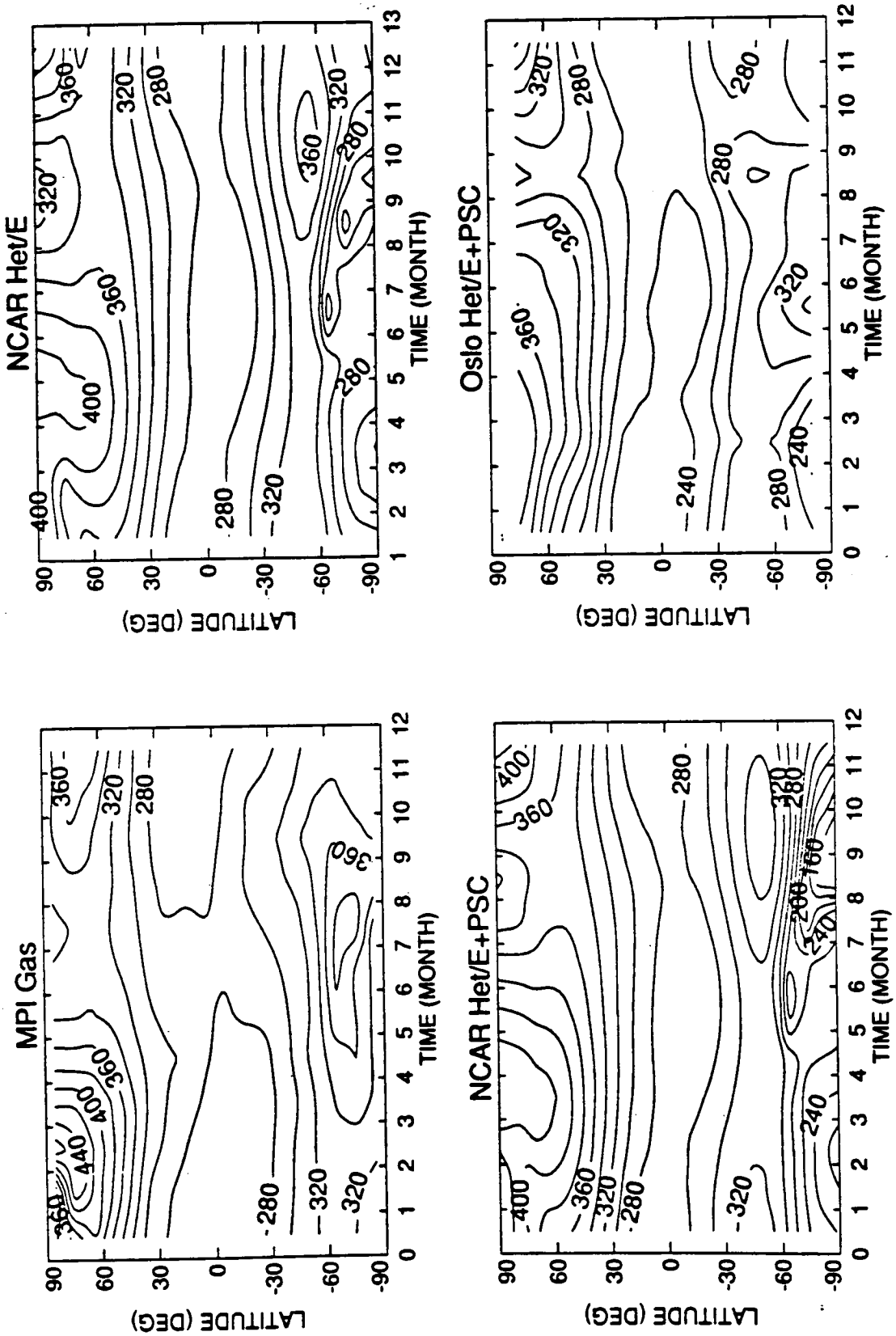

Figure 8-1c Column ozone abundances (Dobson Units) circa 1980 from observations (TOMS) and models.

Hemisphere maximum occurs in late winter to early spring at the pole; the Southern Hemisphere maximum occurs in early spring and is offset from the pole. The tropical minimum follows an annual cycle out of phase with the sun, reaching a minimum in the northern tropics in December. Only models with PSC simulations or specified polar ozone loss show the pattern typical of the Antarctic ozone hole in the Southern Hemisphere.

The contrast in column O_3 among models is large, but within a model the differences between the GAS and HET chemical formulations are usually small (not shown). For the 1980 simulations, most GAS models are no more than 4 percent different than corresponding HET models everywhere except in the Antarctic spring. In general, the differences among models and chemical formulations for column ozone cannot be used to discriminate among the models by comparison with observations for 1979 and 1980 alone. A better chance to test these simulations may be with the decadal trends discussed in the next section. More detailed analyses of the observations, their uncertainties, and year-to-year variations, along with objective measures of model accuracy, are planned as a workshop in 1992.

The distribution of ozone concentrations with altitude (*i.e.*, profiles) as a function of latitude and month can provide an additional test of the stratospheric models. In Figure 8-2, we show a mean measured profile for the month of March by combining observations from the Solar Backscatter Ultraviolet Spectrometer (SBUV) and the Stratospheric Aerosol Gas Experiment (SAGE II) from the early 1980s. This figure also shows results from the various models and chemical formulations as in Figure 8-1. A first-order comparison of the models with the observations shows very good agreement. For example, the largest ozone mixing ratios, about 10 to 11 ppm, are observed at about 33 km over the equator. The models' predictions are slightly less, 8 to 11 ppm, and the maximum occurs 1–2 km lower. In the upper stratosphere away from the poles, there has been a long-standing problem with the prediction of too low ozone mixing ratios, but here we see only a small, possibly systematic underprediction: at 40 km the observations show 8 ppmv and the models vary from 6 to 8 ppm; and at 50 km the observations are about 3 ppmv with the models varying from 2 to 3 ppm. For observations and many models, the 6-ppmv contour closes off the volume from about 60°S to 60°N over the altitude range from about 28 to 40 km. Differences between GAS and HET in the same model would not be readily discernible in these contours. Large differences between models occur in the lower stratosphere (and are readily seen in Figure 8-2) due to variations among models in the rate of mixing and in the location of the tropopause. A more critical comparison and verification of these models awaits the 1992 workshop on models and measurements.

8.3.3 Modeled Ozone Depletion: 1980 to 1990

The observed reductions in column ozone from the Dobson network and the TOMS satellite (see Chapter 2) have focused attention on the model predictions of ozone change over the past two decades (see WMO, 1990a). The recent TOMS picture of the statistically analyzed decadal trend in column ozone (NOT the difference between years 1990 and 1980) is shown in Figure 8-3 along with model simulations of this change. The TOMS analysis has removed the effects of the solar cycle and thus should be directly comparable to the model simulations. The observations show largest decreases at middle and high latitudes during early spring with little or no significant trend in the tropics. The largest ozone depletions (30 percent) are associated with the Antarctic ozone hole, but substantial declines, more than 8 percent, occur in the Northern Hemisphere as far south as 40°N latitude.

Model calculations of the period 1980–1990 with gas phase chemistry only universally show very small decreases, if any, in column ozone: less than 1 percent change over the tropics and much of the mid-latitudes; peak losses of 2 to 3 percent only during late winter poleward of 60° latitude. When the HET chemical formulation is adopted, allowing for reactions on the sulfate layer, model calculations show substantially greater ozone loss for the period 1980–1990. Ozone losses at 45°N latitude in spring range from 3 to 5 percent in the Atmospheric and Environmental Research, Inc. (AER), Goddard Space Flight Center (GSFC), Lawrence Livermore National Laboratory (LLNL), National Center for Atmospheric

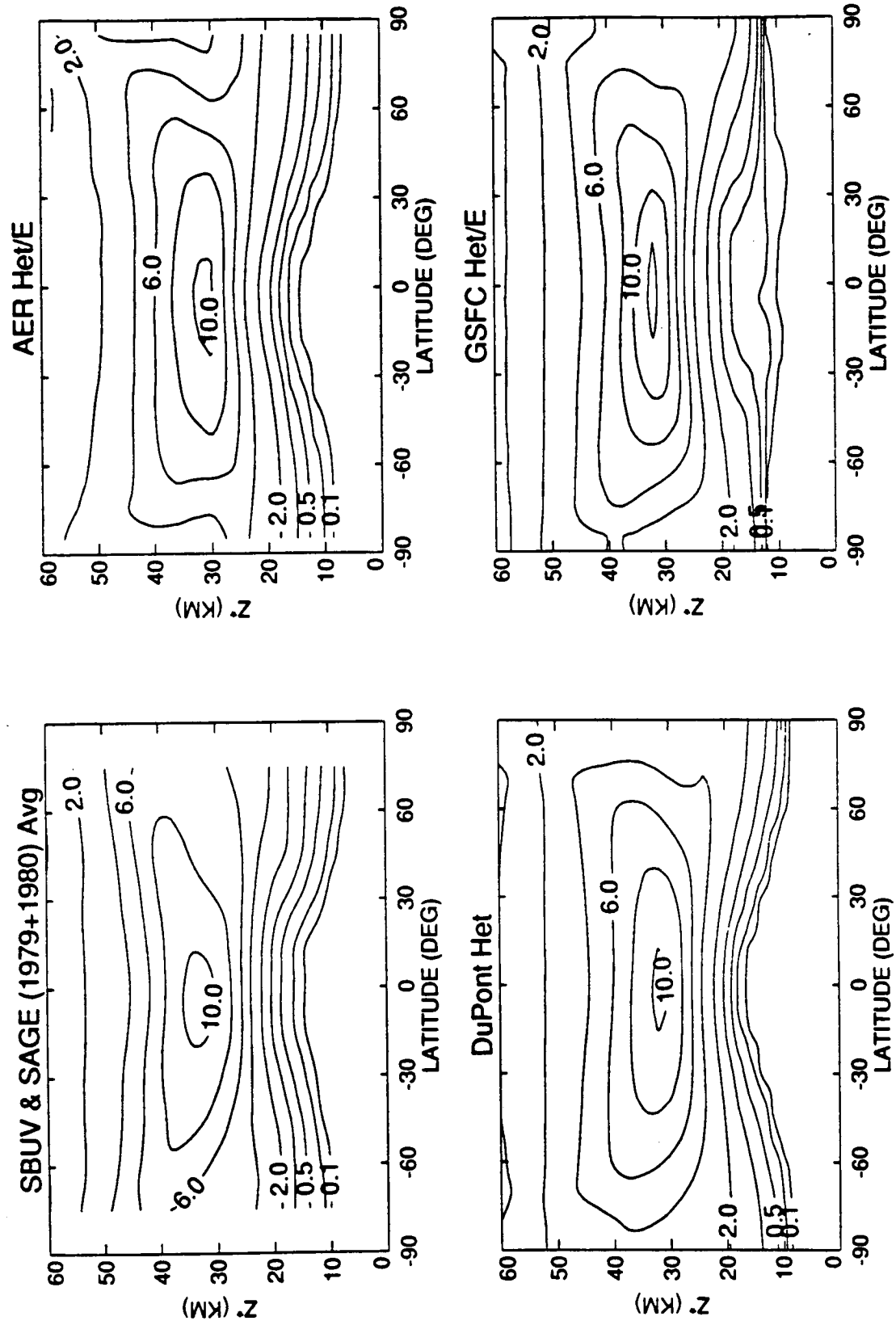

Figure 8-2a Ozone profiles (ppmv mixing ratio) circa 1980 from observations (SBUV) and models.

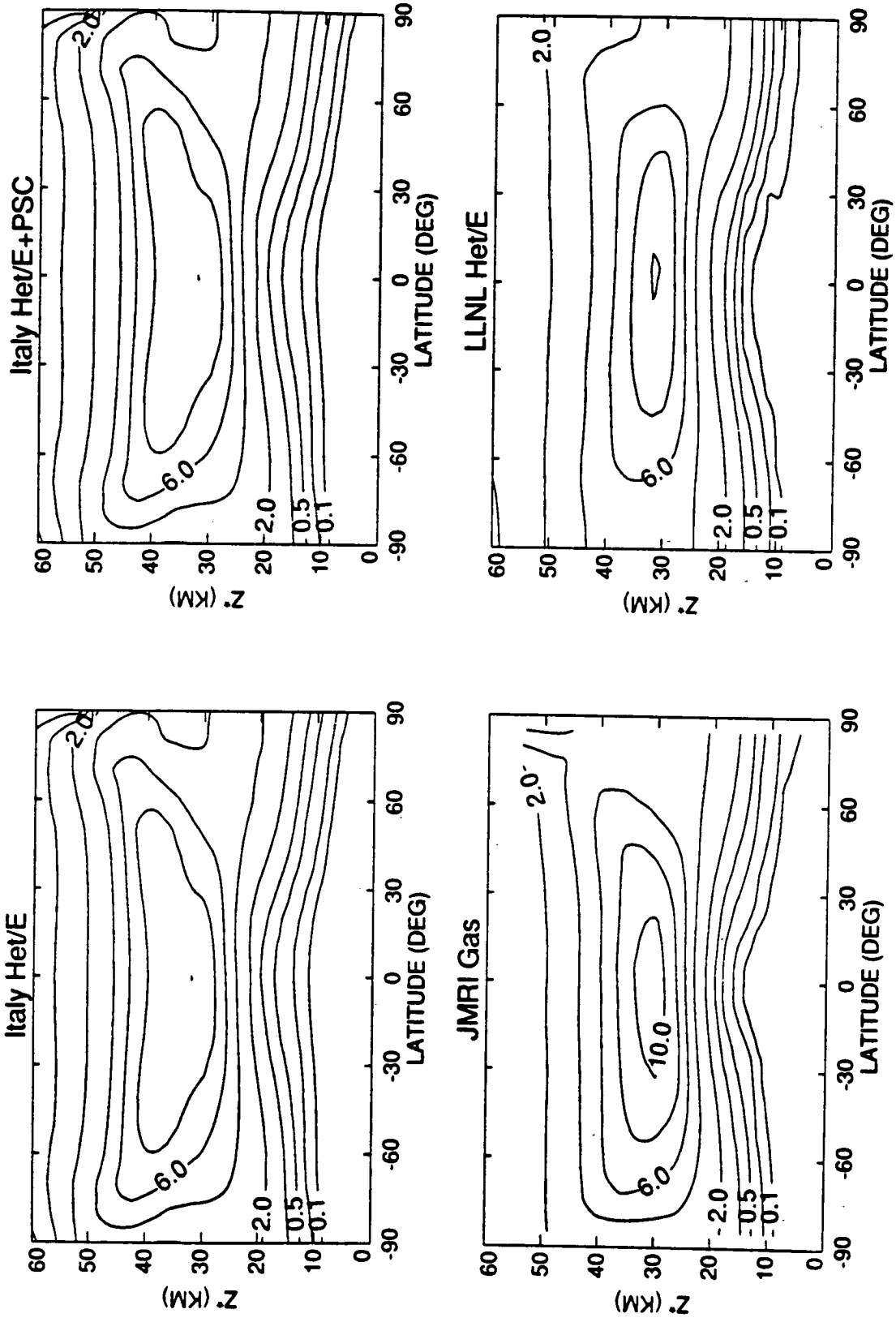

Figure 8-2b Ozone profiles (ppmv mixing ratio) circa 1980 from observations (SBUV) and models.

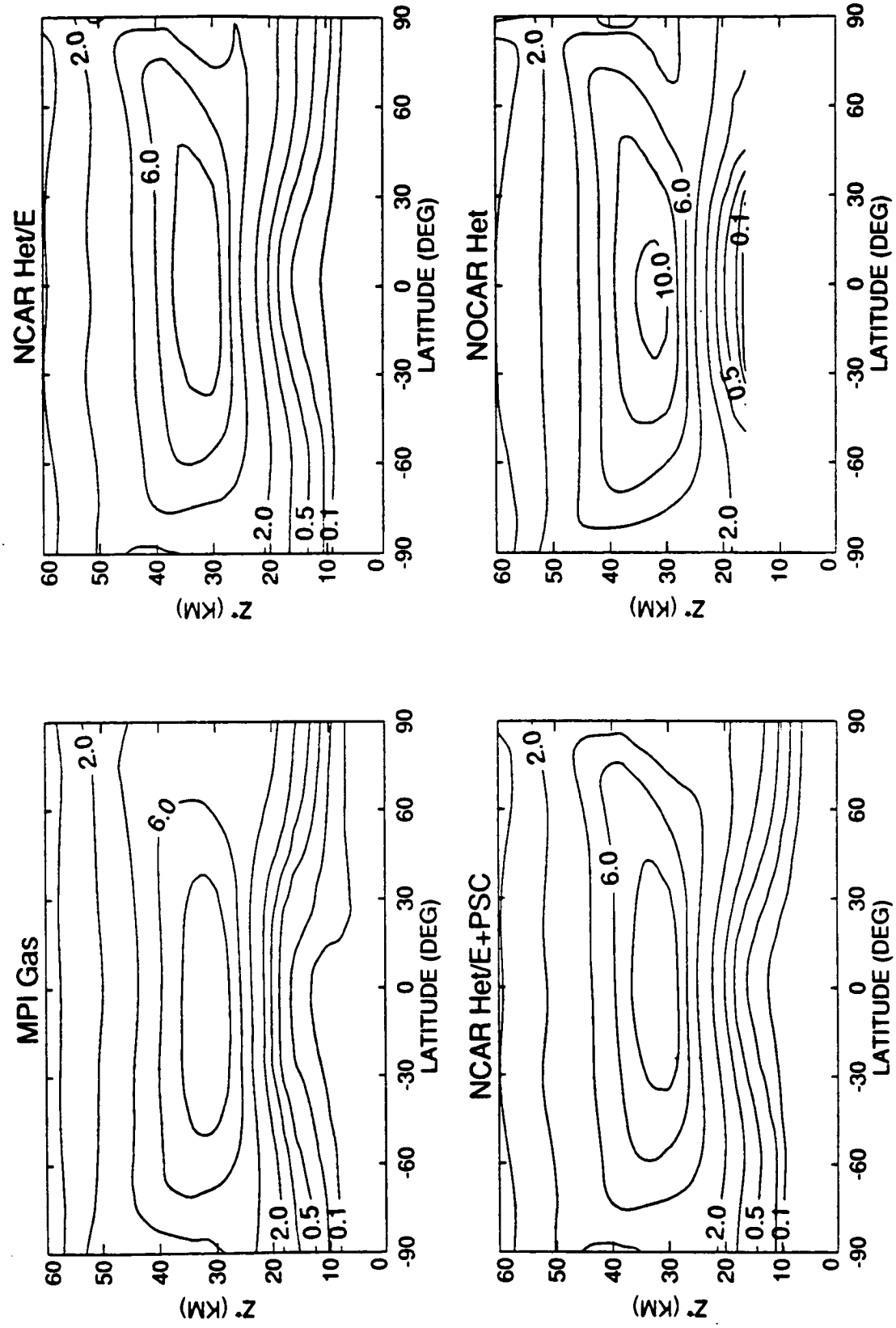

Figure 8-2c Ozone profiles (ppmv mixing ratio) circa 1980 from observations (SBUV) and models.

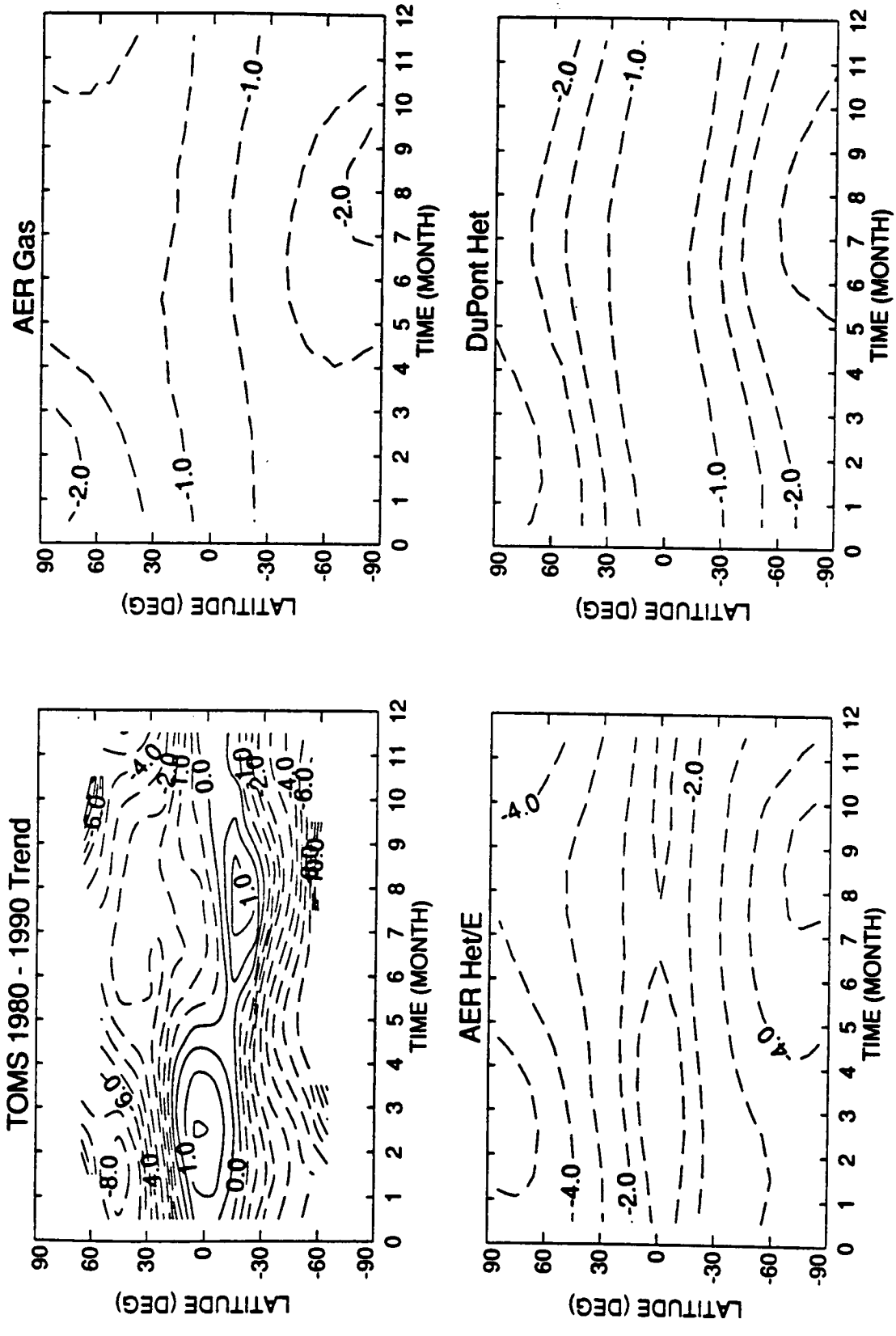

Figure 8-3a Change in column ozone abundances (percent) from 1980 to 1990 based on observations (TOMS) and models.

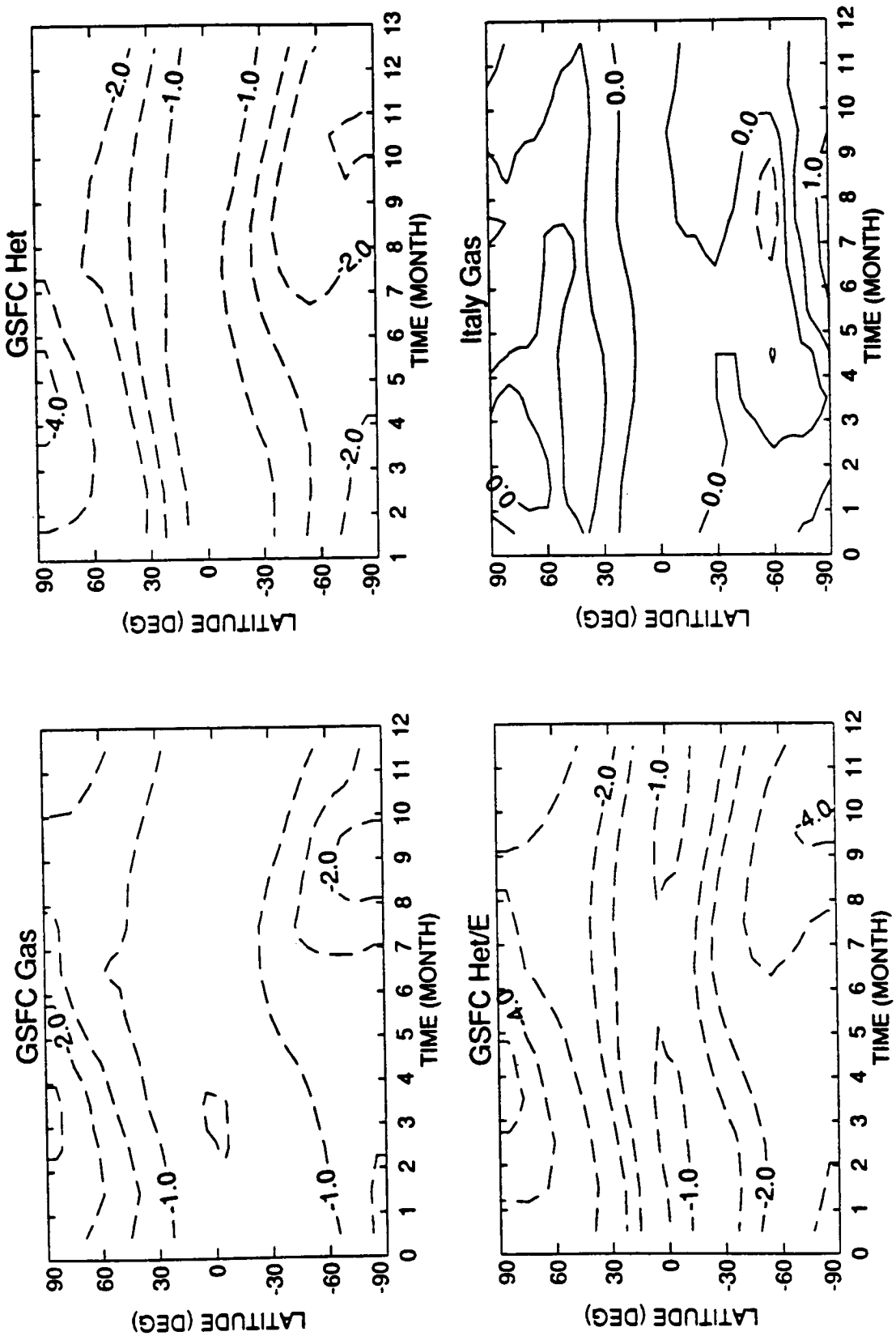

Figure 8-3b Change in column ozone abundances (percent) from 1980 to 1990 based on observations (TOMS) and models.

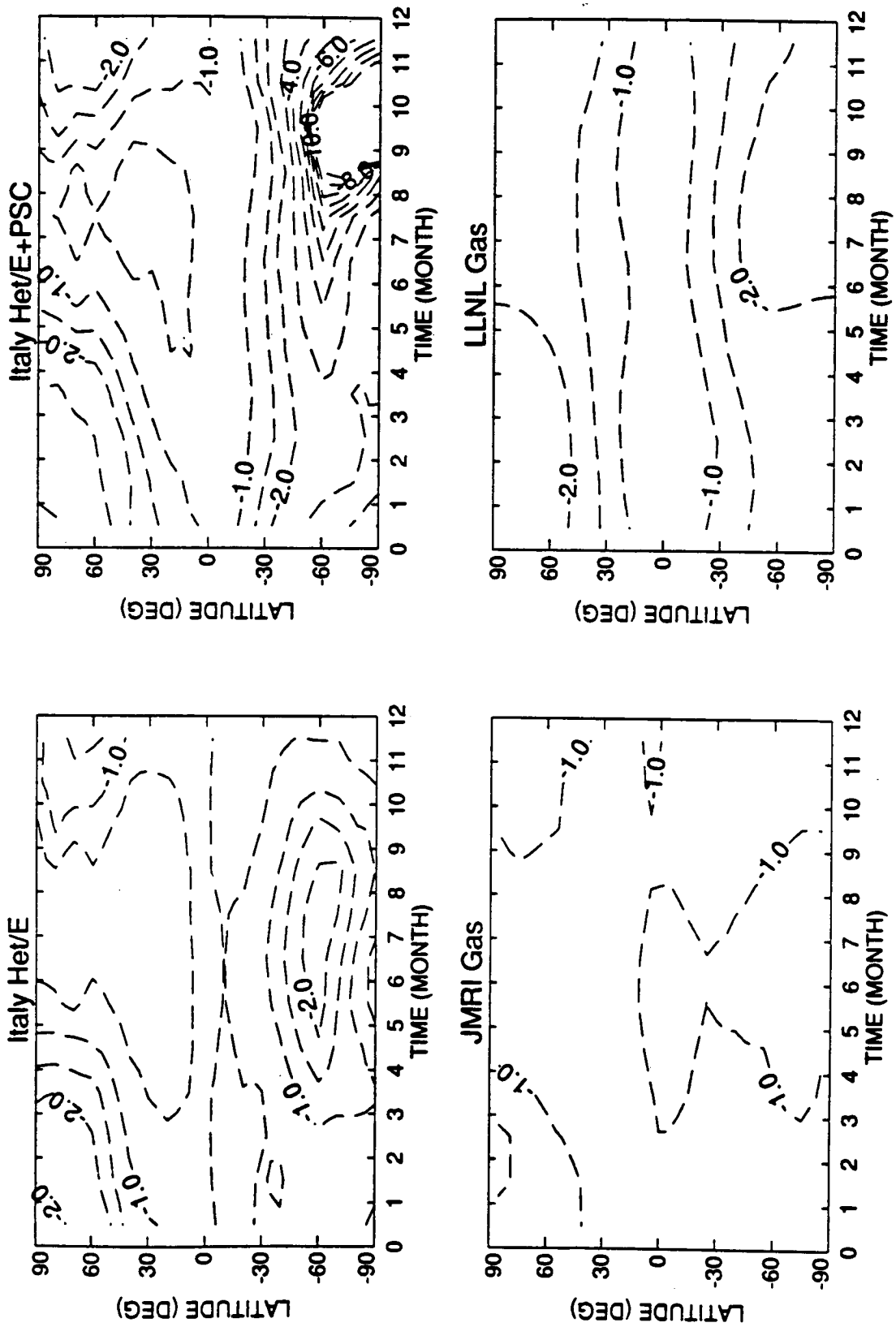

Figure 8-3c Change in column ozone abundances (percent) from 1980 to 1990 based on observations (TOMS) and models.

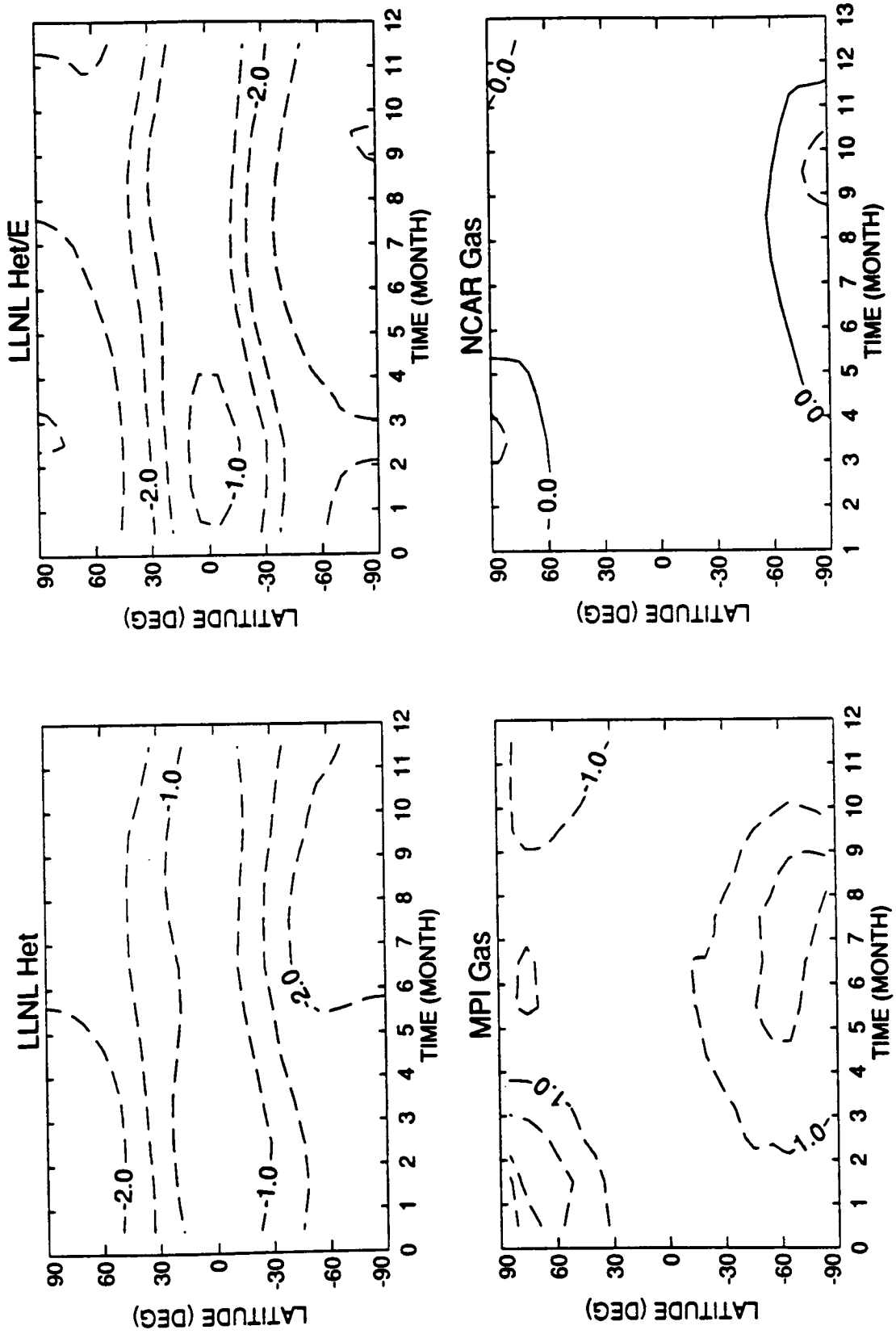

Figure 8-3d Change in column ozone abundances (percent) from 1980 to 1990 based on observations (TOMS) and models.

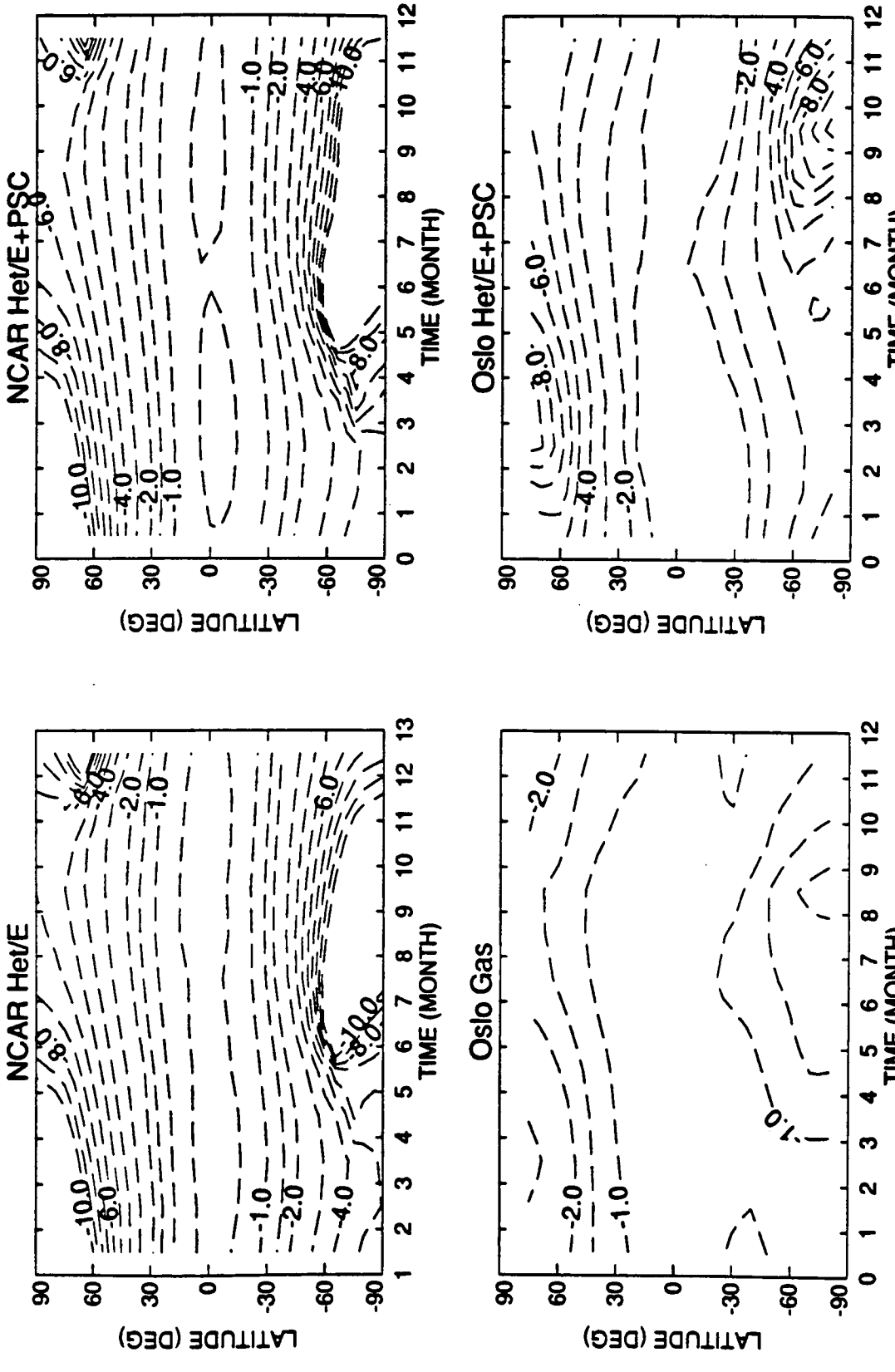

Figure 8-3e Change in column ozone abundances (percent) from 1980 to 1990 based on observations (TOMS) and models.

Research (NCAR), and Oslo models, and they are smaller but of similar pattern in the ITALY model. All HET models predict greater percentage losses at the poles. Most of the HET formulations predict 1 to 2 percent ozone depletion in the tropics over the decade; these values are larger than derived from TOMS, but fall within the quoted uncertainties (see Chapter 2).

The difference in predicted ozone depletion between the upper and lower limits of sulfate aerosol area is of some interest in view of the large variations, factor of 40 or more, in the sulfate layer over the past decade in response to volcanic eruptions. For example, most models (*e.g.*, AER, GSFC, and LLNL) show that the factor of 4 increase in surface area results in about a 1/2 percent larger ozone depletion over most latitudes and seasons. Therefore, model predictions for a 40 percent shift in the baseline value of sulfate layer area over this period would show negligible effects.

In general, the GAS models predict integrated column depletions and vertical profiles of ozone loss from 1980 to 1990 that are much less than those observed at middle latitudes over all seasons in both hemispheres. The HET models simulate most of the observed column ozone loss from 1980 to 1990 for the northern middle latitudes in summer, but only about half of that in winter (see Table 8-A). At high southern latitudes, however, the HET models fail to predict the massive losses associated with the Antarctic ozone hole (PSC chemistry), but still can explain part of the loss at southern mid-latitudes.

Three PSC models incorporate a parametric formulation of the chemistry involving PSCs; however, these PSC simulations in two-dimensional models remain incomplete. While PSC models are still under development, current versions predict greater ozone loss at northern middle latitudes in winter and early spring than do the GAS or HET models. It is possible that the combination of HET and PSC chemistries is synergistic and not linear, and thus, we cannot treat results from the two types of models as additive.

Modeled changes (percent) in the ozone profiles for the decade 1980–1990 are shown in Figures 8-4a-d. The month of March was selected for this comparison because it corresponds generally to the time of maximum ozone loss in the Northern Hemisphere. In this case, the observations are not yet sufficient to report with any degree of certainty the decadal changes in local ozone concentrations resolved latitudinally and monthly. For reference, see Chapter 2 where the observed trends in ozone profiles are reported only at individual stations (Figure 2–12 shows Payerne data) or as averages over latitudes and/or seasons (Figures 2–13 and 2–14 show SAGE data annually averaged).

Ozone depletion from March 1980 to March 1990 is calculated to have a distinct signature or fingerprint. Greatest losses, 12 to 16 percent, occur at high latitudes of both hemispheres (60° to 90° latitude) at the stratopause (40 to 50 km). One exception to this is the LLNL model with a similar pattern, but only 8 percent loss. (The smaller ozone loss in the LLNL model is in part consistent with the temperature feedback included in the model whereby ozone reductions lead to colder temperatures which in turn reduce the rates of ozone loss, especially in the upper stratosphere. When the LLNL model uses fixed temperatures [not shown], its results match those others shown here. However, the NCAR and NOCAR models shown here also include temperature feedback and still predict 12 to 16 percent losses. This discrepancy is unresolved.) Ozone depletion at the stratopause (about 45 km) is predicted to be much smaller in the tropics and at mid-latitudes, where it is slightly larger than, but still within the uncertainty of, the measured decrease (see Chapter 2).

Most models calculate a local ozone enhancement of 1 to 2 percent in the tropics somewhere between 18 and 25 km. This increase in ozone often extends down, into the troposphere, but has little effect on the column because of the small mixing ratios there (see Figure 8-2). At middle latitudes the difference between GAS and HET chemistries shows up clearly in lower stratosphere: in GAS the region 45°N to 90°N between 15 and 25 km has calculated depletions of at most 1 to 2 percent; whereas in HET the depletion in this region is expected to exceed 4 percent. (Not all models match this pattern.) Perhaps one of the most obvious signatures of heterogeneous chemistry (as proposed) is the bimodal pattern of ozone depletion at 50°N to 60°N with a minimum loss near 30 km that appears in all the HET calculations. Some GAS models also show ozone losses in the polar lower stratosphere, extending to mid-latitudes, due to rapid downward transport of ozone depletion from the upper stratosphere.

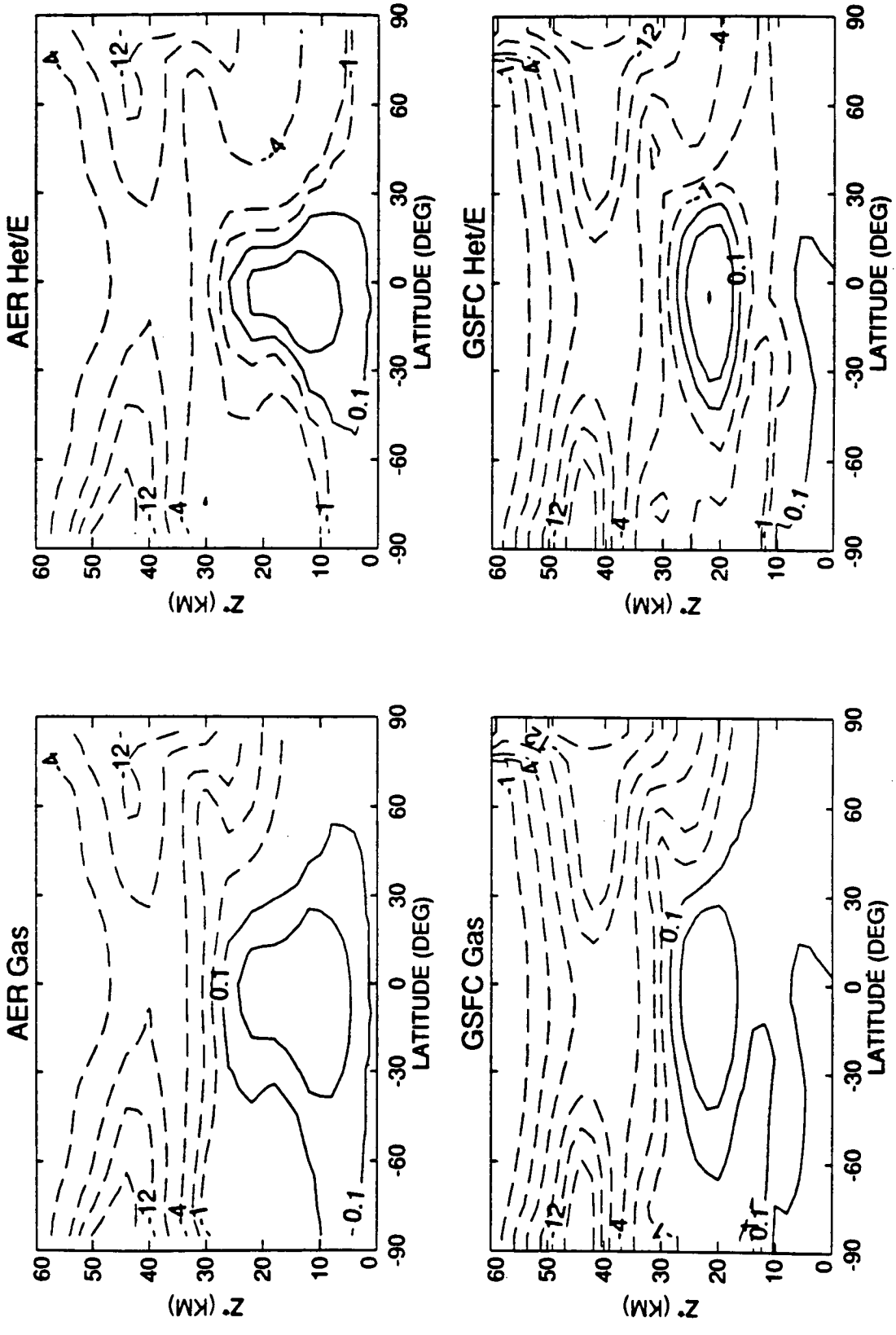

Figure 8-4a Change in ozone profiles (percent) from 1980 to 1990 from models.

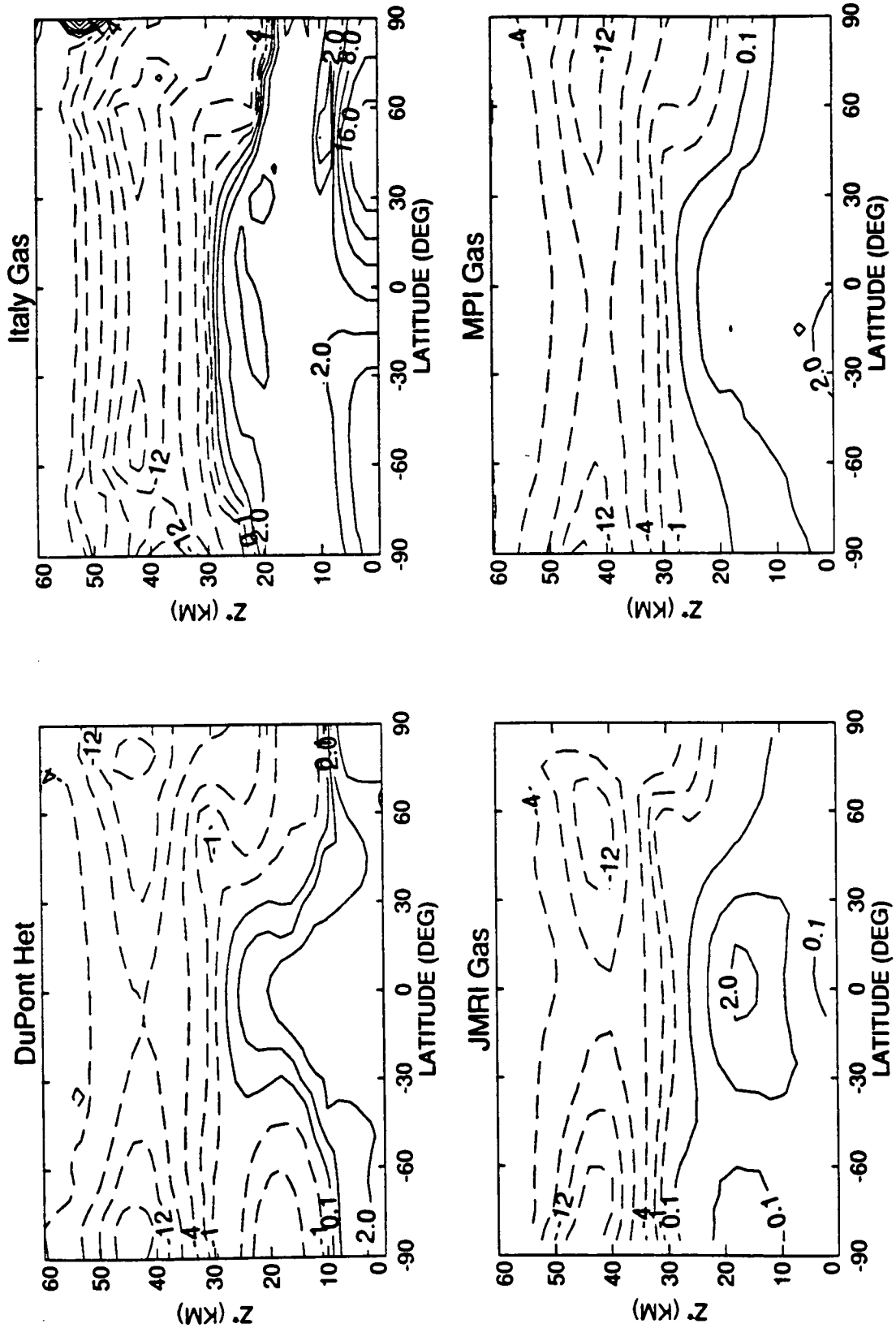

Figure 8-4b Change in ozone profiles (percent) from 1980 to 1990 from models.

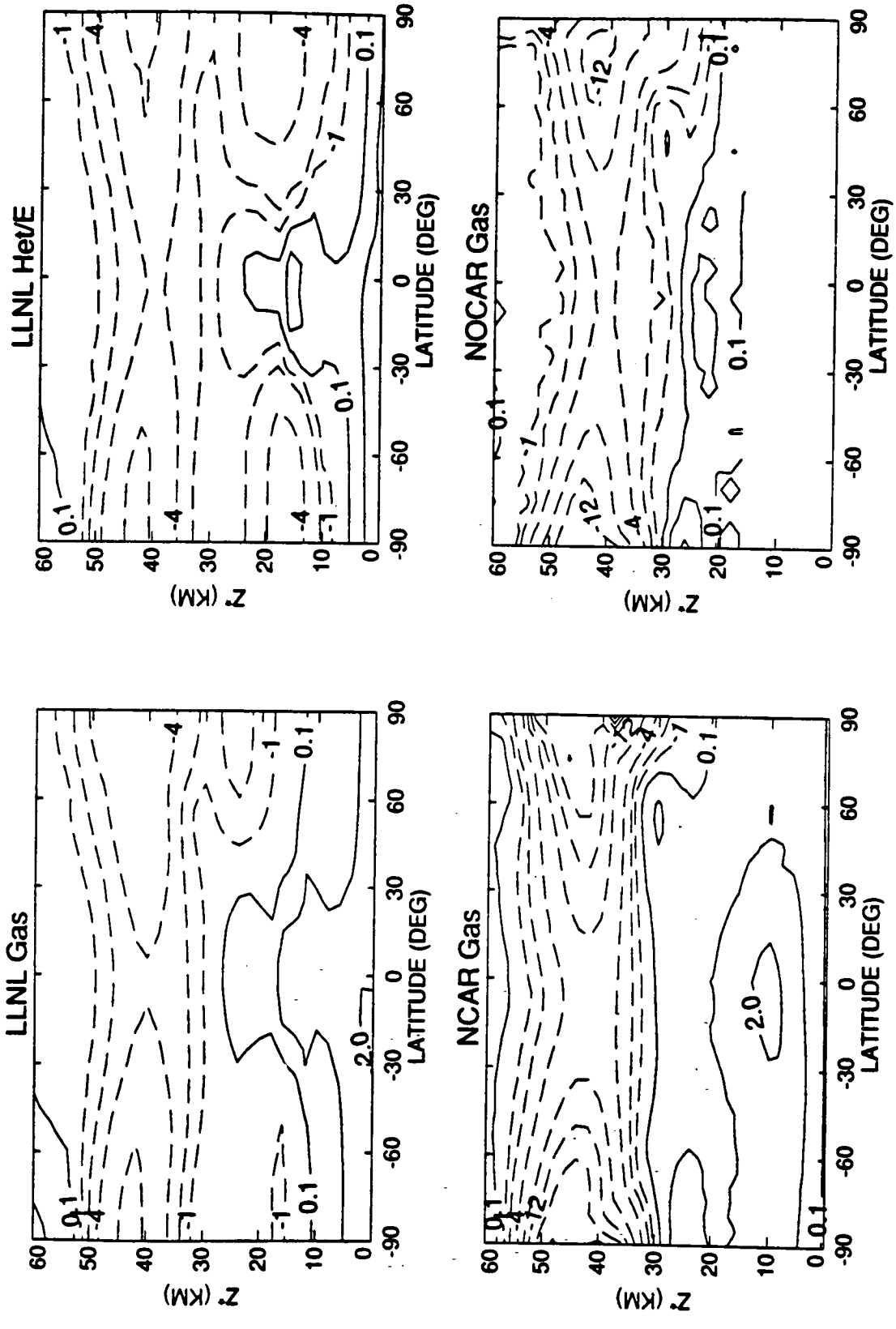

Figure 8-4c Change in ozone profiles (percent) from 1980 to 1990 from models.

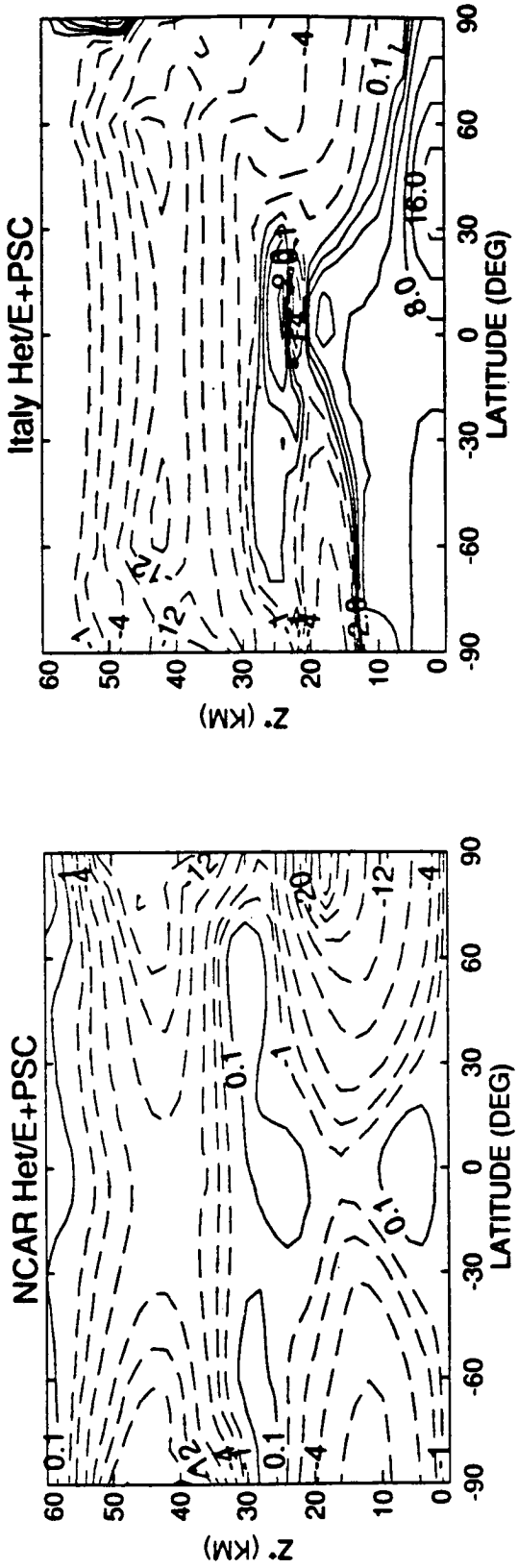

Figure 8-4d Change in ozone profiles (percent) from 1980 to 1990 from models.

Observed changes in ozone profiles over the past decade are not spatially and temporally resolved, as compared with the column changes, to provide a critical test of these simulations (see Chapter 2). Nevertheless, the observed change in ozone profile at mid-latitudes points to two modes of ozone loss, centered separately in the upper and lower stratosphere. The observed loss above 40 km altitude appears to be less than that predicted by models. This discrepancy is worrisome because the presumably well-known gas phase chemistry controls ozone in the upper stratosphere. The disagreement between model simulations and observations may easily fall within the uncertainties of the measurement of such trends (see discussion in Chapter 2). In the lower stratosphere, the agreement with the HET models in March may be fortuitous and cannot be used to verify the current chemical formulation because other mechanisms, particularly processing by PSCs in January and February, may lead to ozone depletion in March. An independent check might be to look for lower stratospheric ozone loss in September, before the occurrence of PSCs, but while the sulfate layer chemistry is active. Model simulations, however, predict a smaller effect and less distinctive signature in September.

8.4 PREDICTING THE FUTURE ATMOSPHERE: 1990–2050

The prediction of the future state of the stratosphere is first examined as semicontinuous time lines of scalar quantities such as chlorine and bromine loading. Then we study the magnitudes and patterns of calculated ozone change as we pass through the maximum in chlorine loading (circa 2000) described in Scenarios A–C.

8.4.1 Time Lines of Change

The chlorine and bromine loading of the atmosphere as defined in the scenarios of Tables 8-3 and 8-6a are plotted in Figures 8-5a and b. These figures include the extension of the scenarios to 2100. Scenario M is an optimistic, unrealizable baseline, assuming that the revised phaseout of the protocol (Table 8-4) meets with absolute global compliance (including all currently unregulated industrial halocarbons). A parallel case shows predictions for the identical scenario, but using the longer lifetimes (*e.g.*, 60 years for $CFCl_3$) adopted in the previous assessments (WMO, 1990b; Prather and Watson, 1990). For chlorine, the effect of CFC lifetimes is not discernible until 2010, but the difference grows steadily. This spread is not an estimate of the uncertainty in predictions of future chlorine loading (see Prather and Watson, 1990), since the uncertainty in CFC lifetimes is greater than the 10 percent

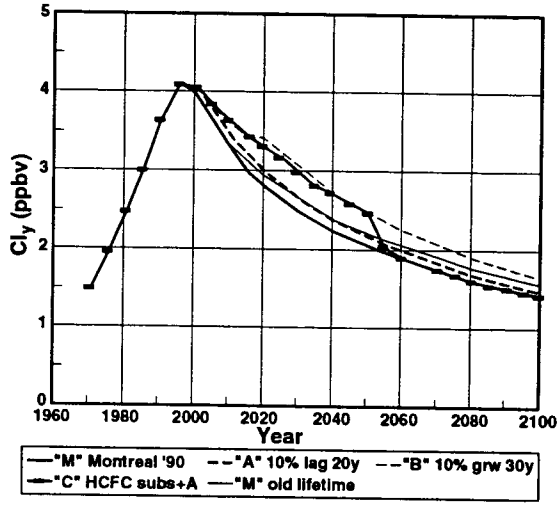

Figure 8-5a Chlorine loading for the basic scenarios (see Table 8-5).

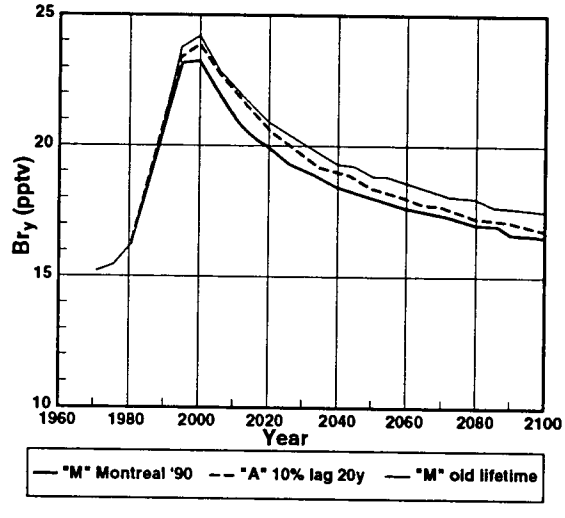

Figure 8-5b Bromine loading for the basic scenarios (see Table 8-5).

difference in these two cases (see Table 8-1). Furthermore, we must fold in the uncertainties in future CFC emissions. In the case of bromine, the uncertainty in halon lifetimes is manifest by the year 2000.

Scenario A, the optimistic phaseout with 10 percent of the market given a 20-year delay, parallels Scenario M with 0.1 to 0.2 ppbv greater chlorine levels throughout most of the 21st century. Scenarios B and C are basically similar out to the year 2050, having the same chlorine loading (up to 0.4 ppbv greater than in A), but from quite a different suite of halocarbons. The chlorine in Scenario B is due to CFCs and is committed for the better part of the century even though emissions cease in the year 2020. By 2050, the difference between Scenarios C and A is due mostly to short-lived HCFCs, and the recovery can be swift, less than 5 years, if emissions are halted. The growth of HCFC substitute H_y in Scenario C continues, perhaps to excess, reaching almost 7 megatons/year in the year 2100; all other scenarios have eliminated halocarbon emissions by the year 2020.

The propagation of chlorine into the stratosphere is shown with the AER and SPB models in Figure 8-6. In steady state, the tropospheric chlorine loading includes all halocarbons and peaks at 4.1 ppbv in 1995. The stratospheric Cl_y mixing ratio is always less than the tropospheric chlorine loading because not all the halocarbons are destroyed. At 40-km altitude, the Cl_y levels peak at 3.9 ppbv about 5 years after the chlorine loading; at 20-km altitude, they may peak a little earlier, but are much lower, about 2 ppbv. Also shown are the chlorine levels calculated with the same model using the steady-state atmospheres prescribed in Table 8-6b. Both approaches lead to similar histories of stratospheric Cl_y.

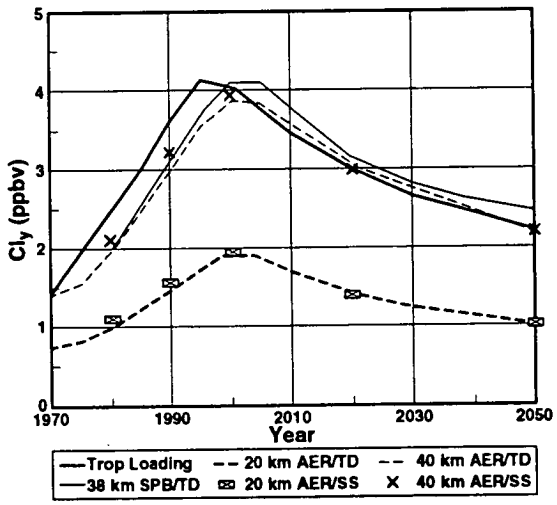

Figure 8-6 Chlorine levels at mid-latitudes (40–50N) in March. The tropospheric chlorine loading is compared with the lag in response predicted with the time-dependent AER results. Steady-state results from AER and SPB model also shown.

A comparison of the AER and GSFC model predictions of Cl_y and Br_y (Br + BrO + HBr + $BrONO_2$ + HOBr + BrCl) in northern mid-latitudes (40°N–50°N) is shown in Figure 8-7 for Scenario A. Both models predict similar magnitudes and time lags

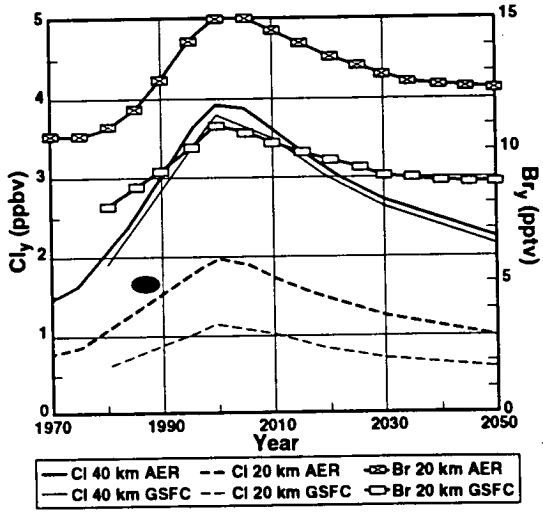

Figure 8-7 Chlorine and bromine levels at 40–50N in March form the AER (thick lines) and GSFC (thin lines) models. Cl_y estimates (oval) at 20 km from Schmidt *et al* (1991).

in Cl_y at 40-km altitude, but the lower stratospheres of these two models are dramatically different as noted in the general intercomparison of ozone profiles. The GSFC model has 30 percent less Br_y and almost 50 percent less Cl_y at 20-km altitude; O_3 levels from the two models (not shown) are, however, similar. At 20 km, it appears that the AER model has more photochemically processed air, while the GSFC model retains more of the chlorine in the form of halocarbons. Such differences should have an impact on the predicted ozone changes.

The impact of the HET chemical formulation is shown in Figures 8-8 for Scenario A with both the AER and GSFC time-dependent calculations. The maximum ozone depletion at 40-km altitude near 45°N latitude differs from model to model but peaks at about 20 percent in the year 2000 and is identical for both GAS and HET chemistries since sulfate layer chemistry takes place only at lower altitudes. At 20-km altitude, the picture is quite different. For GAS, the initial trends from the two models have different signs, but the long-term trends from years 2010 to 2050 is similar. This latter decline (while chlorine is recovering) is attributed to increasing NO_y. For HET, the initial decline in ozone corresponds to the rapid

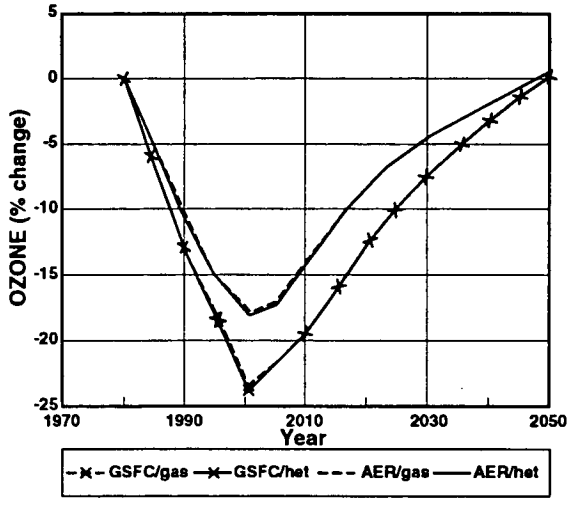

Figure 8-8a Ozone changes (percent) at 40 km, 45N in March from AER (line) and GSFC (X-line) for scenario A using GAS (dashed line) and HET (solid line) models.

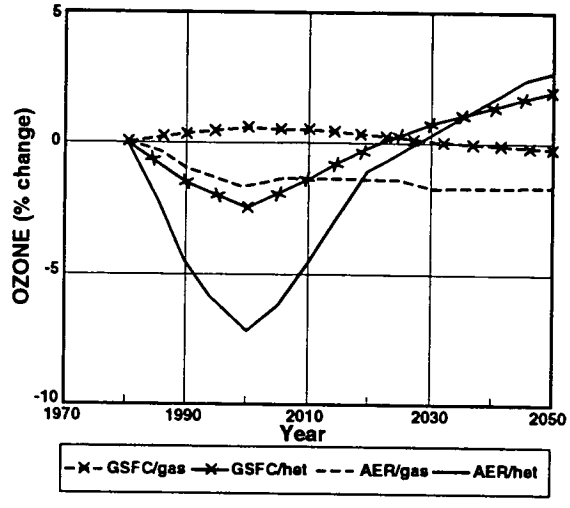

Figure 8-8b Ozone changes (percent) at 20 km, 45N in March from AER (line) and GSFC (X-line) for scenario A using GAS (dashed line) and HET (solid line) models.

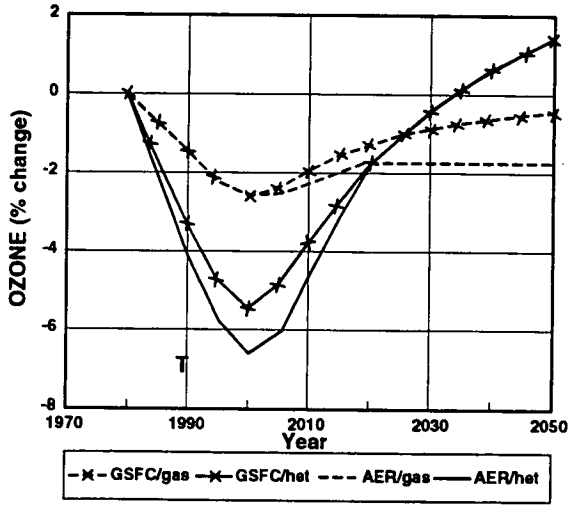

Figure 8-8c Ozone column change (percent) at 45N in March from AER (line) and GSFC (X-line) for GAS (dashed) and HET (solid) models. TOMS trend shown as a 'T'.

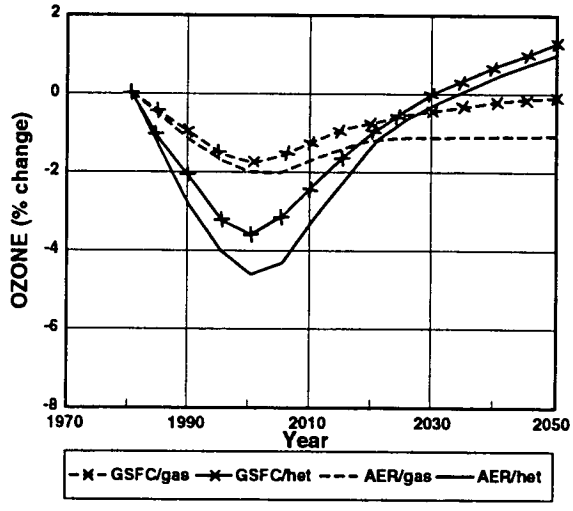

Figure 8-8d Ozone column change (percent) annually averaged Northern Hemisphere, from AER (line) and GSFC (X-line) for GAS (dashed) and HET (solid) models.

rise in Cl_y at 20 km; however, the recovery of O_3 proceeds faster than that of Cl_y because of CH_4 and NO_y increases. The ozone column abundances near 45°N reflect both the 20-km and 40-km patterns; for GAS both models predict a maximum loss of –2.5 percent in the year 2000 followed by a slow recovery; for HET the maximum column loss is about –6 percent and the recovery is much more rapid. In the GAS formulation, the column ozone never recovers because the NO_y increases lead to ozone depletion by 2050. In the HET formulation the recovery of the ozone column is rapid, becoming positive after the year 2030. The average ozone column over the Northern Hemisphere shows a similar history, but with a smaller amplitude.

The recovery of O_3 in the 21st century is clearly different in the GAS and HET chemistries. The explanation comes from an understanding of the relative importance of the different catalytic cycles that destroy ozone in the lower extratropical stratosphere (45°N–90°N, 14 to 23-km). Two models, designated as AER/GSFC, have analyzed the components of ozone loss for the year 2000. For GAS, the NO_y-related cycles account for 57/50 percent of the total, Cl_y-cycles for 6/4 percent, Br_y-cycles (including BrO + ClO) for 4/4 percent, HO_x for 25/30 percent, and O_x (Chapman cycle) for 8/12 percent. The corresponding values for HET are 19/16 percent for NO_y, 18/8 percent for Cl_y, 10/22 percent for Br_y, 45/46 percent for HO_x, and 8/8 percent for O_x. With the traditional GAS chemistry, the NO_y cycles are the most important ozone loss processes in the lower stratosphere, and thus the increase prescribed for N_2O leads to small ozone column reductions in the year 2050, even after Cl_y has recovered. With HET chemistry the impact of the Cl_y changes is amplified, and the recovery to positive values for the ozone column reflects the fact that ozone columns in 1980 (our reference year) are probably depressed by 2 to 4 percent relative to the pre-ozone hole conditions (early 1970s). Also, for HET the changes in N_2O have a much smaller impact on ozone, but CH_4 (through the HO_x chemistry) becomes more important.

Overall, with HET chemistry the role of NO_y in the stratosphere is reduced (Rodriguez *et al.*, 1991; Pitari *et al.*, 1991) because the fraction of NO_y in the active forms, NO and NO_2, is much smaller. The reaction of N_2O_5 on sulfate particles is the critical reaction in HET for most of the models. A sensitivity study with the AER model shows that the much slower $ClONO_2$-sulfate reaction acting alone, or added to the N_2O_5-sulfate reaction, has only a minor impact on ozone: a few tenths of percent in local concentrations and about 0.1 percent in the column. This result is not necessarily universal, since the NCAR model, which includes a parametric model of PSC chemistry, reports that the $ClONO_2$ reaction is important.

The importance of bromine in these calculations is small, almost trivial, for the GAS models, but is enhanced for the HET models. The catalytic loss of O_3 by the BrO + ClO reaction rises as ClO concentrations rapidly increase following the reduction of NO_x by heterogeneous conversion to HNO_3 (Rodriguez *et al.*, 1991). A larger role for the Br_y-catalyzed loss of ozone is predicted for the lower stratosphere (14–23 km) when PSC processing is included, but cannot be quantified from the simulations here.

8.4.2 Patterns of Ozone Change

The largest changes in ozone are predicted to occur in the year 2000 when stratospheric chlorine levels peak in the scenarios adopted here. There is little difference between scenarios in the year 2000 and thus we focus on Scenario A. The predicted ozone column changes from the year 1980 to 2000 are mostly depletions in this case, and their patterns are shown in Figure 8-9. The GAS chemistry models predict modest losses ranging from 0 to 4 percent, whereas the HET models show ozone depletions several times larger. In all cases, the loss is maximal around the winter pole and minimal over the tropics.

The largest difference between Scenarios A, B, and C occurs in the year 2020. Results for the year 2020 are shown in Figure 8-10 for the HET GSFC model. It is important to examine the HET models here, since we know that the GAS models are insensitive to chlorine changes between the years 1980 and 1990 (similar to the spread in chlorine loading between Scenarios A, B, and C in 2020). Scenarios B and C lead to slightly larger column ozone depletions of x–y percent relative to Scenario A, with differences between Scenarios B and C being slight.

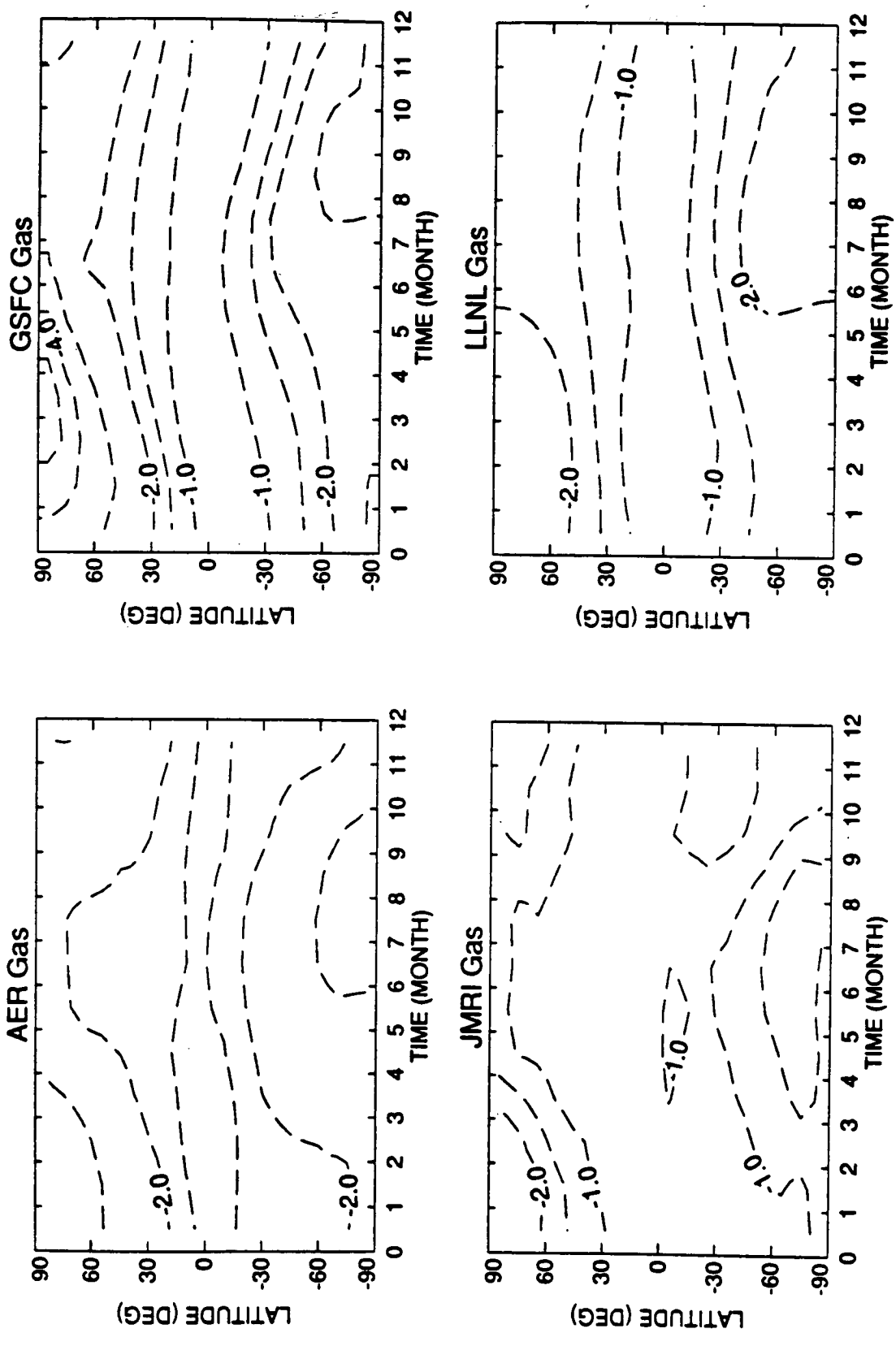

Figure 8-9a Change in column ozone abundances (percent) from 1980 to 2000 based on modeled Scenario A.

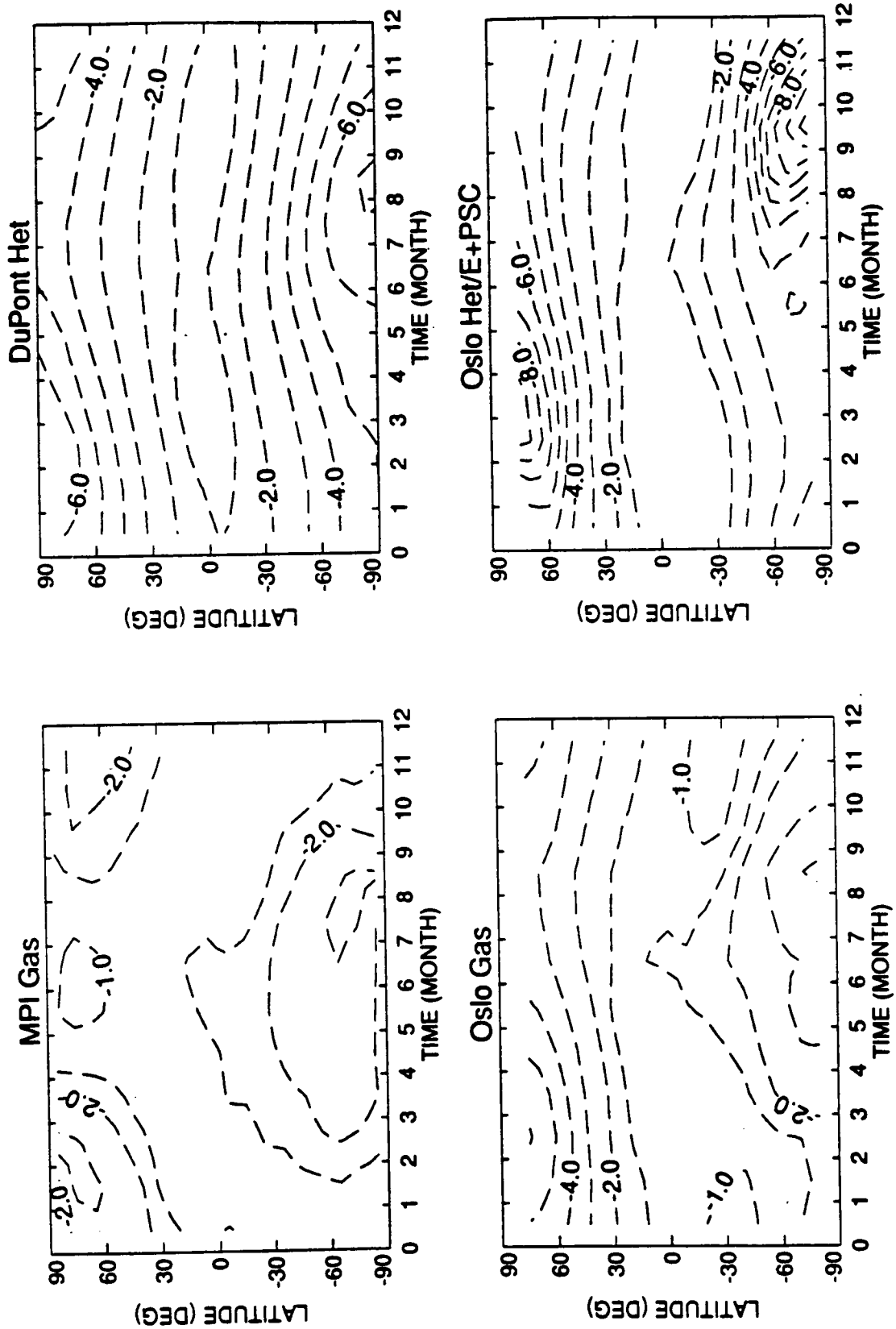

Figure 8-9b Change in column ozone abundances (percent) from 1980 to 2000 based on modeled Scenario A.

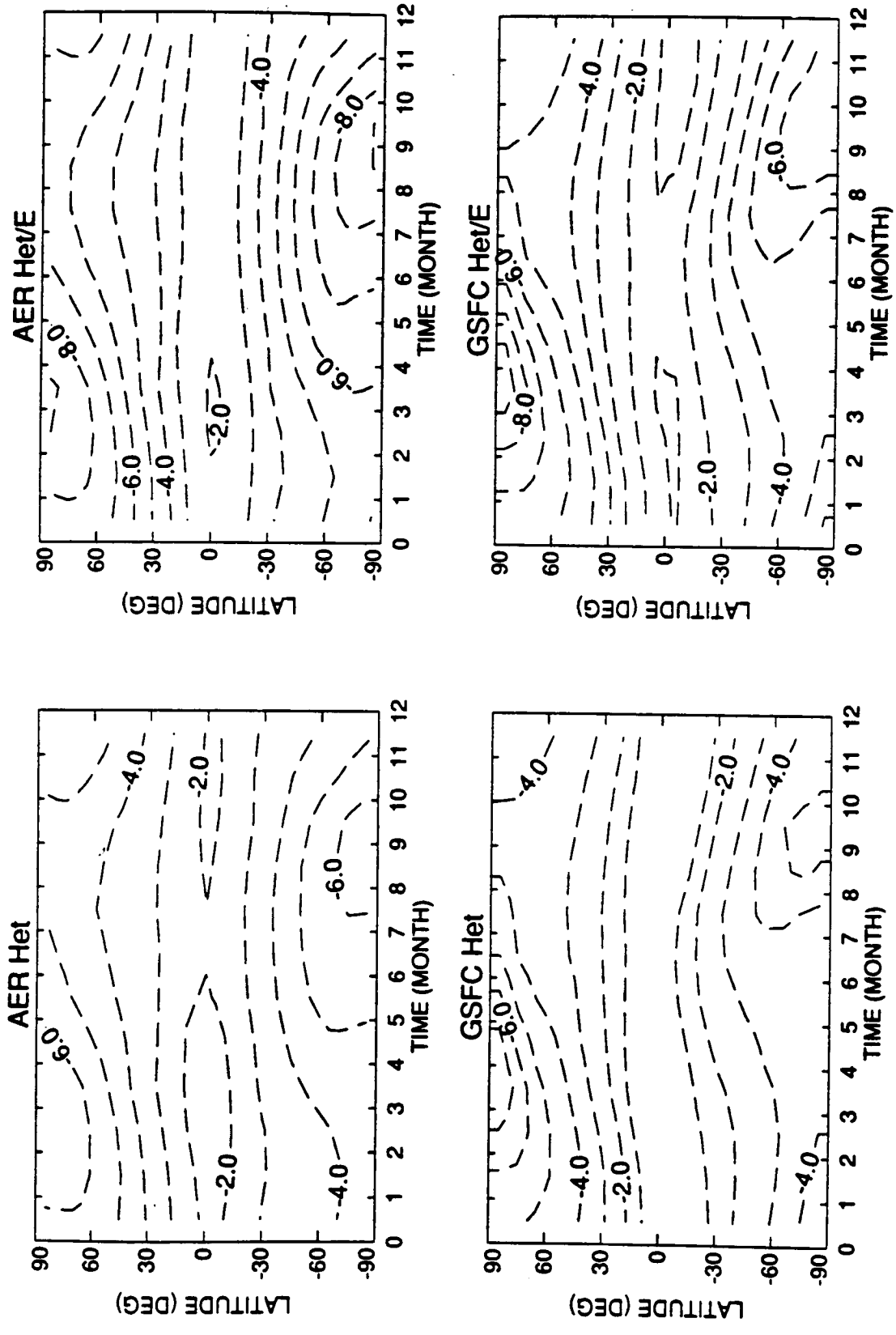

Figure 8-9c Change in column ozone abundances (percent) from 1980 to 2000 based on modeled Scenario A.

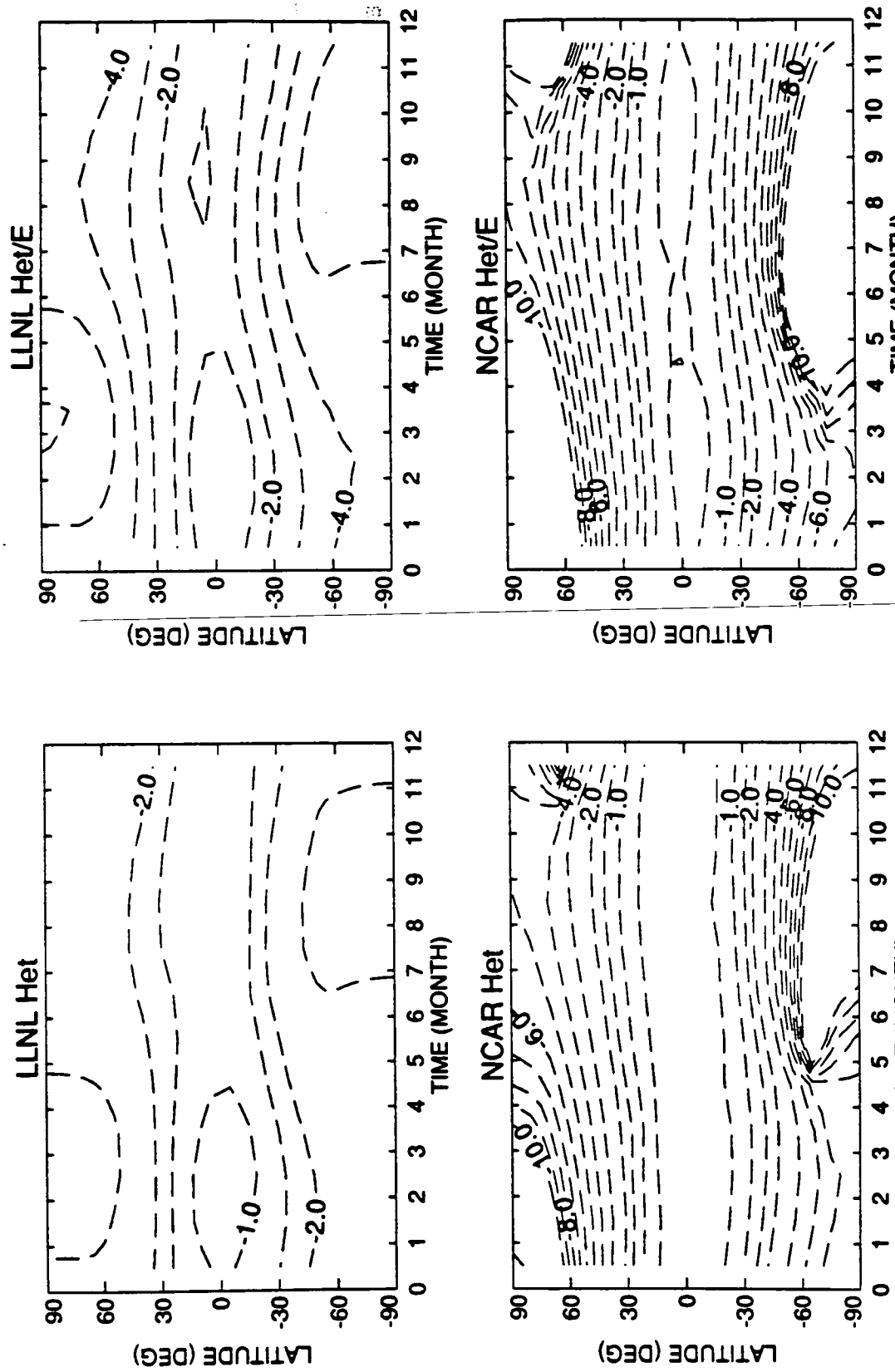

Figure 8-9d Change in column ozone abundances (percent) from 1980 to 2000 based on modeled Scenario A.

The largest differences among the model predictions occurs for the longest time interval, year 1980 to year 2050, where the changes in trace gases are largest. Under these circumstances, the predictions for 2050 depend on competing changes in Cl_y, Br_y, NO_y (through N_2O), CH_4, and stratospheric temperatures (through CO_2 and O_3 changes). Model predictions for the full range of chemical formulations are shown in Figure 8-11. The GAS models agree that perturbations in the tropics should be small, usually less than 1 percent; however, at mid-latitudes and the poles the predictions range from –3 to +4 percent. The HET models all show increases in column ozone of about 2 to 4 percent. This increase is due in part to the choice of 1980 as the reference year, as noted above. Several PSC models included the effects of chemical processing by PSCs (independently, since no method was agreed upon for these scenarios). They also predict a general increase in ozone column everywhere except in the Antarctic spring where the ozone hole still exists, but additional losses relative to the year 1980 are limited.

8.4.3 Peak Chlorine Loading and Integrated Halocarbon Effects

Both predictions and observations indicate that rising chlorine levels in the stratosphere are likely to lead to more extensive and deeper ozone loss. The apparently nonlinear response of ozone to chlorine makes us focus on the maximum levels of stratospheric chlorine. In this section we examine the atmospheric chlorine loading of halocarbons (CL) as a surrogate for chlorine-catalyzed ozone loss in the stratosphere (Prather and Watson, 1990). We recognize that tropospheric chlorine loading from halocarbons will be realized as stratospheric Cl_y with a time delay of 2–4 years and with some systematic reductions in absolute amount due to incomplete oxidation of the halocarbon source gases (*i.e.*, Cl_y is always less than CL). Thus CL is a conservative measure (*i.e.*, upper limit) of the amount of chlorine available to participate in ozone destruction.

Recent work on modeling and data analysis (see Chapter 6) has led to a better determination of the chemically active chlorine (Cl_y) in the lower, middle latitude stratosphere, where the bulk of the ozone loss is now observed. A specific fraction of each halocarbon source molecule is assumed to have been photochemically destroyed and thus contribute to the total Cl_y in the lower stratosphere. Some halocarbons, particularly those with a $-CCl_3$ segment, are readily photolyzed in the lower stratosphere and thus release almost all of their Cl atoms to Cl_y, (see notes to Table 8-B). Others, such as CHF_2Cl, are estimated to have remained mostly intact and release only about a third of their chlorine loading as Cl_y. We define free chlorine (FC), an estimate of Cl_y in the lower stratosphere, as the weighted sum of the chlorine loadings of the source gases.

Bromine-containing halocarbons release active bromine (Br_y) in the stratosphere, which has been measured as BrO and is calculated to contribute significantly to ozone loss over the past decade (see also Chapters 4 and 6). The relative importance, in terms of ozone destruction, of one molecule of Br_y to that of one molecule of Cl_y (defined as α in Chapter 6) varies by more than a factor of 10, depending on the altitude and the absolute amounts of Cl_y present. (When ClO concentrations are high, the ClO-dimer rapidly catalyzes ozone loss and the BrO-ClO cycle is less important; similarly at higher altitudes, the ClO-O reaction dominates. Bromine is relatively most important in the lower stratosphere when ClO levels are less than about 1 ppbv.) Averaging over the lower stratosphere, model results give α ranging from 30 to 120, and we select a value of 40 here to define the free halogen (FH) content of the lower stratosphere (see Table 8-B). Based on observations (see Chapter 6), bromine atoms in the halons and methyl bromide are assumed to be available as stratosphere Br_y, and thus a large part of the halogen-driven destruction of ozone in the lower stratosphere (about 1 ppbv of FH) is due to bromine, predominantly methyl bromide.

The peak chlorine loading is expected to occur between 1995 and 2000 depending on the details of the phaseout of industrial halocarbons. The analysis here pushes the simple model for halogen loading to its limit of credibility, *i.e.*, the model does not include banking of production for later emission and uses a one-year time step. Therefore, we must use these results as a guide to the relative changes in chlorine loading in response to different policy options rather than as a prediction of absolute year-by-year chlorine loading. All of the basic halocarbon scenarios (A, B, and C) show the same peak CL of about 4.13 ppbv, which is 0.05 ppbv greater than Scenario M (absolute global compliance with the protocol, no delays or

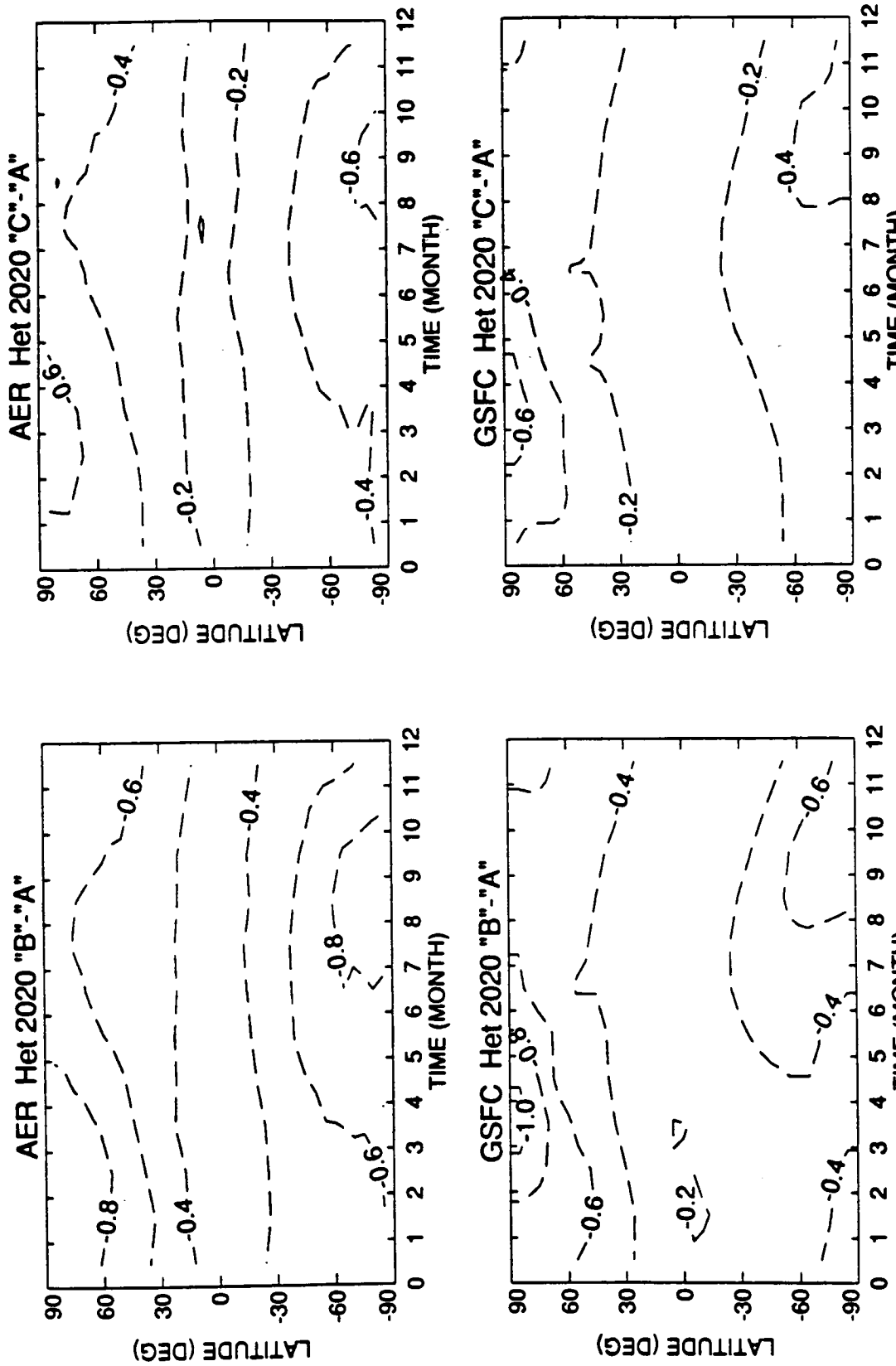

Figure 8-10 Difference in column ozone (percent) between Scenario A, B, & C at 2020 from the AER and GSFC models.

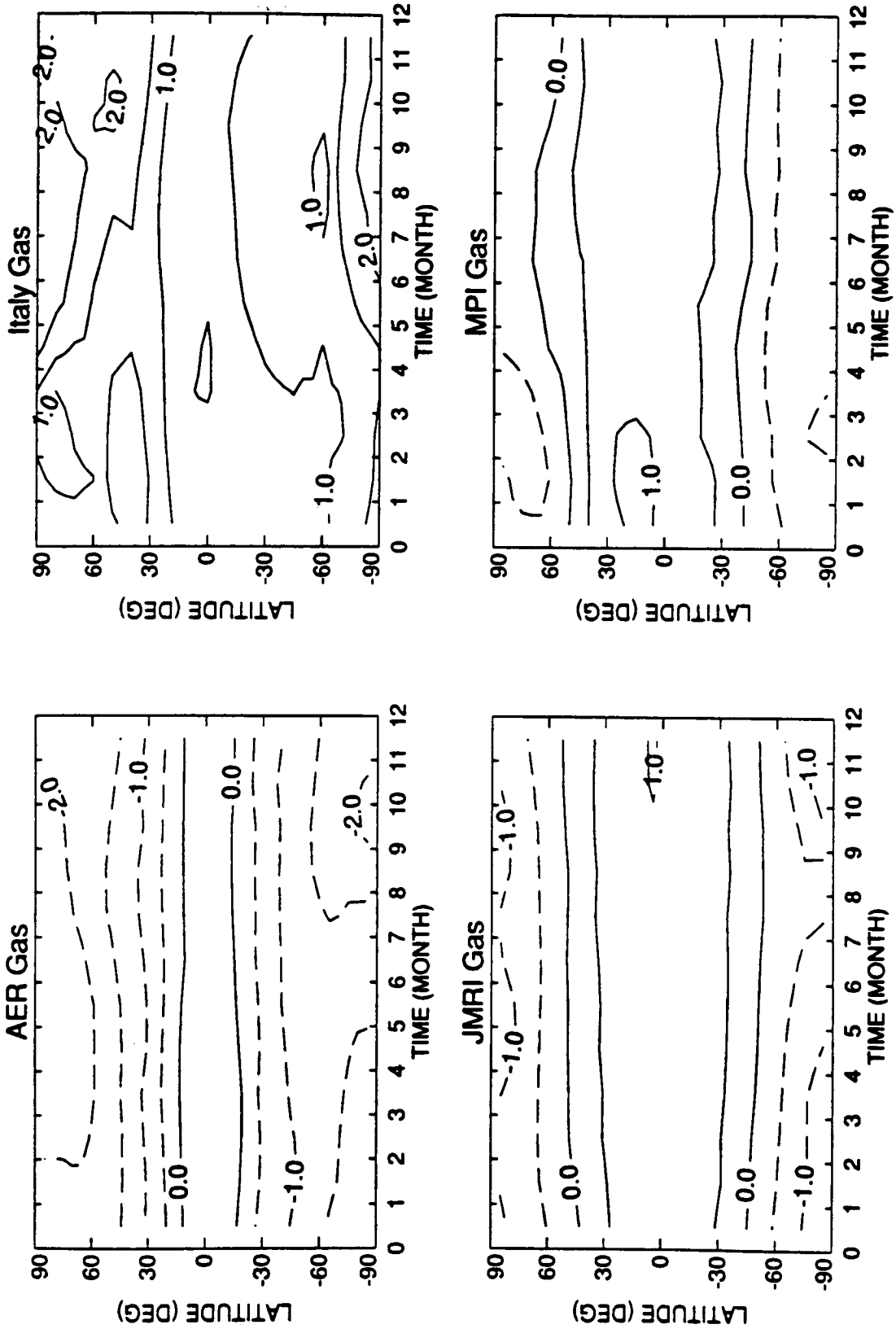

Figure 8-11a Change in column ozone abundances (percent) from 1980 to 2050 based on modeled Scenario A.

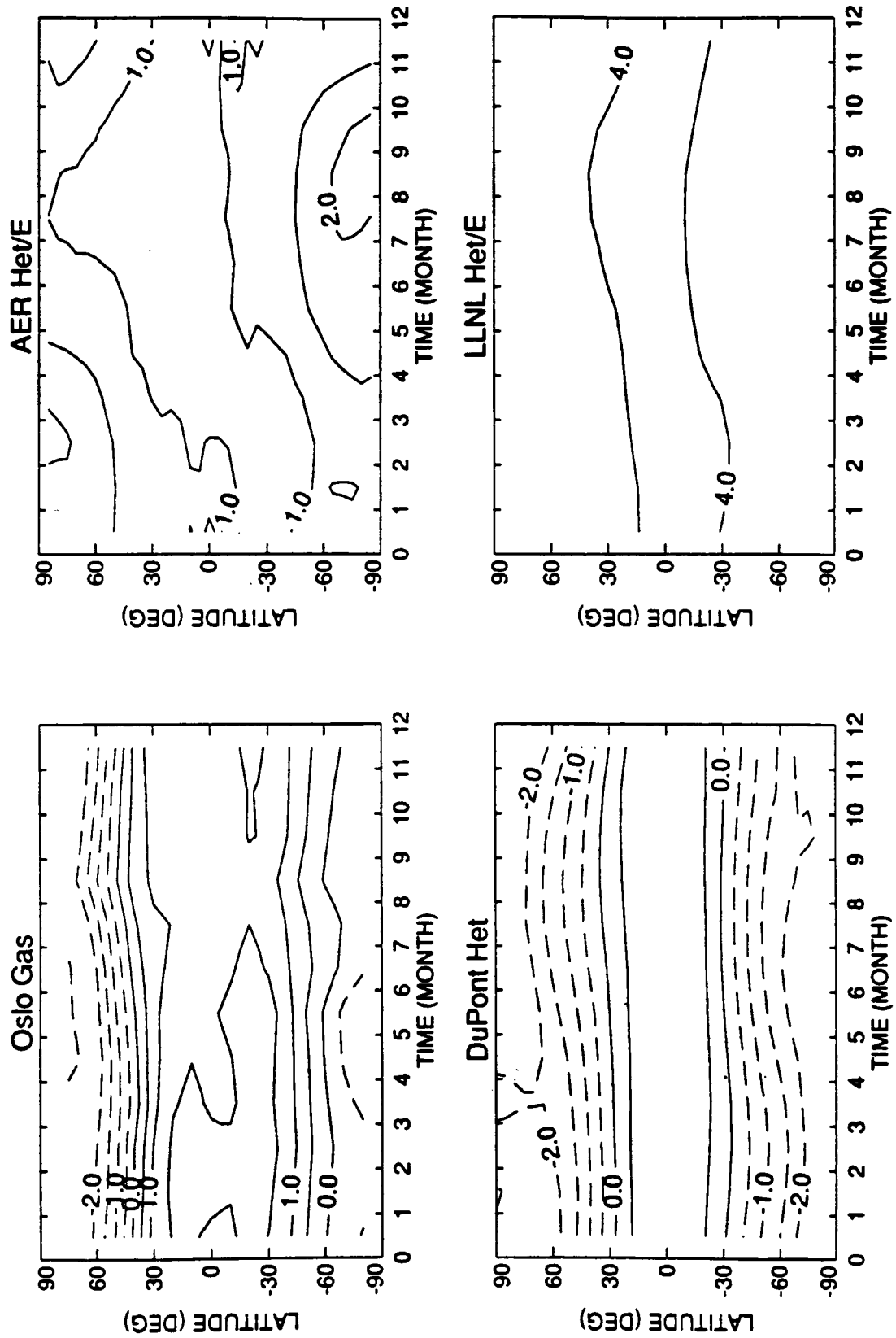

Figure 8-11b Change in column ozone abundances (percent) from 1980 to 2050 based on modeled Scenario A.

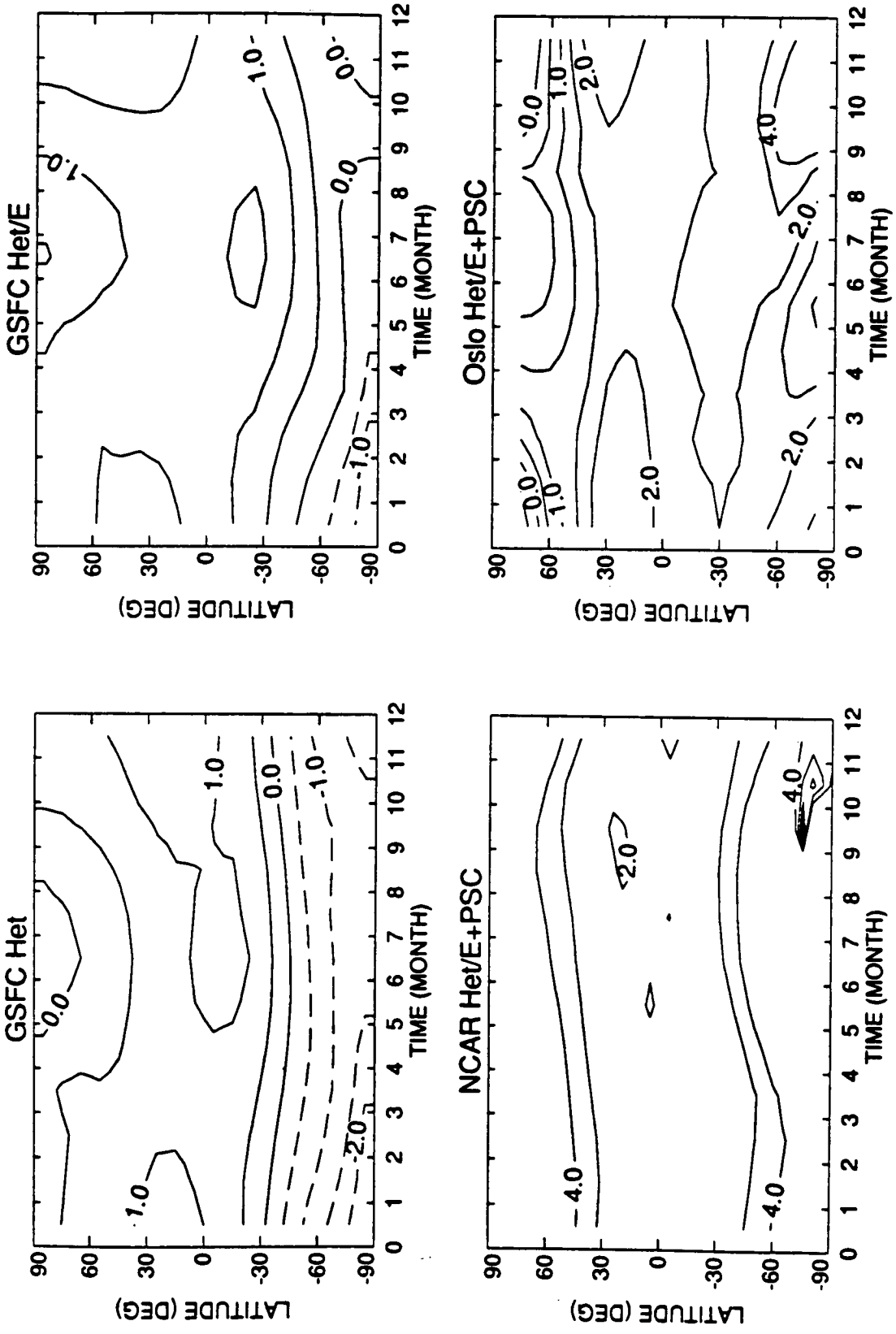

Figure 8-11c Change in column ozone abundances (percent) from 1980 to 2050 based on modeled Scenario A.

substitutions, and eventual phaseout of all chlorinated halocarbons not specifically in the current protocol). A wider variety of options, defined in Table 8-B, is considered here in order to focus on the details of the maximum CL, FC, and FH. The peak CL in the late 1990s may vary over a range of 0.2 ppbv in response to a wide variety of options for halocarbon phaseouts and HCFC substitution. A significant reduction in peak CL (FC and FH also) can be achieved with accelerated phase-out schedules of CFCs, carbon tetrachloride, and methyl chloroform. The times at which CL falls below 3 and 2 ppbv can be shifted by at most 10 years with such an acceleration of the phaseout.

It is important to recognize that the environmental impact of ozone loss, with corresponding enhancement of ultraviolet-B (UVB) exposure, may be cumulative over the years with high ozone depletion. Thus, we define an integral of the chlorine loading (units of ppbv-year) above some threshold as a surrogate for the chronic UVB exposure. The choice of threshold is arbitrary, and a low value such as 1 ppbv would require integration out beyond the 21st century. We focus on the apparently rapid loss of ozone during the 1980s (see Chapter 2), and select 1985 as the threshold year, integrating from 1985 until the values of CL, FC, and FH fall below 3.00, 2.45, and 3.18 ppbv, respectively. The integral CL is more sensitive to the differences between certain policy options: heavy substitution with HCFCs can increase this number by at most 20 percent, whereas accelerated phaseouts can reduce it by as much as 50 percent. Acceleration of the halon phaseout by 3 years would reduce peak bromine loading by 1 pptv (about 4 percent), and thus FH by 0.04 ppbv. Stringent controls on current use of HCFC-22, or on substitution with alternative HCFCs, would not significantly reduce peak chlorine, but would accelerate the decay in chlorine loading in the decades following the peak. Following phaseout of halocarbons, the free chlorine levels drop more rapidly than the chlorine loading because species that contribute most to FC have shorter stratospheric lifetimes (*e.g.*, $CFCl_3$, CCl_4), whereas the longer-lived CFCs have FC/CL ratios much less than 1. Scenarios in Table 8-B show the extreme sensitivity of integral quantities to a range of halocarbon phaseout schedules.

8.5 OPTIONS AND ISSUES TO 2100

These calculations were performed using both the traditional gas phase chemical models and a new heterogeneous formulation that includes the reactions of N_2O_5 and $ClONO_2$ on the background sulfate aerosols. A few models included a parameterization of PSC chemistry, but no agreed-upon approach was taken. Although the new HET models were better able to simulate the recent trends in column ozone over the mid-latitudes, they still do not predict *ab initio* the Antarctic ozone hole. (Furthermore, the current trends might also be explained by an extension of the PSC chemistry mixing to mid-latitudes.) Nevertheless, it is clear from laboratory studies that some form of heterogeneous chemistry on sulfate aerosols should be part of stratospheric models. Based on three-dimensional analysis and model studies (*e.g.*, Lefèvre *et al.*, 1991; Cariolle *et al.*, 1990) it is unlikely that a strictly two-dimensional formalism is adequate to reproduce the chemical processes occurring on PSCs. Zonal asymmetries in PSCs as well as dilution and chemical propagation of O_3 loss from polar regions to mid-latitudes occurs in dimensions and spatial scale not resolved by the current assessment models (*e.g.*, Juckes and McIntyre, 1987; Atkinson *et al.*, 1989; Tuck, 1989; Prather and Jaffe, 1990).

We chose not to examine scenarios for chlorine and bromine loading that continued to increase beyond 4.1 ppbv in 1995. Had we done so, the implications for ozone loss would be severe: the predictions for the year 2000 show that ozone losses may be more than linearly proportional to Cl_y increases, and depletions that were initially limited to the winter pole now extend towards the equator. If halocarbon regulations admit a scenario whereby chlorine increases beyond 5 ppbv, then this assessment must be revisited. It is important to develop a scientifically based measure of cumulative ozone depletion and to relate this to halocarbon loading. In the models and scenarios used here, the impact of bromine increases was not singled out. It appears small, but this may be a major oversight since the greatest effect of Br_y-catalyzed ozone loss would be in PSC chemistry, which we have more difficulty simulating in two-dimensional models.

By the year 2050, we may expect that some residual ozone depletion remains (*e.g.*, the Antarctic

ozone hole, plus some mid-latitude losses), due to chlorine since the tropospheric loading is still expected to exceed 2 ppbv. The model predictions shown here paint a rosier picture by virtue of the choice in trends for N_2O and CH_4 giving predominantly ozone increases relative to the year 1980. One key uncertainty is the importance of N_2O increases: in the AER GAS model, the resulting NO_y increases lead to a 1 to 4 percent additional decrease in column ozone by the year 2050, but in the HET model the impact of N_2O is at most 1 percent. These results point out the importance of the many influences on stratospheric ozone. The greatest uncertainty in predicting ozone in the years 2050 to 2100, providing something like the current Montreal Protocol is in place, will be in predicting the changes in other trace gases (N_2O, CH_4) and climate (CO_2).

REFERENCES

AFEAS, Alternative Fluorocarbon Environmental Acceptability Study, *Scientific Assessment of Stratospheric Ozone: 1989, Vol. II Appendix: AFEAS Report,* Global Ozone Research and Monitoring Project, Report No. 20, World Meteorological Organization, Geneva, 1990.

Atkinson, R.J., W.A. Matthews, P.A. Newman, and R.A. Plumb, Evidence of the middle latitude impact of the Antarctic ozone depletion, *Nature, 340,* 290–293, 1989.

Bruehl, C.P., and P.J. Crutzen, Scenarios of possible changes in atmospheric temperatures and ozone concentrations due to man's activities, estimated with a one-dimensional coupled photochemical climate model, *Climate Dynamics, 2,* 173–203, 1988.

Cariolle, D., A. Lasserre-Bigorry, J F. Royer, and J.F. Geleyn, A general circulation model simulation of the springtime Antarctic ozone decrease and its impact on mid-latitudes, *J. Geophys. Res., 95,* 1883–1898, 1990.

Cunnold, D.M., R.G. Prinn, R.A. Rasmussen, P.G. Simmonds, F.N. Alyea, C.A. Cardelino, A.J. Crawford, P.J. Fraser, and R.D. Rosen, Atmospheric lifetime and annual release estimates for $CFCl_3$ and CF_2Cl_2 from 5 years of data, *J. Geophys. Res., 91,* 10797–10817, 1986.

DeMore, W.B., S.P. Sander, R.F. Hampson, M.J. Kurylo, D.M. Golden, C.J. Howard, A.R. Ravishankara, and M.J. Molina, Chemical kinetics and photochemical data for use in stratospheric models, *JPL Publ. 90–1,* 1990.

Derwent, R.G., and A. Volz-Thomas, The tropospheric lifetimes of halocarbons and their reactions with OH radicals: an assessment based on the concentration of ^{14}CO, in *Alternative Fluorocarbon Environmental Acceptability Study, Scientific Assessment of Stratospheric Ozone: 1989, vol. II, Appendix,* Global Ozone Research and Monitoring Project, Rep. 20, 125–146, World Meteorological Organization, 1990.

Douglass, A.R., C.H. Jackman, and R.S. Stolarski, Comparison of model results transporting the odd nitrogen family with results transporting separate odd nitrogen species, *J. Geophys. Res., 94,* 9862–9872, 1989.

Hofmann, D.J., and S. Solomon, Ozone destruction through heterogeneous chemistry following the eruption of El Chichón, *J. Geophys. Res. 94,* 5029–5041, 1989.

Holton, J.R., On the global exchange of mass between the stratosphere and troposphere, *J. Atmos. Sci, 47,* 392–395, 1990.

IPCC, Intergovernmental Panel on Climate Change, J.T. Houghton, G.J. Jenkins and J.J. Ephraums, eds., *Climate Change: The IPCC Scientific Assessment,* 365 pp., U. Cambridge Press, 1990.

Isaksen, I.S.A., B. Rognerud, F. Stordal, F. Coffey, and W.G. Mankin, Studies of arctic stratospheric ozone in a 2D model including some effects of zonal asymmetries, *Geophys. Res. Lett., 17,* 557–560, 1990.

Jackman, C.H., R.K. Seals Jr., and M.J. Prather, eds., 2D Intercomparison of stratospheric models, *NASA Conference Publication,* CP–3042, 608 pp, 1989a.

Jackman, C.H., A.R. Douglass, P.D. Guthrie, and R.S. Stolarksi, The sensitivity of total ozone and ozone perturbation scenarios in a 2D model due to dynamical inputs, *J. Geophys. Res., 94,* 9873–9887, 1989b.

Jackman, C.H., A.R. Douglass, R.B. Rood, R.D. McPeters, and P.E. Meade, Effect of solar proton events on the middle atmosphere during the past two solar cycles as computed using a 2D model, *J. Geophys. Res., 95,* 7417–7428, 1990.

Juckes, M.N., and M.E. McIntyre, A high-resolution one-layer model of breaking planetary waves in the stratosphere, *Nature, 328,* 590–596, 1987.

Ko, M.K.W., N.D. Sze, M. Livshits, M.B. McElroy, and J.A. Pyle, The seasonal and latitudinal behaviour of trace gases and O_3 as simulated by a 2D model of the atmosphere, *J. Atmos. Sci., 41,* 2381–2408, 1984.

Ko, M.K.W., K.K. Tung, D.K. Weisenstein, and N.D. Sze, A zonal mean model of stratospheric tracer transport in isentropic coordinates: numerical simulations for nitrous oxide and nitric acid, *J. Geophys. Res., 90,* 2313–2329, 1985.

Ko, M.K.W., N.D. Sze, and D.K. Weisenstein, The roles of dynamical and chemical processess in determining the stratospheric concentration of ozone in 1D and 2D models, *J. Geophys. Res., 94,* 9889–9896, 1989.

Krecov, G., and S. Zvenigorodsky, Optical models of the Middle Atmosphere, Ac.Sci.Publ. Nauka, 345 pp., 1990.

Lefèvre, F., D. Cariolle, S. Muller, and F. Karcher, Total ozone from the TIROS operational vertical sounder during the formation of the 1987 "ozone hole," *J. Geophys. Res., 96,* 12893–12911, 1991.

Mahlman, J.D., H. Levy II, and W.J. Moxim, Three-dimensional tracer structure and behavior as simulated in two ozone precursor experiments, *J. Atmos. Sci., 37,* 655–685, 1980.

Montreal Protocol on Substances that Deplete the Ozone Layer, Final Act, UNEP, 1987, revised 1990, London.

Penkett, S.A., B.M.R. Jones, M.J. Rycroft, and D.A. Simmons, An interhemispheric comparison of the concentration of bromine compounds in the atmosphere, *Nature, 318,* 550–553, 1985.

Pitari, G., and G. Visconti, Two-dimensional tracer transport: derivation of residual mean circulation and eddy transport tensor from a three-dimensional model data set, *J. Geophys. Res., 90,* 8019, 1985.

Pitari, G., and G. Visconti, Ozone trend in the Northern Hemisphere: a numerical study, *J. Geophys. Res., 96,* 10931–10940, 1991.

Pitari, G., G. Visconti, and V. Rizi, Sensitivity of stratospheric ozone to heterogeneous chemistry on sulfate aerosols, *Geophys. Res. Lett., 18,* 833–836, 1991.

Prather, M.J., M.B. McElroy, and S.C. Wofsy, Reductions in ozone at high concentrations of stratospheric halogens, *Nature, 312,* 227–231, 1984.

Prather, M.J., and C. M. Spivakovsky, Tropospheric OH and the lifetimes of hydrochlorofluorocarbons (HCFCs), *J. Geophys. Res., 95,* 18723–18729, 1990.

Prather, M., and A. Jaffe, Global impact of the Antarctic ozone hole: chemical propagation, *J. Geophys. Res., 95,* 3473–3492, 1990.

Prather, M.J., and R. T. Watson, Stratospheric ozone depletion and future levels of atmospheric chlorine and bromine, *Nature, 334,* 729–734, 1990.

Prinn, R., D. Cunnold, R. Rasmussen, P. Simmonds, F. Alyea, A. Crawford, P. Fraser, and R. Rosen, Atmospheric trends in methyl chloroform and the global average for the hydroxyl radical, *Science, 238,* 946–950, 1987.

Prinn, R., D. Cunnold, P. Simmonds, F. Alyea, R. Boldi, A. Crawford, P. Fraser, D. Gutzler, D. Hartley, R. Rosen, and R. Rasmussen, Global average concentration and trend for hydroxyl radicals deduced from ALE/GAGE trichloroethane (methyl chloroform) data for 1978–1990, *J. Geophys. Res., 97,* 2445–2461, 1992.

Rodriguez, J.M., K. W. Ko, and N. D. Sze, Role of heterogeneous conversion of N_2O_5 on sulphate aerosols in global ozone losses, *Nature, 352,* 134–137, 1991.

Schmidt, U., and A. Khedim, *In situ* measurements of CO_2 in the winter Arctic vortex and at the middle latitude s: an indicator of the 'age' of stratospheric air, *Geophys. Res. Lett., 18,* 763–766, 1991.

Schmidt, U., R. Bauer, A. Khedim, E. Klein, G. Kulessa, and C. Schiller, Profile observations of long-lived trace gases in the Arctic Vortex, *Geophys. Res. Lett., 18,* 767–770, 1991.

Spivakovsky, C.M., S.C. Wofsy and M.J. Prather, A numerical method for parameterization of atmospheric photochemistry: computation of tropospheric OH, *J. Geophys. Res., 95,* 18433–18439, 1990.

Stordal, F., I.S.A. Isaksen, and K. Horntveth, A diabasic circulation 2D model with photochemistry: simulations of ozone and long-lived tracers with surface sources, *J. Geophys. Res., 90,* 5757–5776, 1985.

Tolbert, M.A., M.J. Rossi, and D.M Golden, Heterogeneous interactions of $ClONO_2$, HCl and HNO_3 with sulfuric acid surfaces at stratospheric temperatures, *Geophys. Res. Lett., 15,* 847–850, 1988.

Tuck, A.F., Synoptic and chemical evolution of the Antarctic vortex in late winter and early spring, 1987, *J. Geophys. Res., 94,* 11687–11737, 1989.

WMO, *Report of the International Ozone Trends Panel: 1988,* Global Ozone Research and Monitoring Project, Report No. 18, World Meteorological Organization, 1990b.

WMO, *Scientific Assessment of Stratospheric Ozone: 1989, Vol. I,* Global Ozone Research and Monitoring Project, Report No. 20, World Meteorological Organization, 1990b.

CHAPTER 9

Predicted Aircraft Effects on Stratospheric Ozone

Authors:

M.K.W. Ko
D. Kley
S. Wofsy
E. Zhadin

Additional Contributors:

C. Johnson
M. Prather
D. Weisenstein
D.J. Wuebbles

Chapter 9

Predicted Aircraft Effects on Stratospheric Ozone

Contents

SCIENTIFIC SUMMARY

Engine emissions from subsonic and supersonic aircraft include oxides of nitrogen (NO_x), water vapor, unburned hydrocarbons, carbon monoxide, carbon dioxide, and sulfur dioxide. Addition of NO_x to the atmosphere is expected to decrease ozone in the stratosphere and increase ozone in the troposphere. Resulting changes in ozone, water vapor, and aerosol loading in the altitudes around the tropopause may have a climatic impact since the response of radiative forcing to changes in concentrations is most sensitive here.

The first step in assessing these effects is to determine quantitatively the changes in background concentrations associated with emitted gases and aerosols. Most of the emissions from the projected supersonic fleet as well as one-quarter to one-half of the emissions from the subsonic fleet are deposited directly into the lower stratosphere, to be redistributed by large-scale transport. Current models cannot accurately simulate the accumulation of emitted materials in the stratosphere and their eventual removal, as much of the injection is close to the tropopause. Model predictions in this chapter are based on simulations from two-dimensional models that assume that the emitted material is zonally mixed. The impact of flight corridor effects on the predictions has not been assessed.

The current fleet of subsonic aircraft may be sufficiently large to have increased background concentrations of NO_x, ozone and the sulfate layer. Gas phase modeling studies predict that the current subsonic aircraft fleet (injection of 2 $Tg(NO_2)$/year) contributes to 5–10 percent of the total amount of ozone in the troposphere around 40°N. These models also predict a decrease in ozone in the lower stratosphere of less than 1 percent. Projected increases in the subsonic fleet could lead to further increases of tropospheric ozone with associated changes in OH and additional (although still small) reduction of ozone in the stratosphere. These estimates are subject to considerable uncertainties due to uncertainties in the magnitude and distribution of emissions and to differences among models. The role of heterogeneous chemical processes in the troposphere needs to be assessed.

The additional impact on ozone from projected fleets of supersonic aircraft [high-speed civil transports (HSCT)] operating in the year 2015 (cruise altitudes around 15, 19, and 22 km) has been examined by a model intercomparison exercise using gas phase models. With the operation of aircraft assumed to be concentrated in the Northern Hemisphere, the largest decrease in local ozone is found poleward of 30°N around the cruise altitude. There is very little increase in upper tropospheric ozone due to HSCT alone because of the reduced ozone flux from the stratosphere. For cruise altitudes below 28 km, the calculated decrease in column abundance of ozone is larger for higher cruise altitudes and larger NO_2 emission indices. The calculated decrease in the Southern Hemisphere is typically a factor of 2 to 3 smaller than that in the Northern Hemisphere. In one of the cases (a fleet of aircraft flying Mach 3.2 between 21 and 24 km with NO_2 emission index of 15 and annual fuel use of 70 Tg per year), the calculated decrease in ozone column abundance at northern mid-latitudes ranges from 7 percent to 12 percent. This spread in model results increases with decreasing cruise altitude and reflects differences in transport and photochemical balance in the various models. In the Mach 2.4 case (cruise altitude of 17-20 km), the range of model-calculated decreases in column abundance in the same region is 2 to 6 percent.

Heterogeneous reactions occurring on polar stratospheric clouds (PSCs) or the global sulfate aerosol layer have a large impact on the ozone chemistry in the lower stratosphere, and hence, the predicted response to supersonic aircraft. If N_2O_5 is converted to HNO_3 via known heterogeneous reactions on the global sulfate layer, the column changes for the Mach 2.4 case from two of the models are calculated to be small (–0.5 to +0.5 percent). At the same time, there is an increase in upper tropospheric ozone of about 5 percent due to HSCT alone. Nevertheless, there could be large and unpredictable changes in ozone if emissions from the aircraft cause enhanced formation of PSCs or increases in the sulfate aerosol loading, leading to repartitioning of the chlorine species and higher concentrations of ClO.

9.1 INTRODUCTION

The possibility that the current fleet of subsonic aircraft may already have caused detectable changes in both the troposphere and stratosphere has raised concerns about the impact of such operation on stratospheric ozone and climate. Recent interest in the operation of supersonic aircraft in the lower stratosphere has heightened such concerns. Previous assessments of impacts from proposed supersonic aircraft have been based mostly on one-dimensional model results although a limited number of multidimensional models were used (CIAP, 1974; COMESA, 1975; COVOS, 1976; Sundararaman, 1984). In the past 15 years, our understanding of the processes that control the atmospheric concentrations of trace gases has changed dramatically (WMO, 1986; WMO, 1990). This better understanding has been achieved through accumulation of kinetic data and field observations as well as development of new models. It would be beneficial to start examining the impact of subsonic aircraft to identify opportunities to study and validate the mechanisms that have been proposed to explain the ozone responses.

The two major concerns are the potential for a decrease in the column abundance of ozone leading to an increase in ultraviolet radiation at the ground, and redistribution of ozone in the lower stratosphere and upper troposphere leading to changes in the Earth's climate. Two-dimensional models (as discussed in Chapters 6 and 8) have been used extensively for ozone assessment studies, with a focus on responses to chlorine perturbations. There are problems specific to the aircraft issues that are not adequately addressed by the current models. This chapter reviews the current status of the research on aircraft impact on ozone with emphasis on immediate model improvements necessary for extending our understanding. The discussion will be limited to current and projected commercial aircraft that are equipped with air-breathing engines using conventional jet fuel. The impacts are discussed in terms of the anticipated fuel use at cruise altitude.

9.2 IMPACT OF AIRCRAFT OPERATION ON ATMOSPHERIC TRACE GASES

Various materials are introduced into the atmosphere associated with the operation of aircraft. Such operation can perturb the ambient concentrations of atmospheric trace gases either by direct injection of specific trace gases (such as H_2O and oxides of nitrogen) or through photochemical reactions of the injected material (such as impact on ozone from injected oxides of nitrogen and nonmethane hydrocarbons). Current analysis indicates that engine effluents have the largest relative impacts while contributions from leakage of fluids (hydraulic and sanitation), fuel dump, chipped paint, and erosion of other components are apparently trivial (see Chapter 2, HSRP [1992]).

9.2.1 Emission Indices

Emissions from engine types are specified in terms of the emission index (EI) for each material, defined as grams emitted per kilogram of fuel burned. Typical EI values for various materials are summarized in Table 9-1. The amount of H_2O and CO_2 emitted associated with fuel combustion are determined by stoichiochemistry with minor variations depending on the saturation of the fuel. Emissions associated with incomplete combustion (CO, unburned hydrocarbons) depend on engine design and operating conditions. Additional emissions such as sulfur and trace metals may come from impurities in the fuel and are conserved during the combustion process. The emitted material that has the largest impact on ozone is oxides of nitrogen (NO_x = NO + NO_2), which are produced predominantly from the reaction of N_2 and O_2 at high temperature in the combustion chamber. NO_x in the engine effluent is typically 85 percent NO and 15 percent NO_2. There has been some confusion on the definition of EI(NO_x) as tailpipe emission for NO has been reported sometimes as mass of NO_2 equivalent without explicitly stating so. The EI for NO_x is defined here in terms of grams of NO_2 equivalent emitted, *i.e.*, 46 gm times the total number of moles of NO plus NO_2 emitted per kilogram of fuel burned. The large range of values quoted for CO, HC, and NO_x in Table 9-1 is mainly caused by different power settings during take off, climb, cruise, and descent. It is interesting to note that the evolution of engine design (more efficient, cleaner burning, high-temperature combustion) in the past decades has decreased EIs for CO and hydrocarbons and increased EI(NO_x).

Table 9-1 Emission index (grams per kilograms of fuel used) of various materials for subsonic and supersonic aircraft for cruise condition. Values in parenthesis are ranges for different engines and operating conditions.

Species [gm molecular weight]	Subsonic Aircraft* Short-Range	Subsonic Aircraft* Long-Range	Supersonic Aircraft†
CO_2 [44]	3160	3160	3160
H_2O [18]	1230	1230	1230
CO [28]	5.9 (0.2-14)	3.3 (0.2–14)	1.5 (1.2–3.0)
HC as methane [16]	0.9 (0.12-4.6)	0.56 (.12–4.6)	0.2 (0.02–0.5)
SO_2 [64]	1.1	1.1	1.0
NO_x as NO_2 [46]	9.3 (6-19)	14.4 (6–19)	Depends on design (5–45)

*Mean (fuel-consumption weighted) emission indices for 1987 based on Boeing (1990). The values were calculated from a data base containing emission indices and fuel consumptions by aircraft types. The difference between short-range (cruise altitude around 8 km) and long-range (cruise altitude between 10 and 11 km) reflects different mixes of aircraft used for different flights.

†Based on Boeing (1990) and Douglas (1990).

9.2.2 Estimates of Perturbations to Background Concentrations

The extent to which the background concentration of a particular trace gas is perturbed by direct injection from aircraft can be obtained by comparing the injection rate with the local budget of the trace gas (*i.e.*, *in situ* photochemical production rate and transport divergence) in the region. The expected increase in concentration is related to the injection rate by the local residence time of the species. For a relatively inert gas injected into the lower stratosphere near the tropopause, the residence time in the stratosphere is about 1 year. If the material is deposited farther away from the tropopause, the residence time is closer to 2 years. Residence time in the upper troposphere is expected to be shorter (1–3 weeks) because of more efficient vertical overturning. Strat-trop exchange also plays an important role in this case because material injected in the tropical upper troposphere could be transported to the stratosphere where the residence time is much longer.

Although estimates exist for the annual mass exchange between the troposphere and the stratosphere, there are large uncertainties concerning the processes responsible for the exchange process (See review in Chapter 5, WMO [1986]). It is particularly important to understand those processes for aircraft operations because specific flight corridors could be adjusted systematically according to local meteorological conditions. For instance, the transverse circulation thought to be associated with jet streams (Krishnamurti, 1961; Mahlman, 1973) would imply downward motion on the cyclonic (poleward) side of the jet core. This would imply that material deposited poleward of the jet core would have shorter residence time than material injected equatorward of the jet core.

The residence time in the lower stratosphere (estimated to be about 1 year) is long enough for the emitted NO_x to be repartitioned to other forms of total odd nitrogen (NO_y) species as dictated by the local conditions. Thus, the NO_x emitted in the stratosphere could be treated as NO_y in model simulations. In contrast, NO_x deposited in the troposphere will remain as NO_x during the 1–3 weeks it stays in the atmosphere. Given the ambient concentrations of various trace gases in the atmosphere, values from Table 9-1 imply that the perturbation on a percentage basis is largest for NO_y and H_2O in the stratosphere. Emitted NO_x is also expected to have a large impact in the upper troposphere. Although any unburned HC may form a large local source of a specific hydrocarbon, its effect on atmospheric chemical cycles is small compared to CH_4.

Recently, Hofmann (1990) suggested that the stratospheric sulfate burden may have been increasing by 5 percent per year in the last decade.

Hofmann (1991) pointed out that fuel use from subsonic aircraft has also increased at the same rate during that period, suggestive that sulfur emission from aircraft engines could be a cause. Estimates based on EI for sulfur are not inconsistent with such a suggestion. However, tests of such ideas must await more careful studies incorporating microphysics of aerosol growth that can translate sulfur emissions to changes in sulfate loading. At present, the budget of the stratospheric sulfate layer is not well understood. Various theoretical estimates suggested that 8×10^7 kg of sulphur per year is needed to sustain the sulfate layer under background (nonvolcanic) conditions. The EI for SO_2 given in Table 9-1 would imply that fuel use in the stratosphere over 10^{11} kg/year would be important (>50 percent) if all the sulfur were deposited in the stratosphere. However, it should be noted that the value cited in Table 9-1 is an upper limit based on fuel standards for engines. Actual sulfur content in the fuel is expected to be smaller since industry prefers low-sulfur fuel, which is less corrosive to the engines.

Other products from engine combustion include carbon soot particles and condensation nuclei (CN). The number of CN has been estimated to be 2–4 x 10^8 particles per kilogram of fuel used (Douglas, 1989). Whether this may lead to additional formation of aerosol particles or polar stratospheric clouds is unclear since such processes are not well understood. It is believed that addition of carbon soot (light-absorbing) particles may also change the optical properties of the atmosphere.

9.3 MODEL STUDIES OF OZONE RESPONSE

As pointed out by Johnston (1971) and Crutzen (1971), increases in the stratospheric concentration of NO_x from engine effluent will lead to an increase in the NO_x-catalyzed ozone removal by the reactions:

$$\begin{aligned} &NO + O_3 \rightarrow NO_2 + O_2 \\ &\underline{NO_2 + O \rightarrow NO + O_2.} \\ &O + O_3 \rightarrow 2O_2, \text{ catalyzed by } NO_x \end{aligned} \qquad (9\text{-}1)$$

However, increases in NO_x may also affect other chemical cycles, leading sometimes to compensating effects. In the troposphere, the increases in NO_x will enhance the following reactions:

$$\begin{aligned} &NO + RO_2^{\cdot} \rightarrow NO_2 + RO \\ &NO_2 + h\nu \rightarrow NO + O \\ &\underline{O + O_2 \rightarrow O_3} \\ &RO_2 + O_2 \rightarrow RO + O_3, \text{ catalyzed by } NO_x \text{ and by } HO_x \text{ and by photons} \end{aligned} \qquad (9\text{-}2)$$

leading to net ozone production. (See Chapter 5 for a more detailed discussion.)

The exact response of ozone depends on the detailed balance of the competing chemical cycles and transport in different regions of the atmosphere. This is one reason why a multidimensional model is necessary for a realistic assessment of the ozone impact. Most of the results presented in this chapter are based on results from two-dimensional models discussed in Chapters 6 and 8 of this report. In interpreting these results, one must be aware of uncertainties normally associated with these models as well as additional points that are specific to the aircraft problem (see reviews by Douglass *et al.*, 1991; Johnston *et al.*, 1991). These are :

- Since the injection is very close to the tropopause, the results are particularly sensitive to how strat-trop exchange is treated in the models. This has not been a major focus of previous efforts in two-dimensional model development.
- Once the engine effluent is deposited along the flight path, it is subject to mesoscale transport before it becomes zonally mixed. In addition, with emissions concentrated at heavily-traveled flight corridors, the emitted material may retain zonally asymmetric features. Questions can be raised whether current two-dimensional models can adequately simulate these effects.
- The response of ozone to emitted NO_x will change if heterogeneous chemistry is occurring. Furthermore, H_2O and NO_x emissions may promote formation of polar stratospheric clouds that activate chlorine-catalyzed ozone depletion. Sulfur emission may lead to enhancement of the sulfate layer. These changes may cause repartitioning of the existing chemical species in the atmosphere and result in a change in ozone unrelated to other injected chemicals.

9.4 EFFECT OF SUBSONIC AIRCRAFT ON OZONE

We will restrict the review to the 10–12 km region near the extratropical tropopause where the emissions from cruising subsonic fleet are expected to have the largest impact. The effect in the lower tro-

posphere is more difficult to predict because of the much larger variabilities in both local conditions and emissions from the aircraft during ascent and descent.

9.4.1 Latitudinal Distribution of Flight Operations and Fuel Use

The current flight scenario was estimated in the Boeing report (Boeing, 1990) based on the 1987 Official Airline Guide (OAG) (see also Chapter 4 in HSRP [1992]). The OAG contains published commercial jetliner flights with the exception of the domestic former Soviet Union, Eastern Europe, and Chinese flights. Short-range travel (< 400 miles) was assumed to occur around altitudes of ≈26,600 ft (8 km). All long-range flight traffic was assumed to occur around 33,000 to 37,000 ft (10 to 11.2 km). The latitudinal distributions of fuel burned are shown in Figure 9-1 for latitudinal bands of 10°. Note that 93 percent of the long-range cruise occurs in the Northern Hemisphere.

Based on the 1987 OAG, the Boeing report estimated the figures for fuel burned for the 1987 fleet to be 1.14 x 10^{10} kg/year for the short-range cruise and 7.24 x 10^{10} kg/year for the long-range cruise. The world consumption of aviation fuel in 1987 was 15.3 x 10^{10} kg (International Energy Annual, 1988). Nuesser and Schmitt (1990) reported a figure of 15.0 x 10^{10} kg for 1988 based on ICAO statistics and information supplied by Lufthansa. Therefore, the Boeing report accounts only for 53 percent of all aviation fuel burned in 1987. HSRP (1992) has estimated that aviation in the former Soviet Union and Eastern Europe could account for 12 percent of the world total, China for 2 percent, and U.S. military and private jet use for 7 percent each. The remaining 19 percent of the world jet fuel usage could be assigned to the sum of charter, cargo, and turboprop aircraft. For comparison, 11 percent of the German Lufthansa fleet fuel consumption was used for cargo flights in 1988 (Reichow, 1990).

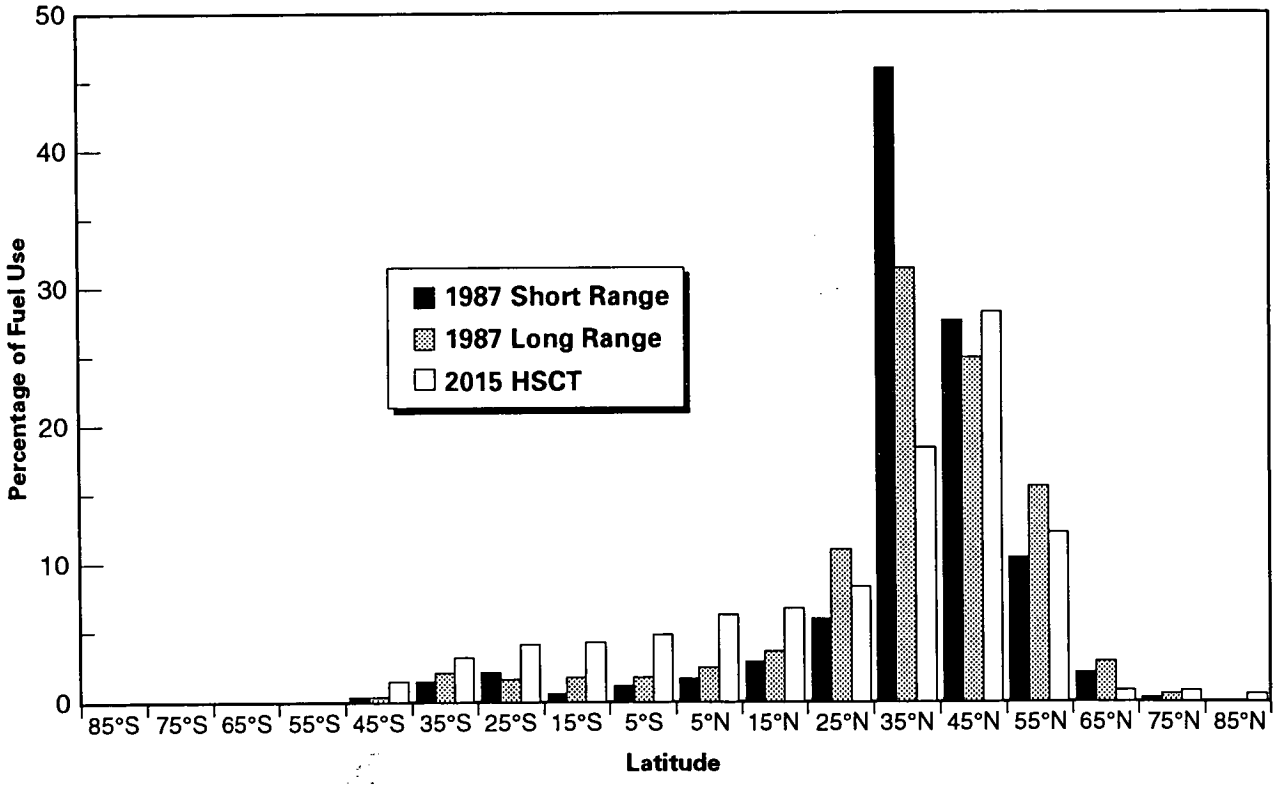

Figure 9-1 Fractional distribution of fuel use as a function of latitude band for 1987 commercial jet air traffic and projected 2015 HSCT aircraft. The fractional distributions sum to 100 percent for each of the three cases.

Table 9-2 Estimates of percentage of fuel burn in the stratosphere for the subsonic fleet.

Month	Cruise Altitude = 10 km		Cruise Altitude = 11 km	
	Latitude of tropopause *λ_T at 10 km (°N)	Portion of Northern Hemisphere fuel burn that occurs in the stratosphere (percent)	Latitude of tropopause *λ_T at 11 km (°N)	Portion of Northern Hemisphere fuel burn that occurs in the stratosphere (percent)
January	38	56	33	72
February	42	41	33	72
March	43	40	34	72
April	46	27	35	72
May	47	26	40	56
June	55	16	45	40
July	65	2	55	16
August	65	2	55	16
September	64	2	50	26
October	58	8	45	40
November	52	16	45	40
December	49	27	40	56
Annual†		22		48

*Based on atmospheric cross sections for the year 1980 (Danielsen *et al.*, 1983).
†Assume same fuel burn for each month

9.4.2 Allocation of Fuel-Related Emission to Troposphere and Stratosphere

The cruise altitude, 10–11 km, is within the stratosphere during certain times of the year. Table 9-2 gives the values for the latitude (λ_T) in the Northern Hemisphere where the tropopause is below and above the cruising altitude to the north and south of λ_T, respectively. Also given is the percent of fuel burned in the Northern Hemisphere that occurs in the stratosphere based on the fuel use distribution given in Figure 9-1. Table 9-2 reveals that, over the course of a full year, 22 and 48 percent of the 1987 Northern Hemisphere fuel burn occurs in the stratosphere for a cruise altitude of 10 and 11 km, respectively. This corresponds to an injection of about 0.2 to 0.5 x 10^9 kg(NO_2) in the Northern Hemisphere stratosphere. The result illustrates that the estimates critically depend on the assumed cruise altitude. A recent case study reported by Schumann and Reinhardt (1991) utilized actual flight paths and tropopause heights along the flight paths as determined by a numerical weather prediction model to calculate the fraction of the time spent in the stratosphere by the flights between Frankfurt and New York in December 1990 and June 1991. The results show that the time fraction depends on actual flight routing designed to avoid the jet stream. Future analysis should take into account these routing practices.

9.4.3 Estimates of Impact on Ozone

9.4.3.1 Impact on Stratosphere

Since part of the flight operation actually occurs within the stratosphere, stratospheric NO_x can be perturbed by materials directly deposited in the stratosphere as well as transport of engine effluents deposited in the tropical troposphere. The amount of NO_x transported from the troposphere is estimated to be small and confined to tropical and subtropical latitudes. Previous work of Ko *et al.* (1986) used a two-dimensional zonal mean model to estimate the bulk transport of lightning-generated NO_x to the lower stratosphere. Results from the same model indicate that the current subsonic fleet may have increased the NO_y concentrations in the lower stratosphere in the Northern Hemisphere by 0.5 ppbv. It is unclear whether measurements can detect an interhemispheric NO_y difference of 0.5 ppbv in the lower stratosphere and ascribe it to specific causes. One may expect a hemispherical asymmetry (with more NO_y

and H_2O in the Northern Hemisphere) to result from the export of denitrified and dehydrated air from the Antarctic ozone hole. Results from the Ko *et al.*, model and from Wuebbles and Kinnison (1990) show that the effect on ozone is small with a decrease in local ozone of less than 1 percent. Clearly, these results can only be considered as rough estimates, as two-dimensional models have limited utility in the description of the small scale features of strat-trop exchange as evident from the fact that they are not capable of accurately modeling the observed water vapor concentration in the lower tropical and subtropical stratosphere.

9.4.3.2 Impact on the Troposphere

The impact of aircraft emissions on the troposphere is to increase the NO_x content of the upper troposphere and to change the ozone concentration. Since ozone production in the current atmosphere is believed to be NO_x-limited, the effect of NO_x emissions is to enhance the ozone concentration.

Kley *et al.* (1981) measured the altitude distribution of NO_x in the upper troposphere and showed that input of NO_x from the stratosphere plus aircraft emissions are large enough to produce the observed increase with altitude of NO_x. Ehhalt *et al.* (1992) have compared measured profiles of NO with NO_x profiles that were calculated based on emission from ground-based and aircraft sources plus natural sources using a simple two-dimensional model. Figure 9-2 shows their measured NO data that were obtained during quasi-meridional flights close to the east coast of North America and to the west coast of Europe. Based on $EI(NO_x) = 10$, they concluded that 30–40 percent of the present-day tropospheric NO_x between 6 and 10 km at northern mid-latitudes results from aircraft emissions. Their figure would increase to 45–60 percent if the values for EIs from Table 9-1 are used.

The effect of aircraft on tropospheric ozone was addressed by Hidalgo and Crutzen (1977), Liu *et al.* (1980), Isaksen (1980), and Derwent (1982). More recent studies include work by Crutzen and Bruehl (1990), Wuebbles and Kinnison (1990), Beck *et al.* (1992), and Johnson and Henshaw (1991). Although the amount of NO_x emissions from aircraft is small compared to surface NO_x emission, the effect on tropospheric ozone and global warming is significant because the amount of ozone produced per unit emission is some 20 times larger for aircraft emission than surface emission, and the change in ozone occurs at altitudes of maximum radiative response (Johnson *et al.*, 1992).

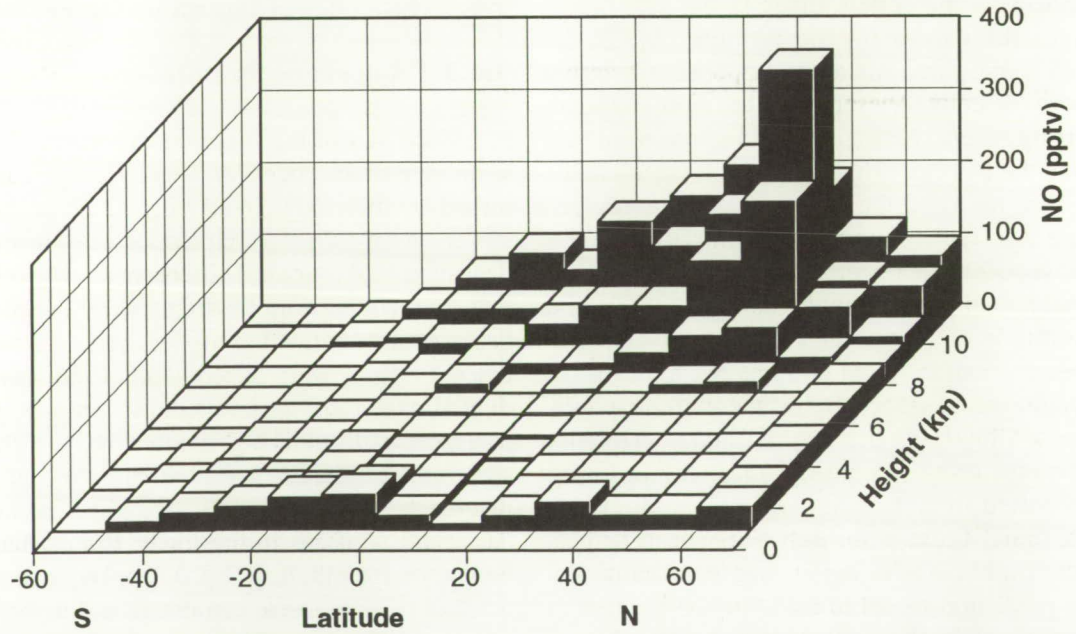

Figure 9-2 Observed distribution of NO from quasi-meridional flights close to the east coast of North America and to the west coast of Europe. The results are reported in Ehhalt *et al.* (1992).

Typical model results indicate that local ozone increases of 3–12 percent between 8 and 12 km for NO_x injections of 1.5–2.0 x 10^9 kg of NO_2 per year. There are associated changes to OH and other species. There has been no concerted effort to understand the differences among the models and there are considerable differences in the distribution of the emissions with height and latitude. Current research effort is being directed to improve the quality of the emissions data base. Finally, the role of heterogeneous reactions in the troposphere has not been explored.

9.5 EFFECT OF SUPERSONIC AIRCRAFT ON OZONE

There are several recent studies of the effects of high-speed aircraft (Johnston *et al.*, 1989; Ko *et al.*, 1991). It is difficult to compare the results since the emission scenarios are different in each study. The High Speed Research Program (HSRP) from National Aeronautics and Space Administration (NASA) organized a model intercomparison workshop in which the modelers were asked to use the same input to perform the simulations. The discussion in this section is based on the results of that workshop. The reader is referred to the workshop report (HSRP, 1992) for additional information.

As an assessment, the result presented here is necessarily interim. These model calculations should be viewed more as sensitivity studies, primarily designed to serve the following purposes:

- Identify parameters that are needed to characterize the ozone response,
- Allow for intercomparison of model predictions,
- Focus on the range of fleet operations and engine specifications giving minimal environmental impact, and
- Provide the basis for future assessment studies.

The basic scenarios were chosen to be as realistic as possible using available information on anticipated technology. They are not to be interpreted as a commitment or goal for environmental acceptability.

It should be emphasized that the calculations reported in HSRP (1992) are performed using gas-phase chemistry only. Heterogeneous chemistry occurring on the global sulfate layer (Weisenstein *et al.*, 1991) and the PSCs is expected to modify the results in a significant way. These effects could be further enhanced if there is an increase in aerosol loading or occurrence of PSCs due to the operation of the HSCT.

9.5.1 Parameters That Affect the Calculated Ozone Response

9.5.1.1 Emission Scenarios

For two-dimensional models that simulate the zonal mean (averaged over longitude) distributions of the trace gases, one must specify the distributions of the emitted materials as functions of latitude, height, and season. The calculations were performed for supersonic fleets with cruise fuel use of 70 x 10^9 kg/year. This corresponds to a realistic fleet of approximately 500 or more aircraft that represents an economically feasible size for the HSCT fleet. Fuel use during takeoff, climb, and descent was ignored in these calculations. The adopted latitudinal distribution of fuel use is given in Figure 9-1. Detailed distribution for any specific fleet will of course depend on flight routes, anticipated demands between city pairs, and routing to avoid sonic booms over land. The chosen distribution is based on two independent studies that take into account each of these concerns (Boeing, 1989, 1990; Douglas, 1989, 1990).

The fuel use is distributed according to projected flight paths and the emitted materials are assumed to be deposited along the flight paths. No adjustment is made to account for the vertical and meridional transport of the plume that may occur in the first few weeks before the emitted material becomes zonally mixed. Aircraft with particular cruise speeds (Mach numbers) operate most efficiently at specific altitudes. The adopted pressure-altitude ranges for each Mach number are 14–17 km for Mach 1.6 cruise, 17–20 km for Mach 2.4 cruise and 21–24 km for Mach 3.2 cruise. The assigned spread in altitude is in accord with possible traffic control and the natural climb of cruise altitudes towards the end of a trip as the fuel is being used up. Fuel use and emissions are assumed to be uniform throughout the year.

The emission indices for various engine effluents were discussed in Table 9-1. Recent modeling results (Johnston *et al.*, 1989; Ko *et al.*, 1991; Wuebbles and

Kinnison, 1990) showed that the main impact on ozone is due to the total amount of NO_x emitted and the altitude of injection. For fixed fuel use, the amount of NO_x emitted is related to the EI(NO_x). The Mach number (*i.e.* altitude of injection) and the EI for NO_x are used as the only two independent parameters in the HSRP scenarios, which represent cases with cruise speeds of Mach 3.2, 2.4, and 1.6, and selected cases with EI(NO_x) ranging from 5 to 45.

9.5.1.2 Background Atmosphere

The predicted HSCT fleet could be fully operational only by about the year 2015 when atmospheric concentrations of several trace gases are expected to be different from what they are today. It was decided that the calculations should be performed relative to a background atmosphere for the year 2015. (See Chapter 8 for a description of the typical 2015 atmosphere.) It is assumed that there will be no reduction in the subsonic fleet with the introduction of the supersonic fleet. Thus, the impact of the supersonic fleet will be compared to the baseline atmosphere that includes a projected subsonic fleet (which is twice the present fleet size) operating in the 2015 background atmosphere.

9.5.2 Model Results Using Gas Phase Chemistry

The modeling groups that participated in the intercomparison are:

AER:	Atmospheric and Environmental Research Inc., M. Ko and D. Weisenstein
GSFC:	NASA Goddard Space Flight Center, C. Jackman, A. Douglass, and K. Brueske
LLNL:	Lawrence Livermore National Laboratory, D. Wuebbles and D. Kinnison
NCAR:	National Center for Atmospheric Research, G. Brasseur
CAMED-P:	University of Cambridge, University of Edinburgh, J. Pyle, R. Harwood, and A. Jones
Oslo:	University of Oslo, I. Isaksen, F. Stordal.

The procedure for this intercomparison assessment made use of the infrastructure set up for previous model intercomparison workshops (see Jackman *et al.*, 1989). Model results were collected in digital format at the Upper Atmosphere Data Program (UADP) at NASA Langley to facilitate comparisons.

Except for the CAMED-P model, the transport circulation and temperatures in the models are fixed so that the effects of dynamical feedbacks are ignored. Changes in O_3 are responses to modifications in the chemical removal rates resulting from aircraft emissions. This, to first order, should be related to the amount of injected NO_y retained in the atmosphere at steady state. Typical residence time of the injected materials depends on the altitude of injection and ranges from 1.7 to 2.6 years for Mach 3.2 injection, 1.1 to 1.5 years for Mach 2.4 injections, and 0.5 to 0.8 years for Mach 1.6 injection. Note that a large residence time implies that the emitted NO_y is retained in the stratosphere for a longer period of time so that more NO_y will be added to the stratosphere at steady state for a particular emission rate. As a result, more O_3 will be removed for the same emission. For instance, the calculated decrease in ozone at northern mid-latitudes for EI (NO_x) = 15 ranges from 7–12 percent for the Mach 3.2 case, as compared with 2–6 percent for the Mach 2.4 case. The residence time could also depend on the time of the year the emissions occur and the actual three-dimensional nature of the flight path. Neither of these is considered in the results discussed here.

The calculated changes in column ozone and in local ozone are shown in Figures 9-3 and 9-4 for the case with Mach 2.4 and EI(NO_x) = 15. The calculated perturbations in global ozone content are summarized in Table 9-3. The following observations can be made about the results:

- The calculated impacts on O_3 are greater for larger EI and higher cruise altitudes. This result applies to all models.
- The magnitudes of the calculated O_3 changes can differ from model to model by significant amounts. The calculated changes in global content differ by a factor of 1.5 for Mach 3.2 cruise, factor of 4 for Mach 2.4 cruise. For the Mach 1.6 case, the calculated ozone responses range from no impact to a decrease of 0.7 percent for EI = 15.
- All models showed large decreases in the region north of 30°N between 10 and 25 km where most of the NO_x emissions are deposited.
- The extent to which the lower stratosphere in the Southern Hemisphere is affected in each

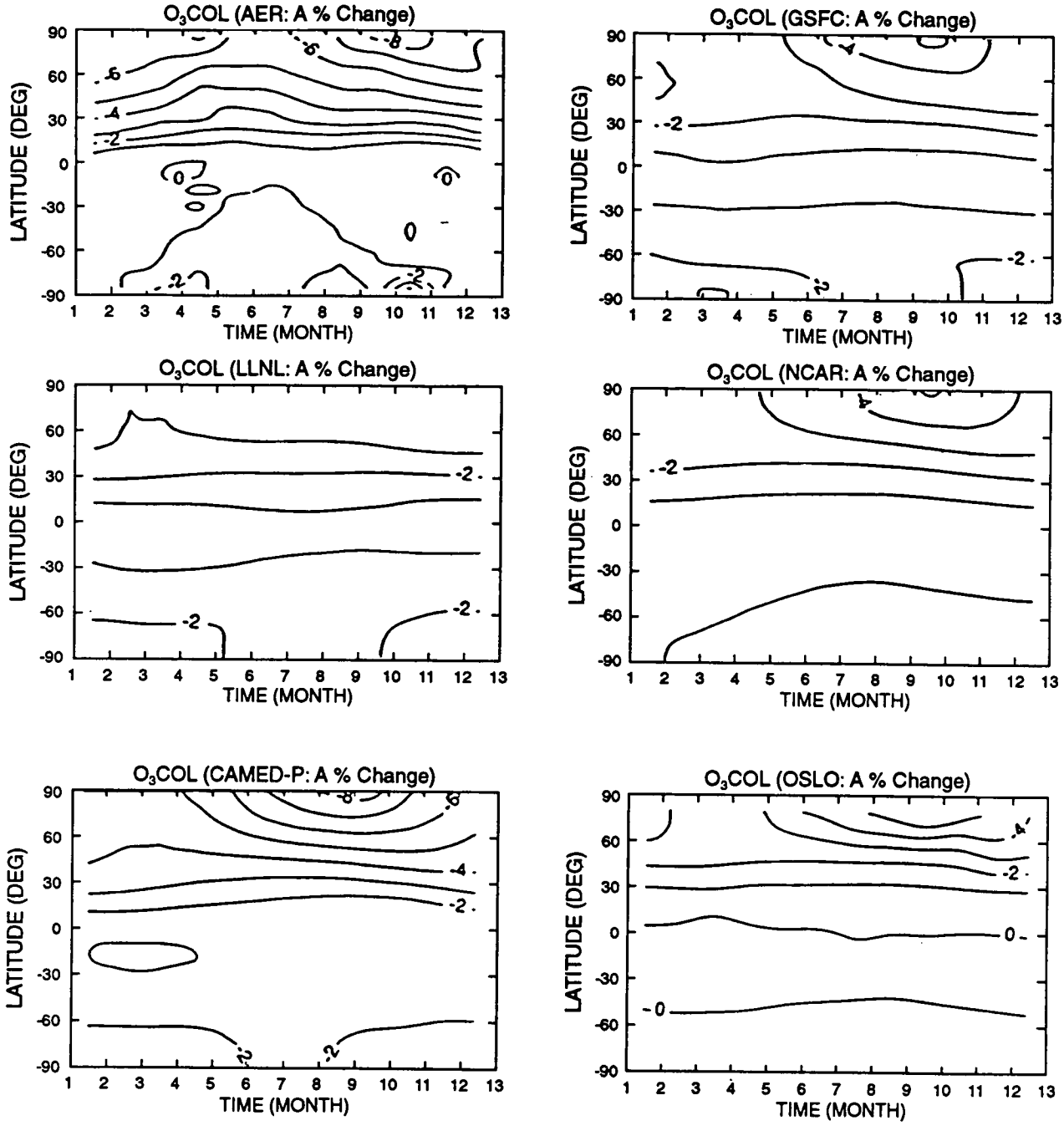

Figure 9-3 Calculated percent changes in the column abundances of O_3 as functions of latitude and season for a fleet of Mach 2.4 supersonic aircraft with $EI(NO_x)$ = 15. The annual fuel use is 70 x 10^9 kg/year. The latitudinal distribution of fuel use is given in Figure 9-1. The percent change is calculated relative to a 2015 atmosphere with a subsonic fleet. The contour interval is one percent.

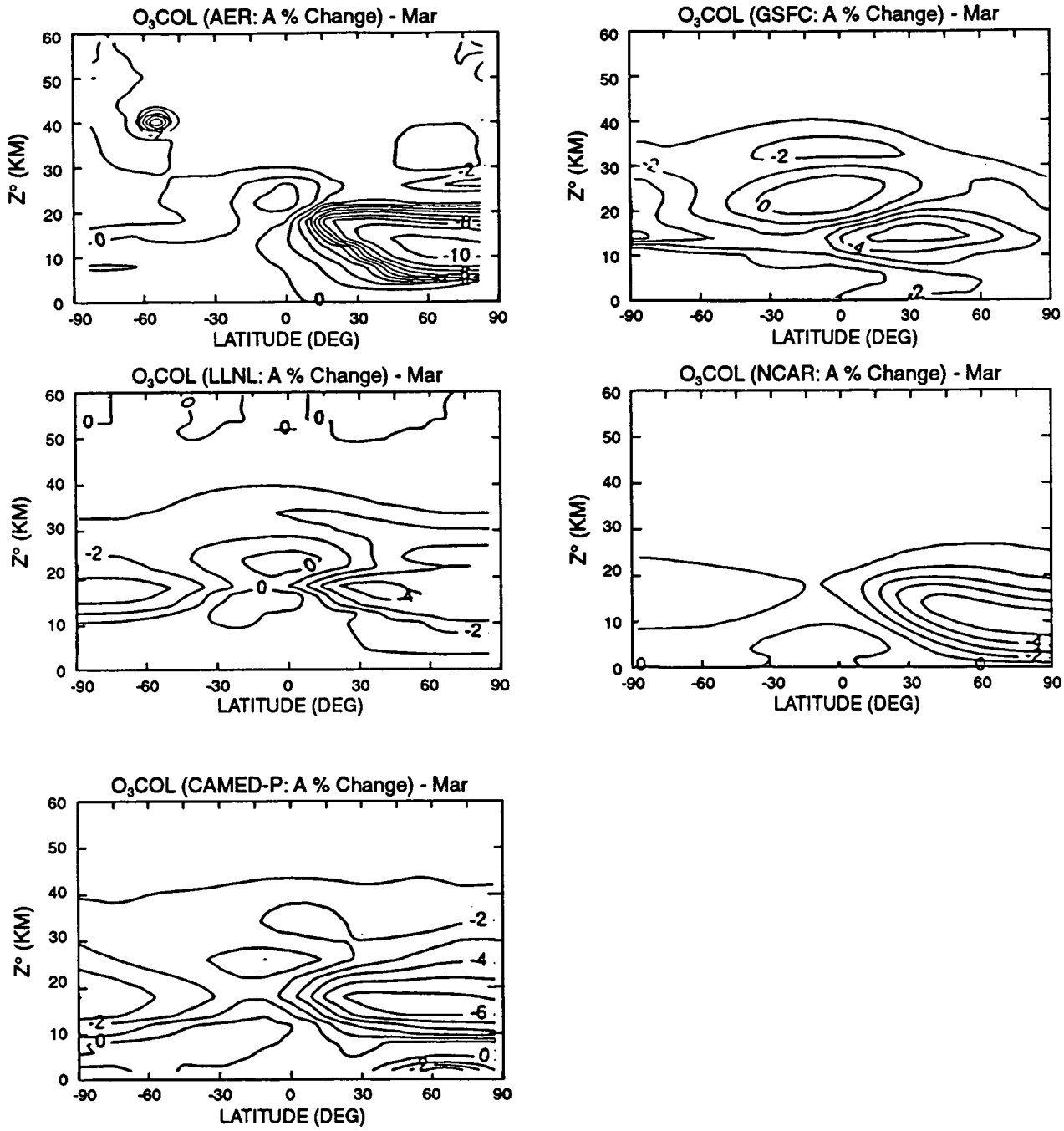

Figure 9-4 Calculated percent changes in the local concentration of O_3 as functions of latitude and height for a fleet of Mach 2.4 supersonic aircraft with $EI(NO_x) = 15$. The annual fuel use is 70 x 10^9 kg/year. The latitudinal distribution of fuel use is given in Figure 9-1. The percent change is calculated relative to a 2015 atmosphere with a subsonic fleet. The contour interval is one percent.

Table 9-3 Calculated percent decrease in annual average of global O_3 content.

	EI = 5			EI = 15			EI = 45
Mach Number	3.2	2.4	1.6	3.2	2.4	1.6	2.4
AER	1.2	0.61	0.11	4.3	2.1	0.40	7.5
CAMED-P				5.3	2.5	0.72	
GSFC	1.2	0.50	0.20	4.1	1.7	0.67	5.9
LLNL	0.9	0.50	0.085	3.4	1.7	0.29	6.1
NCAR	0.78	0.31	0.14	3.5	1.4	0.62	4.7
Oslo	1.2	0.15	0.01	4.1	0.72	.002	3.5

model is related to how efficiently NO_y is transported to the Southern Hemisphere.

- The sensitivity of the ozone response is related to the residence time of injected NO_x.
- The sensitivity of the ozone response to changes in NO_x in the lower stratosphere is different in different models as evident from the fact that the ozone changes normalized by changes in NO_x are different.
- Although changes of ozone in the upper troposphere contribute little to changes in column abundance, such a redistribution could have important implications for the radiative balance in the stratosphere.

9.5.3 Heterogeneous Chemistry in the Atmosphere

The O_3 responses to increases in NO_x shown in the previous section were calculated assuming gas phase reactions only. Heterogeneous reactions occurring on PSCs and on the global sulfate aerosol layer (see Chapters 3 and 4) are likely to change these responses in a significant way. In contrast to the case with chlorine perturbation, where heterogeneous reactions will enhance the ozone depletion, including heterogeneous reactions in the HSCT model calculations will actually give smaller ozone decreases due to NO_x increases. Figure 9-5 shows the change in ozone from the AER

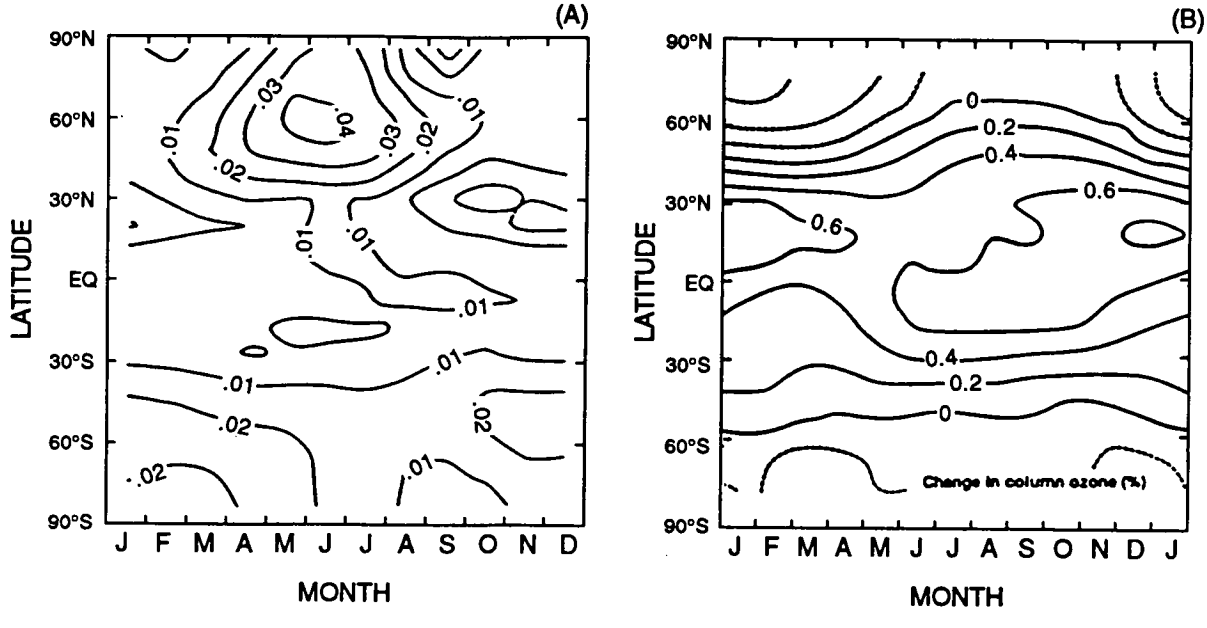

Figure 9-5 Percent changes in column abundance of O_3 calculated with the reaction $N_2O_5 + H_2O$ (aerosol) $\rightarrow$ $2HNO_3$ included. The emission scenario is exactly the same as those described in Figure 9-3. Panel A-result from AER model (Weisenstein *et al.*, 1991) Panel B-result from LLNL model using the lower limit parameterization (see Chapter 8). Note that the parameterization of aerosol collision frequency is not the same in the two models.

model (Weisenstein *et al.*, 1991) and LLNL model, (Wuebbles, private communication) calculated using the same scenario as in Figure 9-3 except that the reaction $N_2O_5 + H_2O \rightarrow 2HNO_3$ is assumed to occur on the global sulfate layer. Note that the calculated ozone change is greatly reduced compared to the results shown in Figure 9-3.

The altered response of ozone to NO_x injection with heterogeneous chemistry included can be explained by changes in the relative contributions of the catalytic cycles to ozone removal (Weisenstein *et al.*, 1991). These cycles involve NO_x, Cl_x, HO_x, O_x, and Br_x radical species. The NO_x cycle accounts for more than half of the ozone loss in both winter and summer with gas phase chemistry only. The effect of the heterogeneous reaction $N_2O_5 + H_2O \rightarrow 2HNO_3$ is to repartition the odd nitrogen family, resulting in NO_x concentrations which are reduced by 80 percent in winter and 40 percent in summer between 10 and 20 km at mid and high latitudes as compared with gas phase-only calculations. Thus the ozone loss due to the NO_x cycle becomes a much smaller fraction of the total ozone loss. Increases in OH and ClO due to inclusion of the heterogeneous reaction cause the contributions from the HO_x and Cl_x cycles to nearly double.

Addition of nitrogen oxides from HSCT emissions results in a 20–30 percent increase in the NO_x cycle with or without the $N_2O_5 + H_2O$ reaction. However, the ozone response is much less sensitive to the NO_x increase with heterogeneous chemistry included because of the reduced role of NO_x in regulating total ozone loss. Furthermore, an increase in the NO_x concentration will enhance the concentration of $ClONO_2$, HNO_3, and HO_2NO_2 and thus reduce the Cl_x and HO_x catalytic destruction of ozone. Depending on the background levels of Cl_x and HO_x and the overall rate of the $N_2O_5 + H_2O$ reaction, HSCT emissions can even result in small ozone increases.

The rates for many heterogeneous reactions have been measured in the laboratory (see Chapter 3). There is no reason to exclude these reactions in model simulations. However, whether they actually occur in the atmosphere and whether there are other significant heterogeneous reactions occurring on aerosol particles are unresolved issues. A concerted campaign of atmospheric measurements of radical species should help to elucidate the role of heterogeneous reactions occurring on aerosol particles and on PSCs in the lower stratosphere where HSCT aircraft will fly.

9.5.4 Future Research

The analysis reported in the HSRP (1992, Chapter 5) suggests that the difference among the model-predicted ozone responses can be understood in terms of the residence time for the injected NO_x and O_3 response sensitivity factor peculiar to each model. One must look for observations in the present atmosphere that can help define these quantities and predict how they may change. Future research should emphasize model developments and acquisition of kinetic data to better define model input and field data for model validation. Specific emphases should be given to the following issues (see also review by Johnston *et al.*, 1991 Douglass *et al.*, 1991).

9.5.4.1 Stratospheric-Tropospheric Exchange

The issue of stratospheric-tropospheric exchange is important for determining the residence time for the injected material and how they are redistributed. Changes in ozone concentration near the tropopause are particularly sensitive to the changes in NO_x in the same region. The ^{14}C data from atmospheric nuclear tests seem ideally suited for deriving stratospheric residence times for comparison with model results (Johnston *et al.*, 1976; Johnston, 1989). Analyses using two-dimensional models has been reported by Shia *et al.* (1989), Jackman *et al.* (1991) and Kinnison *et al.* (1991). Other data such as ^{238}Pu and ^{90}Sr may also be useful (see *e.g.*, Telegadas and List, 1969). Analysis of data for H_2O, O_3, and NO_y near the tropopause may provide clues for the actual mechanisms responsible for the troposphere-stratosphere exchange rate.

9.5.4.2 Ozone Budget in the Lower Stratosphere

To get a handle on the O_3 sensitivity, one can make use of measurement programs that are designed to provide simultaneous observations of many species [such as Atmospheric Trace Molecule Spectroscopy Experiment (ATMOS), balloon measurement campaigns, and aircraft campaigns] to provide directly measured or derived concentrations for the radical

species to define the local chemical removal rates for ozone for the present-day atmosphere. Getting a handle on the removal rate by transport is much more difficult. Application of the data assimilation technique to derive transport wind fields from observations may serve as a starting point for deriving transport fluxes of O_3 in the lower stratosphere.

9.5.4.3 Plume Dispersion and Plume Chemistry

The source function for the emitted materials used in the calculations is assumed to have the same latitude-height distribution as the flight paths, and the chemical composition is assumed to be identical to that of the emission at the tail pipe. Plume subsidence and subsequent dispersion in the first few weeks before the emitted materials become zonally mixed could provide an effective distribution of sources that differs from the flight paths. Chemical transformation, occurring homogeneously and heterogeneously, may alter the composition of the materials.

The possibility that the emitted material may not be well mixed zonally raised the question of the importance of the proper treatment of nonlinear chemistry (Tuck, 1979) and chemical eddies (Pyle and Rogers, 1980). Recent results from Zhadin and Bromberg (1991) showed their treatment of chemical eddies resulted in a decrease in calculated ozone loss due to more efficient removal of NO_x in the lower stratosphere. Resolution of this issue may have to await results from three-dimensional model simulations.

9.5.4.4 Effects of Sulfur and Particulates

One must also consider the possibility that operation of the HSCT may increase the loading and size distribution in the sulfate layer through emissions of sulfur and particulates. The possible climate effects from the change in radiative properties must be considered in conjunction with the effects from ozone redistribution.

9.5.4.5 Effects of PSCs and Coupling to Chlorine Chemistry

The saturation temperature for the formation of PSCs is a direct function of the local concentration of HNO_3 and water vapor (see discussion in Chapter 3). Injection of NO_y and H_2O by HSCT could promote formation of PSCs. A recent study by Peter *et al.* (1991) estimated that there could be a significant increase in the occurrence of type-I and type-II PSCs in the polar region. However, our ability to model PSCs to provide quantitative predictions of future effects remains extremely limited. How this may enhance the ozone removal by the chlorine cycle needs to be investigated.

REFERENCES

Beck J.P., C.E. Reeves, C.A.A.M. deLeeuw, and S.A. Penkett, The effect of aircraft emissions on tropospheric ozone in the Northern Hemisphere, *Atmos. Environment, 26A*, 17-19, 1992.

Boeing Commercial Airplanes, *High-Speed Civil Transport Study, Summary*, NASA Contractor Report 4234, Boeing Commercial Airplanes, New Airplane Development, 1989.

Boeing Commercial Airplane Group, *High-Speed Civil Transport Study, Special Factors*, NASA Contractor Report 181881, National Aeronautics and Space Administration, Langley Research Center, Hampton, Virginia, 1990.

CIAP, *Report of Findings: The Effects of Stratospheric Pollution by Aircraft*, DOT–TSC–75–50, Climatic Impact Assessment Program, U.S. Department of Transportation, Washington, D.C., 1974.

COMESA, *The Report of the Committee on Meteorological Effects of Stratospheric Aircraft*, U.K. Meteorological Office, Bracknell, England, 1975.

COVOS, *Comite d'Etudes sur les Consequences des Vols Stratospheriques, Activities*, Societe Meteorologique de France, Boulogne, France, 1976.

Crutzen, P.J., and C. Bruehl, The atmospheric chemical effects of aircraft operations, in *Air Traffic and the Environment- Background Tendencies and Potential Global Atmospheric Effects*, pp. 96–106, edited by U. Schumann, Springer Verlag, Berlin, 1990.

Crutzen, P.J., Ozone production rates in an oxygen, hydrogen, nitrogen oxide atmosphere, *J.Geophys. Res., 76*, 7311–7327, 1971.

Danielsen, E.F., S.E. Gaines and R.S. Hipskind, *An atlas of objectively analyzed atmospheric cross*

sections 1973–1980, NASA Ames Research Center, 1983.

Derwent, R.G., Two-dimensional model studies of the impact of aircraft exhaust emissions on tropospheric ozone, *Atmos. Environment, 16*, 1997–2007, 1982.

Douglas Aircraft Company, *Study of High-Speed Civil Transport*. NASA Contractor Report 4235, Douglas Aircraft, Company, New Commercial Programs, 1989.

Douglas Aircraft Company, *Procedure for Generating Global Atmospheric Engine Emissions Data from Future Supersonic Transport Aircraft*, NASA Contractor Report 181882, National Aeronautics and Space Administration, Langley Research Center, Hampton, Virginia, 1990.

Douglass, A.R., M.A. Carroll, W.B. DeMore, J.R. Holton, I.S.A. Isaksen, H.S. Johnston, and M.K.W. Ko, *The Atmospheric Effects of Stratospheric Aircraft: A Current Consensus*, NASA Reference Publication 1251 National Aeronautics and Space Administration, Office of Management, Scientific and Technical Information Division, 1991.

Ehhalt, D.H., F. Rohrer, and A. Wahner, Sources and distribution of NO_x in the upper troposphere at northern latitudes, *J. Geophys Res. 97*, 3725–3738, 1992.

Hidalgo, H., and P.J. Crutzen, The tropospheric and stratospheric composition perturbed by NO_x emissions of high-altitude aircraft, *J. Geophys. Res., 82*, 5833–5866, 1977.

HSRP, *The atmospheric effects of stratospheric aircraft: A first program report*, High Speed Research Program Annual Review, NASA reference publication, 1272, National Aeronautics and Space Administration, Washington, D.C., 1992.

Hofmann, D.J., Increase in the stratospheric background sulfuric acid aerosol mass in the past 10 years, *Science, 248*, 996–1000, 1990.

Hofmann, D.J., Aircraft Sulfur emission, *Nature, 349*, 659, 1991.

International Energy Annual, Energy Information Admin., U.S. Dept. of Energy Report DOE/EIA-0219, 1988.

Isaksen, I.S.A., *The tropospheric ozone budget and possible man made effects*, Proceedings of the Quadrennial Ozone Symposium, Vol. II (ed. J. London), 845–852, NCAR, Boulder Colorado, 1980.

Jackman, C.H., R.K. Seals, and M.J. Prather, Editors, *Two-Dimensional Intercomparison of Stratospheric Models*, NASA Conference Publication 3042, Proceedings of a workshop (Virginia Beach, VA, Sept. 11–16, 1988) sponsored by the National Aeronautics and Space Administration, Washington, D.C., Upper Atmosphere Theory and Data Analysis, 1989.

Jackman, C.H., A.R. Douglass, K.S. Bruiske, and S.A. Klein, The influence of dynamics on two-dimensional model results: Simulation of ^{14}C and stratospheric aircraft NO_x injection, *J. Geophys. Res., 96*, 22559-22572, 1991.

Johnson, C. and J. Henshaw, The impact of NO_x emissions from tropospheric aircraft, AEA Environment & Energy, AEA–EE–0127, Harwell Laboratory, U.K., 1991.

Johnson, C., J. Henshaw, and G. McInnes, The impact of aircraft NO_x emissions on tropospheric ozone and global warming, *Nature, 355*, 69-71, 1992.

Johnston, H.S., Reduction of stratospheric ozone by nitrogen oxide catalysts from supersonic transport exhaust, *Science, 73*, 517–522, 1971.

Johnston, H.S., Evaluation of excess carbon-14 and strontium-90 data for suitability to test two-dimensional stratospheric models, *J. Geophys. Res., 94*, 18485–18493, 1989.

Johnston, H.S, D. Kattenhorn, and G. Whitten, Use of excess carbon 14 data to calibrate models of stratospheric ozone depletion by supersonic transports, *J. Geophys. Res., 81*, 368-380, 1976.

Johnston, H.S., D.E. Kinnison, and D.J. Wuebbles, Nitrogen oxides from high-altitude aircraft: An update of potential effects on ozone, *J. Geophys. Res., 94*, 16351–16363, 1989.

Johnston, H.S., M.J. Prather, and R.T. Watson, *The Atmospheric Effects of Stratospheric Aircraft: A Topical Review*, NASA Reference Publication 1250, National Aeronautics and Space Administration, Office of Management, Scientific and Technical Information Division, 1991.

Kinnison, D.E., D.J. Wuebbles, and H.S. Johnston, *Two-dimensional model study of atmospheric transport using Carbon-14 and Strontium-90 as*

inert tracers, Lawrence Livermore National Laboratory Report, Livermore, CA, 1991.

Kley, D., J.W. Drummond, M. McFarland, and S.C. Liu, Tropospheric profiles of NO_x, *J. Geophys. Res., 86,* 3153–3161, 1981.

Ko, M.K., D.K. Weisenstein, N.-D. Sze, R.-L. Shia, J.M. Rodriguez, and C. Heisey, *Effects of Engine Emissions from High Speed Civil Transport Aircraft: A Two-Dimensional Modeling Study, Part I and II,* NASA Contractor Report 4346, National Aeronautics and Space Administration, Office of Management, Scientific and Technical Information Division, 1991.

Ko, M.K.W., M.B. McElroy, D.K. Weisenstein, and N.D. Sze, Lightning: A possible source of stratospheric odd nitrogen, *J. Geophys. Res., 91,* 5395–5404, 1986.

Krishnamurti, T.N., The subtropical jet stream of winter, *J. Meteorol., 18,* 172–191, 1961.

Liu, S.C., D. Kley, M. McFarland, J.D. Mahlman, and H. Levy, On the origin of tropospheric ozone, *J. Geophys Res., 85,* 7546–7551, 1980.

Mahlman, J.D., On the maintenance of polar front jet stream, *J. Atmos. Sci., 30,* 544-557, 1973.

Nuesser, H.G., and A. Schmidt, The global distribution of air traffic at high altitudes, related fuel consumption and trends, pp. 1–11, in *Air Traffic and the Environment-Background Tendencies and Potential Global Atmospheric Effects,* pp. 12–22, Proceedings of DLR International Colloquium, Bonn, Germany, November 15–16, 1990, ed. U. Schumann, Springer-Verlag, Berlin, 1990.

Peter, T., C. Bruehl, and P.J. Crutzen, Increase in the PSC-formation probability caused by high-flying aircraft, *Geophys Res Lett., 18,* 1465–1468, 1991.

Pyle, J.A., and C.F. Rogers, Stratospheric transport by stationary planetary waves: The Importance of chemical processes, *Quart. J. Roy. Meteorol. Soc., 106,* 421–446, 1980.

Reichow, H.P., Fuel consumption and emissions of air traffic, in *Air Traffic and the Environment-Background Tendencies and Potential Global Atmospheric Effects, pp.* 12–22, Proceedings of DLR International Colloquium, Bonn, Germany, November 15–16, 1990, ed. U. Schuman, Springer-Verlag, Berlin, 1990.

Sundararaman, N., The High Altitude Pollution Program (1976-1982), FAA-EE-84-10, U.S. Dept. of Transportation, Federal Aviation Administration, Washington, DC, 1984.

Schumann, U., and M.E. Reinhardt, Studies on the effect of high-flying air-traffic on the atmosphere, *42nd Congress of the International Astronautical Federation,* Oct. 5–11, 1991, Montreal, Canada, 1991.

Shia, R.L., Y.L. Yung, M. Allen, R. Zurek, and D. Crisp, Sensitivity study of advection and diffusion coefficients in a two-dimensional stratospheric model using excess Carbon 14 data, *J. Geophys Res., 94,* 18467–18484, 1989.

Telegadas, K. and R.J. List, Are particulate radioactive tracers indicative of stratospheric motions? *J. Geophys. Res., 74,* 1339–1350, 1969.

Tuck, A.F., A comparison of one-two- and three-dimensional model representations of stratospheric gases, *Phil. Trans. Roy. Soc. London, A290,* 477–494, 1979.

Weisenstein, D., M.K.W. Ko, J.M. Rodriguez, and N.D. Sze, Impact of heterogeneous chemistry on model-calculated ozone change due to HSCT Aircraft, *Geophys. Res. Lett, 18,* 1991–1994, 1991.

WMO, *Atmospheric ozone 1985, assessment of our understanding of the processes controlling its present distribution and change.* World Meteorological Organization, Global Ozone Research and Monitoring Project, Report No. 16, 1986.

WMO, *Scientific Assessment of Stratospheric Ozone: 1989,* World Meteorological Organization, Global Ozone Research and Monitoring Project, Report No. 20, 1990.

Wuebbles, D.J., and D.E. Kinnison, Sensitivity of stratospheric ozone to present and future aircraft emissions, in *Air Traffic and the Environment Background Tendencies and Potential Global Atmospheric Effects,* pp. 96–106, ed. U. Schumann, Springer-Verlag, Berlin, 1990.

Zhadin, F.A., and D.V. Bromberg, The numerical assessments of ozone reduction by stratospheric aircraft in the 2-D model including chemical eddies, *J. of Meteorol. and Hydrol.* USSR, in press, 1991.

CHAPTER 10

Predicted Rocket and Shuttle Effects on Stratospheric Ozone

Authors:

R.S. Harwood
C.H. Jackman
I.L. Karol
L.X. Qiu

Additional Contributors:

M.J. Prather
J.A. Pyle

Chapter 10

Predicted Rocket and Shuttle Effects on Stratospheric Ozone

Contents

SCIENTIFIC SUMMARY

The exhaust products of rockets contain many substances capable of destroying ozone. Although there are over a hundred rocket launches per year worldwide, studies so far have only considered the effects of the less frequent launches of the largest rockets. Most attention has focused on the potential reductions in ozone produced by chlorine compounds from solid fuel rockets. Rockets that release or are expected to release relatively large amounts of chlorine per launch into the stratosphere include NASA's Space Shuttle (68 tons) and Titan IV (32 tons) rockets, and European Space Agency's (ESA's) Ariane–5 (57 tons).

Within a few kilometers of the exhaust trail of these rockets, local ozone may be reduced by as much as 80 percent at some heights for up to 3 hours. Since the rocket trajectory is slanted, the corresponding column ozone loss is computed to be reduced over an area of order of a few hundred square kilometers, but the depletion nowhere exceeds 10 percent. A satellite study of column ozone loss associated with several NASA Space Shuttle launches failed to detect any depletion. Local effects of similar magnitude may also be produced by the NO_x emitted by the Soviet Energy rocket. Recovery of the ozone in the wake is computed to be rapid in all cases. All but a fraction of a percent is predicted to be restored within 24 hours.

The stratospheric chlorine input from a NASA launch rate scenario of nine Space Shuttles and six Titan IV rockets per year is computed to be less than 0.25 percent of the annual stratospheric chlorine source from halocarbons in the present-day atmosphere. If the annual background source from halocarbons is reduced and/or the launch rate increases, the fractional contribution will become larger.

Steady-state model computations using the NASA scenario show increases in the middle to upper stratospheric chlorine amounts by a maximum of about 10 pptv (about 0.3 percent of a 3.3 to 3.5 ppbv background) in the northern middle and high latitudes. Independent steady-state model computations of the effect of 10 ESA Ariane–5 launches per year yield comparable maximum values, but at all latitudes. For both scenarios, corresponding decreases in ozone are computed to be less than 0.2 percent locally in the region of maximum chlorine increase, leading to changes in column ozone of much less than 0.1 percent.

It is not yet possible to quantify with confidence the effects of particulates from the exhausts, principally of Al_2O_3 from the solid-fueled rockets. However, simple steady-state estimates using the NASA scenario suggest increases of the chemically active area of stratospheric aerosols of less than 0.1 percent, so the long-term global impact is likely to be negligible.

10.1—INTRODUCTION

The major chemical effluents of either solid- or liquid-fueled rockets that can potentially perturb stratospheric ozone include chlorine compounds (HCl), nitrogen compounds (NO_x), and hydrogen compounds (H_2 and H_2O). Radicals (Cl, ClO, H, OH, HO_2, NO, and NO_2) formed directly or indirectly from rocket exhaust can cause the catalytic destruction of ozone. Other exhaust compounds that could presumably lead to ozone destruction either by direct reaction with ozone or by providing a surface for heterogeneous processes include the particulates Al_2O_3, ice, and soot.

The possible impact of the exhausts of solid-fuel rockets on the ozone layer was recognized first in the early 1970s when possible effects of supersonic civilian aircraft were also first postulated. Accordingly, they were considered as part of the Climatic Impact Assessment Program (see Hoshizaki, 1975). At that time the effects of the Space Shuttle exhausts were considered to be small; model computations led to the conclusion that (with a launch rate of 60 Space Shuttles per year) the total ozone concentrations would be reduced by about 0.25 percent in the Northern Hemisphere and by about 0.025–0.05 percent in the Southern Hemisphere with an uncertainty of about a factor of three (Potter *et al.*, 1978). Since that study, there has been new knowledge of the chemical reaction rates and changing perceptions of the role of homogeneous and heterogeneous chemical reactions. Accordingly, in this chapter we review more recent assessments. No one has yet studied the effects of the totality of launches, but the effects of the launches of the larger rockets have been assessed by Prather *et al.* (1990a,b), Karol *et al.* (1991), and Pyle and Jones (1991), as described below.

The exhaust plume, including exhausted products and heights of release, is considered in Section 10.2. The exhaust plume spreads out so effects need to be considered at various time and space scales. We loosely devise the categories of (1) local and regional and (2) global scales and consider these in Sections 10.3 and 10.4, respectively. A major uncertainty of the model simulations presented in this chapter concerns the effects of the particulates that are exhausted during rocket launches. These rocket-produced particulates are discussed in Section 10.5. Finally, conclusions are offered in Section 10.6.

10.2 THE EXHAUST PLUME

Several countries have major space launch vehicles including the U.S. (*e.g.*, Space Shuttle, Centaur, Atlas, Titan, and Delta), U.S.S.R. (*e.g.*, Energy and Proton), ESA (*e.g.*, Ariane), Japan (*e.g.*, H–1, H–2, N–2, M–5), and China (*e.g.*, Long March). Some of these launch vehicles depend on solid fuel, some depend on liquid fuel, and others rely on a combination of solid and liquid (*e.g.*, Space Shuttle). The major exhaust products of various solid and liquid systems are shown in Table 10–1.

Each Shuttle launch vehicle uses about 1,000 tons of solid propellant and about 730 tons of liquid propellant (Bennett and Hinshaw, 1991). The solid boosters exhaust their effluents of HCl, Al_2O_3, CO, CO_2, H_2, and H_2O below 50 km, whereas the exhaust products H_2O and H_2 from the main engine (based on liquid propulsion) are primarily injected above 50 km. Most of the constituents exhausted below the tropopause, typically at a height of 15 km for the launch latitudes, are washed out rapidly before they can reach the stratosphere and hence have negligible effect on the ozone layer. Thus the Shuttle exhausts approximately 68 tons of chlorine in the form of HCl per launch above the tropopause (based on Prather *et al.*, 1990a,b, with the tropopause assumed at 15 km). The comparable value for the Titan IV is 32 tons of chlorine, for Ariane–5, 57 tons (based on Pyle and Jones, 1991, with the tropopause assumed at 14 km), and for Energy, zero tons.

A projection of launches in 1991 and 2000 by the four main space agencies involved in chemical rocket launches was recently given by AIAA (1991). Although together the four main space agencies are expected to launch over a hundred rockets in each of these years, most rockets are relatively small and inject only modest amounts of substances in the stratosphere. Large amounts of stratospheric rocket effluents are injected or are expected to be injected by the Space Shuttle, Titan IV, Energy, and Ariane–5 rockets.

NASA (U.S.) is projected to launch six Space Shuttles and four Titan IV rockets in 1991 and 10 Space Shuttles and 10 Titan IV rockets in 2000. Only one launch is projected from the former Soviet Union with the use of the Energy rocket in 1991, and it is unknown how many will be launched in 2000. ESA is developing a new powerful launcher (Ariane–5),

Table 10–1 Examples of Launchers, Chemical Propulsion Systems, and Major Exhaust Products (from Table 1 of AIAA, 1991).

Country	Application	Engine/Motor	Propellant Combination	Exhaust Products
China	Long March	YF–73	O_2/H_2	H_2/H_2O
Europe	Ariane–4	HM7		
	Ariane–5	Vulcain		
U.S.	Centaur	RL10A–3–3A		
	STS	SSME		
	ALS, NLS	STME		
Japan	H–1, H–2	LE–5		
	H–2	LE–7		
U.S.S.R.	Energy	RD-0120		
U.S.	Atlas	MA–5A Sustainer	O_2/RP–1	CO, CO_2, H_2, H_2O
		MA–5A		
	Delta	RS–27A		
Japan	N–2, H–1	MB–3		
U.S.S.R.	Proton	RD–?		
	Energy	RD–170		
China	Long March	YF–22	N_2O_4/Hydrazine (Aerozine 50)	CO, CO_2, H_2, H_2O, N_2, NO_x
Europe	Ariane	Viking		
U.S.	Titan, Delta N–2 (Japan)	AJ10–118		
	Titan	LR–91		
	Titan	LR–87		
U.S.S.R.	Proton	RD–?		
	Proton	RD–253		
Europe	Ariane–4	P9.5	Solid	HCl, Al_2O_3, CO_2, CO, N_2, H_2, H_2O
	Ariane–5	EAP/MPS		
U.S.	STS	RSRM		
		ASRM		
	Titan 34D	UA 1205		
	Titan IV	UA 1207		
	Titan II	Castor		
	Atlas IIAS	Castor 4A		
	Delta 6920	Castor 4A		
	Delta 7920	GEM		
Japan	N–2	Castor 2		
	H–1A	Castor 2		
	H–2	Nissan		
	MU–3S–2	M–13		
		SB–735		
		M–23		
		M–3B		
	M–5	M14		
		M24		
		M34		

which is expected to be launched later this decade. Current understanding of these rocket effluents is based on calculations using combustion chemistry. Experimental verification of the rocket effluent amounts is badly needed.

10.3 LOCAL AND REGIONAL EFFECTS

The substances emitted from rocket exhausts are initially confined to a small volume of atmosphere a few hundred meters wide extending the length of the flight path. This affected volume is then moved away from the vicinity of the launch site by the wind systems and simultaneously distorted and mixed with the surrounding air, so that the contaminated volume increases, while the concentrations of pollutants decrease. This raises the possibility that restricted areas of severely reduced columnar ozone amounts may be found downwind of launch sites for a short period after each launch.

These local and regional effects are in some ways more difficult to calculate than global effects, being very dependent on the meteorological situation prevailing at the time of launch and involving, for the timescales of a few tens of minutes to one day, small-scale mixing processes of which we have limited knowledge. Nonetheless, plausible assumptions are possible that should permit estimates to be made that indicate the order of magnitude of the reductions.

Karol *et al.* (1991) have carried out calculations of the ozone reductions that may be expected during the 24 hours following the launch of both NASA's Shuttle and the Soviet Energy rocket. They use the emissions listed in Table 10–2 and a combination of two models: a box model and a model that allows the plume to diffuse horizontally for different stages of plume-spread. The calculations were performed for two rather different exhaust scenarios for each propulsion system. In addition to gases directly emitted by the exhaust, they have also considered the possibility that nitrogen oxides are produced as a result of the mixing of hot exhaust gases with the surrounding air and that some HCl emitted by the Shuttle is converted rapidly to Cl_2. Of the total gases emitted or produced by the launch, those with significant ozone depletion potentials are listed in table 10–2 for each scenario. The effects of Al_2O_3 particles and heterogeneous chemistry are not included in this calculation.

Table 10–2 Emission scenarios used by Karol *et al.* (1991). The values are the emissions in tons into a layer with top at the height listed.

SHUTTLE				
	Scenario A		Scenario B	
Top of Layer (km)	HCl	NO	Cl_2	NO
4	38.0	22.0	6.1	2.5
8	22.6	13.1	3.9	1.1
16	12.6	6.7	2.6	0.8
24	10.0	3.8	1.9	0.6
32	8.9	2.2	1.2	0.4
40	8.0	1.3	0.9	0.9

ENERGY				
	Scenario A		Scenario B	
Top of Layer (km)	HCl	NO	Cl_2	NO
4	-	28.6	-	0.3
8	-	17.0	-	0.2
16	-	8.7	-	0.2
24	-	4.9	-	0.2
32	-	2.9	-	0.25
40	-	1.7	-	0.3

PREDICTED ROCKET AND SHUTTLE EFFECTS

Figure 10–1 shows the calculated ozone concentration in the exhaust plume, expressed as a ratio of the initial climatological values at several heights for all scenarios. In Scenario A for the Shuttle (Figure 10–1a), 80 to 90 percent of the ozone is destroyed at all levels within a few minutes. Values stay low for about an hour (closer to 2 hours at 40 km) and then recover to be very close to their initial values by the end of the first day. In Scenario B for the Shuttle, the released chlorine products are conceived as being emitted as the more active chlorine gas rather than as hydrogen chloride, though in lesser quantities. As a result, the ozone is completely destroyed in the plume at all heights for a period (Figure 10–1b). In this scenario, the recovery is more rapid than in Scenario A at all heights except at 40 km.

These model simulations of dramatic ozone losses in the first couple of hours after launch have been corroborated by measurements taken after the launch of a different solid rocket (Titan III). The Titan III uses the same oxidizer (ammonium perchlorate) as the Space Shuttle, thus is expected to release HCl in large amounts in the exhaust plume. Ozone reductions greater than 40 percent in the exhaust trail of a Titan III solid rocket at an altitude of 18 km were observed only 13 minutes after launch (Pergament *et al.*, 1977). However, these measurements need to be repeated with modern instruments before confirmation of the theory of rapid, short-lived ozone loss in the plume.

In Scenario A for Energy (Figure 10–1c), the ozone losses are predicted to be comparable to those of the Shuttle for Scenario A, despite the lack of chlorine in the Energy emissions. For Scenario B (Figure 10–1d), however, the reductions are considerably less and the recovery more rapid. Karol *et al.* (1991) were able to show that the ozone reduction by the Shuttle depends on the form in which the chlorine is released. Substituting 10 tons of HCl to 5 tons of Cl_2 (same mass of chlorine) in Shuttle Scenario A at the 24-km level brought rapid total destruction of the ozone at that level. However, the recovery was little affected. A dependency was also demonstrated of the developments in the first two hours or so on whether the Shuttle launch is in daylight or darkness. The dependence is small for the case when the chlorine is all in the form of HCl, but large when it is in the form of Cl_2, the reductions being less than 30 percent for the nighttime case at 24 km.

According to the estimates of Karol *et al.* (1991), the areas affected by the plume are of restricted horizontal extent. The values quoted above are for the plume axis, and the effects fall off rapidly with distance from that axis. Thus, for example, at 24 km in Shuttle Scenario A the distance from the center within which the ozone is destroyed by 10 percent or more is a little over 1 km for the first hour, rising to 4 km in the next 2 hours, after which it shrinks rapidly to zero as the plume recovers to the extent that the reductions nowhere exceed 10 percent.

Aftergood (1991) suggested that there could be a significant "soft spot" or a local decrease in total ozone after a Space Shuttle launch. Since the rocket trajectories through the atmosphere are curved rather than straight up, the calculations of Karol *et al.* (1991) indicate that the maximum depletion of the total ozone column never exceeds 10 percent at any point under the Shuttle plume in the first 2 hours and subsequently falls to much smaller values. Consistent with these model computations, McPeters *et al.* (1991) found no evidence of ozone depletion in a study of TOMS images taken at varying times after eight separate Shuttle launches.

Some laboratory experiments (Gershenzon *et al.*, 1990) suggest that direct thermal decomposition of ozone may occur in high temperature jets. This phenomenon has been observed in O_2–O_3 jets for rather high ozone concentrations relative to O_2; however, the reaction may take place for atmospheric ozone concentrations at sufficiently high temperatures, such as those found in the exhaust plume. This is believed to be a rather short-term effect with recombination of the thermally decomposed products (O and O_2) occurring rapidly after mixing with cooler air.

Regional effects (1000×1000 km^2) due to rocket effluents have been computed [from the Cl_y (Cl, Cl_2, ClO, Cl_2O_2, HCl, HOCl, and $ClONO_2$) perturbation] due to a single Space Shuttle launch using a three-dimensional model (Prather *et al.*, 1990a,b) with a resolution of 8° latitude by 10° longitude. The Cl_y concentration at 40 km, 30°N, 70°W, can increase by a few percent 2 days after the launch, and the corresponding ozone decrease is expected to be less than 1 percent at that height. The subsequent rate at which the chlorine is dispersed depends on season, the summer atmosphere being less dispersive than the winter. After a further 6 days, the peak chlorine concentrations had fallen by a factor of 4 in the January simu-

C-4

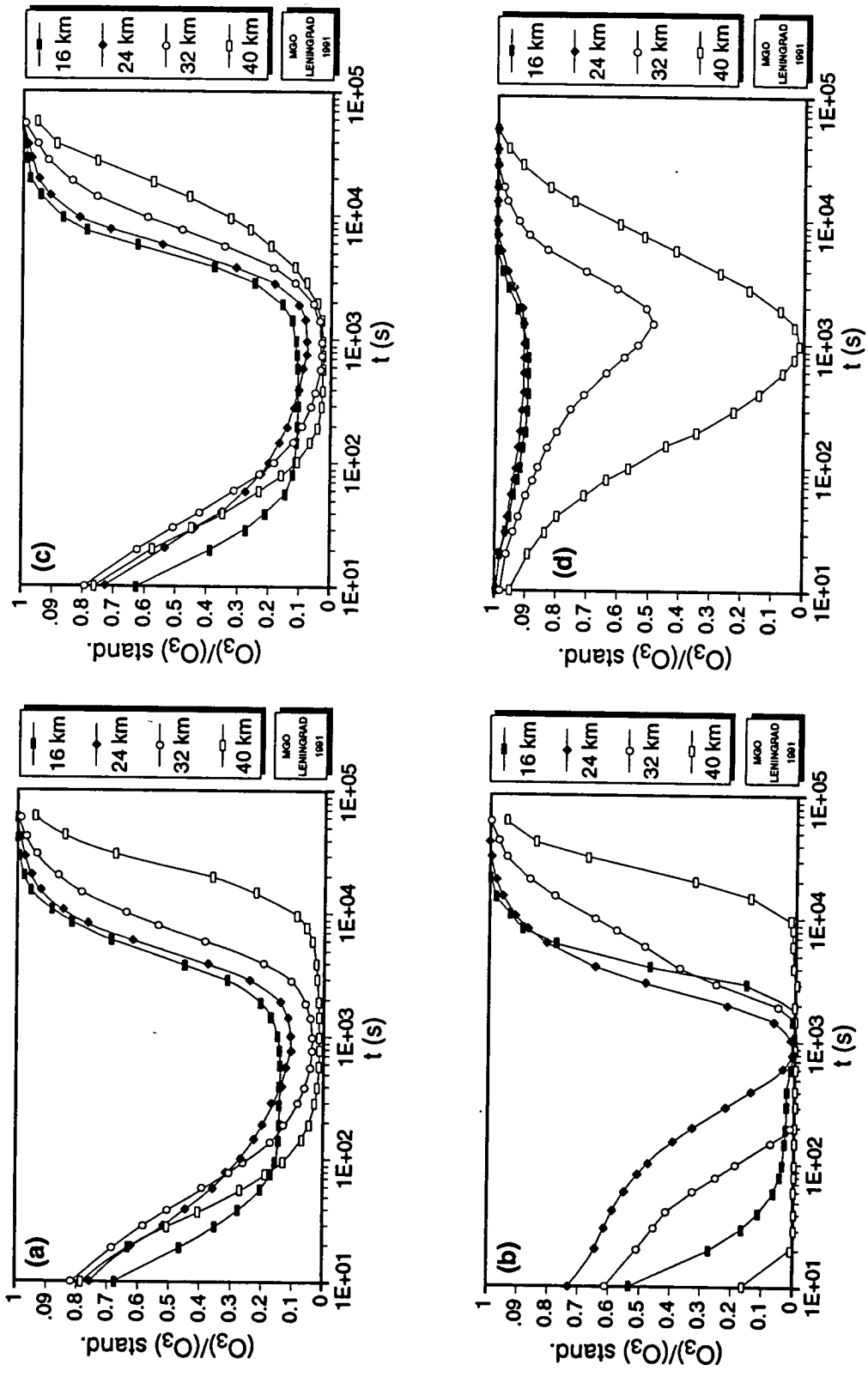

Figure 10–1 Local plume time variations in ozone due to rocket exhausts (Karol *et al.*, 1991). The vertical axis is the ozone amount expressed as a ratio of the initial (standard atmosphere) value. (a) Shuttle Scenario A (see Table 10–2); (b) Shuttle Scenario B; (c) Energy Scenario A; and (d) Energy Scenario B.

lations and a factor of 2 in the July simulations. The Cl_y emitted by the Shuttle becomes spread over all longitudes in about 30 days and is less than 0.15 percent of background levels.

In conclusion, the local plume effect of rocket exhausts has not been extensively studied, but the studies that have been undertaken indicate that rocket exhausts can lead to severe ozone loss over a restricted volume within a few kilometers of the plume axis. The corresponding total reduction of ozone column in the case of the Space Shuttle probably does not exceed 10 percent over an area the size of the TOMS field of view of 40×40 km^2 and is within typical natural variations some 3 hours after launch. During the subsequent few days, chlorine may remain enhanced in the upper stratosphere by a few percent, falling to a few tenths of a percent by the end of the first month. These studies have included homogeneous chemistry only and have employed a limited treatment of mixing processes that spread the plume from a scale of a few 10s of meters to the 1000 km resolved by the three-dimensional models. Further studies are needed to clarify the importance of these restrictions.

10.4 GLOBAL SCALE EFFECTS

After about a month, the effects of a given launch are spread over a sufficiently large portion of the atmosphere and diluted to the stage where they contribute less to any ozone reduction than do the remnants of the previous launches. It thus becomes necessary to consider the cumulative global-scale effect of a series of launches. A natural reference is provided by considering the steady state, which is reached when the annual average rate of increase in chlorine and other active species from exhaust plumes is balanced by the rate at which they or their derived products are removed, mostly by transfer to the troposphere followed by rain-out.

Global effects due to rocket exhausts on Cl_y and ozone concentrations, as affected by Cl_y homogeneous chemistry, have been computed by Prather *et al.* (1990a,b). The steady-state impact of nine Space Shuttles and six Titan IV launches per year on the chlorine loading was assessed with two two-dimensional models and one three-dimensional model. The increased stratospheric loading of chlorine from this U.S. launch scenario is less than 0.25 percent globally of the annual stratospheric chlorine source from halocarbons in the present-day atmosphere.

The corresponding changes in chlorine loading and ozone concentration were calculated using the two-dimensional models. The results from one of these models, the Goddard Space Flight Center (GSFC) model, are shown in Figures 10–2 and 10–3, respectively. Although there were differences of detail, the broad results of changes in chlorine concentrations were similar in all models. Cl_y in the middle to upper stratosphere is computed to increase by a maximum of about 10 pptv (about 0.3 percent of a 3.3 to 3.5 ppbv background) in the northern middle and high latitudes. Compared to the natural source of chlorine from CH_3Cl (Weisenstein *et al.*, 1991) this rocket-induced Cl_y adds about 1.7 percent to a 0.6 ppbv background.

The corresponding maximum ozone depletion was calculated to be less than 0.2 percent at 40 km in the winter hemisphere. Maximum column ozone depletion is computed to be much less than 0.1 percent for this scenario.

Using the same launch scenario, a computation of the total yearly average global stratospheric ozone depletion is found to be about 0.0065 percent (Jackman, C. H., private communication, 1991). The global effects of Space Shuttle launches have also been computed by Karol *et al.* (1991) for both scenarios listed in Table 10–2. Scaling their calculations to an equivalent nine Space Shuttle and six Titan IV launches per year gives a total global ozone depletion of 0.0072 to 0.024 percent.

Pyle and Jones (1991), using a two-dimensional model, assessed the impact of the chlorine from 10 Ariane–5 launches per year. They performed a 20-year simulation, adding the appropriate amount of chlorine for that scenario until a steady state was established in which the results repeated from one year to the next. These computations indicate an effect similar to that reported above for the Prather *et al.* (1990a,b) work on Shuttle and Titan IV launches (*e.g.*, maximum local ozone depletion is around 0.1 percent near 40 km).

In general, the modeling studies discussed above did not quantitatively evaluate the effect of effluents other than chlorine emitted from the rocket exhaust. One exception is Karol *et al.* (1991) who also included NO_x (N, NO, NO_2) injections. None of the studies considered HO_x (H, OH, HO_2), NO_x, and Cl_y in con-

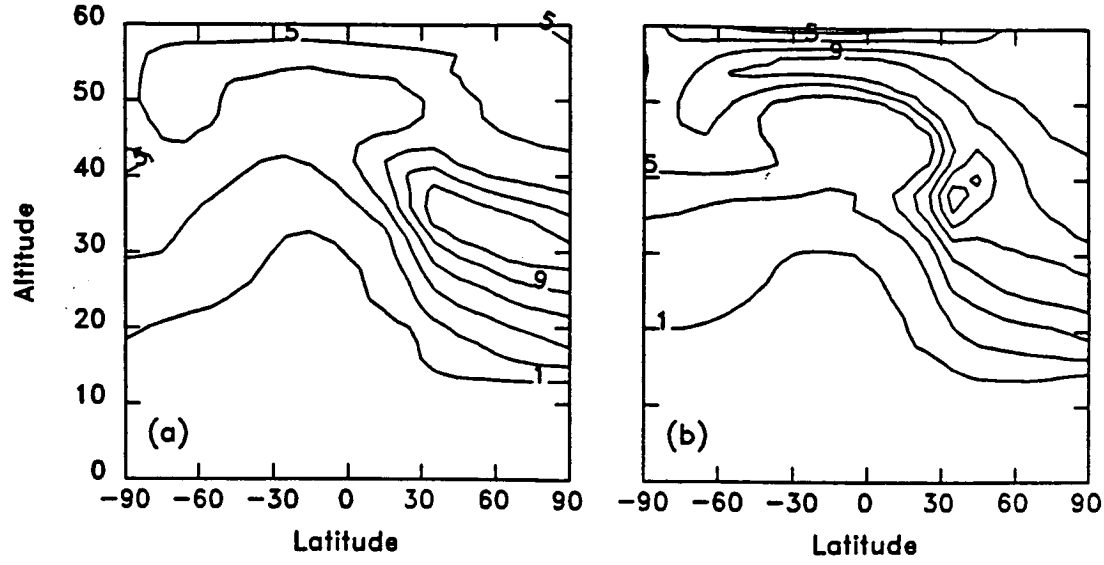

Figure 10–2 Latitude by altitude contours of the perturbation to background Cl_y levels (pptv) for the GSFC model (Prather *et al.*, 1990b) in the steady state for an annual launch scenario of nine Space Shuttles and six Titan IV rockets in (a) January and (b) July.

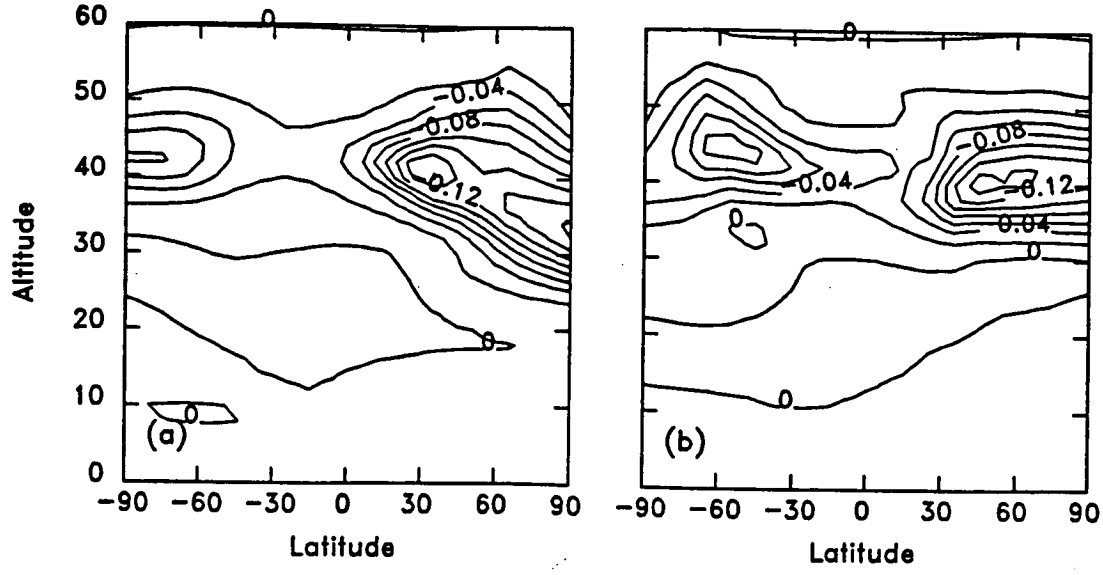

Figure 10–3 Perturbation in ozone (percent) corresponding to Figure 10–2 in (a) January and (b) July.

junction. Bennett and Hinshaw (1991) completed a calculation of the relative contributions of nine Space Shuttle and six Titan IV launches to the stratospheric burdens of the potential ozone destroyers. These were taken to be HO_x (from emitted H_2 and H_2O) and NO_x (from emitted NO) in addition to Cl_y. In this computation, NO_x was increased by 0.0014 percent (though no NO_x production from afterburning was considered), HO_x was increased by 0.0048 percent, and Cl_y was increased by 0.16 percent, all above the global background. These calculations indicate that the rocket-induced Cl_y changes should be the most significant when considering the long-term global effects on stratospheric O_3, so that the omission of other substances in the assessments reported above is not expected to affect the conclusions.

Jackman *et al.* (1991) recently completed a two-dimensional model computation on the effects of HO_x from emitted H_2 and H_2O for a hypothetical National Aerospace Plane (NASP) on stratospheric ozone. A rate of 40 launches per year results in H_2 and H_2O increases of 0.34 and 0.16 percent, respectively, at 35 km altitude and 35°N latitude. This results in an OH increase of 0.1 percent and a corresponding ozone decrease of 0.006 percent at this location. Total global column ozone impact is calculated to be a decrease of less than 0.0002 percent.

None of these calculations have included the impact of heterogeneous chemistry whether on preexisting particles or on the particles emitted in the exhaust. The latter are discussed further below. There is a need for some additional work here. However, a context for interpretation of the importance of rocket exhausts in an atmosphere containing aerosols is provided by comparing the total input of reactive chlorine into the atmosphere from rockets with the inputs from industrial sources.

10.5 EFFECTS OF PARTICULATES

Particulates in the form of Al_2O_3, soot, and ice are released to the atmosphere in chemical rocket launches. Although any chemical rocket launch releases particulates of some form into the atmosphere, most particulate measurements of rocket exhausts are associated with Space Shuttle launches. Measurements have been conducted to obtain samples of the Shuttle-exhausted aluminum oxide particles with the use of aircraft collecting filter samples during descending spiral maneuvers in the exhaust plumes. These measurements show a distribution of particles with significantly more particles below 1 μm than above 1 μm in size (Cofer *et al.*, 1985).

The first observation of Al_2O_3 particles in the stratosphere was reported by Brownlee *et al.* (1976). Zolensky *et al.* (1989) reported an order of magnitude increase in particles above 0.5 μm, which were mostly aluminum rich between 17 and 19 km from 1976 to 1984. These aluminum-bearing particles are thought to be from both the Space Shuttle launches and ablating spacecraft material, with the ablating spacecraft material predominating (Zolensky *et al.*, 1989).

The exhausted particulates may have a large local effect on the stratosphere. Recently, the effect of Al_2O_3 aerosols with a mean radius of 0.1 μm and a sticking coefficient of 5×10^{-5} has been estimated (Karol, I.L., private communication, 1991). These aerosols produce an additional 30 percent ozone depletion in the 400 to 1500 sec time period after emission. Before and after this time period, the additional depletion is mostly less than 5 percent. Since the Al_2O_3 aerosols act as condensation nuclei for sulfate in the stratosphere, it is reasoned that their stratospheric influence after the first 1500 sec will be like those of other resident aerosols.

Aerosols have been implicated in enhancing ozone decrease by chlorine species, even in the absence of polar stratospheric clouds (Hofmann and Solomon, 1989; Rodriguez *et al.*, 1991). Turco *et al.* (1982) has suggested that the Space Shuttle could increase the average ice nuclei concentration in the upper troposphere by a factor of 2. Rough estimates suggest that U.S.-launched rockets increase the global aerosol surface of the unperturbed stratosphere by about 0.1 percent (Prather *et al.*, 1990b; McDonald *et al.*, 1991), therefore, these computations indicate that the global particulate effects of these rocket-produced aerosols could be responsible for about 1/1000th of the current ozone depletion associated with heterogeneous chemistry.

10.6 CONCLUSIONS

Rocket launches can have a significant local effect on the stratosphere by reducing ozone substantially (perhaps >80 percent) within the expanding exhaust plume up to 3 hours after launch. Even when such severe reductions take place, the reduction in

column ozone is probably less than 10 percent over an area a few kilometers by a few tens of kilometers and is generally much smaller. The local-plume ozone reductions decrease to near zero over the course of a day, and the regional effects are smaller than can be detected by satellite observations. Moreover, none of the atmospheric modeling studies that assume the present rate of rocket launches show a significant global impact on the ozone layer (the calculated impact is predicted to be much smaller than the effect of the solar cycle on ozone, for instance). A consideration of the other products of rocket launches that can potentially destroy ozone shows even smaller effects from those substances so far as homogeneous effects are concerned.

These modeling studies are incomplete and, because of the inherent uncertainties, may underestimate or possibly overestimate the ozone depletion expected by rockets. For instance, only one of the above studies considers the potential impact of heterogeneous chemistry. However, the total annual addition to stratospheric chlorine from rocket launches is of the order of 0.25 percent of the global annual stratospheric chlorine source from halocarbons in the present-day atmosphere, so that the global impact of rocketry is a third-order or smaller effect compared with other sources of chlorine. If the annual background source from halocarbons is reduced and/or the launch rate increases, the fractional contribution will become larger.

REFERENCES

Aftergood, S., Comment on "The Space Shuttle's impact on the stratosphere," by Michael J. Prather, *et al.*, *J. Geophys. Res., 96,* 17377, 1991.

AIAA (American Institute of Aeronautics and Astronautics), Atmospheric effects of chemical rocket propulsion, AIAA workshop report, Washington, D.C., October 1, 1991.

Bennett, R.R., and J.C. Hinshaw, The effects of chemical propulsion on the stratospheric ozone, internal report, Thiokol Corporation, Brigham City, Utah, 1991.

Brownlee, D. E., G. V. Ferry, and D. Tomandl, Stratospheric aluminum oxide, *Science, 191,* 1270–1271, 1976.

Cofer, W.R. III, R.J. Bendura, D.I. Sebacher, G.L. Pellett, G.L. Gregory, and G. L. Maddrea, Jr., Airborne measurements of Space Shuttle exhaust constituents, *AIAA J., 23,* 283–287, 1985.

Gershenzon, Y., S. Zvenigorodsky, and V. Rosenshtein, *Adv. in Chemistry (Uspehi Hymii), 59,* 1601–1626, 1990.

Hofmann, D.J., and S. Solomon, Ozone destruction through heterogeneous chemistry following the eruption of El Chichon, *J. Geophys. Res., 94,* 5029–5041, 1989.

Hoshizaki, H. (chairman), Aircraft wake microscale phenomena, Chap. 2, pp. 60–73, in The Stratosphere Perturbed by Propulsion Effluents, *CIAP Monogr. 3,* Climatic Impact Assessment Program, U.S. Dept. of Transportation, Washington, D.C., 1975.

Jackman, C.H., A.R. Douglass, and K.F. Brueske, A simulation of the effects of the National Aerospace Plane testing on the stratosphere using a two-dimensional model, Code 916, NASA/GSFC, Greenbelt, MD 20771, preprint of a report given to the U. S. Air Force, 1991.

Karol, I.L., Y.E. Ozolin, and E.V. Rozanov, Effect of space rocket launches on ozone and other atmospheric gases, paper presented at the European Geophysical Association Conference, Wiesbaden, 1991.

McDonald, A.J., R.R. Bennett, J.C. Hinshaw, and M. W. Barnes: Chemical propulsion and the environment, *Aerospace America,* 32–36, May 1991.

McPeters, R.,M. Prather, and S. Doiron, Reply to "Comment on 'the Space Shuttle's impact on the stratosphere'," *J. Geophys. Res., 96,* 17379–17381, 1991.

Pergament, H.S., R.I. Gomberg, and I.G. Poppoff, Appendix G, NO_x deposition in the stratosphere from the Space Shuttle rocket motors, in NASA Technical Memorandum X–58198—Proceedings of the Space Shuttle Environmental Assessment Workshop on Stratospheric Effects, 1977.

Potter, A.E., Environmental effects of the Space Shuttle, *J. Environ. Sci., 21,* 15–21, 1978.

Prather, M.J., M.M. Garcia, A.R. Douglass, C.H. Jackman, M.K. W. Ko, and N.D. Sze, An assessment of the impact on stratospheric chemistry and ozone caused by the launch of the

Space Shuttle and Titan IV, in Present State of Knowledge of the Upper Atmosphere 1990: An Assessment Report, NASA Reference Publication 1242, 111–122, 1990a.

Prather, M.J., M.M. Garcia, A.R. Douglass, C.H. Jackman, M.K. W. Ko, and N.D. Sze, The Space Shuttle's impact on the stratosphere, *J. Geophys. Res., 95*, 18583–18590, 1990b.

Pyle, J.A., and A.E. Jones, An investigation of the impact of the Ariane–5 launches on stratospheric ozone, prepared for the European Space Agency, 1991.

Rodriguez, J.M., M.K. W.Ko, and N.D. Sze, Role of heterogeneous conversion of N_2O_5 on sulphate aerosols in global ozone losses, *Nature, 352*, 134–137, 1991.

Turco, R.P., O.B. Toon, R.C. Whitten, and R. J. Cicerone, Space shuttle ice nuclei, *Nature, 298*, 830–832, 1982.

Weisenstein, D., M.K.W. Ko, and N.D. Sze, The chlorine budget of the present-day atmosphere: A modeling study, *J. Geophys. Res,.97*, 2547–2559, 1992.

Zolensky, M.E., D.S. McKay, and L.A. Kaczor, A tenfold increase in the abundance of large solid particles in the stratosphere, as measured over the period 1976–1984, *J. Geophys. Res., 94*, 1047–1056, 1989.

CHAPTER 11

Ultraviolet Radiation Changes

Authors:

R.L. McKenzie
M. Ilyas
J.E. Frederick
V. Filyushkin

Additional Contributors:

A. Wahner
P. Muthusubramanian
C.E. Roy
K. Stamnes
M. Blumthaler
S. Madronich

Chapter 11

Ultraviolet Radiation Changes

Contents

SCIENTIFIC SUMMARY

A major consequence of ozone depletion is an increase in solar ultraviolet (UV) radiation received at the Earth's surface. This chapter discusses advances that have been made since the previous assessment (*WMO*, 1990) to our understanding of UV radiation. The impacts of these changes in UV on the biosphere are not included, because they are discussed in the effects assessment (UNEP, 1991). The major conclusions and recommendations are:

- Significant improvements in the UV data base have occurred since the last assessment. Spectral measurements are becoming available, but, to determine trends, long-term accurate measurements of UV are required at unpolluted sites.

- Biologically damaging UV has been observed to more than double during episodes of ozone depletion in Antarctica. Smaller episodic enhancements have been measured in Australia. The observed enhancements are consistent with the results of radiative transfer calculations for clear sky conditions.

- An erythemal Radiative Amplification Factor (RAF) of 1.25 ± 0.20 has been deduced from measurements of ozone and UV at a clean air site. This is in agreement with the RAF derived from model calculations (RAF = 1.1 at 30° N).

- There is an apparent discrepancy between observed UV trends from the Robertson-Berger (RB) network and those calculated from TOMS ozone data. Cloud variability, increases in tropospheric ozone and aerosol extinctions may have masked the UV increase due to ozone depletion. In addition, the data record available for comparison is short, and the instrument calibration (which is critical) is still in question. However, at a high-altitude European observatory, the observed positive trends in UV appear to be larger than expected. Further studies of the effects of cloud and aerosol on UV are required.

- Clear-sky radiative transfer calculations using ozone fields measured by the TOMS instrument show that during the 1980s erythemally active UV has increased significantly at latitudes poleward of 30°, with larger increases in the Southern Hemisphere, particularly at high latitudes.

- Significant increases in UV effects are most likely to appear first in the Southern Hemisphere where in the summer, historical ozone levels are lower and the Earth-Sun separation is a minimum. Further, in the Southern Hemisphere, stratospheric ozone losses are more severe, tropospheric ozone has not increased, and aerosol concentrations are lower.

- Existing chemical models underestimate the changes in the observed ozone fields. Therefore, they cannot be used to accurately predict future changes in UV fields.

11.1 UV MEASUREMENTS AND ANALYSES

11.1.1 Interpretation of Ultraviolet-B (UVB) Time Series Data

The most comprehensive time series of UVB data are those from the Robertson-Berger (RB) network. However, a study by Scotto *et al.* (1988) showed no increase in UVB at U.S. observation sites, despite the decrease in stratospheric ozone. Investigations to understand the reasons for this surprising result have continued. Increases in tropospheric ozone that more than compensated for stratospheric ozone losses were proposed by Brühl and Crutzen (1989). However, recent analyses of TOMS data and tropospheric ozone trends suggest an increase in UVB should still have been observed (UNEP, 1991). Increasing local pollution at the measurement sites has also been suggested. Since the industrial revolution, reductions in Northern Hemisphere UVB have already occurred due to aerosol extinction. The decreases in UVB caused by increases in aerosols since the industrial revolution probably exceed the increases due to ozone depletion (Figure 11-1, from Liu *et al.* [1991]). On a local scale, changes in pollution at the network sites may therefore be significant in the analysis period (1974-1985).

The RB meters have a relatively low sensitivity to ozone depletion. Typically a 1 percent reduction in ozone produces an increase of less than 1 percent in the RB-weighted irradiance (UNEP, 1991), and it is possible that the trends in UVB irradiance measured by the RB network have been masked by natural variability in cloud cover. A study by Beliavsky *et al.* (1991) argues that because of natural cloud variability, decades of data would be required before UVB trends would be detectable without supporting measurements.

Frederick and Weatherhead (1991) have examined RB data from two sites in the U.S. (Bismarck and Tallahassee) at which Dobson ozone data were available (Figure 11-2). They concluded that monthly trends in the RB data are consistent with expectations based on Dobson column ozone measurements for the months of high UVB irradiance, April through September. However, large differences exist between modeled and clear-sky results in the period November

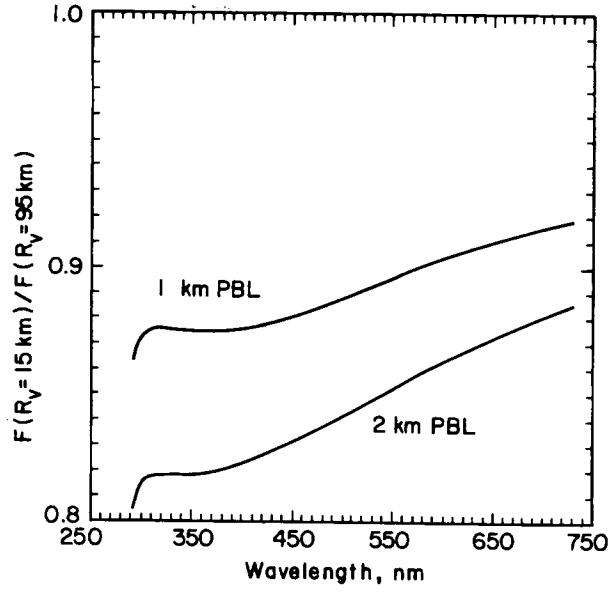

Figure 11-1 Ratio of daily surface solar radiation for 15-km visual range (typical Northern Hemisphere) to that for 95-km visual range (clean air) as a function of wavelength, for assumed aerosol boundary layer heights of 1 and 2 km (from Liu *et al.*, (1991)).

through February. The reason for this discrepancy is unknown at present. We understand that the calibration of this network is currently being evaluated, and a publication is likely to appear. With the information currently available, there are still questions about the calibration of this network.

RB data obtained from the high-altitude European observatory at Jungfraujoch has been used in conjunction with measurements of global radiation (G) between 300 and 2000 nm, to eliminate cloud and aerosol effects, and reveal trends in UVB (Blumthaler and Ambach, 1990). Updated measurements that include data from 1990 (M. Blumthaler, private communication, 1991) are shown in Figure 11-3. The plot shows the departures from the long term mean in the ratio UVB/G. The data show irregular variations, but unlike the U.S. data, there is a superimposed trend, which corresponds to UVB increases of 10 ± 5 percent per decade, which is larger than that expected (Madronich, 1991) from the changes in ozone measured over the same period (Chapter 2). However, the effects of the 1982 El Chichón volcanic eruption on these data may be significant either through its possible influence on

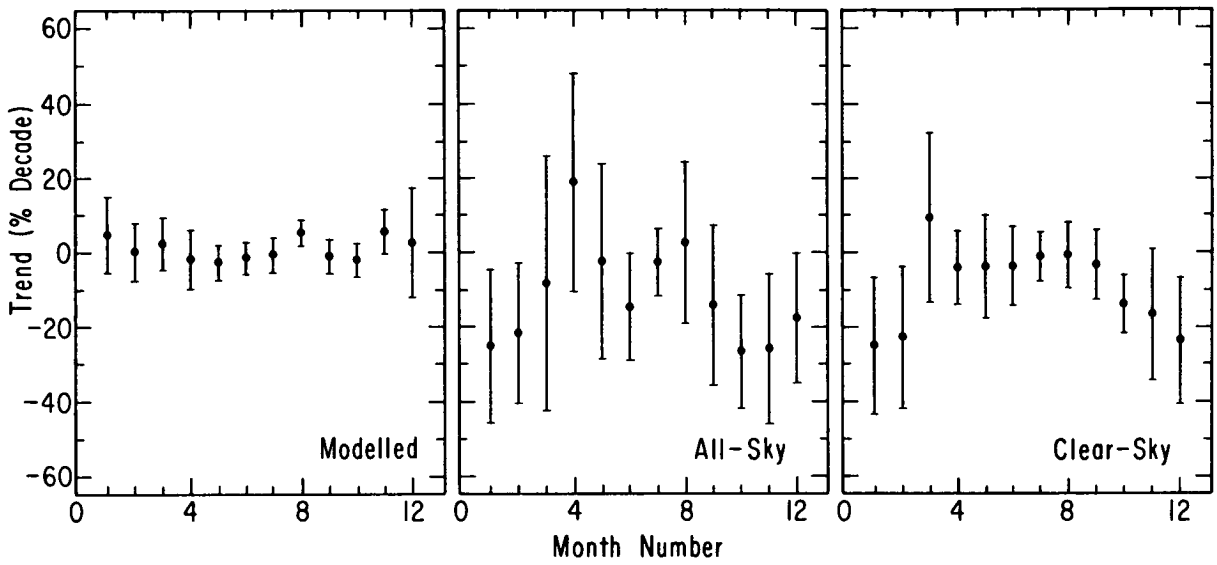

Figure 11-2 Trends by month of the year in the Robertson-Berger (RB) meter data set for Bismarck U.S., derived for the period 1974-1985. Error bars denote 95 percent confidence limits. Left panel: Results derived from radiative transfer calculations using Dobson ozone data as inputs. Center panel: Trends in the entire RB data set, including the influence of clouds. Right panel: Trends in a clear-sky subset of the RB data base (from Frederick and Weatherhead, 1991).

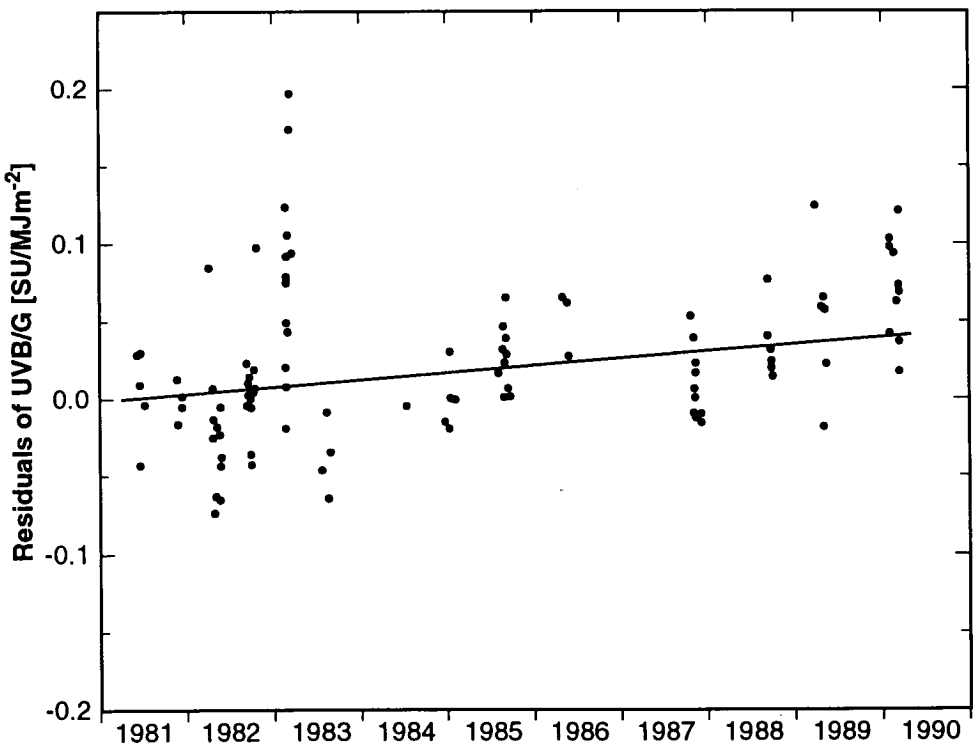

Figure 11-3 Long-term tendency of the residuals from the long-term means of the ratios UVB/G, measured at Jungfraujoch observatory between 1981 and 1990. The regression line is also shown (Blumthaler, private communication, 1991).

ozone that was anomalously low at these latitudes in 1983 (WMO, 1990), or through changes in the wavelength-dependent aerosol optical depth (Kent *et al.*, 1991).

There has been an increasing awareness that spectral measurements are required to study the effects of changes in ozone on UV radiation. The RB response does not accurately represent any of the diverse biological action spectra of interest (UNEP, 1991), whereas spectral data can be accurately convolved with various action spectra. In addition, the spectral information enables greater confidence in instrument calibration, and identification of the reasons for any changes in UV. For example, spectral measurements have enabled ozone column amounts to be deduced, and facilitated determination of cloud and aerosol effects (Stamnes *et al.*, 1990). The time series of UV spectral measurements is too short at present to determine trends, but useful insights have nevertheless been gained already from analyses of this type of data.

11.1.2 Effects of Antarctic Ozone Depletion

In 1988 the National Science Foundation established four sites for monitoring solar UV and visible radiation in the high-latitude Southern Hemisphere. Three of these sites are on the Antarctic continent, at the South Pole, McMurdo, and Palmer Stations, and one is located at Ushuaia, Argentina. Results from McMurdo (Stamnes *et al.*, 1990), and from Palmer Station on the Antarctic peninsula (Lubin *et al.*, 1989; Lubin and Frederick, 1991) have appeared in the literature. To date the focus has been on changes in surface ultraviolet irradiance associated with the springtime depletion in ozone.

The UV radiation field over Antarctica varies with the solar elevation, clouds and haze, and the atmospheric ozone amount. Over Palmer Station (latitude 64.8° S), clouds, in a monthly averaged sense, reduce the surface UV irradiance to approximately 50 to 60 percent of the values that would prevail under perpetually clear skies. The springtime depletion in ozone constitutes a relatively recent perturbation to the highly variable radiation background. The two issues to consider here are (a) the magnitude of the reduction in ozone and (b) the

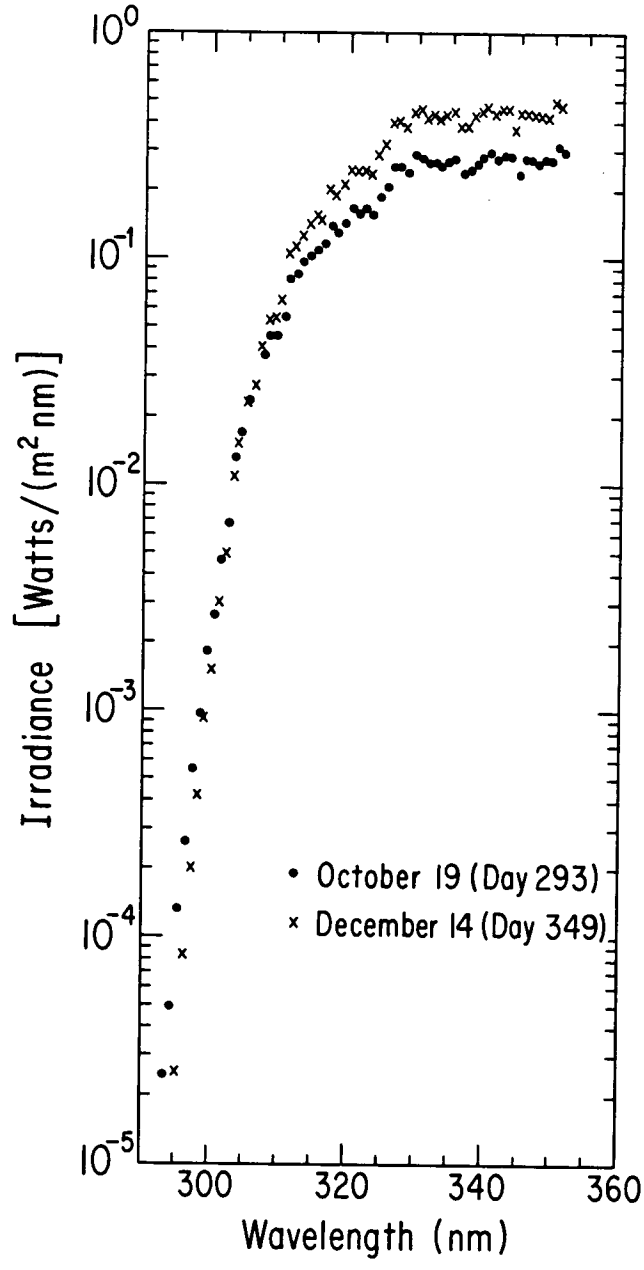

Figure 11-4 Spectra of ultraviolet solar irradiance measured at local noon from Palmer Station, Antarctica, in 1988. Day number 293 (Oct. 19) is the time of minimum ozone, while day number 349 (Dec. 14) is representative of conditions near summer solstice.

timing of the reduction relative to the normal seasonal cycle in solar radiation.

Figure 11-4 presents two spectra of surface UV irradiance measured at local noon from Palmer Station on days number 293 (Oct. 19) and 349 (Dec. 14) of 1988 (Lubin *et al.*, 1989). The former date was the day of minimum ozone, while the latter is near summer solstice. Based solely on solar elevation, one would expect the largest irradiances in December. Figure 11-4 shows this to be the case at wavelengths longer than 315 nm. However, at shorter wavelength, the measured irradiances for October equal and then exceed those in December. This is the manner in which a reduction in ozone appears in UV radiation at the earth's surface. Although the enhanced irradiances exist at wavelengths where the absolute energy flux is small, living cells are quite sensitive to damage in the spectral region from 300 to 315 nm.

The springtime ozone depletion of 1988 had vanished from the Antarctic peninsula by mid-November. However, during 1990 reduced ozone amounts persisted over Palmer Station well into December. The combination of low ozone and high solar elevation led to unusually large irradiances as shown in Figure 11-5 (Frederick and Alberts, 1991). The points denote ratios of the noontime irradiance measured at 306.5 nm, near the peak of the biologically weighted spectrum, to that at 350.0 nm, where absorption by ozone is insignificant. Use of this irradiance ratio removes the influence of clouds, to a

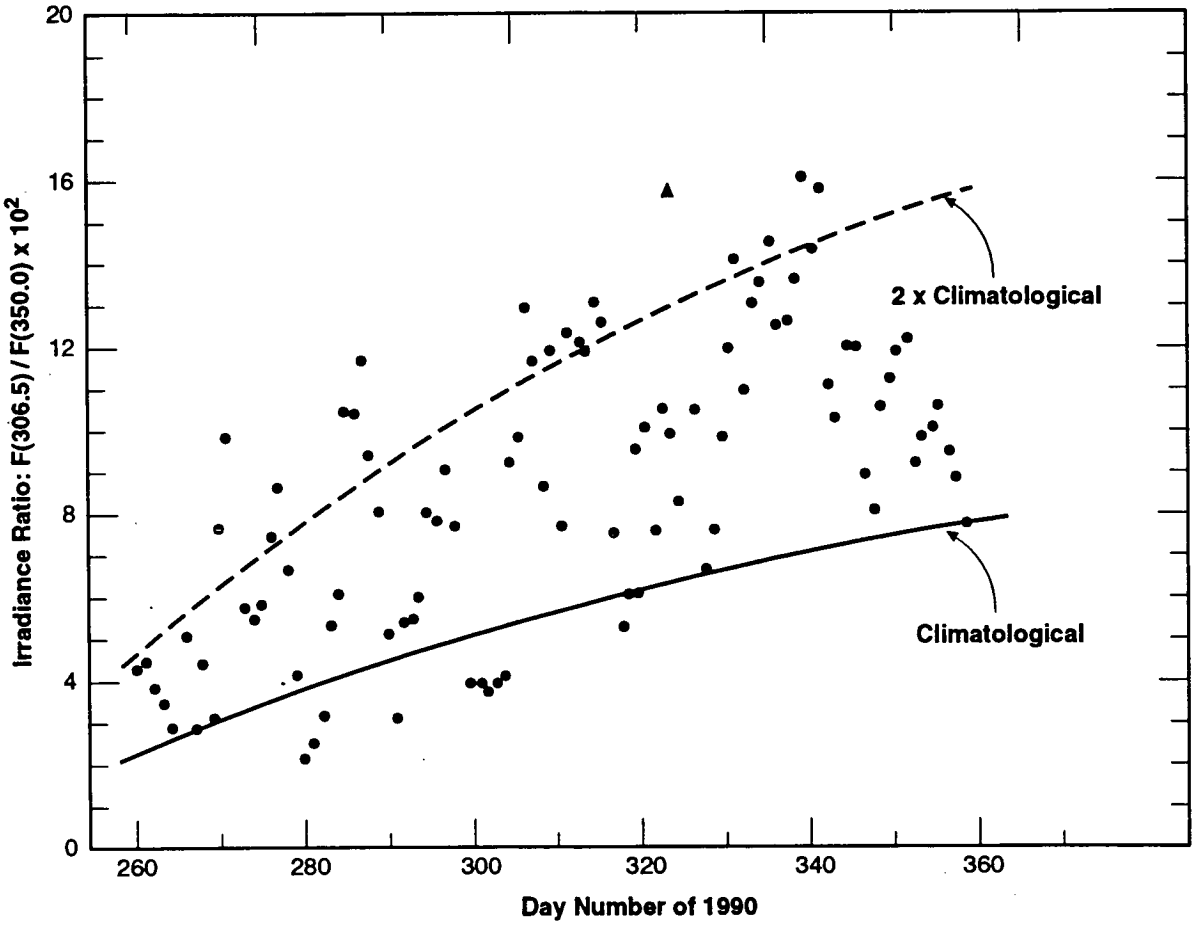

Figure 11-5 Ratios of noontime solar irradiance at 306.5 nm to that at 350.0 nm (points) for the Austral spring of 1990 at Palmer Station. The solid curve labeled "climatological" is a calculation based on ozone amounts that are typical of those in the absence of a depletion. The dashed curve is twice the climatological irradiance ratio.

good approximation, so the points indicate variations associated with ozone only. The solid line represents computed ratios based on the ozone climatology of Nagatani *et al.* (1988) in which any springtime ozone reduction is small. The dashed line indicates double the climatological prediction. Approximately 20 percent of the days during the spring of 1990 had irradiance ratios in excess of the climatological prediction by a factor of 2 or more, and the enhancement persisted into early December when the daylight period is long. Measurements from McMurdo Station during 1990 yielded similar results, with ozone depletions persisting in December to give enhancements in biologically weighted radiation by a factor of three (Stamnes *et al.*, 1991). The variations in observed UVB irradiances in Antarctica have been shown to be consistent with the results of radiative transfer calculations (Stamnes *et al.*, 1990).

The minimum ozone levels over Antarctica occur in October. At this time, solar elevations are relatively low, so that the maximum UV fluxes occur later in the year. However, the transmission of sea-ice has a strong seasonal maximum in spring so that organisms that live under the ice sheet may be at risk (Trodahl and Buckley, 1989). In terms of the potential ecological effects, the duration of the ozone depletion is likely to be an important quantity. When ozone amounts remain low into December, the instantaneous and 24-hour integrated UV irradiances discussed above can be far in excess of the maximum values experienced in Antarctica prior to the 1980s.

11.1.3 Global Effects

UVB perturbations have also been seen at mid-latitudes in the Southern Hemisphere, from episodic intrusions of ozone-poor air from the Antarctic ozone hole. For example, Roy *et al.* (1990) showed an association between high UVB levels in Melbourne, Australia, and ozone-depleted air arriving from Antarctica in late 1987. Figure 11-6 shows the strong anticorrelation between UVB (integrated over the wavelength range 285-315 nm) and ozone. The impacts of the ozone changes on the observed UV are consistent with model predictions, although calculated irradiances are 10 percent smaller.

The Southern Hemisphere is where increases in UV stresses are most likely to appear first. Historically, UV levels there have been high because of the lower ozone amounts in summer compared with the Northern Hemisphere, and because the Earth-Sun separation is smallest in January. Further, in the Southern Hemisphere stratospheric ozone losses are more severe, tropospheric ozone has not increased, and aerosol concentrations are lower (McKenzie, 1991).

In absolute terms, even small percentage decreases in ozone are important in the tropics, since UVB levels there are already large. A 10 percent decrease in ozone in the tropics would lead to a UVB increase that is larger than the total UVB at mid-latitudes (Ilyas, 1989). In view of this sensitivity, more tropical measurements of UV are clearly required, even though the most recent analyses of TOMS satellite ozone indicate that there have been no changes of statistical significance at equatorial latitudes.

11.1.4 Radiative Amplification Factor Deduced from Measurements

A suitable long-term data base does not yet exist to enable global UV trends due to ozone depletion to be determined. It has, however, been demonstrated that under similar observing conditions (*i.e.*, same ozone, sun angle, clear skies), any changes between 1980 and 1988 in the measured spectral distribution of UV at Lauder, New Zealand (45°S, 170°E), were small (Bittar and McKenzie, 1990). Since December 1989, spectral measurements from Lauder have been made routinely at fixed Solar Zenith Angles (SZAs) and near local noon, whenever weather conditions permit. Typical spectra obtained at midday in winter and summer are shown in Figure. 11-7a. The figure also shows the erythemal weighting function (McKinlay and Diffey, 1987) used in the analyses that follow in the remainder of this chapter. The integrated midday erythemal irradiance in winter (Figure 11-7b) is only 10 percent of that in summer, due mainly to differences in the SZA.

Seasonal variations in ozone are large at mid-latitude sites, enabling these measurements to be used to investigate the relationship between UV and ozone (and other factors such as cloud cover and sun angle). Observations obtained at fixed SZAs over a year were used, and variations due to seasonal changes in the Sun-Earth separation were removed using a simple trigonometric correction. Data from 1990

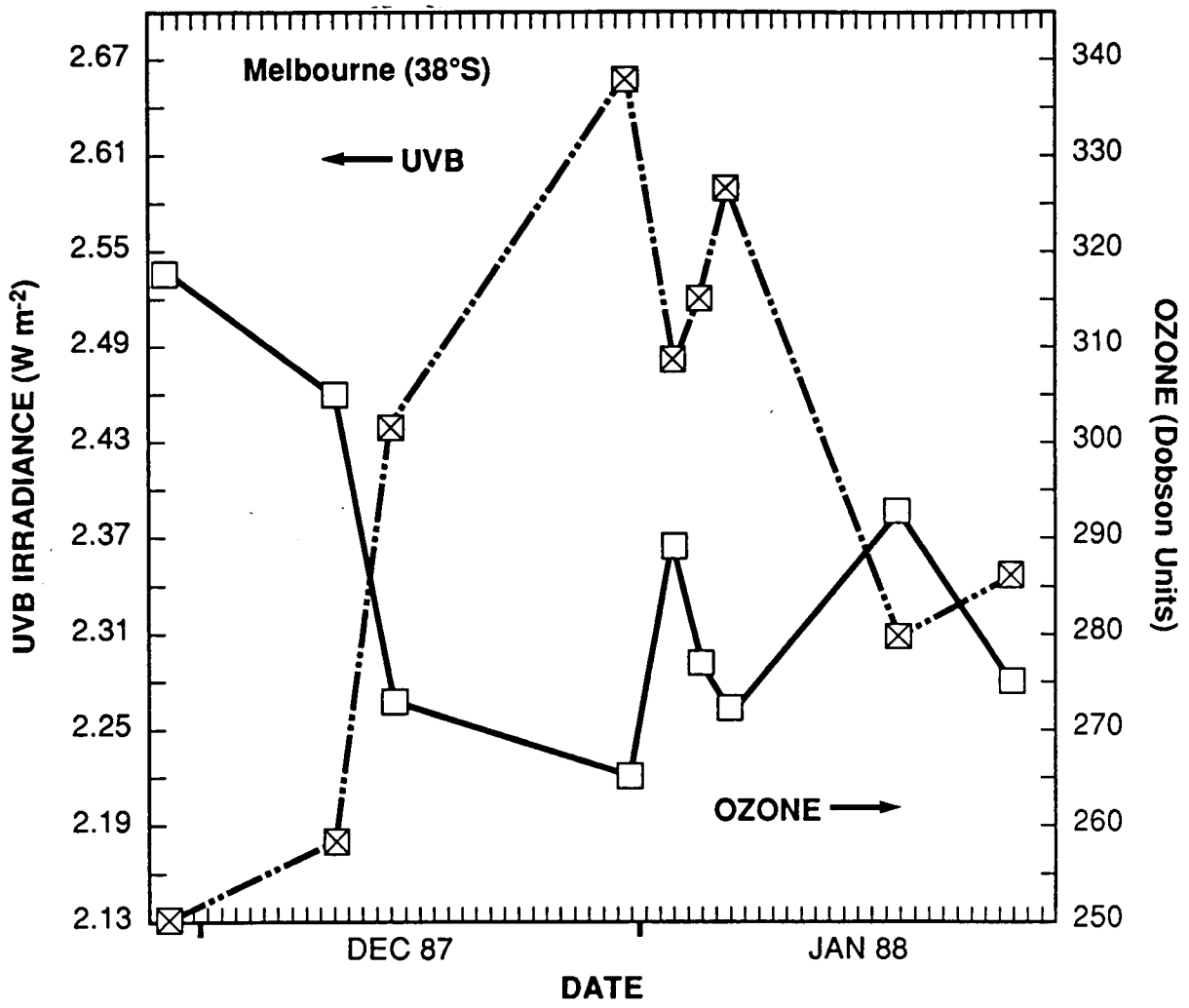

Figure 11-6 Comparison of solar UVB radiation (285 to 315 nm) and ozone at Melbourne, Australia (38° S), during the intrusion of ozone-poor air in December 1987 and January 1988 (from Roy *et al.*, (1990)).

were used in the analysis. In this period, variations in aerosol extinction were relatively small.

Figure 11-8 shows the relationship between ozone column and erythemally weighted UVB for SZA = 60 . The influence of clouds and SZA on UVB dominate over ozone effects. Clouds frequently reduce the irradiances by 50 percent or more (no observations are attempted if rain is imminent). The clear-sky subset of this data was used to deduce the increase in erythemal UV (EUV) that would result from a 1 percent decrease in ozone. This RAF: [RAF = $-(d(EUV)/EUV)/(d(O_3)/O_3)$] was then used to reconstruct the curves in the figure. Similarly, RAFs were derived for other SZAs. Figure 11-9 shows these RAFs as a function of SZA. The spread of results between morning and afternoon UV measurements, and between TOMS and Dobson ozone data, indicates the uncertainty in the measurements. Thus the RAF derived from these measurements is 1.25 ± 0.20 (McKenzie *et al.*, 1991).

The computed daily integrated RAF for this action spectrum at 30°N is 1.1, and is insensitive to cloud and tropospheric aerosol variations (UNEP, 1991). However, the calculated effect of an ozone redistribution from the stratosphere to the troposphere will lead a decrease in UV for small solar zenith angles (Brühl and Crutzen, 1989), but may lead to an increase for large solar zenith angles (Tsay and Stamnes, 1991a). Stratospheric aerosols (from volcanos) have a similar effect (Tsay and Stamnes, 1991b), so that

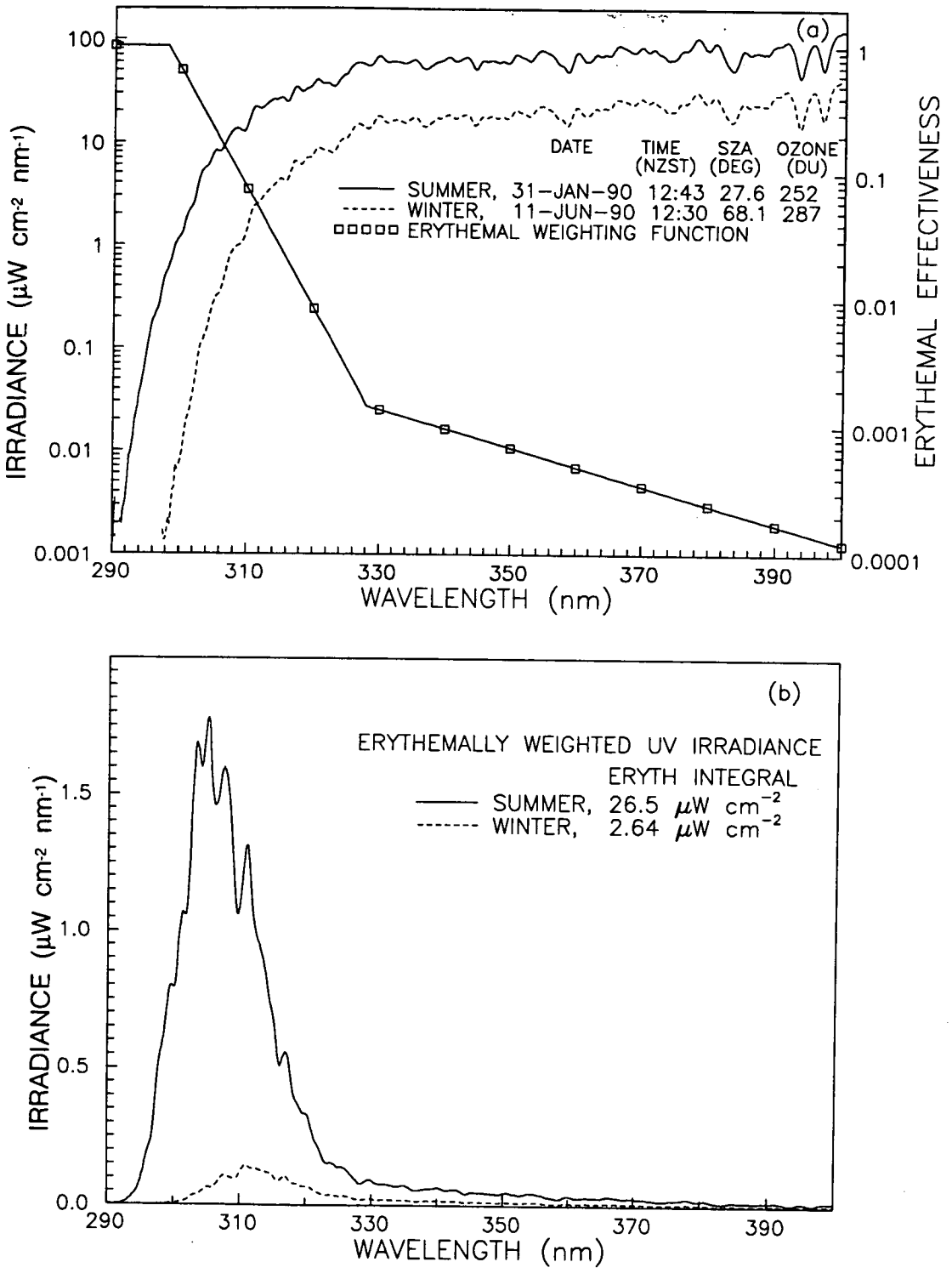

Figure 11-7 (a) Typical noon spectra of UV irradiance at mid-latitudes for summer and winter, showing the erythemal action spectrum used in the calculations that follow, (b) corresponding erythemally weighted irradiances.

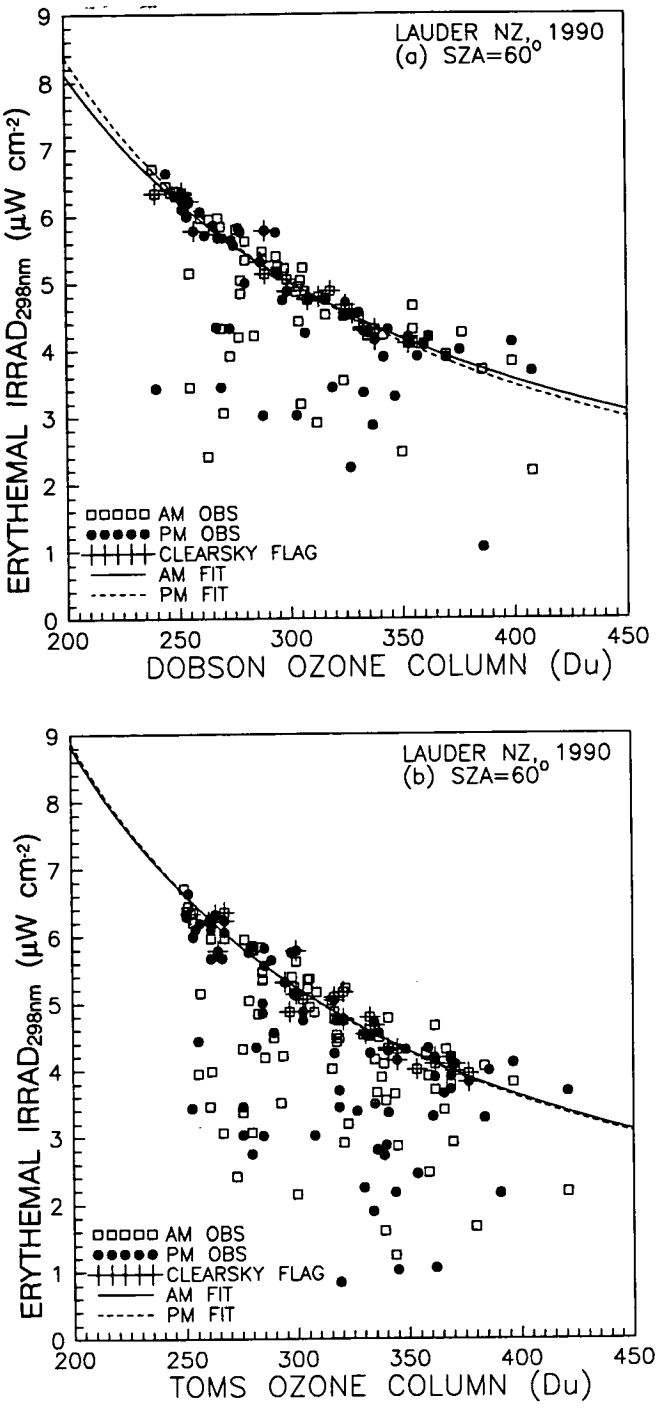

Figure 11-8 Relationship between erythemal UV (EUV) measured at SZA = 60° , and ozone (and cloud) measured at the same site (a) Ozone measured by Dobson, (b) ozone measured by TOMS. Observations that were positively identified as being cloud-free are flagged. The best-fit values of RAF = -[d(EUV)/EUV/d(O_3/O_3)] to these points were found for both morning and afternoon observations, and used to construct the fitted curves shown.

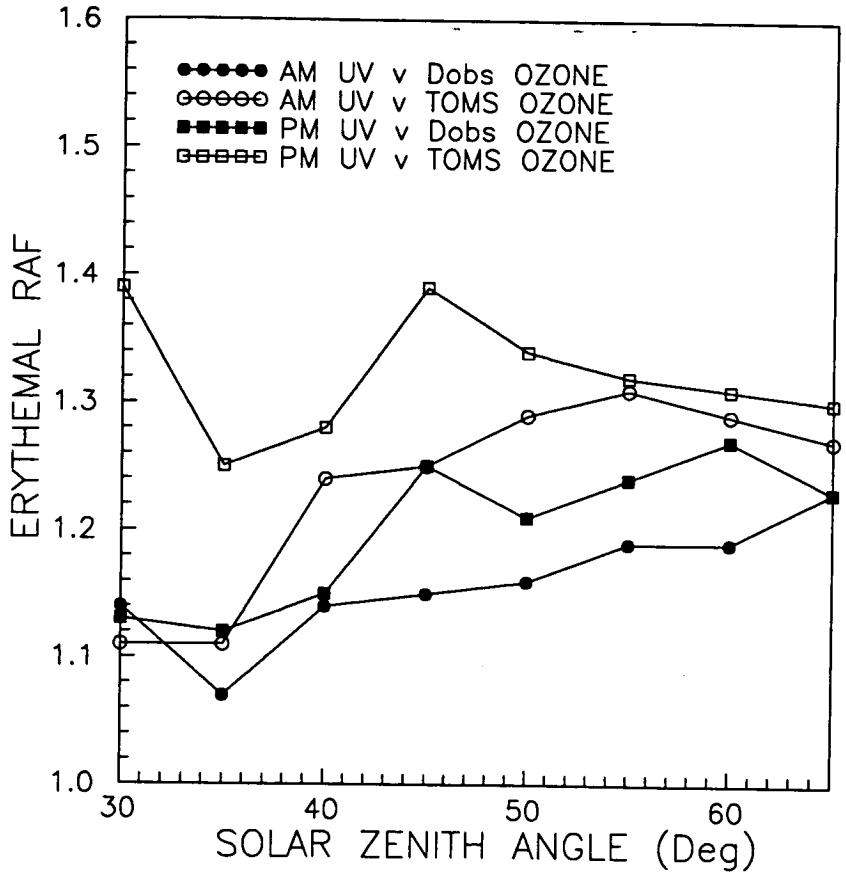

Figure 11-9 RAFs as functions of solar zenith angle, deduced from measurements of erythemally weighted UV irradiance and total ozone. Results have been separated into morning and afternoon observations, and the RAFs are deduced for both Dobson and TOMS ozone measurements.

impacts of ozone vertical redistributions and stratospheric aerosols on UV will depend on latitude and season.

11.2 CHANGES IN ULTRAVIOLET RADIATION BASED ON MEASURED AND COMPUTED OZONE AMOUNTS

11.2.1 Objectives and Limitations

This section presents computed changes in UV irradiances based on ozone values taken from measurements and two-dimensional models. Consistent with the focus of this assessment on the stratosphere, the present work addresses only those changes in UV irradiance related to changes in column ozone. The results should not be interpreted as the changes that would have actually occurred, but rather as the changes that would have occurred if column ozone were the only variable. In particular, the calculations do not account for a change in the partitioning of ozone between the stratosphere and troposphere and assume clear, pollution-free skies. All results were obtained with the radiative transfer model described by Frederick and Lubin (1988).

This analysis reports the erythemal irradiance integrated over the entire daylight period. This is defined by the convolution over wavelength of the action spectrum for erythema (McKinlay and Diffey, 1987) with the computed spectral irradiance incident on the ground integrated from sunrise to sunset. The absolute erythemal irradiance, in joules per square meter of horizontal area, depends on the action

spectrum being normalized to unity at wavelengths less than 298 nm. The extension of the spectrum to 400 nm implies that the weighted irradiance has a weaker sensitivity to changes in ozone than was the case with older action spectra, which terminated at shorter wavelengths. It is important to recognize that the values reported here depend on the action spectrum adopted. While the action spectrum for erythema is a standard reference, it is not appropriate to all biological responses. For example, using the action spectrum appropriate for damage to DNA, the sensitivity to ozone is increased, while for photosynthesis inhibition, the RAF is near 1 (UNEP, 1991). A biologically weighted irradiance provides an index of the radiation dose received by an organism, but quantitative predictions must be based on an established relationship between dose and response. A large percentage change in irradiance may or may not correspond to a large percentage change in biological response. Similarly, small percentage changes in irradiance are not necessarily insignificant. Such considerations receive further attention in the companion "Effects Assessment" document.

Figure 11-10 presents contours of daytime integrated erythemal irradiance as functions of latitude and month. The column ozone values used here are from the TOMS Version 6 data set for the year 1980. The patterns are as expected from the elevation of the sun and the duration of daylight. Large absolute values exist in the tropics and in the summer hemisphere, while a sharp latitudinal gradient exists in winter. These results represent the baseline case against which to measure percentage changes in irradiance over periods of years.

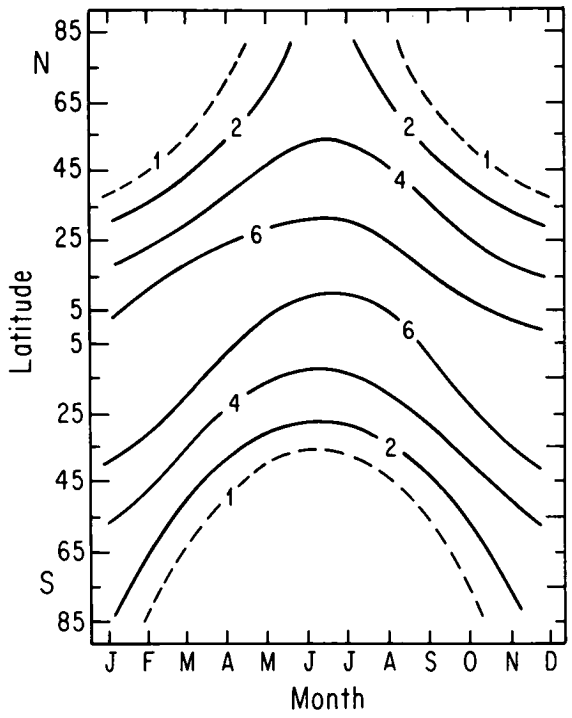

Figure 11-10 Latitudinal and monthly distribution of daytime integrated erythemal irradiance in kilojoules per square meter of horizontal area based on TOMS zonally averaged column ozone measurements from 1980.

11.2.2 Changes in Erythemal Radiation Based on TOMS Ozone Measurements

Figure 11-11 gives the percent change in daytime integrated erythemal irradiance from 1980 to 1990 as functions of latitude and month based on zonally and monthly averaged measurements from TOMS. The results show increases of 8 to 12 percent in the mid- to high-latitude winter and spring of the Northern Hemisphere. The changes from 1980 to 1990 are typically 4 to 8 percent in the northern mid-latitude summer and 4 to 12 percent in the southern summer. Note that the largest percentage changes appear in winter when the absolute irradiances are small. The cross-hatched area in Figure 11-11 is a region of large gradients in irradiance associated with the prolonged Antarctic ozone depletion of 1990. The UV enhancements in this region are in excess of 25 percent.

The annually integrated irradiance is a useful index that incorporates both the large annual cycle in radiation and the seasonal changes in ozone. Figure 11-12 presents the percent change in annually integrated erythemal irradiance between 1980 and 1990 as a function of latitude. The changes are near zero within 30° latitude of the equator but become positive at latitudes poleward of 30° in each hemisphere. The increases reach 10 percent at high northern latitudes. The extended high-latitude, Southern Hemisphere ozone depletion of 1990 led to

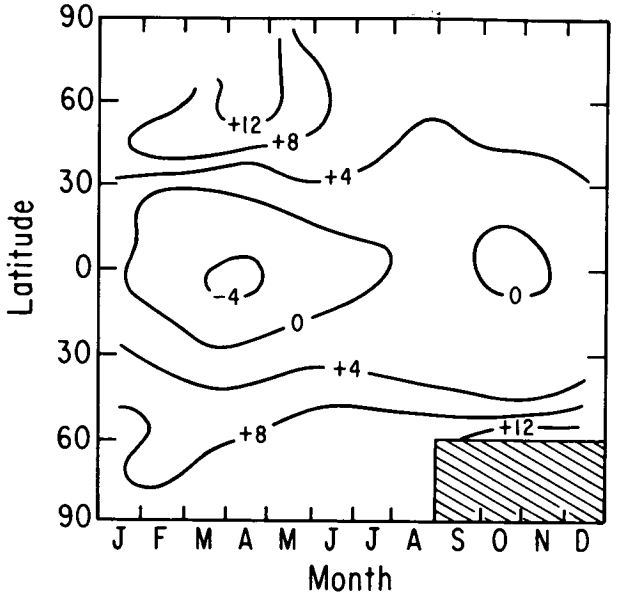

Figure 11-11 Percentage changes in daytime integrated erythemal irradiance as functions of latitude and month based on column ozone changes measured by the TOMS instrument from 1980 to 1990.

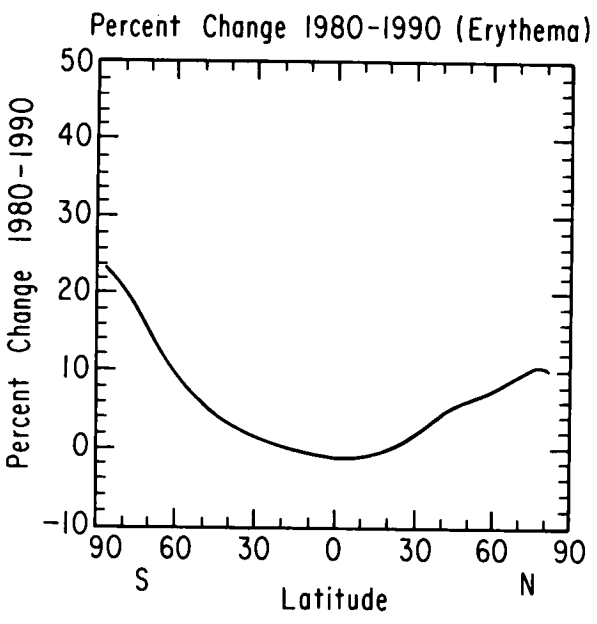

Figure 11-12 Percentage change in annually integrated erythemal irradiance between 1980 and 1990 as a function of latitude.

large ultraviolet irradiances in late spring and early summer. These influence the annually integrated irradiances, giving enhancements of 10 to 24 percent compared with 1980 at latitudes poleward of 60°S.

11.2.3 Predicted Changes in Erythemal Radiation Based on Computed Ozone Values

Current chemical models seriously underestimate the ozone losses observed by TOMS between 1980 and 1990 (see Chapter 2). Therefore they cannot be used to accurately predict future changes in UV fields. Nevertheless, the models are qualitatively in agreement that ozone losses due to atmospheric chlorine will reach a peak around the year 2000, when the peak chlorine loading is expected to maximize given full or near-full compliance with the Montreal Protocol (see Chapter 8, Scenario A). Erythemal UV levels are expected to be enhanced by a factor of two over 1990 levels by 2000, with a gradual reduction thereafter. By 2020, UV levels are expected to have reverted to 1990 levels. It must be stressed, however, that these are crude estimates, because the model simulations are incomplete.

REFERENCES

Beliavsky, A.V., V.M. Zakharov, and G.M. Kruchenitsky, The effect of cloudiness on the detection of UVB irradiance trends caused by total ozone depletion, *Optics of the Atmosphere* (Russian), submitted 1991.

Bittar, A., and R.L. McKenzie, Spectral UV intensity measurements at 45° S: 1980 and 1988, *J. Geophys. Res., 95,* 5597-5603, 1990.

Blumthaler, M., and W. Ambach, Indication of increasing solar UVB radiation flux in alpine regions, *Science, 248,* 206-208, 1990.

Brühl, C., and P.J. Crutzen, On the disproportionate role of tropospheric ozone as a filter against solar UVB radiation, *Geophys. Res. Lett., 16,* 7, 703-706, 1989.

Frederick, J.E., and A.D. Alberts, Prolonged enhancement in surface ultraviolet radiation during the Antarctic spring of 1990, *Geophys. Res. Lett., 18,* 10, 1869–1871, 1991.

Frederick, J.E., and D. Lubin, The budget of biologically active ultraviolet radiation in the Earth-atmosphere system, *J. Geophys. Res., 93,* 3825-3832, 1988.

Frederick, J.E., and E.C. Weatherhead, Temporal changes in surface ultraviolet radiation: a study of the Robertson-Berger meter and Dobson data records, *Photochem. Photobiol.,* submitted 1991.

Ilyas, M. The danger of ozone depletion in the tropics, *Search, 20,* (5), 148-149, 1989.

Kent, G.S., M.P. McCormick, and S.K. Schaffner, Global climatology of the free tropospheric aerosol from 1.0 μm satellite occultation measurements, *J. Geophys. Res., 96,* 5249-5267, 1991.

Liu, S.C., S.A. McKeen, and S. Madronich, Effect of anthropogenic aerosols on biologically active ultraviolet radiation, *Geophys. Res. Lett., 18,* 12, 2265-2268, 1991.

Lubin, D., J.E. Frederick, C.R. Booth, T. Lucas, and D. Neuschuler, Measurements of enhanced springtime ultraviolet radiation from Palmer Station, Antarctica, *Geophys. Res. Lett., 16,* 783-785, 1989.

Lubin, D., and J.E. Frederick, The UV radiation environment of the Antarctic peninsula: The roles of ozone and cloud cover, *J. Appl. Meteor., 30,* 478-493, 1991.

Madronich, S., Implications of recent total atmospheric ozone measurements for biologically active radiation reaching the Earth's surface, *Geophys. Res. Lett., 18,* 12, 2269–2272, 1991.

McKenzie, R.L., Application of a simple model to calculate latitudinal and hemispheric differences in UV radiation, *Weather and Climate, 11,* 3-14, 1991.

McKenzie, R.L., W.A. Matthews and P.V. Johnston, The relationship between erythemal UV and ozone, derived from spectral irradiance measurements, *Geophys. Res. Lett., 18* , 2269–2272, 1991.

McKinlay, A.F., and B.L. Diffey, A reference action spectrum for ultraviolet induced erythema in human skin, in *Human Exposure to Ultraviolet Radiation: Risks and Regulations* (Eds. W. R. Passchler and B. F. M. Bosnajakovic), Elsevier, Amsterdam, 83-87, 1987.

Nagatani, R.M., AJ. Miller, K. W. Johnson, and M.E. Gelman, An eight-year climatology of Meteorological and SBUV ozone data, *NOAA Technical Report NWS, 40,* Camp Springs, MD, 125 pp, 1988.

Roy, C.R., H.P. Gies, and G. Elliot, Ozone depletion, *Nature, 347,* 235-236, 1990.

Scotto J., G. Cotton, F. Urbach, D. Berger, and T. Fears, Biologically effective ultraviolet radiation: surface measurements in the U.S., *Science, 239,* 762-764, 1988.

Stamnes, K., Z. Jin, J. Slusser, C. Booth and T. Lucas, Three-fold enhancements of biologically effective ultraviolet levels at McMurdo Station, Antarctica, during the 1990 ozone "hole," *Geophys. Res. Lett.,* submitted 1992.

Stamnes, K., J. Slusser, M. Bowen, C. Booth, and T. Lucas, Biologically effective ultraviolet radiation, total ozone abundance, and cloud optical depth at McMurdo Station, Antarctica: September 15, 1988 through April 15, 1989, *Geophys. Res. Lett., 17,* 2181-2184, 1990.

Trodahl, H. J., and R. G. Buckley, UV levels under sea ice during the Antarctic spring, *Science, 245,* 194-195, 1989.

Tsay S.-C., and K. Stamnes, UV radiation in the Arctic: The impact of potential ozone depletion and cloud effects, *J. Geophys. Res.,* in press 1991a.

Tsay, S.-C. and K. Stamnes, The stratosphere as a modulator of UV radiation into the biosphere, *Surveys in Geophysics,* in press 1991b.

UNEP *Environmental Effects Panel Report,* Chapter 1, Changes in biologically active ultraviolet radiation reaching the Earth's surface, S. Madronich, L. O. Bjorn, M. Ilyas, and M. M. Caldwell, 1991.

WMO, *Scientific assessment of stratospheric ozone: 1989,* World meteorological organization Global Ozone Research and Monitoring Project, Report No. 20, Eds D. L. Albritton and R. T. Watson, 1990.

APPENDICES

A List Of International Contributors and Reviewers

B List of Figures

C List of Tables

D Major Acronyms and Abbreviations

E Chemical Formulae and Nomenclature

APPENDIX A

OMIT TO END

LIST OF INTERNATIONAL CONTRIBUTORS AND REVIEWERS

CO-CHAIRS

Daniel L. Albritton	National Oceanic and Atmospheric Administration, Boulder, CO	US
Robert T. Watson	National Aeronautics and Space Administration, Washington, DC	US

OZONE PEER-REVIEW MEETING
Les Diablerets, Switzerland
October 14-18, 1991

Daniel L. Albritton	NOAA Aeronomy Laboratory	US
Roger Atkinson	Statewide Air Pollution Research Center	US
Lane Bishop	Allied Signal Inc.	US
Rumen D. Bojkov	World Meteorological Organization	Switzerland
William H. Brune	Pennsylvania State University	US
Bruce Callander	Meteorological Office, IPCC Secretariat	UK
Daniel Cariolle	Meteorologie Nationale EERM/CNRM	France
Marie-Lise Chanin	Service d'Aèronomie du CNRS	France
R. Anthony Cox	Natural Environment Research Council	UK
Vitali Fioletov	Central Aerological Observatory	USSR
Paul J. Fraser	CSIRO	Australia
Sophie Godin	Service d'Aèronomie du CNRS	France
Robert S. Harwood	University of Edinburgh	UK
Abdel Moneim Ibrahim	Egyptian Meteorological Authority	Egypt
Ivar S. A. Isaksen	University of Oslo	Norway
Charles H. Jackman	NASA Goddard Space Flight Center	US
Evgeny A. Jadin	Central Aerological Observatory	USSR
Colin Johnson	Harwell Laboratory	UK
Igor L. Karol	Main Geophysical Observatory	USSR
Jack Kaye	NASA Headquarters	US
James B. Kerr	Atmospheric Environment Service	Canada
Dieter Kley	Kernforschungsanlage Jülich GmbH	Germany
Malcolm K. W. Ko	Atmospheric & Environmental Research, Inc.	US
Michael J. Kurylo	NASA Headquarters/NIST	US
Jane Leggett	Environmental Protection Agency	US

INTERNATIONAL CONTRIBUTORS AND REVIEWERS

Conway B. Leovy	University of Washington	US
Pak Sum Low	Ozone Secretariat, UNEP Headquarters	Kenya
Yoshihiro Makide	University of Tokyo	Japan
W. Andrew Matthews	DSIR Physical Sciences	New Zealand
Mack McFarland	E.I. DuPont de Nemours and Co., Inc.	US
Richard L. McKenzie	DSIR Physical Sciences	New Zealand
Gèrard Mègie	Service d'Aèronomie du CNRS	France
P. Muthusubramanian	Madurari Kamaraj University	India
Michael Oppenheimer	Environmental Defense Fund	US
D. C. Parashar	National Physical Laboratory	India
Stuart A. Penkett	University of East Anglia	UK
Lamont R. Poole	NASA Langley Research Center	US
Michael J. Prather	NASA Goddard Institute for Space Studies	US
Margarita Prendez	Universidad de Chile	Chile
Lian Xiong Qiu	Academica Sinica, Beijing	Peoples Republic of China
V. Ramaswamy	Princeton University	US
A. R. Ravishankara	NOAA Aeronomy Laboratory	US
Joan Rosenfield	NASA Goddard Space Flight Center	US
Nelson Antonio Sabogal	Instituto Colombiano de Hidrologià	Colombia
Eugenio Sanhueza	Instituto Venezolano de Investigaciones Cientificas	Venezuela
Howard Sidebottom	University College Dublin	Ireland
Susan Solomon	NOAA Aeronomy Laboratory	US
Johannes Staehelin	Atmosphärenphysik ETH	Switzerland
Richard S. Stolarski	NASA Goddard Space Flight Center	US
Bhoganahalli Subbaraya	Physical Research Laboratory	India
Guido Visconti	Università degli Studi-l'Aquila	Italy
Andreas Wahner	KFA Jülich	Germany
Wei-Chyung Wang	State University of New York at Albany	US
David A. Warrilow	Department of the Environment	UK
Robert T. Watson	NASA Headquarters	US
Tom Wigley	University of East Anglia	UK
Donald J. Wuebbles	Lawrence Livermore National Laboratory	US
Ahmad Zand	University of Teheran	Iran
Rudi J. Zander	University of Liege	Belgium
Joseph M. Zawodny	NASA Langley Research Center	US
Christos Zerefos	Aristotelian University of Thessaloniki	Greece
Ya-Hui Zhuang	Asian Institute of Technology	Thailand
Sergei Zvenigorodsky	USSR Academy of Sciences	USSR

Chapter 1 Source Gases: Concentrations, Emissions, and Trends

	Chapter Coordinator	
Paul Fraser	CSIRO	Australia
	Lead Authors	
Robert Harriss	University of New Hampshire	US
Yoshihiro Makide	University of Tokyo	Japan
Stuart Penkett	University of East Anglia	UK
Eugenio Sanhueza	Instituto Venezolano de Investigaciones Cientificas	Venezuela
	Contributors	
Fred N. Alyea	Georgia Institute of Technology	US
Don Blake	University of California, Irvine	US
Derek M. Cunnold	Georgia Institute of Technology	US
James W. Elkins	NOAA/CMDL	US
Michio Hirota	Japan Meteorological Agency	Japan
Ronald G. Prinn	Massachusetts Institute of Technology	US
Rei A. Rasmussen	Oregon Graduate Institute for Science & Technology	US
F. Sherwood Rowland	University of California, Irvine	US
Toru Sasaki	Meteorological Research Institute	Japan
H. Scheel	Fraünhofer Institute for Atmos. Env. Research	Germany
Wolfgang Seiller	Fraünhofer Institute for Atmos. Env. Research	Germany
P. Simmonds	University of Bristol	UK
Paul Steele	CSIRO	Australia
Ray F. Weiss	Scripps Institution of Oceanography	US
	Mail Reviewers	
R. Anthony Cox	Natural Environment Research Council	UK
Jack Kaye	NASA	US
Volker Kirchhoff	Atmospheric and Space Science, INPE	Brazil
Henning Rodhe	University of Stockholm	Sweden

Chapter 2 Ozone and Temperature Trends

	Chapter Coordinator	
Richard S. Stolarski	NASA Goddard Space Flight Center	US
	Lead Authors	
Lane Bishop	Allied Signal Inc.	US
Rumen D. Bojkov	World Meteorological Organization	Switzerland
Marie-Lise Chanin	Service d'Aèronomie du CNRS	France
Vitali Fioletov	Central Aerological Observatory	USSR
Sophie Godin	Service d'Aèronomie du CNRS	France
Volker Kirchhoff	Atmospheric and Space Science, INPE	Brazil
Joseph M. Zawodny	NASA Langley Research Center	US
Christos Zerefos	Aristotelian University of Thessaloniki	Greece

	Contributors	
William Chu	NASA Langley Research Center	US
John DeLuisi	NOAA/CMDL	US
Anne Hansson	Atmospheric Environment Service	Canada
James Kerr	Atmospheric Environment Service	Canada
Evgeny Lysenko	Central Aerological Observatory	USSR
M. Patrick McCormick	NASA Langley Research Center	US
Paul Newman	NASA Goddard Space Flight Center	US
Margarita Prendez	Universidad de Chile	Chile
Johannes Staehelin	Atmosphärenphysik ETH	Switzerland
Bhoganahalli Subbaraya	Physical Research Laboratory	India
	Mail Reviewers	
Neil Harris	Department of the Environment	UK
William Hill	University of Wisconsin-Madison	US
A. J. Miller	NOAA National Meteorological Center	US

Chapter 3 Heterogeneous Processes: Laboratory, Field, and Modeling Studies

	Chapter Coordinator	
Lamont R. Poole	NASA Langley Research Center	US
	Lead Authors	
Rod L. Jones	University of Cambridge	UK
Michael J. Kurylo	National Institute of Standards and Technology	US
Andreas Wahner	KFA Jülich	Germany
	Contributors	
Jack G. Calvert	National Center for Atmospheric Research	US
A. Fried	National Center for Atmospheric Research	US
David J. Hofmann	NOAA/CMDL	US
Leon F. Keyser	Jet Propulsion Laboratory	US
Charles E. Kolb	Aerodyne Research	US
M.-T. Leu	Jet Propulsion Laboratory	US
Mario J. Molina	Massachusetts Institute of Technology	US
M. C. Pitts	Hughes STX	US
A. R. Ravishankara	NOAA Aeronomy Laboratory	US
L. W. Thomason	NASA Langley Research Center	US
Margaret A. Tolbert	SRI, International	US
Doug R. Worsnop	Aerodyne Research, Inc.	US
	Mail Reviewers	
Robert F. Hampson	National Institute of Standards and Technology	US
O. Brian Toon	NASA Ames ResearchCenter	US
Steve Wofsy	Harvard University	US

Chapter 4 Stratospheric Processes: Observations and Interpretation

	Chapter Coordinator	
William H. Brune	Pennsylvania State University	US
	Lead Authors	
Guy Brasseur	National Center for Atmospheric Research	US
R. Anthony Cox	Natural Environment Research Council	UK
Anne Douglass	NASA Goddard Space Flight Center	US
W. Andrew Matthews	DSIR Physical Sciences	New Zealand
Alan O'Neill	Robert Hooke Institute	UK
Margarita Prendez	Universidad de Chile	Chile
Jose M. Rodriguez	Atmospheric & Environmental Research, Inc.	US
Bhoganahalli Subbaraya	Physical Research Laboratory	India
Richard Turco	University of California, Los Angeles	US
Rudi J. Zander	University of Liege	Belgium
Xiuji Zhou	State Meteorological Administration	Peoples Republic of China
	Contributors	
J. Austin	Meteorological Office	UK
Malcolm K. W. Ko	Atmospheric & Environmental Research, Inc.	US
Michael J. Prather	NASA Goddard Institute for Space Studies	US
A. R. Ravishankara	NOAA Aeronomy Laboratory	US
Mark R. Schoeberl	NASA Goddard Space Flight Center	US
Susan Solomon	NOAA Aeronomy Laboratory	US
Adrian F. Tuck	NOAA Aeronomy Laboratory	US
	Mail Reviewers	
Daniel Cariolle	Meteorologie Nationale EERM/CNRM	France
Mack McFarland	E.I. DuPont de Nemours and Co., Inc.	US
John A. Pyle	University of Cambridge	UK
Christos Zerefos	Aristotelian University of Thessaloniki	Greece

Chapter 5 Tropospheric Processes: Observations and Interpretation

	Chapter Coordinator	
Ivar S. A. Isaksen	University of Oslo	Norway
	Lead Authors	
Roger Atkinson	Statewide Air Pollution Research Center	US
J. A. Fuglestvedt	University of Oslo	Norway
Colin Johnson	Harwell Laboratory	UK
Yuan-Pern Lee	National Tsing Hua University, Taiwan	Republic of China
Jos. Lelieveld	Max-Planck Institute for Chemistry-Mainz	Germany
Howard Sidebottom	University of Dublin	Ireland
Anne Thompson	NASA Goddard Space Flight Center	US

	Contributors	
T. Berntsen	University of Oslo	Norway
William H. Brune	Pennsylvania State University	US
Jack Kaye	NASA Headquarters	US
Michael Oppenheimer	Environmental Defense Fund	US
	Mail Reviewers	
Paul J. Crutzen	Max-Planck Institute for Chemistry-Mainz	Germany
Volker Kirchhoff	Atmospheric and Space Science - INPE	Brazil
Stuart Penkett	University of East Anglia	UK

Chapter 6 Ozone Depletion and Chlorine Loading Potentials

	Chapter Coordinator	
Susan Solomon	NOAA Aeronomy Laboratory	US
	Lead Authors	
John A. Pyle	University of Cambridge	UK
Donald J. Wuebbles	Lawrence Livermore National Laboratory	US
Sergei Zvenigorodsky	USSR Academy of Sciences	USSR
	Contributors	
Peter Connell	Lawrence Livermore National Laboratory	US
Donald A. Fisher	E.I. DuPont de Nemours and Co., Inc.	US
Malcolm K. W. Ko	Atmospheric & Environmental Research, Inc.	US
Frode Stordal	Norwegian Institute for Air Research	Norway
Debra Weisenstein	Atmospheric & Environmental Research, Inc.	US
	Mail Reviewers	
Guy Brasseur	National Center for Atmospheric Research	US
Michael J. Prather	NASA Goddard Institute for Space Studies	US

Chapter 7 Radiative Forcing of Climate

	Chapter Coordinator	
V. Ramaswamy	Princeton University	US
	Lead Authors	
Conway Leovy	University of Washington	US
Henning Rodhe	University of Stockholm	Sweden
Keith Shine	University of Reading	UK
Wei-Chyung Wang	State University of New York at Albany	US
Donald J. Wuebbles	Lawrence Livermore National Laboratory	US
	Contributors	
M. Ding	State University of New York at Albany	US
Jae A. Edmonds	Department of Energy	US

Paul Fraser	CSIRO	Australia
Keith Grant	Lawrence Livermore National Laboratory	US
Colin Johnson	Harwell Laboratory	UK
D. Lashof	National Resources Defense Council	US
Jane Leggett	Environmental Protection Agency	US
Jos. Lelieveld	Max-Planck Institute for Chemistry-Mainz	Germany
M. Patrick McCormick	NASA Langley Research Center	US
Abraham Oort	NOAA Geophysical Fluid Dynamics Laboratory	US
M. D. Schwartzkopf	NOAA Geophysical Fluid Dynamics Laboratory	US
A. Sutera	University of Camerino	Italy
David A. Warrilow	Department of the Environment	UK
Tom Wigley	Meteorological Office	UK
	Mail Reviewers	
Jeffrey Kiehl	National Center for Atmospheric Research	US
Joan Rosenfield	NASA Goddard Space Flight Center	US

Chapter 8 Future Chlorine- Bromine-Loading and Ozone Depletion

	Chapter Coordinator	
Michael J. Prather	NASA Goddard Institute for Space Studies	US
	Lead Authors	
Abdel Moneim Ibrahim	Egyptian Meteorological Authority	Egypt
Toru Sasaki	Meteorological Research Institute	Japan
Frode Stordal	Norwegian Institute for Air Research	Norway
Guido Visconti	Università degli Studi-lAquila	Italy
	Model Contributors	
Guy Brasseur	National Center for Atmospheric Research	US
Christoph H. Brühl	Max-Planck Institute für Chemie	Germany
Donald A. Fisher	E.I. DuPont de Nemours and Co., Inc.	US
Ivar S. A. Isaksen	University of Oslo	Norway
Charles H. Jackman	NASA Goddard Space Flight Center	US
Evgeny A. Jadin	Central Aerological Observatory	USSR
Malcolm K. W. Ko	Atmospheric & Environmental Research, Inc.	US
Toru Sasaki	Meteorological Research Institute	Japan
Susan Solomon	NOAA Aeronomy Laboratory	US
Guido Visconti	Università degli Studi-lAquila	Italy
Donald J. Wuebbles	Lawrence Livermore National Laboratory	US
Sergei Zvenigorodsky	USSR Academy of Sciences	USSR
	Mail Reviewers	
Daniel Cariolle	Meteorologie Nationale EERM/CNRM	France
Paul Fraser	CSIRO	Australia
Charles H. Jackman	NASA Goddard Space Flight Center	US

Mack McFarland	E.I. DuPont de Nemours and Co., Inc.	US
Susan Solomon	NOAA Aeronomy Laboratory	US

Chapter 9 Predicted Aircraft Effects on Stratospheric Ozone

Chapter Coordinator

Malcolm K. W. Ko	Atmospheric & Environmental Research, Inc.	US

Lead Authors

Evgeny A. Jadin	Central Aerological Observatory	USSR
Dieter Kley	Kernforschungsanlage Jülich GmbH	Germany
Steve Wofsy	Harvard University	US

Contributors

Colin Johnson	Harwell Laboratory	UK
Michael J. Prather	NASA Institute for Space Studies	US
D. Weisenstein	Atmospheric & Environmental Research, Inc.	US
Donald J. Wuebbles	Lawrence Livermore National Laboratory	US

Mail Reviewers

W. Andrew Matthews	DSIR Physical Sciences	New Zealand
K. Stamnes	University of Alaska	US
Froide Stordal	Norwegian Institute for Air Research	Norway

Chapter 10 Predicted Rocket and Shuttle Effects on Stratospheric Ozone

Chapter Coordinator

Charles H. Jackman	NASA Goddard Space Flight Center	US

Lead Authors

Robert S. Harwood	University of Edinburgh	UK
Igor L. Karol	Main Geophysical Laboratory	USSR
Lian Xiong Qiu	Academia Sinica	Peoples Republic of China

Contributors

Michael J. Prather	NASA Goddard Institute for Space Studies	US
John A. Pyle	Cambridge University	UK

Mail Reviewers

Ivar S.A. Isaksen	Univeristy of Oslo	Norway
Harold S. Johnston	Univeristy of California, Berkeley	US
Michael Oppenheimer	Environmental Defense Fund	US
Donald J. Wuebbles	Lawrence Livermore National Laboratory	US

Chapter 11 Ultraviolet Radiation Changes

Chapter Coordinator

Richard L. McKenzie	DSIR Physical Sciences	New Zealand

Lead Authors

V. Filyushkin	Central Aerological Observatory	USSR
John E. Frederick	University of Illinois-Chicago	US
Mohammad Ilyas	University of Science of Malaysia	Malaysia

Contributors

M. Blumthaler	University of Innsbruck	Austria
Sasha Madronich	National Center for Atmospheric Research	US
P. Muthusubramanian	Madurai Kamaraj University	India
Colin E. Roy	Australian Radiation Laboratory	Australia
K. Stamnes	University of Alaska	US
Andreas Wahner	KFA Jülich	Germany

Mail Reviewers

Vyacheslav Khattatov	Central Aerological Observatory	USSR
Michael J. Prather	NASA Goddard Institute for Space Studies	US
Frode Stordal	Norwegian Institute for Air Research	Norway

EDITORS

Daniel A. Albritton	Co-Chair - NOAA	US
Robert T. Watson	Co-Chair - NASA	US
Susan Solomon	Preprint - NOAA Aeronomy Laboratory	US
Robert F. Hampson	National Institute of Standards & Technology	US
Flo Ormond	NASA	US

EDITORIAL STAFF

Earth Science Support Office
Kris Wheeler
Editor: Jan Timmons
Graphics: Lori Kissinger

CONFERENCE COORDINATION AND DOCUMENTATION

Rumen D. Bojkov	WMO	Switzerland
Marie-Christine Charriere	WMO	France
Flo Ormond	NASA	US
N. Plock	NOAA	US
Shelagh Varney	Meteorological Office	UK
Jeanne Waters	NOAA	US

Appendix B

List of Figures

FIGURES

FIGURES

FIGURES

Appendix C

List of Tables

TABLES

APPENDIX D

Major Acronyms and Abbreviations

AAOE	Airborne Antarctic Ozone Experiment
AASE	Airborne Arctic Stratospheric Expedition
AER	Atmospheric and Environmental Research, Inc.
AERE	Atomic Energy Research Establishment (UK)
AFCRL	Air Force Cambridge Research Laboratories
AFEAS	Alternative Fluorocarbon Environmental Acceptability Study
AFGL	Air Force Geophysical Laboratory
AGU	American Geophysical Union
AIAA	American Institute of Aeronautics and Astronautics, Inc.
ALE/GAGE	Atmospheric Lifetime Experiment-Global Atmospheric Gases Experiment
AMAP	Association for Meteorology and Atmospheric Physics
ARC	Ames Research Center (NASA)
ATMOS	Atmospheric Trace Molecule Spectroscopy
AVHRR	Advanced Very High Resolution Radiometer
BaU	Business as Usual
BLP	Bromine Loading Potential
BOIC	Balloon Ozone Intercomparison Campaign
BUV	Backscatter Ultraviolet Spectrometer
CAMED-P	University of Cambridge and University of Edinburgh
CCN	Cloud Condensation Nuclei
CFC	Chlorofluorocarbon
CFM	Chlorofluoromethane
CHEOPS	CHemistry of Ozone in the Polar Stratosphere
CIMO	Commission on Instrument and Method of Observation
CIRA	COSPAR International Reference Atmosphere
CLP	Chlorine Loading Potential
CMA	Chemical Manufacturers Association
CMDL	Climate Monitoring and Diagnostics Laboratory (NOAA, U.S.)
CMRN	Cooperative Meteorological Rocketsonde Network
CNRS	Centre National de la Recherche Scientifique (France)
COSPAR	Committee on Space Research
CPOZ	Compressed Profile Ozone
CSIR	Council for Scientific and Industrial Research Organization (South Africa)
CSIRO	Commonwealth Scientific and Industrial Research Organization (Australia)
DCA	Detector capsule assembly
DU	Dobson Unit

ACRONYMS

ECC	Electrochemical cell (ozonesonde)
ECMWF	European Center for Medium-Range Weather Forecasts
EGA	Emissivity growth approximation
EI	Emission Index
EMR	Electromagnetic radiation
ENSO	El Niño-Southern Oscillation
EOS	Earth Observing System
ERBS	Earth Radiation Budget Satellite
ERL	Environmental Research Laboratory (NOAA)
ESA	European Space Agency
EUV	Erythemal UV
FDH	Fixed Dynamical Heating
FGGE	First GARP Global Experiment
FIAER	Fraunhofer Institute for Atmospheric Environmental Research (Germany)
FOV	Field of view
GAGE	Global Atmospheric Gases Experiment
GARP	Global Atmospheric Research Program
GFDL	Geophysical Fluid Dynamics Laboratory
GHRS	Goddard High Resolution Spectrograph
GIT	Georgia Institute of Technology (United States)
GMCC	Geophysical Monitoring for Global Change (NOAA)
GMT	Greenwich Mean Time
GSFC	Goddard Space Flight Center (NASA)
GWP	Global Warming Potential
HCFC	Hydrochlorofluorocarbon
HFC	Hydrofluorocarbon
HIRS	High Resolution Infrared Radiation Sounder
hPa	hectoPascal
HSCT	High Speed Civil Transports
HSRP	High Speed Research Program
IAGA/IAMAP	International Association for Geomagnetism and Aeronomy/International Association for Meteorology and Atmospheric Physics
ICAO	International Civil Aviation Organization
ICSU	International Council of Scientific Unions
IFC	Inflight calibrator
IFOV	Instrument field of view
IGY	International Geophysical Year
INPE	Brazilian space agency
IOC	International Ozone Commission
IPCC	Intergovernmental Panel on Climate Change
IPV	Isentropic potential vorticity
IR	Infrared

JPL	Jet Propulsion Laboratory
LAMAT	LIMS Map Archival Tapes
LaRC	Langley Research Center (NASA)
LASP	Laboratory for Atmospheric and Space Physics (University of Colorado)
LIMS	Limb Infrared Monitor of the Stratosphere
LLNL	Lawrence Livermore National Laboratory
LRIR	Limb Radiance Inversion Radiometer
LTE	Local Thermodynamic Equilibrium
MAP	Middle Atmosphere Program
MLS	Mid-Latitude Summer
MPIA	Max Planck Institute for Aeronomy (Germany)
MRI	Meteorological Research Institute (Japan)
MSU	Microwave Sounding Unit
NASA	National Aeronautics and Space Administration
NASP	National Aerospace Plane
NBS	National Bureau of Standards (now NIST)
NCAR	National Center for Atmospheric Research (U.S.)
NDSC	Network for the Detection of Stratospheric Change
NESDIS	National Environmental Satellite Data and Information Service
NILU	Norsk Institute for Luftforskning (Oslo)
NIR	Near infrared
NIST	National Institute of Standards and Technology (formerly NBS) (U.S.)
NMC	National Meteorological Center
NMHCs	Non-methane hydrocarbons
NOAA	National Oceanic and Atmospheric Administration
NOAA/AL	National Oceanic and Atmospheric Administration/Aeronomy Laboratory
NOAA-CMDL	National Oceanic and Atmospheric Administration—Climate Monitoring and Diagnostics Laboratory
NOZE	National Ozone Expedition
NPL	National Physical Laboratory (United Kingdom)
NRC	National Research Council
NRL	Naval Research Laboratory
NSSDC	National Space Science Data Center
OAG	Official Airline Guide
ODP	Ozone Depletion Potential
ODW	Ozone Data for the World
OEDC	Organization for Economic Cooperation and Development (Paris, France)
OGC	Oregon Graduate Center (now OGIST) (U.S.)
OGIST	Oregon Graduate Institute for Science and Technology
OGO	Orbiting Geophysical Observatory
OPT	Ozone Processing Team
OTP	Ozone Trends Panel

PAN	Peroxyacetyl nitrate
PMR	Pressure Modulated Radiometer
PMT	Photomultiplier tube
PNW	Pacific North West region of the United States
PPN	Peroxypropionyl nitrate
PSCs	Polar Stratrospheric Clouds
PV	Potential Vorticity
QBO	Quasi-Biennial Oscillation
RAF	Radiative Amplification Factor
RAOB	Rawinsonde Observation
RB	Robertson-Berger Network
ROCOZ	Rocket Ozonesonde
SAGE	Stratospheric Aerosol and Gas Experiment
SAM II	Stratospheric Aerosol Measurement
SAMS	Stratospheric and Mesospheric Sounder
SAO	Smithsonian Astrophysical Observatory (Cambridge, MA)
SBUV	Solar Backscatter Ultraviolet Spectrometer
SCOSTEP	Scientific Committee on Solar Terrestrial Physics
SCR	Selective Chopper Radiometer
SIO	Scripps Institution for Oceanography
SIRIS	Stratospheric InfraRed Interferometer Spectrometer
SME	Solar Mesosphere Explorer
SMM	Solar Maximum Mission
SOI	Southern Oscillation Index
SPEs	Solar Proton Events
SSU	Stratospheric Sounding Unit
SZAs	Solar Zenith Angles
THIR	Temperature Humidity Infrared Radiometer
TIROS	Television and Infrared Observation Satellite
TOMS	Total Ozone Mapping Spectrometer
TOVS	TIROS Operational Vertical Sounder
UADP	Upper Atmosphere Data Program
UARS	Upper Atmosphere Research Satellite
UCI	University of California at Irvine (United States)
UEA	University of East Anglia (United Kingdom)
UKMO	United Kingdom Meteorological Office
UNEP	United Nations Environment Program
UT	University of Tokyo (Japan)
UV	Ultraviolet
UVB	Ultraviolet-B

UVS	Ultraviolet Spectrometer
UVSP	Ultraviolet Spectrometer and Polarimeter
VTPR	Vertical Temperature Profile Radiometer
WMO	World Meteorological Organization
WODC	World Ozone Data Center

Appendix E

Chemical Formulae and Nomenclature

Symbol	Name	Symbol	Name
O	Atomic oxygen	CH_2O	Formaldehyde
O_2	Molecular oxygen	CH_3CHO	Acetaldehyde
O_3	Ozone	$(CH_3)_2CO$	Acetone
O_x	Odd oxygen (O, $O(^1D)$, O_3)	CH_3O_2H	Methyl hydroperoxide
N_2	Molecular nitrogen	CH_2CHCHO	Acrolein
N_2O	Nitrous oxide	C_2Cl_4	Tetrachloroethylene
NO	Nitric oxide	CH_3Cl	Methyl chloride
NO_2	Nitrogen dioxide	CH_2Cl_2	Dichloromethane
NO_3	Nitrogen trioxide, nitrate radical	$CHCl_3$	Chloroform, trichloromethane
		CFC	Chlorofluorocarbon
NO_y	Odd nitrogen (NO, NO_2, NO_3, N_2O_5, $ClONO_2$, HNO_4, HNO_3)	HC	Hydrocarbon
		NMHC	Nonmethane hydrocarbons
		PAN	Peroxyacetylnitrate
NO_x	Oxides of nitrogen (NO, NO_2, NO_3)	CH_3CCl_3	Methyl chloroform
		C_2F_6	Hexafluoroethane
N_2O_5	Dinitrogen pentoxide	CCl_4	Carbon tetrachloride
HNO_2, HONO	Nitrous acid	CCl_3F	Trichlorofluoromethane (CFC–11)
HNO_3, $HONO_2$	Nitric acid		
HNO_4, HO_2NO_2	Peroxynitric acid	CCl_2F_2	Dichlorodifluoromethane (CFC–12)
NH_3	Ammonia		
H_2O	Water vapor	$CClF_3$	Chlorotrifluoromethane (CFC–13)
H_2O_2	Hydrogen peroxide		
OH, HO	Hydroxyl radical	CF_4	Tetrafluoromethane
HO_2	Hydroperoxyl radical	$CHCl_2F$	Dichlorofluoromethane (HCFC–21)
HO_x	Odd hydrogen (OH, HO_2, H_2O_2)	$CHClF_2$	Chlorodifluoromethane (HCFC–22)
CO	Carbon monoxide	CCl_2FCClF_2	Trichlorotrifluoroethane (CFC–113)
CO_2	Carbon dioxide		
CS_2	Carbon disulfide	$CClF_2CClF_2$	Dichlorotetrafluoroethane (CFC–114)
COS, OCS	Carbonyl sulfide		

CHEMICAL FORMULAE AND NOMENCLATURE

SO_2	Sulfur dioxide
SF_6	Sulfur hexafluoride
H_2SO_4	Sulfuric acid
HF	Hydrogen fluoride
HCl	Hydrogen chloride
HCN	Hydrogen cyanide
HOCl	Hypochlorous acid
Cl	Chlorine atom
ClO	Chlorine monoxide
$ClONO_2$, $ClNO_3$	Chlorine nitrate
Cl_x	Odd chlorine, inorganic chlorine
CH_4	Methane
C_2H_6	Ethane
C_3H_8	Propane
C_2H_4	Ethylene
C_2H_2	Acetylene
$CClF_2CF_3$	Chloropentafluoroethane (CFC–115)
CF_3CF_3	Hexafluoroethane
CH_3CN	Methyl cyanide
CH_3I	Methyl iodide
Br	Bromine atom
BrO	Bromine monoxide
Br_x	Odd bromine, inorganic bromine
$CBrF_3$	Trifluorobromomethane
$CHBr_3$	Bromoform, tribromomethane
CH_3Br	Methyl bromide
CH_2Br_2	Dibromomethane
$CHBr_2Cl$	Dibromochloromethane
$C_2H_4Br_2$	Dibromoethane
$CBrClF_2$	Halon 1211
CF_3Br	Halon 1301